Biophysics II

Introduction:
Biomolecular Spectroscopy – How Biomolecules Interact with Light

Uli Nienhaus

Prof. G. U. Nienhaus, Vorlesungsunterlagen Biophysik II, SS 2023.
Nur zum KIT-internen, vorlesungsbegleitenden Gebrauch.
Weitergabe und anderweitige Nutzung verboten.

Angewandte Physik – Biophysik

Lehrveranstaltungen im Sommersemester 2023:

- Vorlesung Biophysik II (zweigeteilt für Chem. Biol.-Master)
  (Gerd Ulrich Nienhaus, SR 6-1, Mi. / Fr. 9:45 – 11:15)

- Übungen zur Vorlesung
  (G. U. N. mit Dr. Gernot Guigas, 2 SWS, Do. 9:45 – 11:15)

- Seminar zur Vorlesung (für Physik-Master Ergänzungsfach)
  (G. U. N. mit Dr. Gernot Guigas, Vortrag zu ausgewähltem Thema, Dauer 30 min, nach Vereinbarung)

- Hauptseminar „Konformationsdynamik in Biomolekülen“
  (G. U. N. mit Dr. Andrei Kobitski, Prof. Wolfgang Wenzel)

Biophysik-Lehrveranstaltungen

Einbettung in die Studiengänge:

Experimentelle Biophysik für Physiker als

- Schwerpunktfach (12 ECTS): Vorlesung + Übungen + Prüfung
- Ergänzungsfach (14 ECTS): Vorlesung + Übungen + Seminar + Prüfung
- Nebenfach (8 ECTS): Vorlesung + Übungen

Experimentelle Biophysik für Chemische Biologen

- Vorlesung + Prüfung (Übungen optional)

Biophysik-Übungen

Leitung:
Dr. Gernot Guigas
gernot.guigas@kit.edu

Anmeldung

- ILIAS - Übung zur Experimentellen Biophysik - SS 2023
- Passwort: Golgi_2023
- Hier auch Download von Vorlesungsfolien und Skripten

Ausgabe der Übungsblätter

- jeden Dienstag in ILIAS - Übungen zur Experimentellen Biophysik - SS 2023

Abgabe der bearbeiteten Übungsblätter

- am Dienstag der Folgewoche vor 10 Uhr, in ILIAS - Übung zur Experimentellen Biophysik - SS 2023

Besprechung der Übungsblätter

- jeden Donnerstag, 9:45 – 11:15 Uhr in Seminarraum 6-2 (6. Stock, Physikhochhaus)
- Termin der 1. Übung: Do, 27.04.2023

Vorleistung zur Prüfung

- Erfolgreiche Bearbeitung von 75% der Übungsaufgaben
- Regelmäßiges Präsentieren von Lösungen an der Tafel

Programm der Biophysik-Vorlesung

Im Rahmen der Vorlesungssequenz Biophysik I und II wird eine **Einführung in die molekularen Grundlagen der Lebensvorgänge** gegeben. In der Vorlesung Biophysik I werden zunächst die verschiedenen Arten von Biomolekülen vorgestellt und ihre **strukturellen und dynamischen Eigenschaften** diskutiert. Ferner wird ein Überblick über die **physikalischen Methoden zur Bestimmung der Struktur von Biomolekülen** gegeben. Darauf aufbauend werden in der Vorlesung Biophysik II **spektroskopische Methoden** eingeführt, mit denen sich **Strukturänderungen** beobachten lassen. Anschließend werden die physikalischen Prinzipien erörtert, auf denen wichtige biomolekulare Prozesse (Ligandenbindung, Energie- und Elektronentransfer bei der Photosynthese) beruhen. Es werden folgende Themenbereiche behandelt:

A. Biomoleküle

1. Proteine
2. Nukleinsäuren
3. Lipide und Membranen

B. Strukturbestimmung

4. Optische Mikroskopie
5. Röntgenstrukturanalyse
6. Elektronenmikroskopie
7. Neutronenbeugung
8. XAS

C. Spektroskopische Methoden

9. Strukturbestimmung mit NMR
10. Wechselwirkung von EM-Strahlung mit Biomolekülen
11. Chromophore in Biomolekülen
12. Zeitauflösende Absorptionsspektroskopie
13. Fluoreszenzspektroskopie
14. Schwingungsspektroskopie (IR/Raman)

D. Biomolekulare Funktion

15. Ligandenbindung an Hämproteinen
16. Reaktionstheorie
17. Dynamik der Konformationsänderungen
18. Bioenergetik
19. Elektronentransfer-Theorie
20. Energie- und Elektronentransfer bei der Photosynthese

Biophysikalische Forschung am Institut

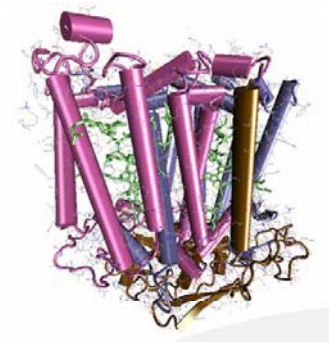

Fluorescence Microscopy

- Microscopy hardware
- Quantitative analysis tools
- Nanostructured surfaces

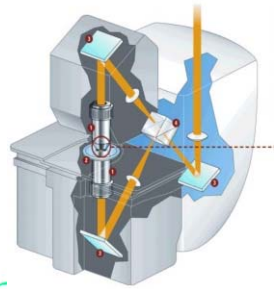

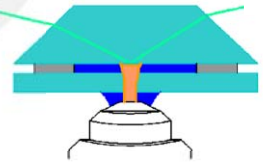

Biomolecular Structure-Dynamics-Function Studies

- Spectroscopy
- Crystallography
- Single molecule fluorescence

Fluorescent Probes

- Synthetic dyes
- Quantum dots
- Fluorescent proteins

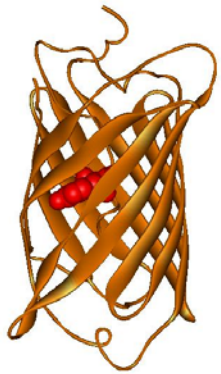

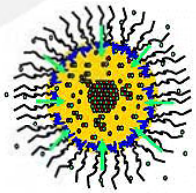

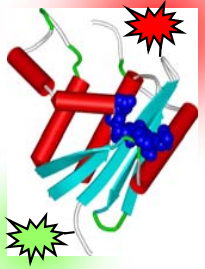

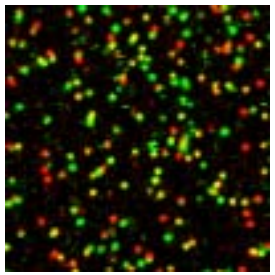

Imaging Applications

- Biology
- Medicine
- Pharmacology (HTS, HCS)

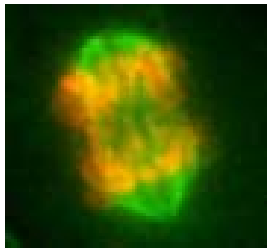

What is "Biophysics" ?

- Understanding life's processes as they happen in space and time ...
  - Molecular biophysics
  - Cell biophysics
  - Neurobiophysics
  - Biomechanics
  - Evolution
  - Radiation biophysics
  - ...
  - ...

The Feynman Lectures on Physics

... the full appreciation of natural phenomena, as we see them, must go beyond physics in the usual sense. We make no apologies for making these excursions into other fields, because the separation of fields, as we have emphasized, is merely a human convenience, and an unnatural thing. Nature is not interested in our separations, and many of the interesting phenomena bridge the gaps between fields. ...

R.P. Feynman in
"The Feynman Lectures on Physics",
Vol. I, Chapter 35

Why should a physicist study biomolecules ?

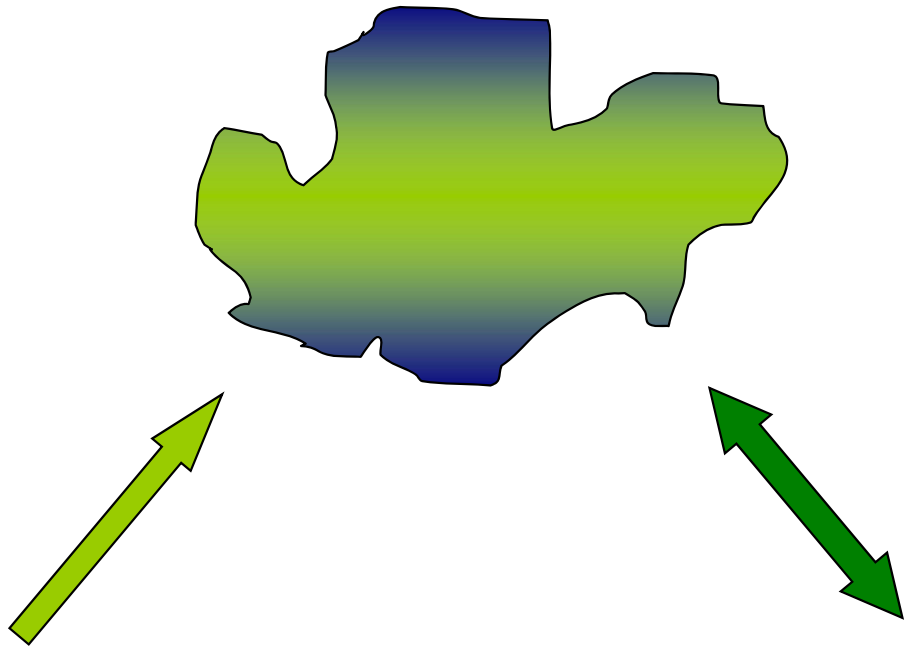

How does it work?

Physical concepts and laws in complex and living biosystems

Biophysics

Biological Physics

Complex Systems

Glasses
Spin glasses
Polymers
Biomolecules

- wide distributions of characteristic time scales
- Non-Arrhenius T dependence
- Metastability

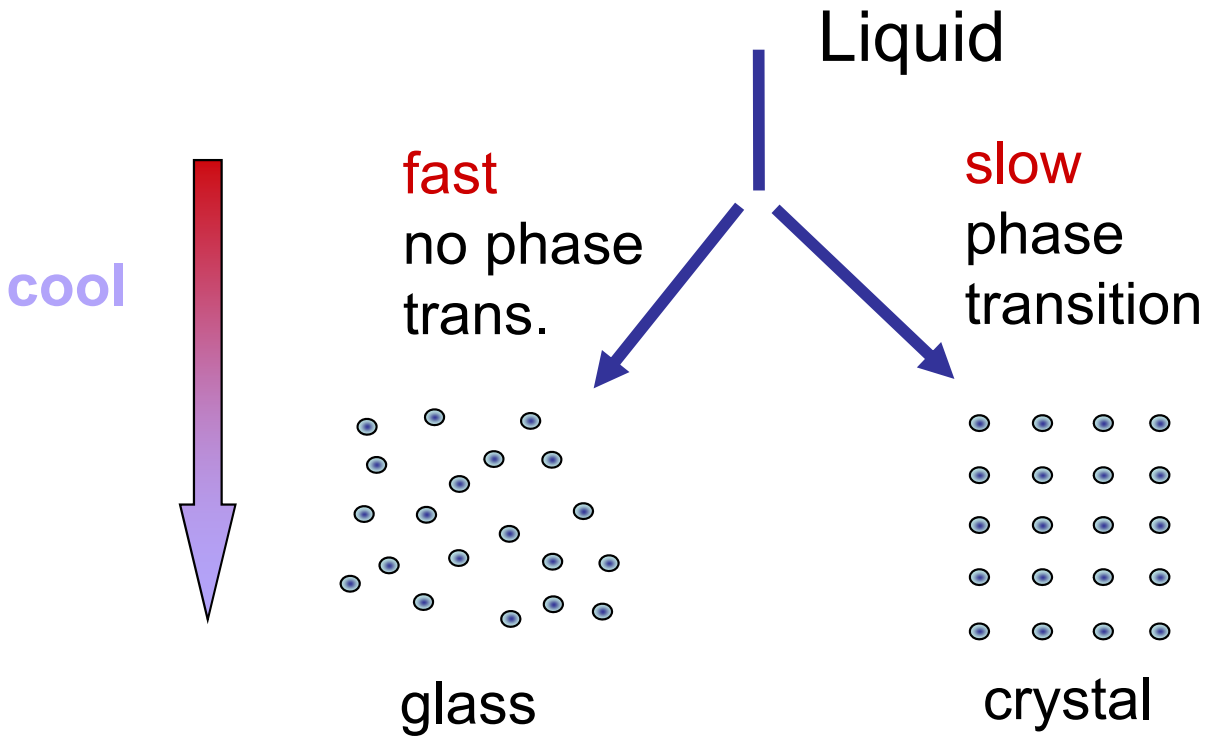

Energy Levels and Landscapes

„Simple system"

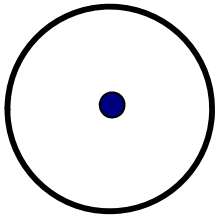

atom
nucleus

„Complex system"

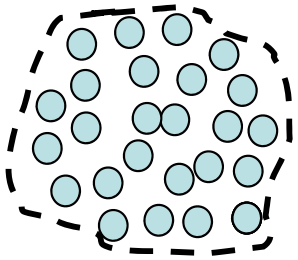

liquid
droplet

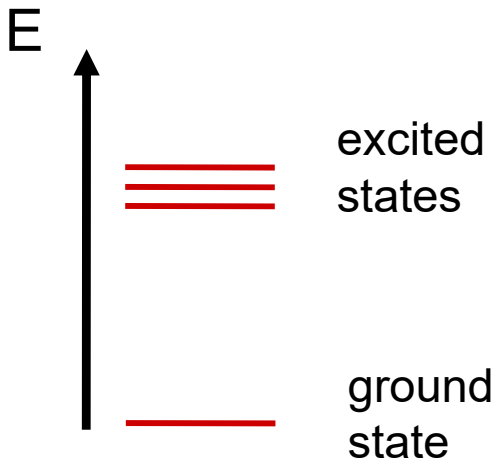

ground state <u>not</u>
degenerate

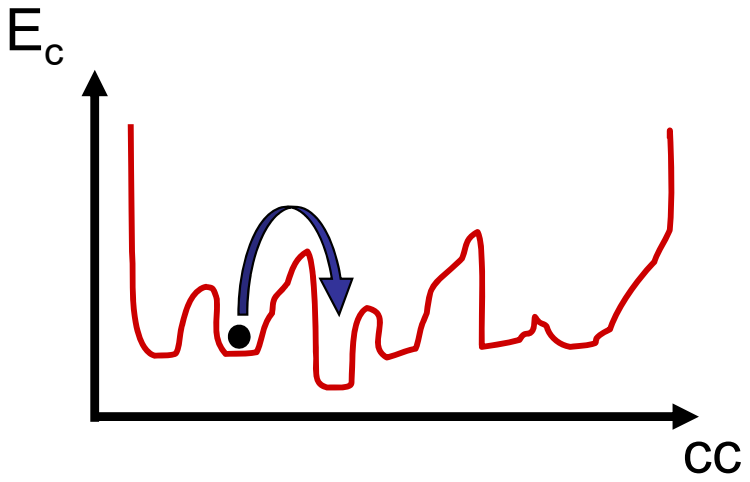

Many „ground states"
of nearly equal energies.

Disorder and Frustration

Crystal

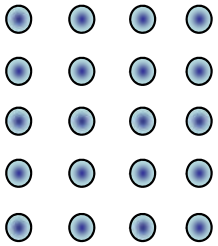

symmetry
periodicity

Liquid/
Glass

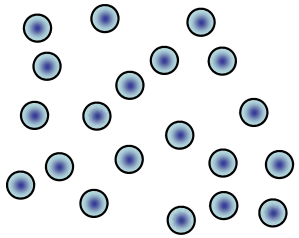

randomness
aperiodicity

Frustration

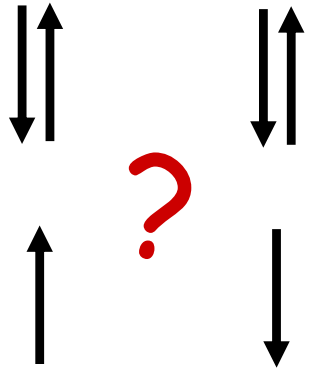

spin
glass

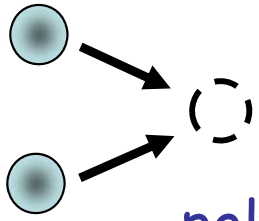

polymer:
Competition for
vacant sites
(steric constraints)

Diversity and Unity of Life

- Perplexing variety

  form, size, organizational level, ecological niche, ...

- Unifying principles

  same building blocks
  Cells contain nucleic acids, proteins, machinery for regulation, reproduction, repair, motion, similar metabolism, steady flux of energy and materials required to 'defeat' 2nd law of thermodynamics.

  evolved from the same ancestor
  genome comparison – evolutionary record, examples representative

Hierarchy of Living Systems

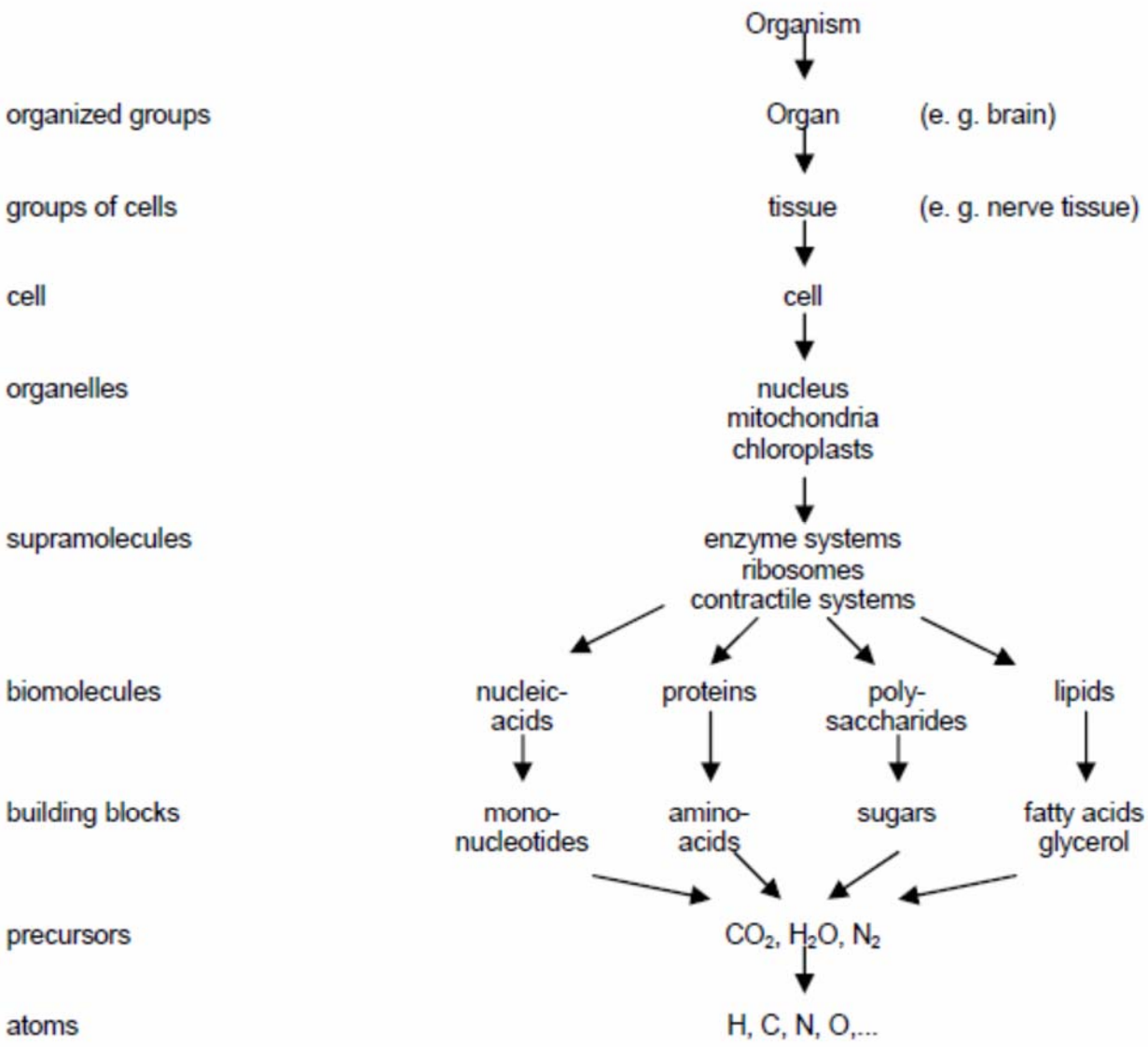

…from Organisms to Atoms

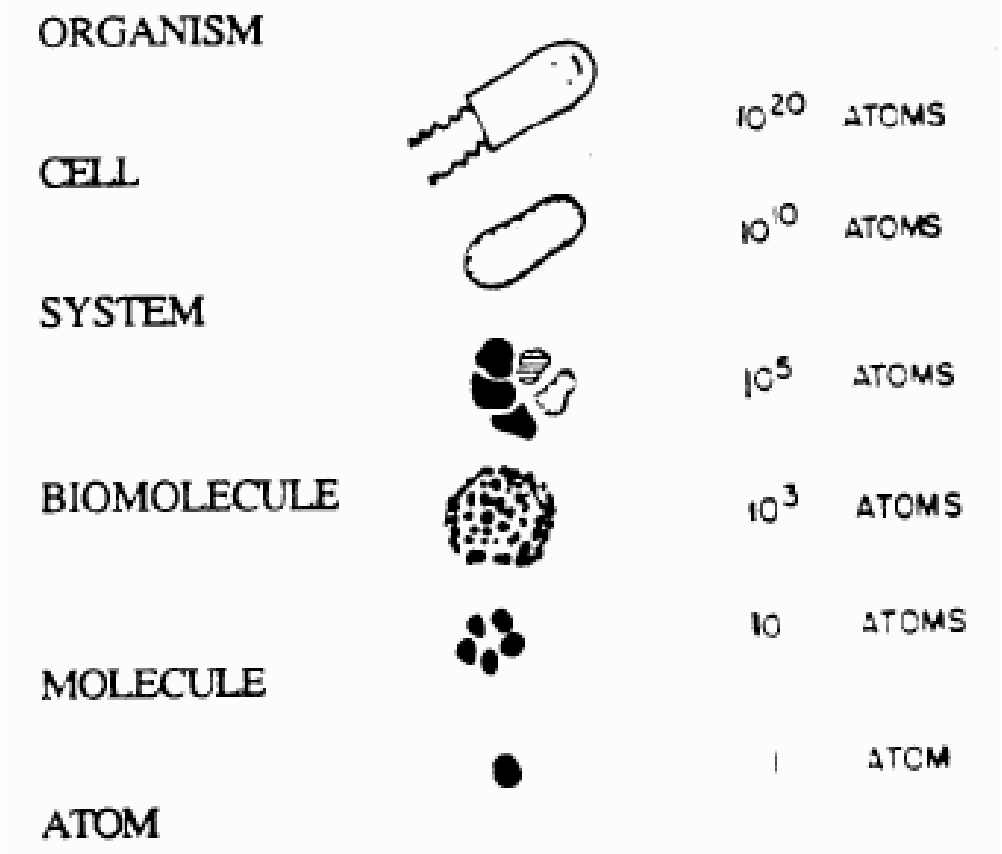

Simple Example: Virus

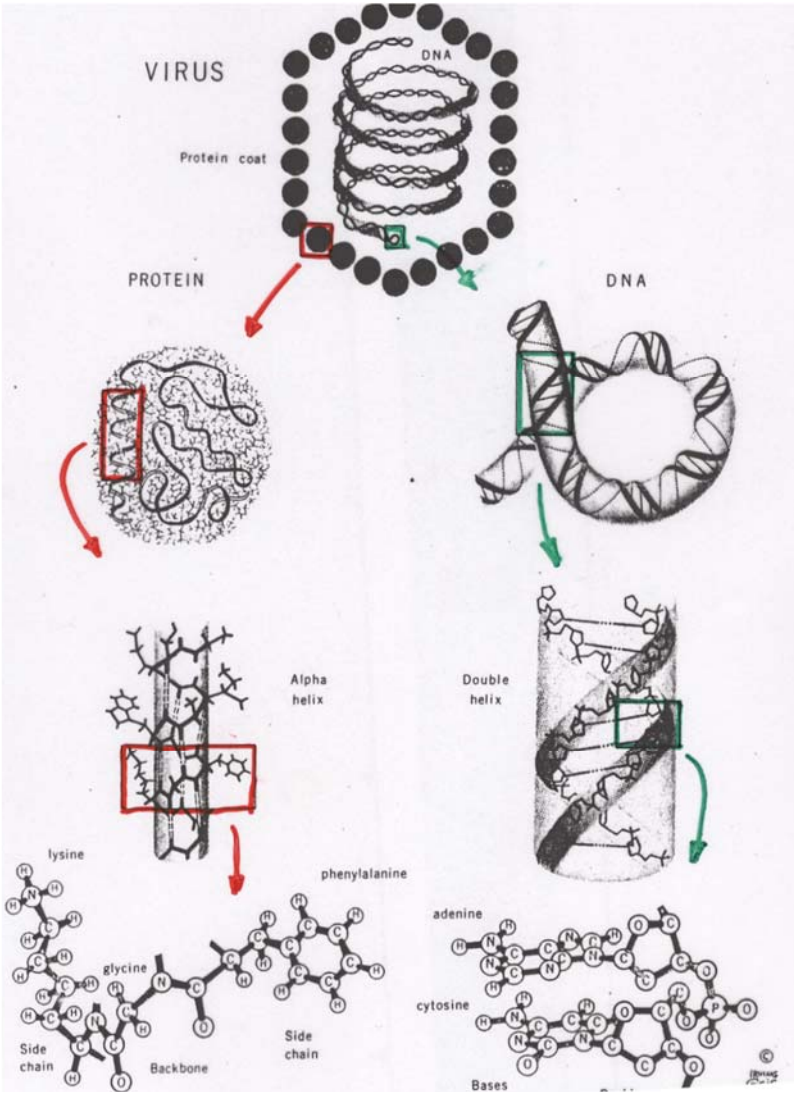

Biomolecules

- Proteins
- Nucleic Acids
- Lipids
- Polysaccharides

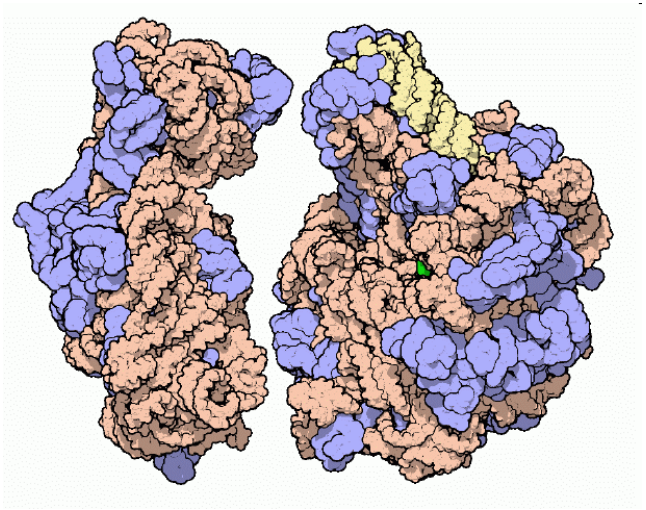

Ribosome

DNA

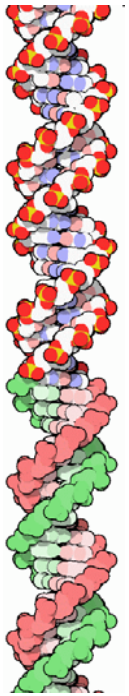

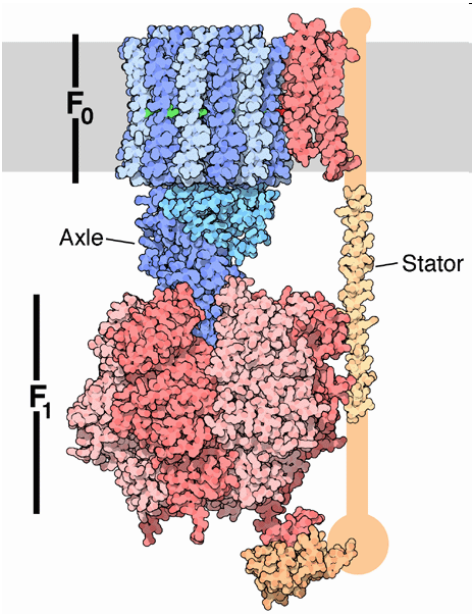

ATP Synthase

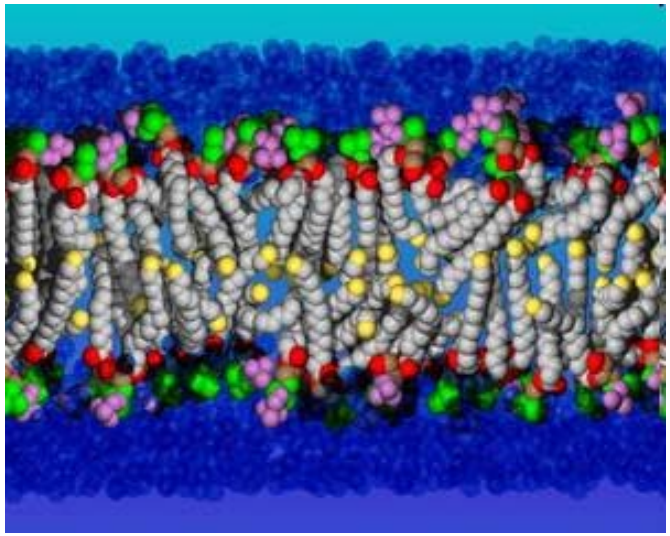

Lipid Bilayer

Polysaccharides

Biological molecules: exciting physical systems

- mesoscopic size – importance of thermal fluctuations
- statistical physics (order/disorder phenomena, protein/RNA/DNA folding)
- complexity and hierarchy of structures
- quantum physics (electron/energy transfer, spectroscopy)
- information storage/transfer (genomics, evolution)

Molecular Biophysics

- Understand structure-function relation in biological macromolecules that support and control processes of life:

  Nucleic acids - genetic information ...and much more!
  Proteins - functional processes
  Lipid membranes - compartment formation
  Polysaccharides - diverse functions

- Main disciplines:

  Biology, biochemistry, biophysics, medicine, pharmacology, materials science, ...

- Major contributions of Physics:

  Theoretical concepts
  Experimental tools
  Computation

Structure Determination

X-ray crystallography:
Analysis of diffraction pattern generated by interaction between X-rays and the electron density within a protein crystal.
‚Snapshot of the average structure‘

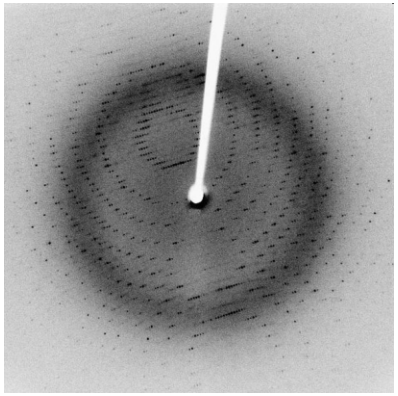

3Clpro
(SARS protease)

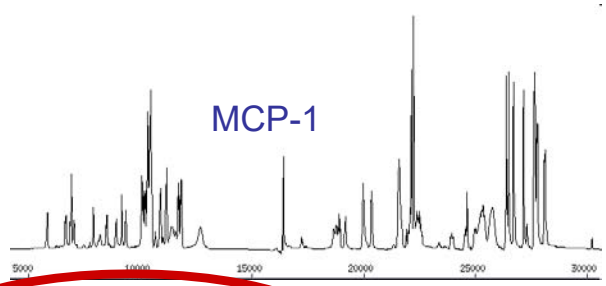

NMR Spectroscopy
measures distances between atomic nuclei rather than the electron density in a molecule.
No crystallization necessary.
Observation of dynamics, not only structure

Cryo-electron microscopy
can resolve macromolecular complexes (size 5 – 10 nm) deposited as single layers or arranged in thin slices.

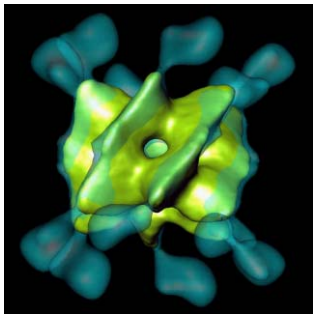

CaM kinase II

Spectroscopy

- studying the properties of matter through its interaction with different frequency components of the electromagnetic spectrum.
- observing the interaction of light with different degrees of freedom of the molecule. Each type of spectroscopy—different light frequency—gives a different picture → ***the spectrum***.

Nature of interaction with matter (simplified):

X-rays cause electronic transitions from low-lying closed shells of atoms.
UV – visible radiation causes outer electron transitions in atoms and molecules.
IR causes vibrational transitions in molecules.
Microwave radiation causes rotational transitions in molecules,
and can flip electron spins (**ESR**).
Radio waves can flip nuclear spins (**NMR**).

Biophysics II

Protein Basics

Part 1a

Uli Nienhaus

Prof. G. U. Nienhaus, Vorlesungsunterlagen Biophysik II, SS 2023.
Nur zum KIT-internen, vorlesungsbegleitenden Gebrauch.
Weitergabe und anderweitige Nutzung verboten.

Biomolecules

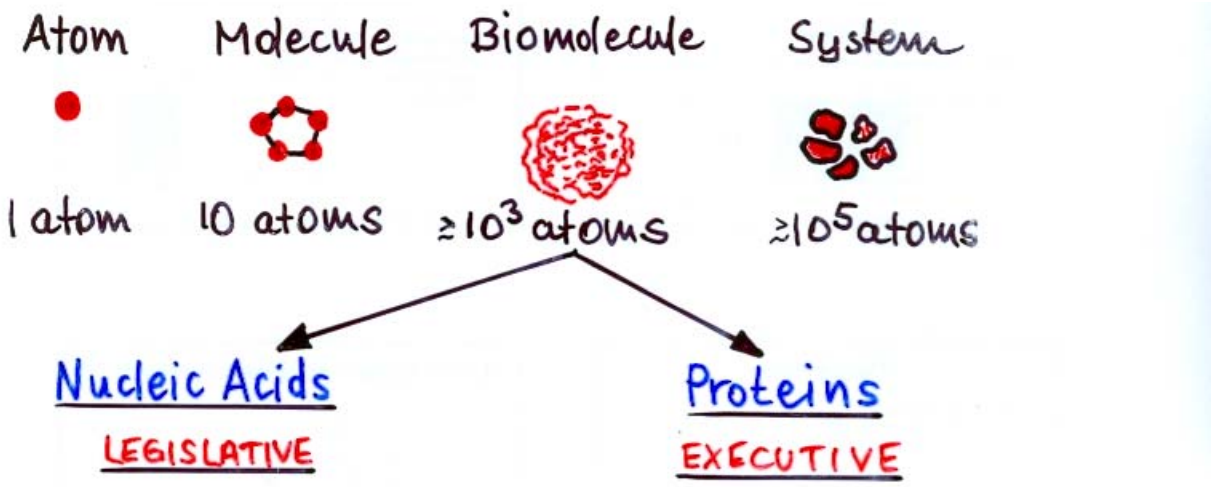

Protein Biosynthesis:
DNA → mRNA → protein

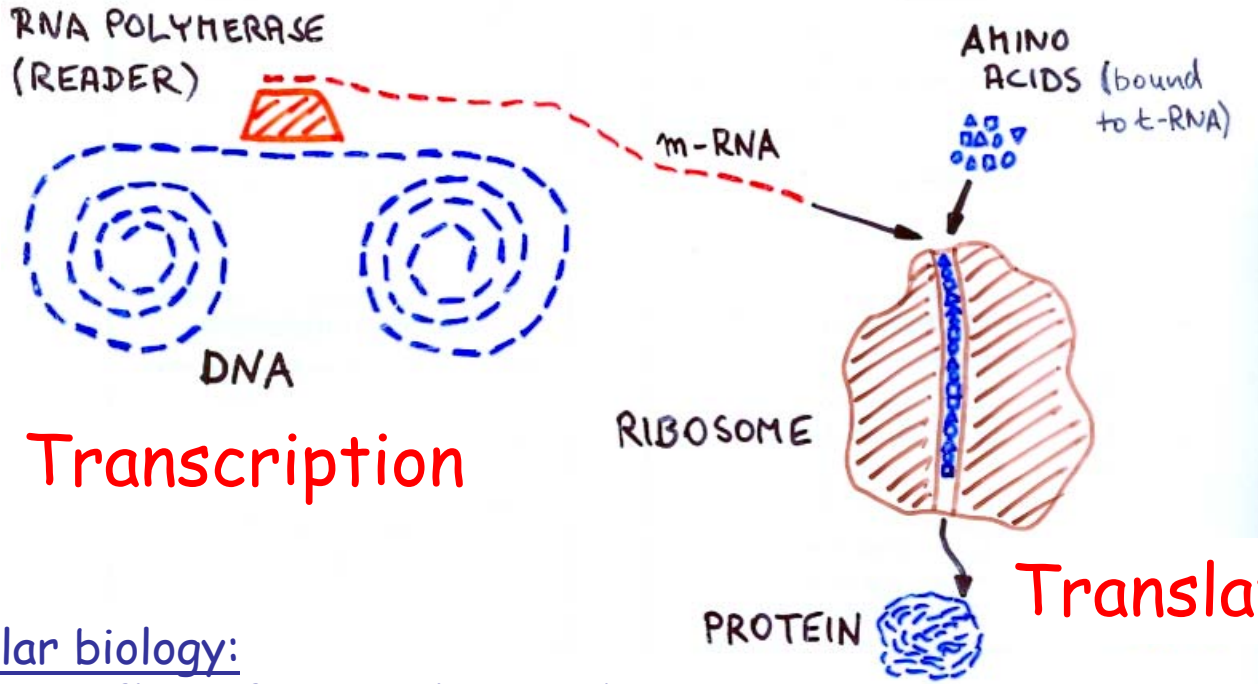

Transcription

Translation

Central dogma of molecular biology:
Sequence information always flows from nucleic acids to proteins but never back from there (Francis Crick, 1957).

Information & Construction

Living systems - store information how to assemble

Parts
Assembler (self-reproducing)

Information Content

Information capacity $N_{\lambda\nu} = \lambda^{\nu}$ (λ - basis, ν - digits)

System	basis	digits	$N_{\lambda\nu}$	$bits_2$
Four-letter words	26	4	26^4	~ 18.8
Small protein	20	100	20^{100}	~ 432
Nucleic acid (3 mm)	4	10^7	$4^{10\hat{}7}$	= $2 \cdot 10^7$

Proteins have diverse functions

- Enzymes: Lysozyme
  Ribonuclease
  Alcohol dehydrogenase
- Storage: Ferritin
  Albumin
- Transport: Hemoglobin
  Hemocyanin
- Protection: Immunoglobulins
  Fibrinogen
- Light harvesting: Rhodopsin
  Reaction Center
- Light production: Luciferase
- Structure: Collagen
  α-Keratin
- Hormones: Insulin

Proteins are folded polymer chains

Primary structure

backbone

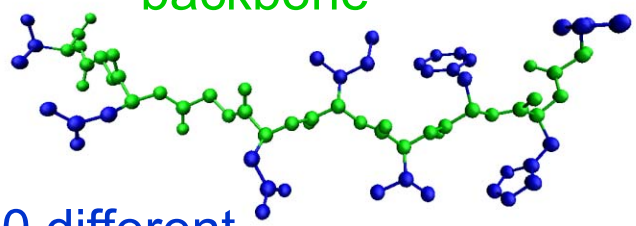

20 different sidechains

Building blocks:

20 different amino acids

side chain

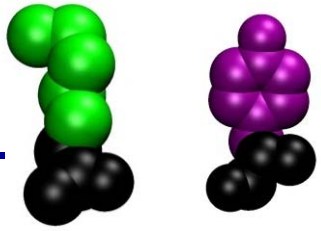

backbone

Secondary structure

H-bonds

α-helix
β-sheet

Tertiary structure

Sequence determines 3D structure

- van der Waals (vdW)
- H-bonds
- hydrophobic interactions
- charge interactions
  (salt bridges) ⊕ … ⊖
- (covalent)

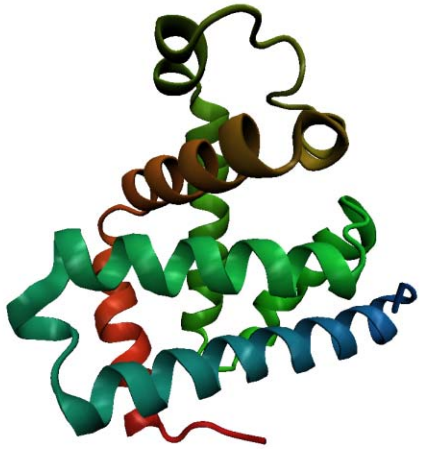

myoglobin

Self-organized nanostructures

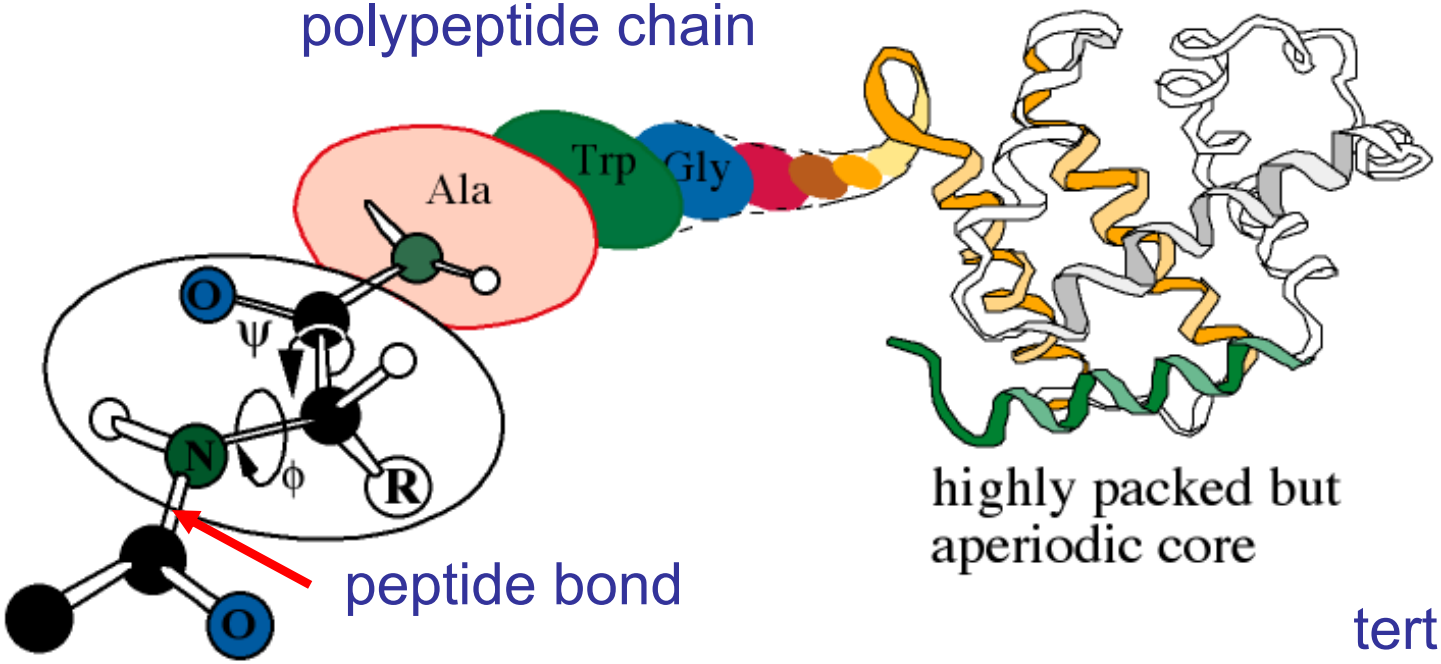

secondary structure
(here all α-helix)

tertiary structure:
- tightly packed (vdW)
- hydrophobic core

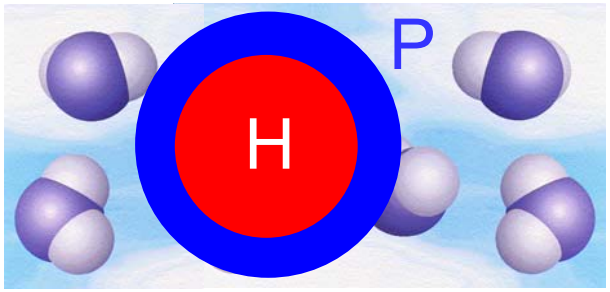

"Oil drop model, HP model"
H: Hydrophobic, P: Polar

Self-organized nanostructure:
1D sequence encodes 3D architecture
'2nd half of genetic code'

Self-assembly of proteins – Anfinsen's experiment

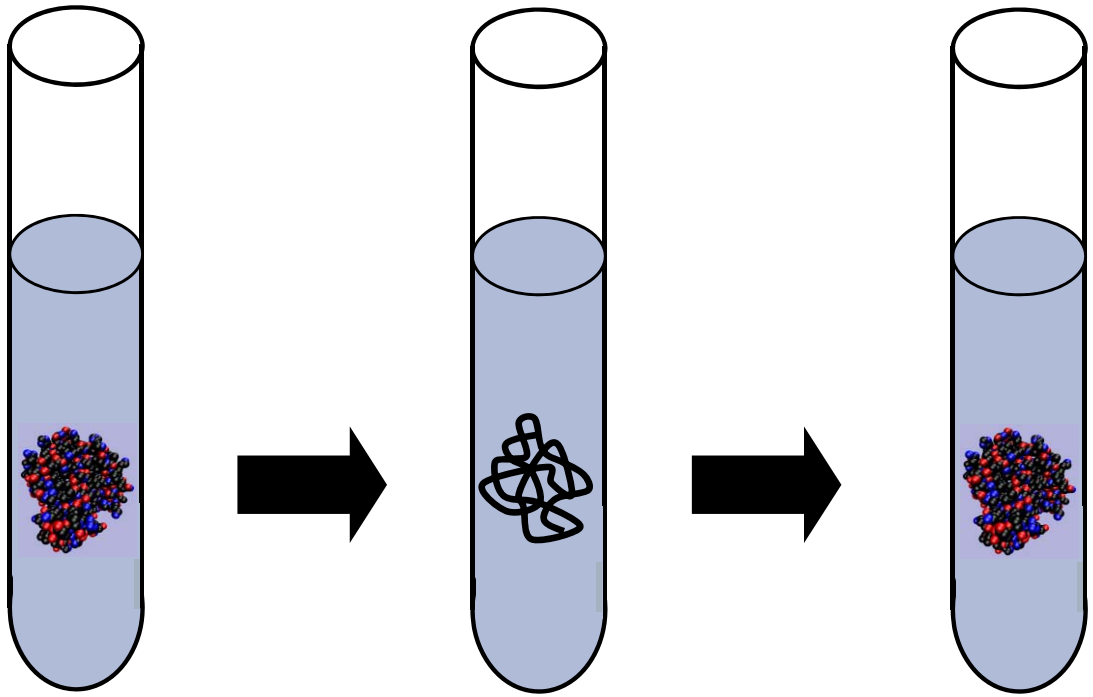

Native conditions (buffer solution) | **Chemical denaturant (Urea, GdmCl, H^+)** | **Native conditions (buffer solution)**

Thermodynamic Hypothesis:

The native conformation of a protein is adopted spontaneously. The correct 3D structure is already encoded in the sequence of amino acids.

C. B. Anfinsen, "Principles that govern the folding of protein chains." *Science* **181** (1973) 223.

Protein folding

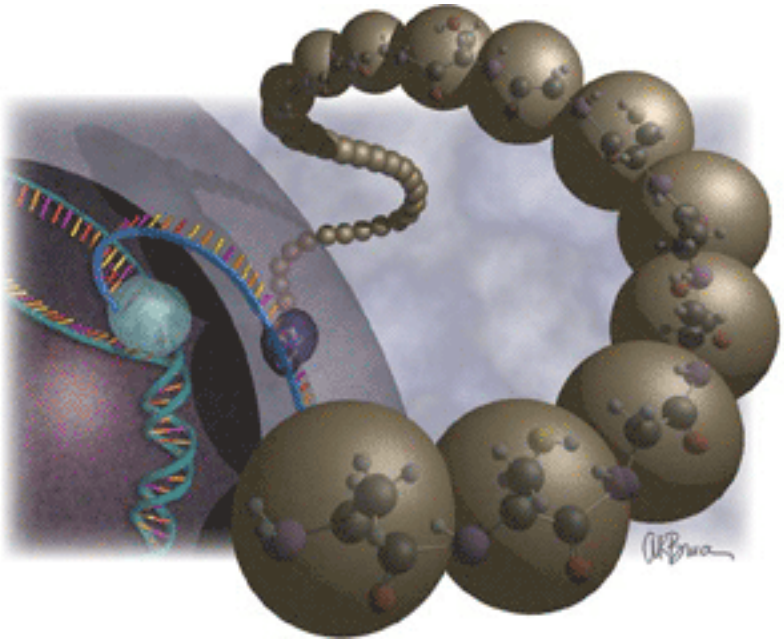

‘soft’ phase transition

Jones et al., *Proteins* **61** Suppl 7 (2005) 143.

Misfolded proteins:

non-functional, can be causing disease (formation of amyloid fibrils, e.g., BSE, CJD, Alzheimer’s disease)

Proteins are marginally stable,
$\Delta G \approx -20 \ldots -50$ kJ/mol

Protein folding

- Huge number of possible chain conformations ($W \approx 10^{100}$ for a protein with 100 amino acids).
- Folding decreases number of available conformations substantially.
- Free energy minimum is typically found on sub-second time scales.

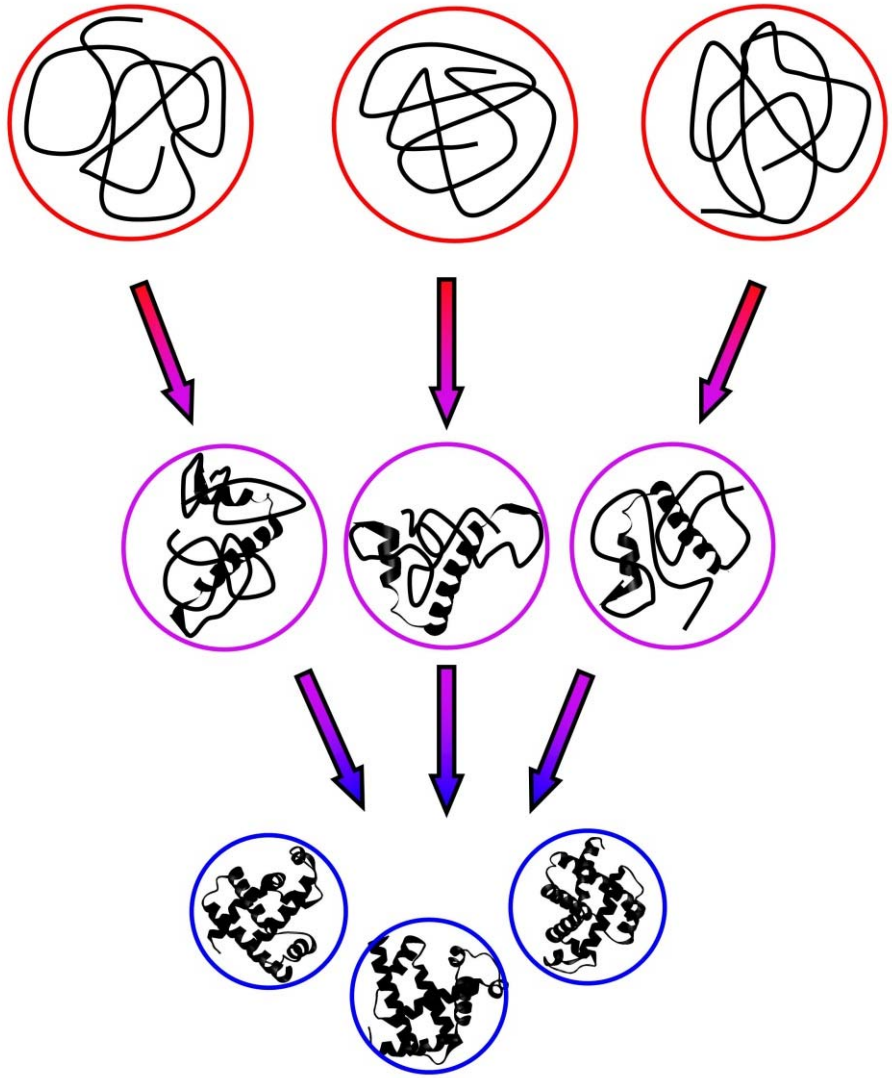

Levinthal's Paradox

How can the polypeptide chain find its folded state in view of the vast number of unfolded chain conformations?

Random search: $\tau_{fold} \geq W\tau_0$ → with realistic W and $\tau_o \approx 10^{-11}$ s, random search takes much longer than the age of the universe!!

Possible Solutions:

- A (mechanically, chemically or thermally) unfolded chain may not be a random coil but may retain residual structure
- Biased search instead of random search

C. Levinthal, "How to fold graciously", in "Mössbauer spectroscopy in biological systems", Proceedings of a meeting held at Allerton House, Monticello, Illinois, edited by P. Debrunner, J. C. M. Tsibris and E. Münck, p. 22. University of Illinois Press (1969).

Funnel-shaped protein energy landscape

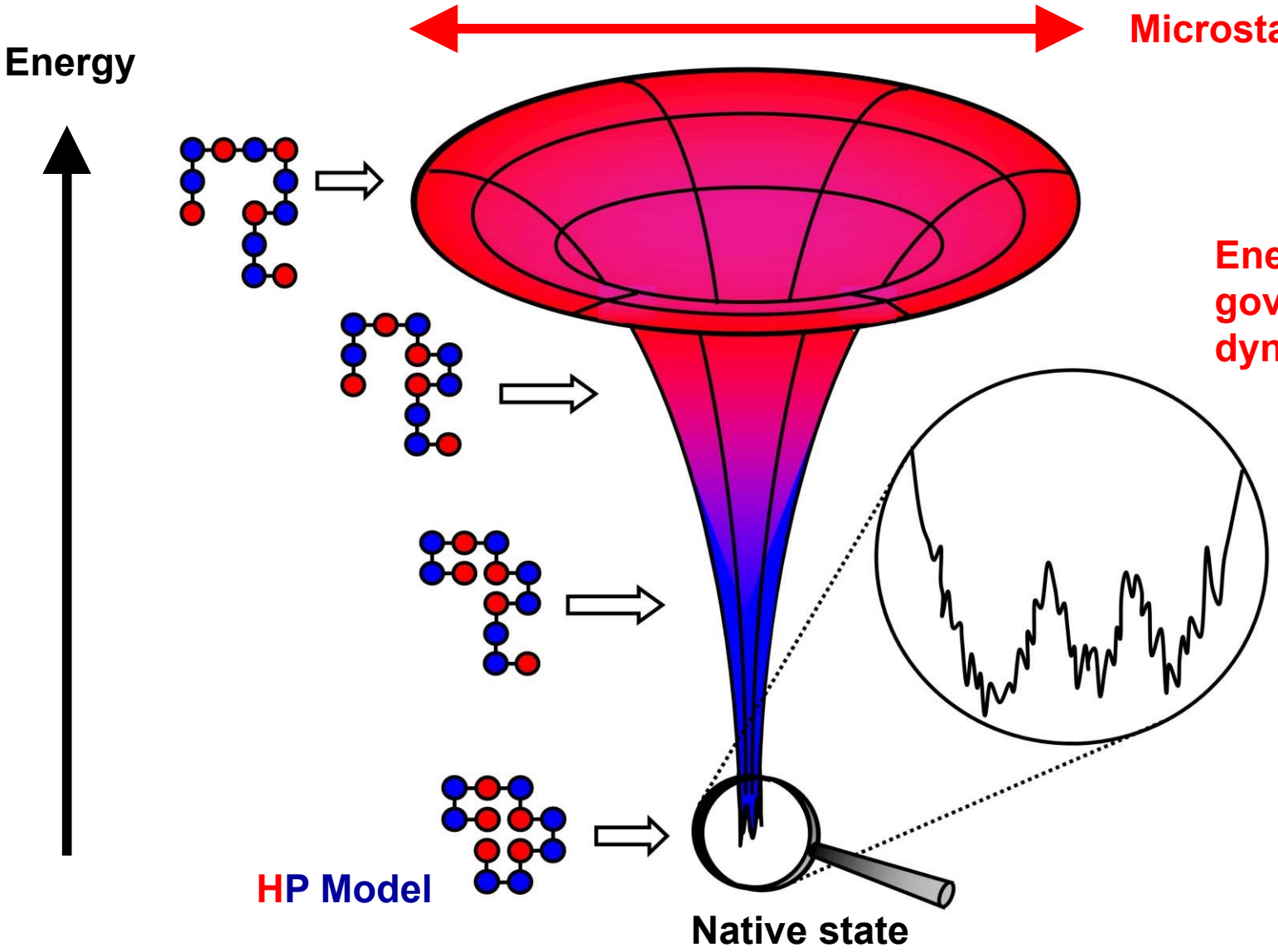

Energy landscape governs structure, dynamics, function

Nienhaus and Young, Encyc. Appl. Phys. 15 (1996) 163.

Onuchic
Wolynes
Bryngelson
Luthey-Schulten
Go
Dill
Thirumalai
Shakhnovich

Energy landscapes

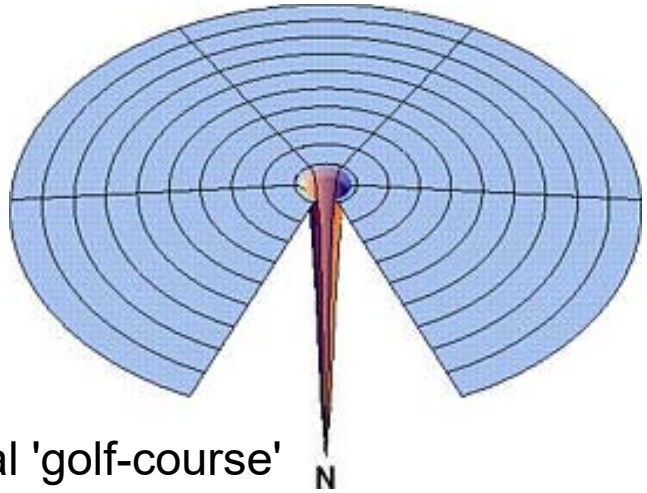

Levinthal 'golf-course' landscape

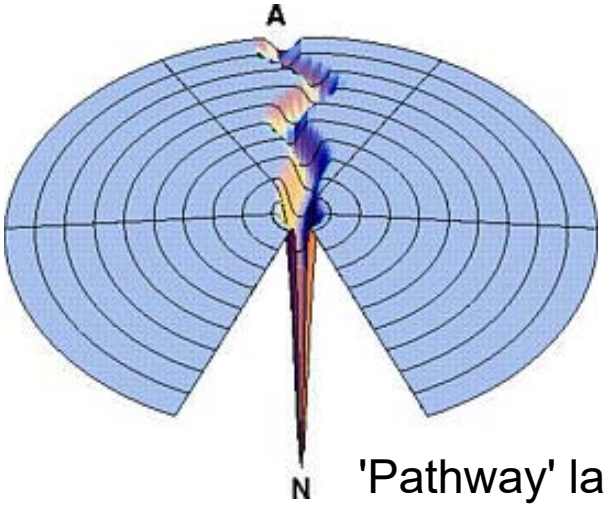

'Pathway' landscape

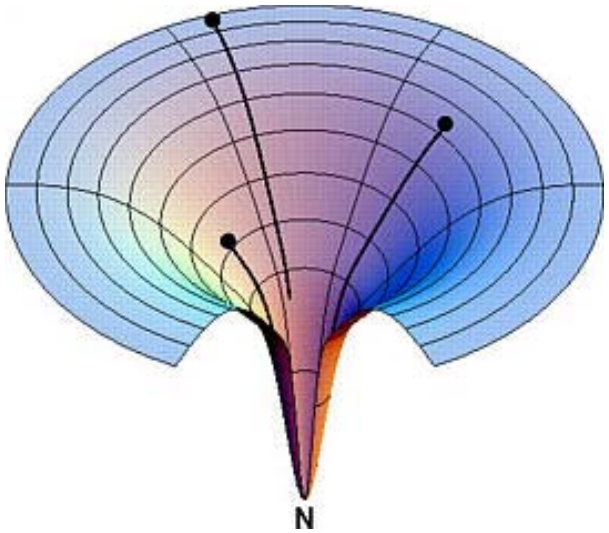

Smooth funnel landscape

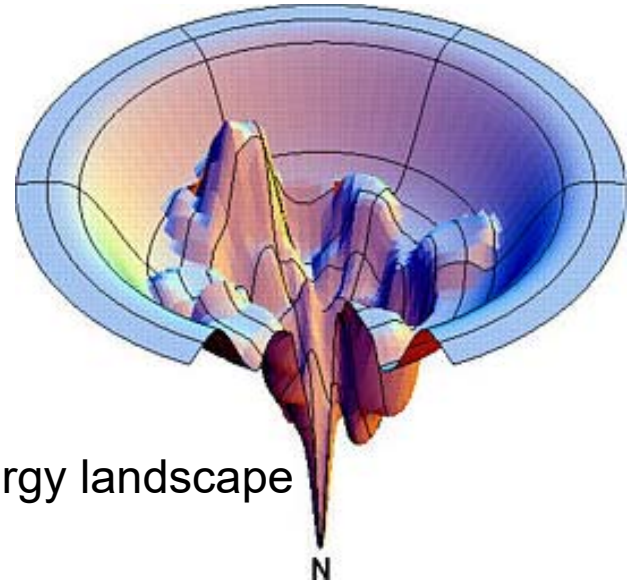

Rugged energy landscape

Dill & Chan, *Nature Struct. Biol.* **4** (1997) 10-19.

Packing density of folded proteins

- Closest packed spheres 0.74
- Closest packed inf. cylinders 0.91
- Homogeneous solid 1.00

← proteins

organic crystals: 0.70 … 0.78

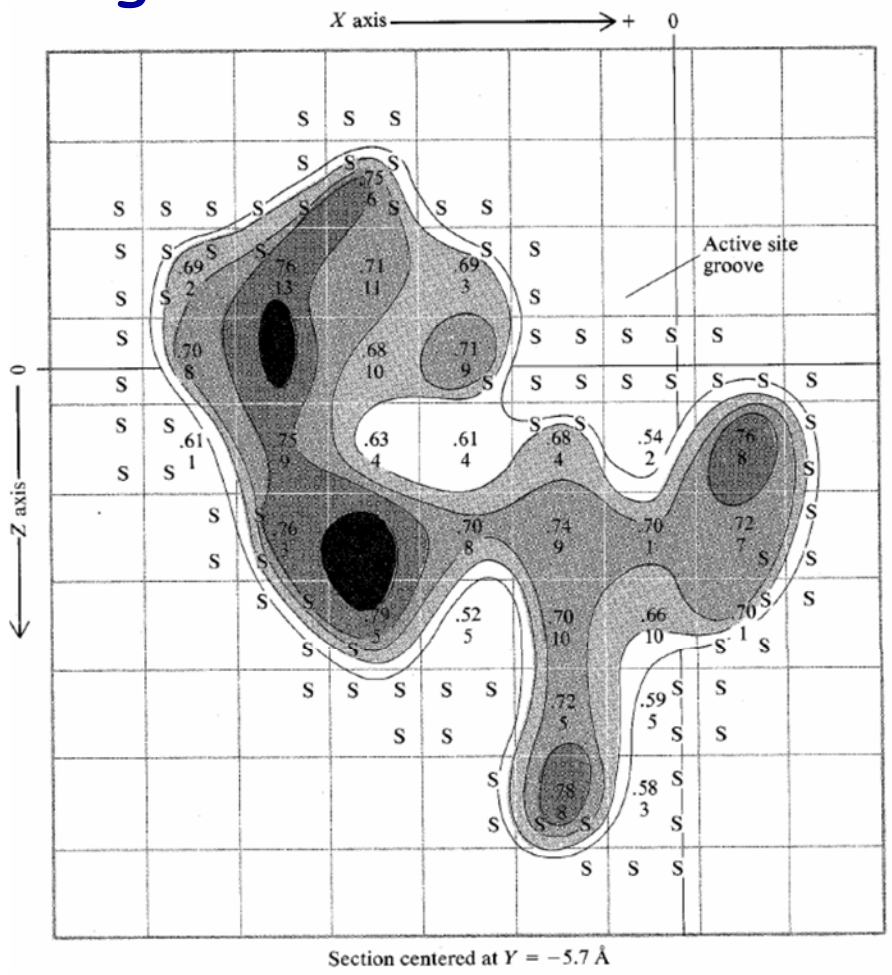

Section through the center of bovine pancreatic ribonuclease S:

3D grid of 5.6 A spacing superimposed.

Number of atoms with center inside cube are shown.

Also shown is the average packing density.

Hypothetical layer of solvent molecules (S) defines surface.

F.M. Richards, J. Mol. Biol. 82:1 (1974)

Cavities in myoglobin

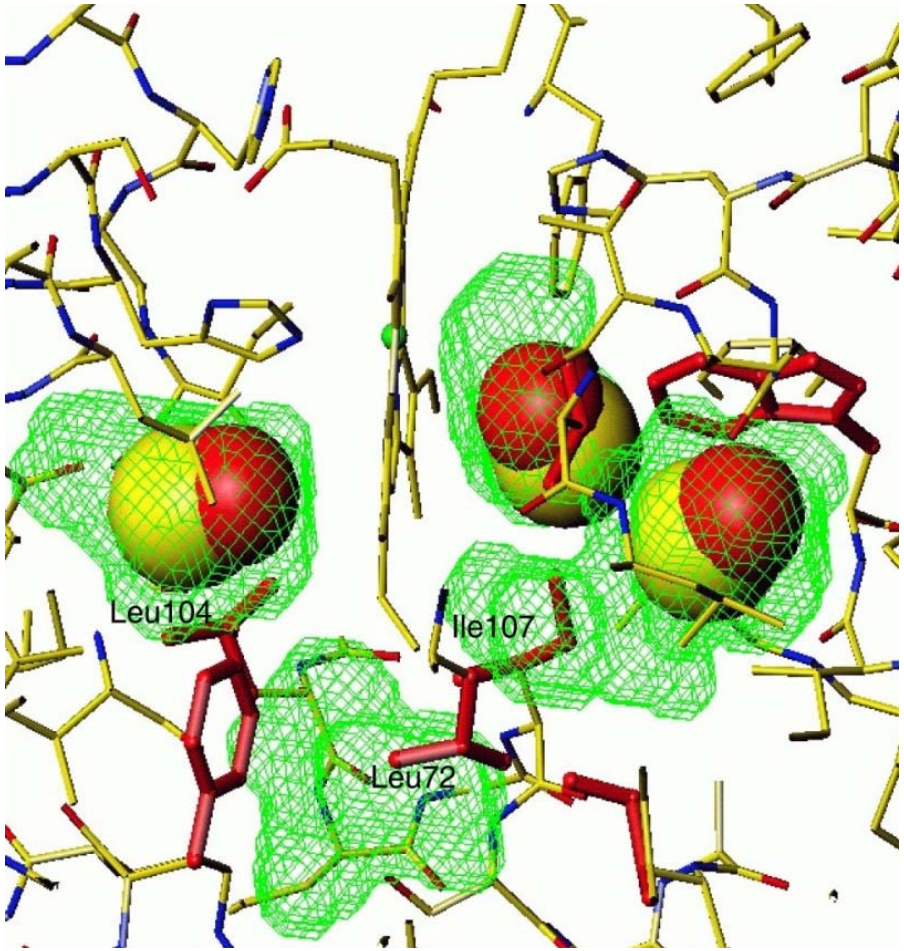

Ancient Greek philosopher Aristotle:
"**Nature abhors a vacuum.**"

Ostermann et al., Nature 404 (2000), 205-208

Polypeptides

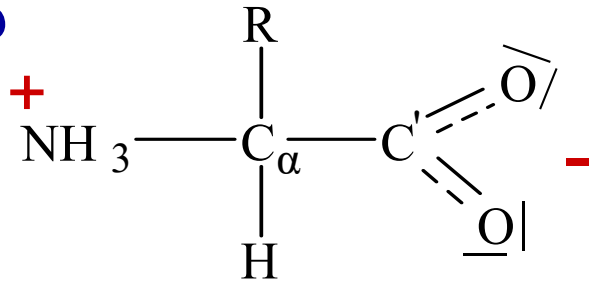

- Linear chains of α-amino acids
- 20 different side chains R
- Central carbon C_α tetrahedrally coordinated (sp^3)

$\Theta = 109.47° = \arccos(-1/3)$

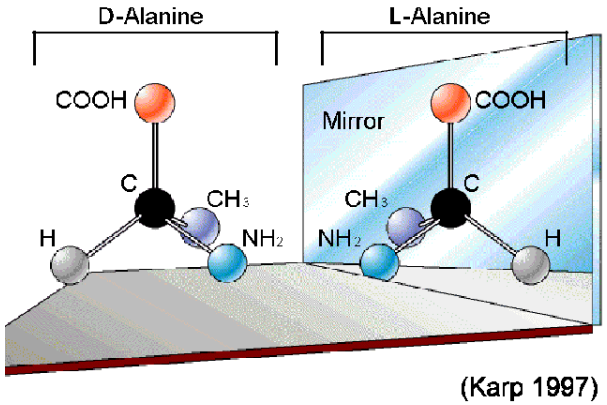

(Karp 1997)

Two distinct mirror images (enantiomers), only L-AA used in protein biosynthesis

peptide bond

Polymerisation

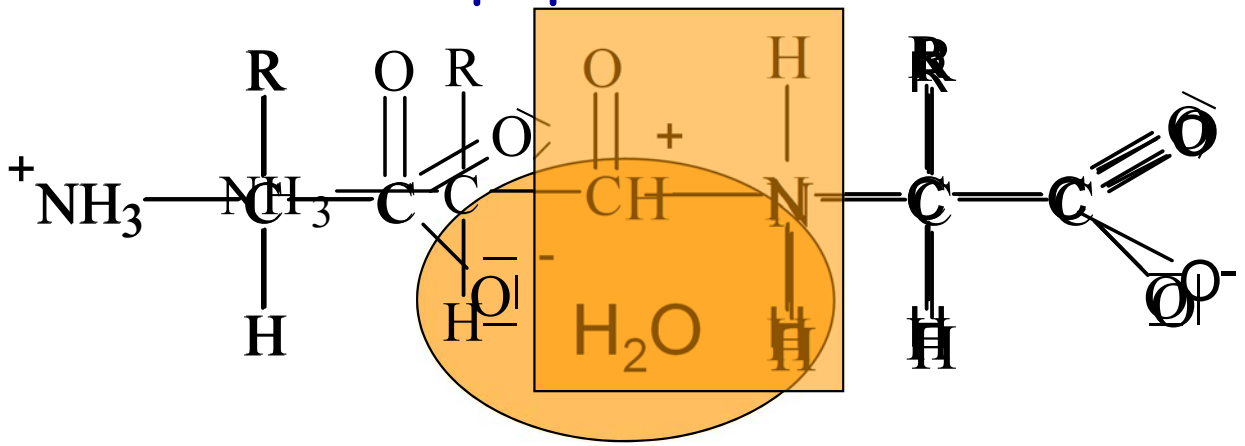

Peptide bond properties

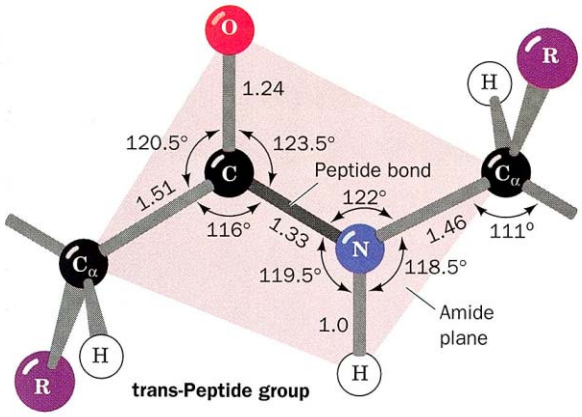

- Partial double-bond character ⟶ planarity

  $E = 88 \sin 2\theta$ [kJ/mol]
- 2 angles needed to specify backbone conformation
- Large dipole moment : p = 3.7 D (HCl : 1.03D)

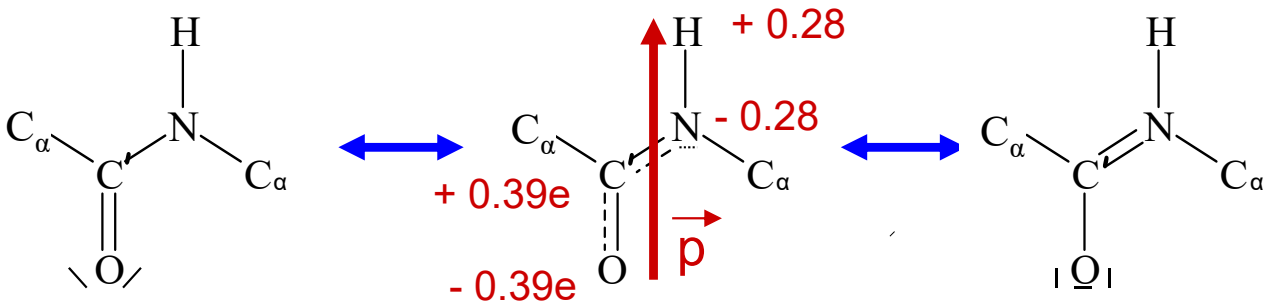

Bond lengths [Å]

Peptide		Normal
1.24	C = O	1.21
1.32	**C′ - N**	**1.47**
------	C = N	1.27
1.46	N - C_α	1.47
1.51	C_α – C′	1.54

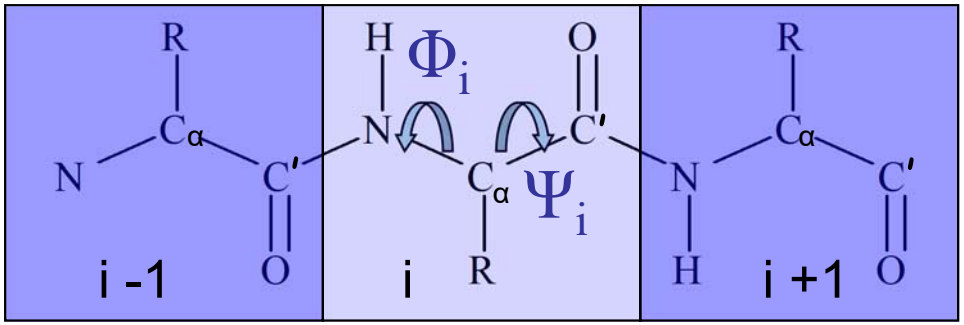

Amide planes

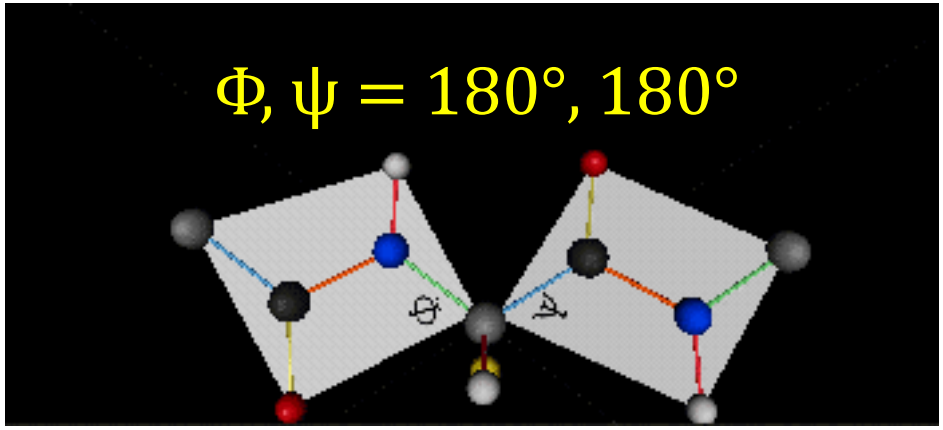

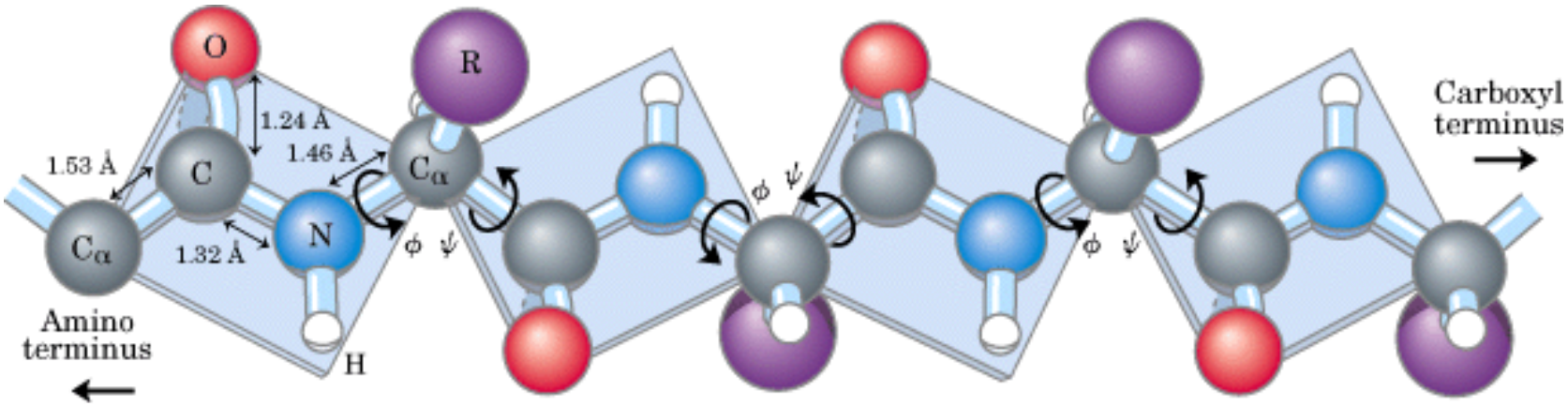

Amino acids

The 20 standard proteinogenic amino acids can be classified according to different properties:

- non-polar side chains
- polar side chains
  - neutral
  - charged

Non-polar side chains

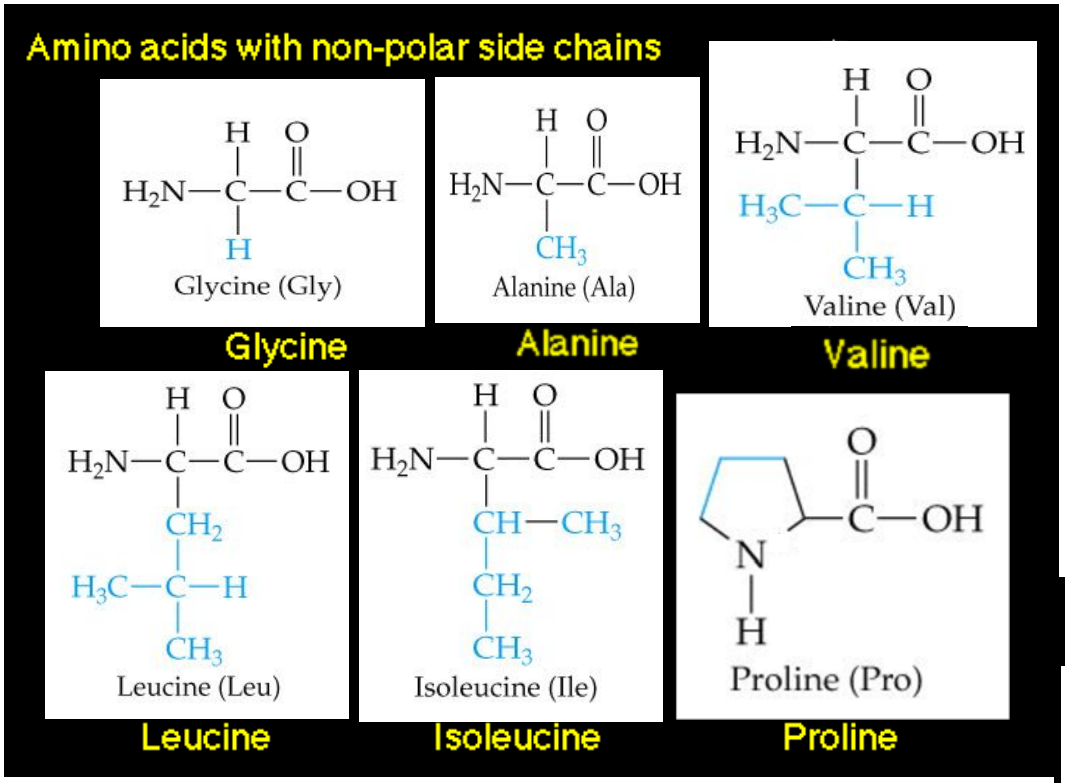

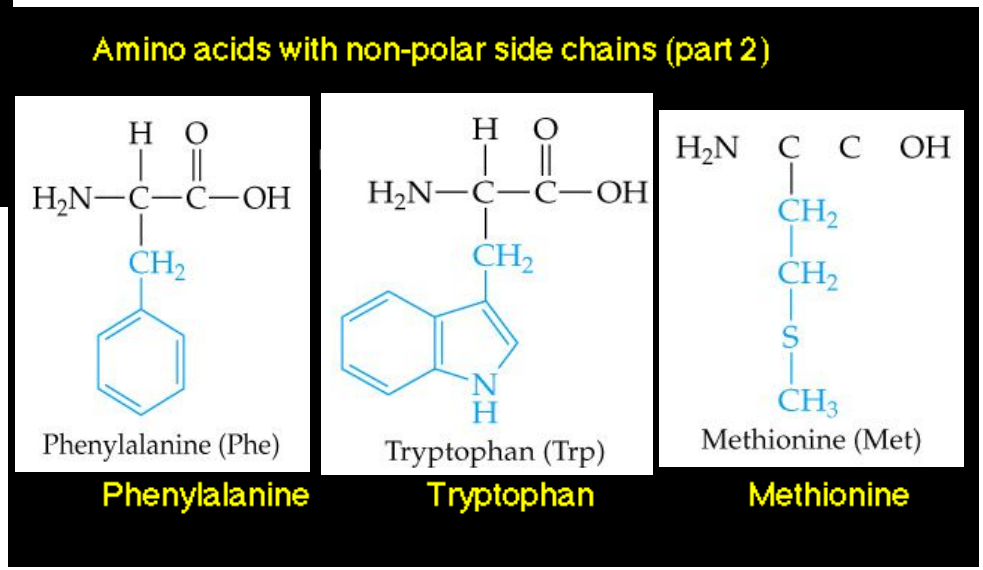

Polar (uncharged) side chains

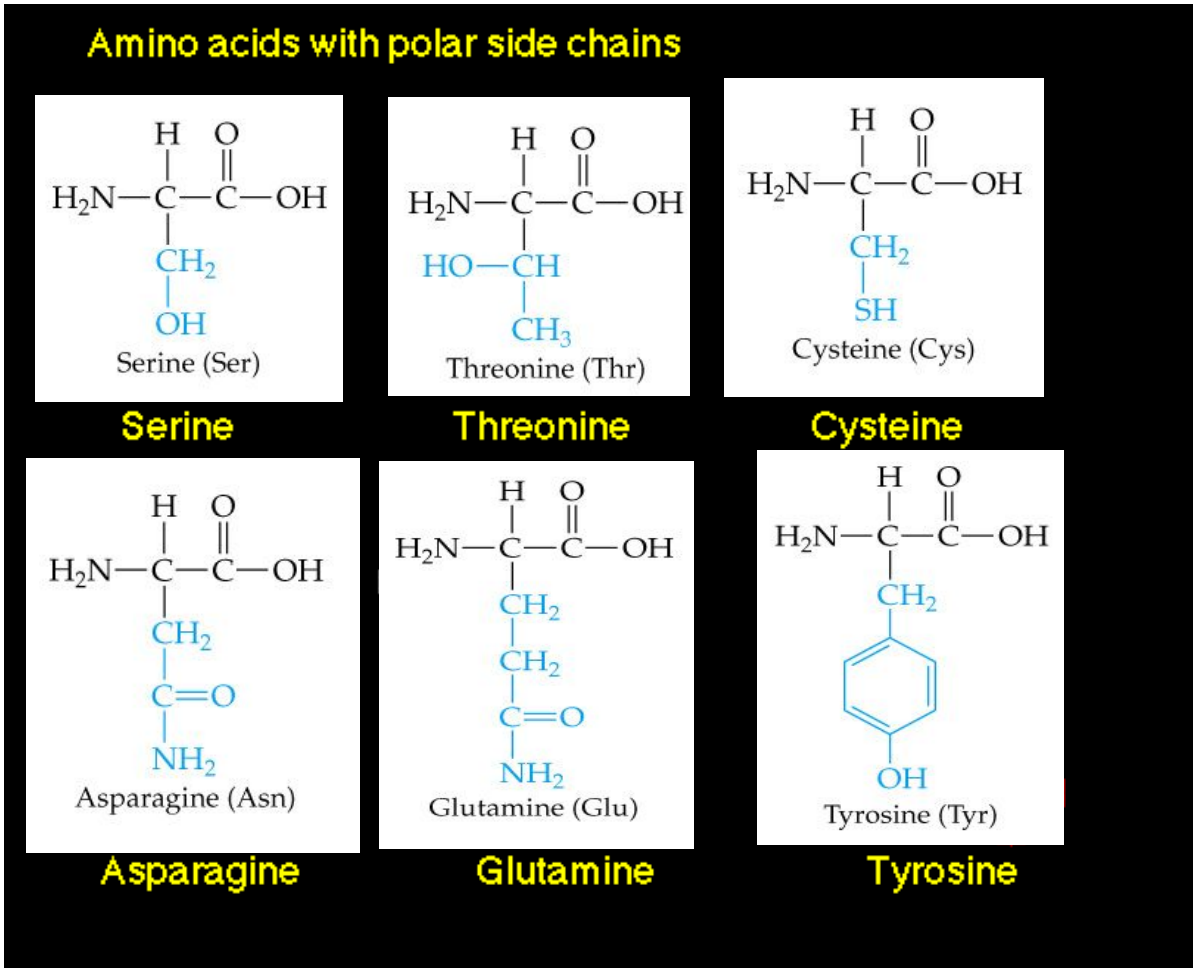

Cys is typ. charged at pH > ~8.5 !!!

Tyr is non-polar!!!

Charged side chains

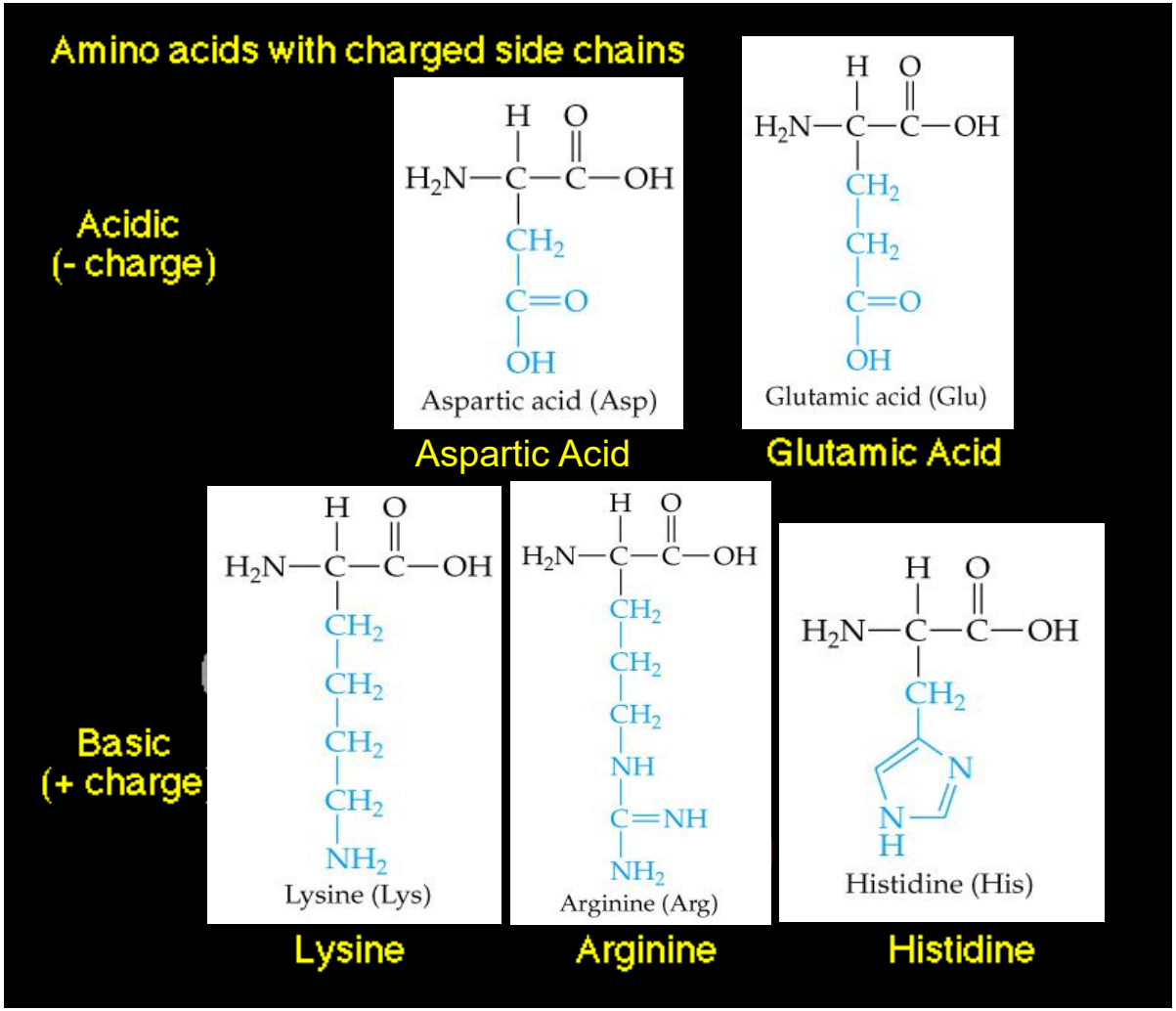

His is typically neutral at pH 7

(pos. charged below pH 6, with both N atoms protonated)

Polarity of amino acid side chains

Quantitative approach: measure solubilities in H_2O
"like dissolves like"

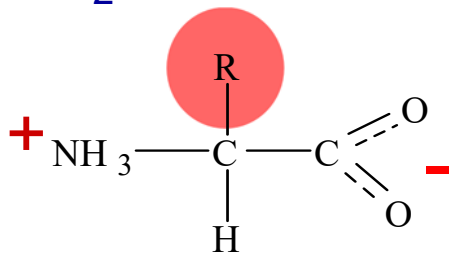

problems:

1. amino acids are zwitterions
2. solubility measures equilibrium
   $AA_{solution} \leftrightarrow AA_{cryst}$, not gas!

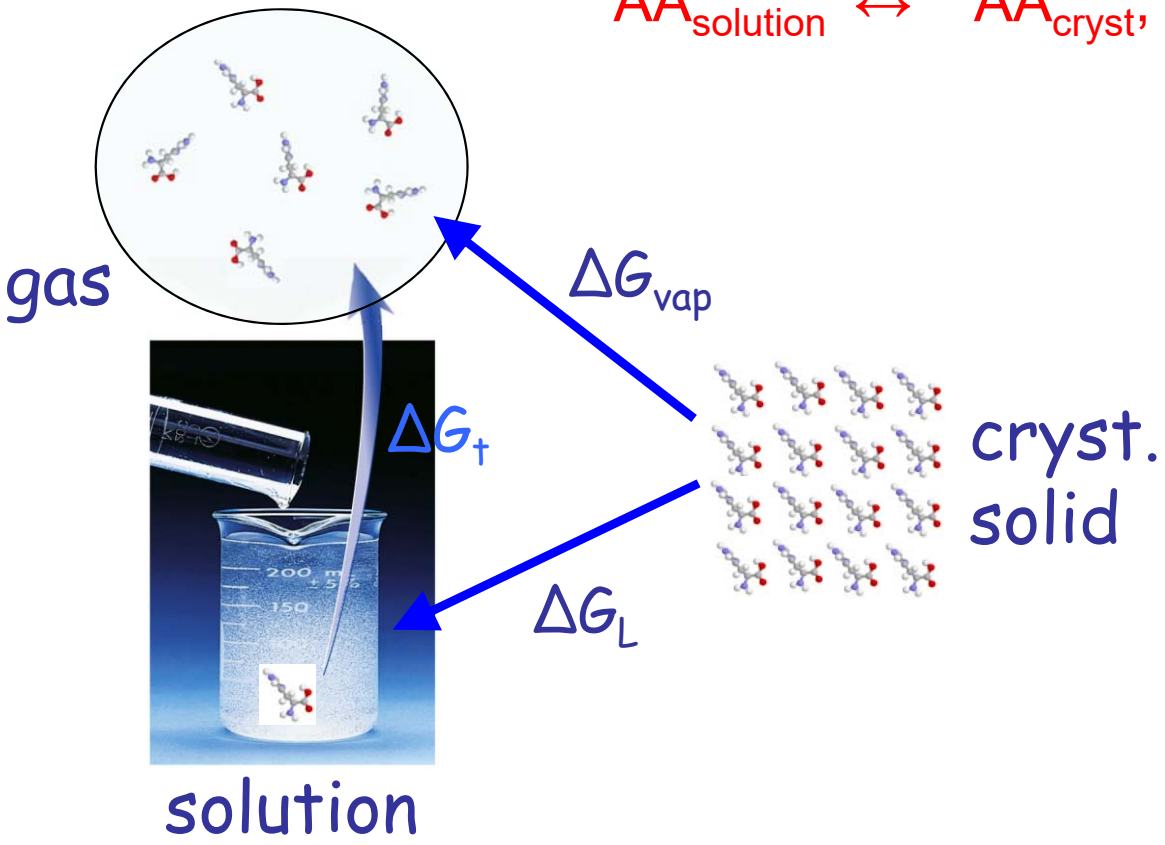

$$\frac{[L]}{[S]} = K_L = e^{-\Delta G_L / RT}$$

$$S \rightleftharpoons L$$

Polarity of amino acid side chains

Solution (Tanford): compare solubilities in H_2O (polar solvent) with EtOH (less polar)

1. calculate $\Delta G_{transfer}$ EtOH ⟶ H_2O
2. subtract ΔG_t of glycine to obtain side chain contribution only

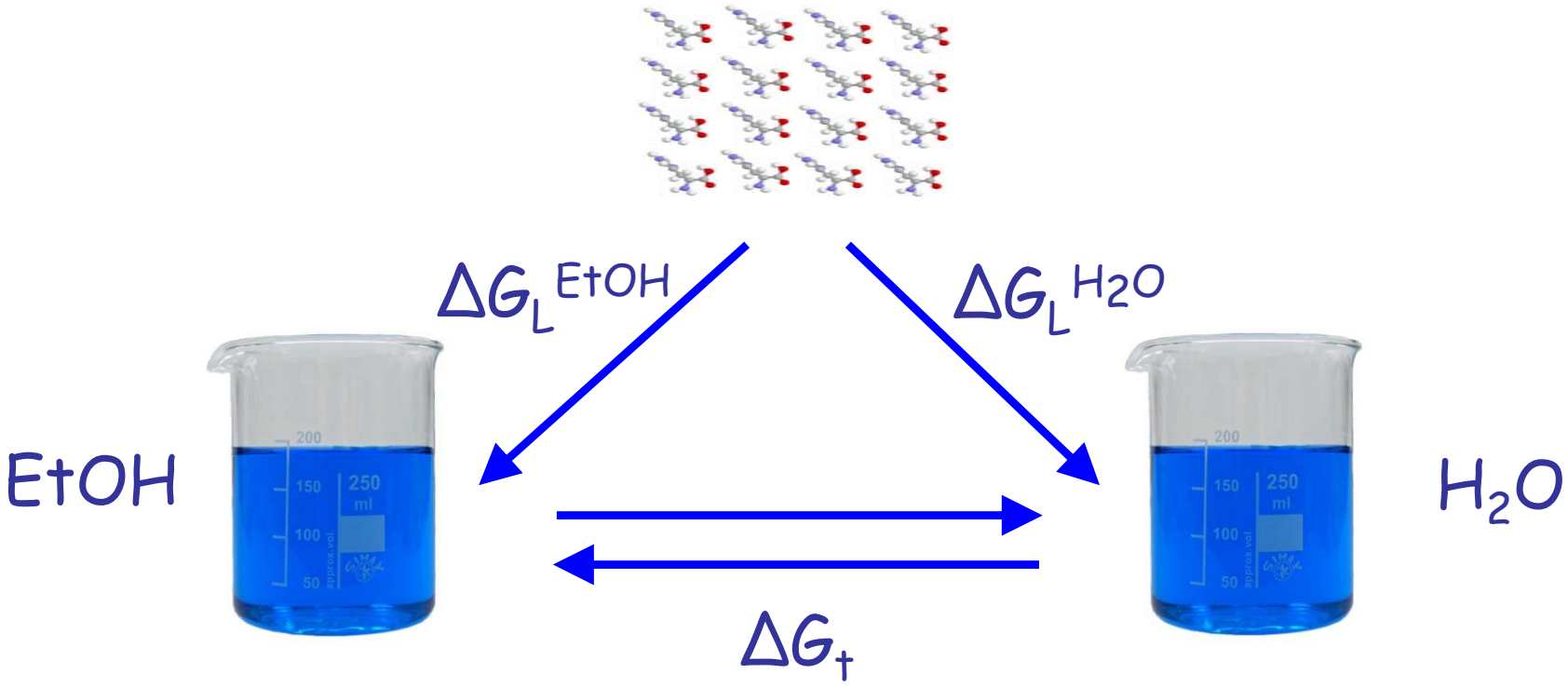

Polarity of amino acid side chains

Example

Gly : ΔG_t = -19.4 kJ/mol

Phe : ΔG_t = - 8.3 kJ/mol

Phe side chain : ΔG_t = + 11.1 kJ/mol

ΔG_t is positive, Phe side chain does not like to dissolve in polar solvent!

Cantor & Schimmel

Table 2-4
Classification of amino acid properties

Residue	Type	Zwitterion solubility, 25°C (moles/kg)	Side chain transfer ΔG_t, EtOH → H_2O (kcal/mole)
Trp	Nonpolar	0.07	3.00
Ile	Nonpolar	0.26	2.95
Tyr	Nonpolar‡	<0.00	2.85
Phe	Nonpolar	0.17	2.65
Leu	Nonpolar	0.16	2.40
Val	Nonpolar	0.50	1.70
Met	Nonpolar	0.38	1.30
Cys*	Nonpolar	<0.00	1.00
Ala	Nonpolar	1.86	0.75
Gly	Nonpolar‡	3.33	0.00
His	Ambiguous	ND	ND
Pro	Polar‡	14.1	2.60
Ser	Polar	4.02	ND
Thr	Polar	ND	0.45
Asn	Polar	0.19	ND
Gln	Polar	0.29	ND
Asp	Charged	0.04†	ND
Glu	Charged	0.06†	ND
Lys	Charged	3.95§	1.50
Arg	Charged	4.06§	0.75

* Data shown are actually 1/2 cystine.
† With side chain protonated; without a proton, the value is much higher.
‡ Usually.
§ HCl salts.
ND = No data.

Classification

Nonpolar	Polar	Charged
Trp	(Pro)	Asp
Ile	Ser	Glu
Tyr	Thr	Lys
Phe	Asn	Arg
Leu	Gln	
Val		
Met		
Cys		
Ala		
Gly		

increasing hydrophobicity

Primary structure

What can be learned from studies of the amino acid sequence ?

- Position of important residues
- Polarity of protein
- Secondary structure prediction
- 3D structure (≥2020: successful AI approaches, AlphaFold2, RoseTTAFold etc.)
- Evolution

Occurrence of different amino acids

Leu, Ala, Gly are common amino acids

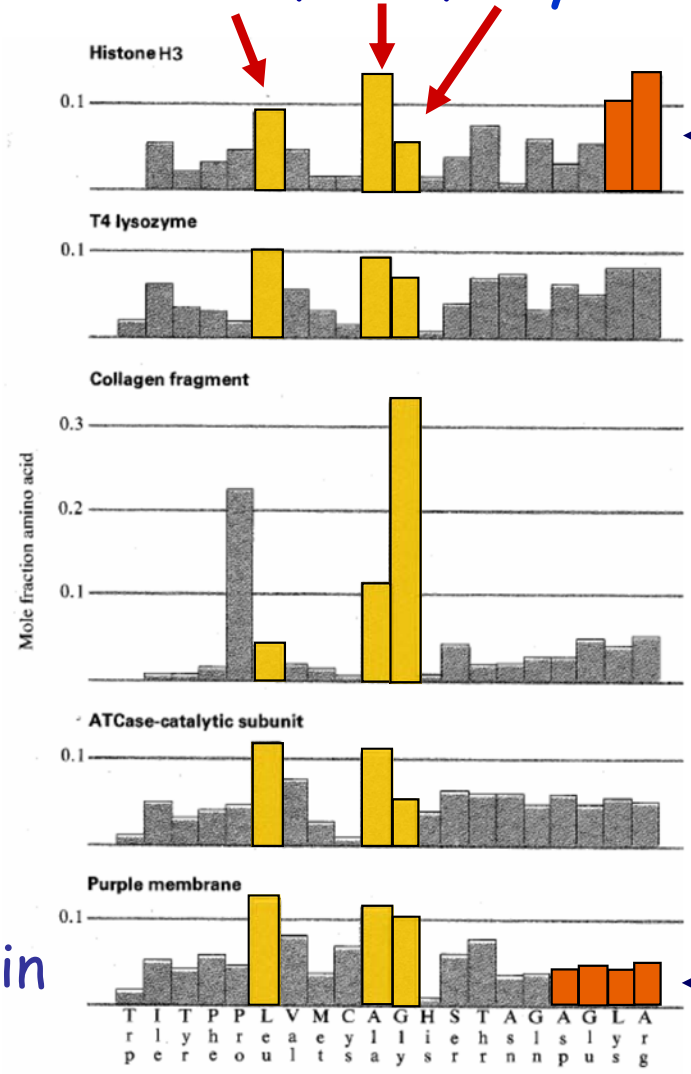

large number of positively charged amino acids

Bacteriorhodopsin

small number of polar amino acids

Addenda

Addendum I:
Properties of water, hydrophobic effect, hydrophobic interactions

Addendum II:
Acids and bases, acid-base properties of amino acids, charge interactions

Some key properties of water

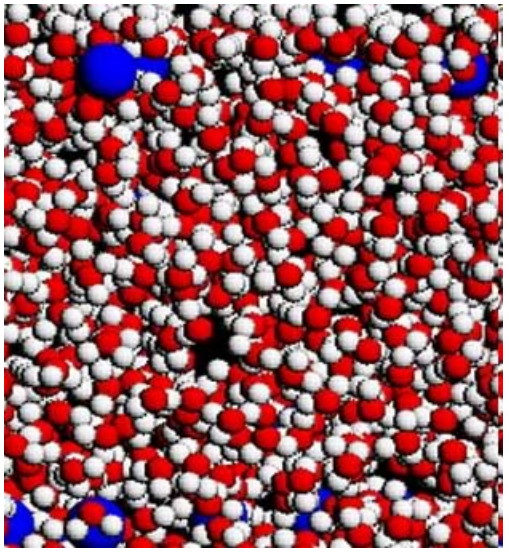

Life depends on the peculiar properties of water. Bulk water properties derive from the structure and interactions of water molecules:

<u>strong dipole:</u>

$p = 6.2 \times 10^{-30}$ Cm = 1.85 D (debye)

<u>interactions:</u>

hydrogen bonding, van der Waals interactions

<u>solid water (ice):</u>

4 H-bonds in tetrahedral geometry

<u>liquid water:</u>

Compromise between enthalpy and entropy: At room T, ~ 3.5 H-bonds are maintained (strong cohesion, high melting point), but bonding pattern fluctuates.

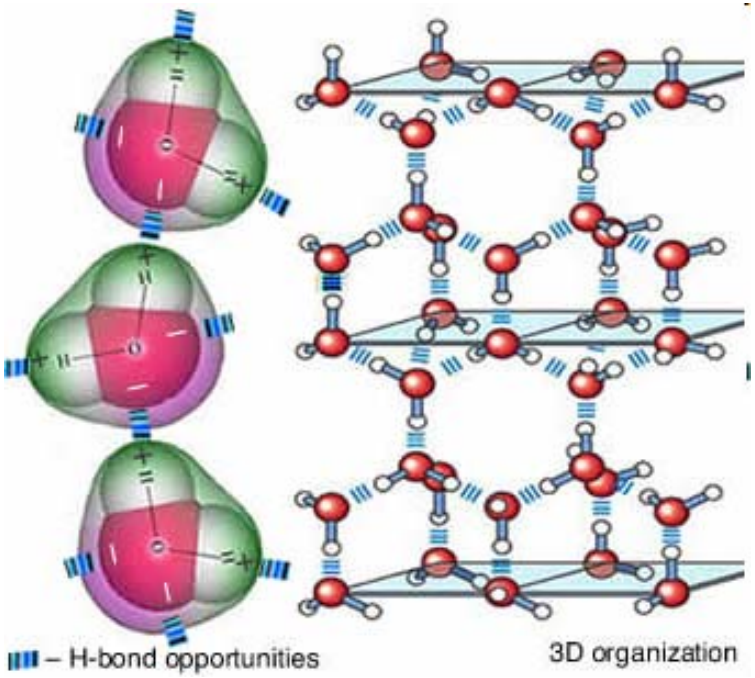

Ice structure

Hydrophobic effect

Solvation of small nonpolar molecules ($R < 5$Å)

~4 H-bonds maintained – but reordering of H-bonds, restricted water dynamics, **entropy** cost

Solvation of large nonpolar clusters ($R > 10$Å)

~1 H-bond per water molecule is sacrificed - **enthalpy** cost

Solvation free energy: scaling with radius R

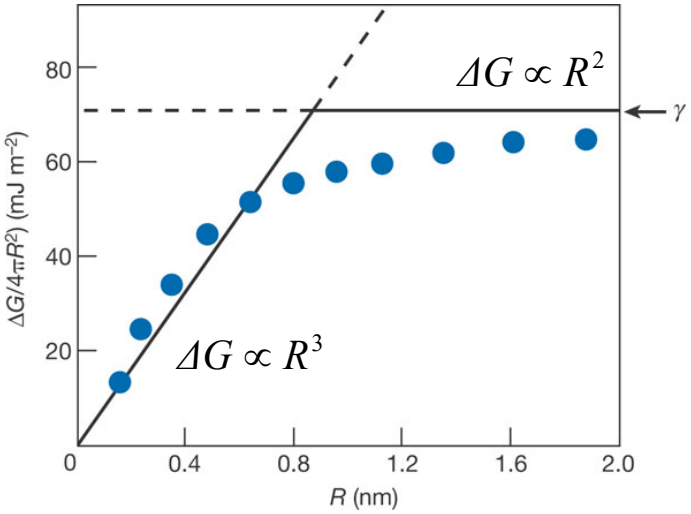

$$\Delta G = \Delta H - T\Delta S$$

$$K = \frac{[\text{Solute}_{\text{H2O}}]}{[\text{Solute}]} = \exp[-\Delta G / RT]$$

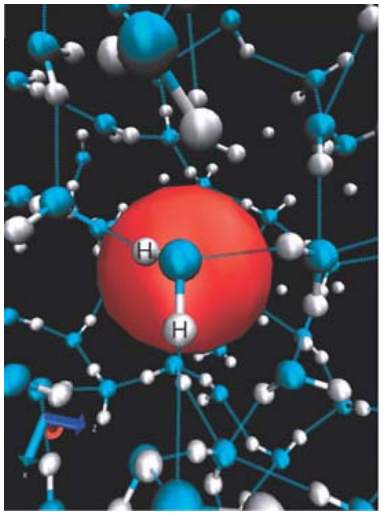

Clathrate cage

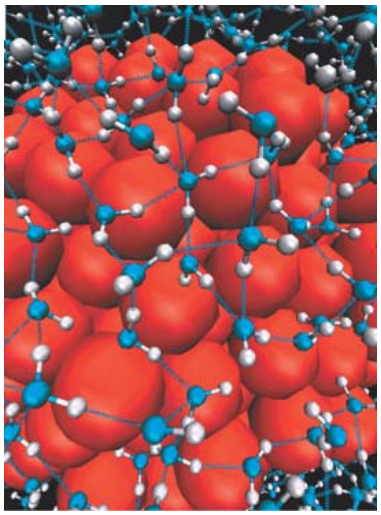

D. Chandler, Nature 437, 640-647 (2005)

Hydrophobic interaction

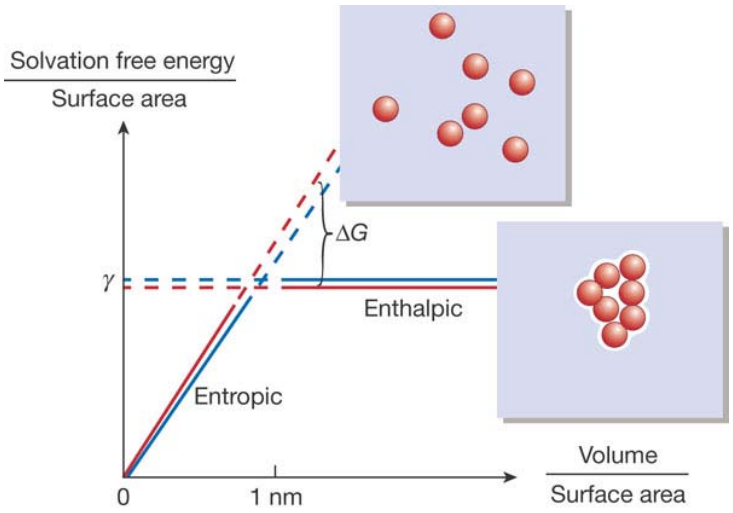

Non-polar moieties will cluster to minimize water perturbation: water-mediated interaction.

Hydrogen bonds will be formed upon dissolving (macro-)molecules with polar atoms (e.g., O, N).

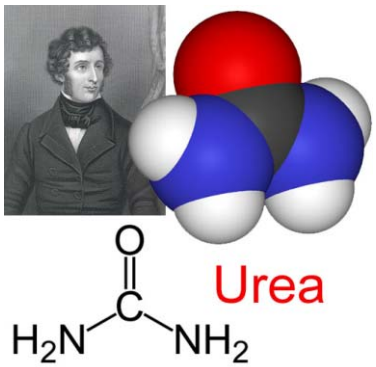

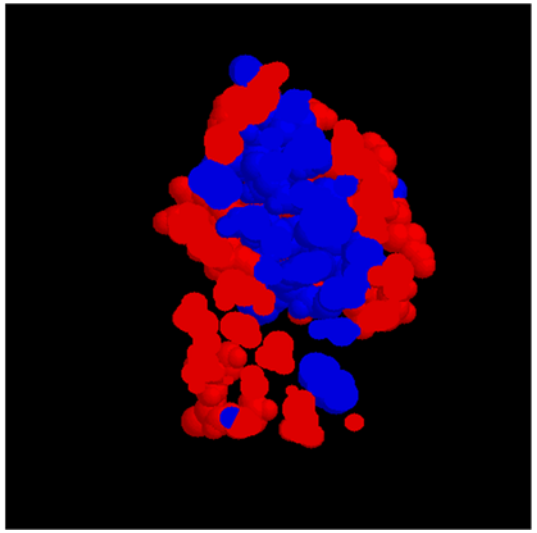

'Oil drop model' of the structure of lysozyme

http://course1.winona.edu/sberg/ANIMTNS/lysox-an.gif

Brief survey of acids and bases

Ionization of residues is crucial for stability and function of proteins.

- Definitions: Acid : proton donor (Brønsted, Lowry)
  Base : proton acceptor

$$A \rightleftharpoons B + H^+$$

- Acids and bases appear as conjugate pairs: NH_4^+/NH_3
  H_2O/OH^-
- Some molecules act both as acids and bases, e.g., amino acids.
- Ionization of water:

$$H_2O \rightleftharpoons OH^- + H^+ \quad \text{(or eq.: } 2\ H_2O \rightleftharpoons OH^- + H_3O^+\text{)}$$

- Equilibrium dissociation coefficient: $K = \dfrac{[H^+][OH^-]}{[H_2O]}$

Acids and bases

- Ion product of water:
  $[H_2O]$ = 55.55 M @ 298 K, 1 atm, practically constant in dilute solutions →

$$K \cdot [H_2O] = K_w = [H^+] \cdot [OH^-] = 10^{-14}\ M^2$$

- pure water: $[H^+] = [OH^-] = 10^{-7}$ M
- acid solution: $[H^+]$ large
- base solution: $[OH^-]$ large
- Definition:

$$pH = -\log [H^+]$$
$$pOH = -\log [OH^-]$$

$$pH + pOH = 14$$

Quantification of H^+-binding strength

For an acid dissociation,

$$AH \rightleftharpoons A^- + H^+,$$

the equilibrium dissociation coefficient is $K = \frac{[A^-][H^+]}{[AH]}$

and pK = -log K

Henderson-Hasselbalch equation: $pH = pK - \log \frac{[AH]}{[A^-]}$

Free energy of ionization (proton dissociation):

$$\Delta G_{ioniz} = \Delta G^0 + RT \ln \frac{[H^+][A^-]}{[HA]}$$

R: gas constant
T: temp. in K

ΔG^0 refers to standard state: 1 M.

ΔG_{ioniz} = 0 in equilibrium: $\Delta G^0 = -RT \ln K$

$= 2.303 \cdot RT \cdot pK$

Amino acids – acid/base titration

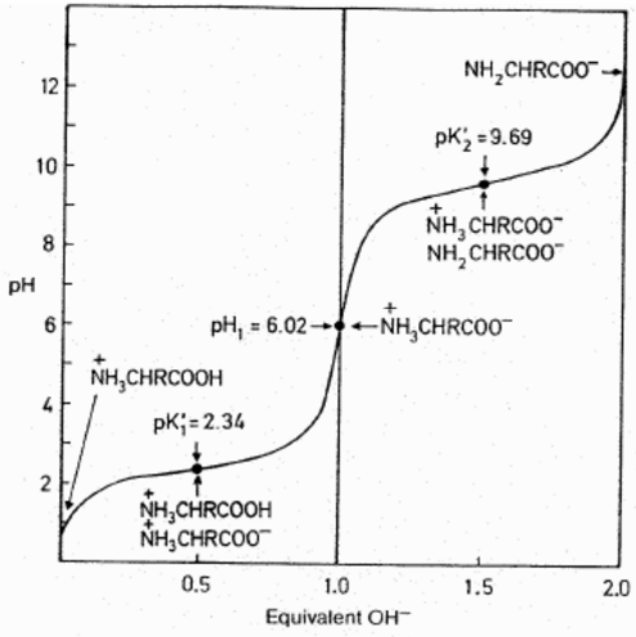

Alanine :

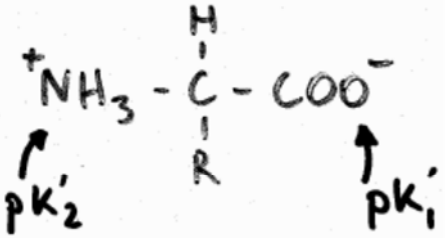

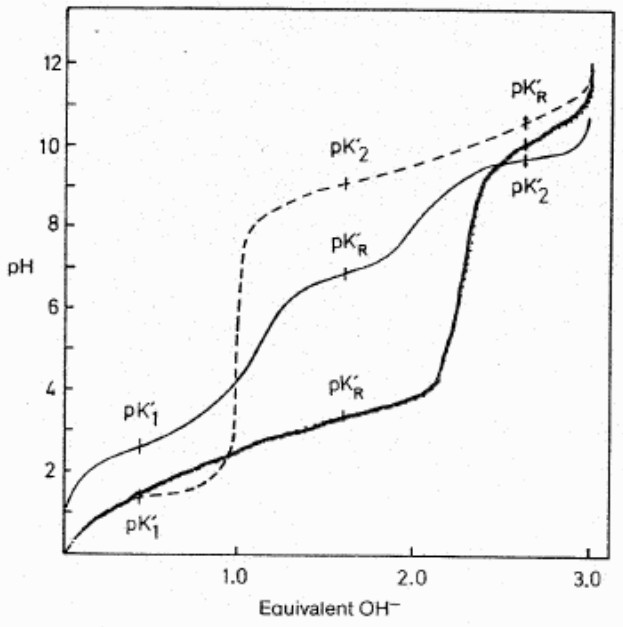

Glutamic acid :

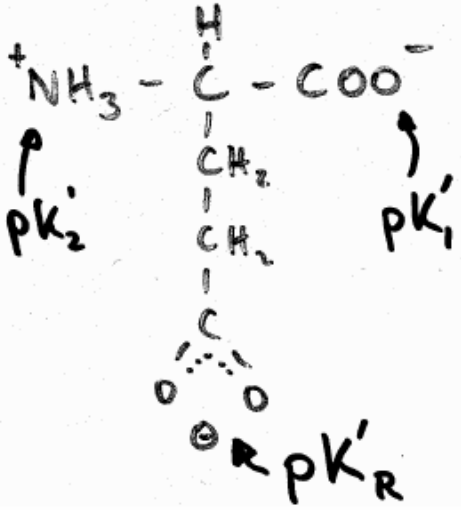

Acid-base properties of amino acids

Amino acid	α-COOH	α-NH_3^+	Side chain	pK_a in amino acid	Expected pK_a in a protein
Alanine	2.3	9.9	—	—	—
Arginine	1.8	9.0	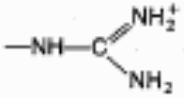	12.5	⩾12
Asparagine	2.0	8.8	—	—	—
Aspartic acid	2.0	10.0	—COOH	3.9	4.4–4.6
Cysteine	1.8	10.8	—SH	8.3	8.5–8.8
Glutamic acid	2.2	9.7	—COOH	4.3	4.4–4.6
Glutamine	2.2	9.1	—	—	—
Glycine	2.4	9.8	—	—	—
Histidine	1.8	9.2	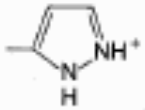	6.0	6.5–7.0
Isoleucine	2.4	9.7	—	—	—
Leucine	2.4	9.6	—	—	—
Lysine	2.2	9.2	—NH_3^+	10.8	10.0–10.2
Methionine	2.3	9.2	—	—	—
Phenylalanine	1.8	9.1	—	—	—
Proline	2.0	10.6	—	—	—
Serine	2.1	9.2	—	—	—
Threonine	2.6	10.4	—	—	—
Tryptophan	2.4	9.4	—	—	—
Tyrosine	2.2	9.1	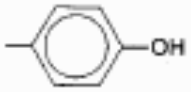	10.9	9.6–10.0
Valine	2.3	9.6	—	—	—

NOTE: The pK_a values in most cases are at 25°C. The expected pK_a values in proteins are determined from model compounds in which titration of side chains is decoupled from charge effects of α-substituents.

Additional interactions

In biomolecules, ionization of one group is often coupled to other groups:

$$\Delta G_{tot} = \Delta G_{int} + \Delta G_{ioniz}$$

$$\Delta G_{tot} = \Delta G_{int} + \Delta G^0 + RT \ln \frac{[H^+][A^-]}{[HA]}$$

In equilibrium:

$$\Delta G_{tot} = 0$$

Then, the apparent pK is

$$pK' = \frac{\Delta G^0 + \Delta G_{\text{int}}}{2.303RT}$$

Example:

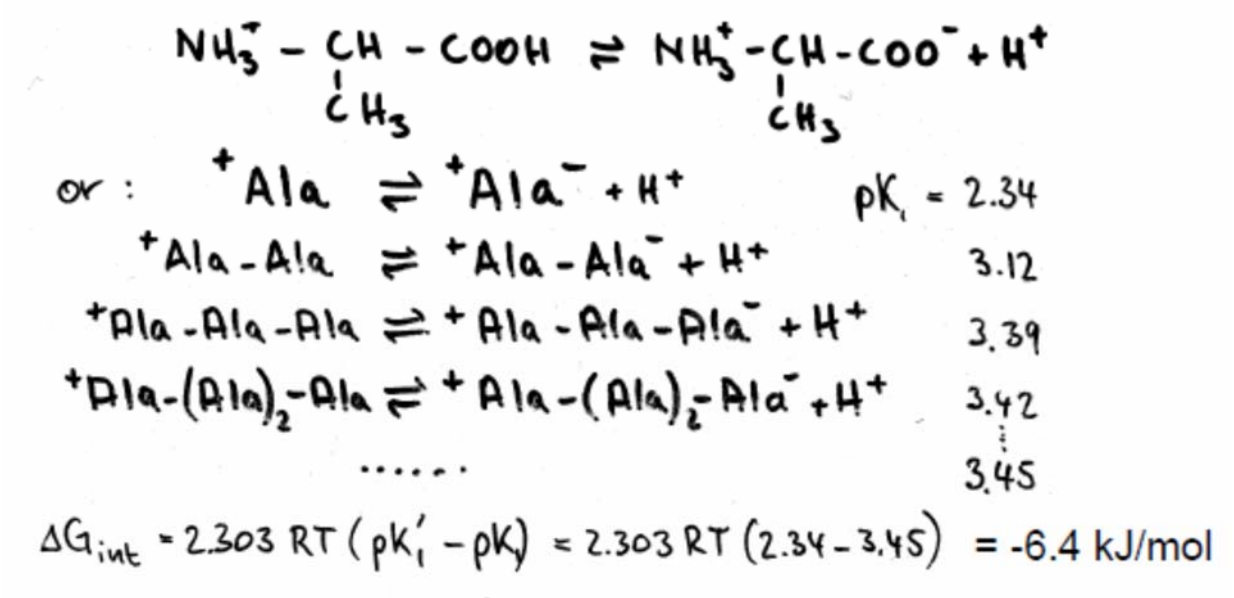

Biophysics II

Protein Secondary Structure
Part 1b

Prof. G. U. Nienhaus, Vorlesungsunterlagen Biophysik II, SS 2023.
Nur zum KIT-internen, vorlesungsbegleitenden Gebrauch.
Weitergabe und anderweitige Nutzung verboten.

Polypeptide Conformations

Not all Φ and Ψ angles are possible!

(a)

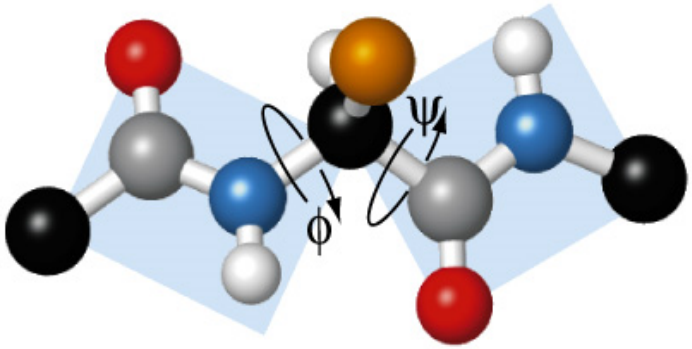

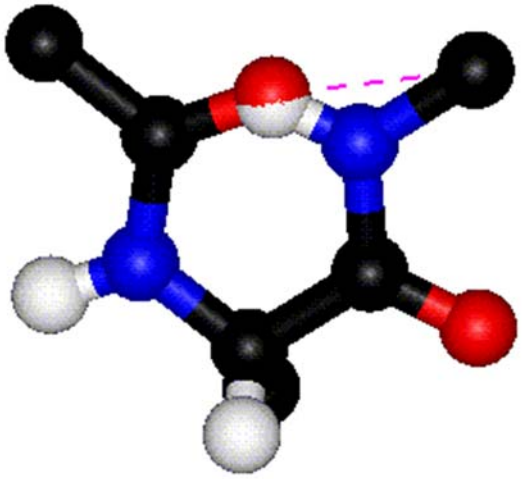

Ψ angle rotation

(b)

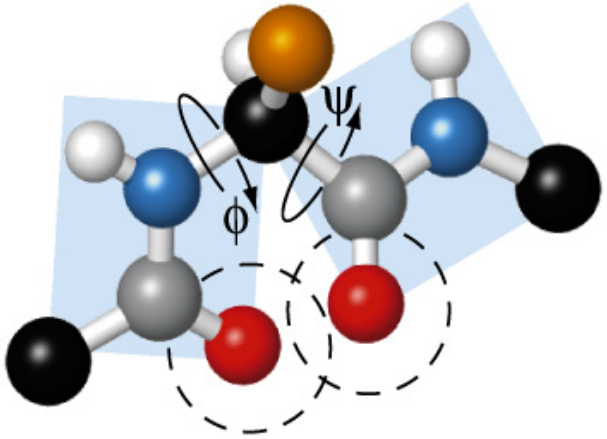

α-carbon
Carbonyl carbon
Hydrogen
Nitrogen
Oxygen
Side chain

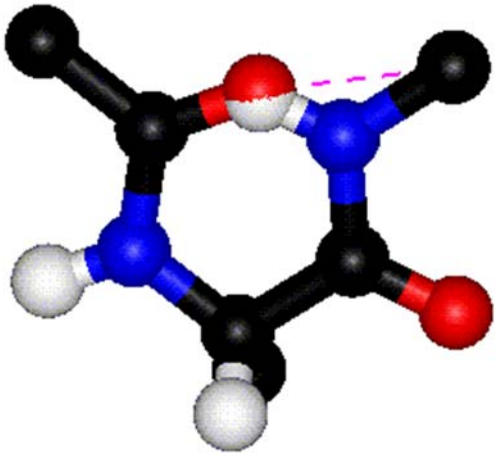

Φ angle rotation

Helices

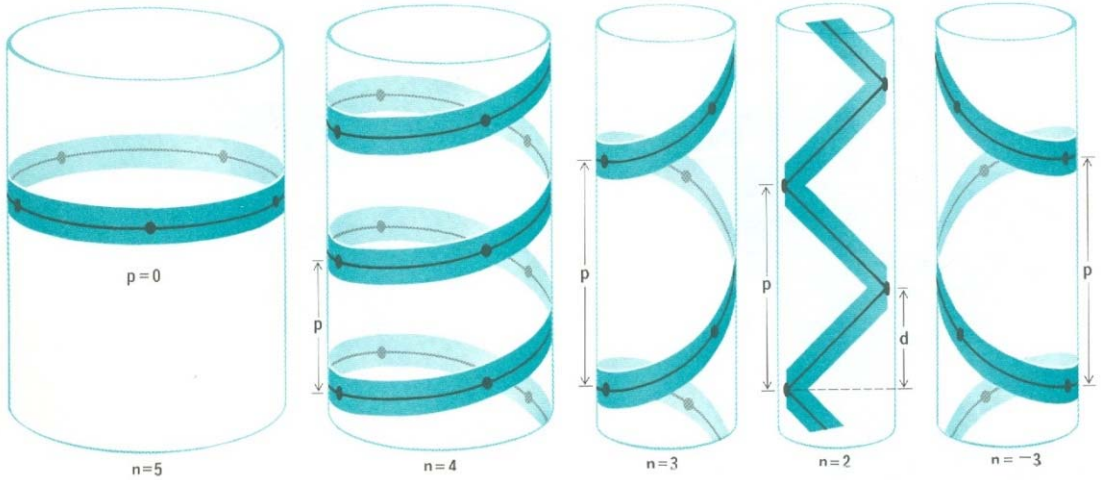

p = pitch
n = # a.a. per turn
d = rise = p/n

Subtract 180° for ψ (due to a redefinition)!

→

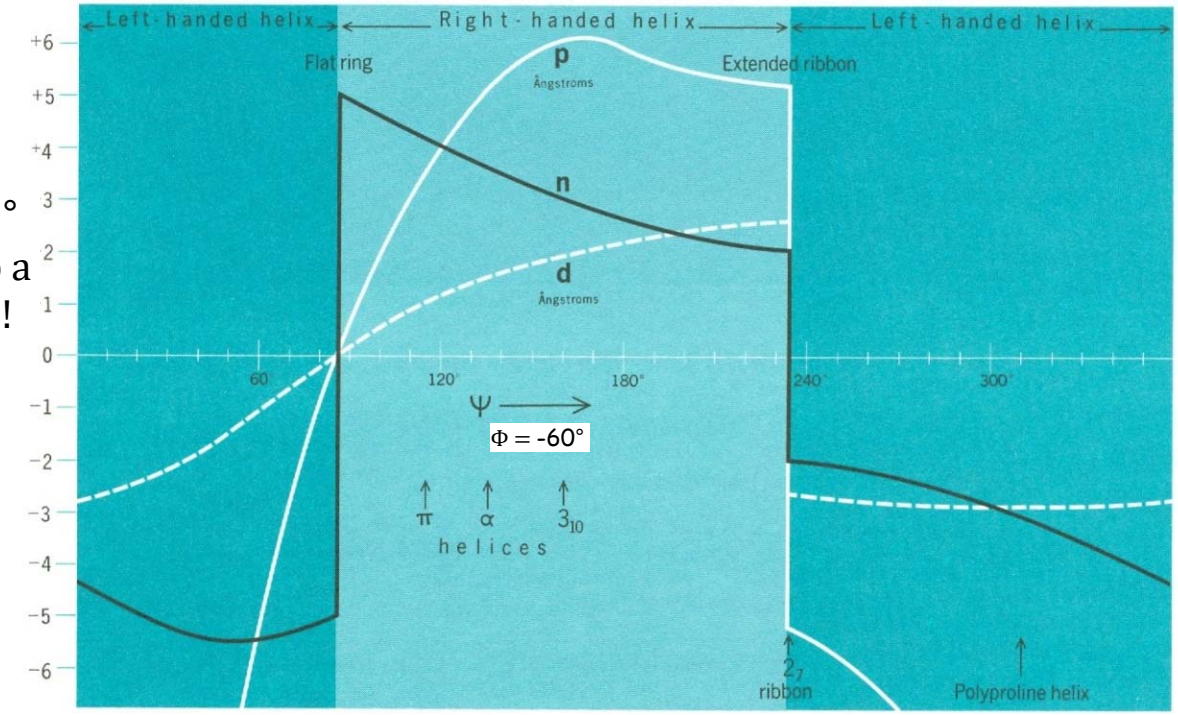

Plot of n, d, *and* p *versus* ψ *for* φ = -60°, *with several important helices marked.*

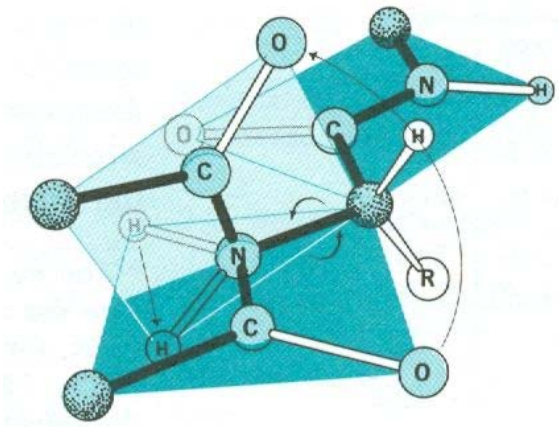

Φ = - 60°
Ψ = 180°

α-helix

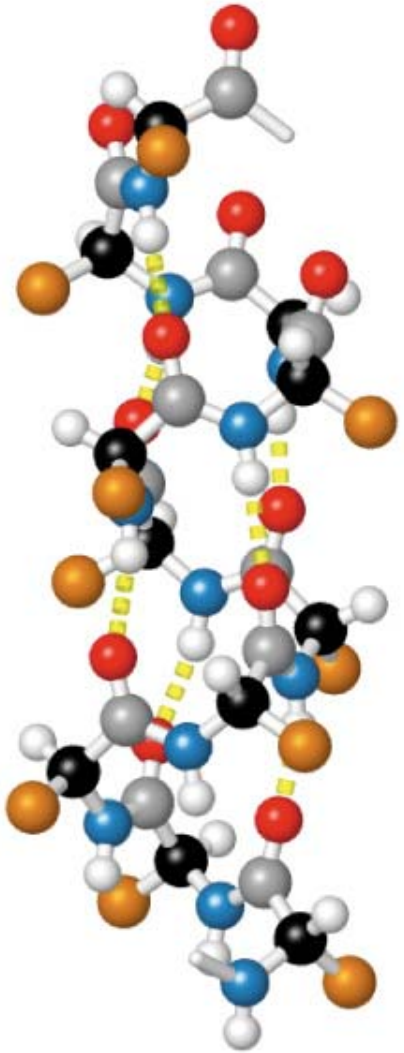

Right-handed α-helix

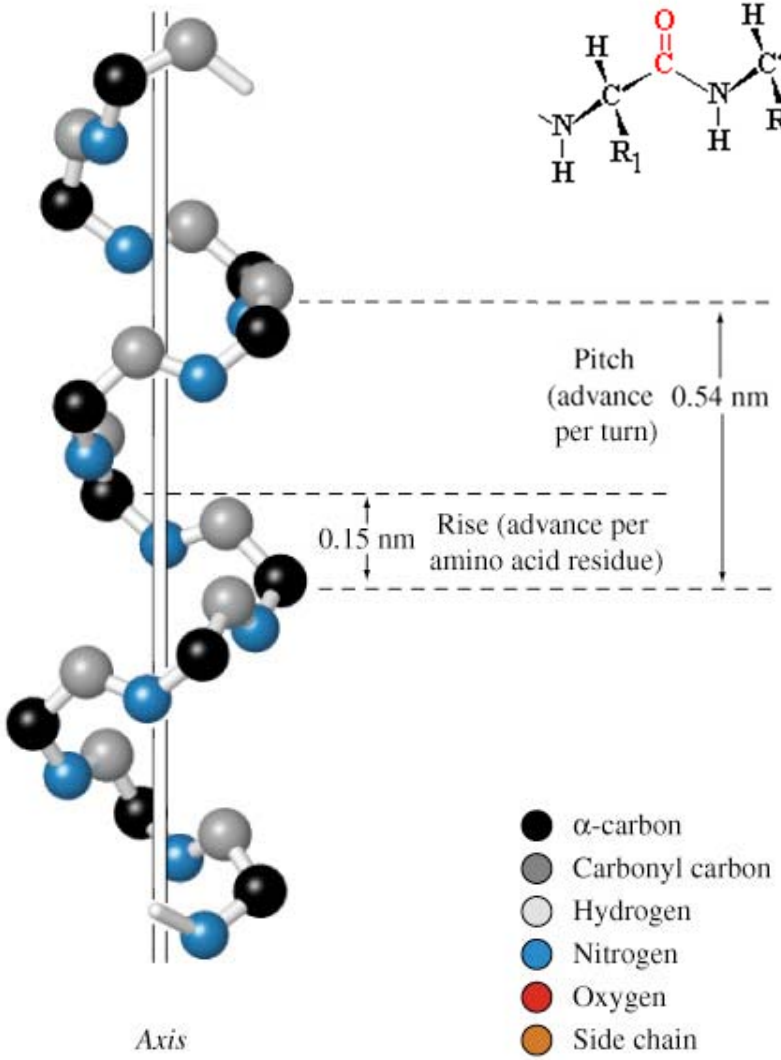

Axis

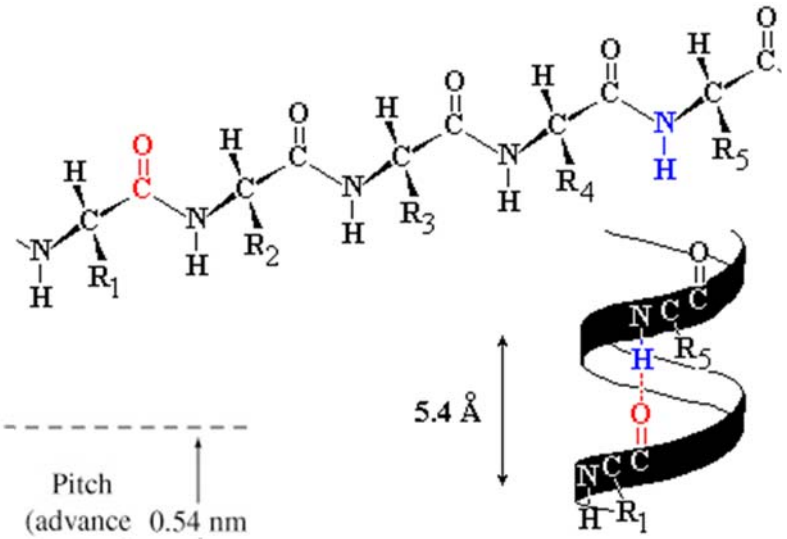

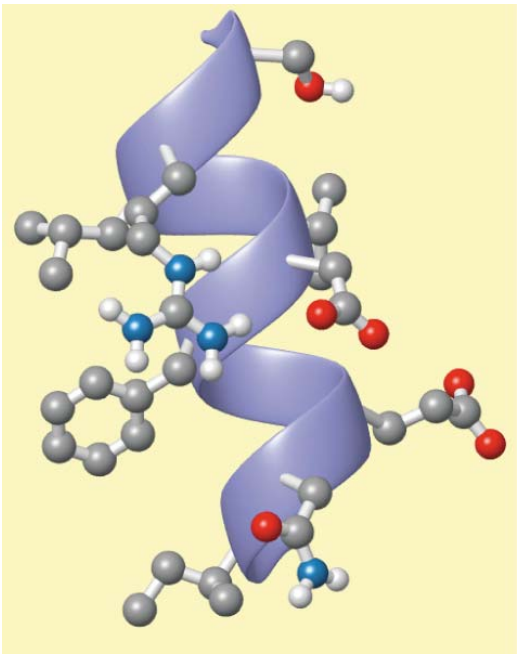

Helices

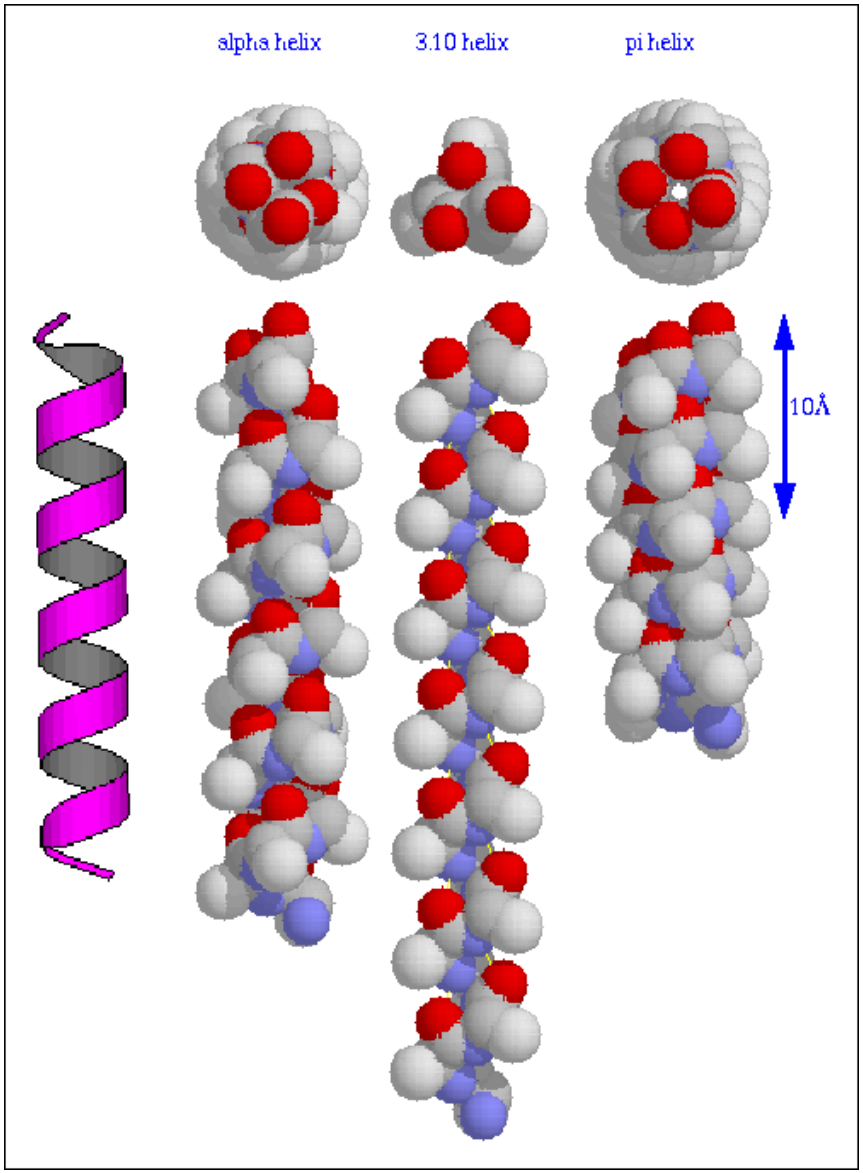

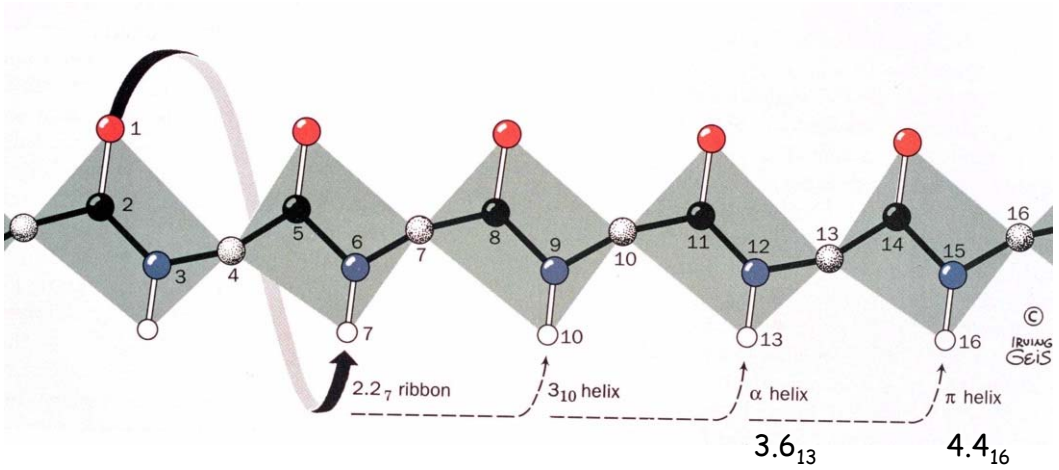

Helix nomenclature: N_m

with N = # res. per turn

m = # atoms connecting H-bond

β-pleated sheets

parallel
β-sheet

antiparallel
β-sheet

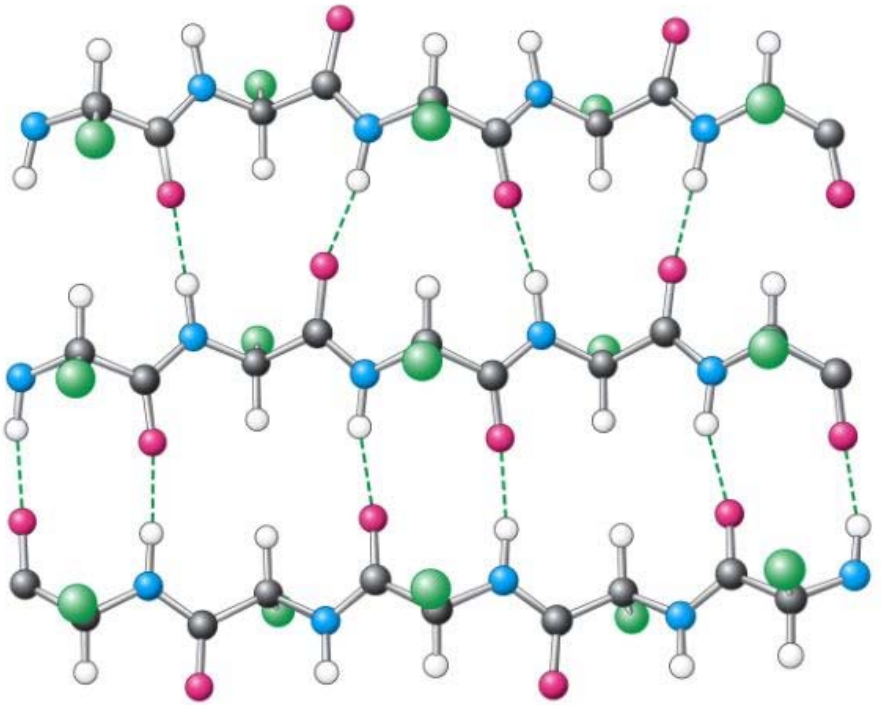

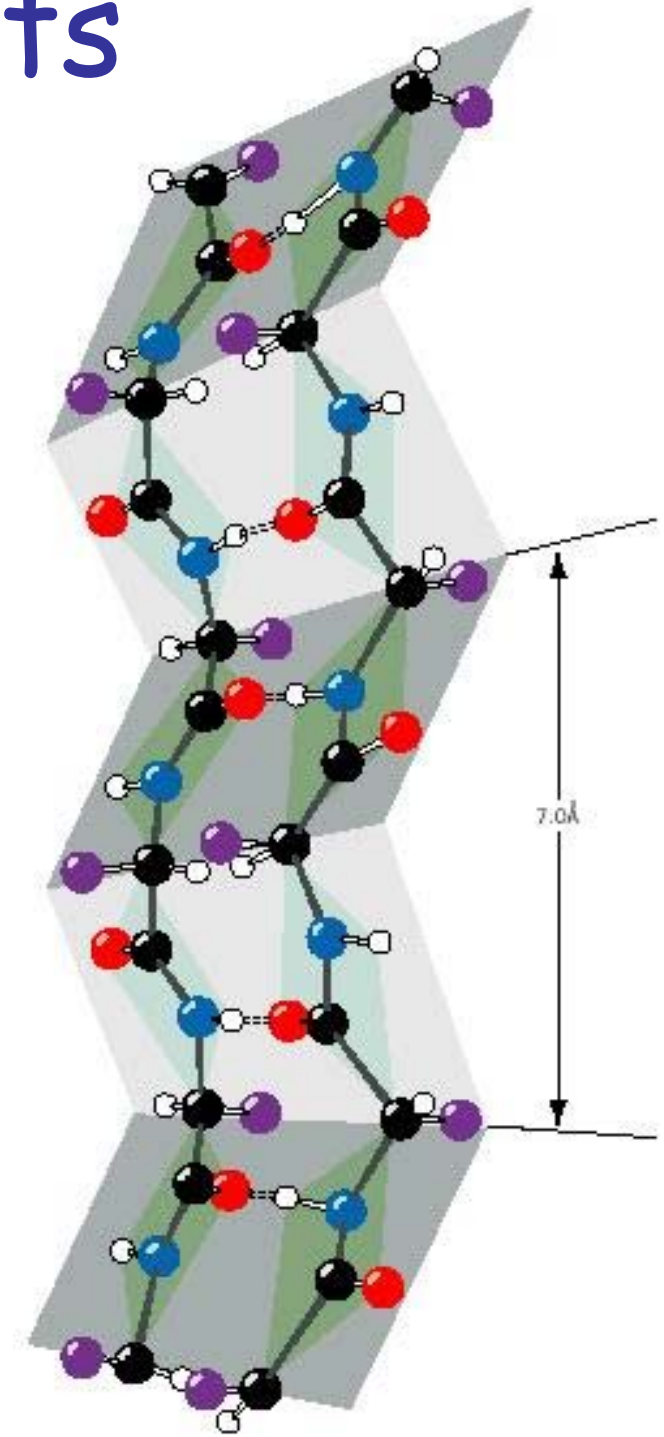

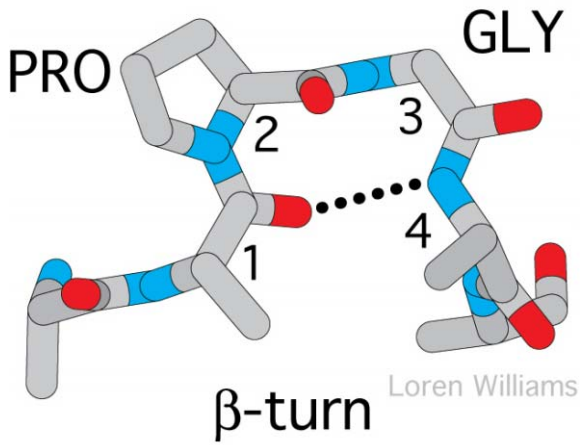

Examples

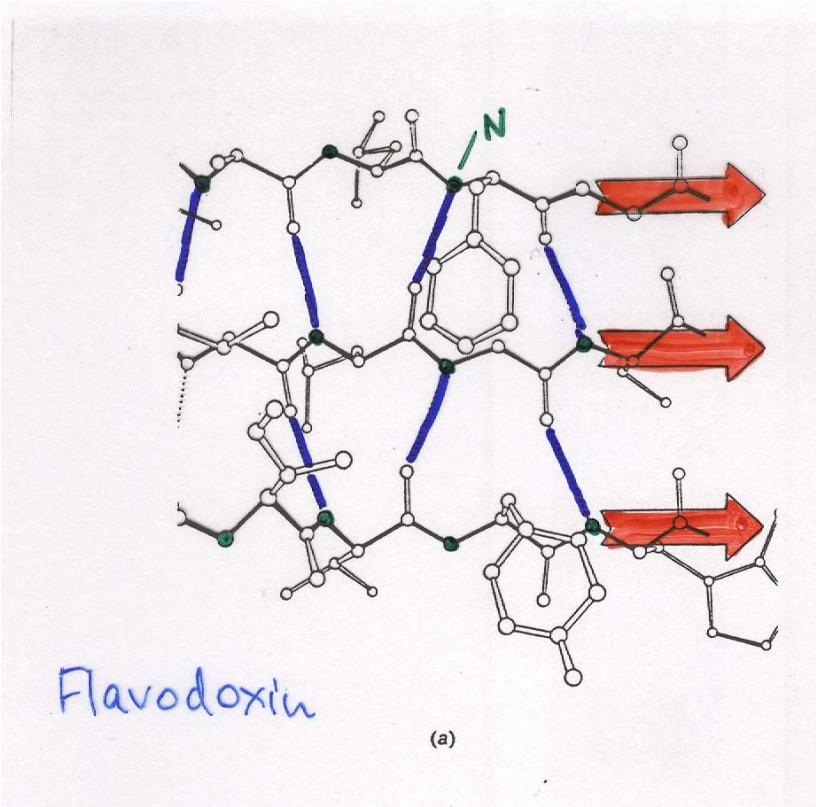

Flavodoxin

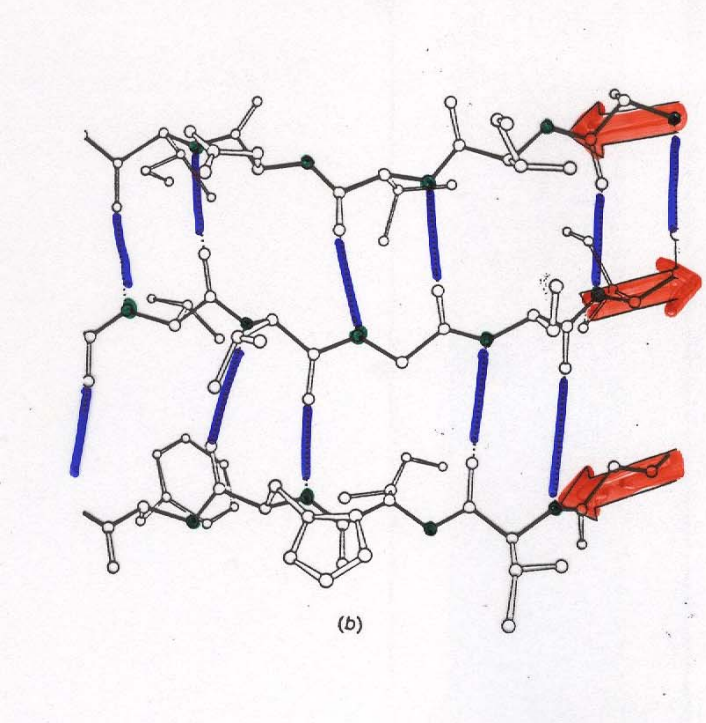

Cu, Zn SOD

Ramachandran Plot

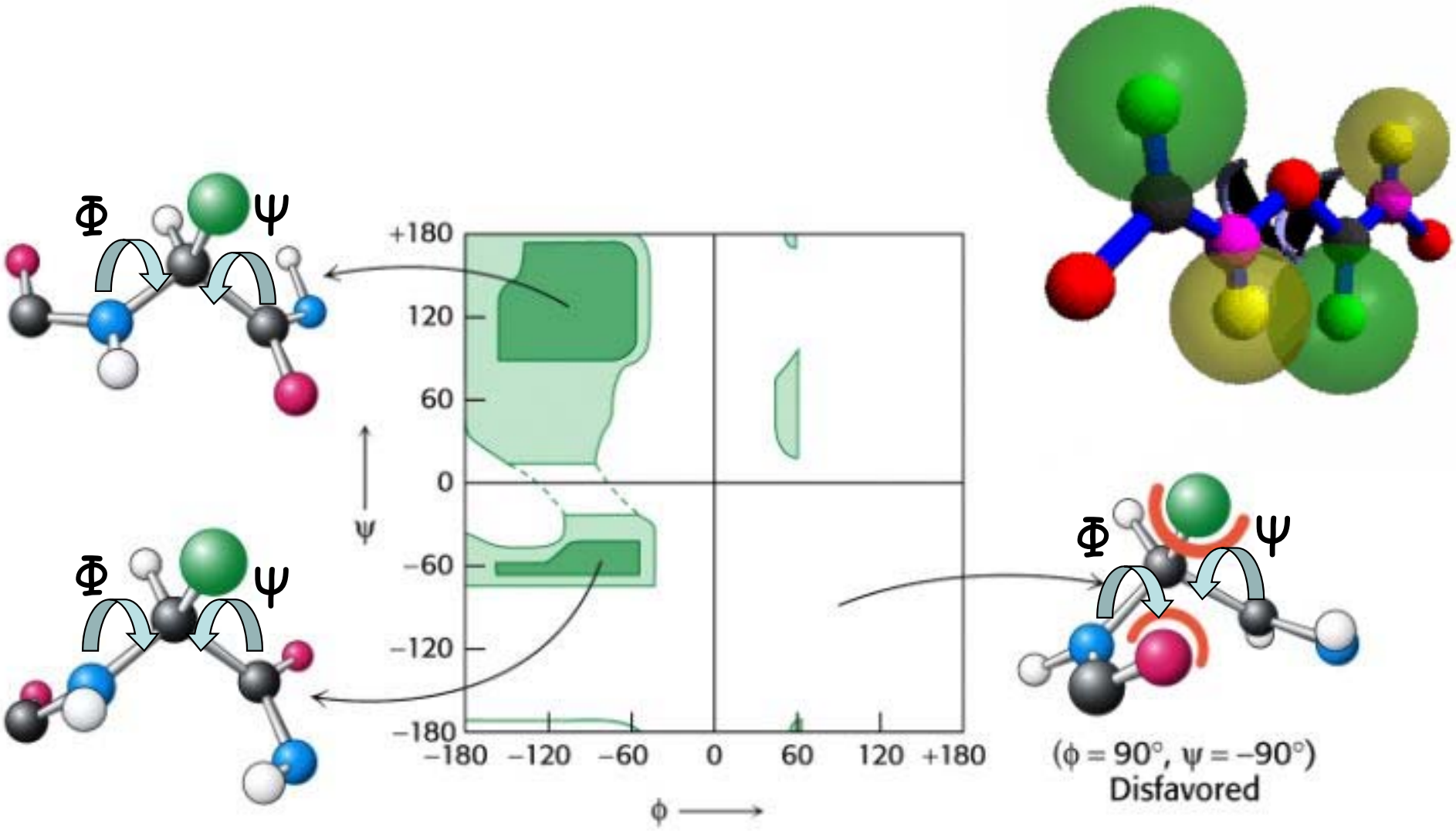

Ramachandran, Ramakrishnan & Sasisekharan (1963) *J. Mol. Biol.* 7, 95-99.

Ramachandran Plot

Φ, Ψ of residues in a single protein

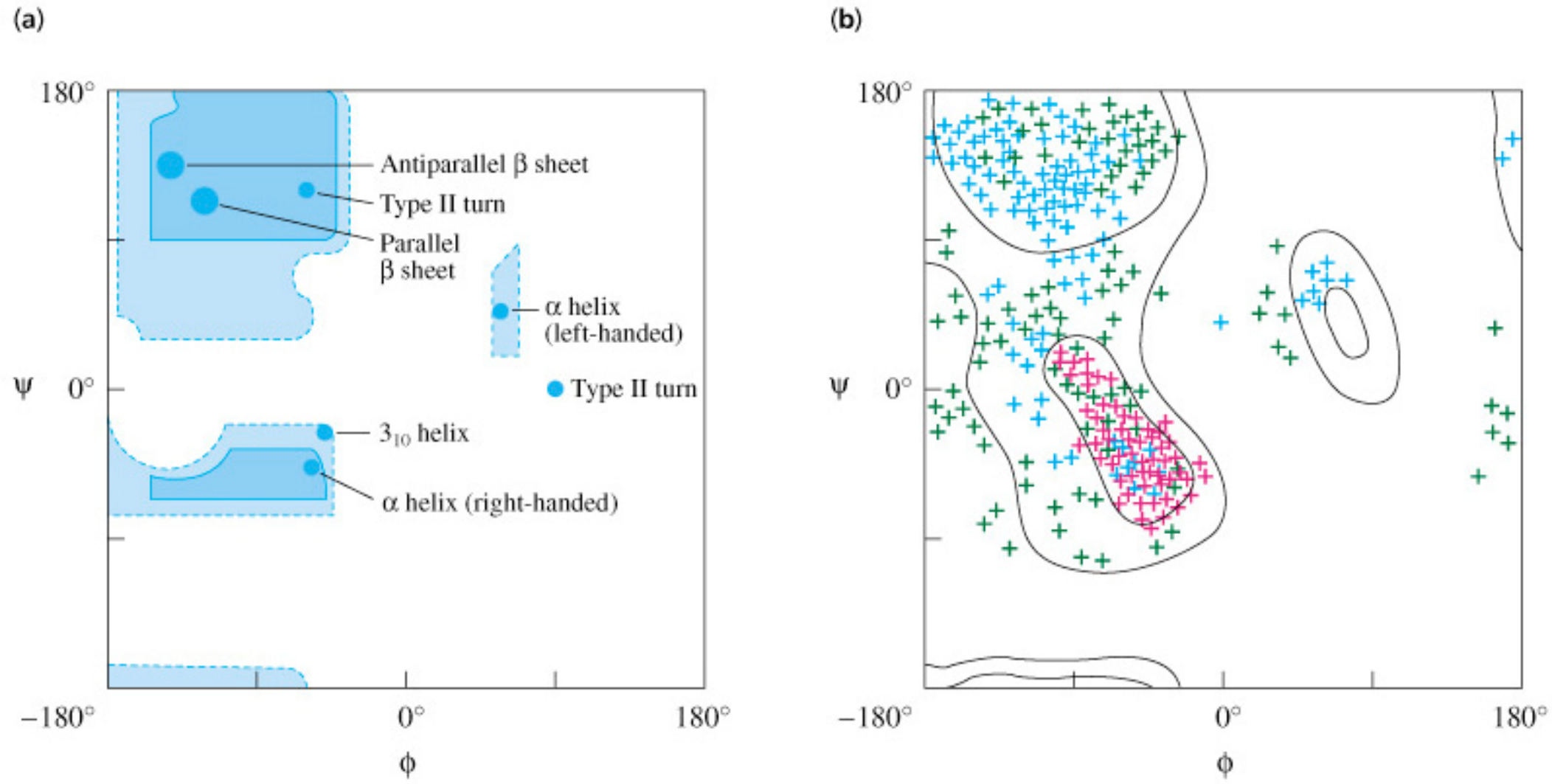

Ramachandran Plot

Φ, Ψ of three important amino acids in many protein structures

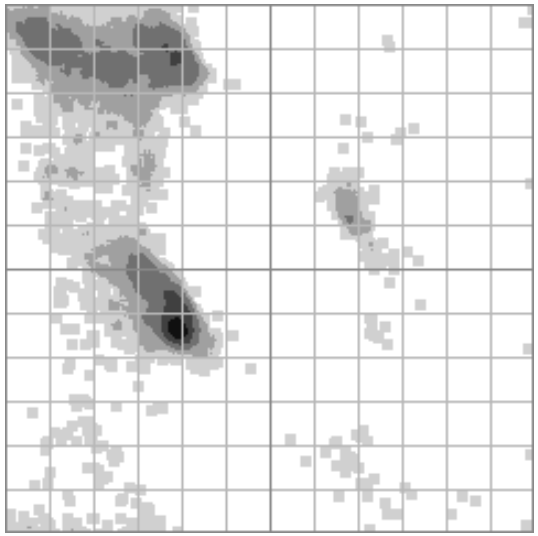

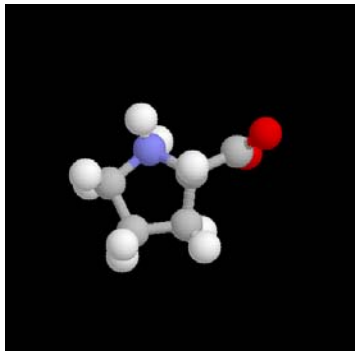

proline

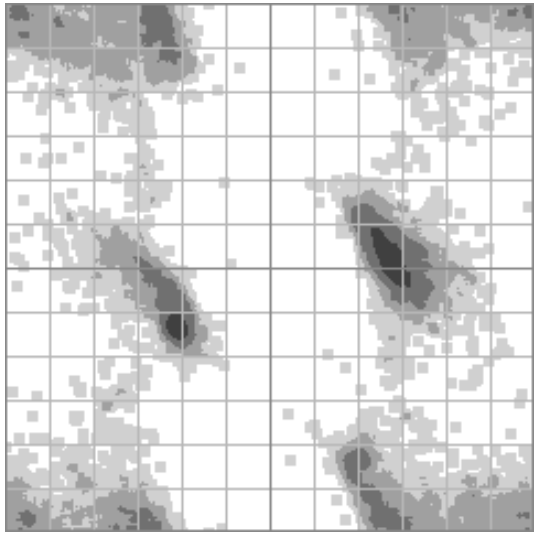

alanine

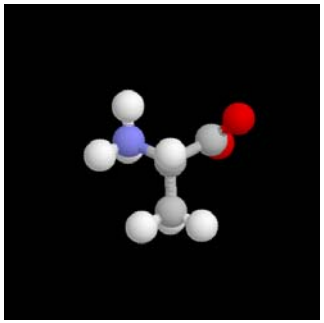

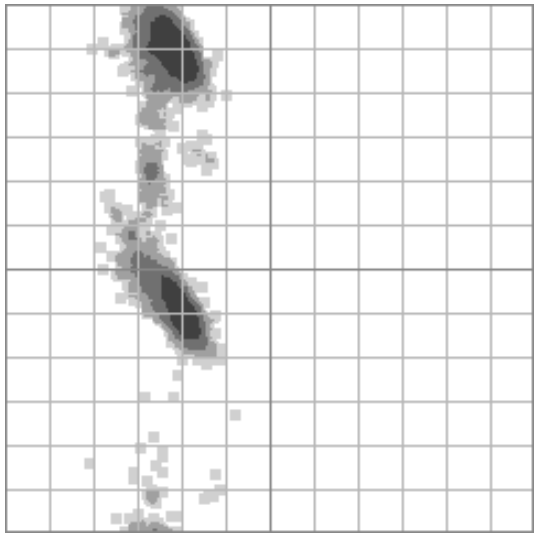

glycine

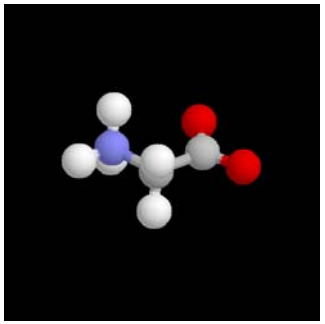

Interactions

Type of interaction		Interaction energy $w(r)$
Covalent	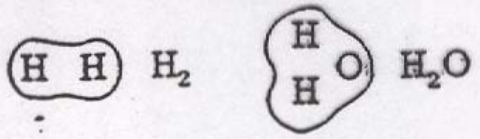	Complicated, short range
Charge–charge	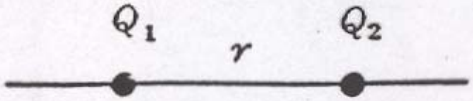	$Q_1Q_2/4\pi\varepsilon_0 r$ (Coulomb energy)
Charge–dipole	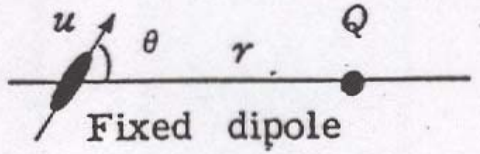	$-Qu\cos\theta/4\pi\varepsilon_0 r^2$
	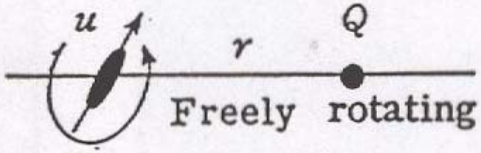	$-Q^2u^2/6(4\pi\varepsilon_0)^2kTr^4$
Dipole–dipole	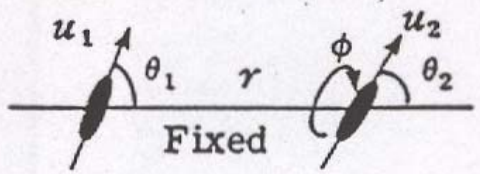	$-u_1u_2[2\cos\theta_1\cos\theta_2 - \sin\theta_1\sin\theta_2\cos\phi]/4\pi\varepsilon_0 r^3$
	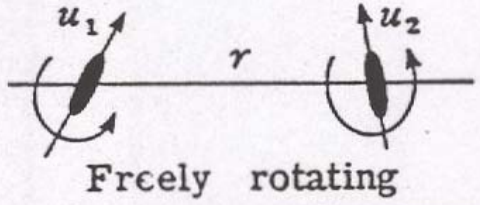	$-u_1^2u_2^2/3(4\pi\varepsilon_0)^2kTr^6$ (Keesom energy)

Interactions

Polarizability α

Charge–nonpolar	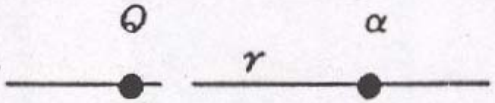	$-Q^2\alpha/2(4\pi\varepsilon_0)^2r^4$
Dipole–nonpolar	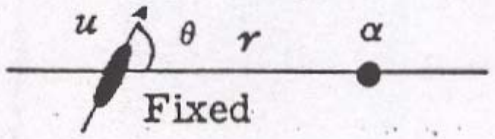	$-u^2\alpha(1+3\cos^2\theta)/2(4\pi\varepsilon_0)^2r^6$
	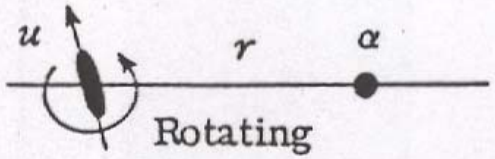	$-u^2\alpha/(4\pi\varepsilon_0)^2r^6$ (Debye energy)
Two nonpolar molecules	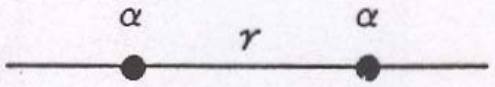	$-\left(\frac{3}{4}\right)\frac{h\nu\alpha^2}{(4\pi\varepsilon_0)^2r^6}$ (London dispersion energy)
Hydrogen bond	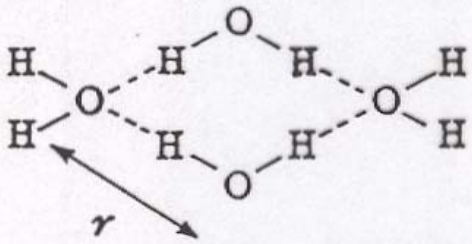	Complicated, short range, energy roughly proportional to $-1/r^2$

Conformational energies

1. Non-bonded interaction

$$E_{kl}(\phi_i;\psi_i) = \frac{a_{kl}}{r_{kl}^{m}} - \frac{b_{kl}}{r_{kl}^{6}}$$

k,l pairs of atoms
m = 9…12

London dispersion energy

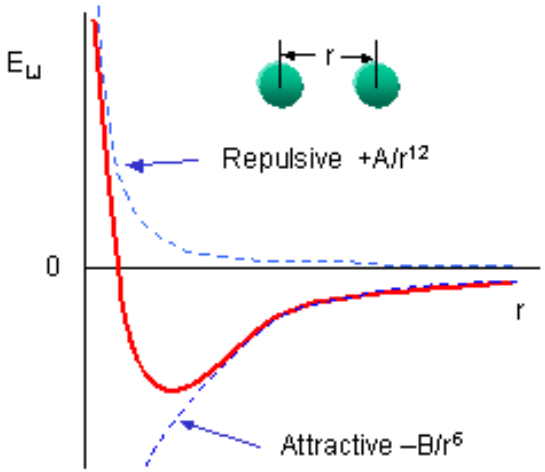

2. Dipolar interaction

$$E_d = \frac{1}{4\pi\varepsilon_0\varepsilon}\left[\frac{\vec{\mu}_A\cdot\vec{\mu}_B}{r^3} - \frac{3(\vec{\mu}_A\cdot\vec{r})(\vec{\mu}_B\cdot\vec{r})}{r^5}\right]$$

or $$E_d = \frac{1}{4\pi\varepsilon_0\varepsilon}\sum_{ij}\frac{q_i q_j}{r_{ij}}$$

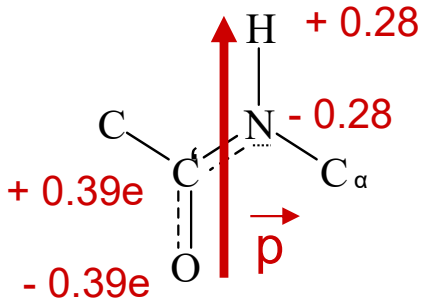

3.7 D

1 D = 3.3 x 10^{-30} Cm

1 eÅ = 4.8 D

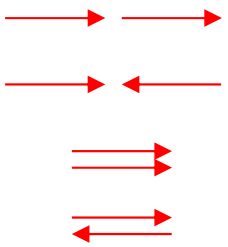

-5.6 kJ/mol

+5.6 kJ/mol

+2.8 kJ/mol

-2.8 kJ/mol

1 D, 5Å distance

Conformational energies

3. Torsional potential

$$E_{tor} = \frac{E_{\phi}^{0}}{2}\left(1+\cos 3\phi\right) + \frac{E_{\psi}^{0}}{2}\left(1+\cos 3\psi\right)$$

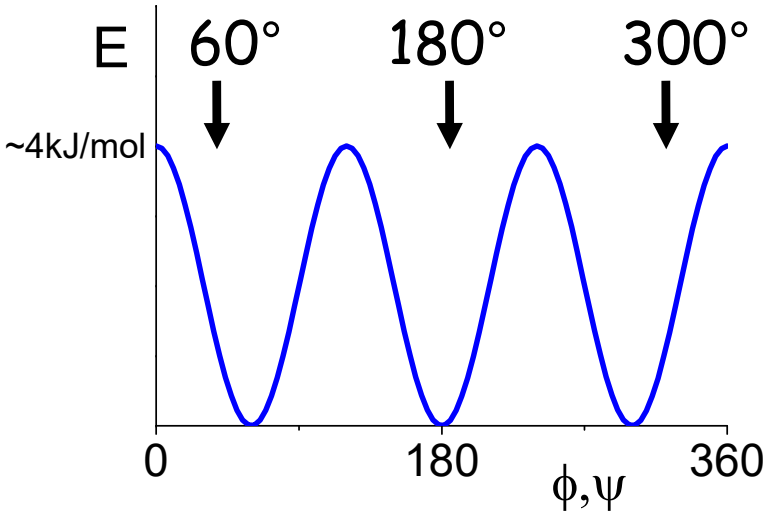

Total energy

$$E_{tot}\left(\phi_i,\psi_i\right) = \sum_{k,l} E_{kl}\left(\phi_i,\psi_i\right) + E_d\left(\phi_i,\psi_i\right) + E_{tor}\left(\phi_i,\psi_i\right)$$

H-bonds, side-chain interactions and solvent interactions are all neglected in this simple model!!!

Glycine

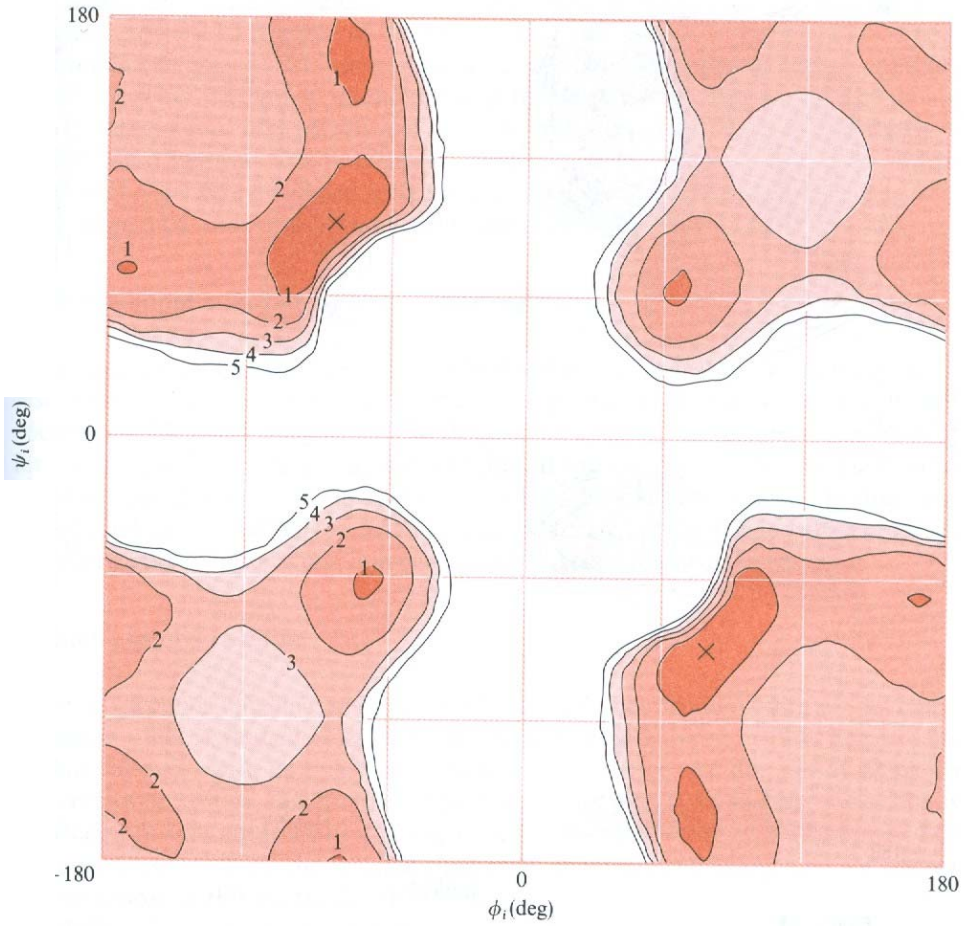

Contour map of E_{tot} in 1 kcal/mol intervals

- Relatively large allowed regions
- Regions extend toward Φ, Ψ = 0

→ Compact folds

Alanine

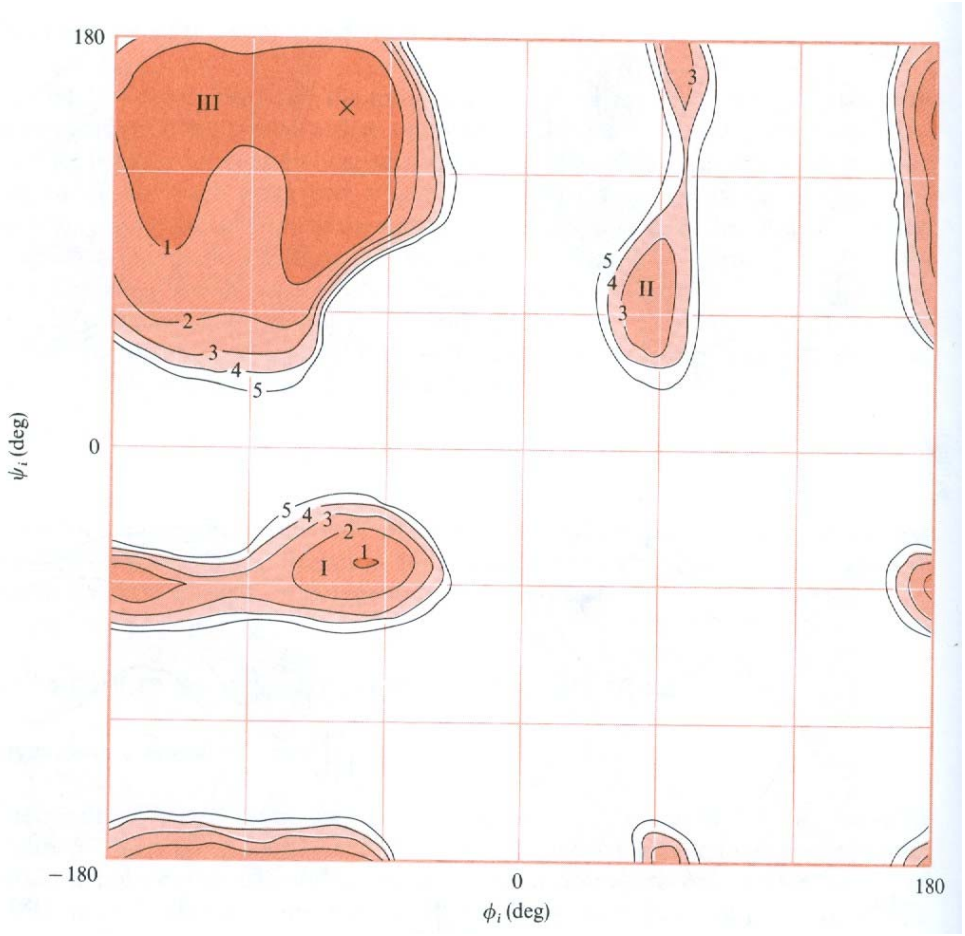

Contour map of E_{tot} in 1 kcal/mol intervals

- typical pattern of amino acids
- those branched at β-carbon have smaller allowed regions.

Proline

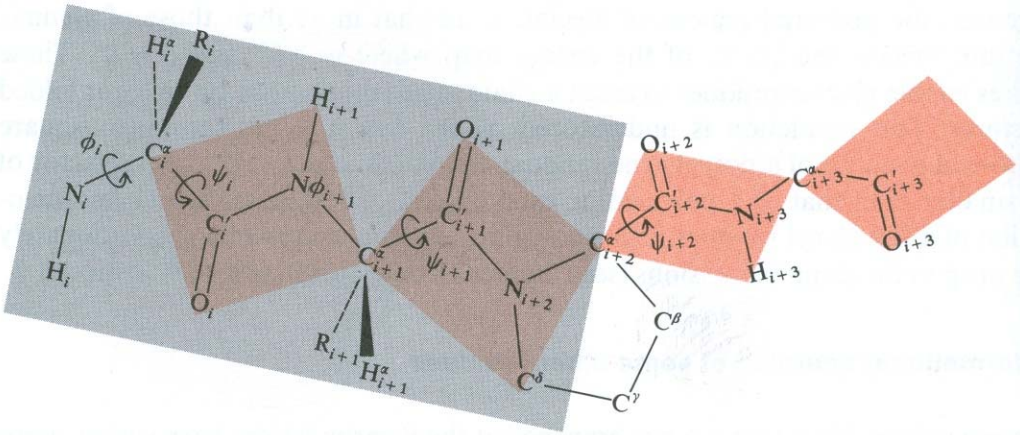

Figure 5-9

Schematic illustration of a polypeptide chain containing an isolated proline residue. [After P. R. Schimmel and P. J. Flory, *J. Mol. Biol.* 34:105 (1968).]

ϕ angle fixed at -60° in proline

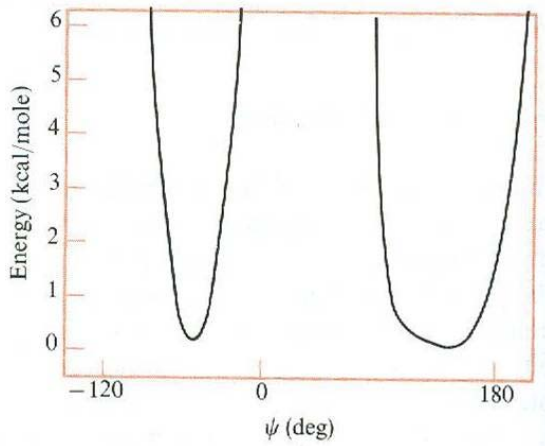

Figure 5-10

Plot of conformational energy versus ψ for an isolated proline within a polypeptide chain. [After P. R. Schimmel and P. J. Flory, *J. Mol. Biol.* 34:105 (1968).]

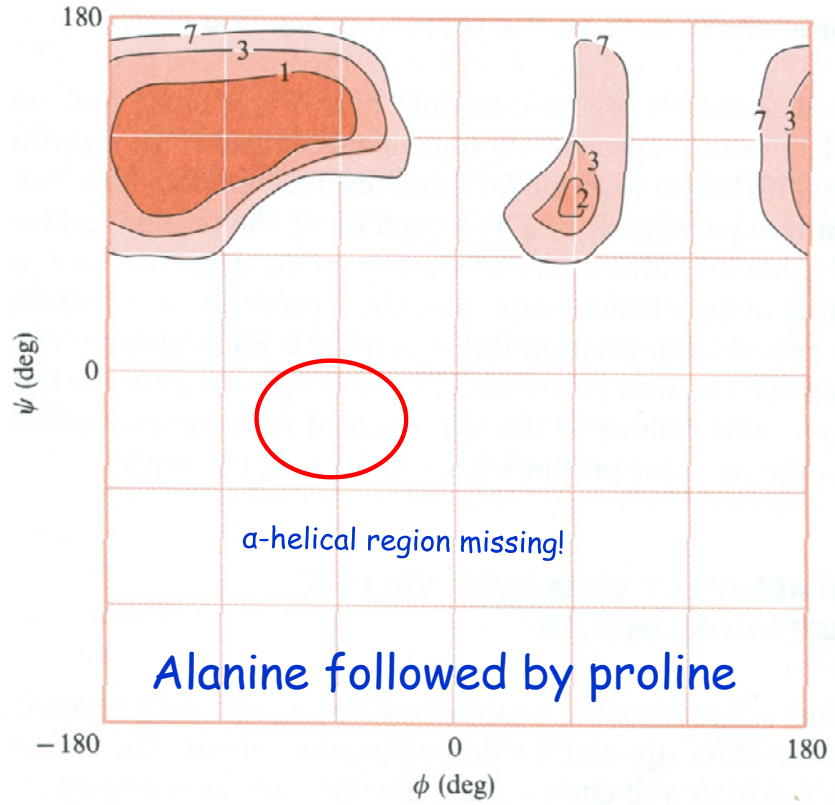

Figure 5-11

Energy contour diagram for an L-alanyl residue that is succeeded by proline. [After P. R. Schimmel and P. J. Flory, *J. Mol. Biol.* 34:105 (1968).]

Proline prevents preceding residue from adopting a-helical conformation

Secondary Structure in Proteins

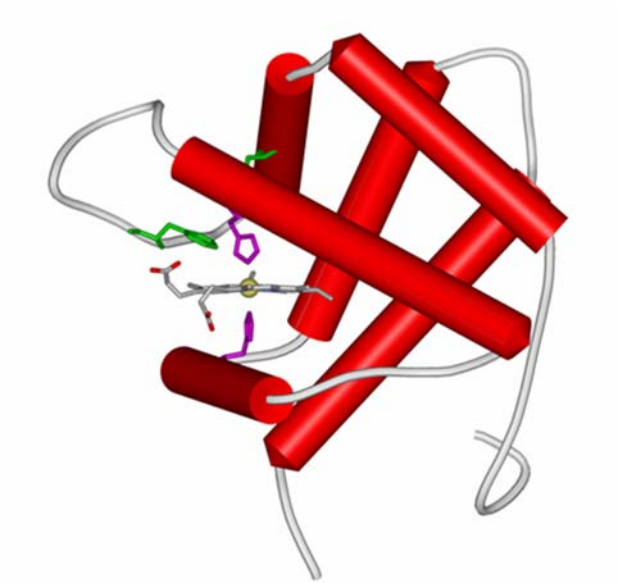

Neuroglobin

only α-helices

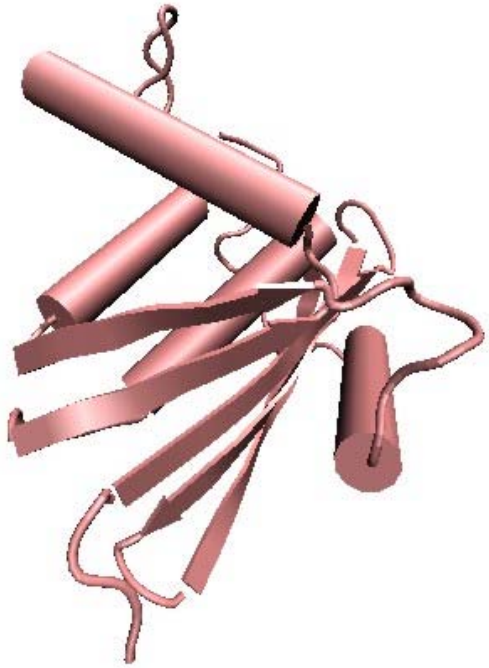

RNase H

α-helices and
β-sheets

Fibronectin domain III_{10}

only β-sheets

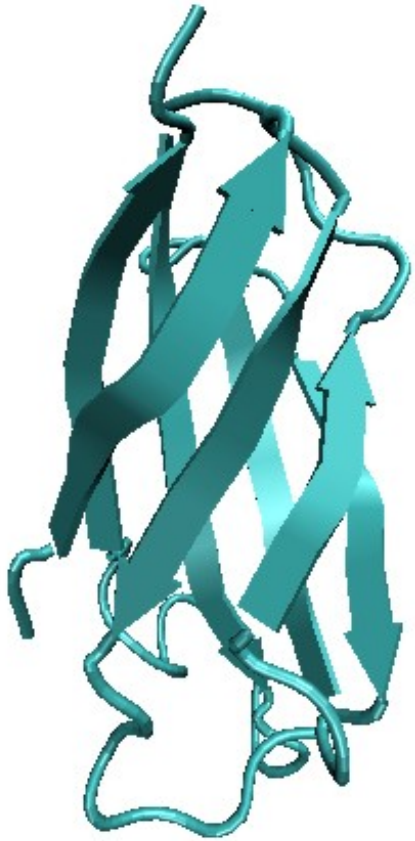

Biophysics II

Protein Tertiary and Quaternary Structure
Part 1c

Prof. G. U. Nienhaus, Vorlesungsunterlagen Biophysik II, SS 2023.
Nur zum KIT-internen, vorlesungsbegleitenden Gebrauch.
Weitergabe und anderweitige Nutzung verboten.

Fibrous Proteins

(a) Collagen

Copyright © Pearson Education, Inc., publishing as Benjamin

intermediate in complexity between secondary and tertiary structure of globular proteins

α-keratin
α-helical (coiled coil)

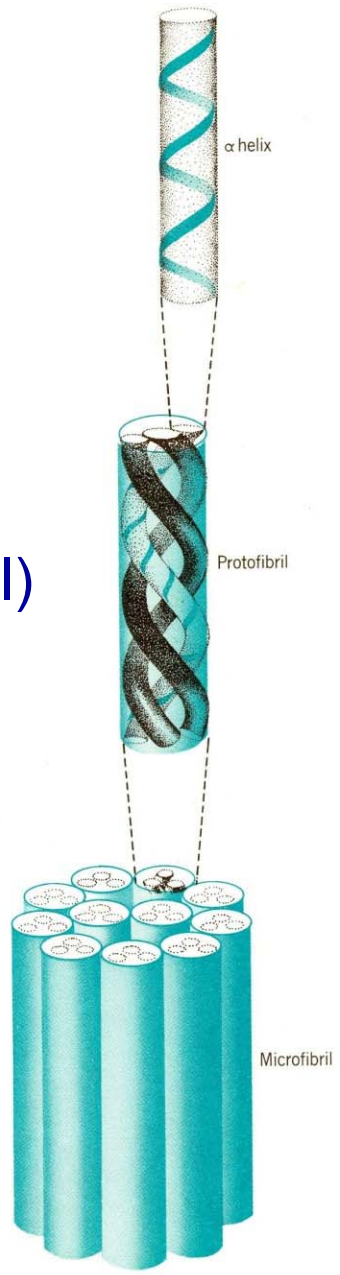

The assembly of hair keratin.

macrofibril
↓
cell
↓
hair fiber

α-keratin: α-helical
silk: β-sheet
collagen: poly-Pro triple helix
sequence: Gly-Pro-X or Gly-X-Hyp

Silk

Predominant sequence $(Gly\text{-}Ser\text{-}Gly\text{-}Ala\text{-}Gly\text{-}Ala)_n$

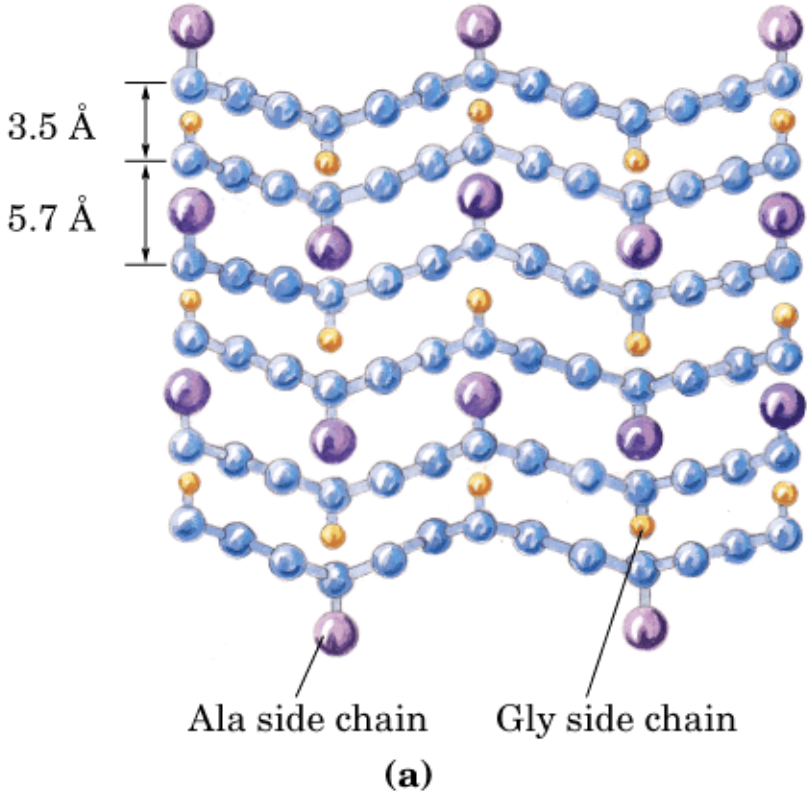

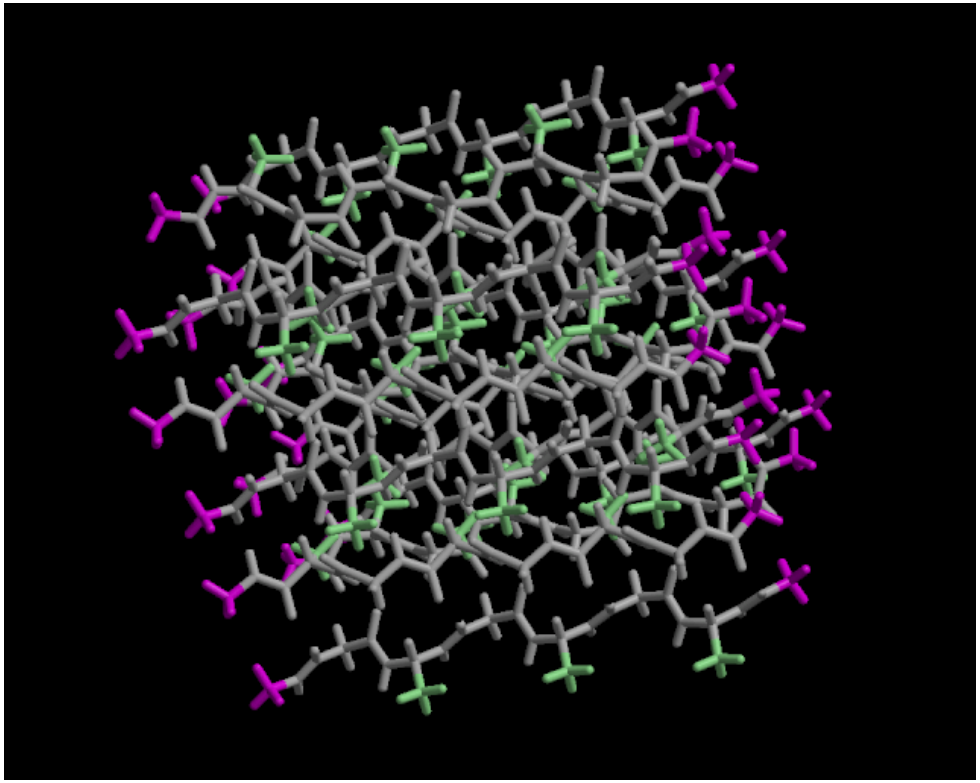

Globular Proteins

Tertiary Structure

Models to represent the structure:

- space-filling models
- no H atoms
- backbone (+ sidechains)
- only α-carbons
- secondary structure “cartoons”

Models of Globular Proteins

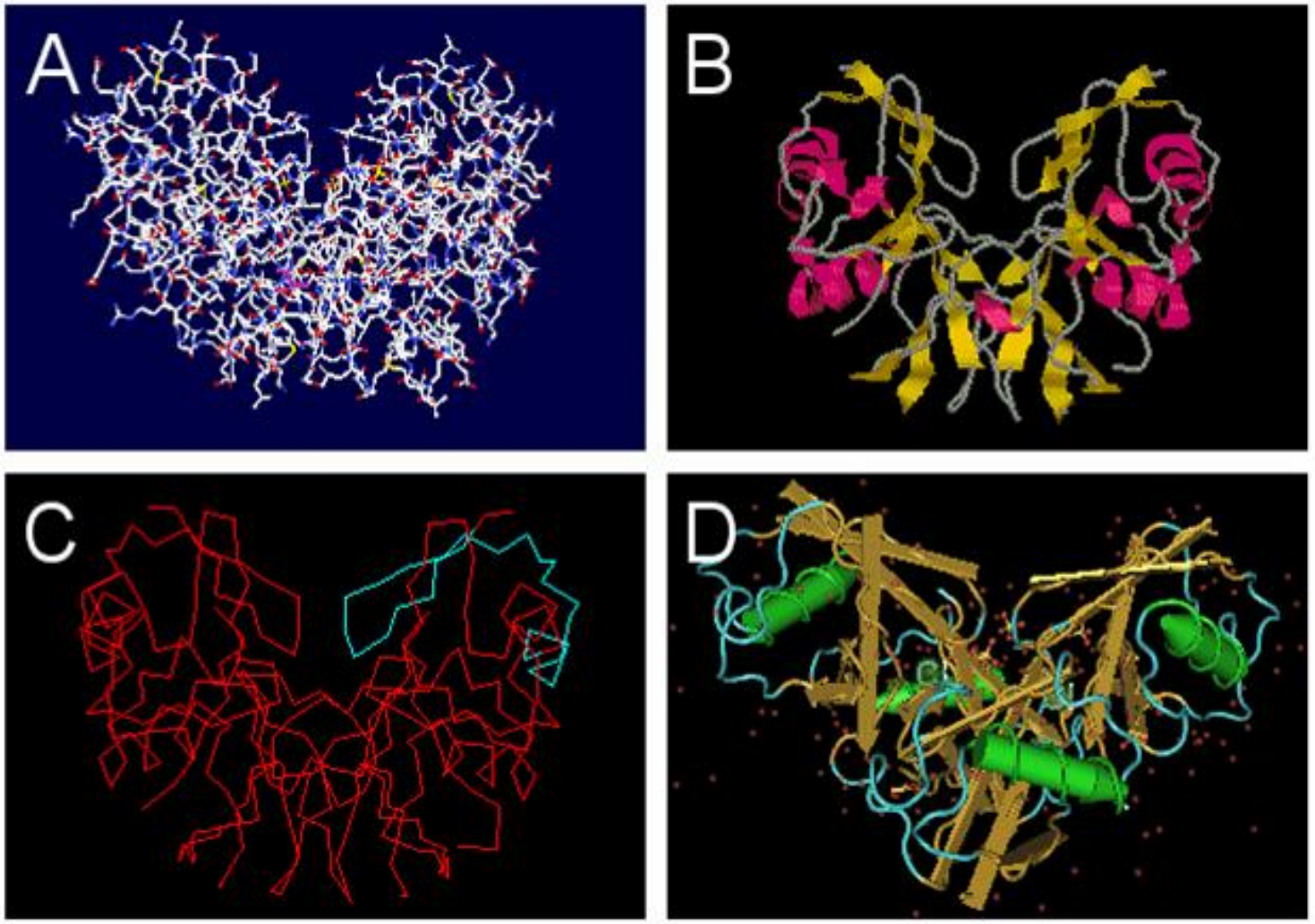

Different protein structural depictions of the ubiquitin-like signalling protein, Nedd8 (PDB ID: 1NND).

(A) illustrates classical ball and stick mode,
(B) cartoon mode,
(C) a wireframe α-carbon trace, with a small section of the structure highlighted in blue, and
(D) a hybrid display with amino acid chains in cartoon mode and non-amino acid atoms in space-filling mode.

Space-filling Models: Hexokinase

Open conformation

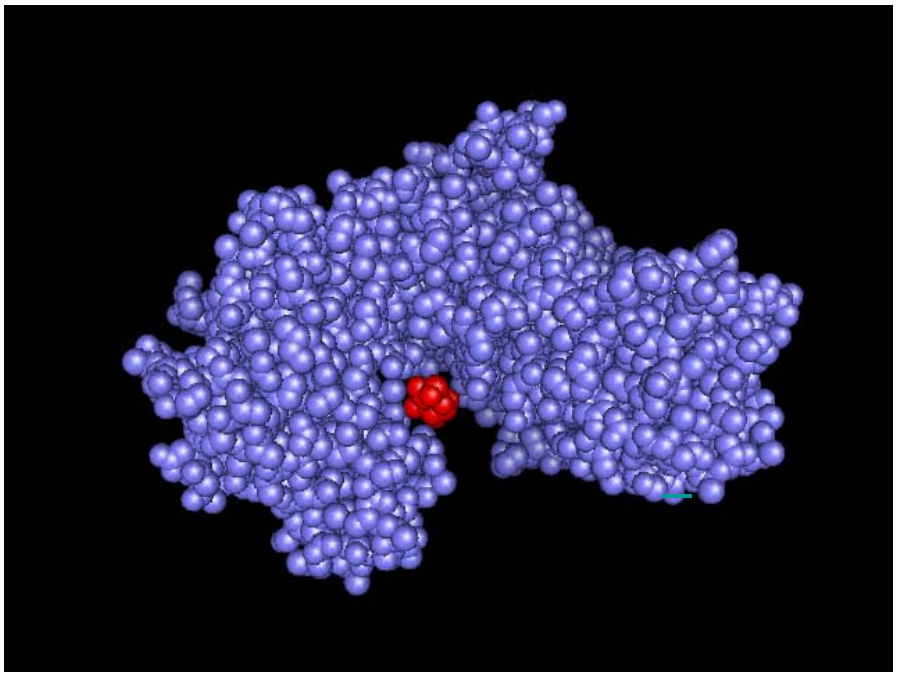

Closed conformation

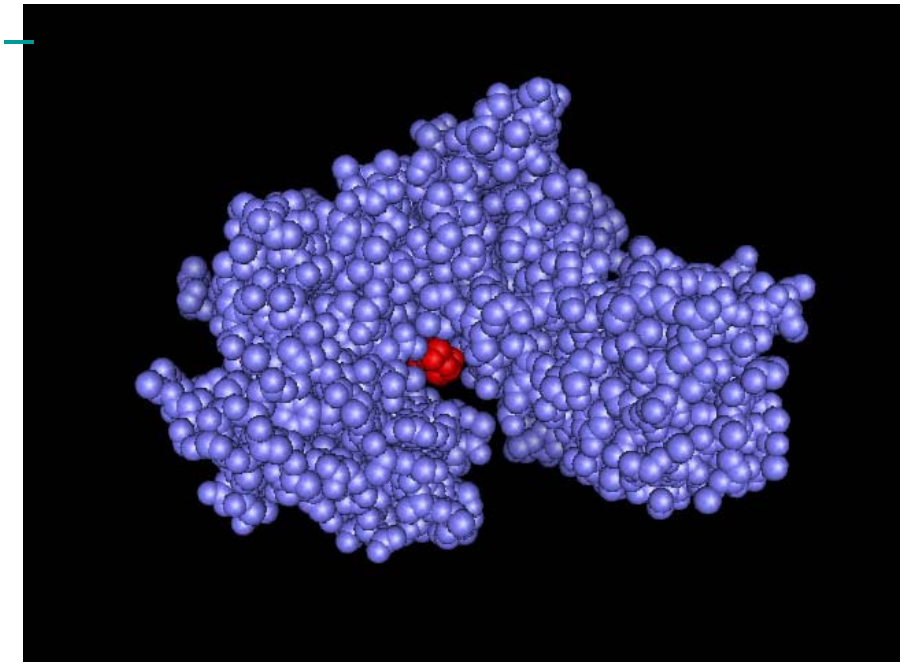

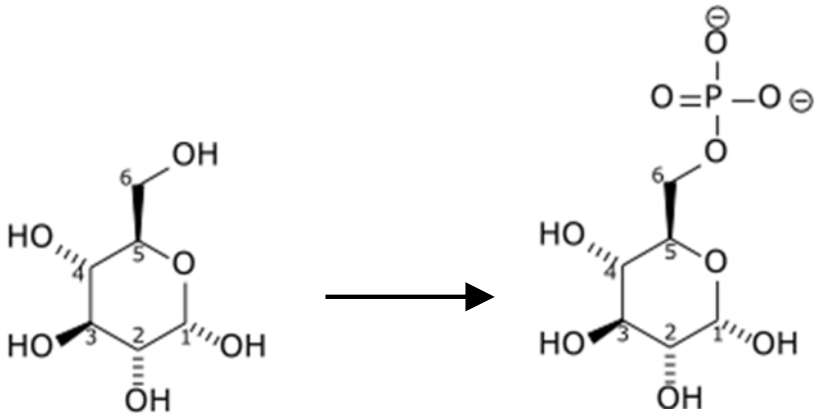

Glucose **Glucose 6-phosphate**

Cartoons of Globular Protein Folds

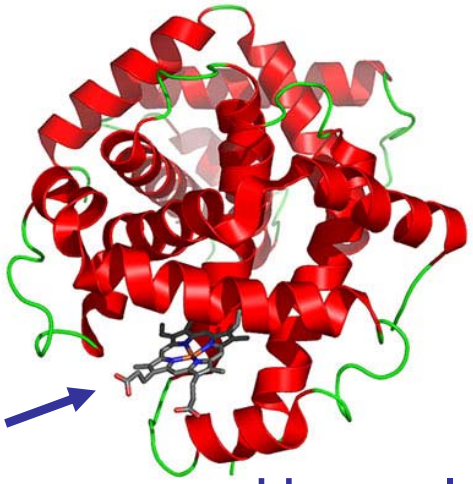

heme prosthetic group

Hemoglobin

Lactate dehydrogenase

NAD cofactor

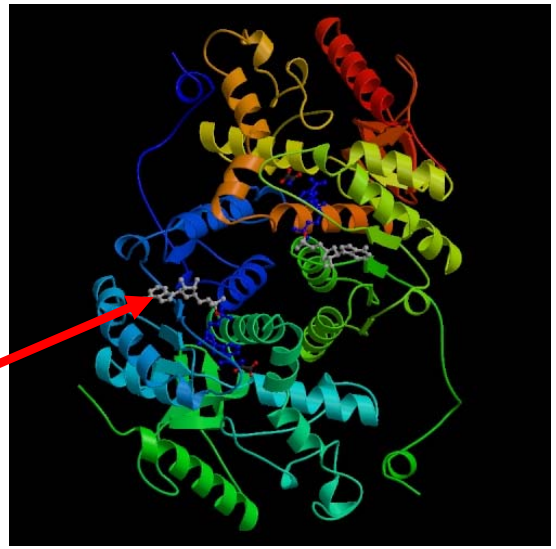

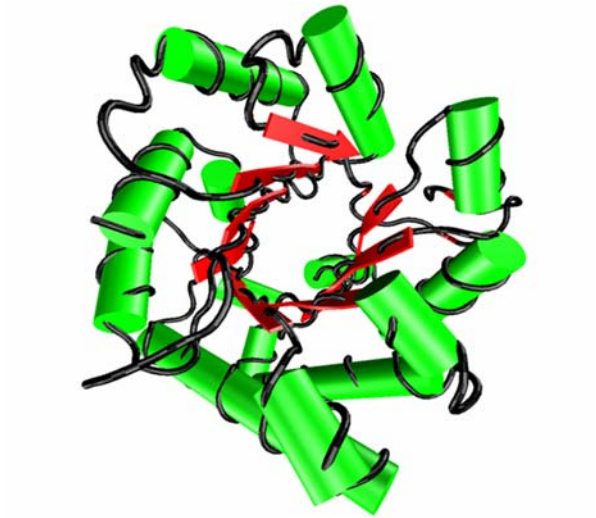

Triose phosphate isomerase

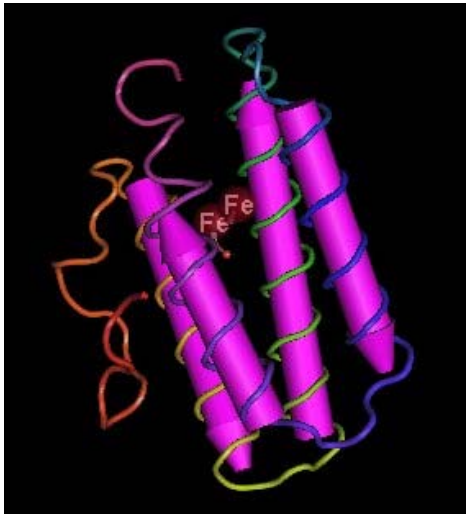

Hemerythrin

Evolution of Structure: Ferredoxin

Ferredoxin

electron transfer protein
e.g., in photosynthesis

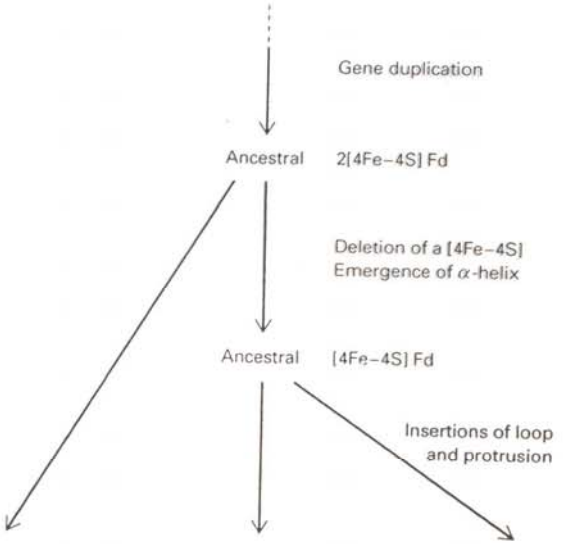

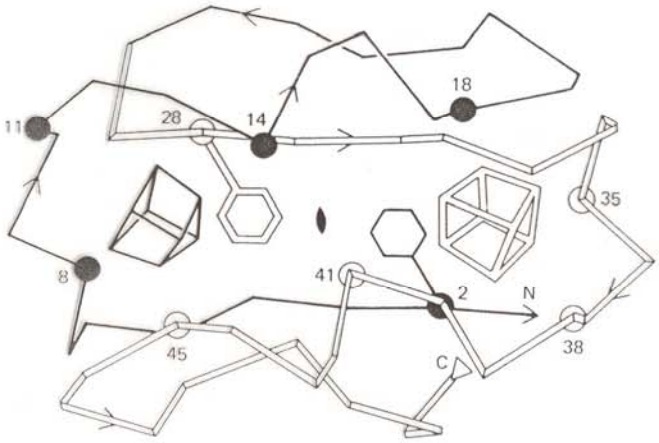

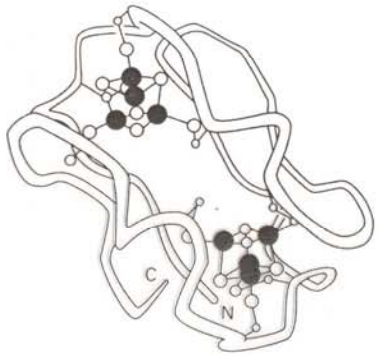

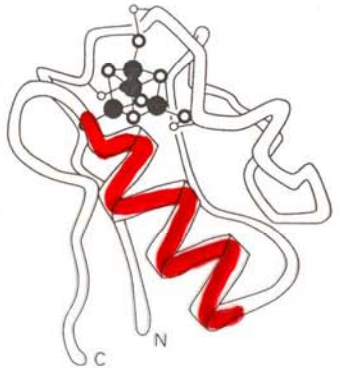

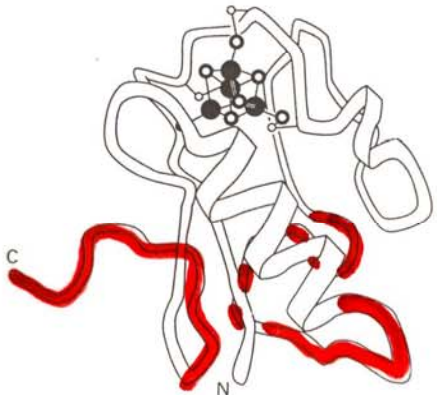

Bonds Stabilizing Tertiary Structure

- Van der Waals interactions
- H bonds between peptide units

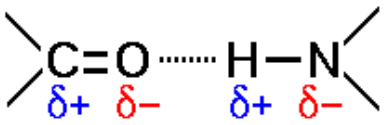

main chain carbonyl and amide

- H bonds between amino acid side chains

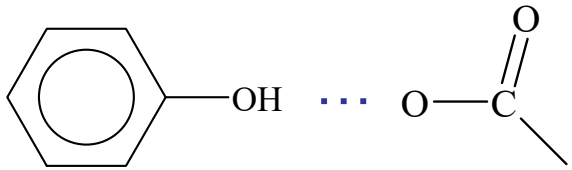

- Charge interactions (ionic bonds, salt bridges)

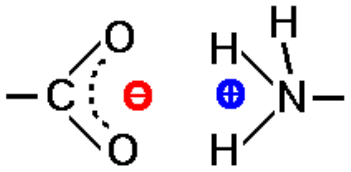

carboxyl group and amino group

- Hydrophobic interactions
- Covalent bonds (rare, mostly disulfide bonds)

Environment of Individual Residues

- dihedral angles (Φ,Ψ) in the “predicted” region (distorted amino acids often have special functions)
- charged residues on surface, usually clustering avoided, particular charge distributions play functional roles
- non-polar residues everywhere, mostly towards the inside, exception: membrane proteins
- hydrogen bonds satisfied

General Properties of Folded Chains

- no general rule for content of α-helix or β-sheet
  - proteins with only α-helices
  - proteins with only β-sheets
  - all combinations

- characteristics of a typical α-helix
  - 10 – 12 residues
  - length ~15 Å

- characteristics of a typical β-sheet
  - four or more strands
  - 20 – 40 residues
  - barrel/sandwich structures

- super-secondary structure

- domain structure

- quaternary structure

Super-Secondary Structure

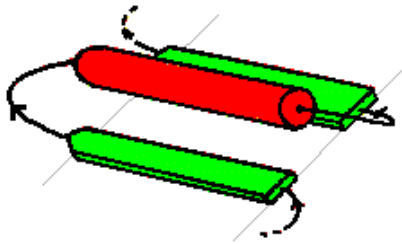

The right–handed beta–alpha–beta unit. The helix lies above the plane of the strands.

The Rossman fold

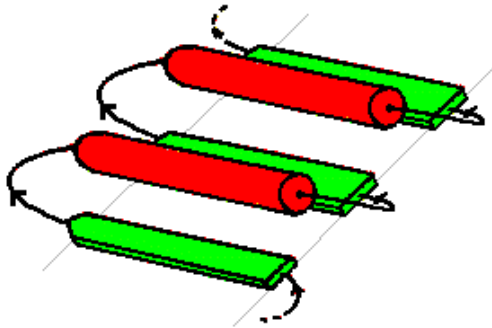

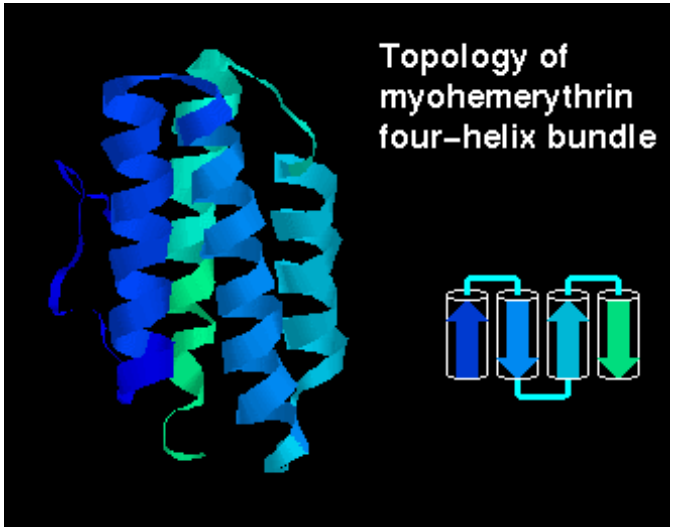

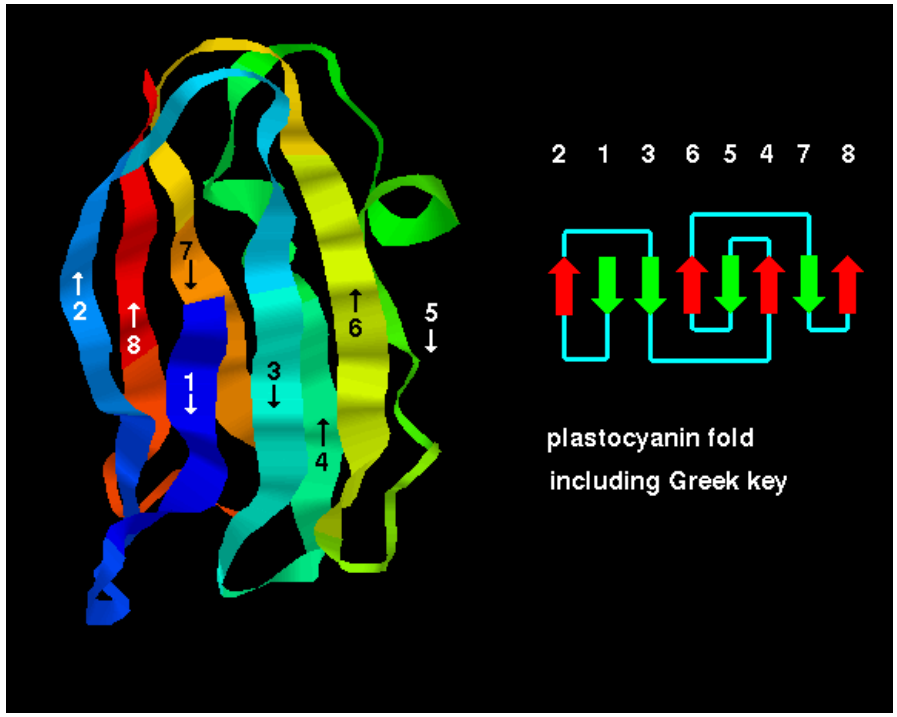

Domain Structure: Immunoglobulin G

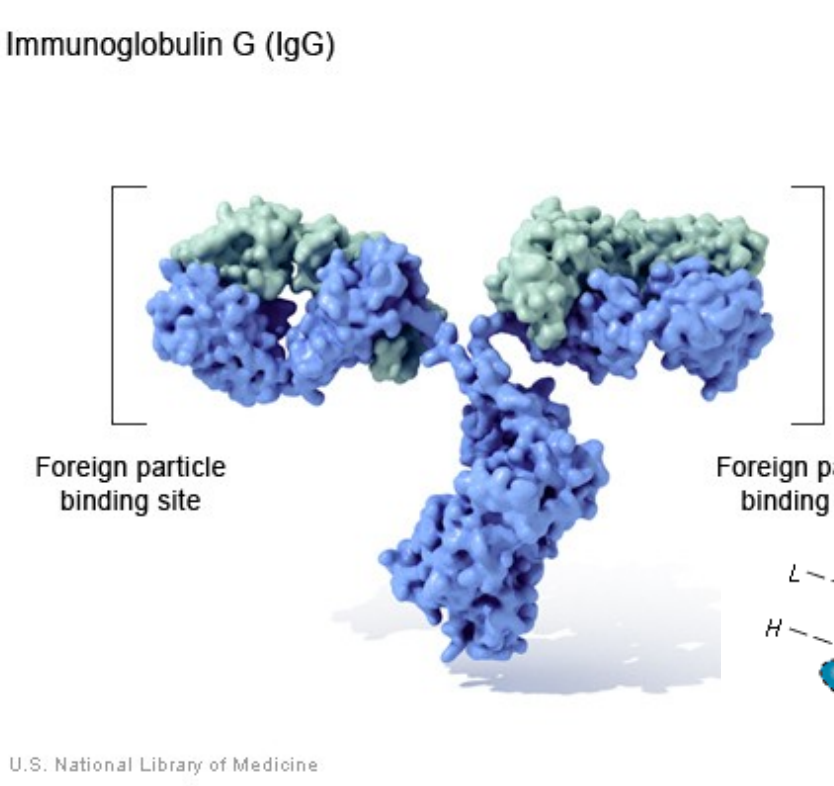

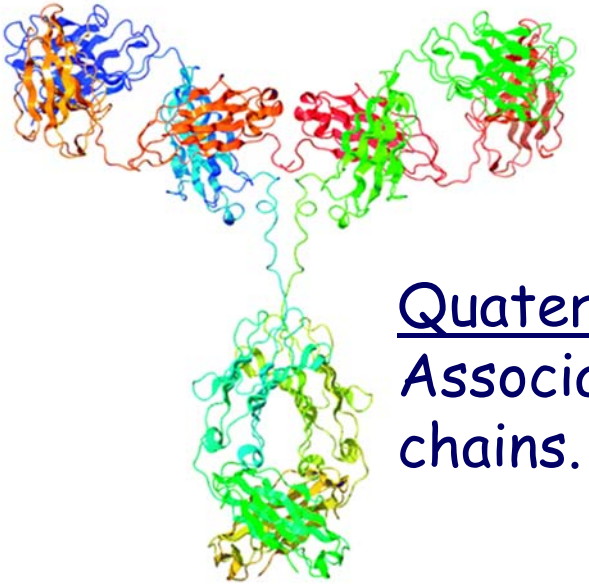

Quaternary structure: Association of folded chains.

Domain: thermodynamically stable part of a poly-peptide chain

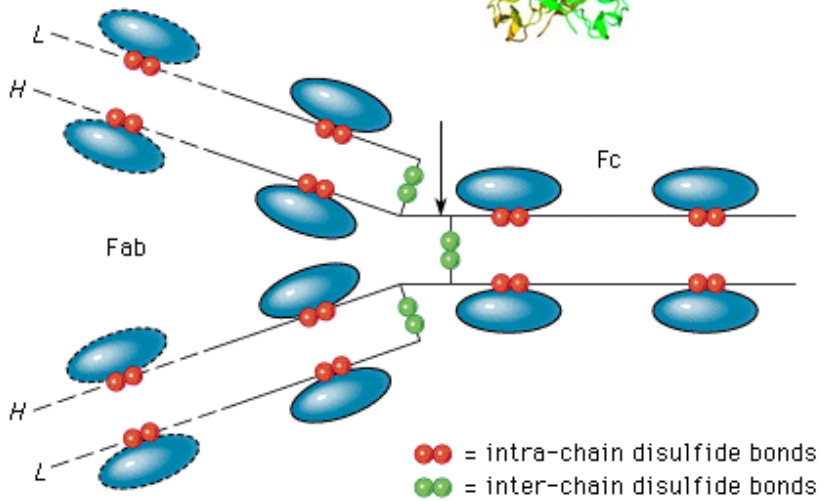

Two heavy chains (*H*) and two light chains (*L*) are linked to each other by inter-chain disulfide bonds. Intra-chain disulfide bonds cause loops to form in the 12 peptide portions, each of which contains about 110 amino acid residues. The 12 peptide regions have cystine residues at similar positions and other similarities in their amino acid sequences. The broken lines represent variable portions and the solid lines represent constant portions of the chains. Specific sites that bind antigens are formed by the variable portions. The vertical arrow indicates cleavage of the IgG molecule into two Fab fragments and one Fc fragment by the action of the enzyme papain.

©1997 Encyclopaedia Britannica, Inc.

Membrane Proteins: Bacterial Reaction Center

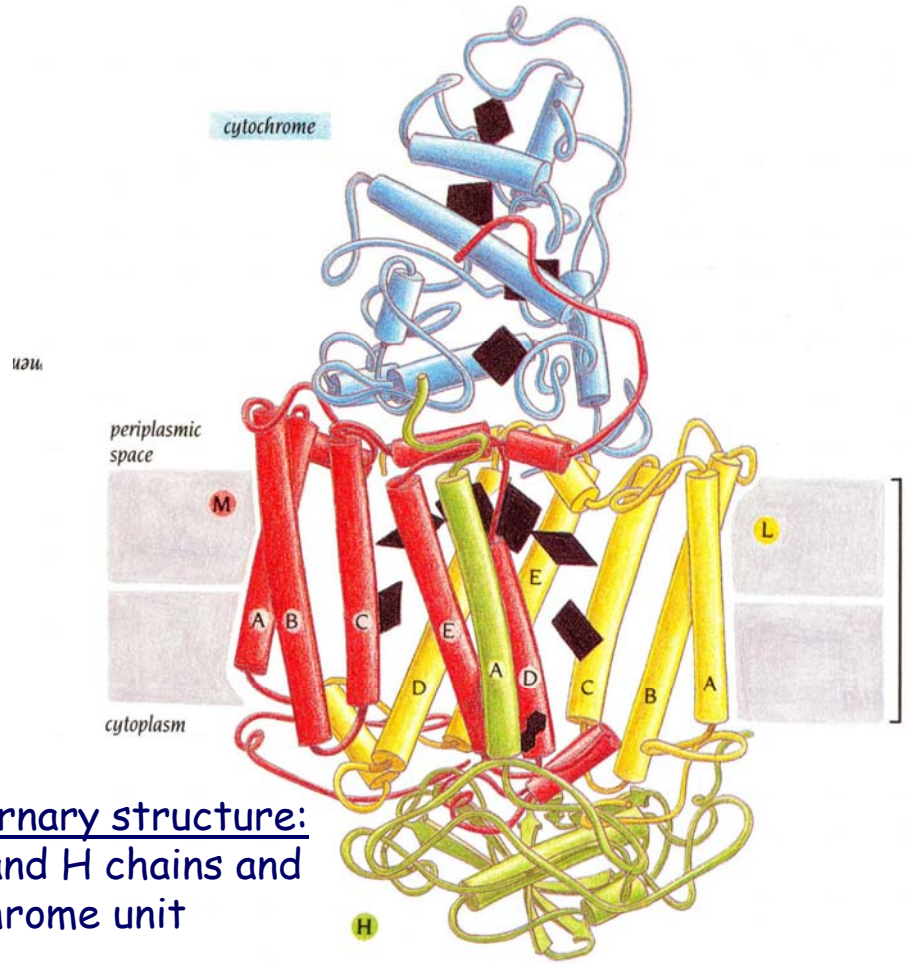

Quaternary structure:
L, M, and H chains and cytochrome unit

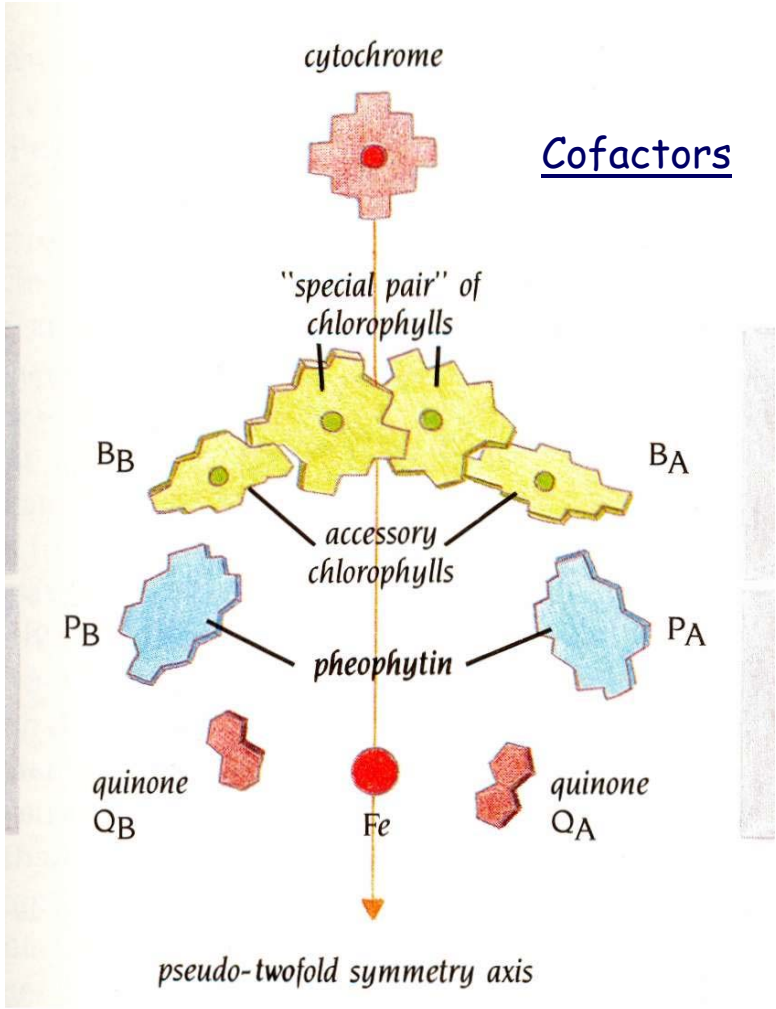

charge separation device ("solar cell") in photosynthesis

Membrane Proteins

Bacteriorhodopsin

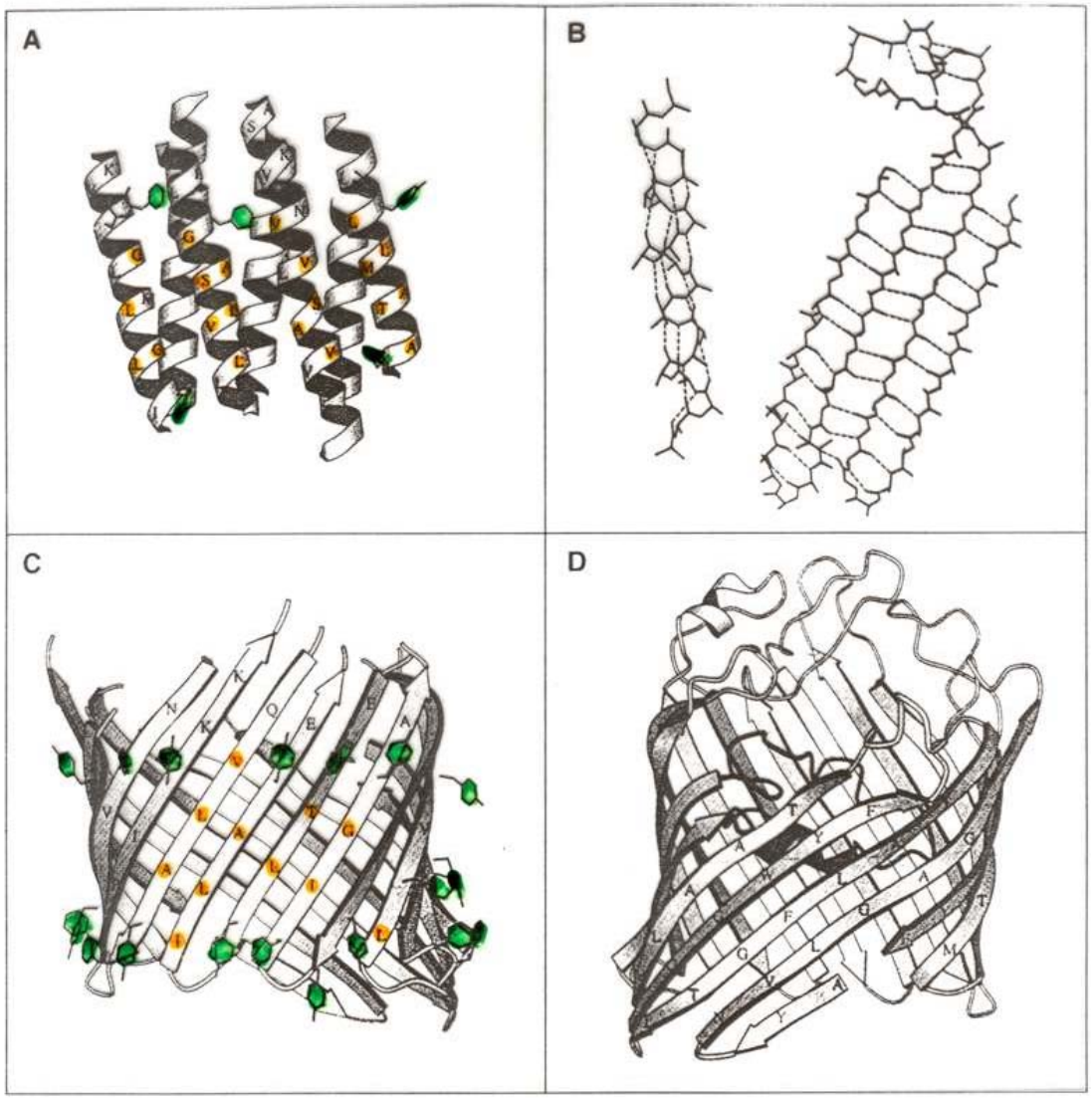

A: bR α-helices
B: β strands

Porin monomer

Porin monomer

Protein Structures

Some proteins with very different sequences (and function) have similar tertiary structure

- IgG domains, Cu-Zn superoxide dismutase, azurin
- NAD-dependent dehydrogenases

…

Are only a few patterns stable?
How many are there ?

- As of Sunday, April 23, 2023
  there are **203,863** structures in the PDB
- Classification emerges
  (~500 different domain structures known)

Tertiary structure is dynamic

- molecular dynamics calculations
- solution vs. crystal structures

Quaternary Structure

Typically non-covalent assemblies of subunits

- definite stoichiometry
  - Homodimers α-α
  - Heterodimers αβ, $\alpha_2\beta_2$
  - large numbers of 12 – 48 – 60 subunits
- indefinite polymers

Subunit assemblies

- each subunit is asymmetric
- only point rotation, no mirror or inversion symmetry (→ chirality)

Symmetries

1. Cyclic, C_n symmetry
2. Dihedral, D_n symmetry (at least one C_2 axis perpendicular to C_n axis)
3. Cubic symmetry (at least four C_3 axes),
   tetrahedron, octahedron / cube, icosahedron

Quaternary Structure

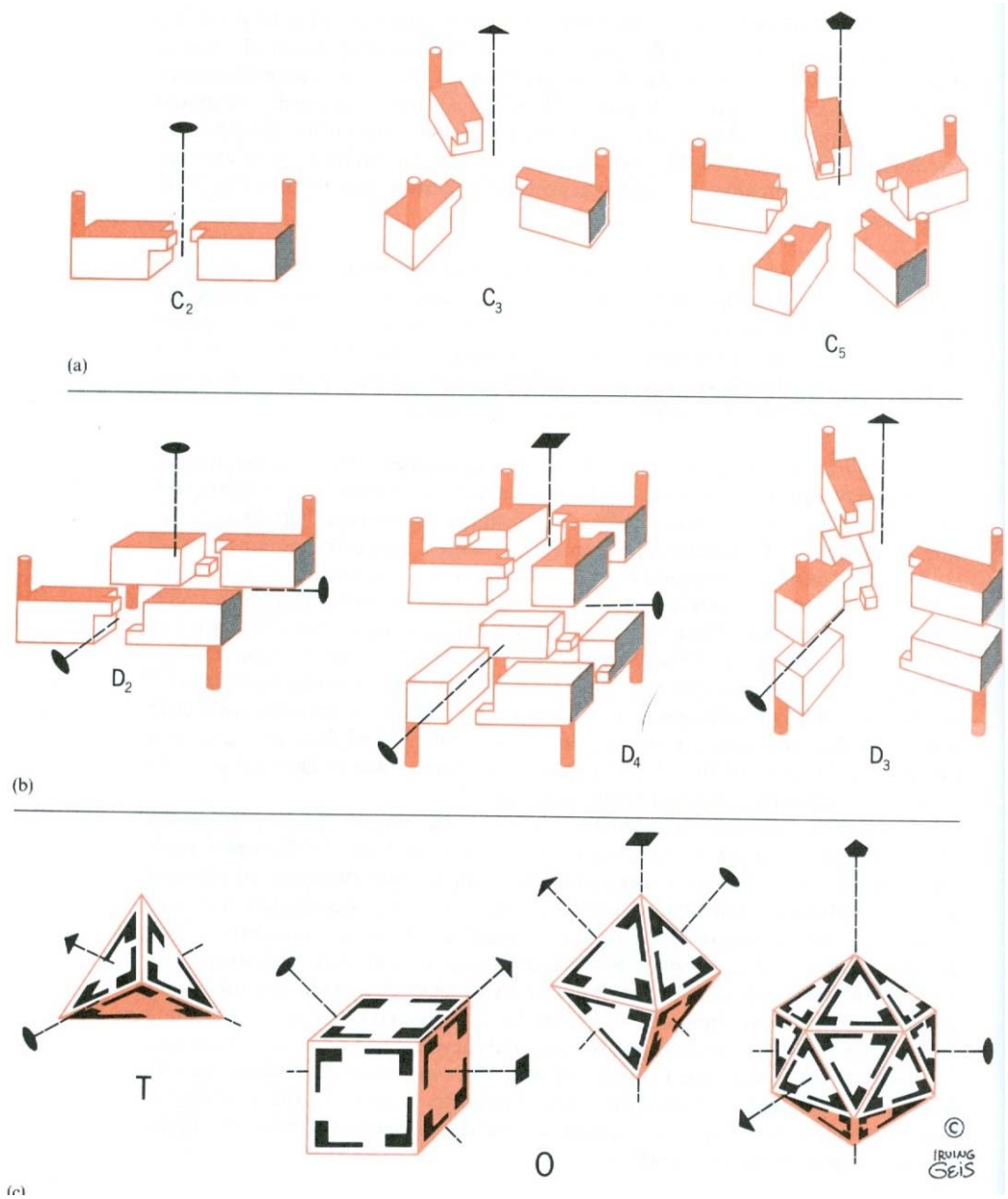

Quaternary Structure

From **Protein Structure and Function** by Gregory A Petsko and Dagmar Ringe

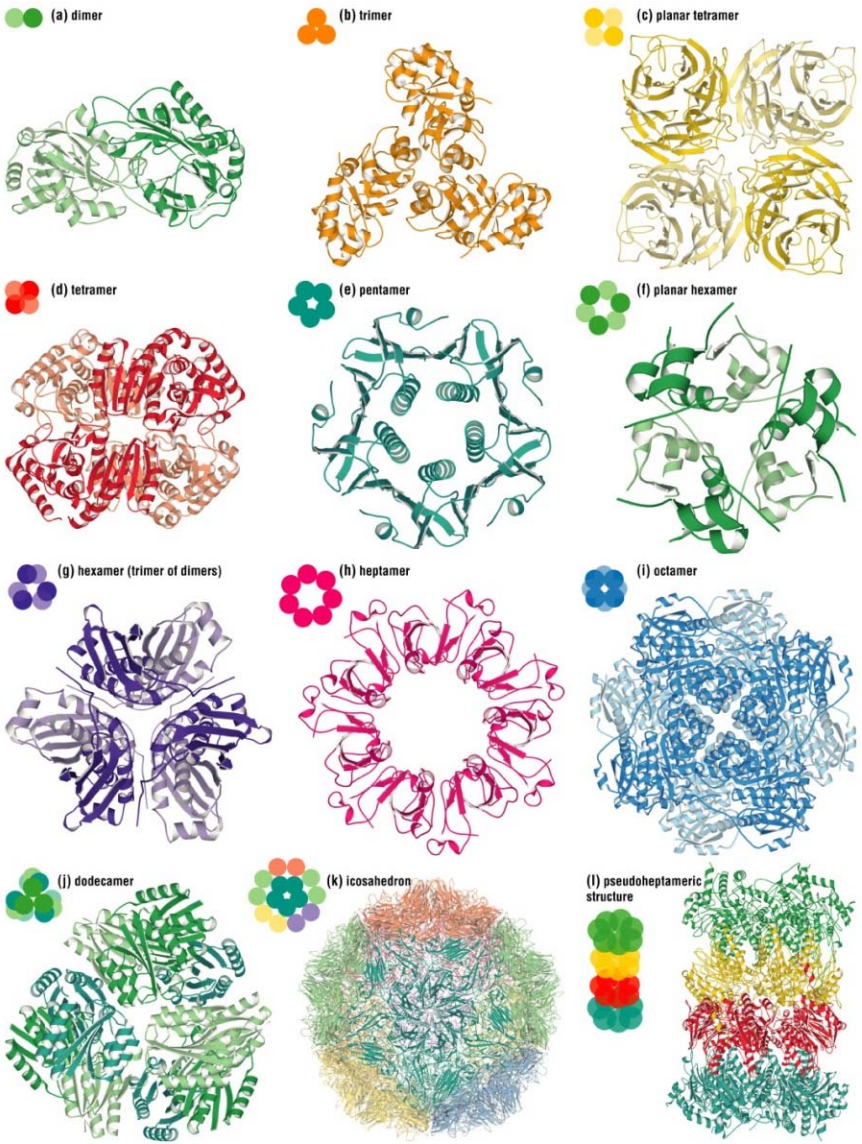

© 1999–2004 New Science Press

Viruses

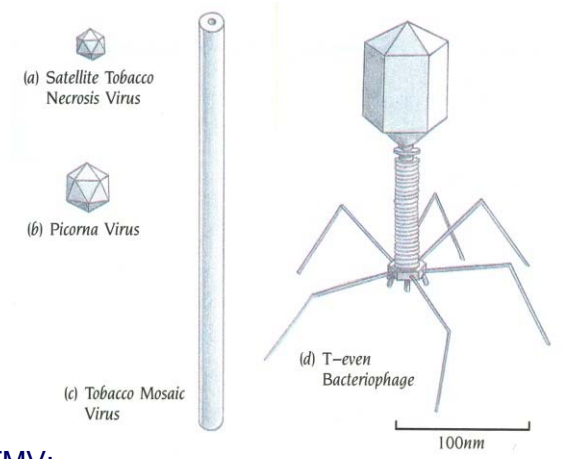

Figure 11.1 Viruses vary in size and shape from the simplest satellite viruses (a) that need another virus for their replication to the T-even bacteriophages (d) that have developed sophisticated mechanisms for injecting DNA into bacteria. Four different virus particles are shown in correct relative scale.

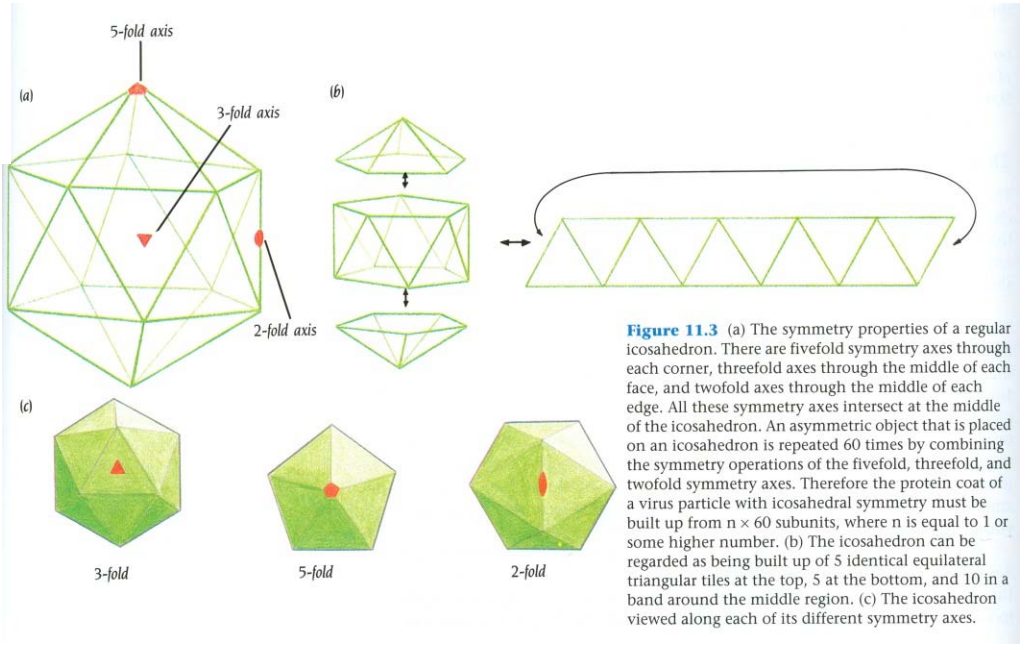

Figure 11.3 (a) The symmetry properties of a regular icosahedron. There are fivefold symmetry axes through each corner, threefold axes through the middle of each face, and twofold axes through the middle of each edge. All these symmetry axes intersect at the middle of the icosahedron. An asymmetric object that is placed on an icosahedron is repeated 60 times by combining the symmetry operations of the fivefold, threefold, and twofold symmetry axes. Therefore the protein coat of a virus particle with icosahedral symmetry must be built up from n × 60 subunits, where n is equal to 1 or some higher number. (b) The icosahedron can be regarded as being built up of 5 identical equilateral triangular tiles at the top, 5 at the bottom, and 10 in a band around the middle region. (c) The icosahedron viewed along each of its different symmetry axes.

TMV:
18 nm x 300 nm
6400 RNA nucleotides
2130 copies of a single capsid protein

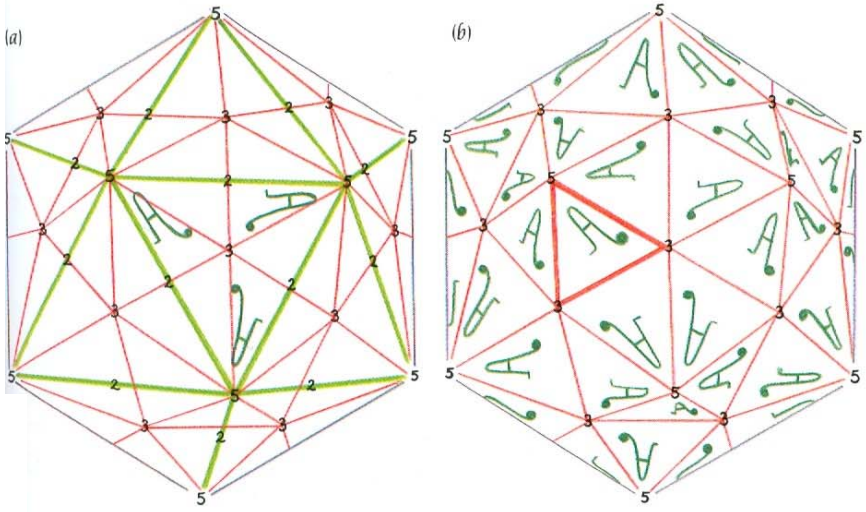

Figure 11.5 Schematic illustration of the way the 60 protein subunits are arranged around the shell of satellite tobacco necrosis virus. Each subunit is shown as an asymmetric A. The view is along one of the threefold axes, as in Figure 11.3a. (a) Three subunits are positioned on one triangular tile of an icosahedron, in a similar way to that shown in 11.4a. The red lines represent a different way to divide the surface of the icosahedron into 60 asymmetric units. This representation will be used in the following diagrams because it is easier to see the symmetry relations when there are more than 60 subunits in the shells. (b) All subunits are shown on the surface of the virus, seen in the same orientation as 11.4a. The shell has been subdivided into 60 asymmetric units by the red lines. When the corners are joined to the center of the virus, the particle is divided into 60 triangular wedges, each comprising an asymmetric unit of the virus. In satellite tobacco necrosis virus each such unit contains one polypeptide chain.

Biophysics II

Nucleic Acids / Protein Biosynthesis
Part 1d

Uli Nienhaus

Prof. G. U. Nienhaus, Vorlesungsunterlagen Biophysik II, SS 2023.
Nur zum KIT-internen, vorlesungsbegleitenden Gebrauch.
Weitergabe und anderweitige Nutzung verboten.

Nucleic Acids and Proteins in Life's Key Processes

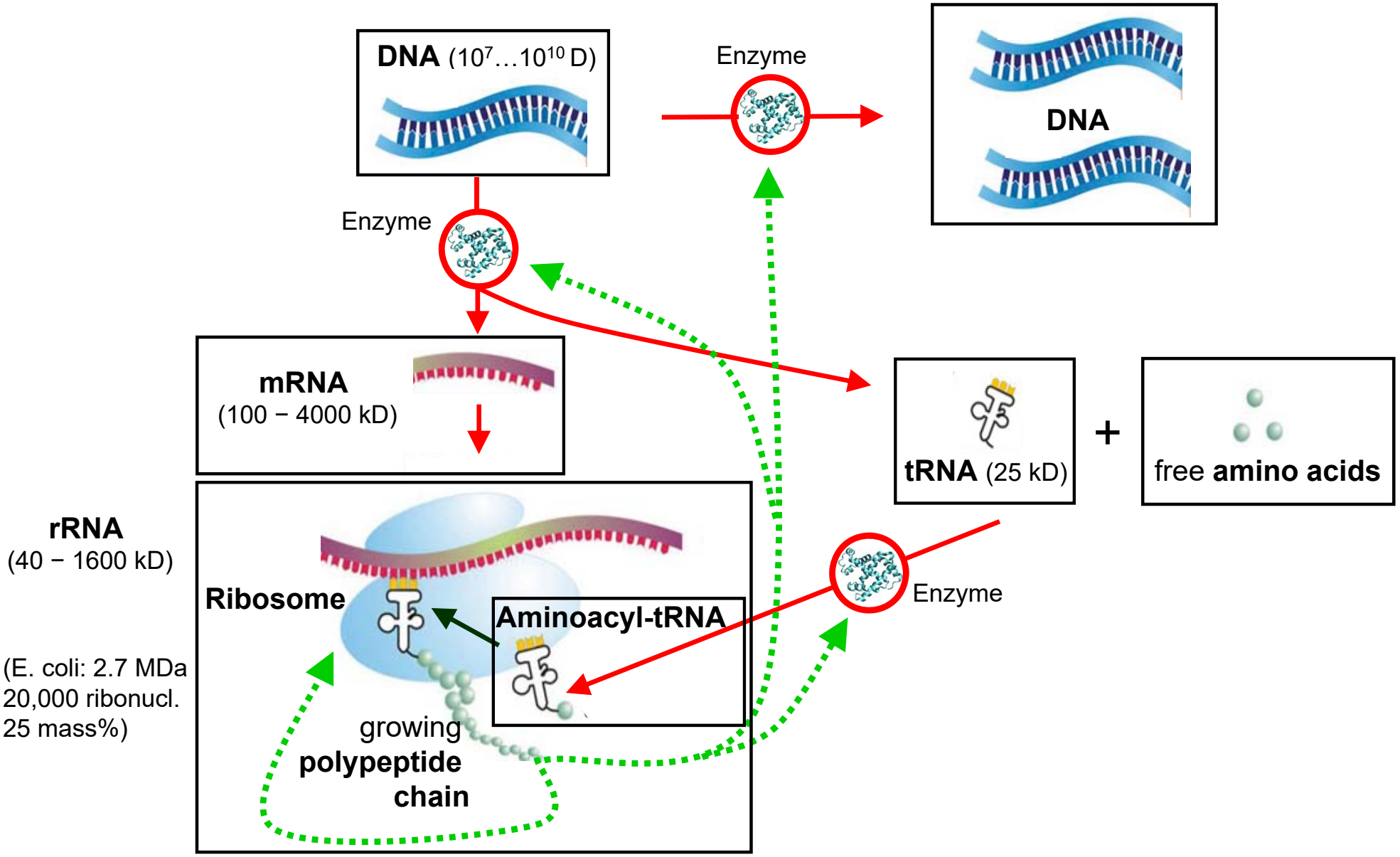

Nucleic Acids: Primary Structure

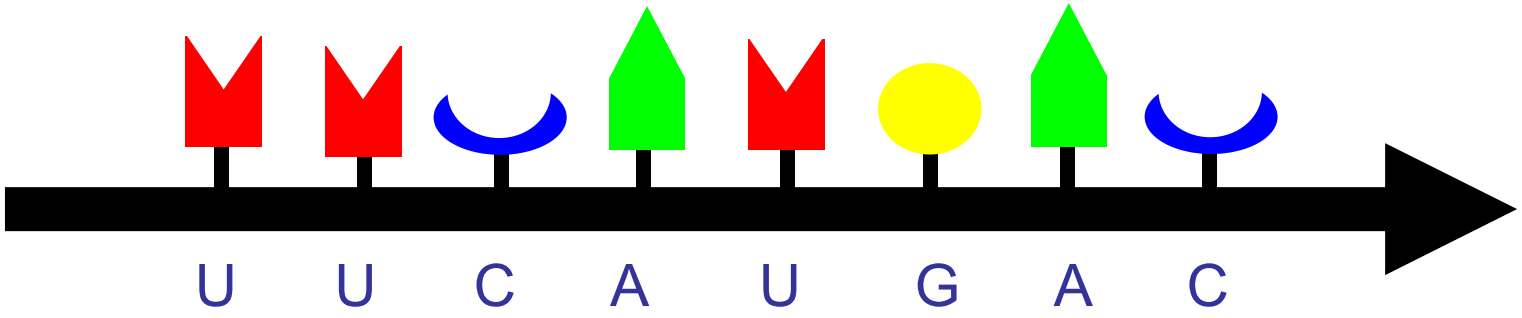

Mononucleotide

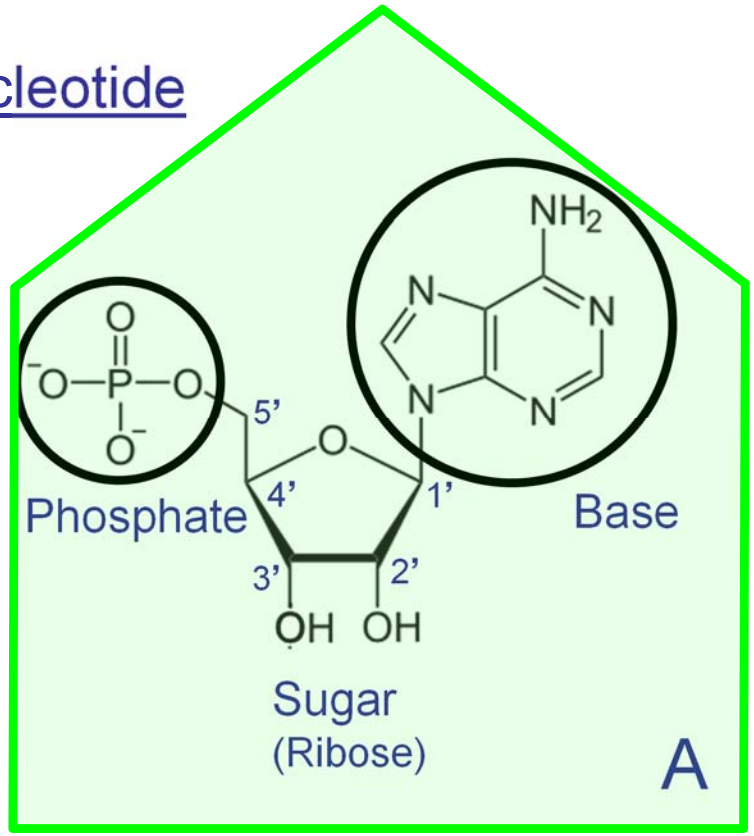

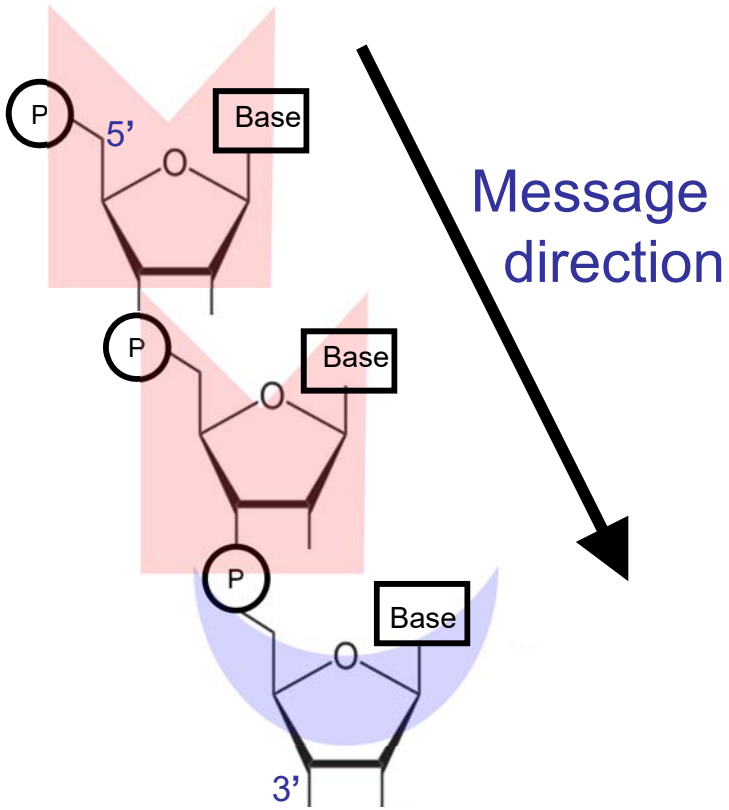

Nucleic Acids: Primary Structure

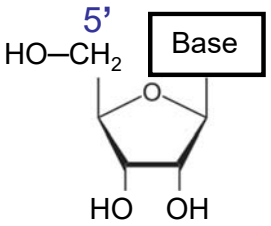

nucleoside
N

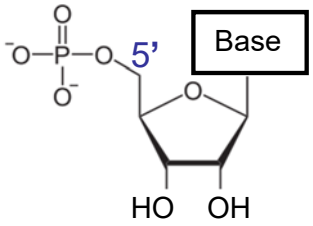

5'-nucleotide
pN

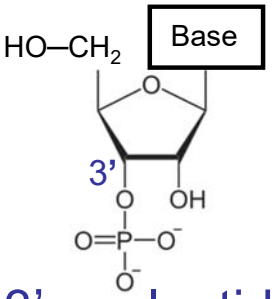

3'-nucleotide
Np

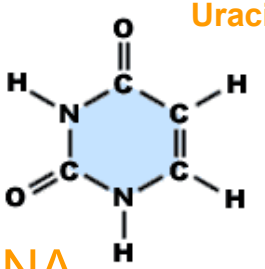

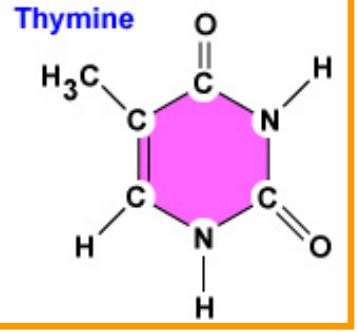

Nitrogenous Bases of DNA

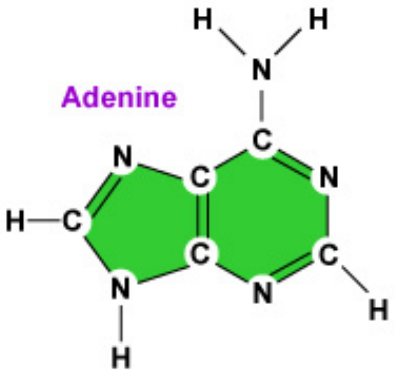

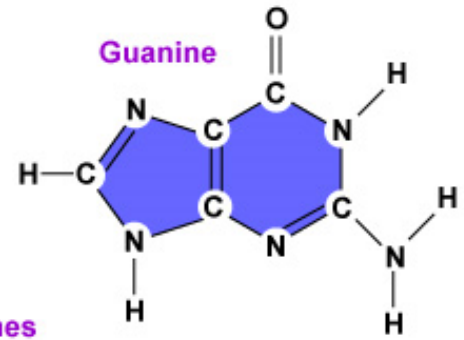

Sugars

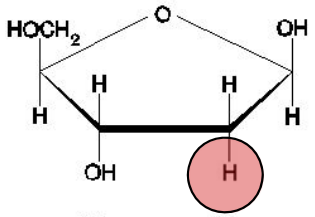

D - Deoxyribose

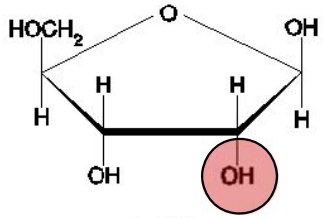

D - Ribose

Nucleic Acids: Nomenclature

Bases:

adenine, guanine, cytosine, thymine (uracil)

(Deoxy)ribonucleosides (base + sugar):

adenosine, guanosine, cytidine, thymidine (uridine)

Nucleoside-5'/3'-phosphate: nucleotide

(Deoxy)nucleotide units in RNA (DNA):

adenylate, guanylate, cytidylate, thymidylate (uridylate)

Watson-Crick Base Pairing

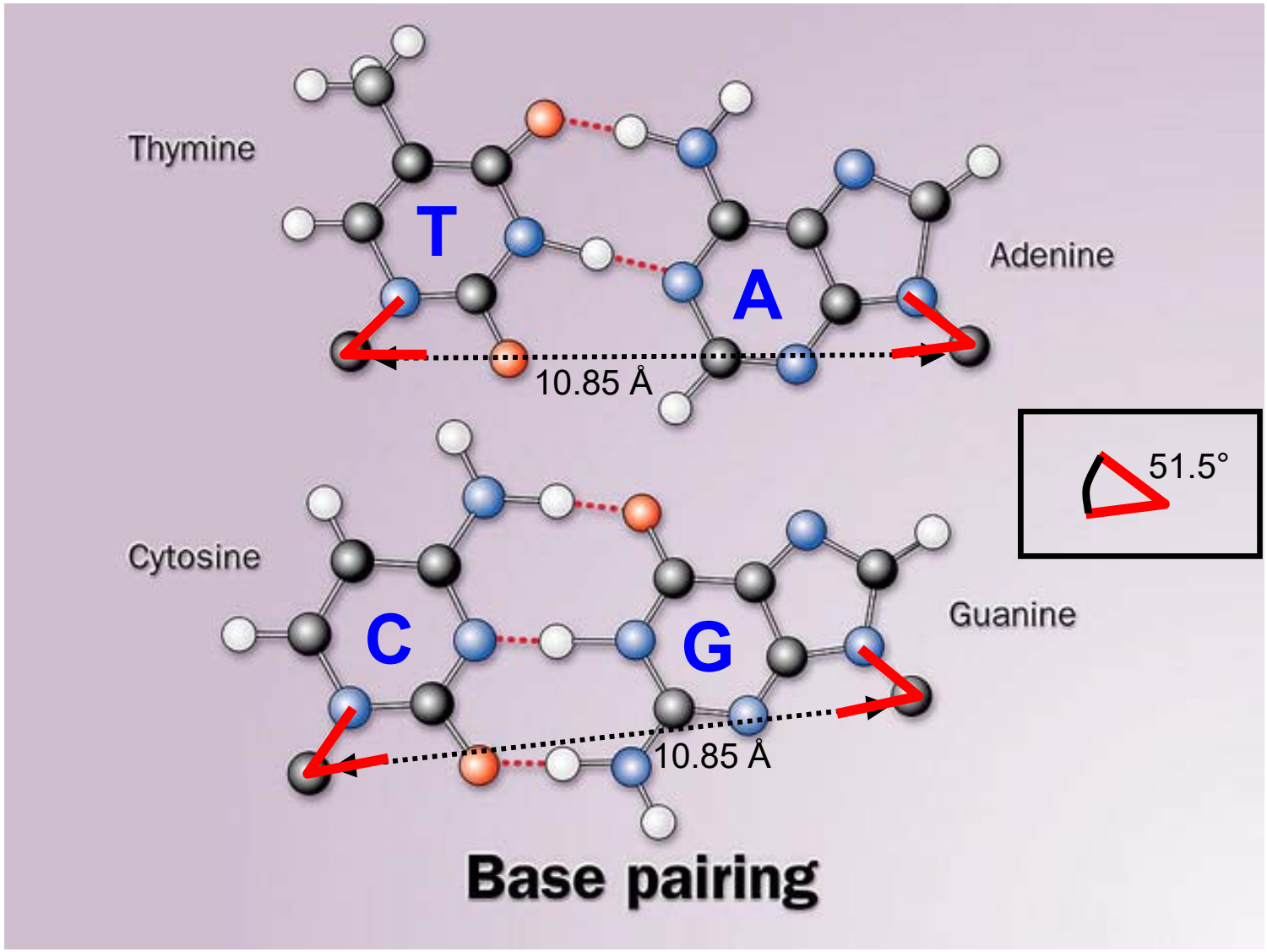

Secondary Structure of DNA

22 Å

Double Helix

1 turn = 10 base pairs = 34 Å

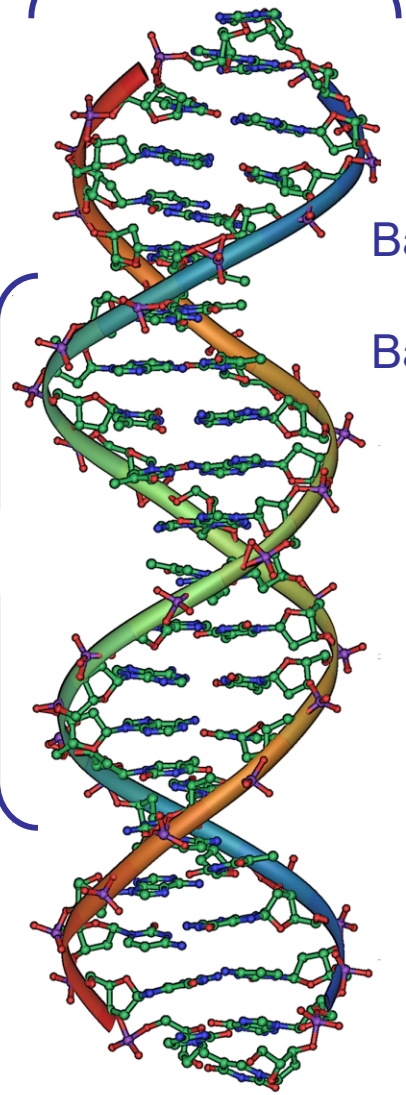

Base pairing
- hydrogen bond formation

Base stacking
- hydrophobic interactions
- induced dipolar coupling

Watson/Crick, 1953

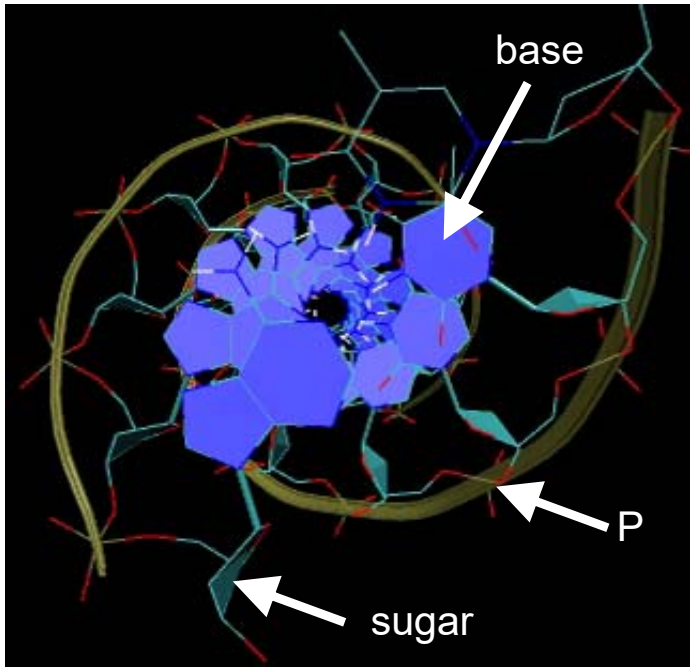

View along one strand of a DNA double helix
(bases inside, sugar/phosphate backbone outside)

DNA Conformations

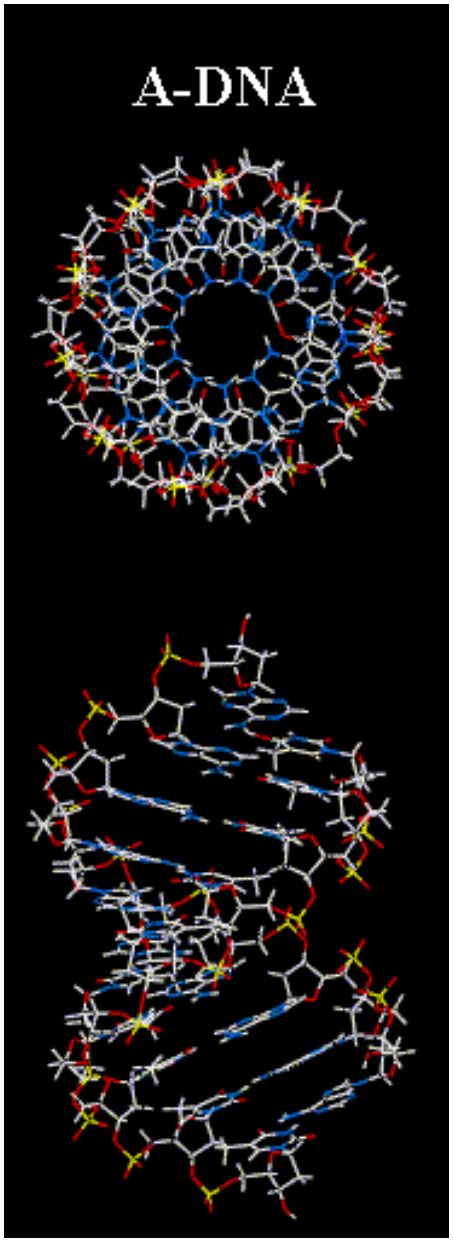

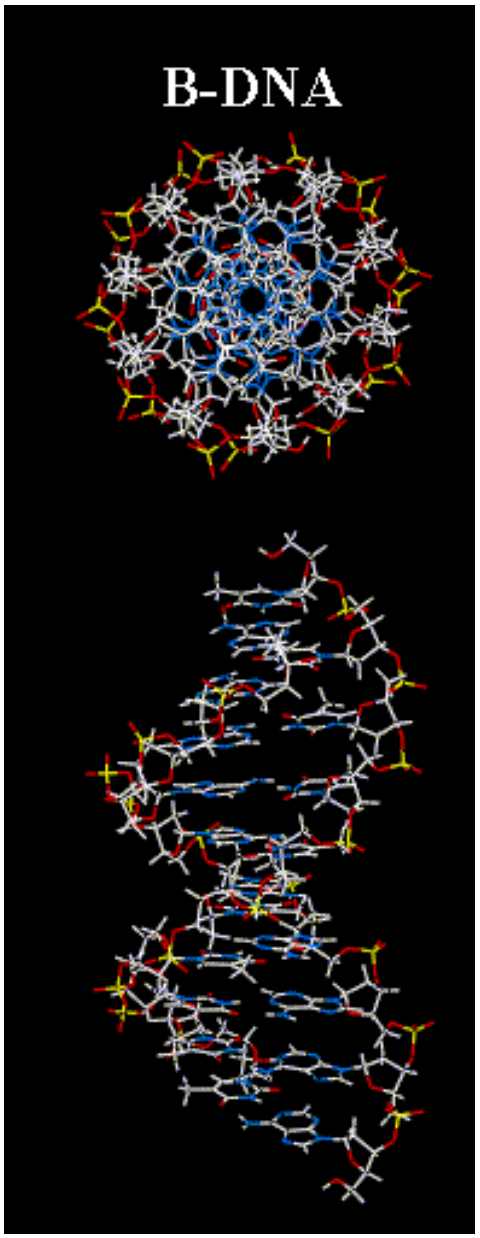

DNA Conformations

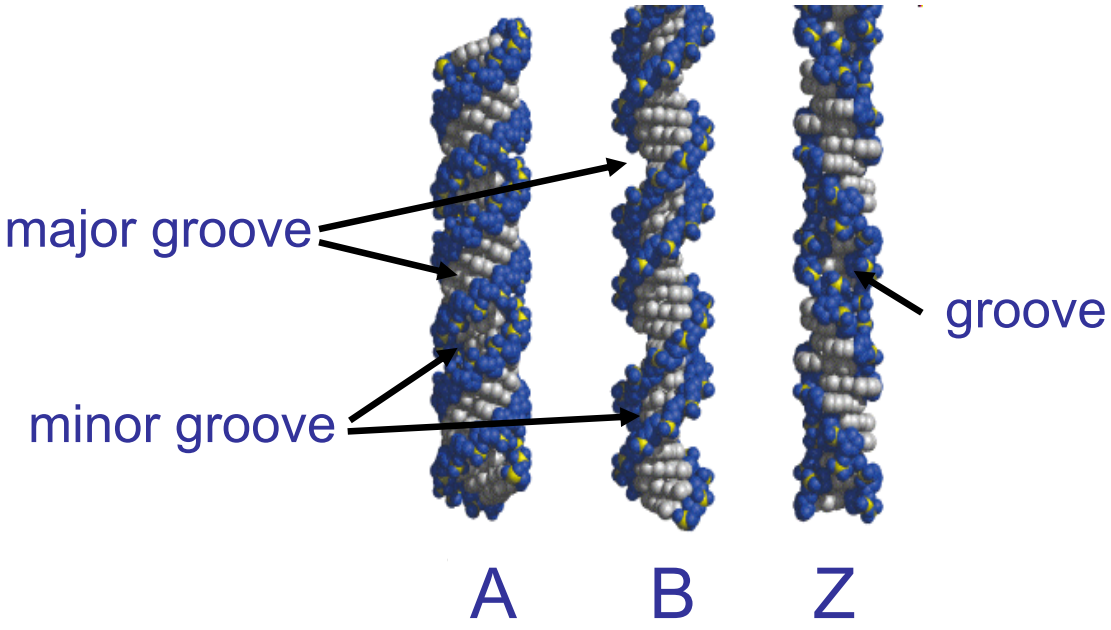

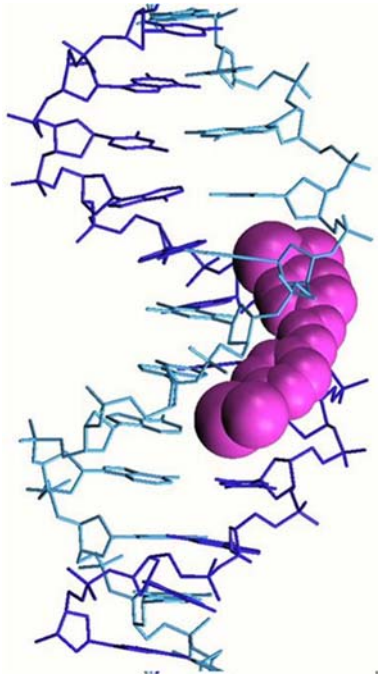

Structure of a DNA oligonucleotide with a drug (shown in pink) bound in the minor groove.

Transfer-RNA (t-RNA): Tertiary Structure

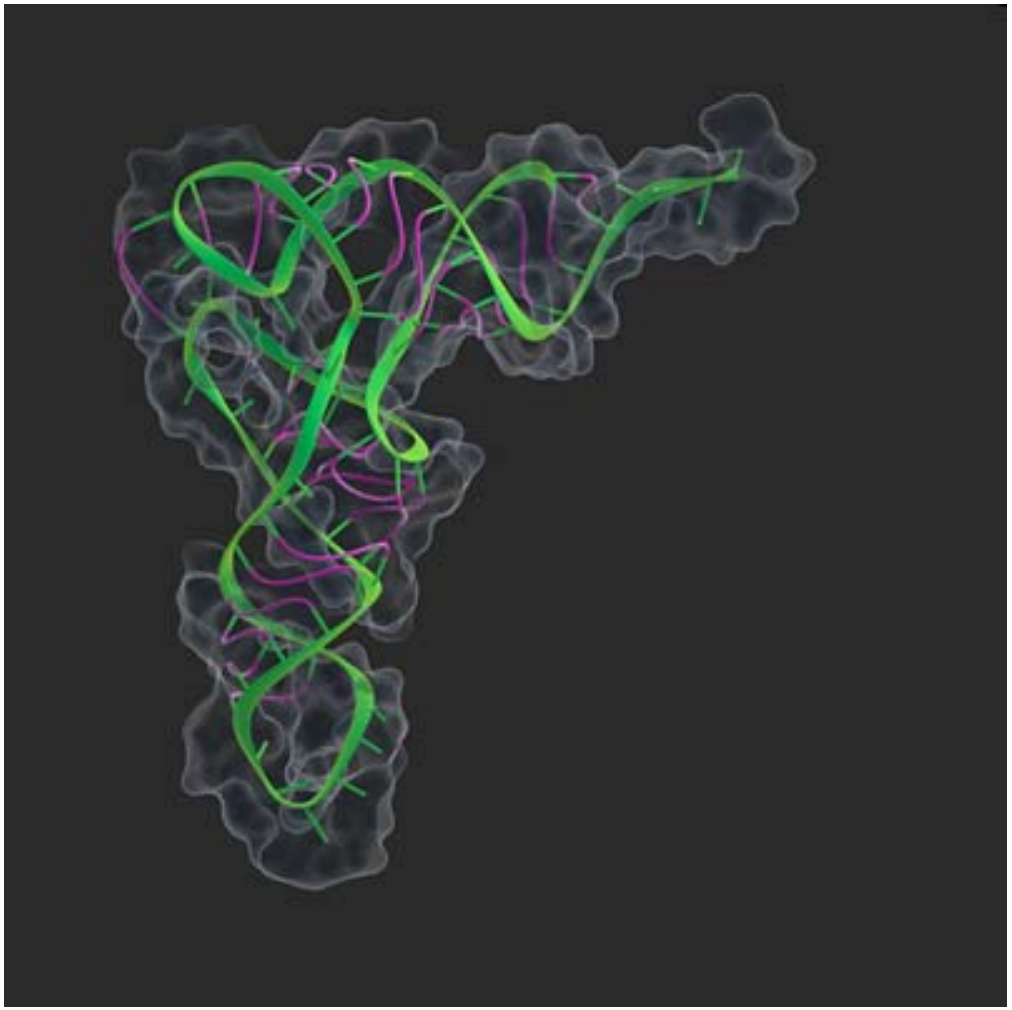

Transfer-RNA (t-RNA)

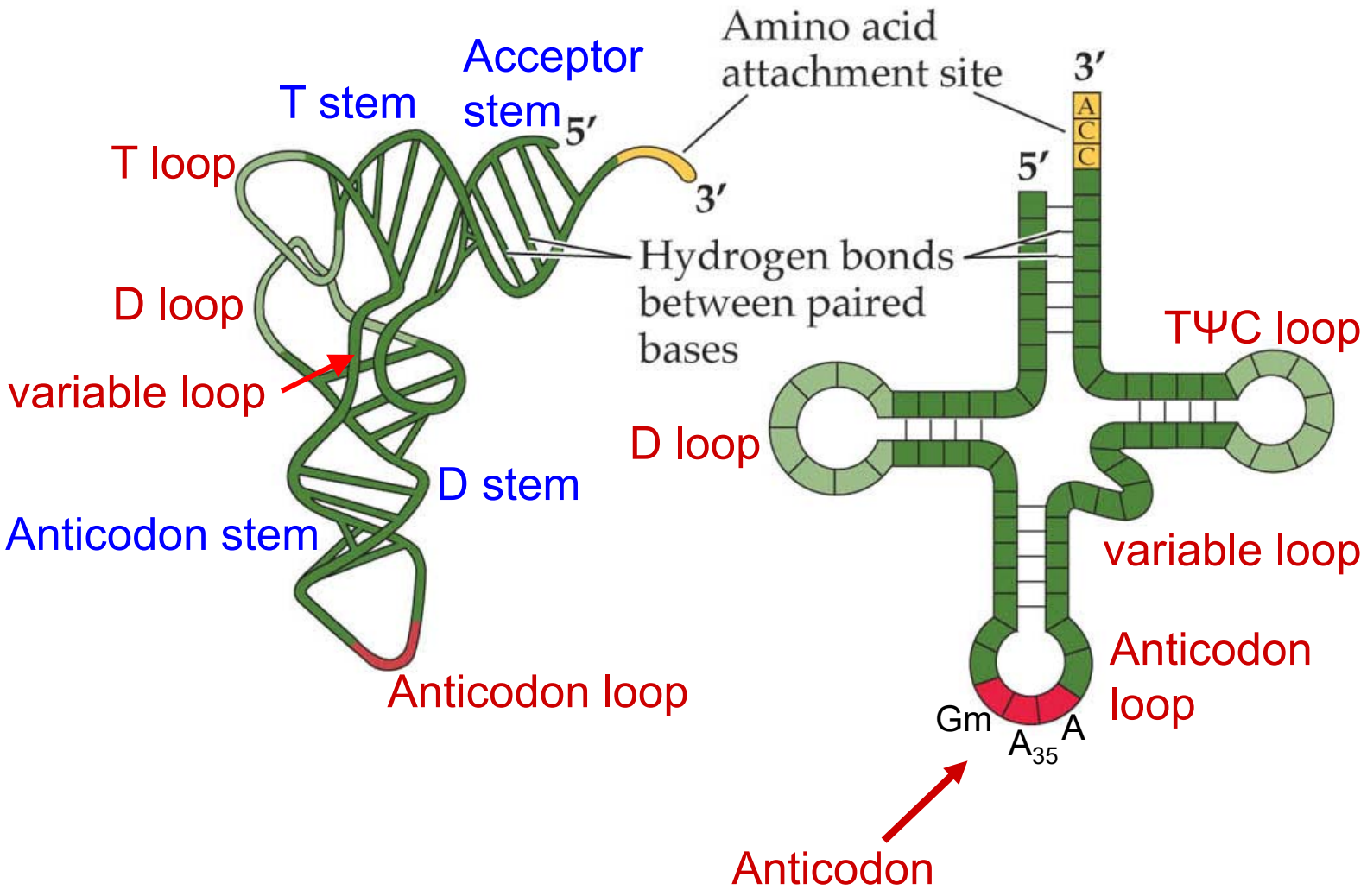

LIFE: THE SCIENCE OF BIOLOGY, Seventh Edition, Figure 12.7 Transfer RNA

© 2004 Sinauer Associates, Inc. and W. H. Freeman & Co.

t-RNA: Base Pairing

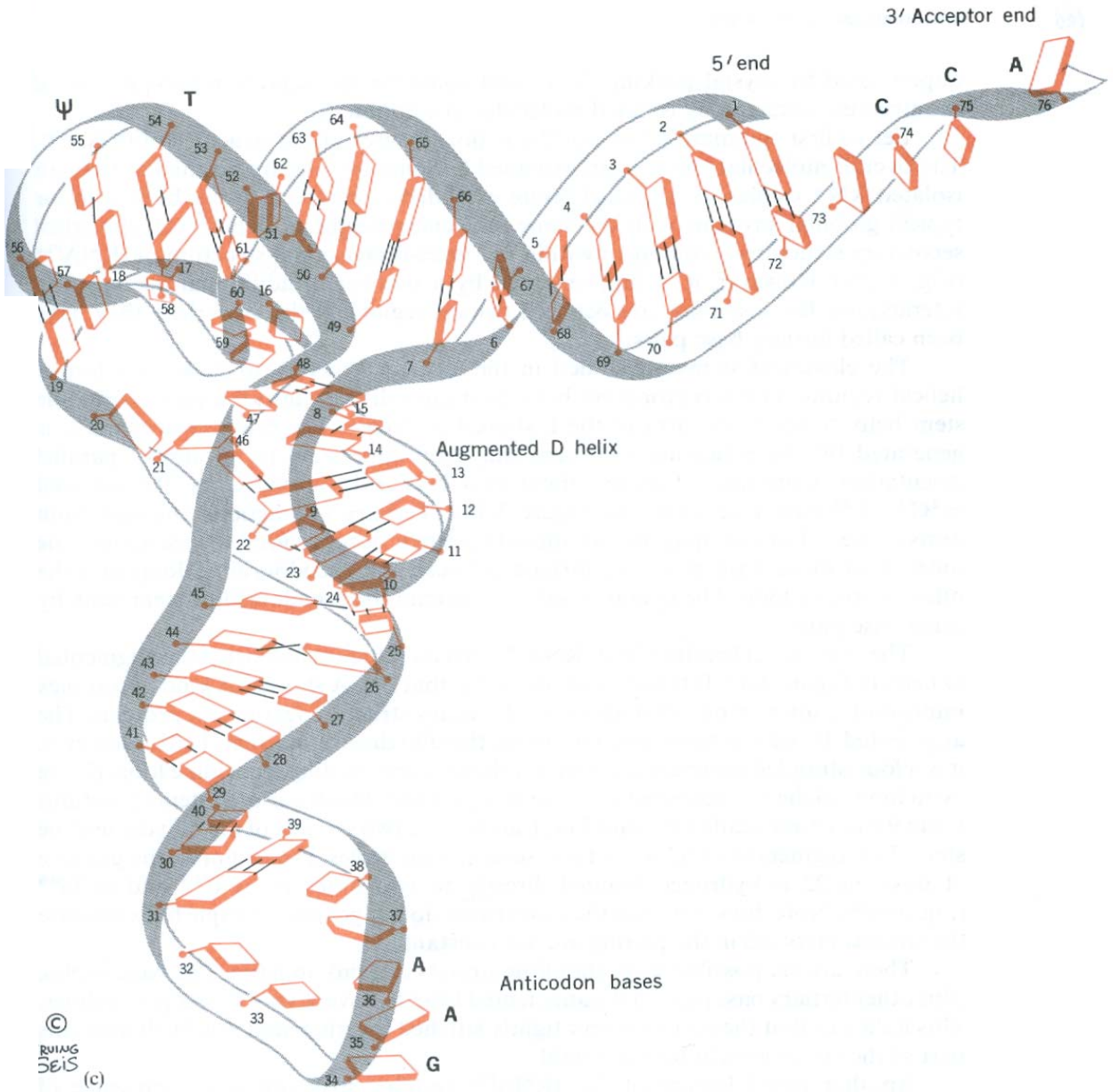

t-RNA Aminoacylation

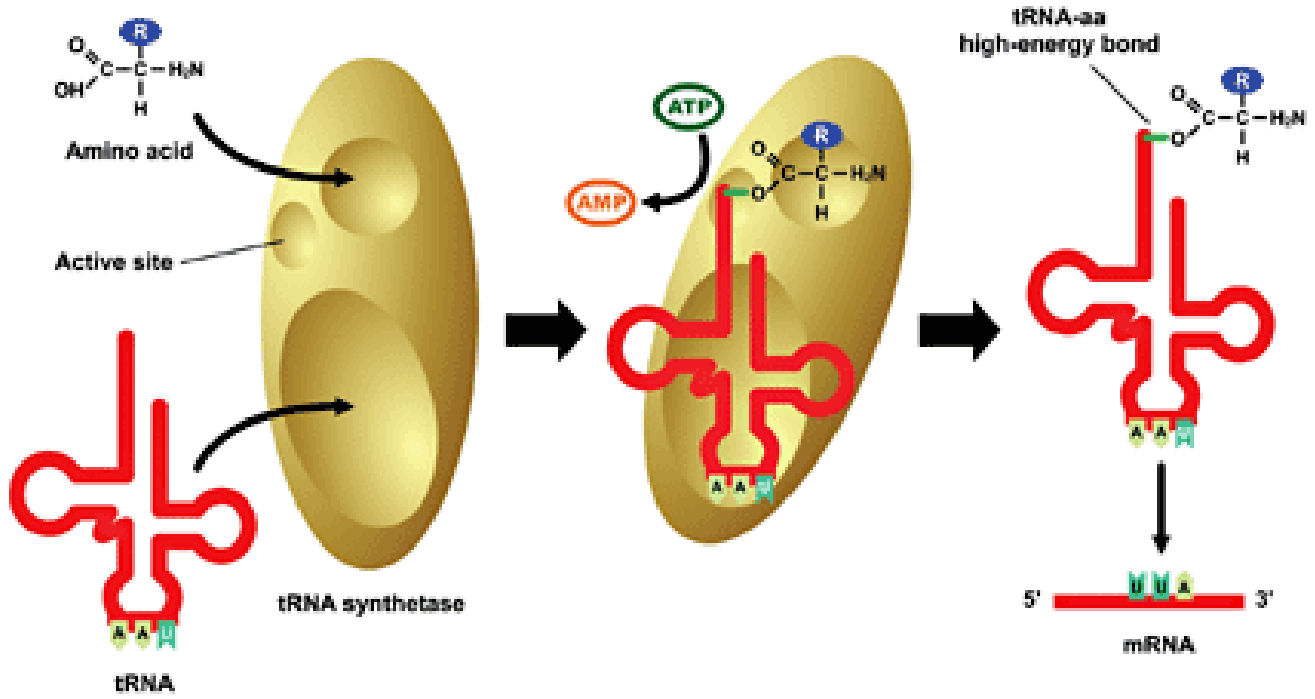

At least 20 different aminoacyl-tRNA synthases exist which link amino acids specifically to the t-RNAs

Class I: 2' esters
Class II: 3' esters

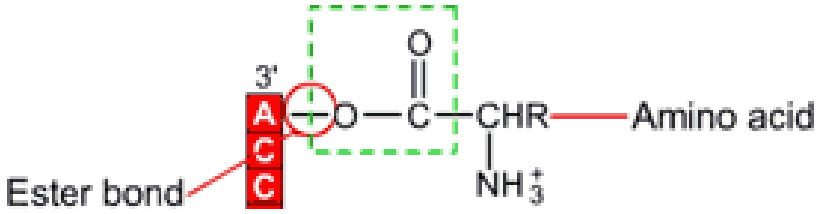

Protein Synthesis

Transcription

- RNA polymerase synthesizes messenger RNA (mRNA) from DNA template.
- One subunit recognizes start signals on DNA.
- Binding of RNA polymerase locally unfolds DNA.
- There are also stop signals on the DNA.

Translation at the Ribosome

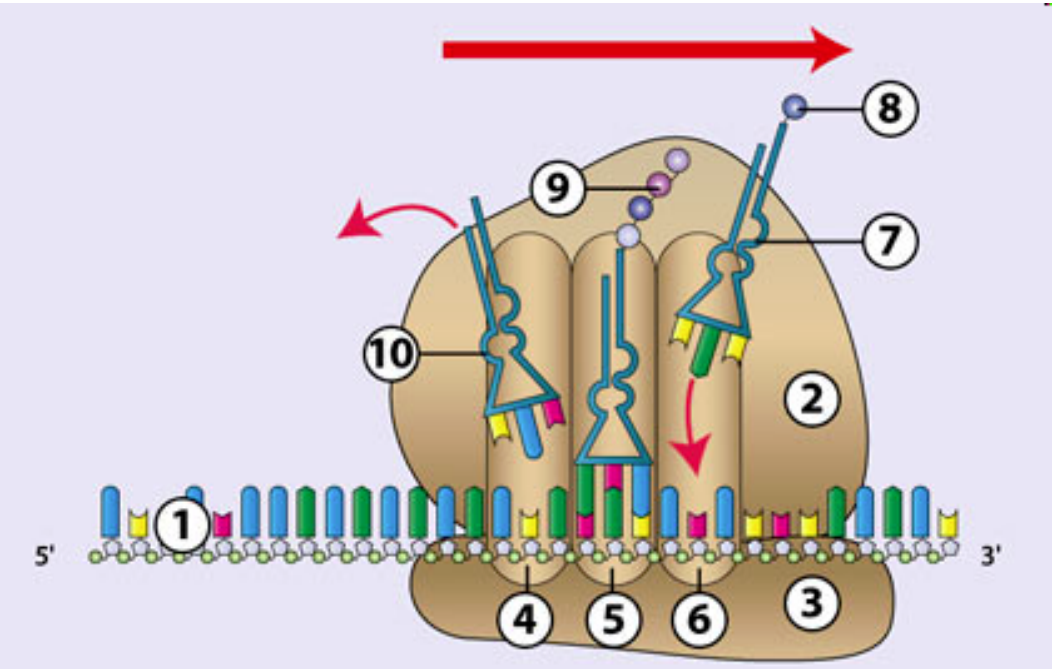

E P A

1 mRNA
2 large ribosome subunit
3 Small ribosome subunit
4 E site (exit site, binds free tRNA))
5 P site (binds peptidyl-tRNA)
6 A site (binds aminoacyl-tRNA)
7 tRNA loaded with amino acid
8 Amino acid
9 Peptide chain
10 unloaded tRNA

Translation

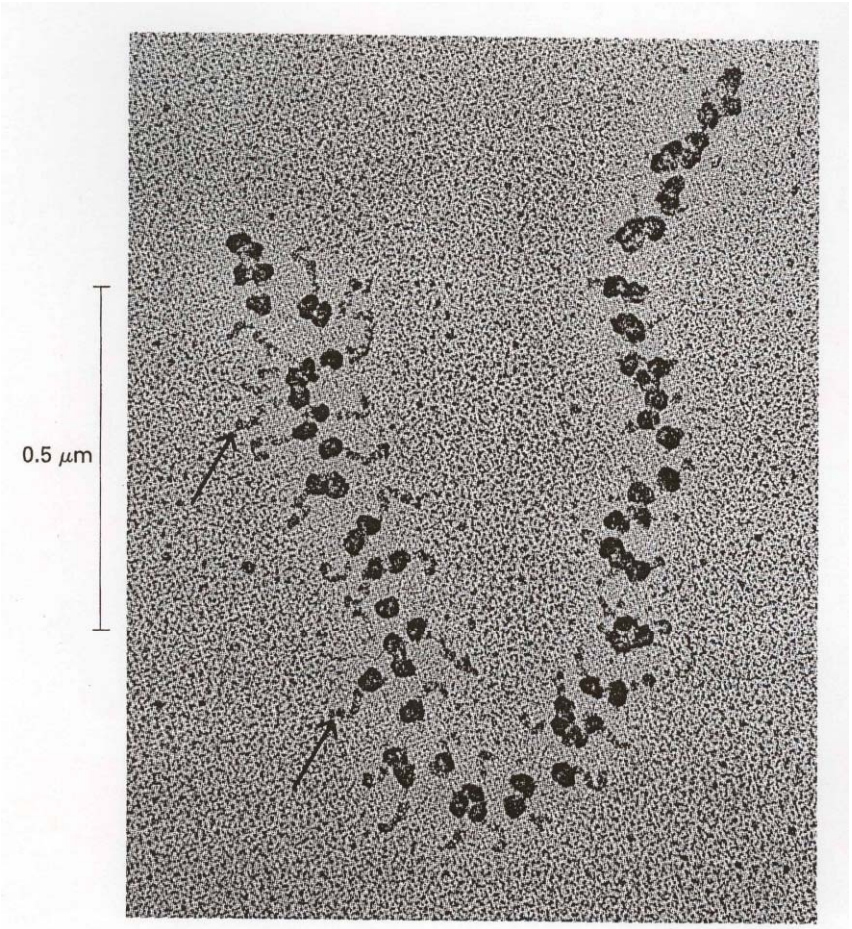

Translation of an mRNA. This electron micrograph shows a series of ribosomes on an mRNA molecule. Nascent polypeptide chains (marked by arrows) emerge from the ribosomes. [After C. Francke, J.-E. Edström, A.W. McDowall, and O.L. Miller, Jr. *EMBO J.* 1(1982):59.]

The Genetic Code

Relationship between base sequence of DNA and amino acid sequence of proteins.

- The code is (nearly) universal.
- Three bases code for one amino acid.
  → redundancy: 64 codes for 20 amino acids.
- The code is sequential, non-overlapping.

Why is a degenerate code advantageous ?

- Minimizes effect of mutations.
- Permits alteration of base composition without altering amino acid sequence.

The Genetic Code

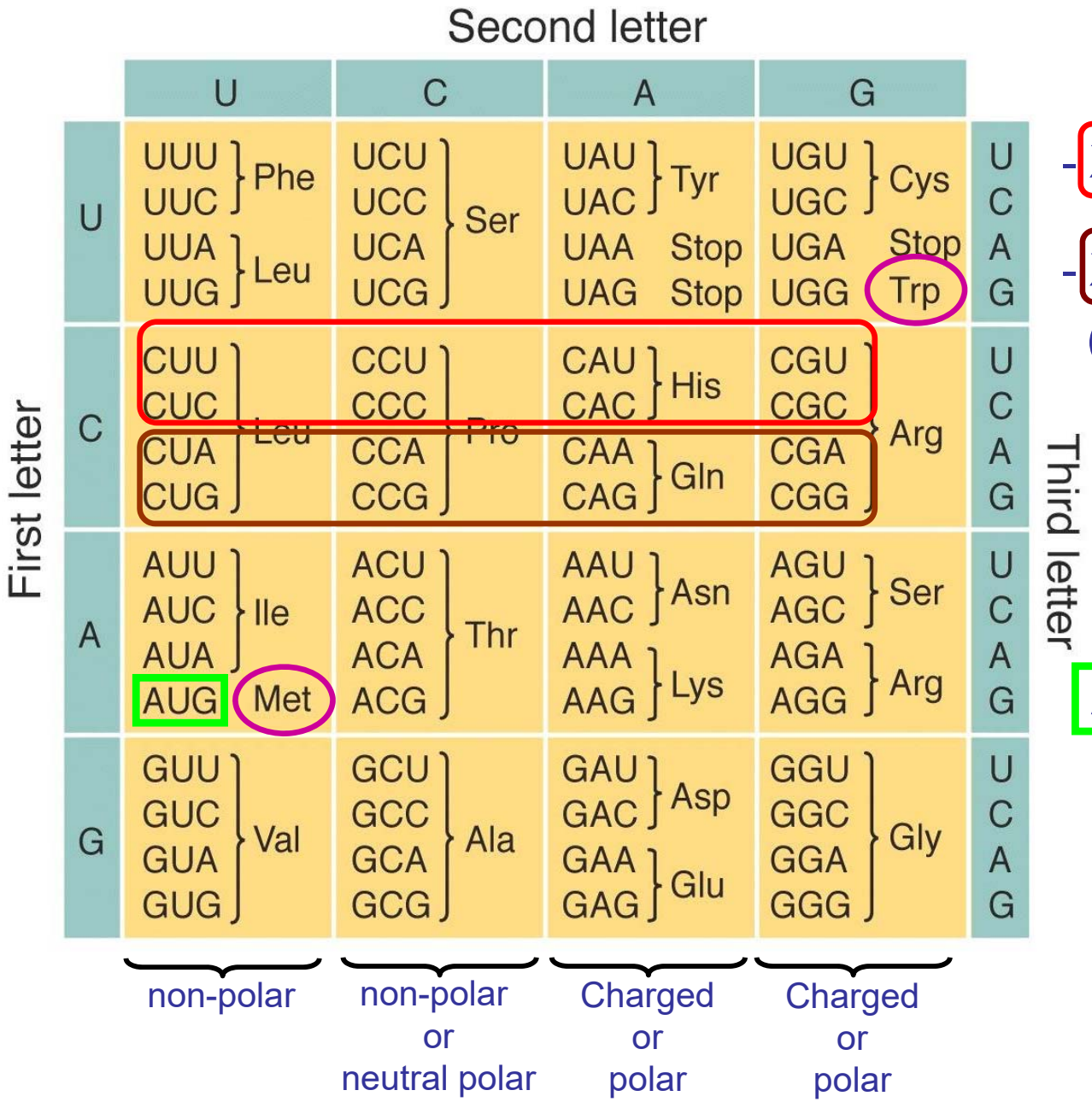

- XYC/XYU code for the same aa.
- XYG/XYA code for the same aa. (except Trp, Met)

AUG also part of start sequence

Human mitochondria use 'special code':
UGA: STOP → Trp
AUA: Ile → Met
AGA: Arg → Stop
AGG: Arg → Stop

Biophysics II

Molecular Orbitals – Linear Combination of Atomic Orbitals (LCAO)

Uli Nienhaus

Prof. G. U. Nienhaus, Vorlesungsunterlagen Biophysik II, SS 2022.
Nur zum KIT-internen, vorlesungsbegleitenden Gebrauch.
Weitergabe und anderweitige Nutzung verboten.

LCAO Molecular Orbitals

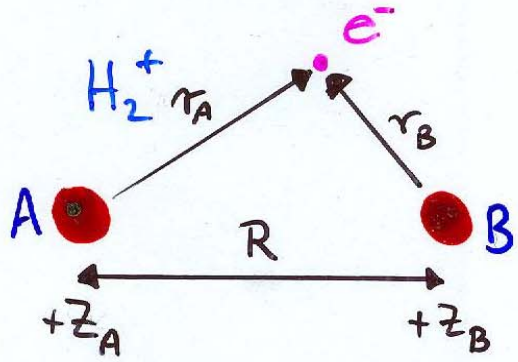

Assumptions:

① Keep R fixed (BOA)

② neglect e^- e^- interaction → H_2^+

$$H = \frac{-\hbar^2}{2m_e}\nabla^2 - \frac{e^2}{4\pi\varepsilon_0}\left[\frac{Z_A}{r_A} + \frac{Z_B}{r_B} - \frac{Z_A Z_B}{R}\right]$$

LCAO : $\psi_e = c_1\phi_A + c_2\phi_B$

assume real c_1, c_2, ϕ_A, ϕ_B

Normalization :

$$1 = \int (N\psi^*)\, N\psi \, d^3\vec{r} = N^2\int\left(c_1^2\phi_A^2 + 2c_1c_2\phi_A\phi_B + c_2^2\phi_B^2\right)d^3\vec{r}$$

$$= N^2\left(c_1^2 + 2c_1c_2 S + c_2^2\right)$$

$$S = \int \phi_A \phi_B \, d^3\vec{r}$$

↳ overlap integral

$S = 0$: ⊥ ; $S = 1$: identity

Energy expectation value:

$$\langle E \rangle = \frac{\int \psi^* H \psi \, d^3\vec{r}}{\int \psi^* \psi \, d^3\vec{r}} = \frac{c_1^2 H_{AA} + 2c_1 c_2 H_{AB} + c_2^2 H_{BB}}{c_1^2 + 2c_1 c_2 S + c_2^2}$$

$$H_{kl} = \int \phi_k^* H \phi_l \, d^3\vec{r}$$

H_{AA}, H_{BB} Coulomb integral

H_{AB} – resonance integral (exchange integral)

($= H_{BA}$, hermitian)

$\langle E \rangle$ will be a minimum for proper choice of c_1, c_2

$$\Rightarrow \frac{\partial E}{\partial c_1} = \frac{\partial E}{\partial c_2} = 0$$

Secular eqs.

$$c_1 (H_{AA} - E) + c_2 (H_{AB} - SE) = 0$$

$$c_1 (H_{AB} - SE) + c_2 (H_{BB} - E) = 0$$

(Variation theorem)

Eliminate c_1, c_2:

$$\begin{vmatrix} H_{AA} - E & H_{AB} - SE \\ H_{AB} - SE & H_{BB} - E \end{vmatrix} = 0$$

→ 2 solutions, E_b, E^*

simplest case: $H_{AA} = H_{BB}$ homonuclear diatomic

$$E_b = \frac{H_{AA} + H_{AB}}{1+S} \qquad E^* = \frac{H_{AA} - H_{AB}}{1-S}$$

$$\psi_b = \frac{1}{\sqrt{2+2S}}(\phi_A + \phi_B)$$

$$\psi^* = \frac{1}{\sqrt{2-2S}}(\phi_A - \phi_B)$$

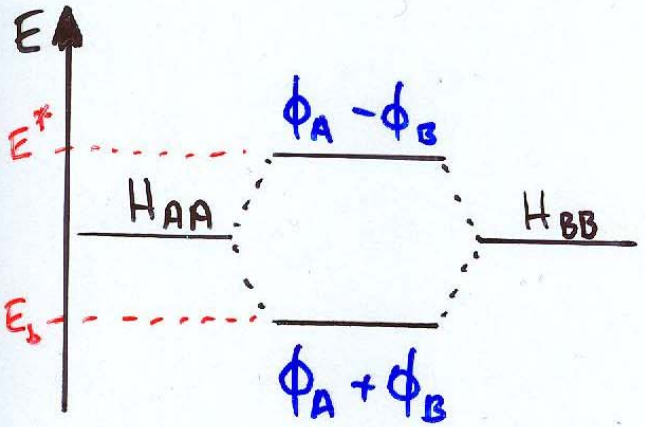

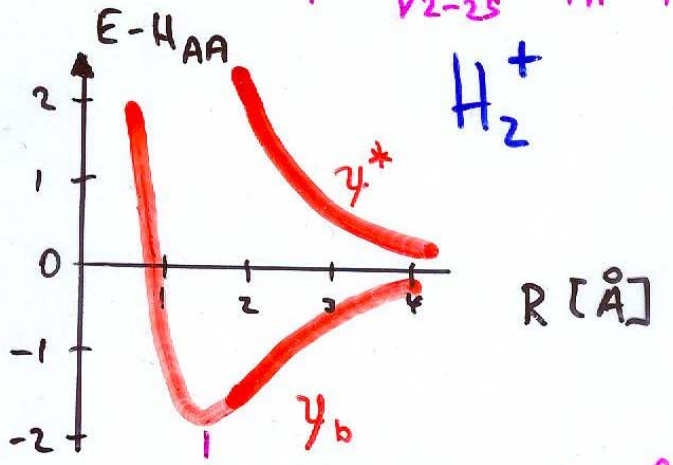

H_2^+

minimum @ −1.76 eV, 1.3 Å

exp −2.79 1.06

Energy diagram (Homodimer)

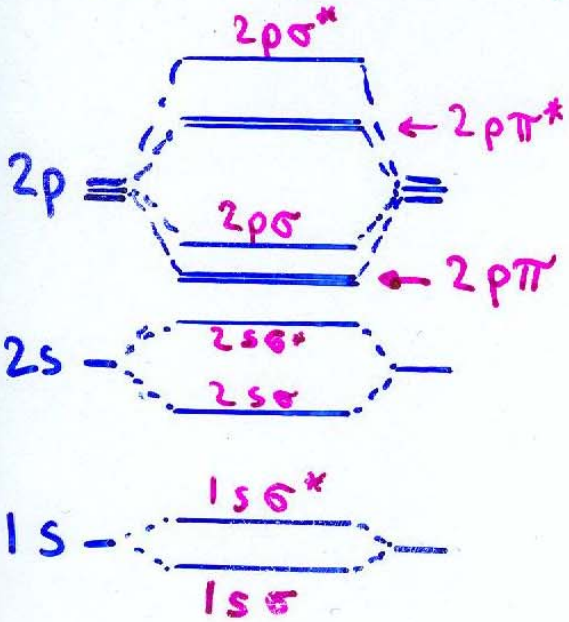

N_2 : 14 electrons

O_2 : 16 electrons

$p\pi^*$: $p_A - p_B$

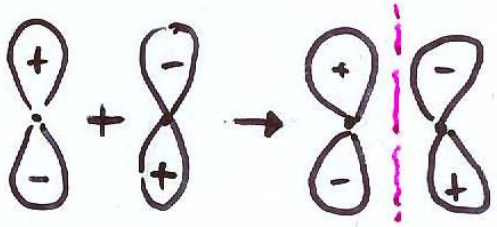

$p\pi$: $p_A + p_B$

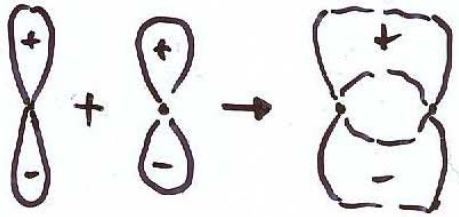

$p\sigma^*$: $p_A - p_B$

$p\sigma$: $p_A + p_B$

$s\sigma^*$: $s_A - s_B$

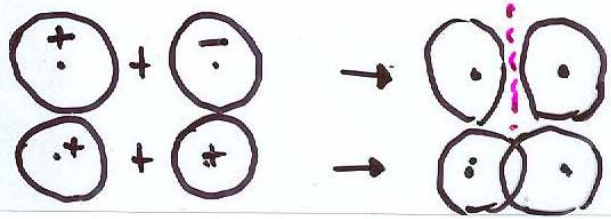

$s\sigma$: $s_A + s_B$

Hybridization

- chemical bonds can involve more than one orbital of each atom:

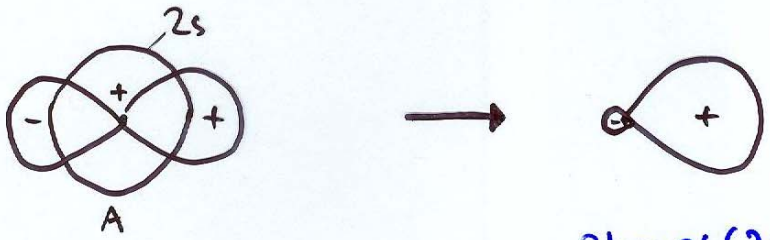

$$\psi = \psi(2s) \pm \lambda \psi(2p)$$

See our discussion of MOs in formaldehyde

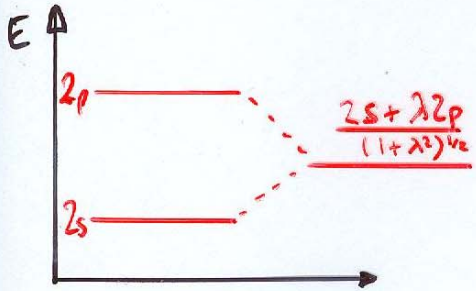

- Hybridization is not a new physical effect, but merely a transformation of H-like orbitals.
- many ways of mixing orbitals : sp^3, sp^2, sp ...
- in general, variational calculation to minimize energy needed to find proper linear combination.

sp^3 Hybridization

Carbon: $1s^2\ 2s^2\ 2p^2$

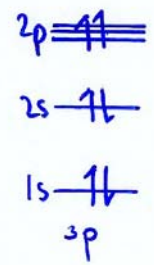

2 bonds expected, but often
4 equivalent bonds observed : CH_4
→ would need ^5S state : $1s^2\ 2s^1\ 2p^3$
+ 4.2 eV

Slater / Pauling :

$$\psi_i = a_i|s\rangle + b_i|p_x\rangle + c_i|p_y\rangle + d_i|p_z\rangle \qquad i = 1 \ldots 4$$

orthonormality:

$$a_i a_j + b_i b_j + c_i c_j + d_i d_j = \delta_{ij}$$

sp^3:

$$|1\rangle = \frac{1}{\sqrt{4}}\left(|s\rangle + |p_x\rangle + |p_y\rangle + |p_z\rangle\right)$$
$$|2\rangle = \frac{1}{\sqrt{4}}\left(|s\rangle + |p_x\rangle - |p_y\rangle - |p_z\rangle\right)$$
$$|3\rangle = \frac{1}{\sqrt{4}}\left(|s\rangle - |p_x\rangle + |p_y\rangle - |p_z\rangle\right)$$
$$|4\rangle = \frac{1}{\sqrt{4}}\left(|s\rangle - |p_x\rangle - |p_y\rangle + |p_z\rangle\right)$$

CH_4 tetrahedral

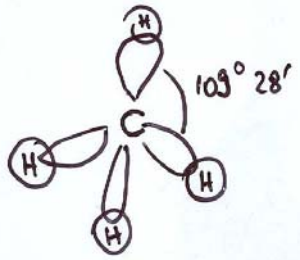

sp^2

Ethylene:

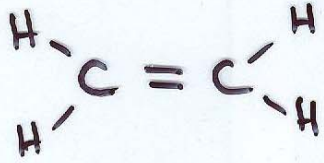

planar, non-rotatable

$$|1\rangle = |p_z\rangle$$

$$|2\rangle = \frac{1}{\sqrt{3}}|s\rangle + \sqrt{\frac{2}{3}}|p_x\rangle$$

$$|3\rangle = \frac{1}{\sqrt{3}}|s\rangle - \frac{1}{\sqrt{6}}|p_x\rangle + \frac{1}{\sqrt{2}}|p_y\rangle$$

$$|4\rangle = \frac{1}{\sqrt{3}}|s\rangle - \frac{1}{\sqrt{6}}|p_x\rangle - \frac{1}{\sqrt{2}}|p_y\rangle$$

side view

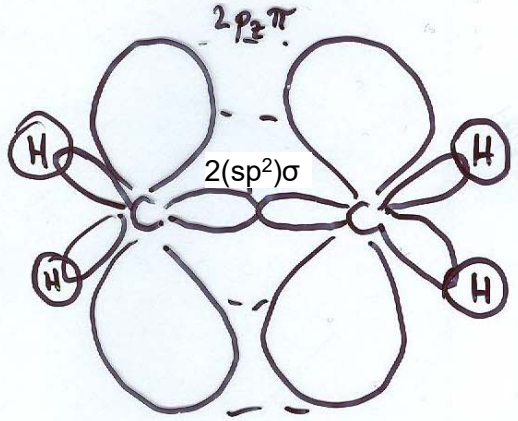

top view

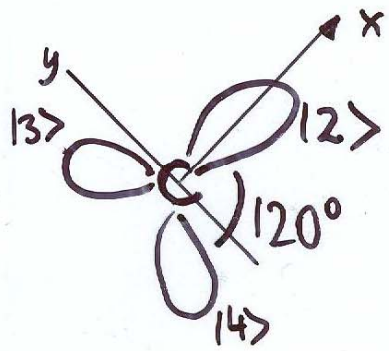

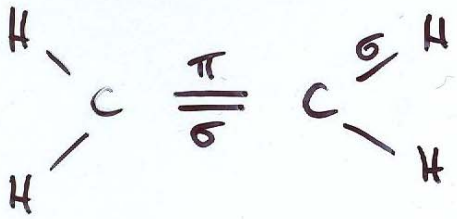

sp

acetylene $H-C\equiv C-H$ linear

$|1\rangle = |p_z\rangle$

$|2\rangle = |p_y\rangle$

$|3\rangle = \frac{1}{\sqrt{2}}(|s\rangle - |p_x\rangle)$

$|4\rangle = \frac{1}{\sqrt{2}}(|s\rangle + |p_x\rangle)$

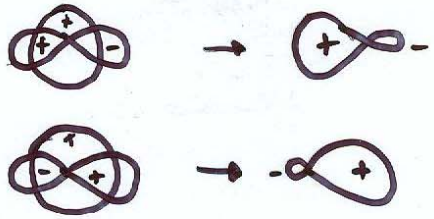

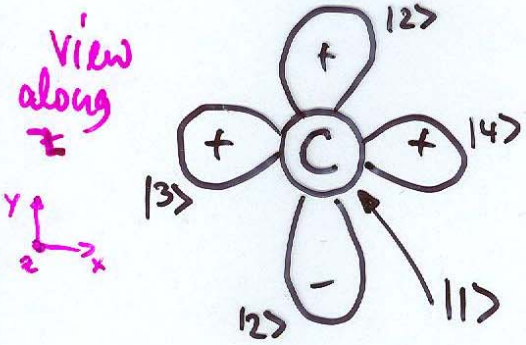

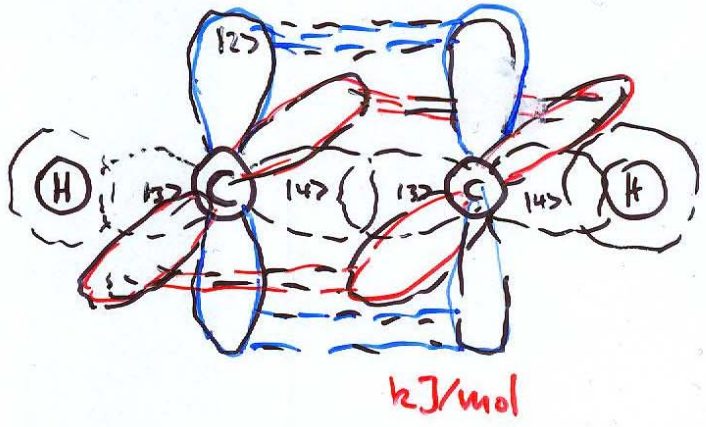

kJ/mol

Energetics :

	σ bond	C–C	348	Δ = 334
σ + π	"	C=C	682	
σ + π + π	"	C≡C	962	Δ = 280

Biophysics II

Introduction:
How Proteins Interact with Light

Uli Nienhaus

Prof. G. U. Nienhaus, Vorlesungsunterlagen Biophysik II, SS 2023.
Nur zum KIT-internen, vorlesungsbegleitenden Gebrauch.
Weitergabe und anderweitige Nutzung verboten.

Light as a Classical Wave

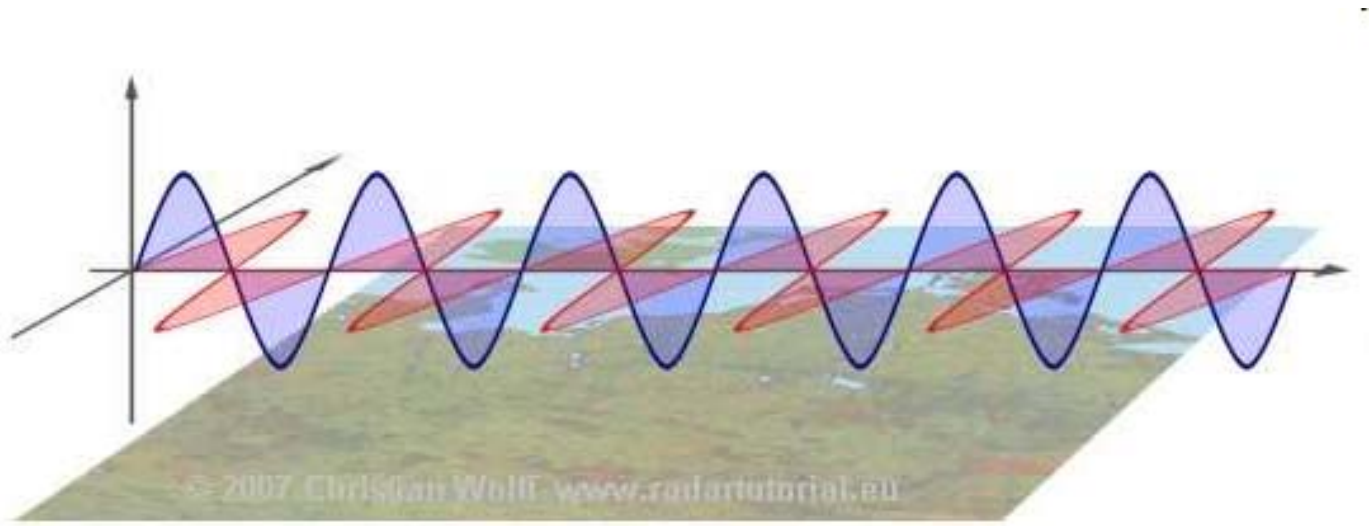

Classical description: Electromagnetic wave

$$\vec{E}_x(z,t) = \hat{x}E_0 \cdot \cos(kz - \omega t)$$

$$k = \frac{2\pi}{\lambda} \qquad \omega = \frac{2\pi}{T}$$

A harmonic wave is characterized by amplitude, wavenumber and frequency

Light as a Classical Wave

Linear polarization

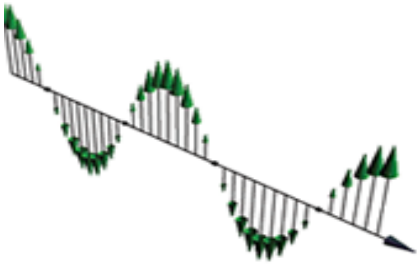

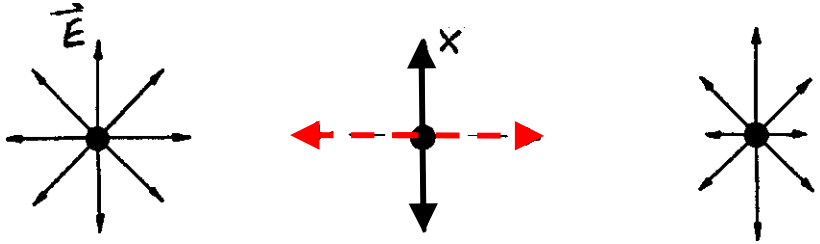

Unpolarized x-polarized partially polarized

y-polarized

Circular polarization

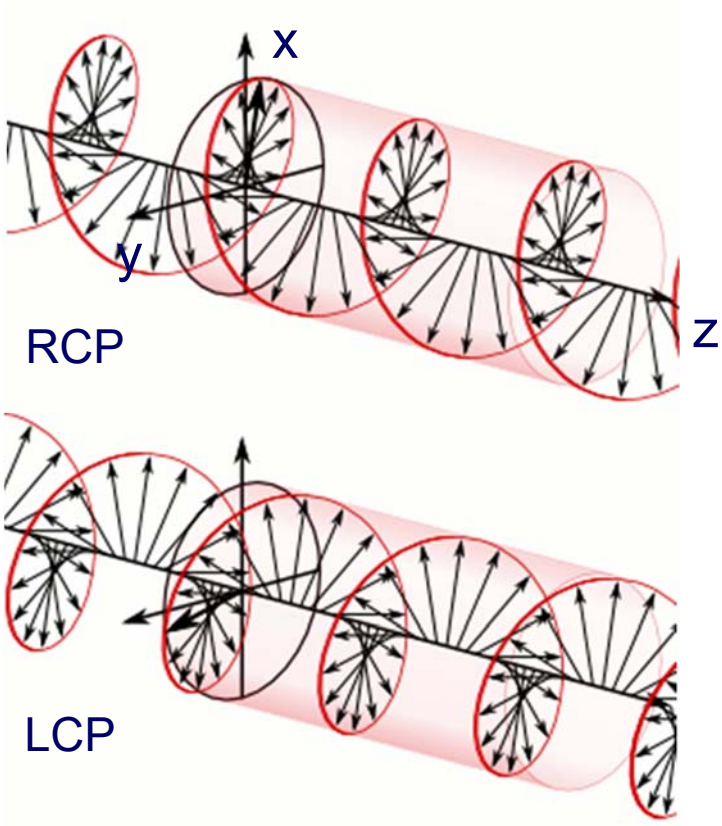

$$\vec{E}\ (z_0,t) = \frac{1}{2}\left(\hat{x}E_0\cos(\omega t) \pm \hat{y}E_0\sin(\omega t)\right)$$

Photons

Quantum-mechanical description: Light as particles (photons)

$$E = h\nu = \hbar\omega$$

$$p = \frac{E}{c} = \frac{h}{\lambda} = \hbar k$$

Photons are characterized by energy, momentum and spin (±1)

$$\nu = \frac{c}{\lambda} \qquad c \equiv 2.99792458 \cdot 10^8 \text{ m/s}$$

Energy in wavenumber units (spectroscopy):

$$\tilde{\nu} = \frac{k}{2\pi} = \lambda^{-1} \quad [\text{cm}^{-1}]$$

Example:

$\lambda = 10^{-6}$ m $\longrightarrow$ $\tilde{\nu} = 10^4$ cm^{-1}

Spectrum of Electromagnetic Radiation

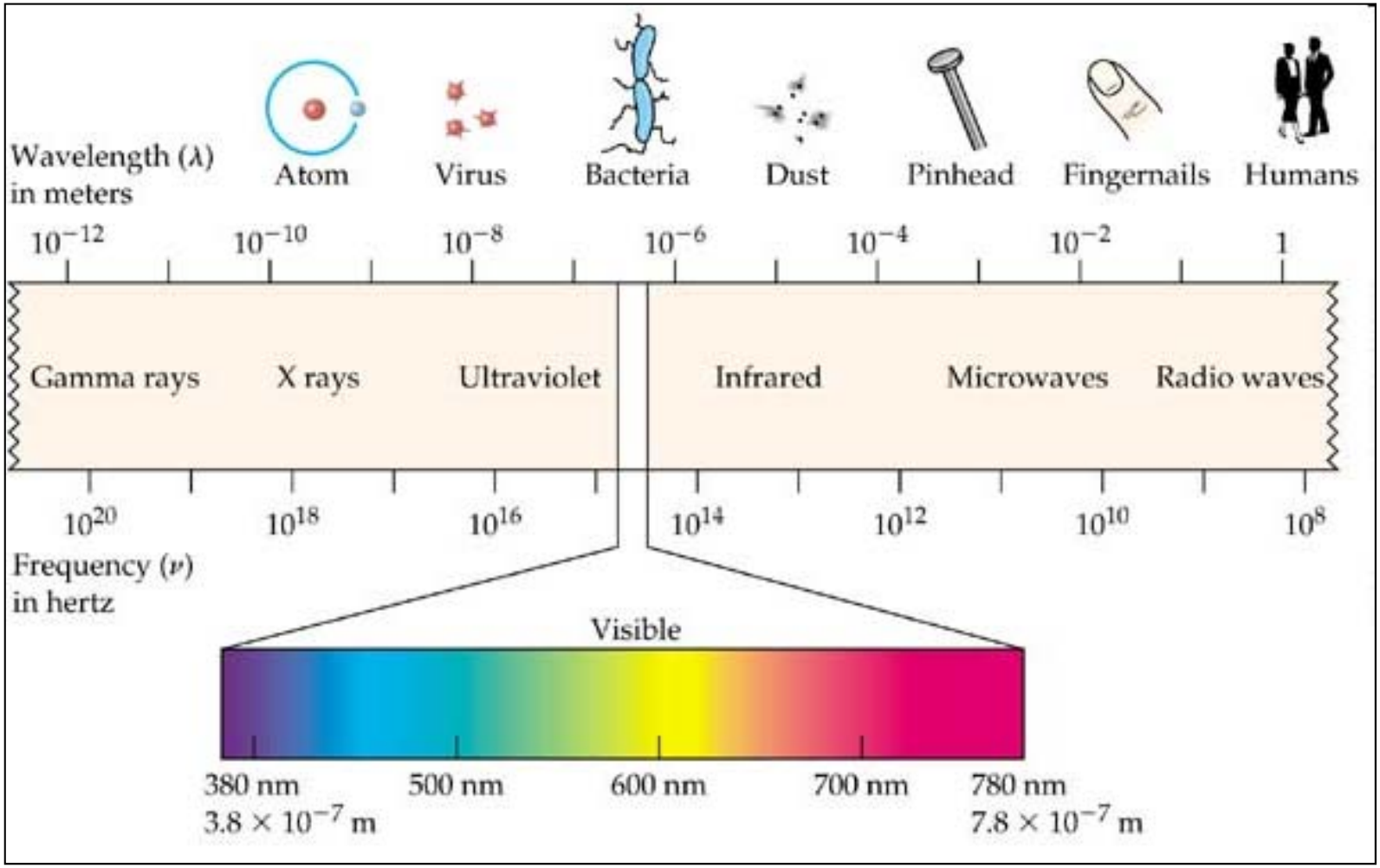

Interaction Processes

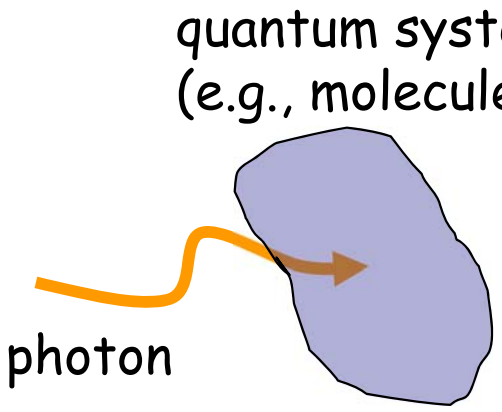

$$E = h\nu = \hbar\omega = h\frac{c}{\lambda}$$

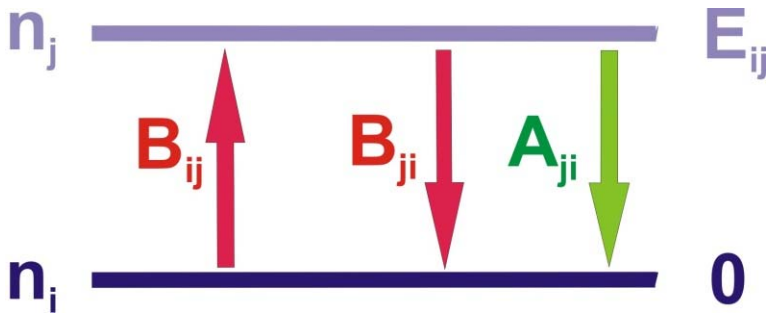

A, B: Einstein coefficients

- Three processes:
  - induced absorption (with rate coefficient B_{ij})
  - induced emission (B_{ji}) in the direction of the incoming radiation
  - spontaneous emission (A_{ji}), direction of emitted photon depends on properties of the system

Einstein Coefficients

- Connection between Einstein coefficients:

$$B_{ij} = B_{ji}$$ microreversibility

$$\frac{n_j}{n_i} = \exp(-E_{ji} / kT)$$ Boltzmann equation

spectral energy density

$$I(\omega_{ij}) = \frac{\omega_{ij}^2}{\pi^2 c^3} \frac{1}{e^{\hbar\omega_{ij}/kT} - 1} \hbar\omega_{ij}$$

DOS

Planck's law

cmp. Rayleigh-Jeans law:

$$I(\omega_{ij}) = \frac{\omega_{ij}^2}{\pi^2 c^3} kT$$

$$I(\omega_{ij}) B_{ij} n_i = I(\omega_{ij}) B_{ji} n_j + A_{ji} n_j$$ Thermal equilibrium

$$\rightarrow A_{ji} = \frac{\hbar\omega_{ij}^3}{\pi^2 c^3} B_{ij}$$

Density of states (DOS):

$$D'(\omega) = \frac{1}{V_x}\frac{dN}{d\omega} = \frac{1}{V_x}\frac{d}{d\omega}\frac{V_x V_p}{h^3} = \frac{d}{d\omega}\frac{\frac{4\pi}{3}\frac{h^3}{\lambda^3}}{h^3} = \frac{\omega^2}{2\pi^2 c^3}$$

$$D(\omega) = 2D'(\omega) = \frac{\omega^2}{\pi^2 c^3}$$ (2 polarizations)!

Line Widths

- Assume: $n_j = n_j(0), \qquad n_i = 0 \quad @t = 0$

$$n_j(t) = n_j(0)\, e^{-A_{ji}t}$$

$$\tau = A_{ji}^{-1}$$

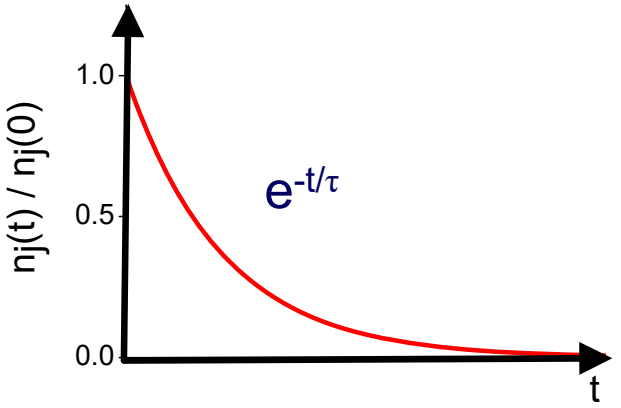

- Line width: $\Gamma\tau = \hbar$

$$\Gamma = \hbar\, A_{ji}$$

Heisenberg uncertainty relation
→ "natural linewidth"

- Line shape:

$$I(\omega) = \frac{1}{(\omega - \omega_{ij})^2 + \left(\frac{\Gamma}{2}\right)^2}$$

Lorentzian (Fourier transform of $e^{-t/\tau}$)

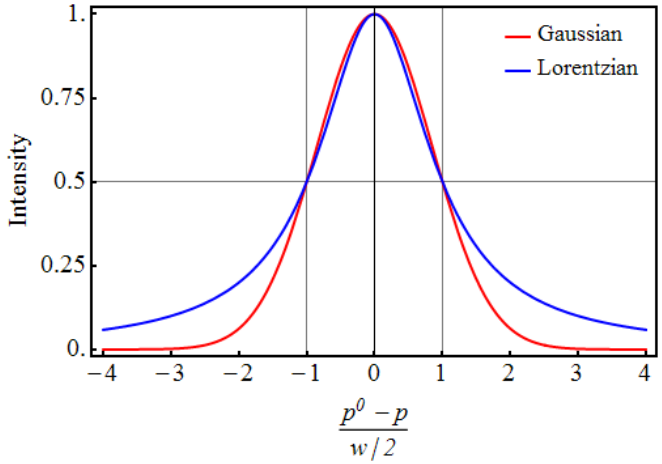

- Broadening effects:

- Molecular motion (Doppler effect)
- Structural heterogeneity
- Environmental effects (solvent)

Induced Absorption I

- Proper derivation needs QED
- Simple derivation treats EM field classically as a weak (first-order) perturbation of a given charge distribution

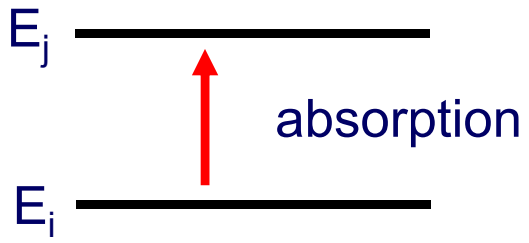

- without EM field

$$H\Psi_i = E_i\Psi_i$$
$$H\Psi_j = E_j\Psi_j$$

time-independent Schrödinger equation

- with EM field

$$H \rightarrow H' = H + V(t)$$

$$V(t) = -\vec{\mu}\cdot\vec{E}_0\cos\omega t$$
$$= -\frac{1}{2}\vec{\mu}\cdot\vec{E}\left(e^{i\omega t} + e^{-i\omega t}\right)$$

electric dipole interaction

stimulated emission/absorption

$$\Psi(t) = C_i(t)\Psi_i(t) + C_j(t)\Psi_j(t)$$

Induced Absorption II

- time-dependent Schrödinger equation

$$\left[H + V(t)\right]\Psi(t) = i\hbar \frac{\partial}{\partial t}\Psi(t)$$

$$= i\hbar \frac{\partial}{\partial t}\left[C_i(t)\Psi_i e^{-iE_i t/\hbar} + C_j(t)\Psi_j e^{-iE_j t/\hbar}\right]$$

- differentiate, cancel terms of time-independent S.E.:

$$V(t)\Psi(t) = i\hbar \frac{\partial C_i}{\partial t}\Psi_i e^{-iE_i t/\hbar} + i\hbar \frac{\partial C_j}{\partial t}\Psi_j e^{-iE_j t/\hbar}$$

- multiply from left with ψ_j^* and integrate over all space (in bracket notation):

$$i\hbar \frac{\partial C_j}{\partial t} = \left\langle \Psi_j \middle| V \middle| \Psi_i \right\rangle C_i e^{i(E_j - E_i)t/\hbar} + \left\langle \Psi_j \middle| V \middle| \Psi_j \right\rangle C_j$$

Induced Absorption III

- Initial conditions: $C_i = 1$, $C_j = 0$

$$i\hbar \frac{\partial C_j}{\partial t} = \left\langle \Psi_j \left| V \right| \Psi_i \right\rangle e^{i\Delta E t/\hbar}$$

- Integrate from $t' = 0 \rightarrow t$

$$C_j(t) = \frac{i}{2\hbar} \left\langle \Psi_j \left| \vec{\mu} \right| \Psi_i \right\rangle \vec{E}_0 \int_0^t e^{i(\Delta E - \hbar\omega)t'/\hbar} dt'$$

$$= \frac{1}{2} \left\langle \Psi_j \left| \vec{\mu} \right| \Psi_i \right\rangle \vec{E}_0 \frac{e^{i(\Delta E - \hbar\omega)t/\hbar} - 1}{(\Delta E - \hbar\omega)}$$

$$\left| C_j \right|^2 = \left| \left\langle \Psi_j \left| \vec{\mu} \right| \Psi_i \right\rangle \vec{E}_0 \right|^2 \cdot \underbrace{\frac{\sin^2\left[(\Delta E - \hbar\omega)t/2\hbar\right]}{(\Delta E - \hbar\omega)^2}}$$

$$\int_{-\infty}^{\infty} \frac{\sin^2 ax}{x^2} dx = \pi |a|$$

Exposure to spectral continuum

Induced Absorption IV

- Probability of absorption of light from a spectral continuum

$$\frac{dP_j}{dt} = \frac{d}{dt}\int_{-\infty}^{\infty} |C_j|^2 d\omega = \left|\langle \Psi_j | \vec{\mu} | \Psi_i \rangle \vec{E}_0\right|^2 \cdot \frac{\pi}{2\hbar^2}$$

$$\frac{dP_j}{dt} = B_{ij} I(\omega)$$

$$I(\omega) = \frac{1}{8\pi}\left|\vec{E}_0(\omega)\right|^2$$

Energy density (cgs) !

$$B_{ij} = \left|\langle \Psi_j | \vec{\mu} | \Psi_i \rangle \vec{E}_0\right|^2 \cdot \frac{4\pi^2}{\hbar^2} \cdot \frac{1}{\left|\vec{E}_0\right|^2}$$

$$B_{ij} = \frac{4}{3}\frac{\pi^2}{\hbar^2}\left|\langle \Psi_j | \vec{\mu} | \Psi_i \rangle\right|^2$$

average over all orientations (for a randomly oriented sample)!

Induced Absorption V

Rate of energy removal from the incident radiation: $\frac{dP_j}{dt} = \frac{4}{3}\frac{\pi^2}{\hbar^2}\left|\left\langle \Psi_j \left| \vec{\mu} \right| \Psi_i \right\rangle\right|^2 I(\omega)$

It depends on (isotropic sample!)

1. Incident spectral density, *I*(ω)
2. $D_{ij} \equiv \left|\left\langle \Psi_j \left| \vec{\mu} \right| \Psi_i \right\rangle\right|^2$

   $= 9.18 \cdot 10^{-3} n \int \frac{\varepsilon(\nu)}{\nu} d\nu$ [D²]

Transition dipole strength

ε: extinction coefficient
n: index of refraction

1 D = 10^{-18} esu cm
1 eÅ = 4.8 D

Empirical definition of the extinction coefficient ε: $\frac{dI}{I} = \varepsilon' C\, dl \Rightarrow \boxed{A(\nu) = \log\frac{I_0}{I} = \varepsilon(\nu) C l}$

Lambert–Beer law

C: concentration
l: path length

Molecular Energy Levels

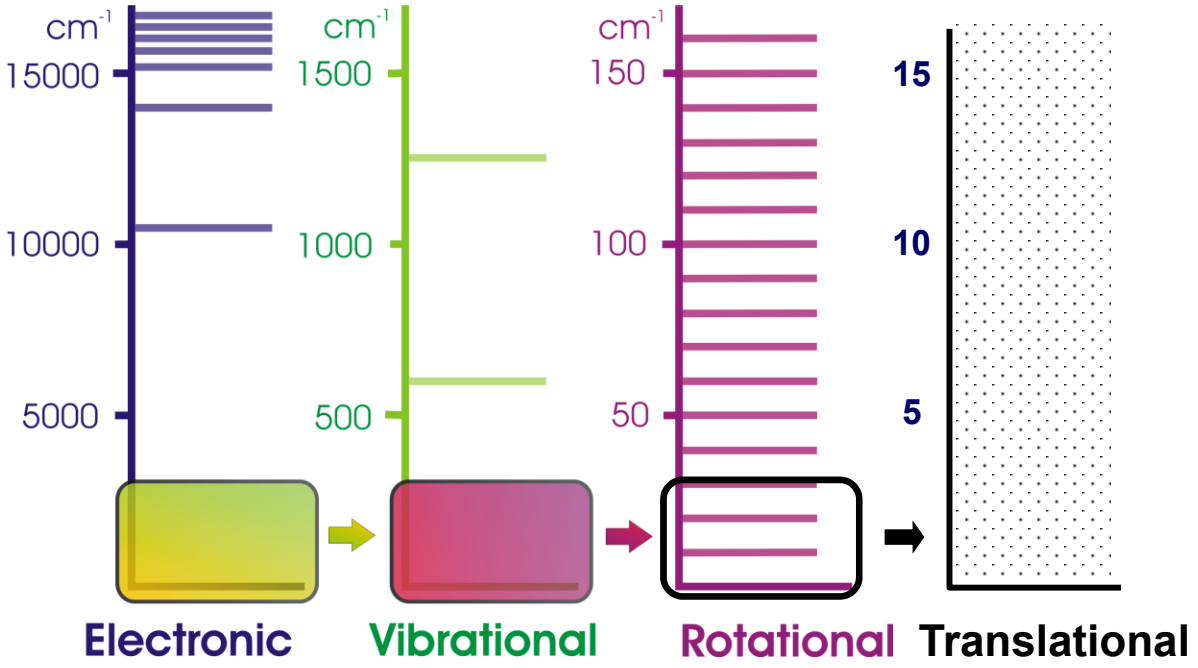

Population in thermal equilibrium:

$$\frac{n_j}{n_i} = e^{-\Delta E / kT}$$

kT = 200 cm^{-1} @ room temperature

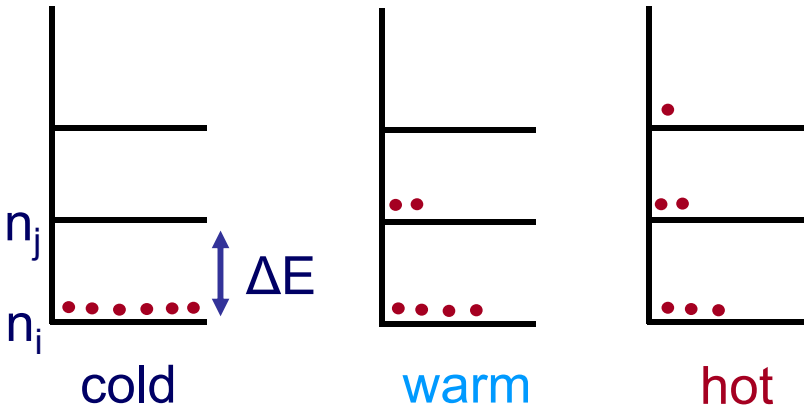

Electronic Transitions I

Electronic transitions occur predominantly via electric dipole interaction.

$$\frac{dP_j}{dt} \propto \left| \left\langle \psi_j \left| e\vec{r} \right| \psi_i \right\rangle \cdot \vec{E} \right|^2$$

EM field

transition dipole moment

Parity: $\mathscr{P}_j \cdot \mathscr{P}_i = -1$

Selection rules: $\Delta E = h\nu$

$$\Delta l = \pm 1$$

The two rules represent energy and angular momentum conservation in the photon-molecule collision. Note that the photon is a spin 1 particle! Forbidden transitions 'violate' the selection rules.

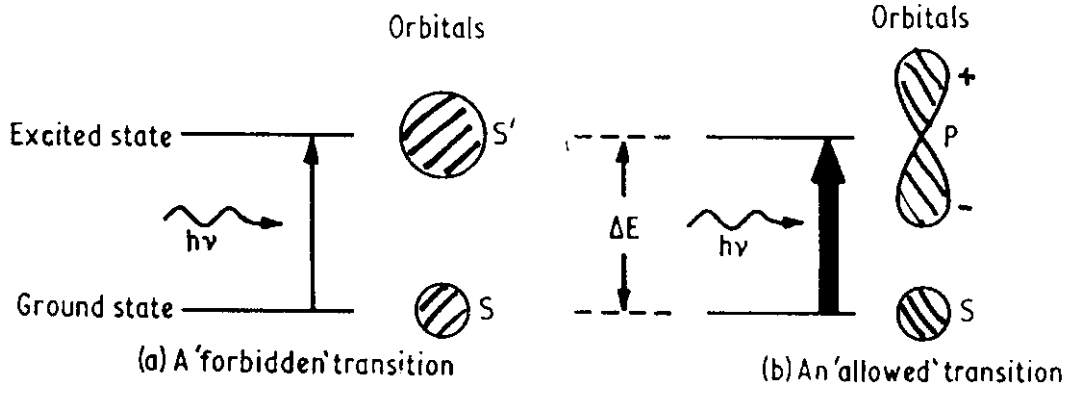

Electronic Transitions II

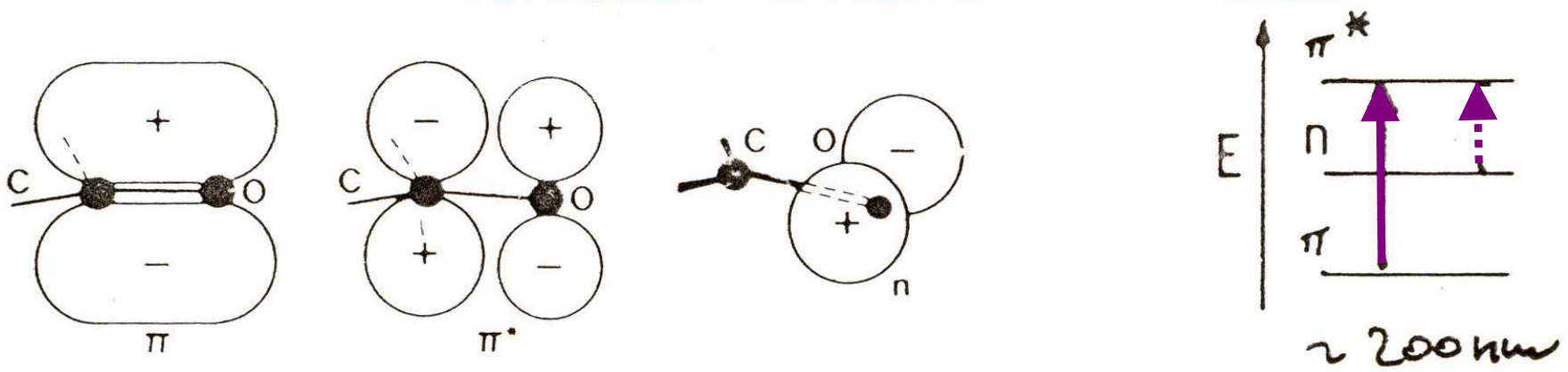

π, π*, and n molecular orbitals of the C=O group and their relative energies.

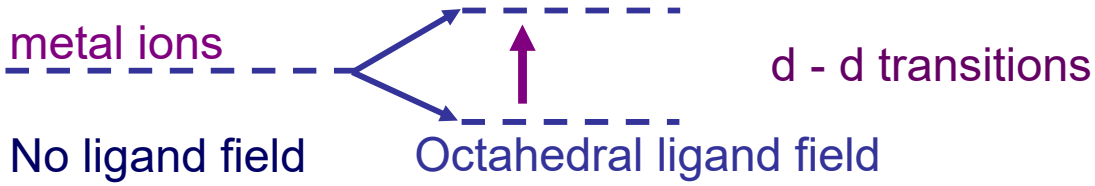

d-orbitals

Electronic Transitions III

Far UV: ≤ 200 nm	- amino acid side chains, backbone
Near UV: 200 – 400 nm	- small conjugated systems (Tyr, Trp, Phe, pyrolle …)
Visible/NIR: 400 – 700+ nm	- metal d-d transitions (weak, forbidden)
	- charge transfer (ligand-metal / metal ligand)
	- large aromatic structures (conjugated π-electron systems, e.g., heme, chlorophyll, retinal): absorption wavelength depends on degree of delocalization

Free Electron Model I

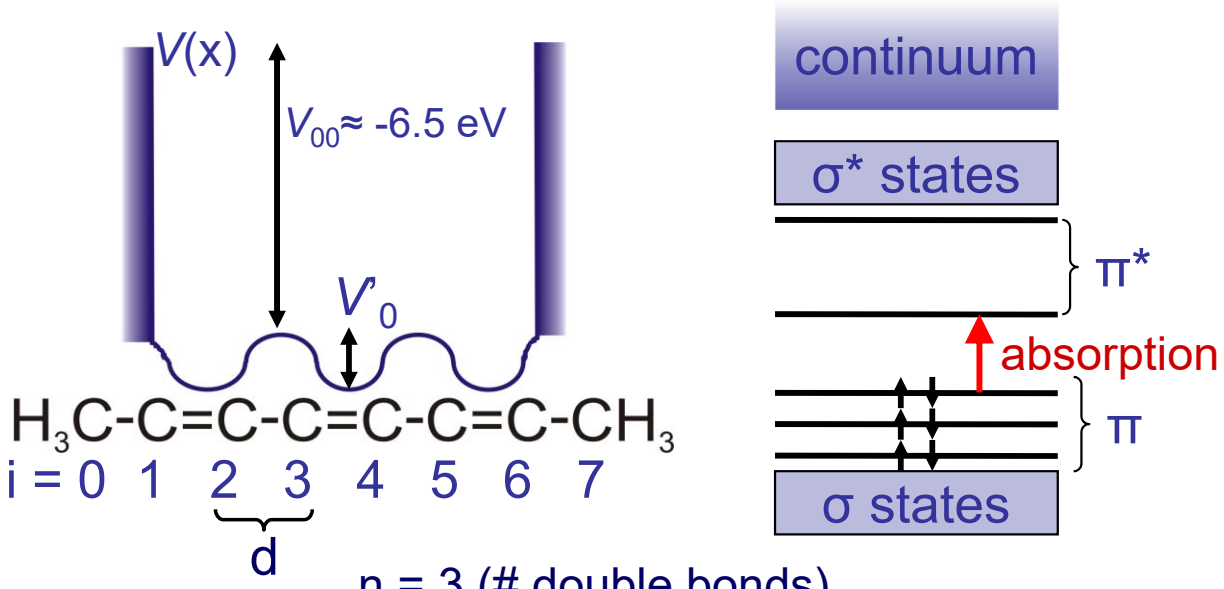

n = 3 (# double bonds)

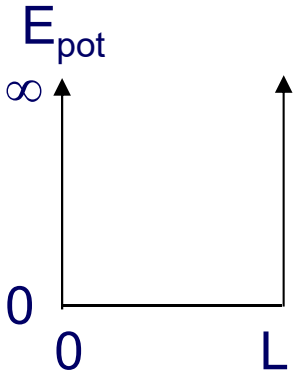

Particle in a box, L = (2n+1)d, flat bottom

S.E.: $\frac{-\hbar^2}{2m_e}\frac{d^2\Psi(x)}{dx^2} = E\,\Psi(x)$

quantum # r = 1, 2, 3…

$$\Psi_r(x) = \sqrt{\frac{2}{(2n+1)d}}\sin\frac{\pi r x}{(2n+1)d} \qquad E_r = \frac{h^2 r^2}{8m_e d^2 (2n+1)^2}$$

Free Electron Model II

More realistically: R(–C=C–) = 1.35 Å
R(–C–C–) = 1.46 Å

➔ wiggly bottom

$$\Delta E = E_{r+1} - E_r = \frac{h^2}{8m_e d^2}\frac{(2r+1)}{(2n+1)^2} + 0.83\left(1-\frac{1}{2n}\right)V_0'$$

correction factor, V_0' = 2.45 eV

Hans Kuhn, J. Chem. Phys. 17 (1949) 1198.

Lowest energy absorption band: here 3 → 4; r = n (in general)

$$\Delta E_{abs} = \frac{h^2}{8m_e d^2}\frac{1}{2n+1}$$

$$\lambda_{abs} = \frac{hc}{\Delta E_{abs}} = \frac{8m_e cd}{h}\cdot \underbrace{d(2n+1)}_{L}$$

Delocalized Electron Systems: Conjugated Hydrocarbon Chains

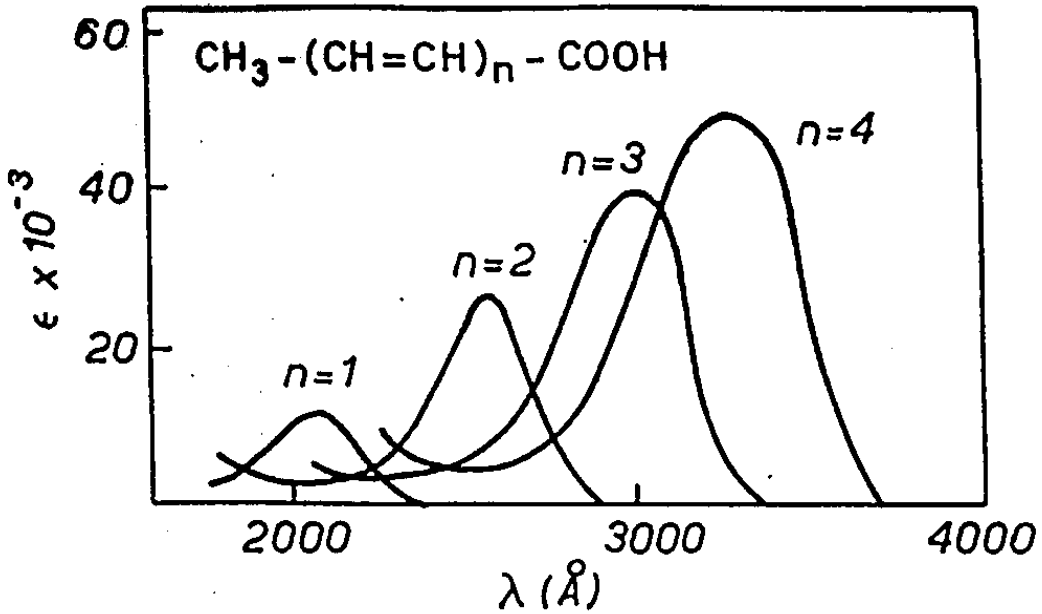

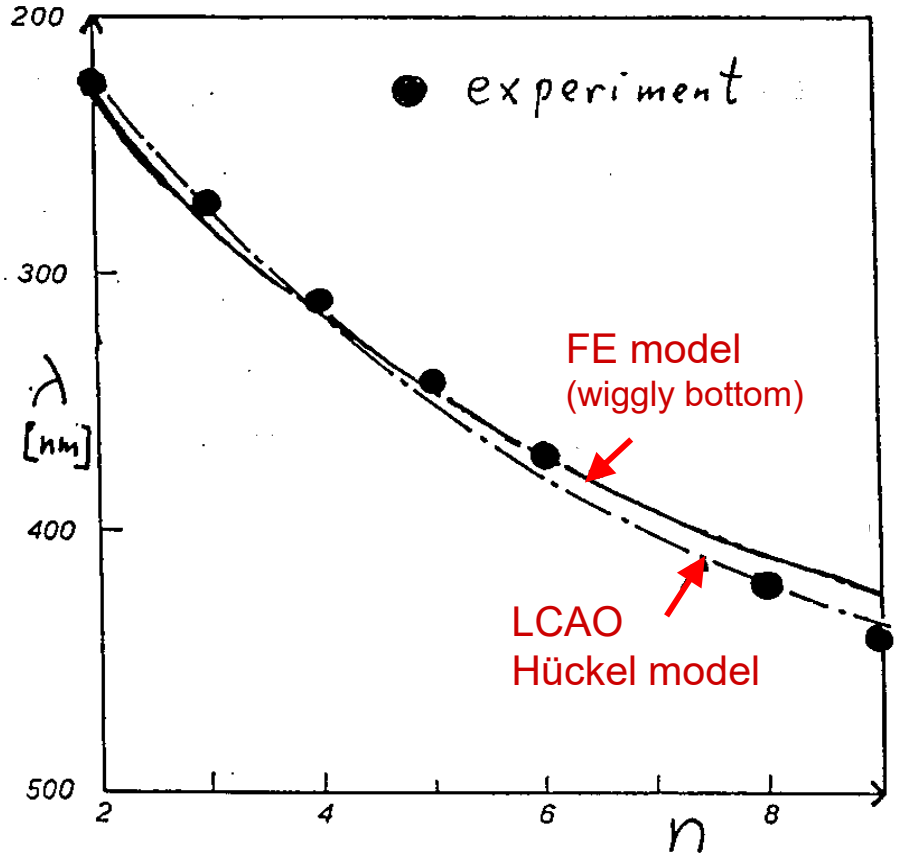

Heme-Light Interaction I

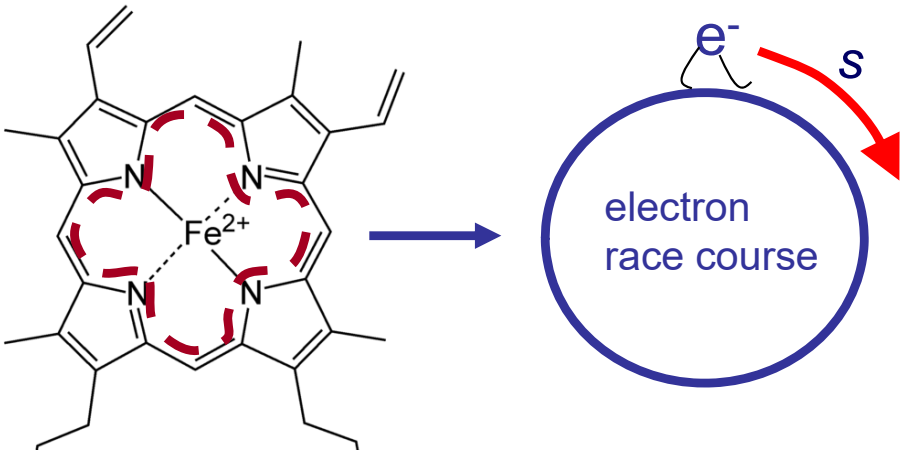

- Heme: Fe^{2+}
- Chlorophyll: Mg^{2+}
- Vitamin B12: Co^{2+}

Simplest model of electronic structure:

-1D electron gas

-18 free electrons:

12 C × 1 = 12 bound @ Fe^{2+}

4 N × 2 = 8

20 - 2 = 18

- Schrödinger Equation:

$$-\frac{\hbar^2}{2m_e}\frac{d^2\Psi}{ds^2} = E\Psi$$

kinetic energy

$$T = \frac{L^2}{2I} = \frac{r^2 p^2}{2m_e r^2}$$

- periodic boundary conditions:

$$\Psi(s) = \Psi(s+L)$$

L: circumference

$$\Psi(s) = N\exp(2\pi i m s / L)$$

Quantum number *m* = 0, ±1, ± 2, ± 3…

Heme-Light Interaction II

- insertion of ψ into Schrödinger Eq.:

$$E_m = \frac{2\pi^2\hbar^2}{m_e L^2} m^2$$

m: orbital angular momentum quantum #

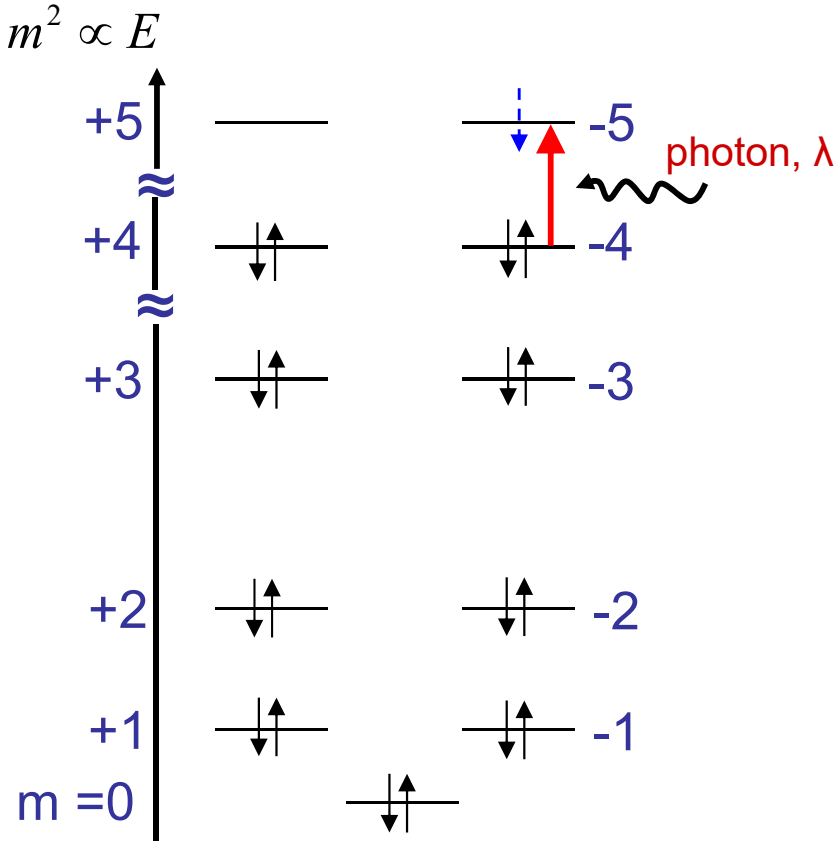

C - C C - N

L = 8 × 1.4 Å + 8 × 1.3 Å ≈ 22 Å

Heme contains altogether 18 delocalized electrons (20 π – 2(Fe^{2+})).

$$\Delta E_{4\to5} = \hbar\omega = \frac{hc}{\lambda} = E_5 - E_4$$

$$\lambda = \frac{m_e c L^2}{9\pi\hbar} = 440 \text{ nm}$$ purple

Electronic Transitions between Molecular Orbitals

Formaldehyde

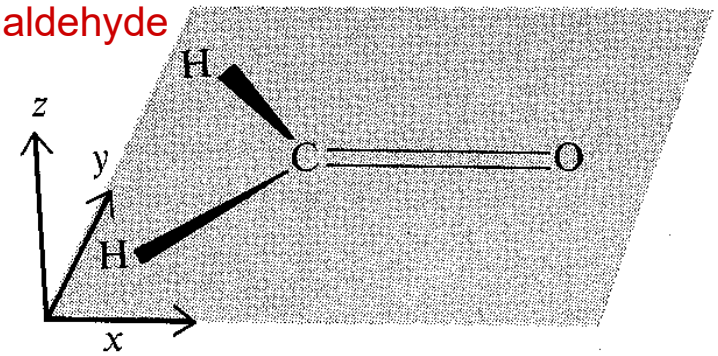

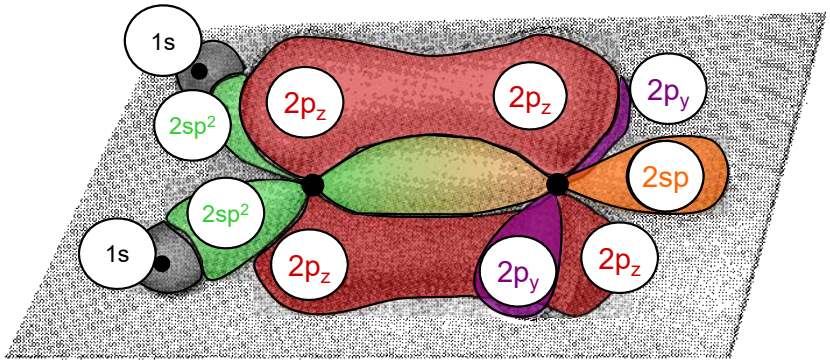

H → 1s

C → $1s^2\ 2s^2\ 2p_x\ 2p_z$ → $1s^2\ 2(sp^2)^3\ 2p_z$ Hybridization!

O → $1s^2\ 2s^2\ 2p_x\ 2p_y^2\ 2p_z$ → $1s^2\ 2(sp)^3\ 2p_y^2\ 2p_z$ Hybridization!

According to more recent MO calculations (2013)

σ bonds between C-H, σ bond between the third $2sp^2$ orbital of C with 2sp of O. A π bond is formed from $2p_z$ of C and O. Two electrons remain in the $2p_y$ orbital of O (lone pair).

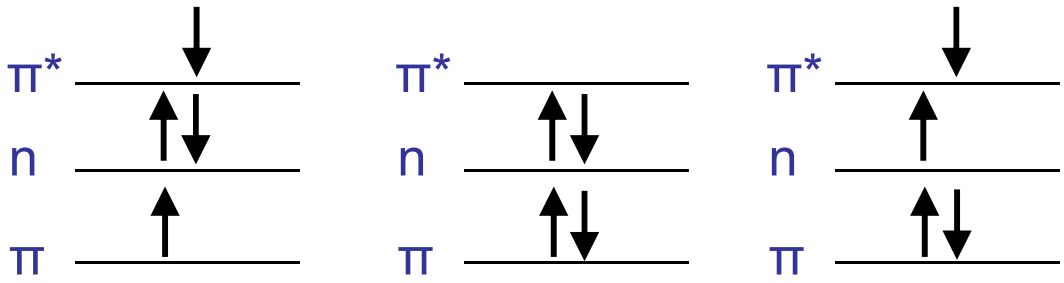

excited state
π → π*

ground state

excited state
n → π*

Linear combination of atomic orbitals (LCAO)

$$\Psi_{\pi} = 2p_z(C) + 2p_z(O)$$

$$\Psi_{\pi^*} = 2p_z(C) - 2p_z(O)$$

Transition Dipole Moments - Symmetries

Evaluation of $\langle \Psi_{\pi^*} | \vec{\mu} | \Psi_{\pi} \rangle$ and $\langle \Psi_{\pi^*} | \vec{\mu} | \Psi_{n} \rangle$ from symmetry

Example: $\langle \Psi_{\pi^*} | \vec{\mu}_{\|\vec{x}} | \Psi_{\pi} \rangle = \int \Psi^*_{\pi^*} e\,\vec{x}\,\Psi_{\pi}\, d^3\vec{r}$

If integrand is even → matrix element non-zero
If integrand is odd → matrix element = 0 (i.e., transition is forbidden)

Function:	Viewed along: *x* axis	Viewed along: *y* axis	Symmetry reflected through: *xy*	*xz*	*yz*
Molecular orbitals					
π		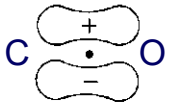	Odd	Even	Even
π^*	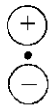	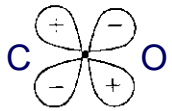	Odd	Even	Odd
n	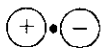		Even	Odd	None
Dipole operators					
$\underset{\sim}{\mu}_x$		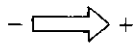	Even	Even	Odd
$\underset{\sim}{\mu}_y$			Even	Odd	Even
$\underset{\sim}{\mu}_z$	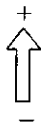	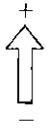	Odd	Even	Even

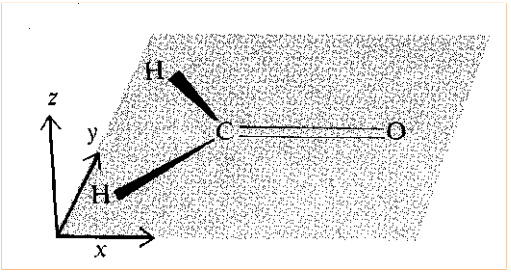

Results

π → π*

1. $\langle \pi | \underset{\sim}{\mu_x} | \pi^* \rangle$ is not zero – the product of the symmetries of π, π^*, and μ_x is even, whether we reflect through the xy, yz, or xz planes;
2. $\langle \pi | \underset{\sim}{\mu_y} | \pi^* \rangle$ is zero because the net symmetry is odd when reflected through either the xz or the yz plane;
3. $\langle \pi | \underset{\sim}{\mu_z} | \pi^* \rangle$ also is zero because it has odd symmetry when reflected through either the xy or yz plane.

n → π*

1. $\langle n | \underset{\sim}{\mu_x} | \pi^* \rangle$ is zero because it has odd symmetry when reflected in either the xy or the xz plane;
2. $\langle n | \underset{\sim}{\mu_y} | \pi^* \rangle$ is zero because it is odd in the xy plane;
3. $\langle n | \underset{\sim}{\mu_z} | \pi^* \rangle$ is zero because it is odd in the xz plane.

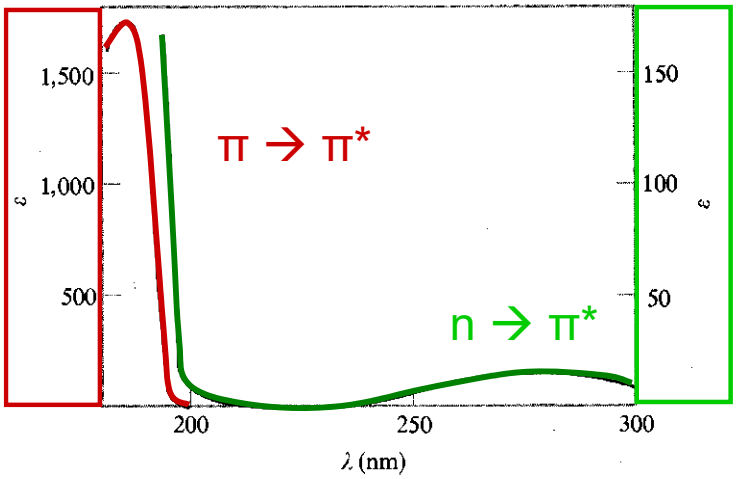

Absorption spectrum of acetone (CH3-CO-CH3) in n-hexane.

Solvent Polarity Effects

- Intensity, band shape, peak wavelength of absorption bands depend on solvent.
- Quantitative analysis of solvent effects is very difficult.
- In general, the presence of solvent lowers the energy levels.
- To produce a band shift, ground state and excited state levels must be shifted to a different extent.
- Solvent configuration minimizes the ground state energy.
- Excitation $\tau = 10^{-15}$ s, configurational changes cannot occur, but the electronic polarizability of the solvent can respond.
- The state with the highest dipole moment will be preferentially lowered by a polar solvent; this is almost always the excited state → red shift on π → π* transition.

  (when solvent polarizability dominates)
- For an n → π* transition, the lone pair orbital often hydrogen-bonds to the solvent. In this case, a blue shift occurs.

$\Delta E_\pi < \Delta E_{\pi^*}$

$\Delta E_n > \Delta E_{\pi^*}$

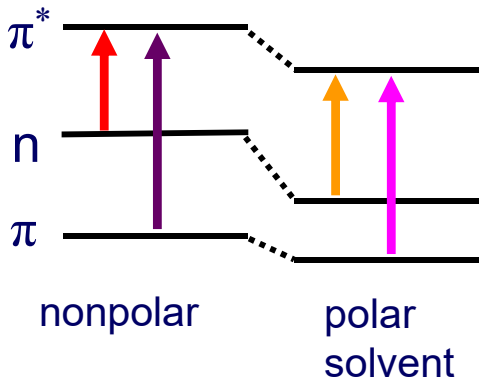

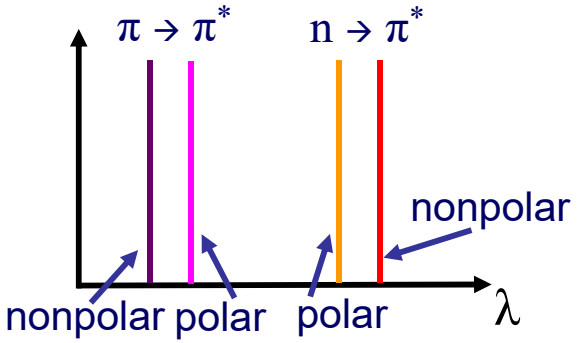

Coupling to Vibrations (classical)

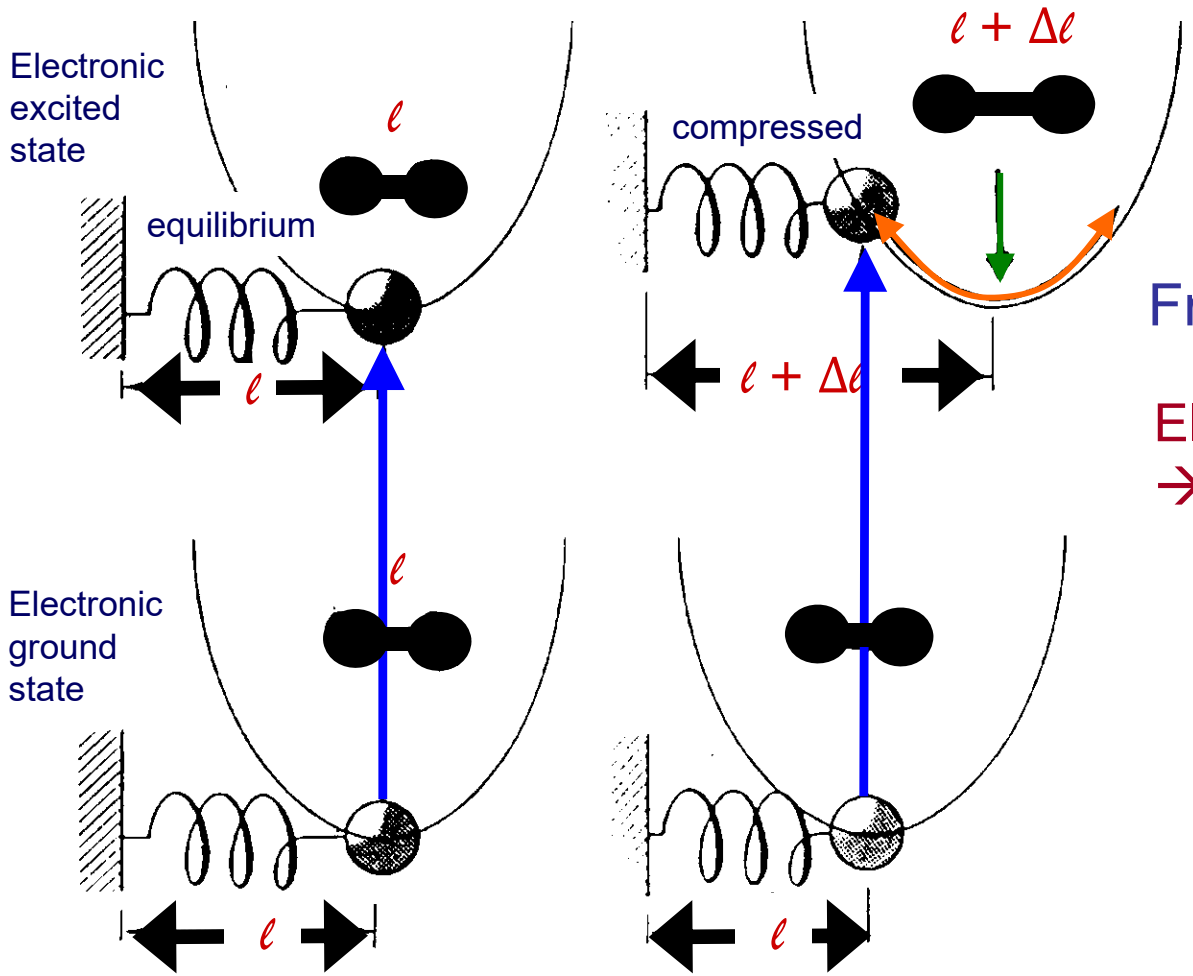

Franck-Condon principle:

Electrons move faster than nuclei
→ vertical transitions!

$$\tau_{exc} \sim 1 \text{ fs}$$

$$\tau_{vib} \geq 10 \text{ fs}$$

Coupling to Vibrations (QM)

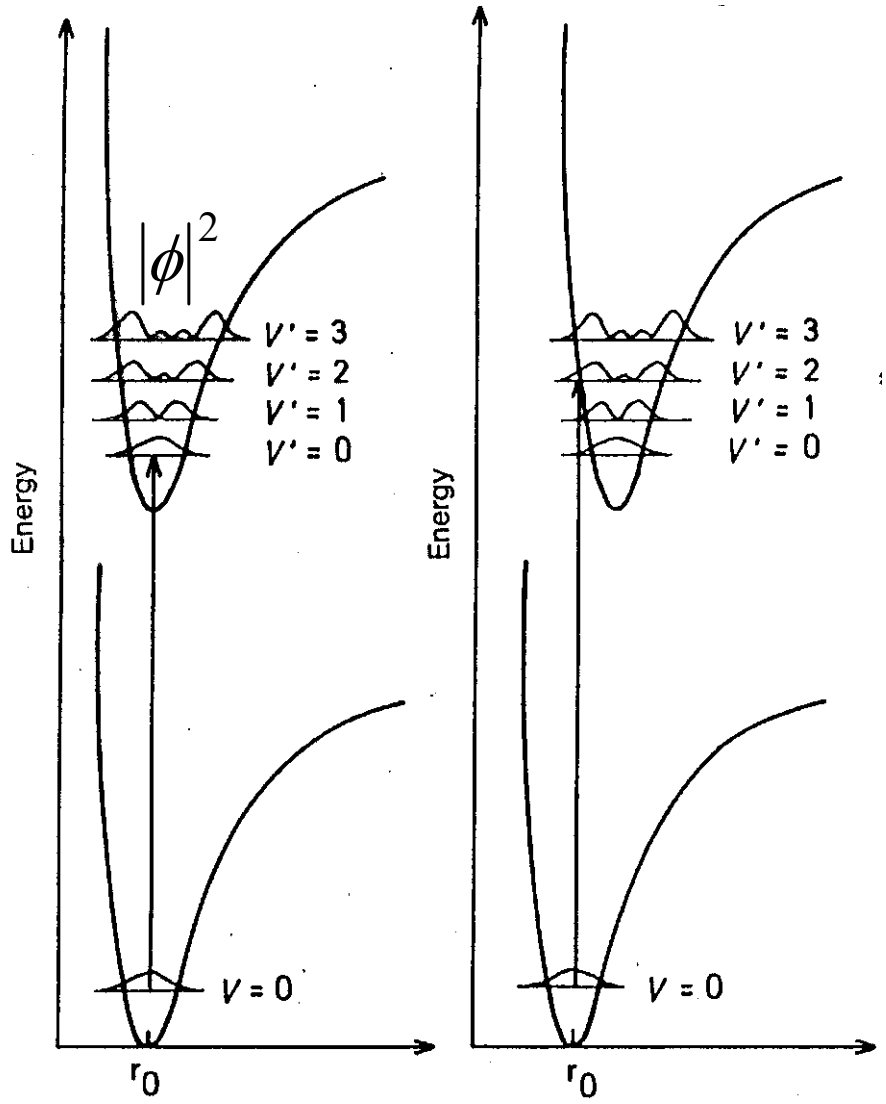

Internuclear distance:

equal in upper and lower states

greater in upper than in lower states

Born-Oppenheimer Approximation:
(BOA)

$$\Psi(\vec{r},\vec{R}) = \Psi_e(\vec{r},\vec{R})\,\phi_N(\vec{R})$$

electronic wavefunction

nuclear wavefunction

Franck-Condon Factor

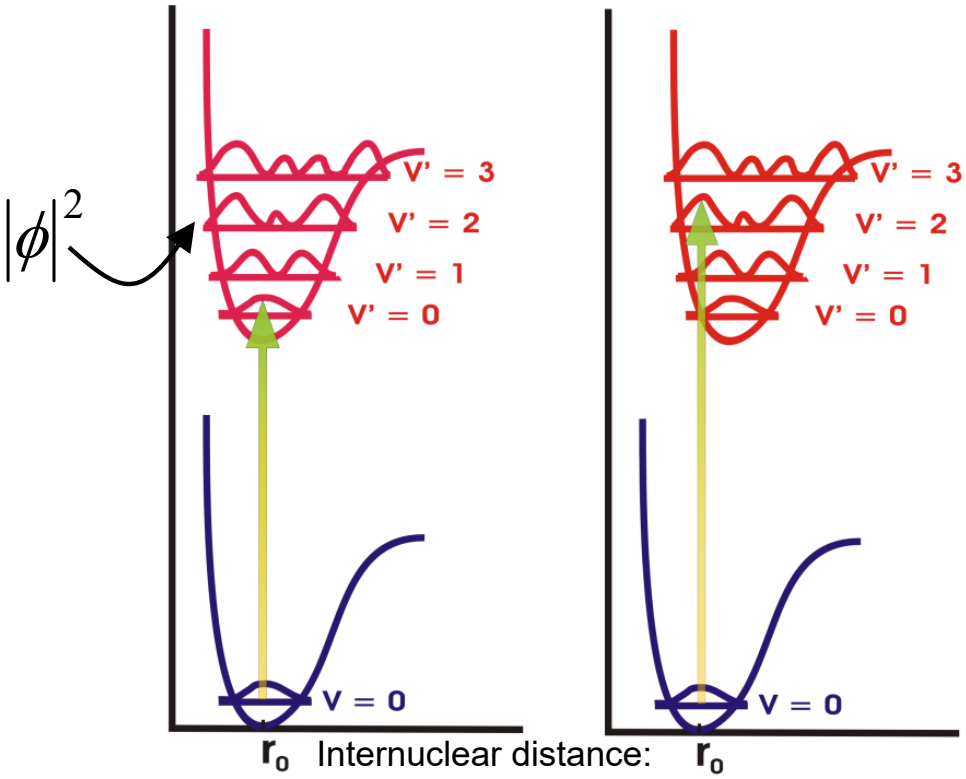

$$\vec{\mu} = -\langle j | e\vec{r} | i \rangle$$

$$= -e \iint \Psi_j^*(\vec{r}) \phi_j^*(\vec{R}) \vec{r} \Psi_i(\vec{r}) \phi_i(\vec{R}) d^3\vec{r} d^3\vec{R}$$

$$= -e \int \Psi_j^*(\vec{r}) \vec{r} \Psi_i(\vec{r}) d^3\vec{r} \cdot \int \phi_j^*(\vec{R}) \cdot \phi_i(\vec{R}) d^3\vec{R}$$

Franck-Condon factor

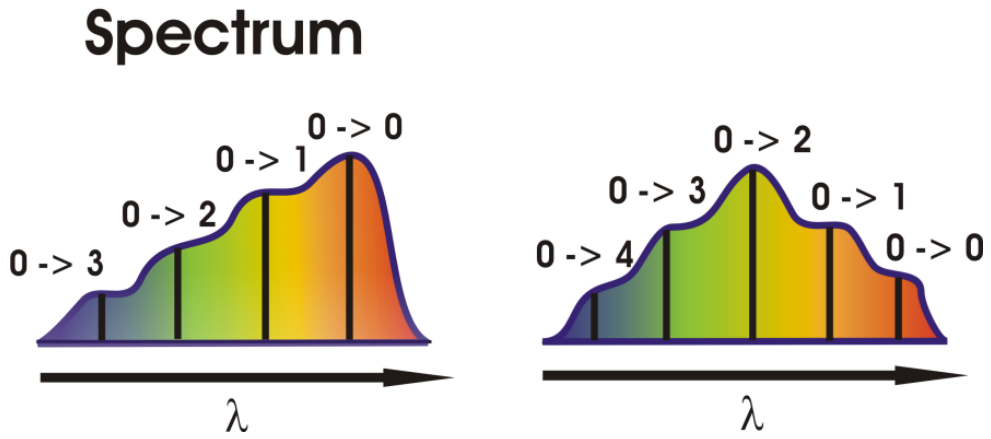

The Franck-Condon factor indicates the overlap of the nuclear wavefunctions of the two states involved in the electronic transition.

Energy Levels of Small Molecules

BOA: $\Psi = \Psi_e(r;R)\cdot\phi_n(R)$

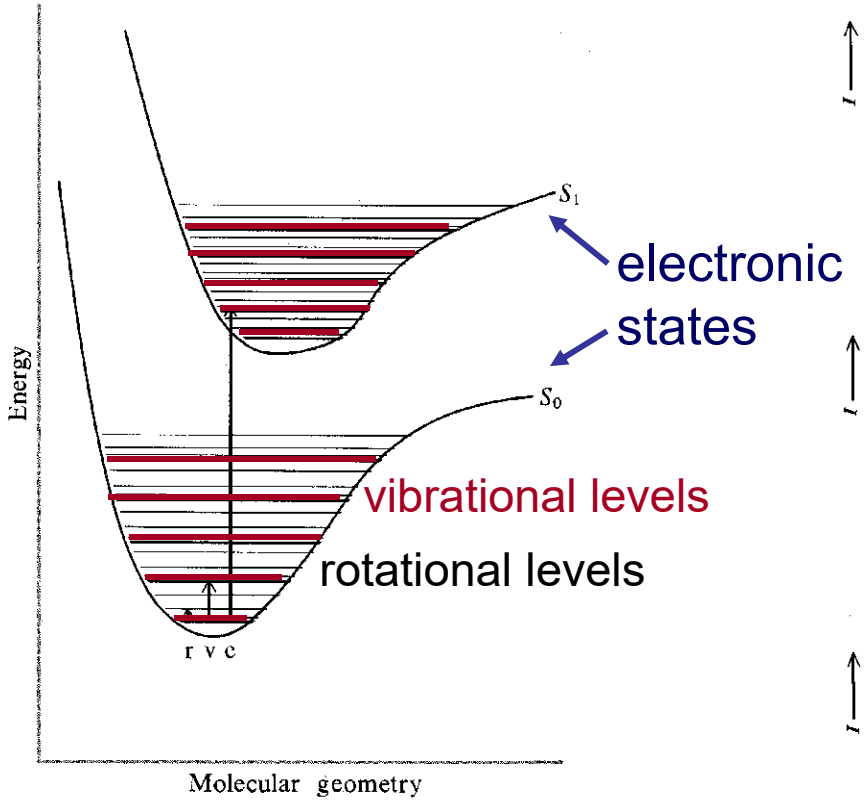

These bands are mainly vibronic in nature (C_6H_6 has 30 vibrational modes)

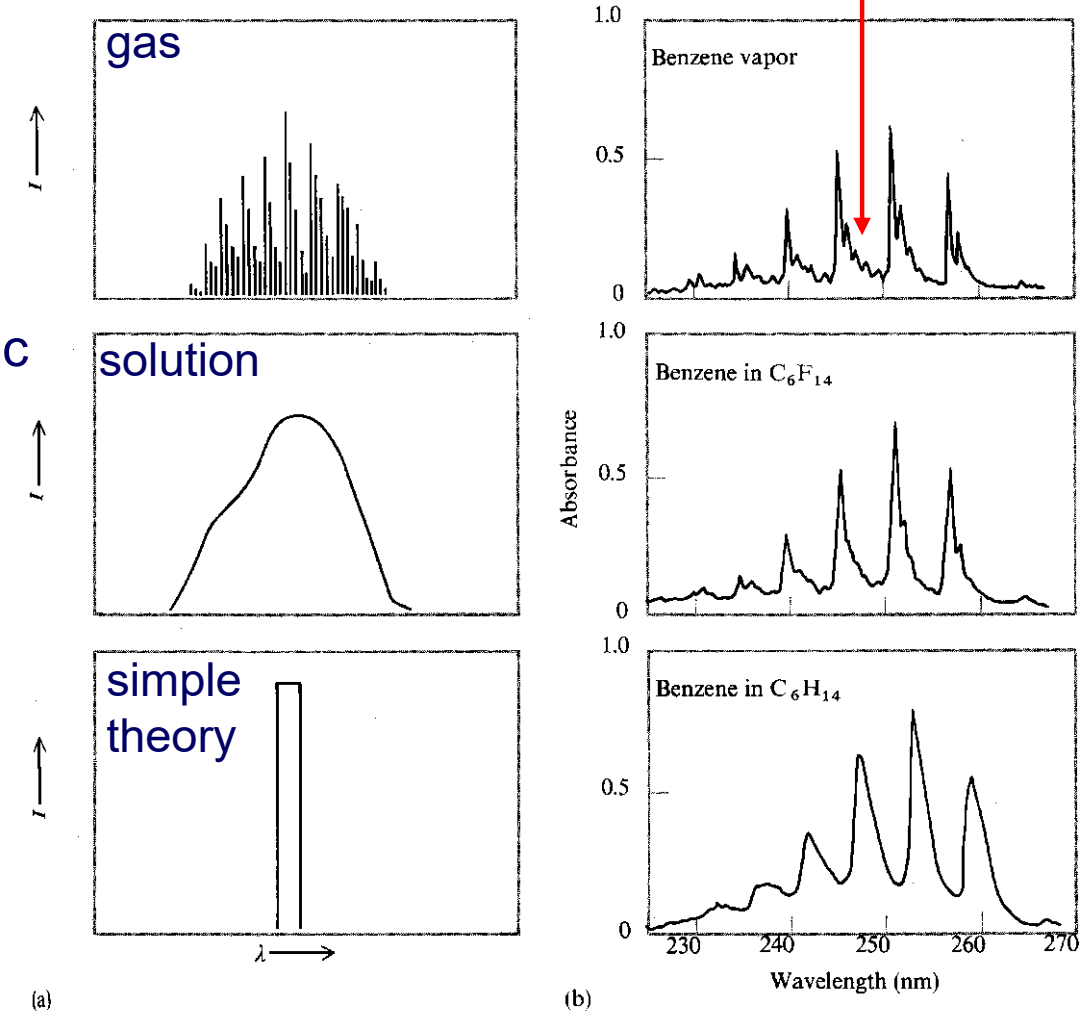

solvent broadening

Jablonski Diagram

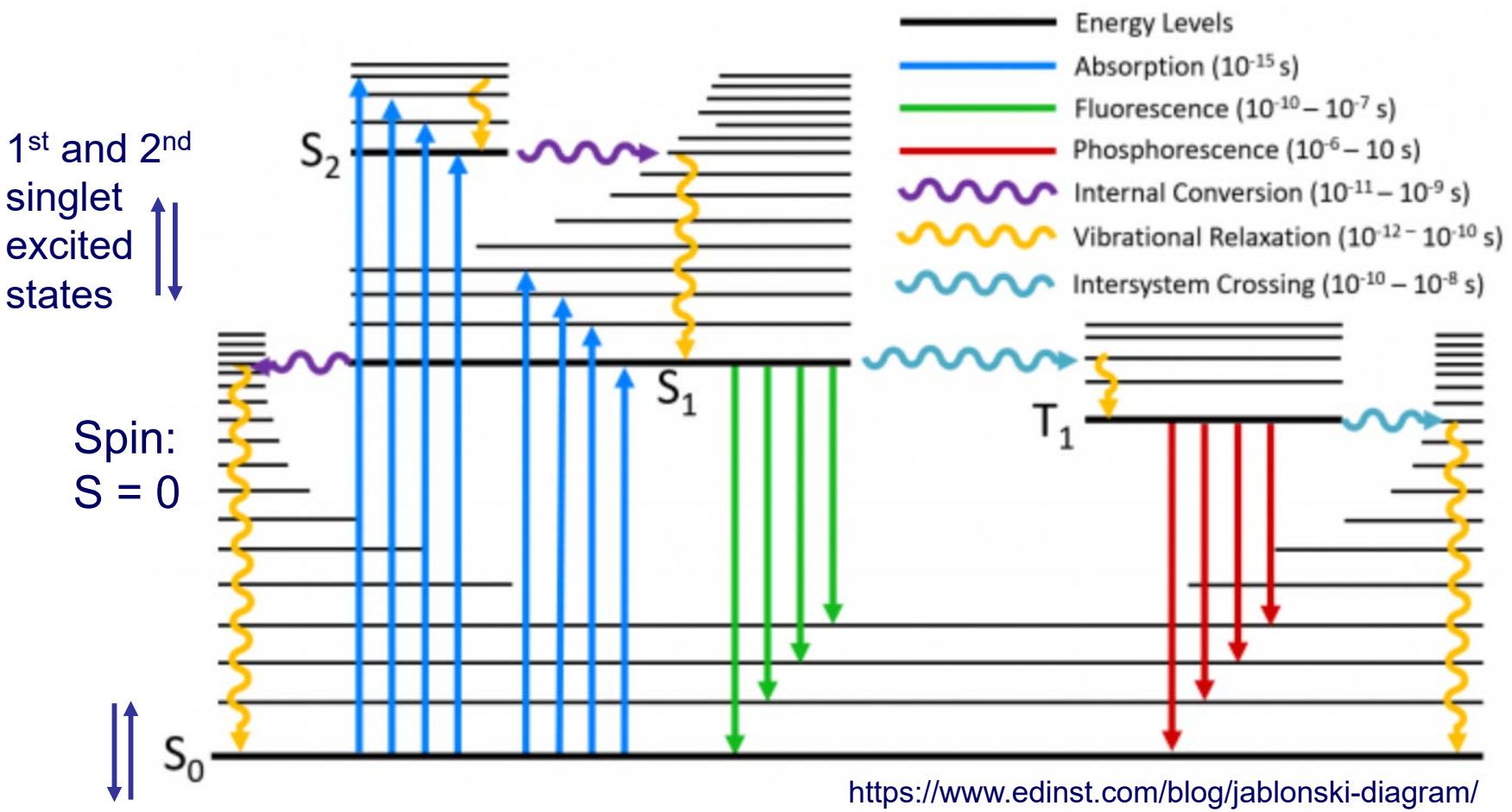

1st and 2nd singlet excited states

Spin: S = 0

triplet state: S = 1 m_s = -1, 0, 1

Singlet ground state

https://www.edinst.com/blog/jablonski-diagram/

Internal conversion: non-radiative change of electronic state

Fluorescence/Phosphorescence

Fluorescence

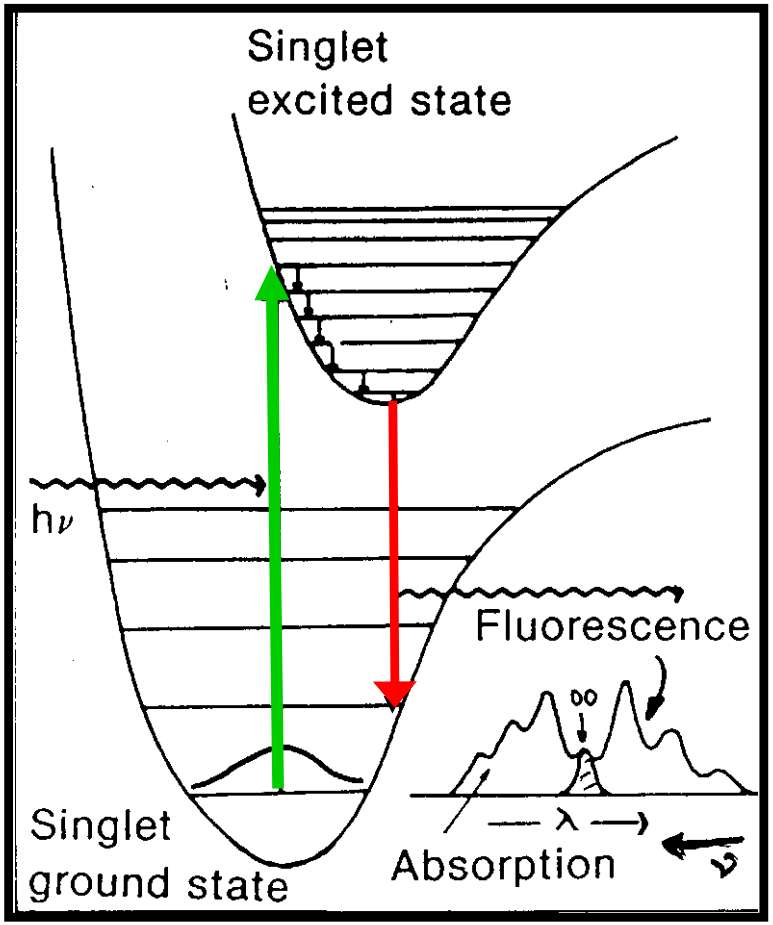

Phosphorescence

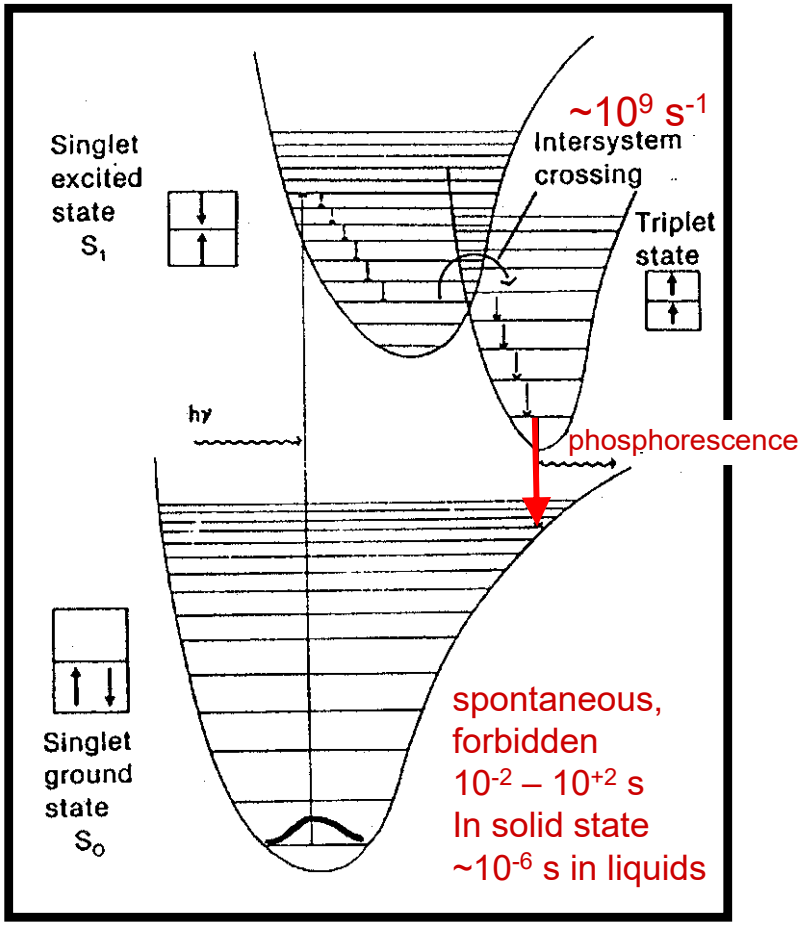

Biophysics II

Introduction:
How Proteins Interact with Light

Uli Nienhaus

Prof. G. U. Nienhaus, Vorlesungsunterlagen Biophysik II, SS 2023.
Nur zum KIT-internen, vorlesungsbegleitenden Gebrauch.
Weitergabe und anderweitige Nutzung verboten.

Absorption Spectroscopy

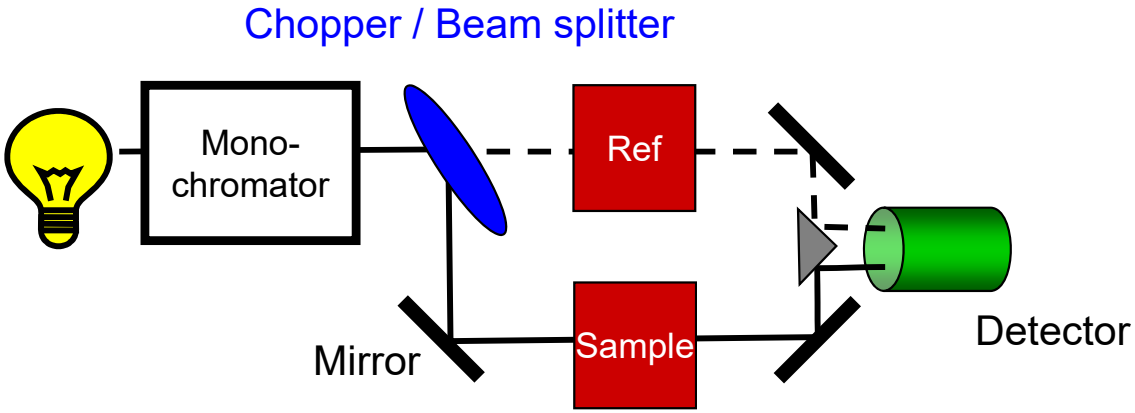

Applications:

- measure concentrations
- structural information
- ionization
- chemical modification
- solvent influence
- conformational changes
- unfolding
- ligand binding
- …

Dual Beam Spectrometer:

$$I(l) = I_0 \cdot 10^{-\varepsilon l c}$$

$$A = \log \frac{I_0}{I(l)} = \varepsilon l c$$

path length

concentration

extinction coefficient

Beer-Lambert law

Absorption Spectra: Examples

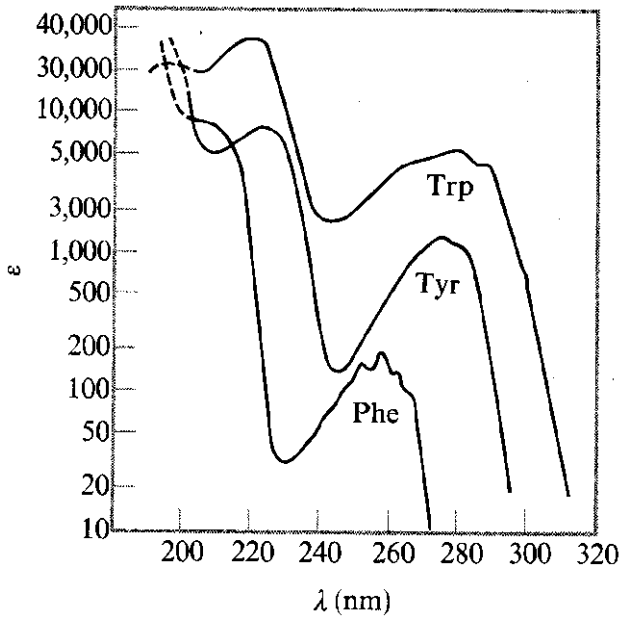

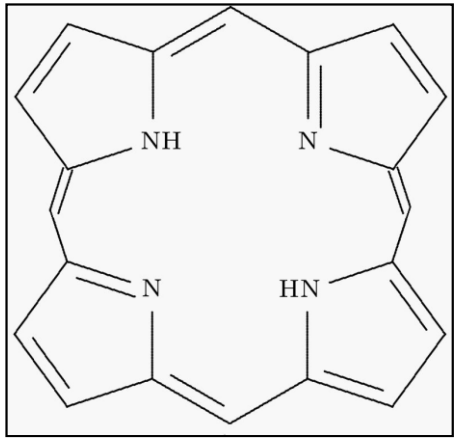

Spectrum of metal porphyrin (here: heme)

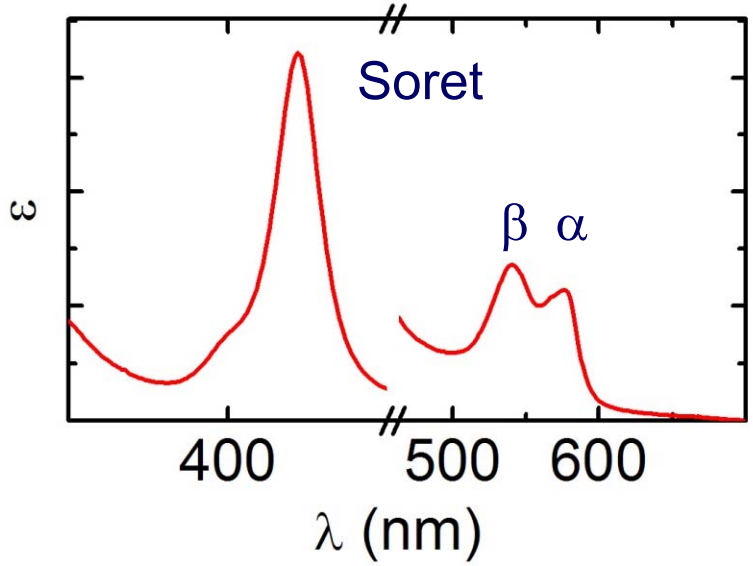

Aromatic amino acids:

1 mg/ml protein (rule of thumb!)

→ 1 OD @ 280 nm

→ 3 OD @ 230 nm

Peptide Bond Absorption

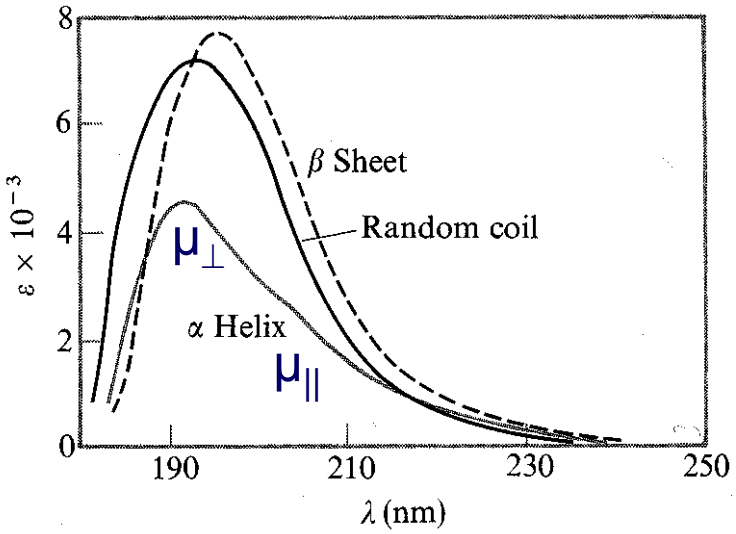

Absorption spectrum of poly-L-lysine in aqueous solution:

random coil pH 6.0, 25°C;
α-helix pH 10.8, 25°C;
β-sheet pH 10.8, 52°C.

(Rosenbeck and Doty, PNAS, 47,1775 (1961))

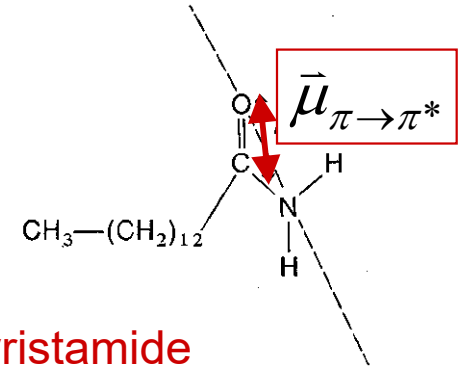

myristamide

n → π*: 210 – 220 nm, weak, ε_{max}= 100 [M^{-1} cm^{-1}]
π → π*: 190 nm ε_{max}= 7000 [M^{-1} cm^{-1}]
(n → σ*): 175 nm

Exciton Splitting

Interactions between identical chromophores (example: dimer)

$$\psi_{A\pm} = \frac{1}{\sqrt{2}}\left(\psi_{1a} \pm \psi_{2a}\right)$$

Hamiltonian: $H = H_1 + H_2 + V$

$$V = \frac{\vec{\mu}_1 \cdot \vec{\mu}_2}{R_{12}^3} - 3\frac{\left(\vec{\mu}_1 \cdot \vec{R}_{12}\right)\left(\vec{\mu}_2 \cdot \vec{R}_{12}\right)}{R_{12}^5}$$

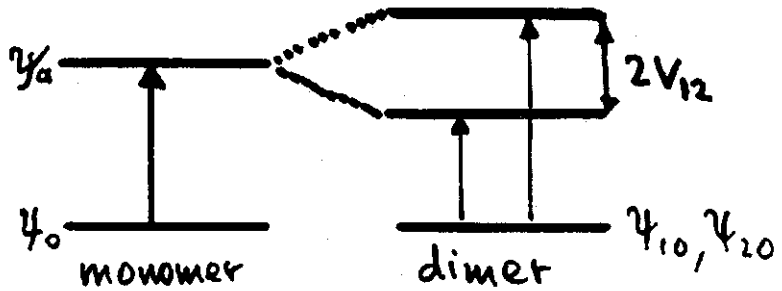

Interaction leads to level splitting:

$$E_+ = E_a + V_{12}$$
$$E_- = E_a - V_{12}$$

$$V_{12} = \left\langle \psi_{1a} \middle| V \middle| \psi_{2a} \right\rangle$$

$$\psi_0 = \phi_{10}\phi_{20}$$
$$\psi_{1a} = \phi_{1a}\phi_{20}$$
$$\psi_{2a} = \phi_{10}\phi_{2a}$$

Intensity of lines

$$D_{0A\pm} = \left| \left\langle \psi_0 \middle| \vec{\mu}_1 + \vec{\mu}_2 \middle| \psi_{A\pm} \right\rangle \right|^2 = D_{0a} \pm D_{0a}\cos\theta_{12}$$

dipole strength

Pyridine Dimer Geometries

Transition dipole orientations shown for $\psi_0 \rightarrow \psi_{A+}$

To obtain band intensity, add vectors and square the magnitude!

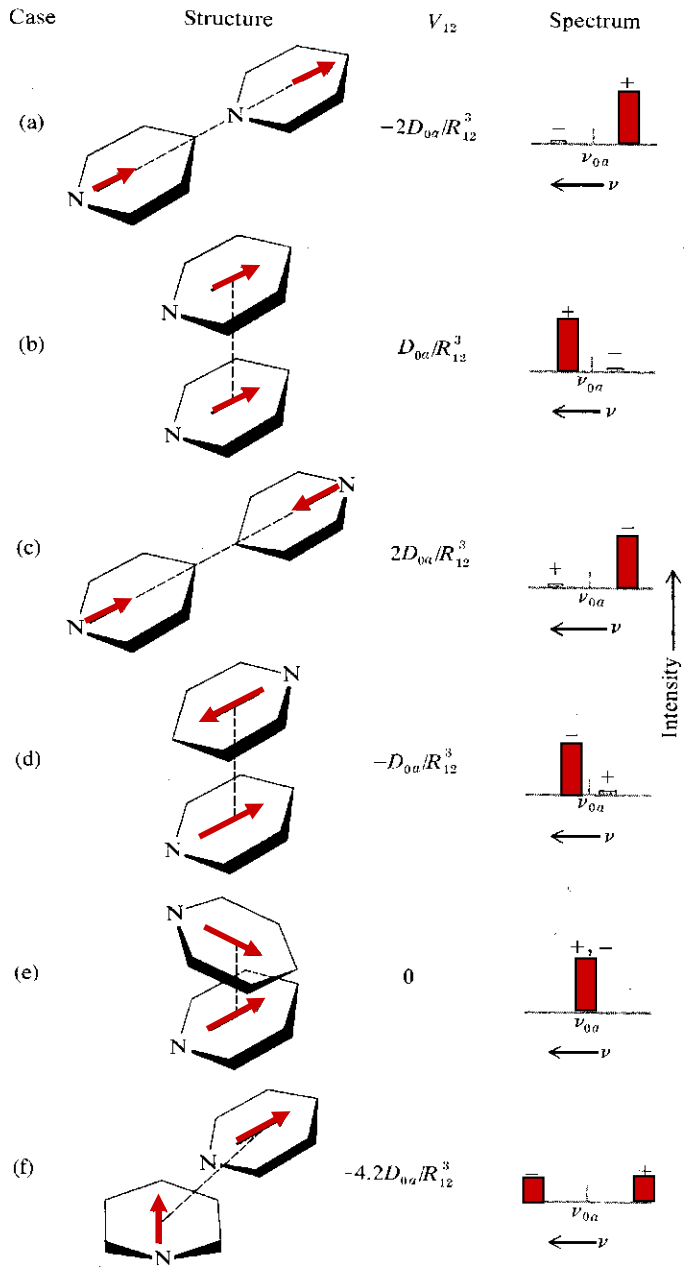

stacked, 90°

90°, in plane

cos θ = 1
$D_{0A+} = 2D_{0a}$
$D_{0A-} = 0$

cos θ = –1
$D_{0A+} = 0$
$D_{0A-} = 2D_{0a}$

cos θ = 0
and
$V_{12} = 0$

cos θ = 0
$V_{12} \neq 0$ (neg.)

Exciton Splitting: Example

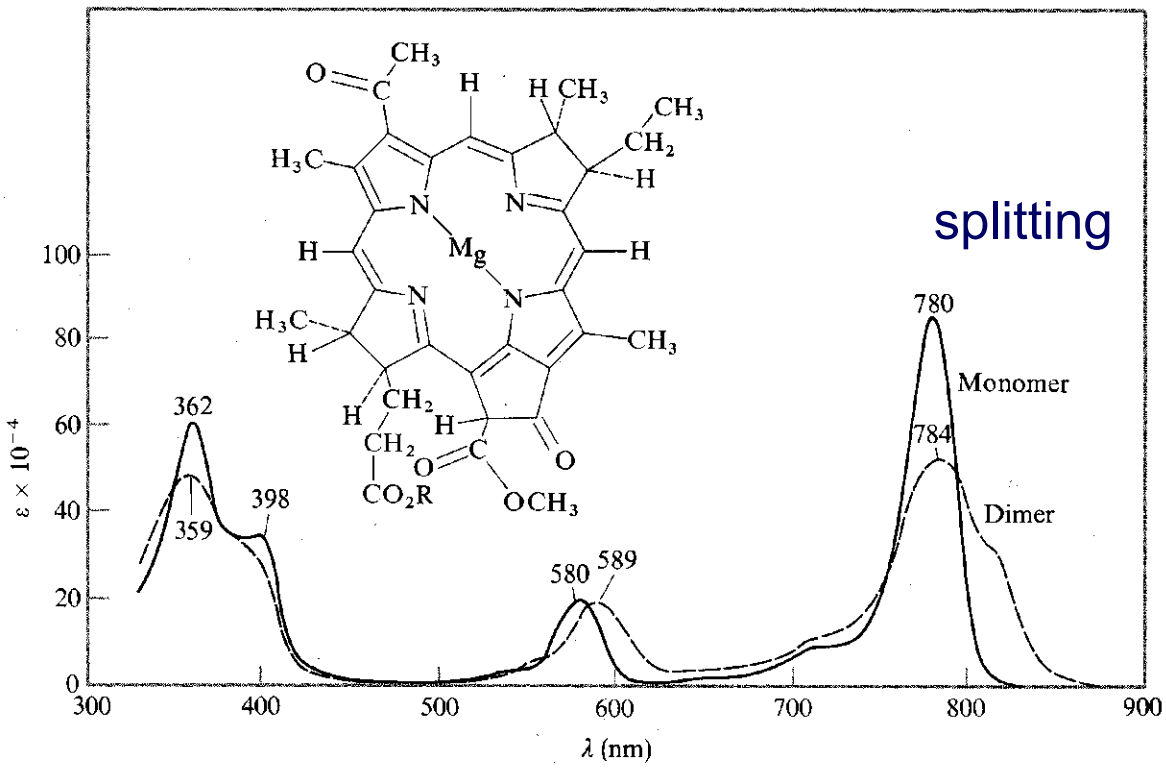

Monomer and dimer spectra of solutions of bacteriochlorophyll

Hypochromism and Hyperchromism

-Hypochromism ("less color") signifies that the absorption of the sample is less than that of the constituent parts.

-Hyperchromism ("more color") is the opposite effect.

-Hypo-/Hyperchromism is the result of the interaction of one particular electronically excited state of a given chromophore and different excited states of neighboring chromophores.

- Qualitatively:

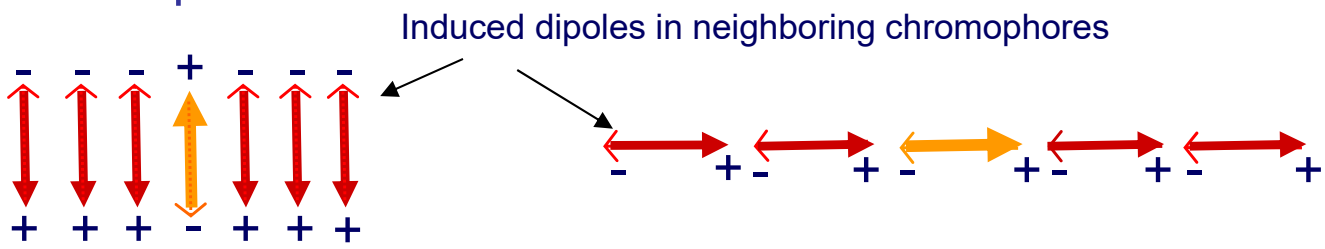

Hypochromism

Hyperchromism

(for excitation of lowest-energy electronic absorption band, so higher excited states will be in phase)

Linear Dichroism

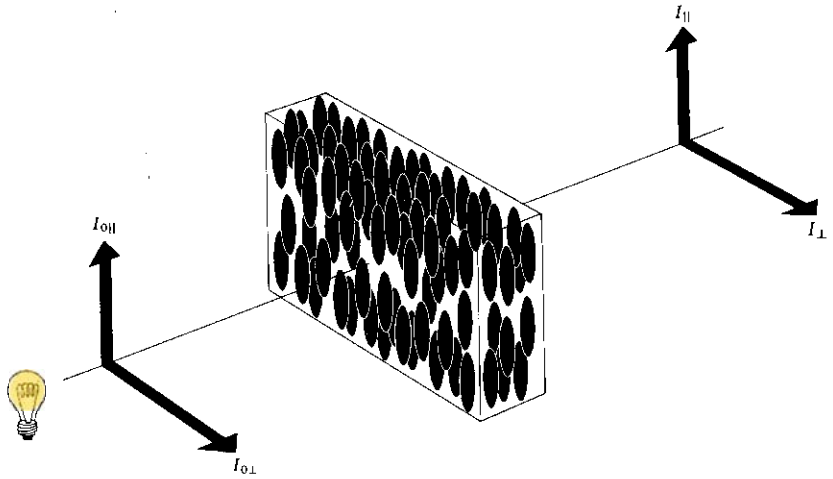

Absorption $\propto \left| \langle \psi_a | \vec{\mu} | \psi_0 \rangle \cdot \vec{E}_0 \right|^2$

In solution (unoriented samples), absorption is independent of polarization.

Oriented samples show linear dichroism: $A_{\parallel} \neq A_{\perp}$

→ structural information (films, crystals)

Dichroic ratio $d = \dfrac{A_{\parallel} - A_{\perp}}{A_{\parallel} + A_{\perp}}$

Linear Dichroism of the α-helix

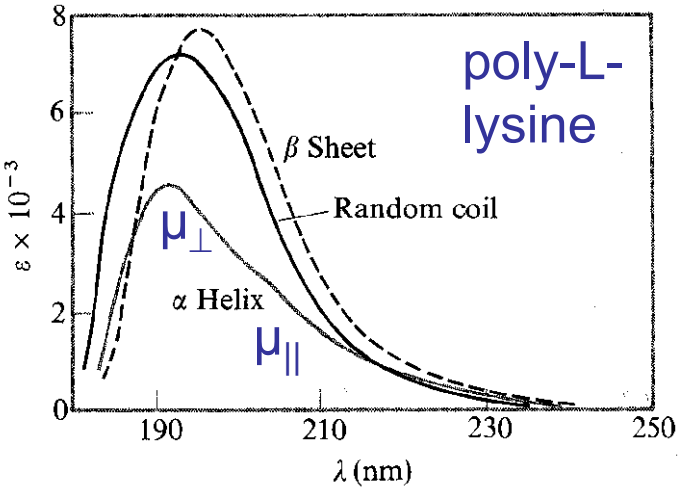

Three collective transition moments due to excitonic coupling

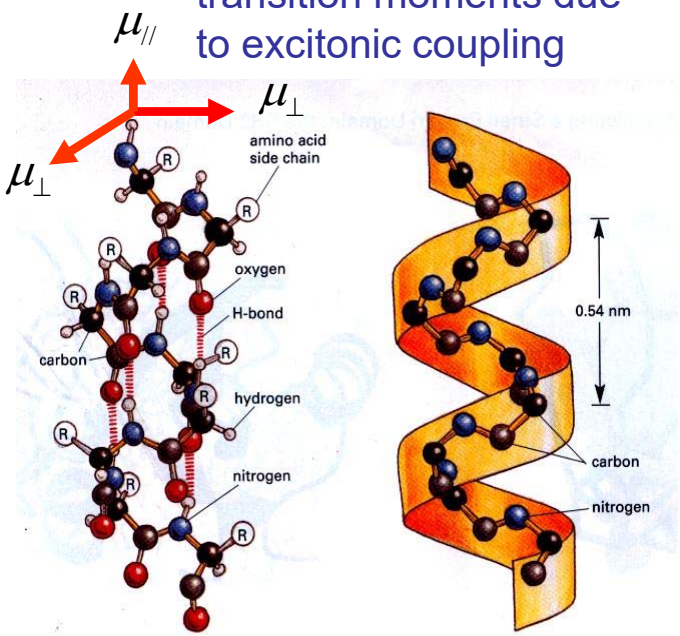

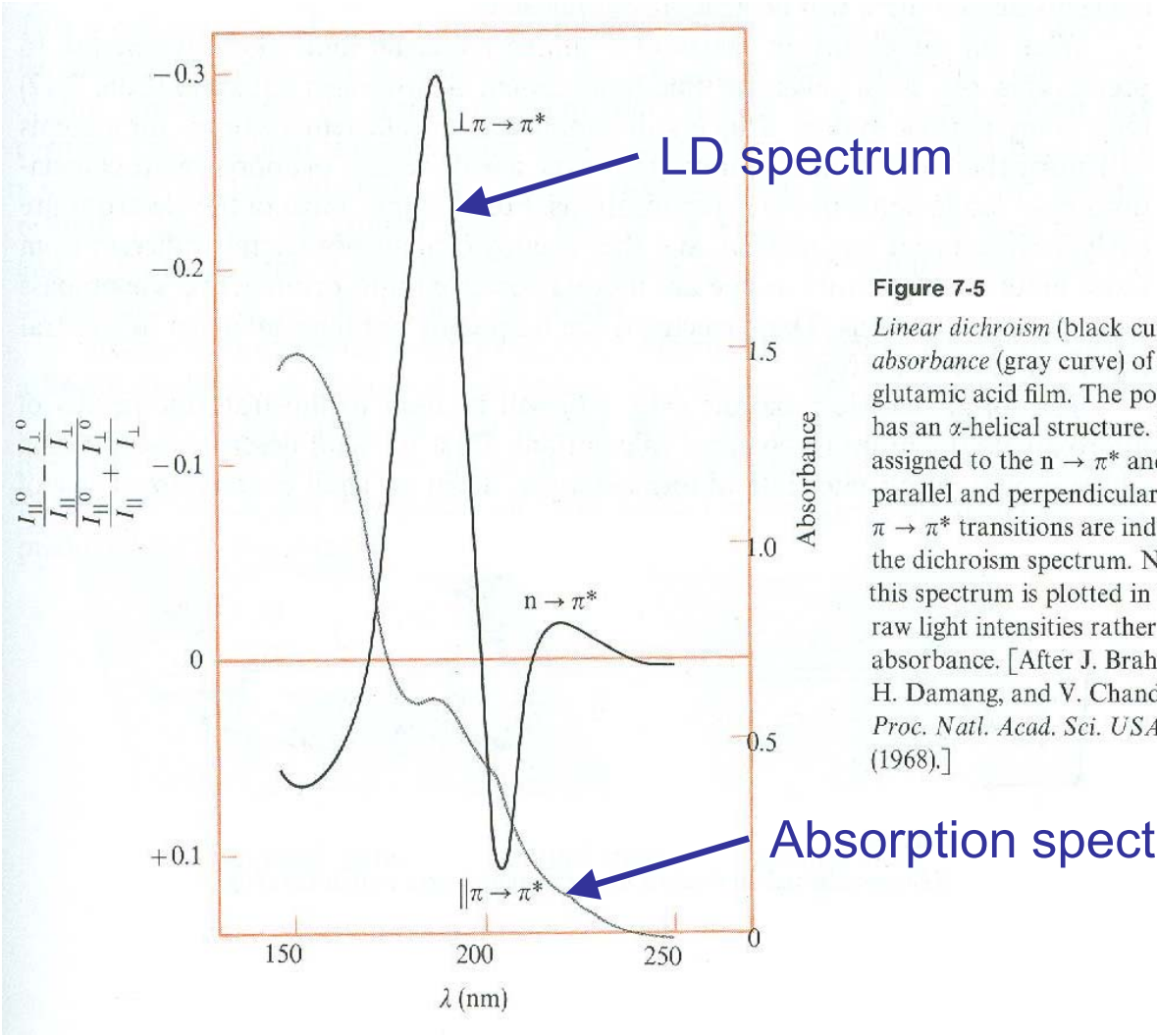

Figure 7-5

Linear dichroism (black curve) *and absorbance* (gray curve) of a poly-L-glutamic acid film. The polypeptide has an α-helical structure. Bands assigned to the n → π* and to the parallel and perpendicular polarized π → π* transitions are indicated on the dichroism spectrum. Note that this spectrum is plotted in terms of raw light intensities rather than absorbance. [After J. Brahms, J. Pilet, H. Damang, and V. Chandrasekharan, *Proc. Natl. Acad. Sci. USA* 60:1130 (1968).]

Optical Activity I

Optically active samples affect LCP and RCP light differently

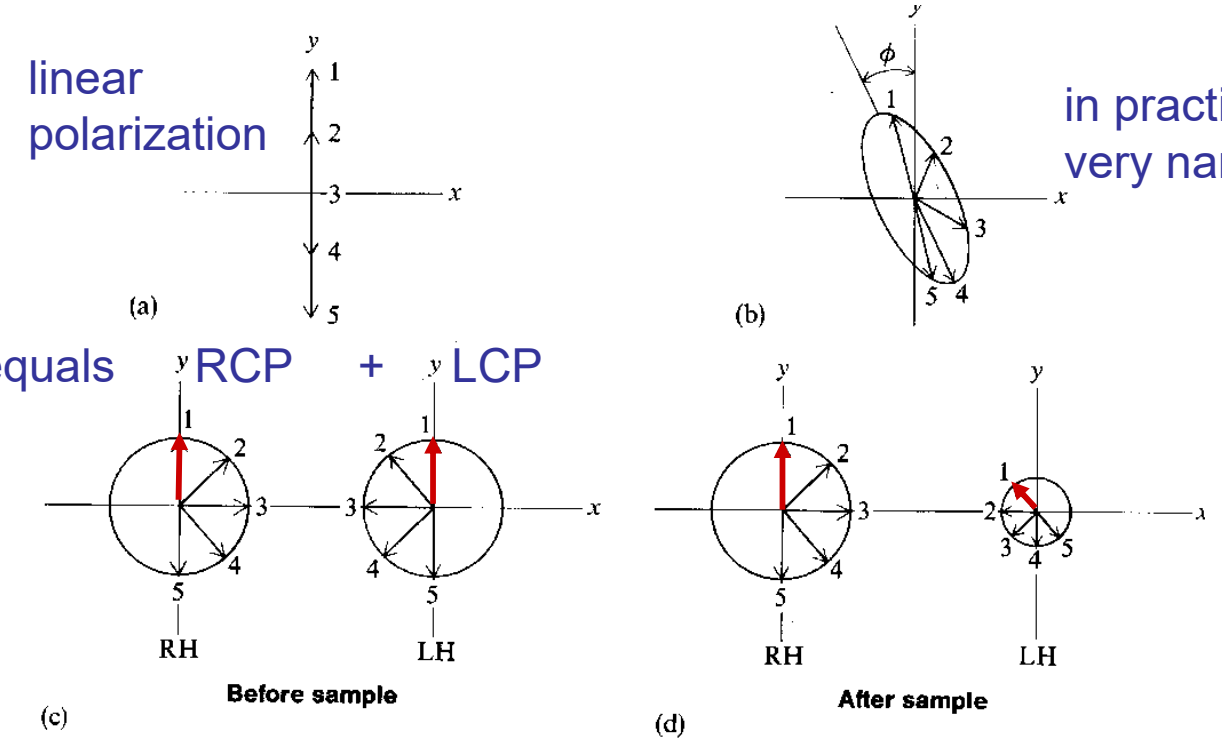

Two (coupled) effects:

- Refractive indices n_R and n_L are different (speed of light is different)
  ➔ polarization plane rotates by an angle Φ, Optical Rotatory Dispersion (ORD).
  (circular birefringence)

- Absorbances A_L and A_R for LCP and RCP are different, Circular Dichroism (CD).
  (ellipticity)

Optical Activity II

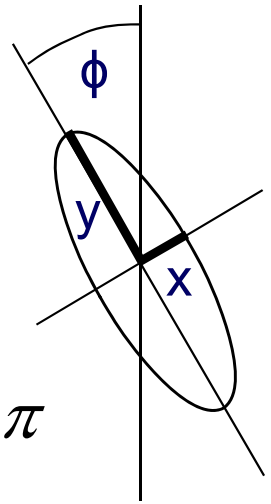

-Ellipticity: $\theta = \arctan\frac{x}{y}$

-Circular dichroism $\theta = 2.303(A_L - A_R)\cdot 180°/4\pi$

-Optical rotatory dispersion $\phi = (n_L - n_R)\frac{l}{\lambda}180°$

-Circular birefringence $n_L \neq n_R$

Small, difficult to measure directly!

Optical Activity III

Chromophores that lack symmetry show optical activity: "Chirality"

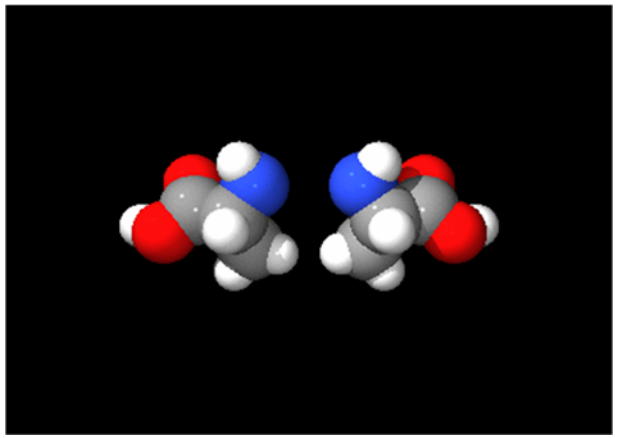

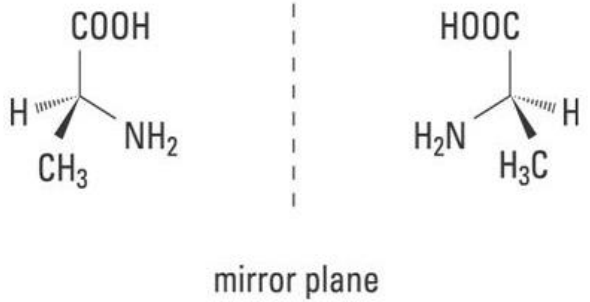

D-Alanine L-Alanine

Rotational strength: $R = \frac{3hc}{8\pi^3 N_A} \int \frac{[\theta(\lambda)]}{\lambda} \, \mathrm{d}\lambda$

molar ellipticity

$R = \mathrm{Im}\langle \psi_0 | \vec{\mu} | \psi_a \rangle \langle \psi_a | \vec{m} | \psi_0 \rangle$

electric dipole transition

magnetic dipole transition

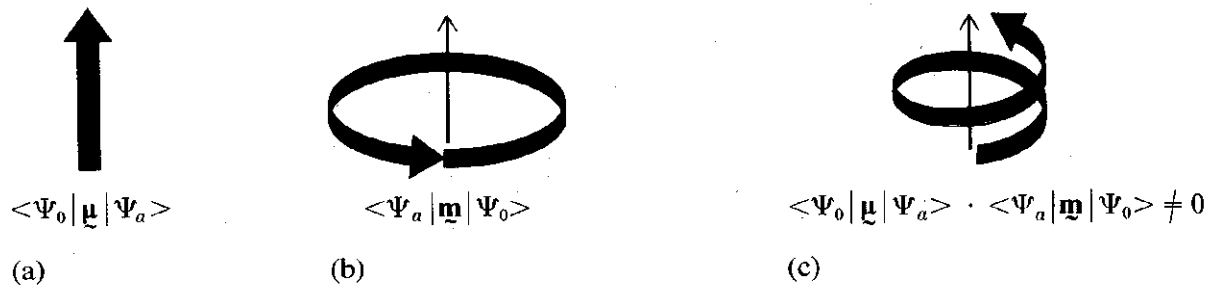

Pure electronic abs. Pure magnetic abs. Optical activity

Circular Dichroism

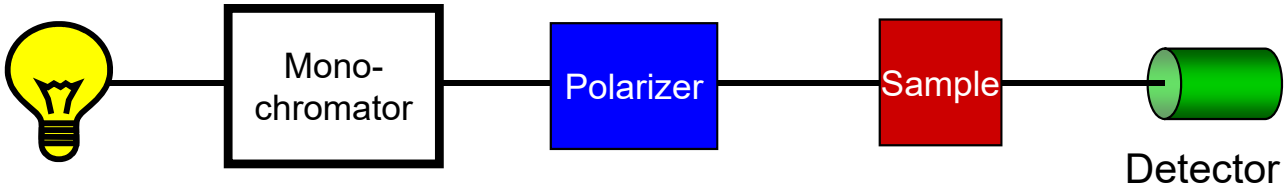

Polarizer: Quarter-wave modulator converts linear polarization into RCP or LCP – either Pockels cell or stress-plate modulator.

Measurement involves exposing the sample alternately to LCP and RCP light and recording $\Delta A = A_L - A_{R,}$ typically 0.03 – 0.3%.

Usually, the result is given in "ellipticity", i.e., the arc tangent of the ratio of the minor axis to the major axis of the polarization ellipse:

$$\theta = 2.303\,(A_L - A_R)\cdot 180^\circ / 4\pi$$

Molar ellipticity at wavelength λ:

$$[\theta]_\lambda = 100\,\theta / C\,l \qquad \left[\frac{\mathrm{deg}\cdot\mathrm{cm}^2}{\mathrm{decimol}}\right] \qquad [\theta]_\lambda \approx 3300\,\Delta\varepsilon_\lambda$$

C: concentration in [mol/l]

l : path length in [cm]

Examples

intrinsic
optical activity

extrinsic, or induced
optical activity

Poly-L-lysine

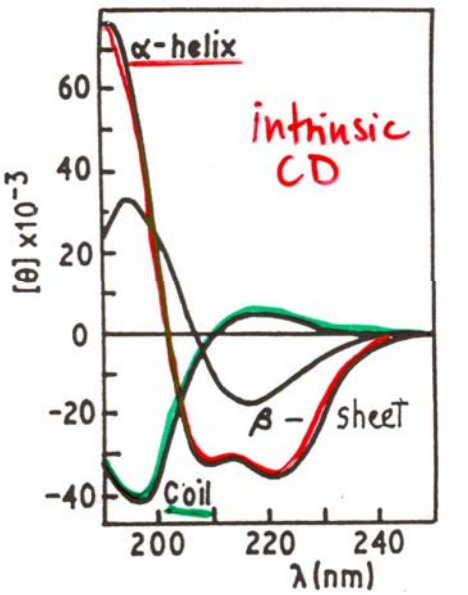

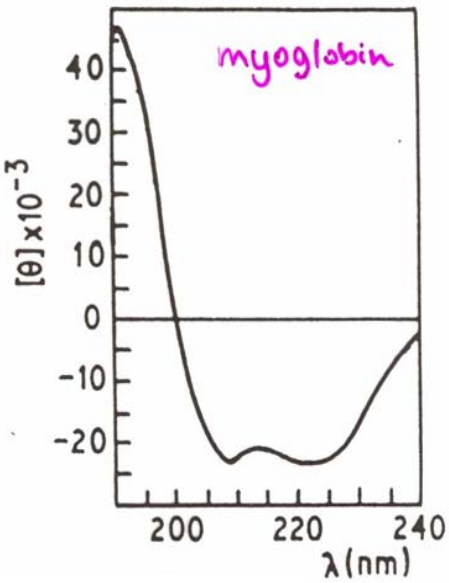

Peptide group CD allows estimation of secondary structure content:

$$\theta = c_1\theta_\alpha + c_2\theta_\beta + c_3\theta_{coil}$$

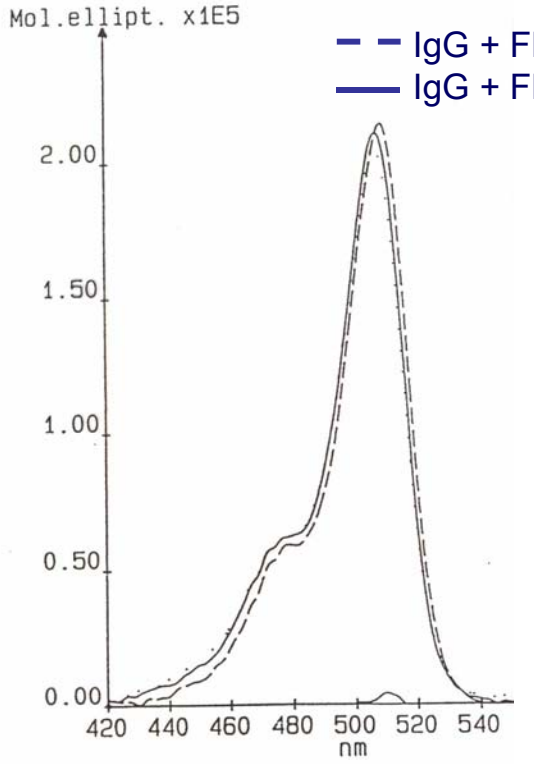

Optical activity of fluorescein is induced by binding to an antibody

Biophysics II

Fluorescence Spectroscopy

Uli Nienhaus

Prof. G. U. Nienhaus, Vorlesungsunterlagen Biophysik II, SS 2023.
Nur zum KIT-internen, vorlesungsbegleitenden Gebrauch.
Weitergabe und anderweitige Nutzung verboten.

Jablonski Diagram

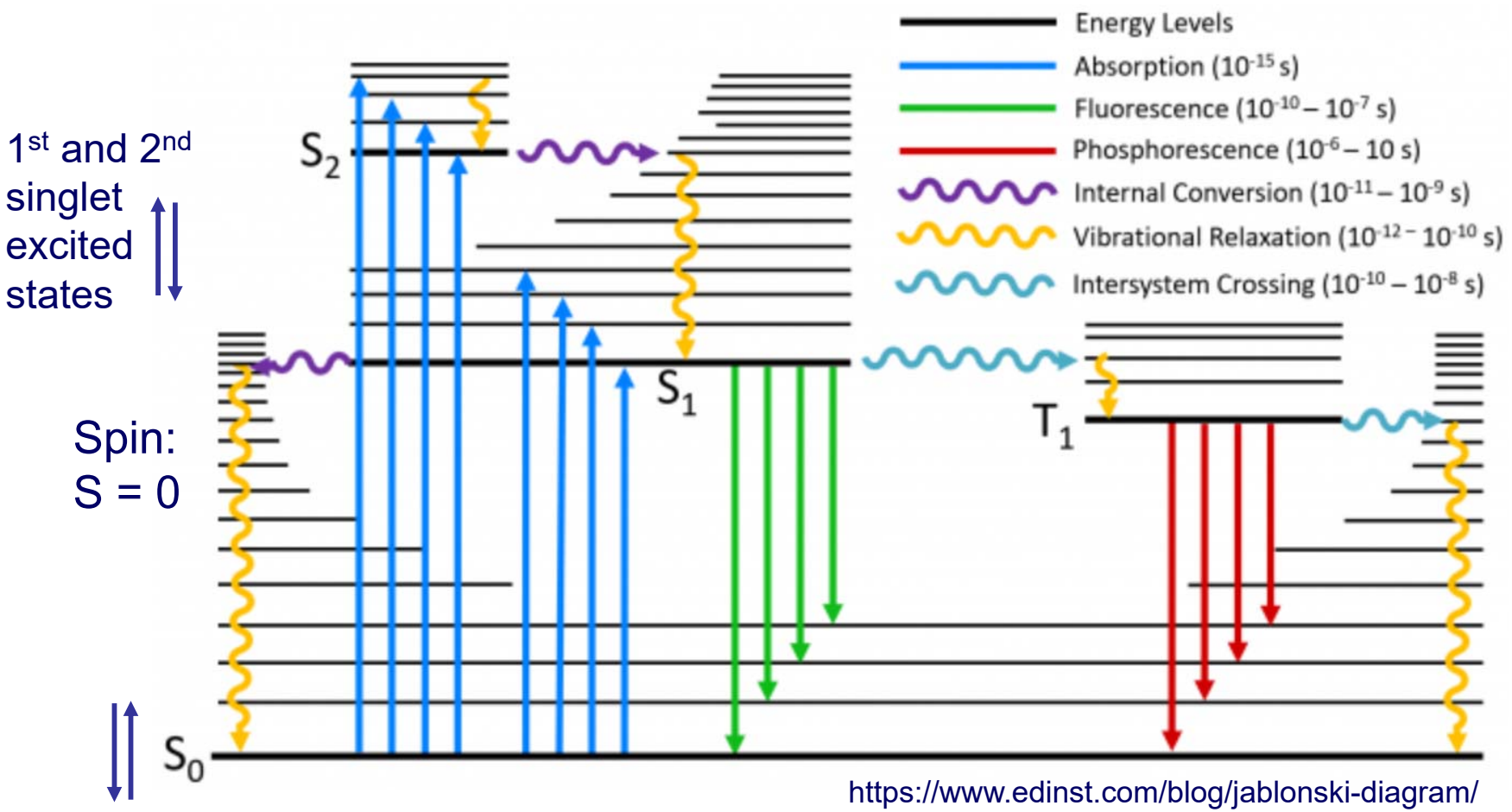

1st and 2nd singlet excited states

Spin: S = 0

triplet state: S = 1 m_s = -1, 0, 1

Singlet ground state

https://www.edinst.com/blog/jablonski-diagram/

Internal conversion: non-radiative change of electronic state

Processes Competing with Fluorescence

Internal Conversion

- Change of electronic state followed by energy loss due to excitation of vibrational modes or collision with solvent molecules. Both processes are enhanced at higher temperature.

Intersystem Crossing

- Singlet to triplet conversion ($S_1 \rightarrow T_1$, forbidden transition), deexcitation by photon emission (phosphorescence) competes with non-radiative decay (ISC $T_1 \rightarrow S_0$ + vibrations).

Quenching

- Some molecules, e.g., ground state radicals (O_2, NO), can convert a singlet to a triplet excited state in a bimolecular reaction (collisional or dynamic quenching).

$$S_1 + Q \xrightarrow{k_q} T_1 + Q$$

($^3Q \rightarrow {}^1Q$ for O_2)

- nonfluorescent complex formation (static quenching).

$$F + Q \underset{}{\overset{K}{\rightleftharpoons}} FQ$$

Time Dependence of Fluorescence Decay

If only fluorescence is present: $-\frac{dn(S_1)}{dt} = k_R\, n(S_1)$

$$n(S_1) = n(S_1(t=0)) \cdot e^{-k_R t}$$

$$k_R = A_{10} = \frac{\hbar\omega^3}{\pi^2 c^3} B_{10} \qquad k_R = \frac{1}{\tau_R}$$

Einstein coefficients

τ_R: radiative lifetime, 10^{-10}…10^{-6} s

If other deexcitation mechanisms contribute: $-\frac{dn(S_1)}{dt} = \left(\sum_{all\ processes} k\right) n(S_1) = k_F\, n(S_1)$

$$k_F = k_R + k_{ic} + k_{is} + k_q[Q]$$

k_F	k_R	k_{ic}	k_{is}	$k_q[Q]$
rate coefficient for depletion of S_1 state	photon emission	internal conversion	intersystem crossing	quenching

$$\phi_F = \frac{k_R}{k_F}$$ quantum yield of fluorescence: $0 \le \phi_F \le 1$

Spectral Properties

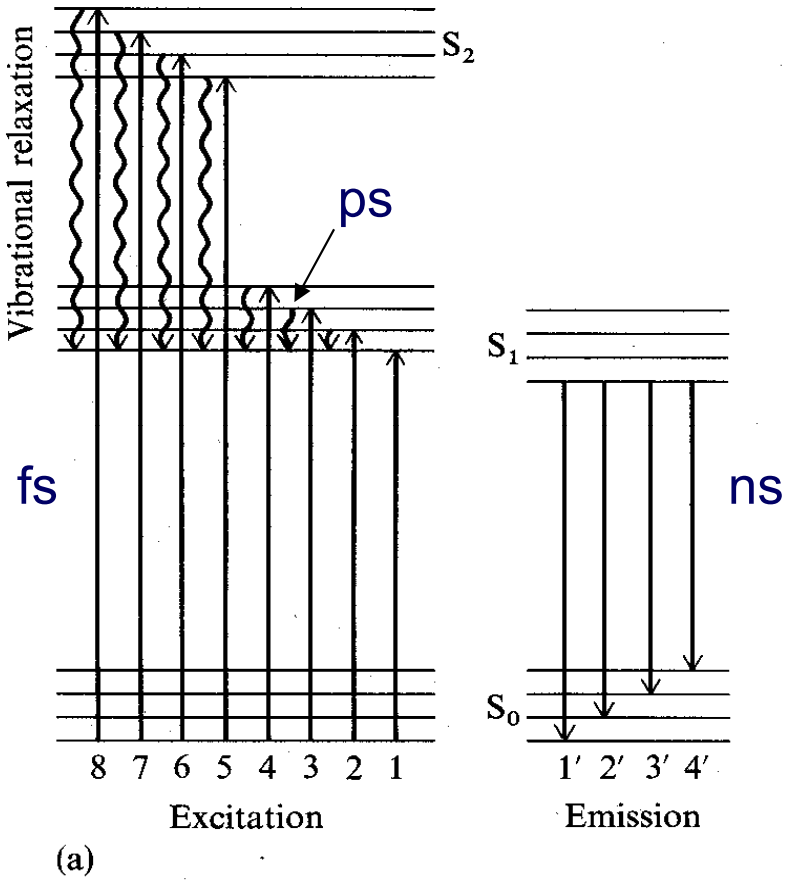

Kasha's rule:
Polyatomic molecular entities in condensed phases luminesce with appreciable yield only from the lowest excited state of a given multiplicity.

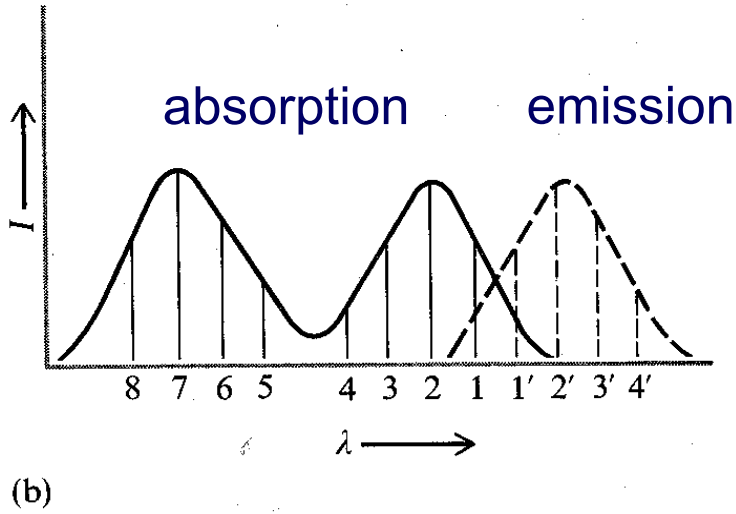

Vibrational deexcitation is faster than the lifetime of the excited state

- Fluorescence spectrum is independent of the excitation wavelength.
- The shape of the emission band is the mirror image of the absorption band, provided that ground and excited state have similar vibronic structure.

Stokes Shift: $\lambda_{em} > \lambda_{abs}$

Static Stokes shift:

- The fluorescence peak is shifted to the red from the excitation peak due to vibrational relaxation in the excited state.

Dynamic Stokes shift:

- The fluorescence peak is usually significantly shifted to the red from the absorption peak (by 20 – 50 nm, ~1000 cm^{-1}) because of solvent reorientation in the excited state.

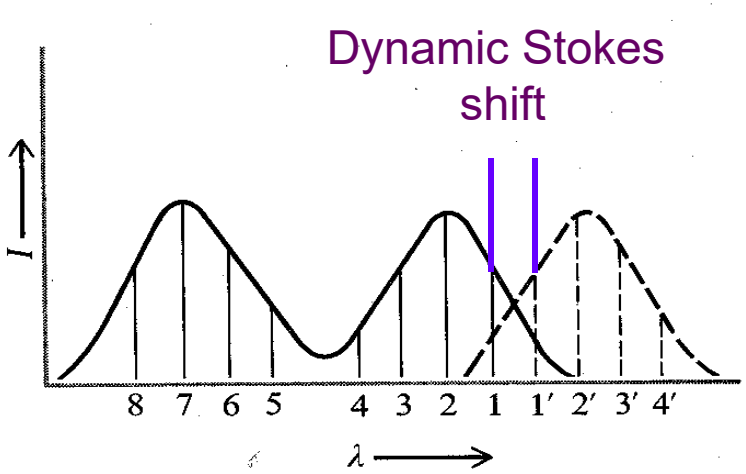

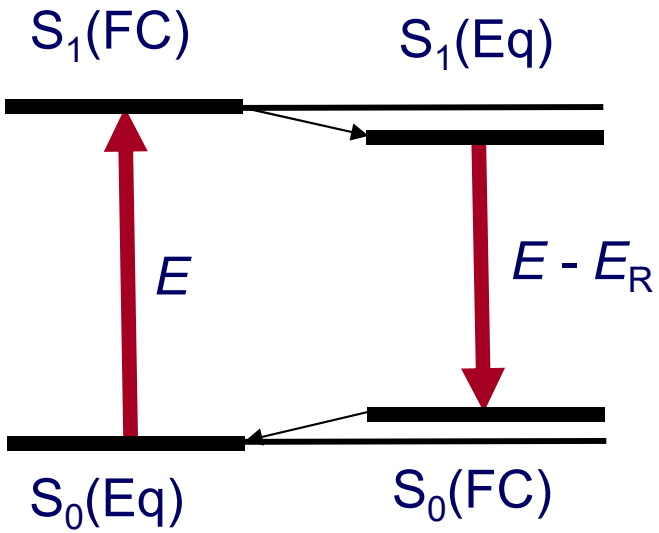

Fluorescence Spectroscopy

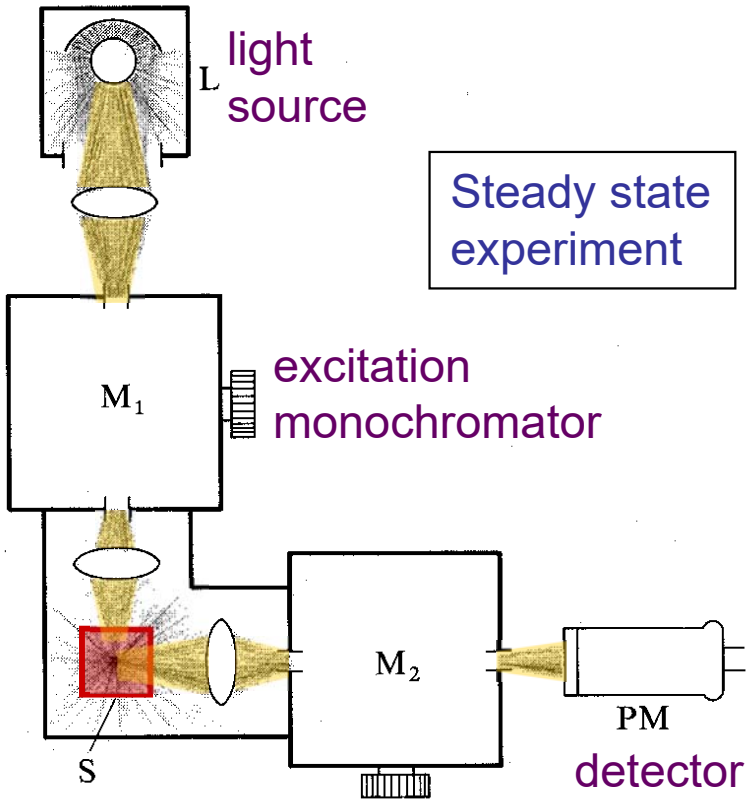

Measured quantities:

1. Fluorescence intensity, f(λ)
2. Fluorescence polarization
3. Fluorescence lifetime
4. Fluorescence quantum yield

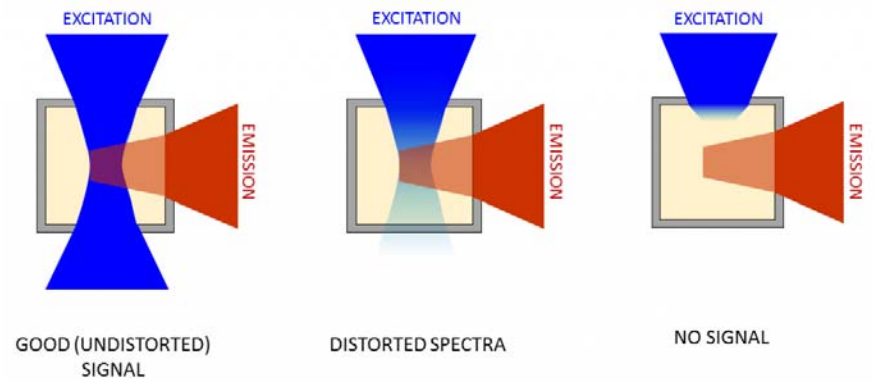

Inner Filter Effect (IFE)

primary IFE: attenuated emission
secondary IFE: distorted spectra

Fluorescence is a very sensitive method; bulk solution measurements can be done at low concentrations (~10^{-9} M)

(6×10^{11} particles/ml)

https://www.edinst.com/blog/inner-filter-effect/

Steady State Measurements

Excitation spectrum

- Emission monochromator is fixed at maximum emission, excitation monochromator is scanned across the absorption band (equivalent to measuring the absorption spectrum for a pure compound).

Emission spectrum

- Excitation monochromator is fixed at maximum absorption, the emission monochromator is scanned across the emission band.

Quantum yields / lifetimes

- Absolute quantum yield determinations are difficult because one has to precisely measure the rate of absorption and emission. In practice, quantum yields are often measured relative to known standards.
- Quantum yields are related to lifetimes: $\phi = \frac{\tau_F}{\tau_R}$
- Lifetimes can be measured directly only with time-resolved experiments.
  - → collision rates with quenchers
  - → energy transfer rates
  - → excited state reactions
  - → lifetimes are needed to calculate rotational correlation times from fluorescence anisotropy.

Intrinsic Fluorescent Probes

Substance	Conditions	Absorption λ_{max} (nm)	Absorption $\varepsilon_{max} \times 10^{-3}$	Fluorescence§ λ_{max} (nm)	Fluorescence§ ϕ_F	τ_F (nsec)	Sensitivity $\varepsilon_{max}\phi_F \times 10^{-2}$
Tryptophan	H_2O, pH 7	280	5.6	348	0.20	2.6	11.
Tyrosine	H_2O, pH 7	274	1.4	303	0.14	3.6	2.0
Phenylalanine	H_2O, pH 7	257	0.2	282	0.04	6.4	0.08
Y base	Yeast $tRNA^{Phe}$	320	1.3	460	0.07	6.3	0.91
Adenine	H_2O, pH 7	260	13.4	321	2.6×10^{-4}	<0.02	0.032
Guanine	H_2O, pH 7	275	8.1	329	3.0×10^{-4}	<0.02	0.024
Cytosine	H_2O, pH 7	267	6.1	313	0.8×10^{-4}	<0.02	0.005
Uracil	H_2O, pH 7	260	9.5	308	0.4×10^{-4}	<0.02	0.004

Molecular brightness (sensitivity): $\varepsilon_{max} \times \phi_F$

Extrinsic Fluorescent Probes

Probe*	Uses	Absorption λ_{max} (nm)	Absorption $\varepsilon_{max} \times 10^{-3}$	Emission§ λ_{max} (nm)	Emission§ ϕ_F	Emission§ τ_F (nsec)	Sensitivity $\varepsilon_{max}\phi_F \times 10^{-2}$
Dansyl chloride	Covalent attachment to protein: Lys, Cys	330	3.4	510	0.1	13	3.4
1,5-I-AEDANS	Covalent attachment to protein: Lys, Cys	360	6.8	480	0.5	15	34
Fluorescein isothiocyanate (FITC)	Covalent attachment to protein: Lys	495	42	516	0.3	4	116
8-Anilino-1-naphthalene sulfonate (ANS)	Noncovalent binding to proteins	374	6.8	454	0.98	16	67
Pyrene, and various derivatives	Polarization studies on large systems	342	40	383	0.25	100	100
Ethenoadenosine, and various derivatives	Analogs of nucleotides bind to proteins, incorporate into nucleic acids	300	2.6	410	0.40	26	10
Ethidium bromide	Noncovalent binding to nucleic acids	515	3.8	600	~1	26.5	38
Proflavine monosemicarbazide	Covalent attachment to RNA 3′-ends	445	15	516	0.02	—	30

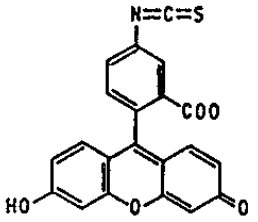

FITC

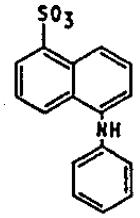

ANS

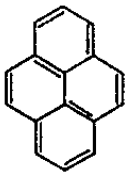
Pyrene

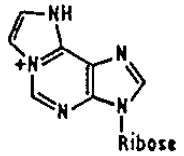

Ethenoadenosine

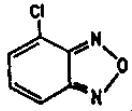

NBD

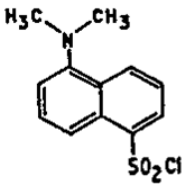

Dansyl chloride

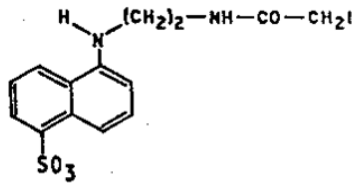

1,5-I-AEDANS

coenzymes: FAD, NADH, porphyrin
analogs: ε-ATP, εNADH

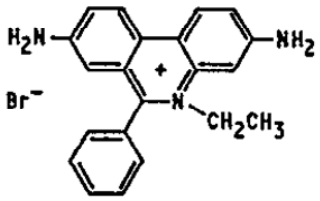

Ethidium bromide

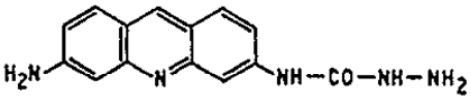

Proflavine monosemicarbazide

Fluorescence Markers

Quantum dots

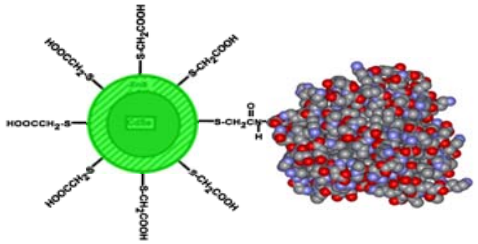

Organic dyes (Cy dyes, Alexa, …)

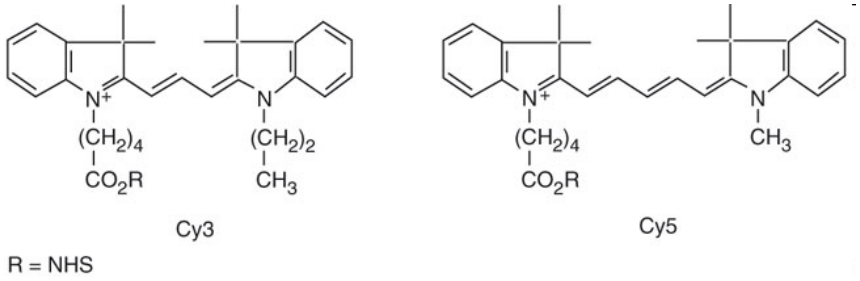

Fluorescent proteins (GFP, eqFP611, IrisFP…)

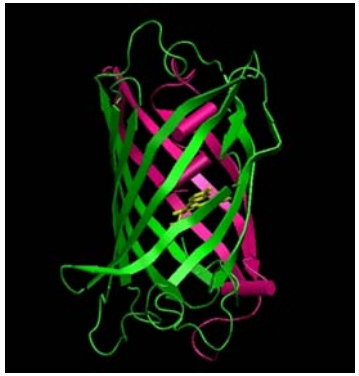

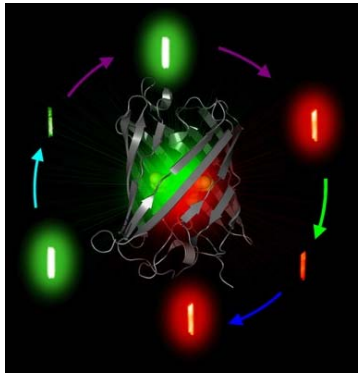

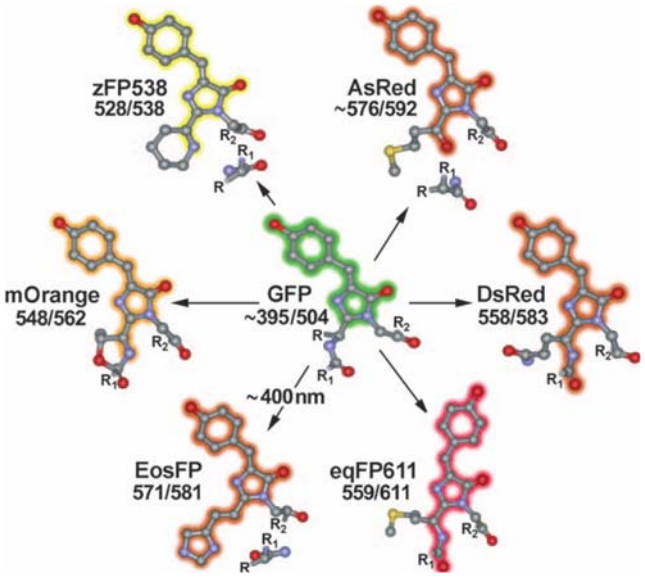

Fluorescence – Sensitivity to Environment

- Solvent relaxation
- Chemical reactions
  - protonation
  - ligand binding
- Changes in orientation
- Quenching

ANS:	ϕ	λ_{max} (nm)
in water	0.004	515
In apoMb	0.98	454

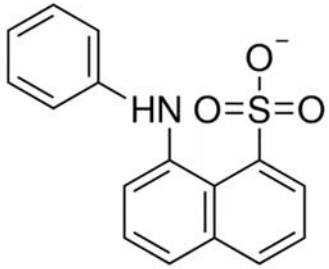

Dynamic (Collisional) Quenching

$$\frac{\text{Fluorescence w/o quencher}}{\text{Fluorescence w/ quencher}} = \frac{\phi_0}{\phi} = \frac{k_R/(k_R + k_{ic} + k_{is})}{k_R/(k_R + k_{ic} + k_{is} + k_q[Q])}$$

Stern-Volmer equation

$$\frac{F_0}{F} = \frac{\phi_0}{\phi} = 1 + \frac{k_q}{k_R + k_{ic} + k_{is}}[Q] = 1 + k_q\tau_0[Q]$$

Collision with quencher molecule

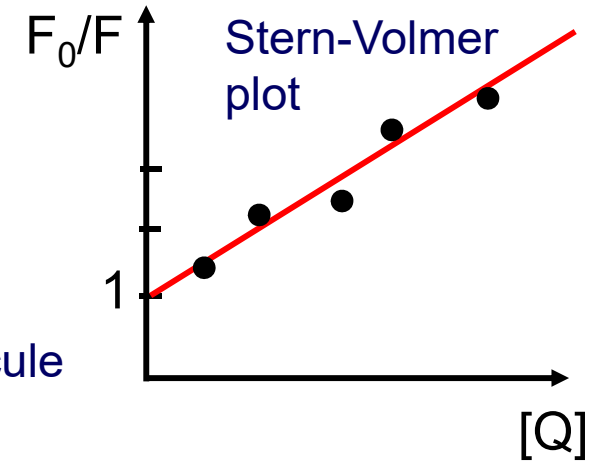

Static and Dynamic Quenching I

Dynamic/Collisional Quenching

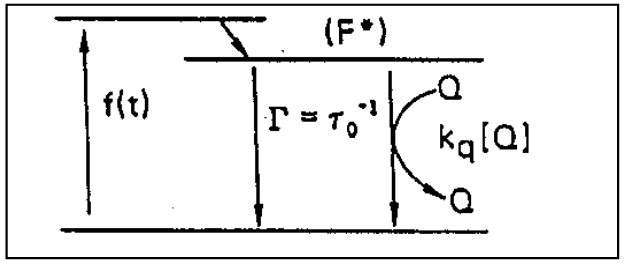

$$\frac{F_0}{F} = 1 + k_q \tau_0 [Q] = \frac{\tau_0}{\tau} \qquad \tau_0 = \tau_F \left([Q] = 0\right)$$

Collision frequency:

$$Z = k_0 [Q]$$

[cm] [cm²/s]

[M⁻¹s⁻¹] $$k_q = \gamma k_0 = \gamma \frac{4\pi N_A}{1000} (R_f + R_q)(D_f + D_q)$$

quenching efficiency

Smoluchowski equation

Static Quenching

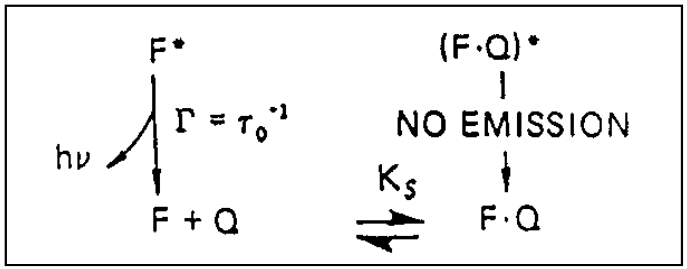

$$[F_0] = [F] + [F \cdot Q]$$

Law of mass action

$$K = \frac{[F \cdot Q]}{[F][Q]} = \frac{[F_0] - [F]}{[F][Q]} = \frac{[F_0]}{[F][Q]} - \frac{1}{[Q]}$$

$$\Rightarrow \quad \frac{F_0}{F} = 1 + K[Q]$$

intensity ratio

- same dependence on [Q]
- distinguish through temperature/viscosity variation in steady state or lifetime measurements.

Stokes-Einstein equation $$D = \frac{kT}{6\pi\eta R}$$

Static and Dynamic Quenching II

Collisional Quenching

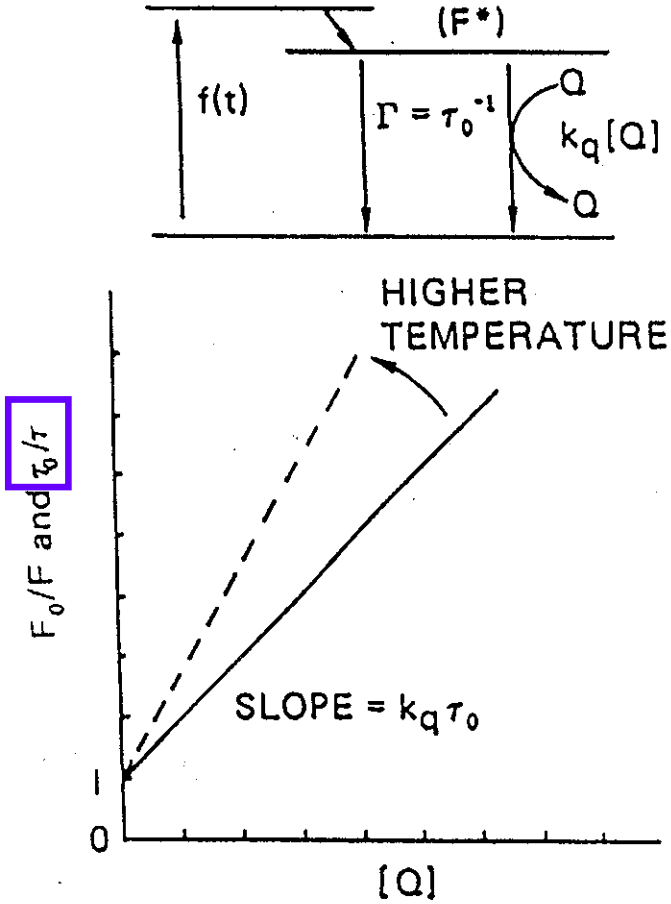

Static Quenching

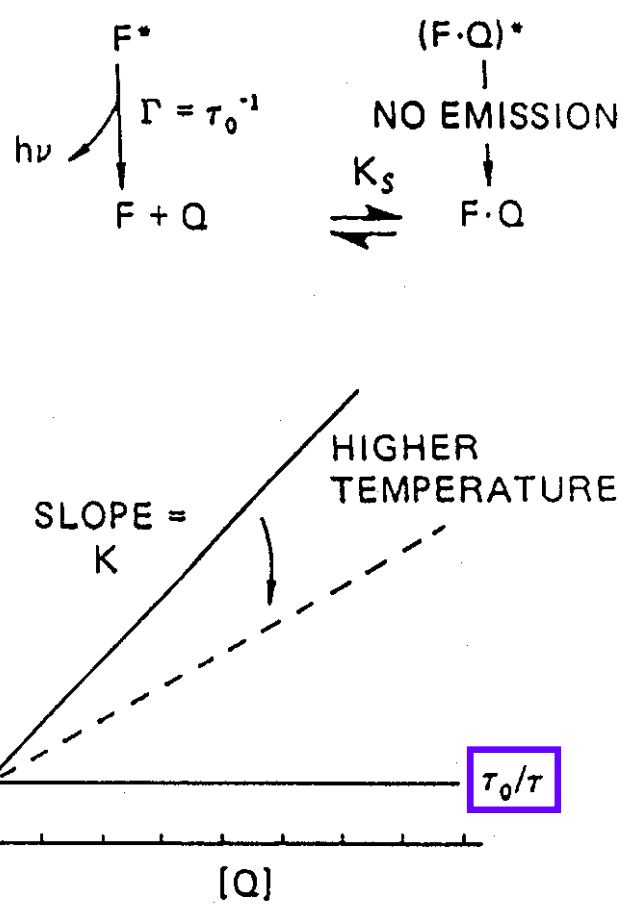

Singlet-Singlet Energy Transfer

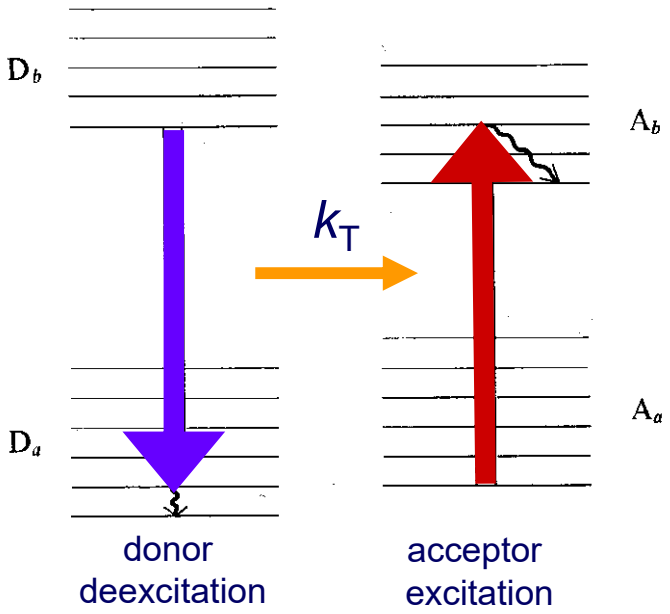

Pair of fluorophores ('donor' / 'acceptor')
very weak coupling, 10 Å ≤ R ≤ 100 Å

$$D^* + A \underset{\text{----}}{\overset{k_T}{\rightleftharpoons}} D + A^*$$

Transfer efficiency: $$E = \frac{k_T}{k_T + k_R^D + k_{ic}^D + k_{is}^D}$$

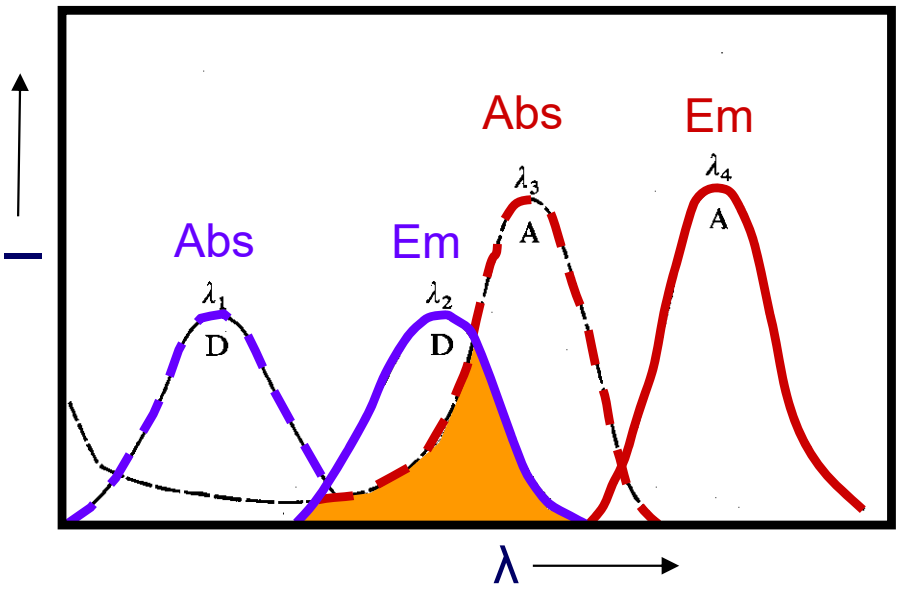

$$\frac{\phi_{D,A}}{\phi_D} = \frac{k_R^D/(k_R^D + k_{ic}^D + k_{is}^D + k_T)}{k_R^D/(k_R^D + k_{ic}^D + k_{is}^D)} = 1 - E = \frac{\tau_{D,A}}{\tau_D}$$

Excitation spectrum
measured at λ_4 has two peaks due to
donor and acceptor absorption.

Förster Theory of Singlet-Singlet Energy Transfer I

weak coupling → Fermi's Golden Rule:

$$k_T(\nu) \propto \left| \left\langle \psi_D \psi_{A^*} \middle| V \middle| \psi_{D^*} \psi_A \right\rangle \right|^2$$

at light frequency ν!!

with dipole-dipole coupling operator:

$$V = \frac{\vec{\mu}_D \cdot \vec{\mu}_A}{R^3} - \frac{3(\vec{\mu}_D \cdot \vec{R})(\vec{R} \cdot \vec{\mu}_A)}{R^5} = \kappa \frac{|\vec{\mu}_D| \cdot |\vec{\mu}_A|}{R^3}$$

geometry lumped into constant κ

introducing V in $k_T(\nu)$:

$$k_T(\nu) \propto \left| \frac{\kappa}{R^3} \left\langle \psi_D \psi_{A^*} \middle| |\vec{\mu}_D| \cdot |\vec{\mu}_A| \middle| \psi_{D^*} \psi_A \right\rangle \right|^2$$

$$\propto \frac{\kappa^2}{R^6} \left| \left\langle \psi_D \middle| \vec{\mu}_D \middle| \psi_{D^*} \right\rangle \right|^2 \left| \left\langle \psi_{A^*} \middle| \vec{\mu}_A \middle| \psi_A \right\rangle \right|^2$$

donor dipole strength D_D

acceptor dipole strength D_A

Förster Theory of Singlet-Singlet Energy Transfer II

- acceptor absorption:

$$D_A \propto B_{ij} \propto \int \varepsilon_A(\nu)\nu^{-1}\,\mathrm{d}\nu$$

$$\phi_D = \frac{k_{R,D}}{k_{F,D}} = \frac{\tau_D}{\tau_R}$$

- donor emission at frequency ν:

$$D_D \propto B_{ji} \propto A_{ji}\nu^{-3} = \tau_R^{-1}\nu^{-3} = \frac{\phi_D}{\tau_D}\nu^{-3}$$

- integrating over all frequencies yields:

normalized fluorescence emission

$$k_T \propto \frac{\kappa^2}{R^6}\frac{\phi_D}{\tau_D}\int \varepsilon_A(\nu) f_D(\nu)\nu^{-4}\,\mathrm{d}\nu$$

Theodor Förster
Ann. Physik
2 (1948) 55.

problem: κ cannot be determined directly from the experiment ($0 \le \kappa^2 \le 4$).
Fortunately, errors in κ enter only as $(\kappa^2)^{1/6}$ into the distance determination.

Interchromophore Distances from Energy Transfer Efficiencies

Förster theory: $k_T = \frac{1}{\tau_D}\left(\frac{R_0}{R}\right)^6$

$R_0 = 9.78\times10^3 (J\,\kappa^2\, n^{-4}\, \phi_D)^{1/6}$ [Å], Förster radius

$J = \int \varepsilon_A(\lambda) f_D(\lambda) \lambda^4 \,\mathrm{d}\lambda$ [M^{-1} cm^3]

normalized on wavelength scale

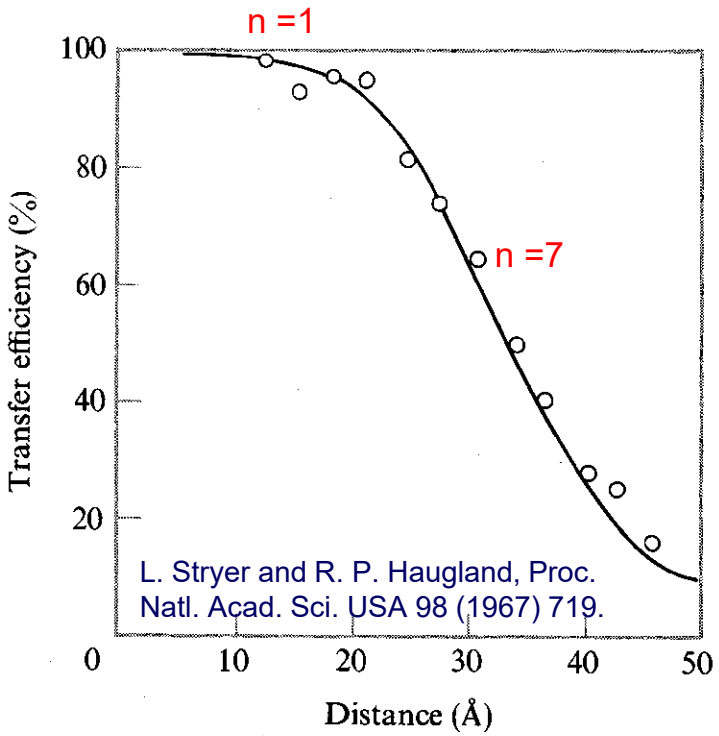

Example: oligomer with n = 1 to 12.

Dansyl – (Pro)$_n$ – NH – NH – CO – NH – Naphtyl

A ← D

J : spectral overlap between donor and acceptor
n : index of refraction – in medium: V→V/n^2
Φ_D : donor quantum yield w/o acceptor
κ^2 : geometric factor (= 2/3 for fast tumbling)

Efficiency: $E = \frac{k_T}{k_T + \tau_D^{-1}} = \frac{R_0^6}{R_0^6 + R^6}$

Detection efficiency

$\gamma = \frac{\eta_A \Phi_A}{\eta_D \Phi_D}$

Experimentally: $E = \frac{I_A}{I_A + \gamma I_D}$ ratiometric

$E = 1 - \frac{\tau_{D,A}}{\tau_D}$ lifetime

Fluorescence Polarization I

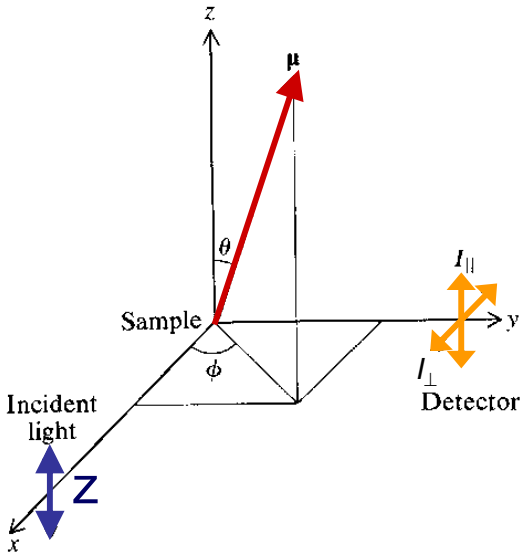

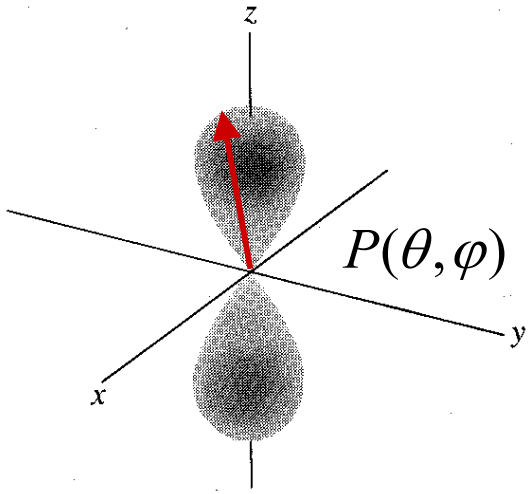

For a rigid, isotropic sample:

Probability of excitation: $P \approx \left|\vec{\mu}\cdot\vec{E}\right|^2 \approx \cos^2\theta$ photoselection

Probability of exciting molecules with μ-angles within θ to $\theta + d\theta$, Φ to $\Phi + d\Phi$:

$$P(\theta,\phi)\,d\theta\,d\phi \approx \cos^2\theta \underbrace{\sin\theta\,d\theta\,d\phi}$$

surface element dS on unit sphere

Fluorescence Polarization II

Fraction of entire population (normalization):

independent of Φ

$$W(\theta,\phi)\,\mathrm{d}\phi\,\mathrm{d}\theta = \frac{P(\theta,\phi)\,\mathrm{d}\phi\,\mathrm{d}\theta}{\int_0^{\pi}\mathrm{d}\theta\int_0^{2\pi}\mathrm{d}\phi\,\cos^2\theta\sin\theta} = \frac{3}{4\pi}\cos^2\theta\sin\theta\,\mathrm{d}\theta\,\mathrm{d}\phi$$

$I_{||}$ is the intensity polarized along z. If emission and absorption dipoles are parallel:

probability of emission: $\left|\vec{\mu}\cdot\hat{z}\right|^2 \propto \cos^2\theta$

- not always the case!

$$I_{||} \propto \left|\vec{\mu}\cdot\hat{z}\right|^2 \propto \int_0^{2\pi}\mathrm{d}\phi\int_0^{\pi}\mathrm{d}\theta\cos^2\theta W(\theta,\phi) = \frac{3}{4\pi}\int_0^{2\pi}\mathrm{d}\phi\int_0^{\pi}\mathrm{d}\theta\cos^4\theta\sin\theta = \frac{3}{5}$$

$I_{\perp}$ is polarized along x:

$$I_{\perp} \propto \left|\vec{\mu}\cdot\hat{x}\right|^2 \propto \int_0^{2\pi}\mathrm{d}\phi\int_0^{\pi}\mathrm{d}\theta(\sin\theta\cos\phi)^2 W(\theta,\phi) = \frac{1}{5}$$

probability of emission: $\left|\vec{\mu}\cdot\hat{x}\right|^2 \propto (\sin\theta\cos\phi)^2$

Fluorescence Polarization III

Polarization: $$P = \frac{I_{\parallel} - I_{\perp}}{I_{\parallel} + I_{\perp}}$$

Anisotropy: $$A = \frac{I_{\parallel} - I_{\perp}}{I_{\parallel} + 2I_{\perp}}$$

For rigid systems with parallel emitting and absorbing dipoles:

$$P = \frac{1}{2} \qquad A = \frac{2}{5}$$

For rigid systems with angle ξ between absorption and emission dipoles:

$$P_0 = \frac{3\cos^2\xi - 1}{\cos^2\xi + 3}$$

limiting polarization, -1/3 < P_0< 1/2

$$A_0 = \frac{3\cos^2\xi - 1}{5} = \frac{2P_0}{3 - P_0}$$

limiting anisotropy, -1/5 < A_0< 2/5

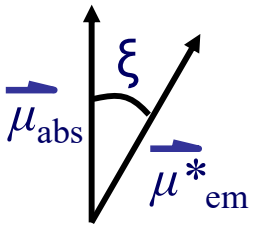

In the presence of motion, molecules change orientation during the time they reside in the excited state. Consider pulsed excitation at t = 0. The early emission is polarized with P_0. Subsequently, rotations will depolarize the emission.

Rotational Motion I

- Rotational motion can be described by Brownian dynamics of the transition dipole moment for emission. For a spherical particle:

2. Fick's law $$\frac{\mathrm{d}W(\theta,\phi,t)}{\mathrm{d}t} = D_{rot}\nabla^2 W(\theta,\phi,t) = \frac{kT}{6V_h\eta}\nabla^2 W(\theta,\phi,t)$$

viscosity

hydrated volume

- Solve DEQ with the boundary condition

$$W(\theta,\phi,0) = \frac{3}{4\pi}\cos^2\theta\sin\theta$$

- To calculate the emission intensity, we must also account for population decay, so that the probability density for finding excited molecules at θ, Φ at time t is

$$W(\theta,\phi,t)e^{-t/\tau_F}$$

Rotational Motion II

probability of emission along z ($\cos^2\theta$ for $\xi = 0$)
or x ($\sin^2\theta \cos^2\Phi$ for $\xi = 0$)

The intensity is given by $I_a(t) = \int_0^{2\pi} \mathrm{d}\phi \int_0^{\pi} \mathrm{d}\theta\, P_a(\theta,\phi,\xi)\, W(\theta,\phi,t)\, e^{-t/\tau_F}$

axis

$$\Rightarrow I_{\parallel}(t) = \left[\frac{1}{3} + \frac{4}{15} e^{-6D_{rot}t}\, \frac{3\cos^2\xi - 1}{2}\right] e^{-t/\tau_F}$$

$$\Rightarrow I_{\perp}(t) = \left[\frac{1}{3} - \frac{2}{15} e^{-6D_{rot}t}\, \frac{3\cos^2\xi - 1}{2}\right] e^{-t/\tau_F}$$

anisotropy $A(t) = \frac{2}{5} e^{-6D_{rot}t}\, \frac{3\cos^2\xi - 1}{2} = \frac{I_{\parallel} - I_{\perp}}{I_{\parallel} + 2I_{\perp}}$

independent of lifetime!

$A(0) = A_0$; $A(\infty) = 0$

rotational correlation time $\tau_c = 1 / (6\, D_{rot}) \approx 10$ ns for 25 kDa protein, 20°C, water

$$\tau_c = \frac{V_h \eta}{kT}$$

Time-Resolved Anisotropy Decay

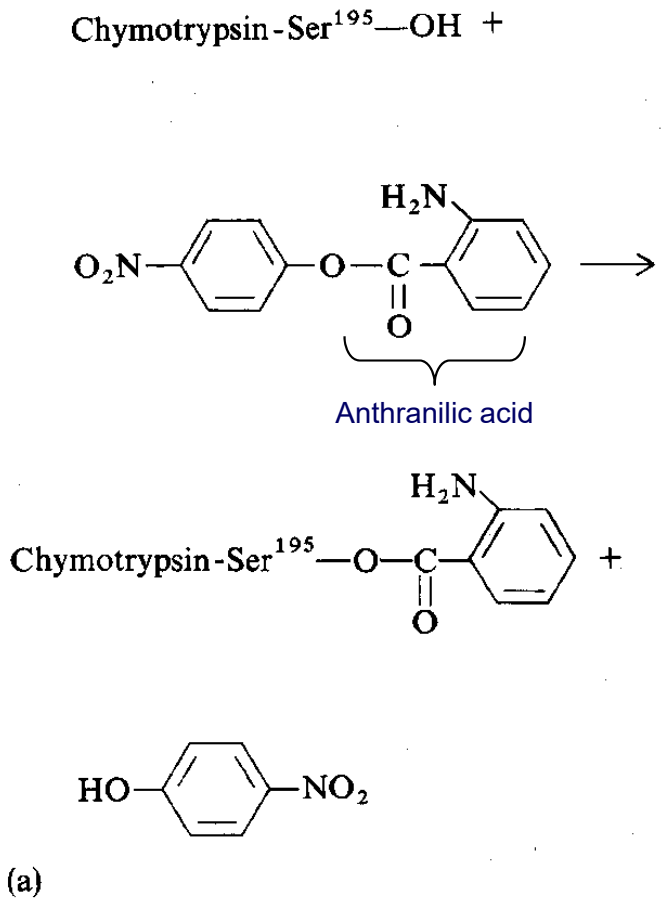

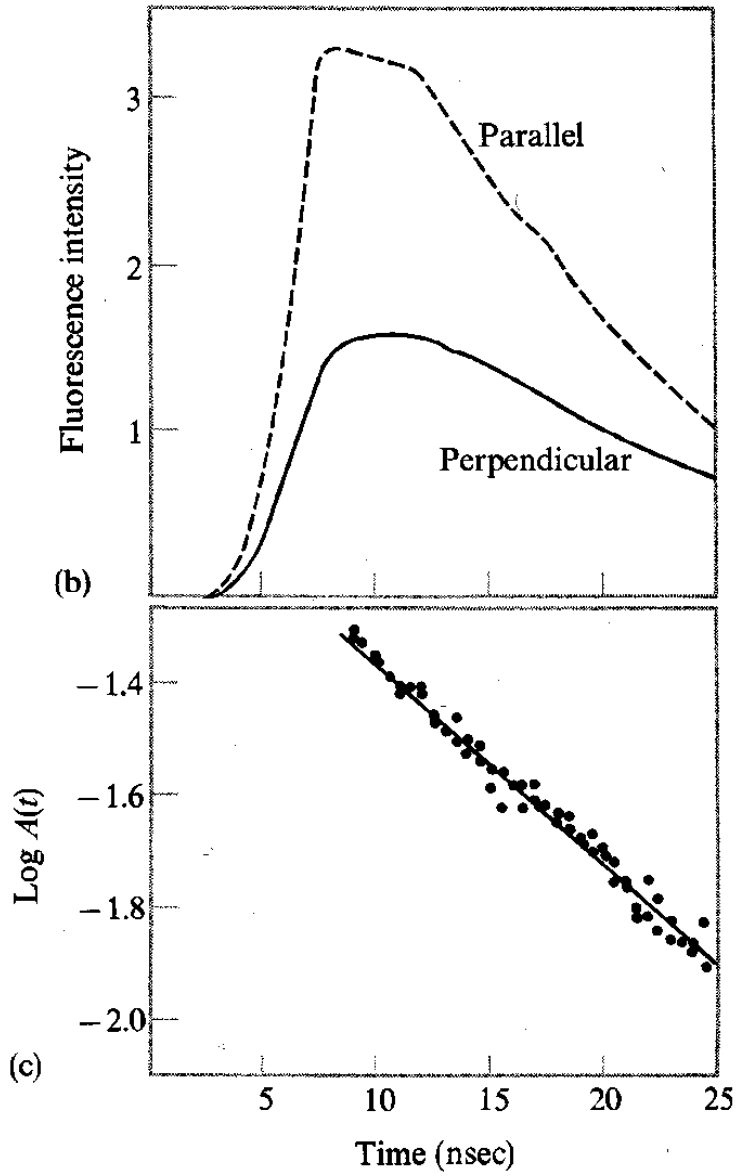

Example: anthraniloyl-Ser^{195}-α-chymotrypsin

L. Stryer, Science 162 (1968) 526.

Steady-State Anisotropy Decay

Steady-state measurements: $\bar{I}_{\parallel} = \tau_F^{-1} \int_0^{\infty} I_{\parallel}(t)\,\mathrm{d}t$ $\bar{I}_{\perp} = \tau_F^{-1} \int_0^{\infty} I_{\perp}(t)\,\mathrm{d}t$

$$\bar{A} = \frac{\int_0^{\infty} A(t)I(t)dt}{\int_0^{\infty} I(t)dt} = \frac{\int_0^{\infty} A_0 \exp(-t/\tau_c) I_0 \exp(-t/\tau_F)dt}{\int_0^{\infty} I_0 \exp(-t/\tau_F)dt} = \frac{A_0 I_0 / (1/\tau_F + 1/\tau_c)}{I_0/(1/\tau_F)}$$

Perrin equation $\boxed{\frac{1}{\bar{A}} = \frac{1}{A_0}(1 + \tau_F/\tau_c)}$

using $\tau_c = \frac{V_h \eta}{kT}$: $\frac{1}{\bar{A}} = \frac{1}{A_0}\left(1 + \frac{\tau_F k}{V_h} \cdot \frac{T}{\eta}\right)$

Perrin equation applies to spherical molecules.
General case: Weber-Perrin equation

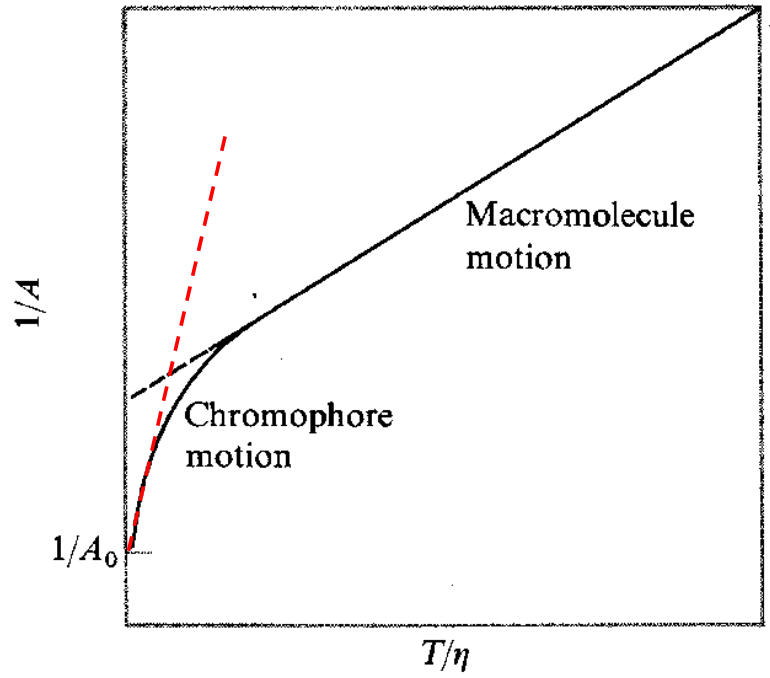

Lifetime Measurements I

Time-correlated single photon counting (TCSPC):

adjust light level to count ~1 photon per 20 laser flashes

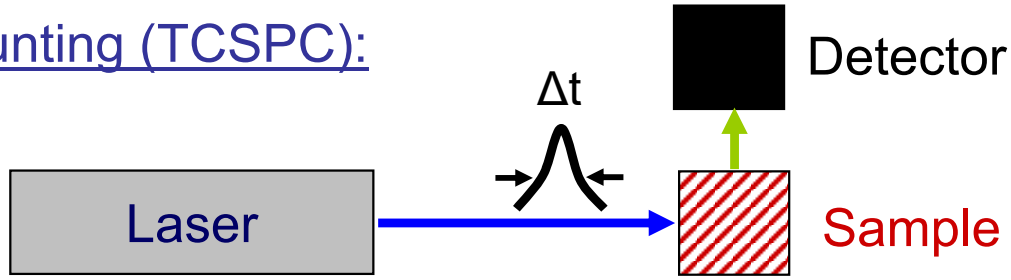

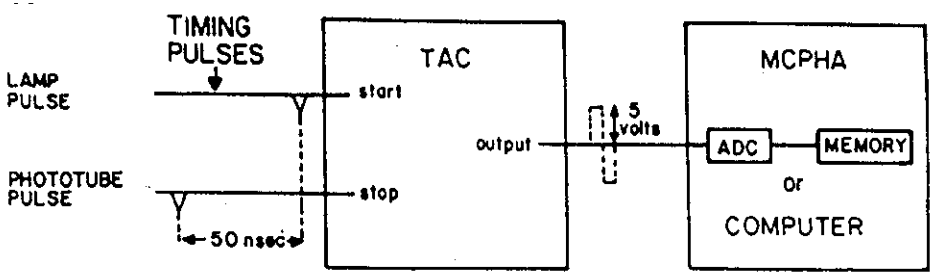

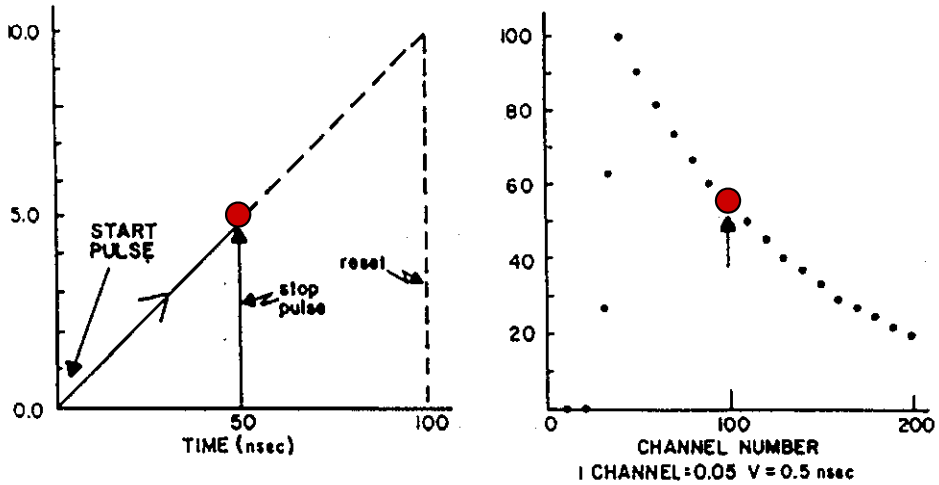

TNS: 6-(p-toluidino)-2-naphthalene sulfonic acid

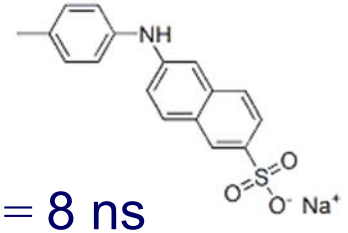

laser pulse shape

$\tau = 8$ ns

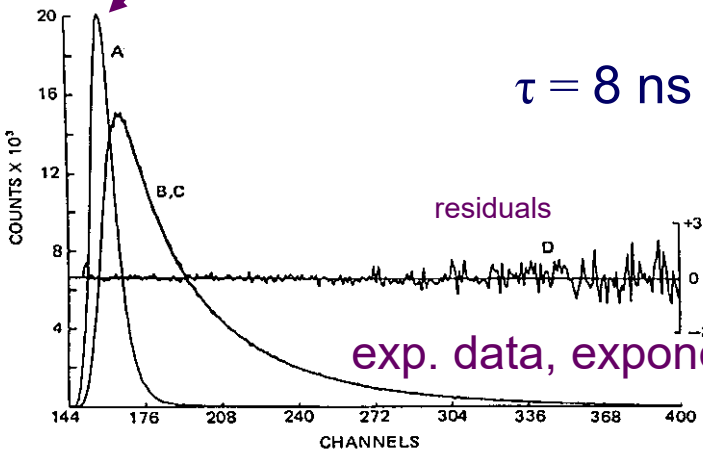

exp. data, exponential fit

Lifetime Measurements II

Phase Fluorometry:

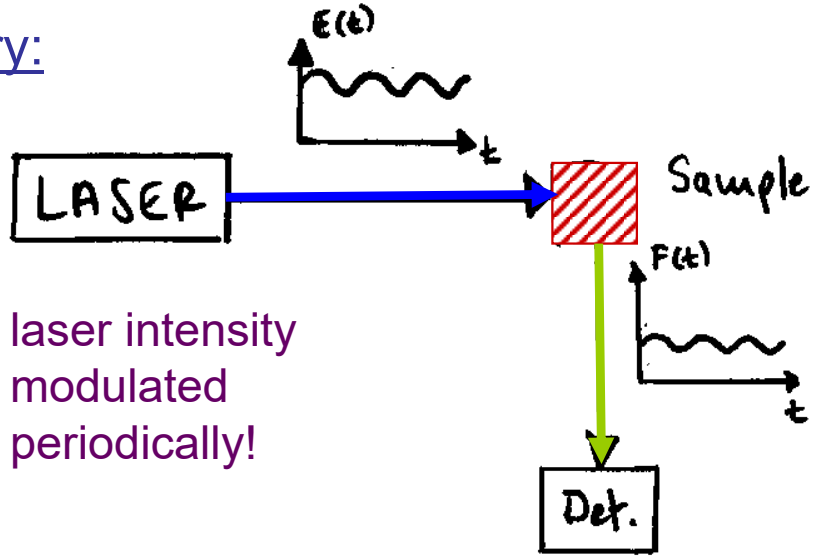

laser intensity
modulated
periodically!

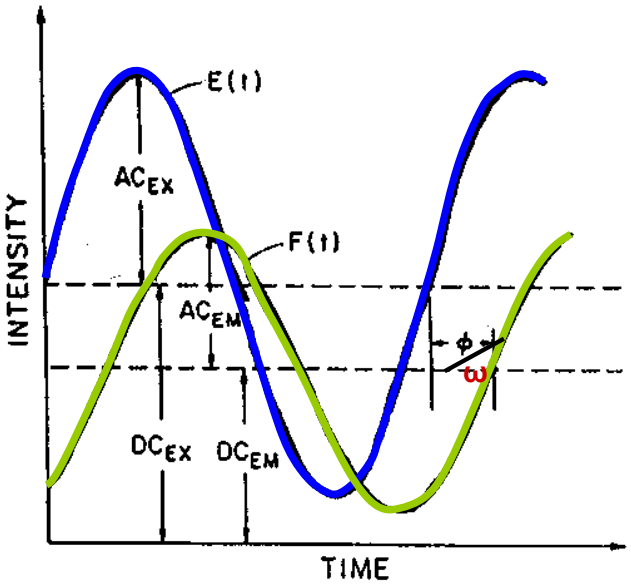

E(*t*): excitation intensity
F(*t*): fluorescence intensity

Linear response: $F(t) = \chi(\omega)E(t)$

$$= \left|\chi(\omega)\right| E_0 e^{-i(\omega t - \varphi(\omega))}$$

$$\chi(\omega) = \left|\chi(\omega)\right| e^{i\varphi(\omega)} = \chi'(\omega) + i\chi''(\omega)$$

$$\left|\chi(\omega)\right| = \sqrt{\chi^* \chi} = \sqrt{\chi'^2 + \chi''^2}$$

$$\varphi(\omega) = \arctan \frac{\chi''(\omega)}{\chi'(\omega)}$$

Lifetime Measurements III

Time response of system (fluorophore) to a δ-perturbation:

$$\tilde{\chi}(t) = \frac{1}{\tau} e^{-t/\tau} \quad \Rightarrow \quad \chi(\omega) = \mathrm{FT}(\tilde{\chi}(t)) = \frac{1}{1 - i\omega\tau} = \boxed{\frac{1 + i\omega\tau}{1 + \omega^2\tau^2}}$$

$$\varphi(\omega) = \arctan \frac{\chi''(\omega)}{\chi'(\omega)} = \arctan \omega\tau_p$$

demodulation

$$|\chi(\omega)| = \sqrt{\chi^* \chi} = \sqrt{\frac{1}{1 + \omega^2\tau_M^2}} = M = \frac{\text{fluorescence modulation}}{\text{excitation modulation}} = \frac{AC_{EM}}{AC_{EX}}$$

Single lifetime: $\tau_p = \tau_M$, frequency independent

more than one: $\tau_p \neq \tau_M$, frequency dependent

Time-resolved Fluorescence

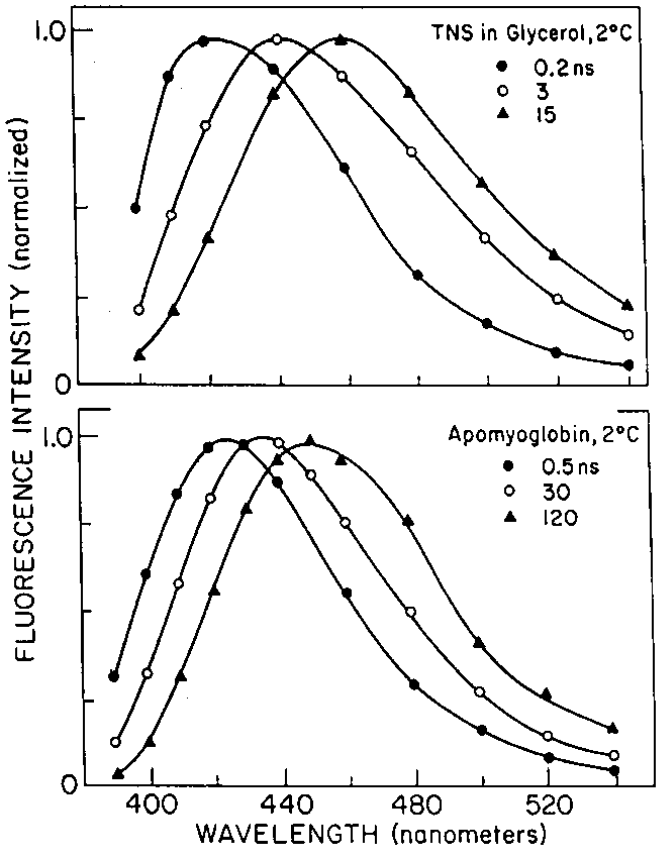

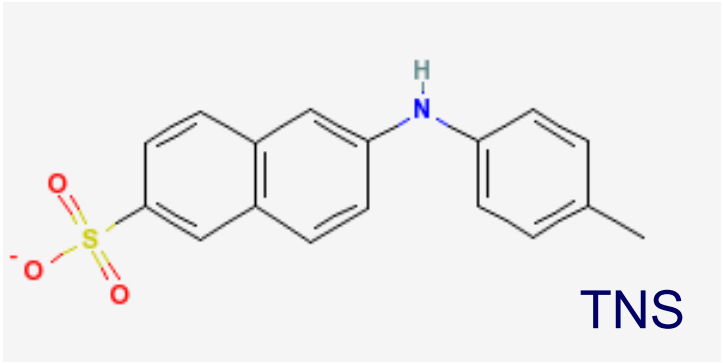

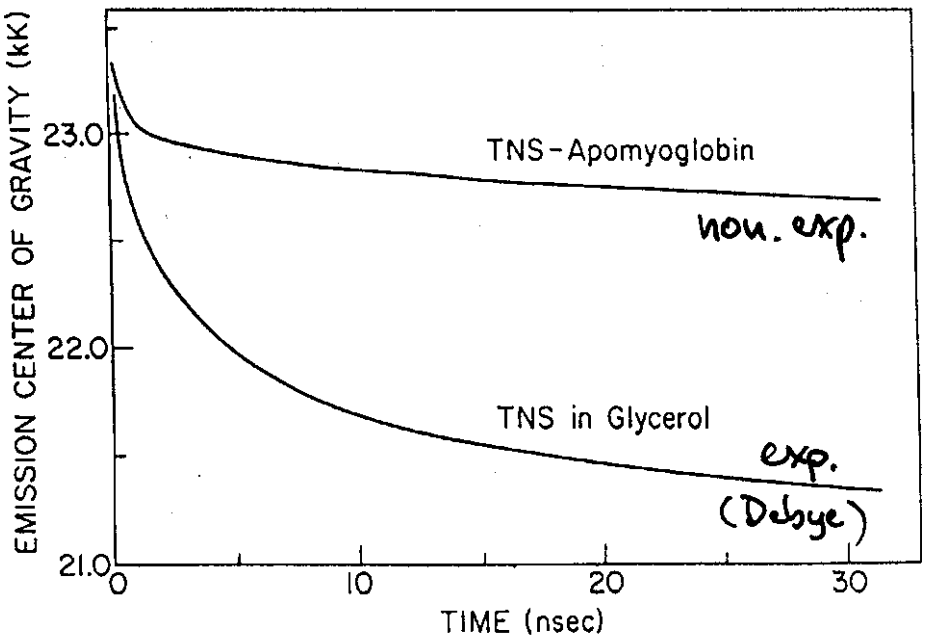

Lakowicz et al., J. Biol. Chem. 259 (1984) 10967

Intrinsic Fluorescence of Proteins

- Tryptophan and tyrosine residues are fluorescent.
- Anisotropy decay measures rotational dynamics.
- Lifetime can serve as an indicator of protein conformations.
- Light with $\lambda > 295$ nm excites only tryptophan.
- NATA (N-acetyl-tryptophan-amide) decays exponentially ($\tau = 3.1$ ns) in water.
- NATA and tryptophan show complex decays in viscous solvents.
- A mixture of fluorophores usually displays a multi-exponential decay with the number of decay constants = number of components of the mixture.
- A single fluorophore in different micro-environments may be considered as a mixture of fluorophores.
- Origin of distributed lifetimes: static or dynamic heterogeneity.

Fluorescence Decay of Single Tryptophan Proteins I

	τ_1 nsec	τ_2 nsec	τ_3 nsec
Apo-azurin	4.9		
Nuclease B	5.1		
Melittin	3.1		
Basic Myelin	4.7	1.97	
Holo-azurin	4.8	0.18	
Glucagon	3.3	1.1	
Adenocorticotropin	5.1	2.0	
Nuclease	5.7	2.0	
RNAse T1	3.3	1.5	
HSA	7.8	3.3	
PLA2	7.2	2.9	0.96
Tuna-Met-MB	2.17	0.132	0.031
Tuna-Apo-MB	2.81	0.33	

$$I(t) = a_1 e^{-t/\tau_1} + a_2 e^{-t/\tau_2} + a_3 e^{-t/\tau_3} + \ldots.$$

Note: 1) Changes in τ
2) Heterogeneity of the decay

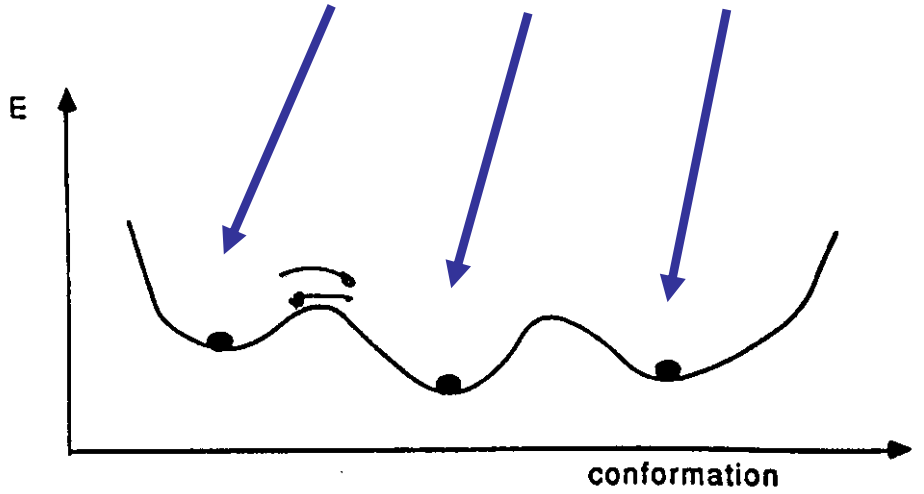

Fluorescence Decay of Single Tryptophan Proteins II

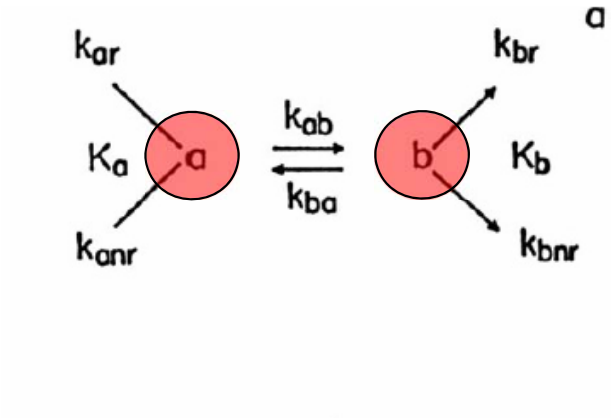

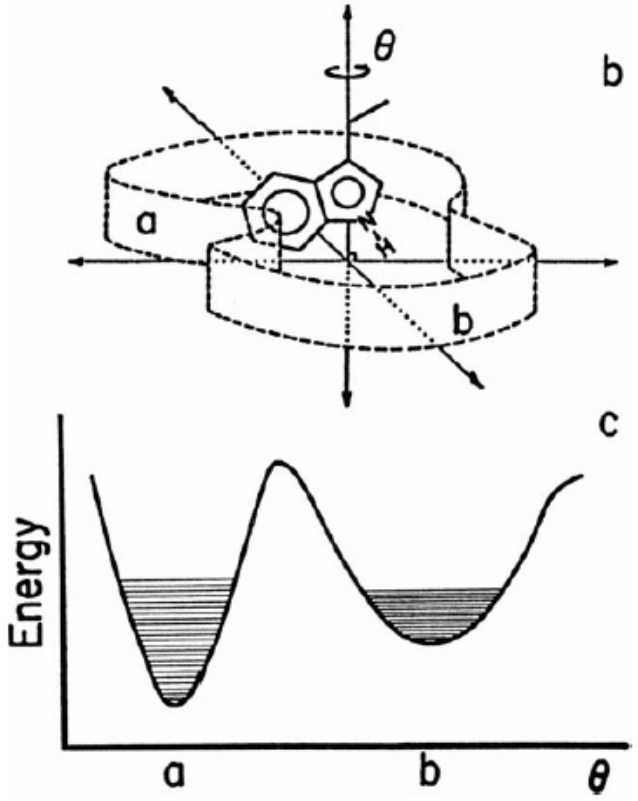

FIGURE 1 (*a*) Interconverting and decaying two state system. k_{ar}, k_{br}, k_{anr}, k_{bnr}, k_{ab}, and k_{ba} are the radiative decay, nonradiative decay, and interconverting rate constants, respectively, of states a and b. $K_a = k_{ar} + k_{anr}$ and $K_b = k_{br} + k_{bnr}$. (*b*) Schematic representation of a tryptophan residue in a protein. The energy of the residue is a function of the coordinate θ. (*c*) Relative potential energy surface in one dimension as a function of the conformational coordinate θ. Energy substates are represented by horizontal lines.

BIOPHYS. J.
Volume 51 (1987) 597-604.

Analysis of Fluorescence Decay with Lifetime Distributions

Sum of exponentials

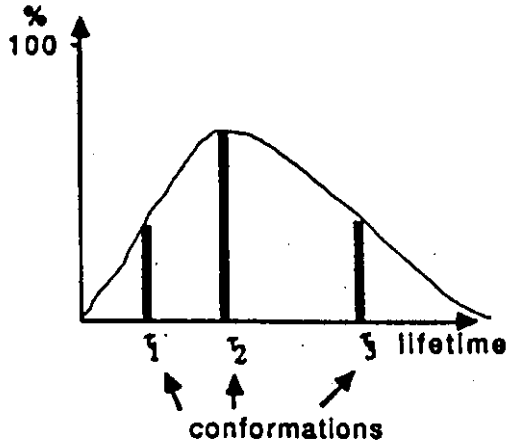

$$I(t) = \sum_i a_i e^{-t/\tau_i}$$

Distributions

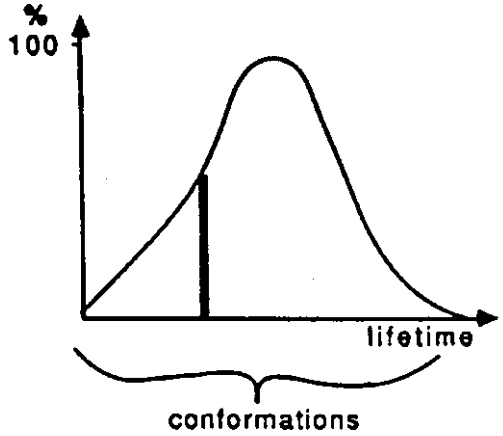

$$I(t) = \int_0^\infty f(\tau) e^{-t/\tau}\, \mathrm{d}\tau$$

Analysis of azurin lifetimes (–48°C in 80% glycerol)

Exponentials	τ	f	χ^2
1	4.78		321
2	5.443		
	0.838	0.146	63
3	10.11	0.392	
	3.11	0.552	
	0.42	0.056	7.1
4	322	0.030	
	8.11	0.451	
	2.88	0.465	
	0.42	0.054	2.9
	Center	Width	Fraction
Gaussian Distributions	4.37	2.41	0.948
(χ^2 = 3.0)	0.174	0.27	0.052

Biophysics II

Molecular Vibrations and Infrared Spectroscopy

Uli Nienhaus

Prof. G. U. Nienhaus, Vorlesungsunterlagen Biophysik II, SS 2023.
Nur zum KIT-internen, vorlesungsbegleitenden Gebrauch.
Weitergabe und anderweitige Nutzung verboten.

Molecular Vibrations I

Simple example – diatomic molecule

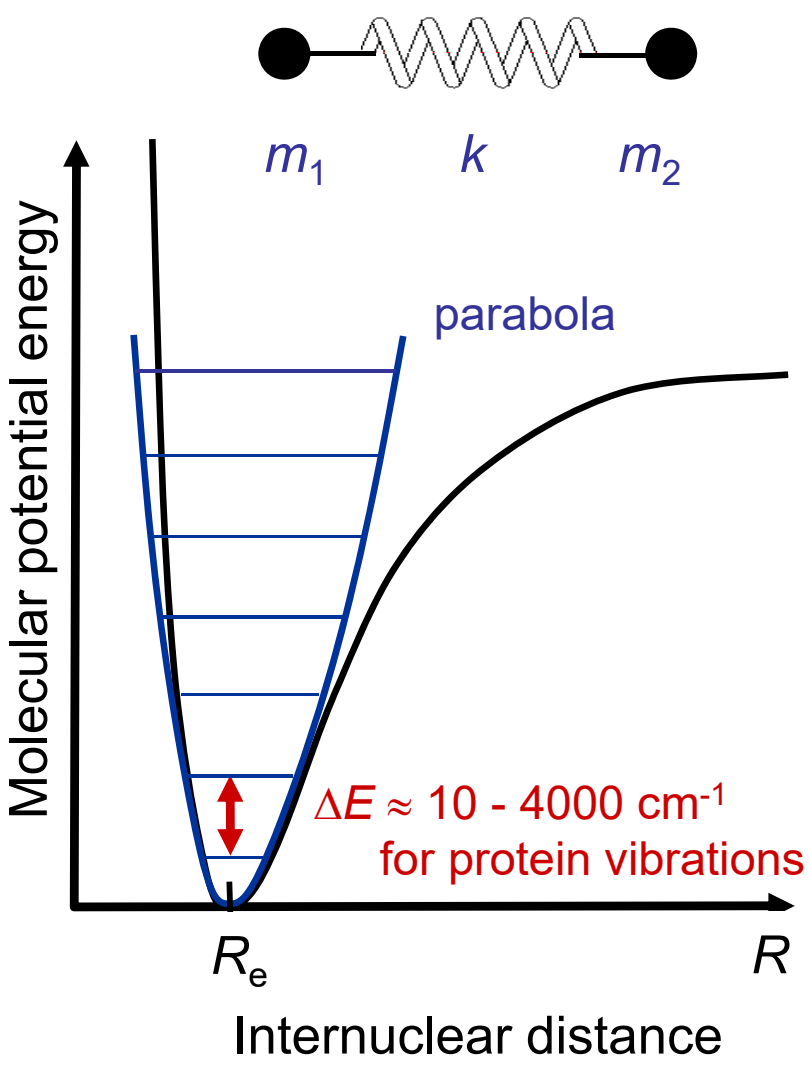

Harmonic oscillator:

$$E_{pot} = \frac{1}{2} k \left(R - R_e\right)^2$$

$$E_n = \left(n + \frac{1}{2}\right)\hbar\omega = \left(n + \frac{1}{2}\right) h\nu$$

$$\omega = \sqrt{\frac{k}{\mu}}$$ ← spring constant ← reduced mass $\quad \frac{1}{\mu} = \frac{1}{m_1} + \frac{1}{m_2}$

→ The greater the mass and the weaker the bond, the lower ω

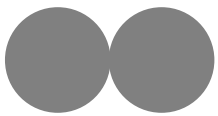

H_2: 2 g/mol
4111 cm^{-1}, T = 8 fs

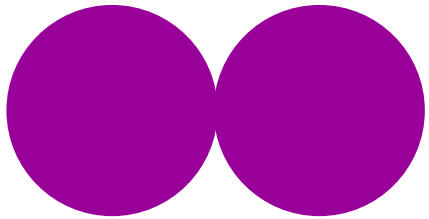

I_2: 254 g/mol

Molecular Vibrations II

Vibrational amplitudes:

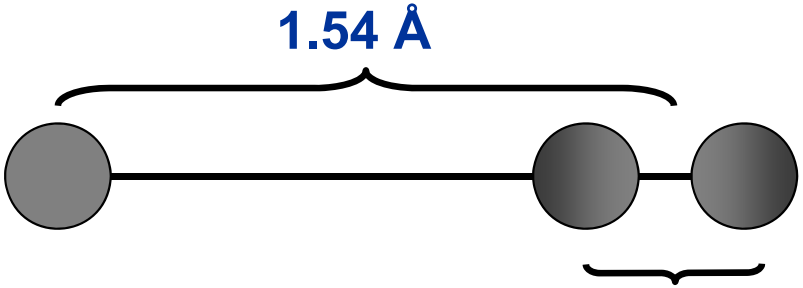

stretching vibration

For a C-C bond with a length of 1.54 Å, the variation is ~0.1 Å.

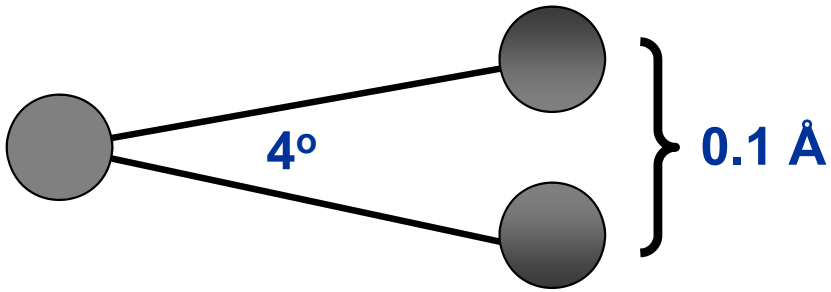

bending vibration

For C-C-C bond angle, a change of 4° is typical, creating a shift of a carbon atom by ~0.1 Å.

Molecular Vibrations III

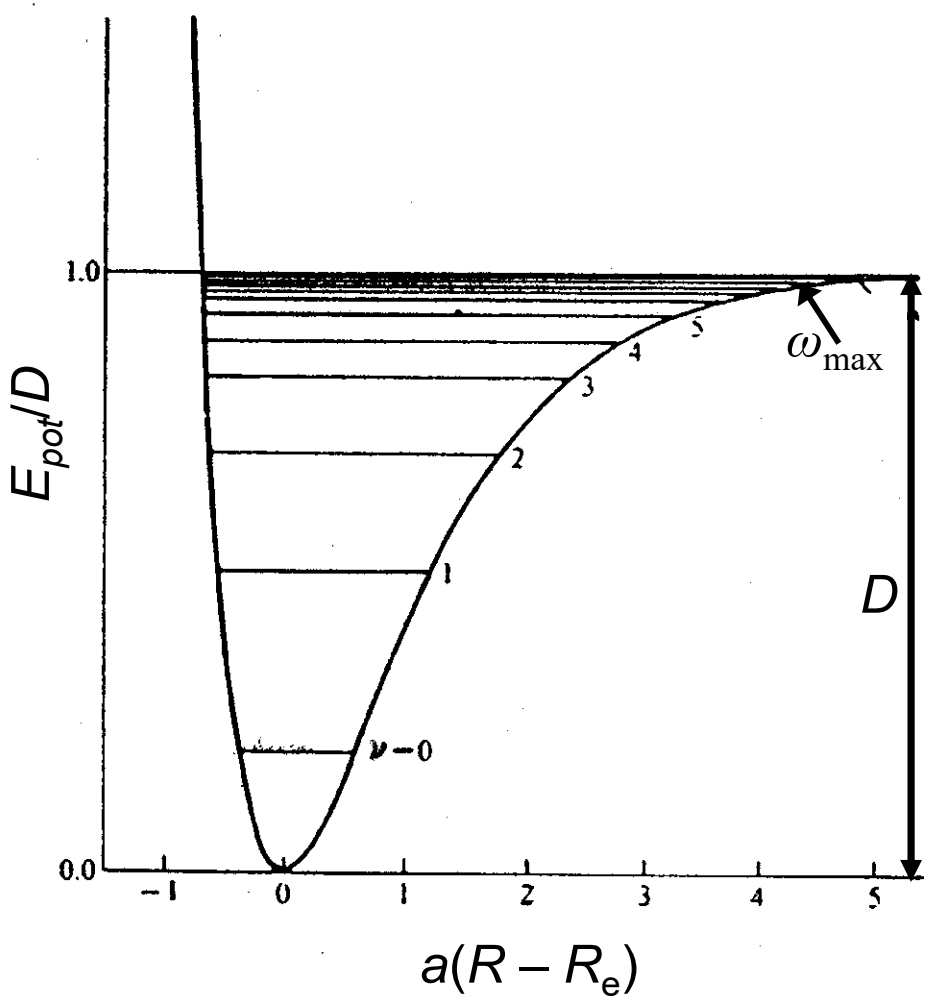

Better approximation than harmonic oscillator:

Morse potential

$$E_{pot} = D\left[1-\exp\left[-a\left(R-R_e\right)\right]\right]^2$$

$$E_n = \left(n+\frac{1}{2}\right)\hbar\omega - \left(n+\frac{1}{2}\right)^2 x_e \hbar\omega$$

$$x_e = \frac{\hbar a^2}{2m\omega}$$ anharmonicity coefficient

Coupling between Vibrations and Electromagnetic Radiation I

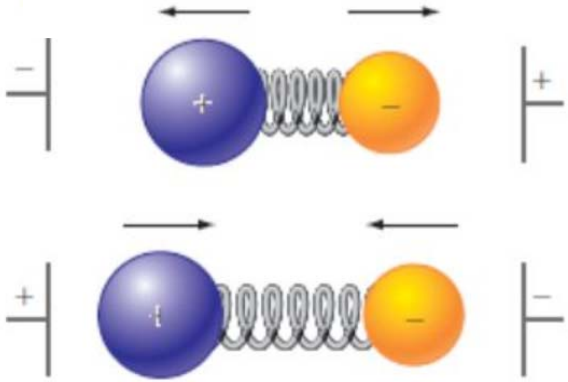

Classically: Light couples to a vibration if the electric dipole moment changes with nuclear position.

Quantum mechanics:

electronic nuclear BOA!

- transition:

$$\psi_0(\vec{r},\vec{R})\,\phi_v(\vec{R}) \;\rightarrow\; \psi_0(\vec{r},\vec{R})\,\phi_{v'}(\vec{R})$$

- dipole operator:

$$\hat{\mu}(\vec{r},\vec{R}) = \sum_{electrons} -e_i\vec{r}_i + \sum_{nuclei} Z_i e_i \vec{R}_i$$

- transition dipole:

$$\begin{aligned}\vec{\mu}_{v\rightarrow v'} &= \iint \psi_0^*(\vec{r},\vec{R})\,\phi_{v'}^*(\vec{R})\,\hat{\mu}(\vec{r},\vec{R})\,\psi_0(\vec{r},\vec{R})\,\phi_v(\vec{R})\,d^3\vec{r}\,d^3\vec{R}\\ &= \int \phi_{v'}^*(\vec{R})\left(\int \psi_0^*(\vec{r},\vec{R})\hat{\mu}(\vec{r},\vec{R})\psi_0(\vec{r},\vec{R})d^3\vec{r}\right)\phi_v(\vec{R})\,d^3\vec{R}\\ &= \int \varphi_{v'}^*(\vec{R})\,\hat{\mu}_{el}(\vec{R})\,\varphi_v(\vec{R})\,d^3\vec{R}\end{aligned}$$

Coupling between Vibrations and Electromagnetic Radiation II

- Taylor expansion of electric dipole moment operator:

$$\hat{\mu}_{el}\left(\vec{R}\right) = \hat{\mu}_{el}\left(\vec{R}_0\right) + \left.\frac{\partial \hat{\mu}_{el}}{\partial \vec{R}}\right|_{\vec{R}_0} \left(\vec{R} - \vec{R}_0\right) \ldots$$

- transition moment: $\vec{\mu}_{v \to v'} = \int \varphi_{v'}^{*}(\vec{R})\, \hat{\mu}_{el}(\vec{R})\, \varphi_{v}(\vec{R})\, d^3\vec{R}$

Orthogonality of harmonic oscillator wavefunctions (Hermite polynomials)

$$= \vec{\mu}\left(\vec{R}_0\right) \int \varphi_{v'}^{*}(\vec{R})\, \varphi_{v}(\vec{R})\, d^3\vec{R} + \left.\frac{\partial \vec{\mu}_{el}}{\partial \vec{R}}\right|_{\vec{R}_0} \int \varphi_{v'}^{*}(\vec{R})\, \vec{R}\, \varphi_{v}(\vec{R})\, d^3\vec{R}$$

- final result:

$$\left\langle \psi_0 \varphi_{v'} \left| \vec{\mu} \right| \psi_0 \varphi_{v} \right\rangle = \left.\frac{\partial \vec{\mu}_{el}}{\partial \vec{R}}\right|_{\vec{R}_0} \cdot \left\langle \varphi_{v'} \left| \vec{R} \right| \varphi_{v} \right\rangle$$

change of dipole moment with change of nuclear position

non-zero for $v' = v \pm 1$ (selection rule!)

Molecular Vibrations: Examples

IR inactive

N – N

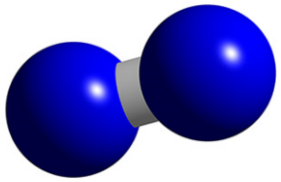

$\nu = 2358.6\ cm^{-1}$

$O^{-} - C^{++} - O^{-}$

symmetric stretch

$\nu = 1353.6\ cm^{-1}$

IR active

$H^{+} - Cl^{-}$

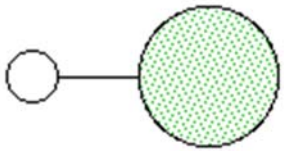

$\nu = 2991\ cm^{-1}$

asymmetric stretch

$\nu = 2396.3\ cm^{-1}$

bending

$\nu = 672.6\ cm^{-1}$

Complex Molecules

N atoms $\rightarrow$ 3N degrees of freedom of motions

Center-of-mass translation: 3 degrees of freedom
Rotation around the center-of-mass : 3 degrees of freedom (2 for linear molecules)

$\Rightarrow$ 3N – 6 normal modes of vibration (3N – 5 for a linear molecule)

Many “localized modes” exist:

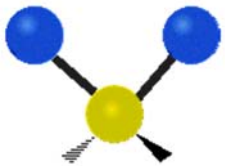

Wagging

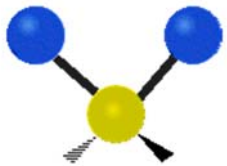

Rocking

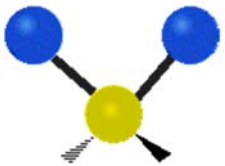

Scissoring

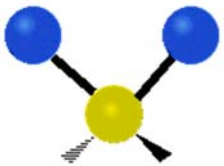

Symmetric stretching

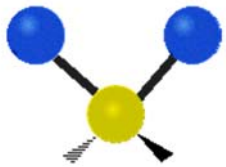

Twisting

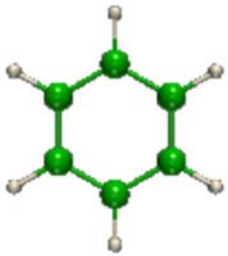

Breathing

Infrared (IR) Spectra of Macromolecules

IR Spectra show many broad, overlapped bands:

- fingerprint region 400 – 1800 cm^{-1}
- H stretch 2400 – 4000 cm^{-1}

For band assignment:

- Select bands in unpopulated regions:
  - di-/tri-atomic ligands 1800 – 2400 cm^{-1}
    (e.g., CO, NO, CN^-, N_3^-)
- Difference spectroscopy:
  - isotope effect
  - photolysis
  - pH change

Examples of Group Frequencies

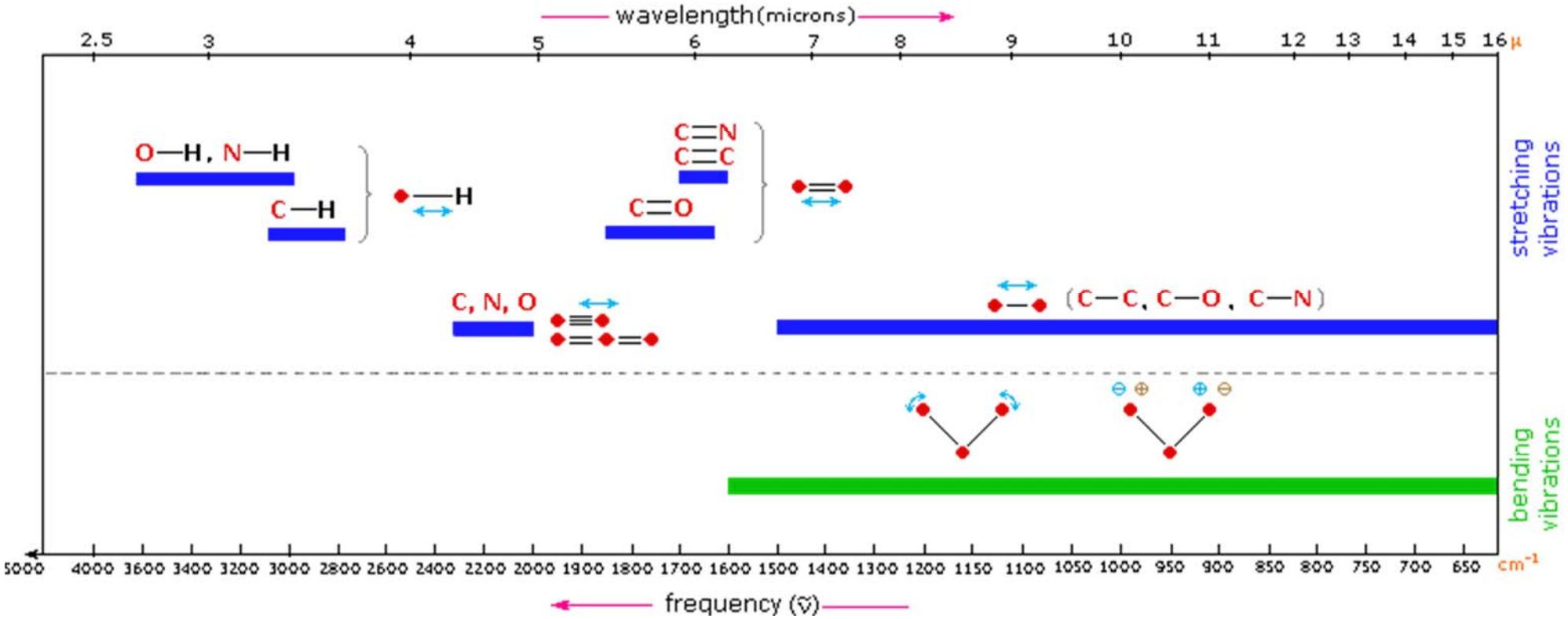

General Trends:

i) Stretching frequencies can be higher than bending frequencies.

ii) Bonds to hydrogen have higher stretching frequencies than those to heavier atoms.

iii) Triple/double/single bonds have high/medium/low stretching frequencies, respectively.

Water Absorption

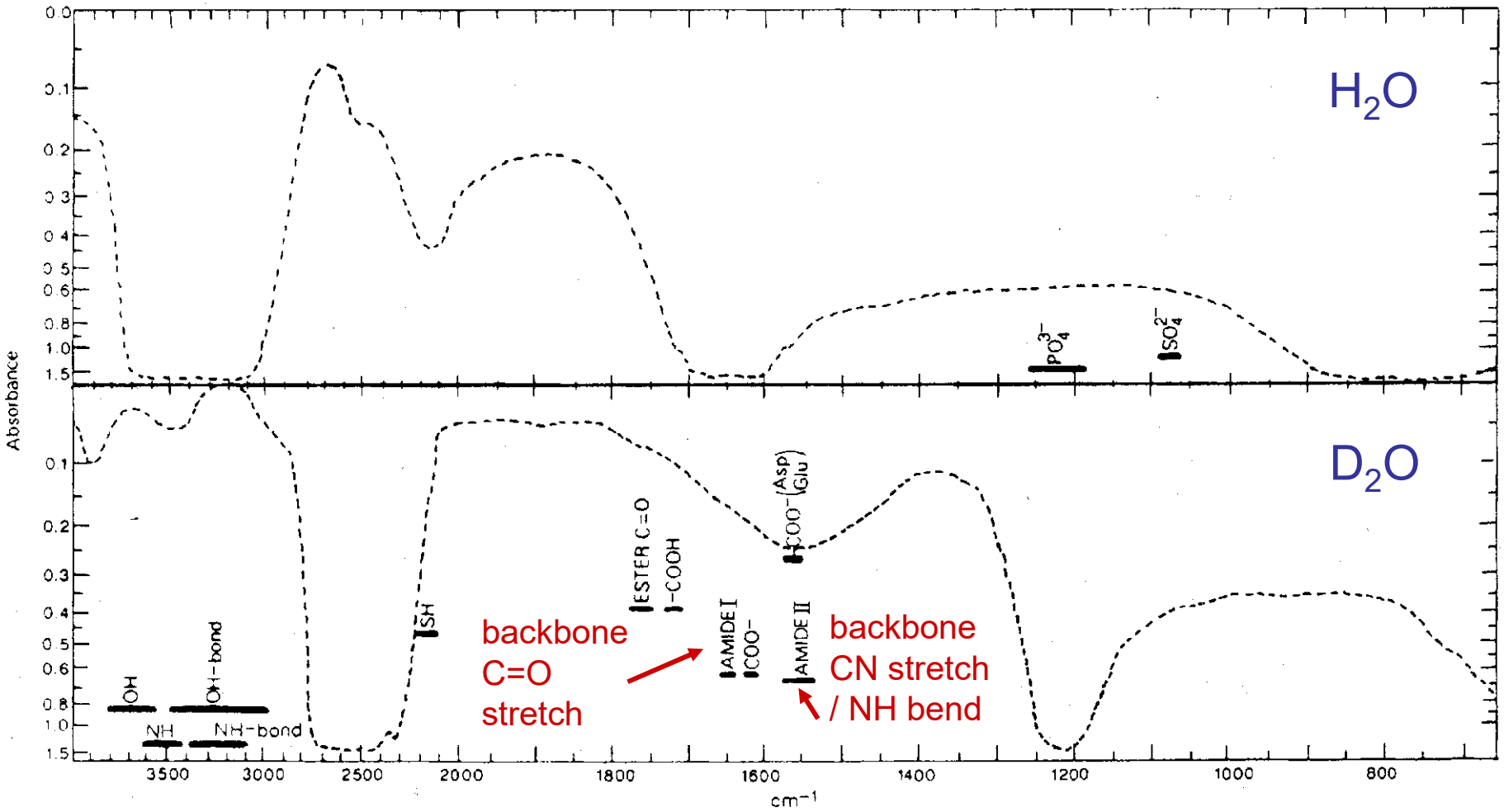

Some representative characteristic group frequencies and typical infrared absorbance spectra of H_2O and D_2O.

IR – Spectroscopy: Apparatus I

1. Dispersive Spectrometer

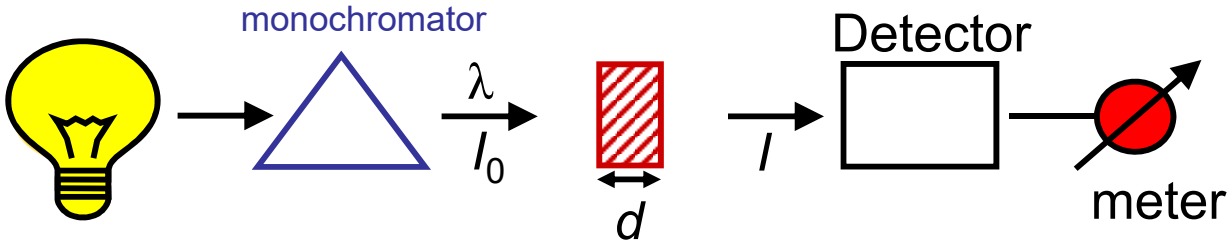

I / I_0 = Transmittance T = $10^{-\varepsilon c d}$

A = Absorbance

Lambert-Beer $A = -\log_{10} T = \varepsilon c d$

extinction coefficient

sample thickness

concentration

Infrared:

Light source optimized for IR, special detectors, window materials CaF_2, NaCl (no glass), reflecting optics (mirrors).

Typical path lengths *d* for aqueous samples: 5 – 100 µm (water absorption!)

IR – Spectroscopy: Apparatus II

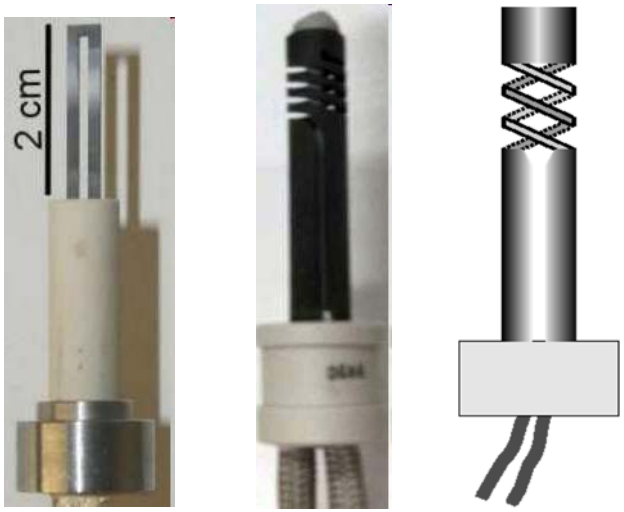

Source: Globar
SiC @ 1100°C

Detectors:

MCT (HgCdTe)
cooled with liquid N_2

also: InSb, InGaAs…..

Liquid Samples (~2 µl)

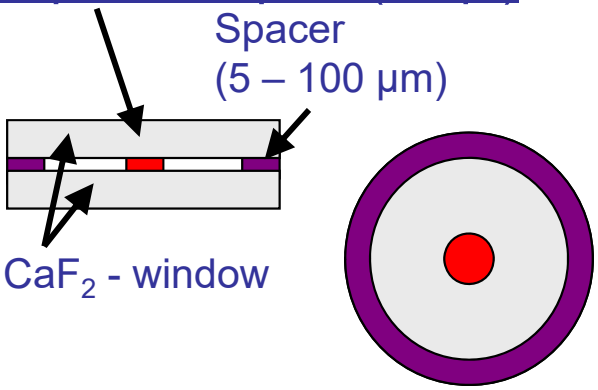

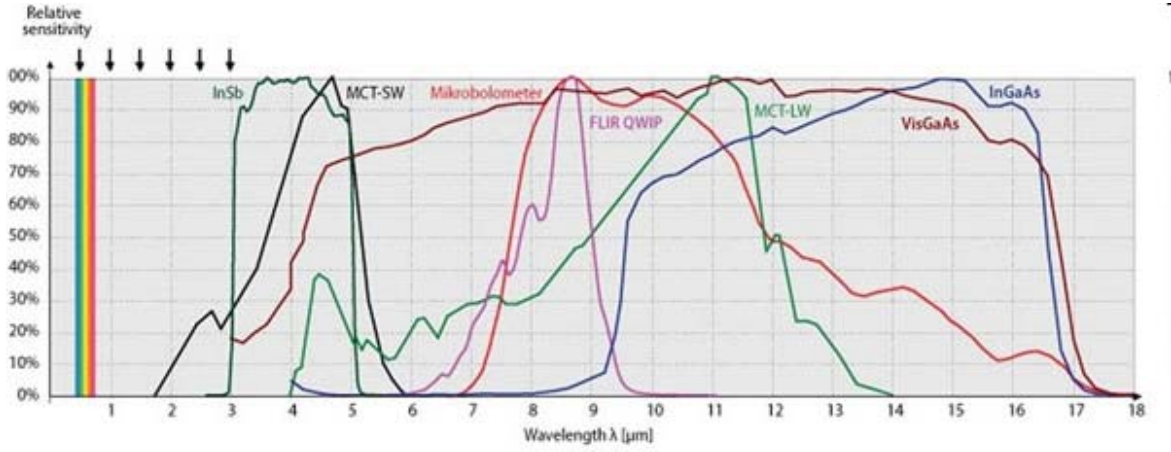

IR – Spectroscopy: Apparatus III

2. Fourier Transform IR (FTIR) Spectrometer

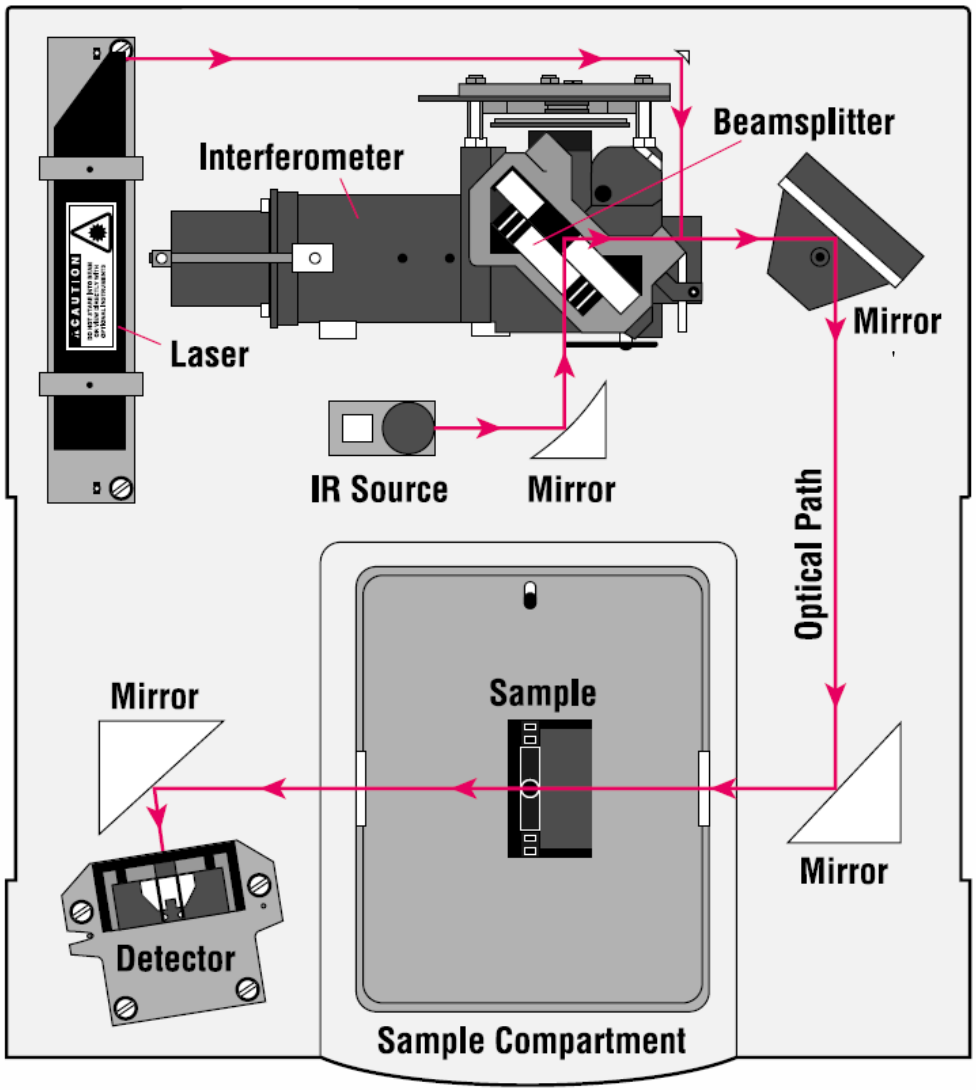

FTIR advantages over dispersive instruments:

1) Felgett's advantage: multiplexing - all frequencies are measured simultaneously

2) Jacquinot's advantage: throughput larger - no slits or apertures necessary

3) Connes's advantage: wavenumber stability - HeNe reference laser (632.8 nm)

Michelson Interferometer I

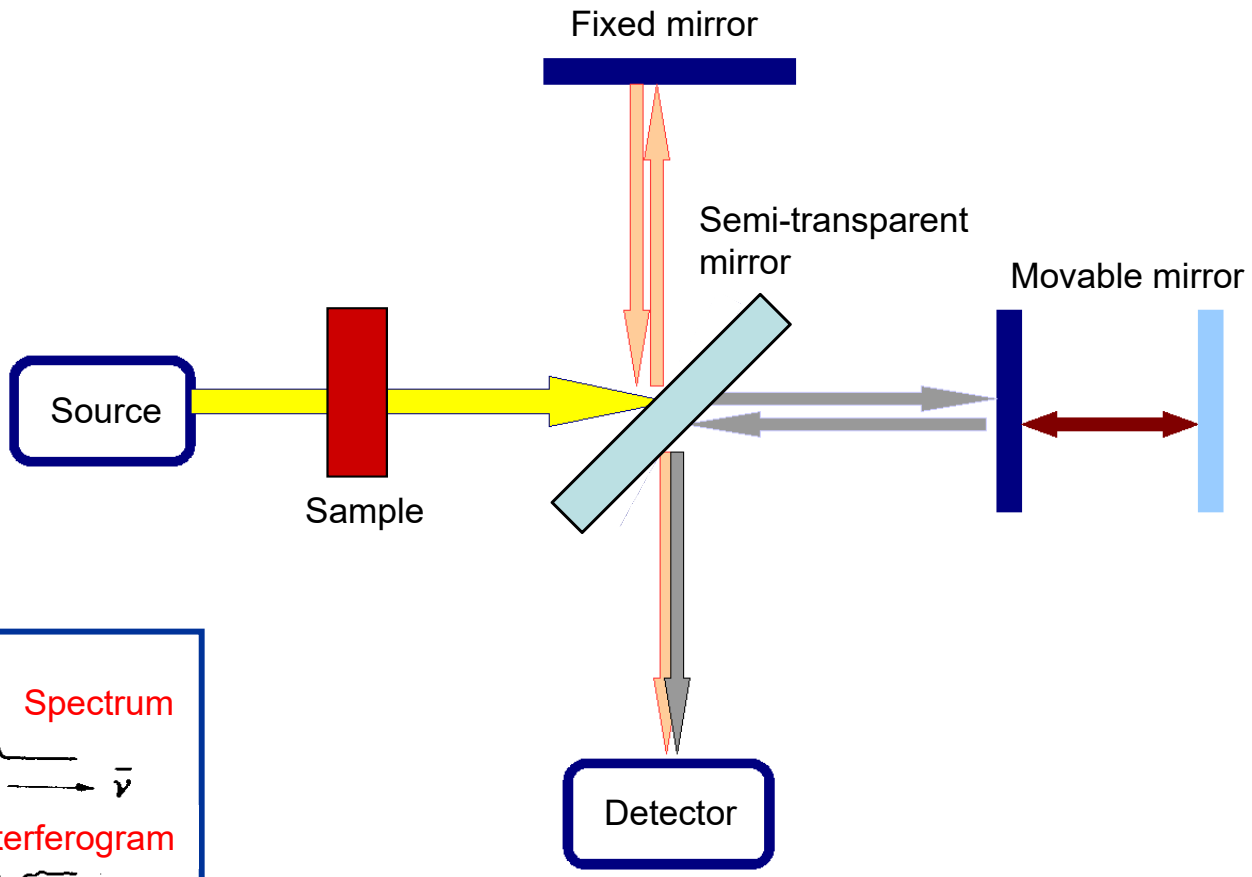

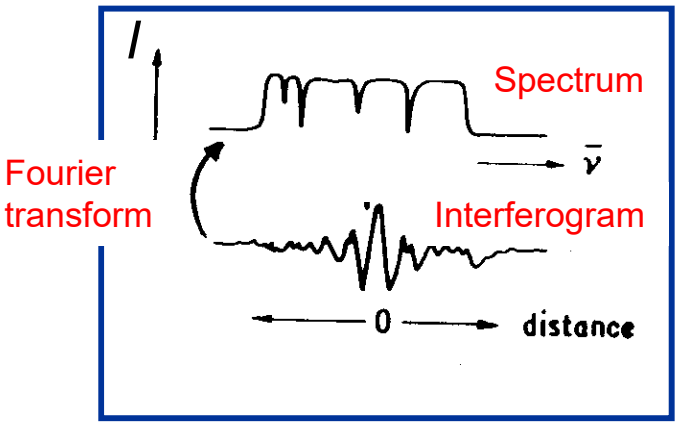

Interferogram, i.e., intensity as a function of the mirror position

$$S(\tilde{\nu}) = \int I(x) e^{2\pi i \tilde{\nu} x} dx$$

Transmission spectrum, i.e., intensity as a function of wavenumber

Michelson Interferometer II

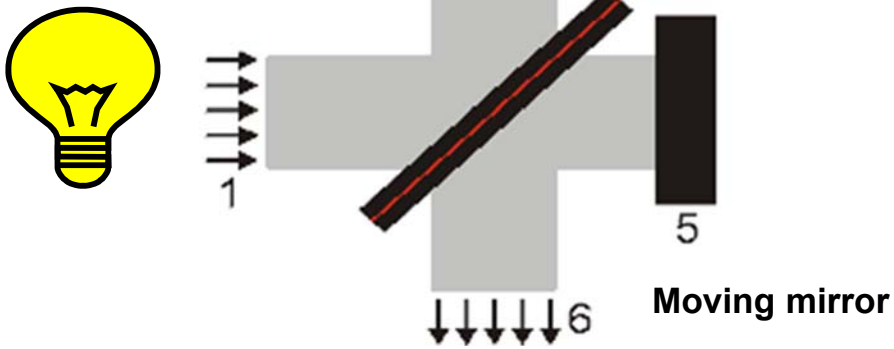

Detector

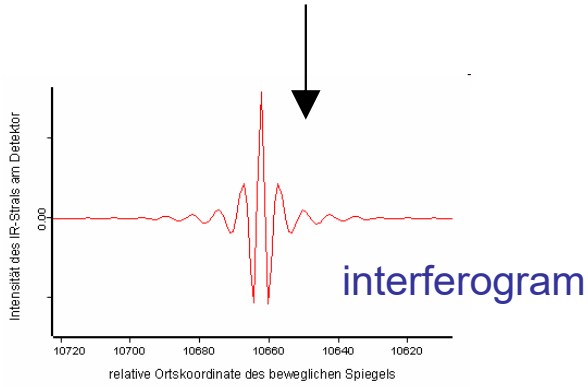

interferogram

Monochromatic Interference

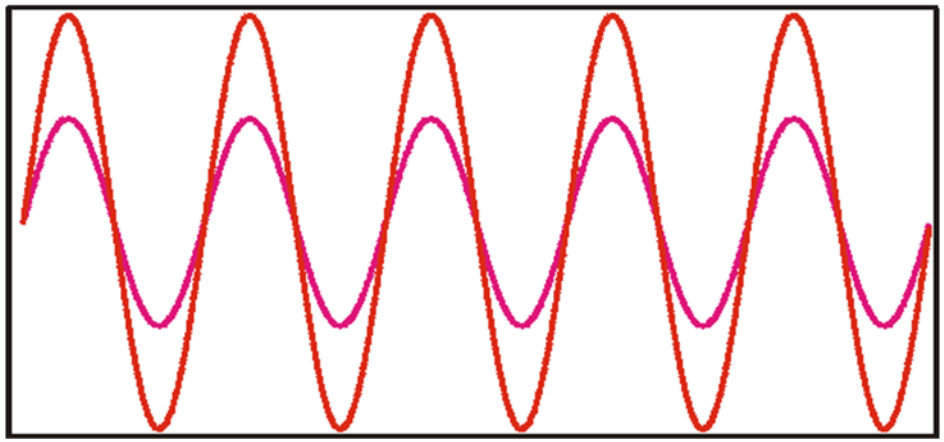

Gray: Reference / fixed mirror
Pink: moving mirror
Red: sum

time

Polychromatic Interference

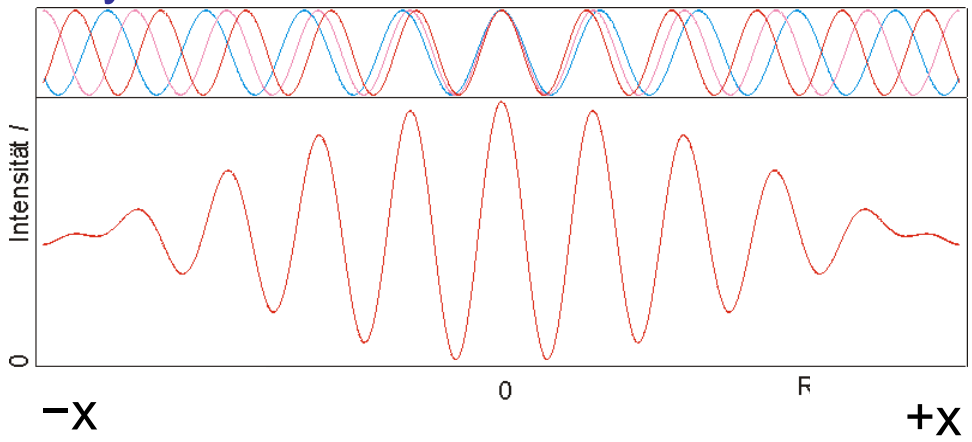

http://www.ir-spektroskopie.de/spec/ftir-prinzip/index.html

FTIR I

EM wave amplitude (norm.): $A = e^{i(kx'-\omega t)} = e^{2\pi i(\tilde{\nu}x'-\nu t)}$

Michelson interferometer: path difference *x*

$$A(x,\tilde{\nu}) = \frac{1}{2}\left[e^{2\pi i\tilde{\nu}x_0} + e^{2\pi i\tilde{\nu}(x_0+x)}\right]$$

$$= \frac{1}{2}e^{2\pi i\tilde{\nu}x_0}\left[1+e^{2\pi i\tilde{\nu}x}\right]$$

$$I(x,\tilde{\nu}) = A^*(x,\tilde{\nu})A(x,\tilde{\nu}) = \frac{1}{2}\left[1+\cos 2\pi\tilde{\nu}x\right]$$ (at the detector)

Spectral distribution $S(\tilde{\nu})$: light source spectrum plus sample absorption

$$I(x) = \int_0^\infty I(x,\tilde{\nu})S(\tilde{\nu})d\tilde{\nu}$$

$$= \frac{1}{2}\underbrace{\int_0^\infty S(\tilde{\nu})d\tilde{\nu}}_{I(0)} + \frac{1}{2}\int_0^\infty \cos(2\pi\tilde{\nu}x)S(\tilde{\nu})d\tilde{\nu}$$

Fourier cosine integral

FTIR II

Fourier inversion:

$$S(\tilde{\nu}) = \int_0^{x_{max}} \left[2I(x) - I(0) \right] \cos(2\pi\tilde{\nu}x)\, dx$$

In practice, mirror motion is limited to x_{max} $\Rightarrow$ resolution limit:

$$\delta\tilde{\nu} \geq \frac{1}{2\, x_{max}}$$

$\Rightarrow$ for a resolution of 1 cm^{-1}: x_{max} = 0.5 cm.

Simple Fourier Transforms

Wavenumber range:

$$\tilde{\nu}_{\max} - \tilde{\nu}_{\min} = \Delta\tilde{\nu} = \frac{1}{2\delta x}$$

Sampling (Nyquist) theorem

Resolution: $\delta\tilde{\nu} = \frac{1}{2\Delta x}$

resolution determined by range of mirror displacement

Uncertainty relation!

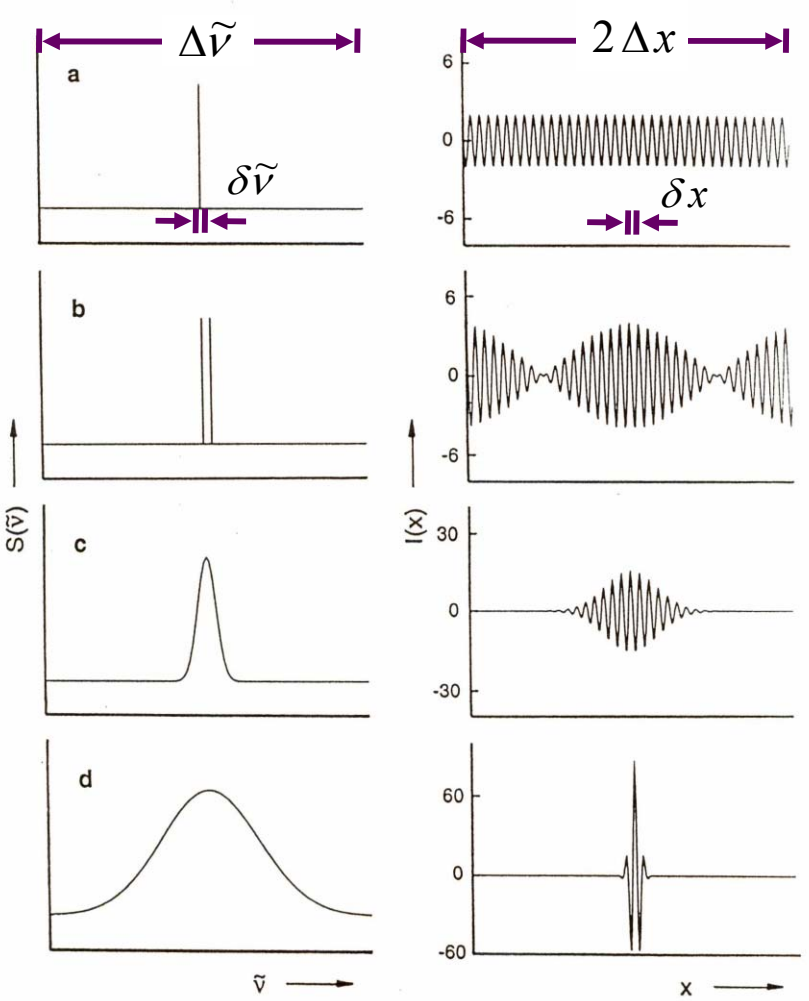

Apodization

- limited scan range affects line shapes (side lobes appear)!

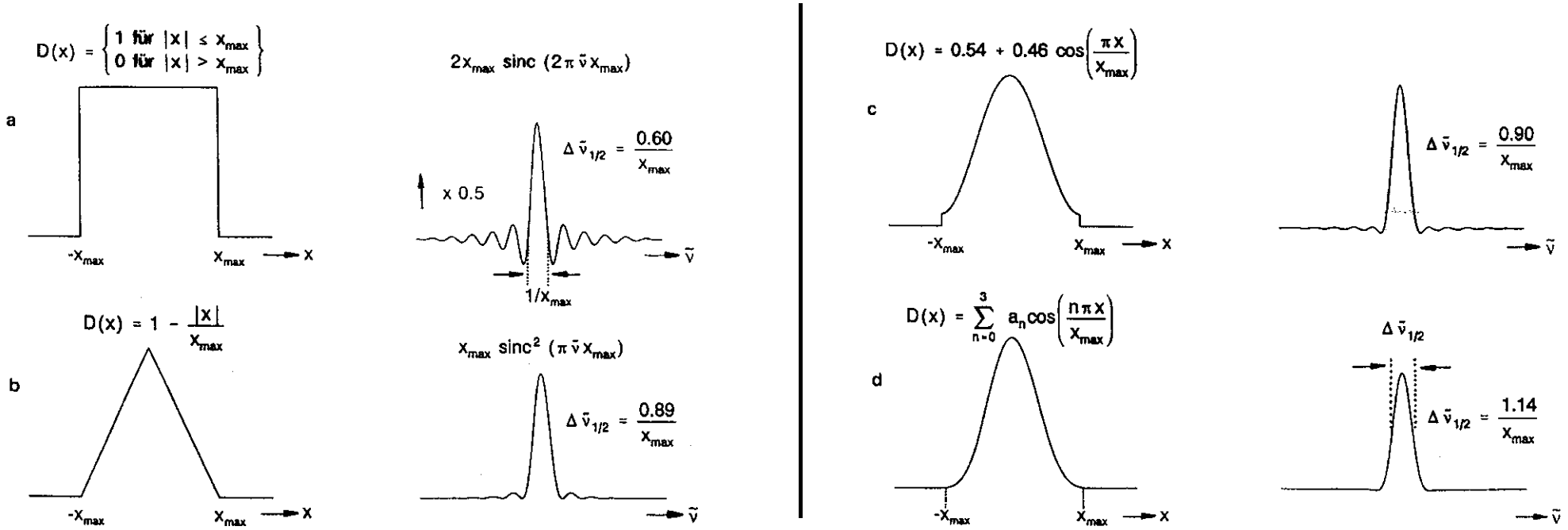

$$I'(x) = I(x) \cdot D(x) \quad \rightarrow \quad S(\tilde{\nu}) = S'(\tilde{\nu}) * D(\tilde{\nu})$$

$I'(x)$	$I(x)$	$S(\tilde{\nu})$	$S'(\tilde{\nu})$
employed in Fourier transform	measured $I(x)$ ($-x_{max} \le x \le x_{max}$)	spectrum after Fourier transform	ideal spectrum

Single Beam Spectra

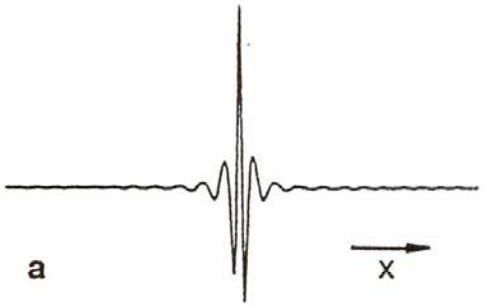

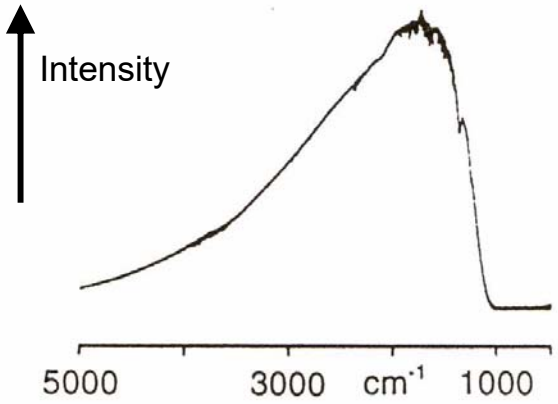

empty spectrometer, purged with N_2:
broad spectrum
→ narrow interferogram

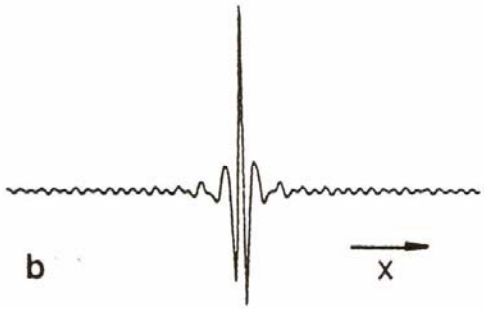

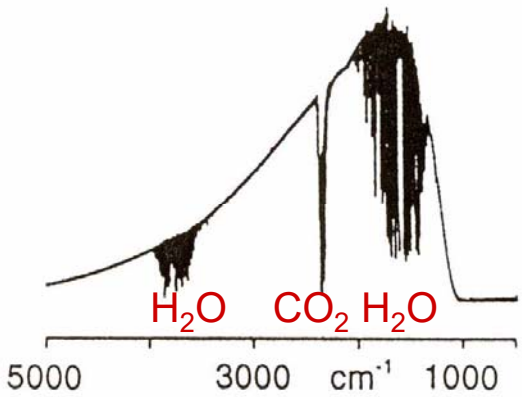

Empty spectrometer, not purged:
'air' absorbs: sharp features
→ broad component in interferogram

Transmittance Spectra

Single-beam spectra:

① empty KBr holder (‘background’)

② caffeine sample

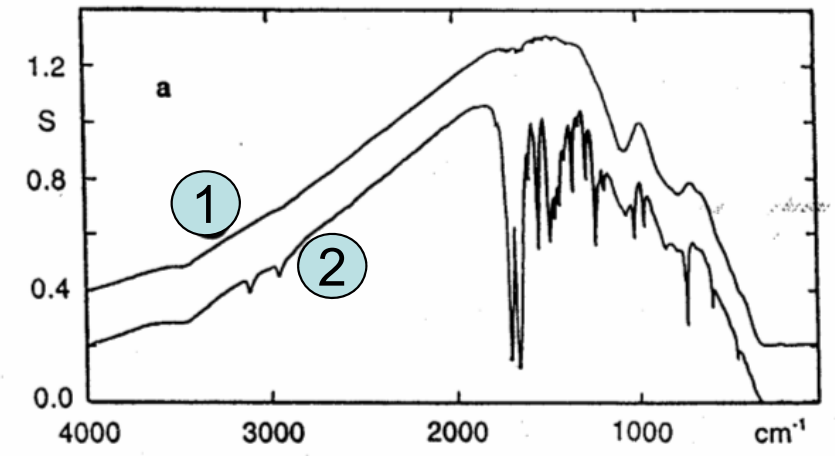

Transmittance spectrum:

$\tau = I / I_0$

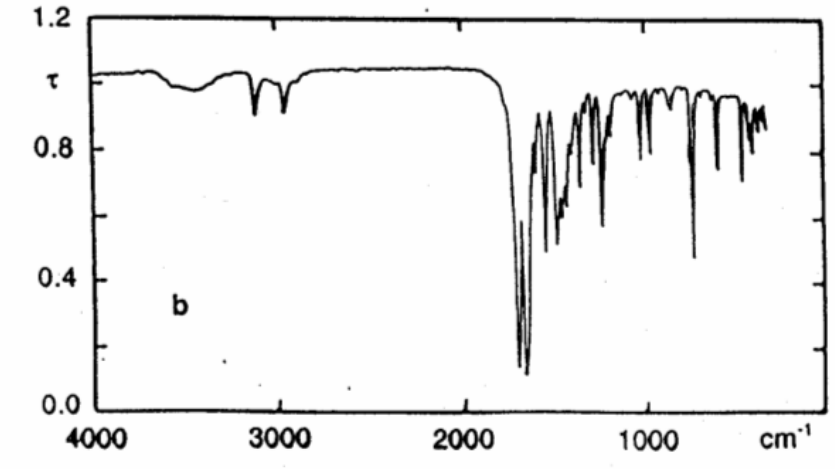

Absorbance:

$A = -\log \tau$

Photolysis Difference Spectroscopy I

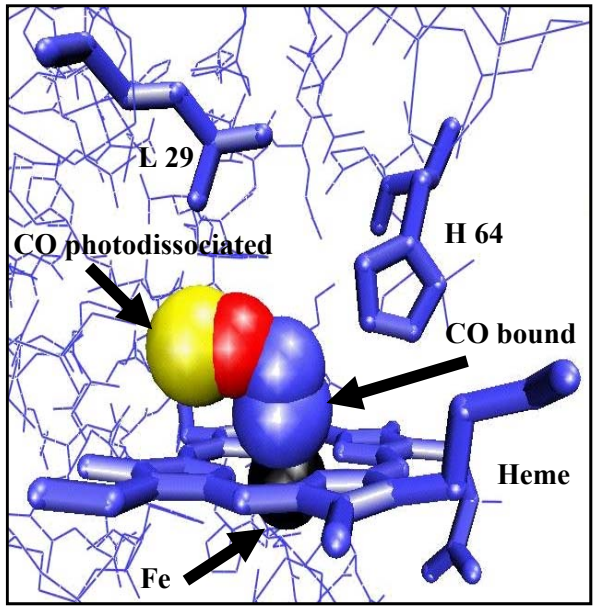

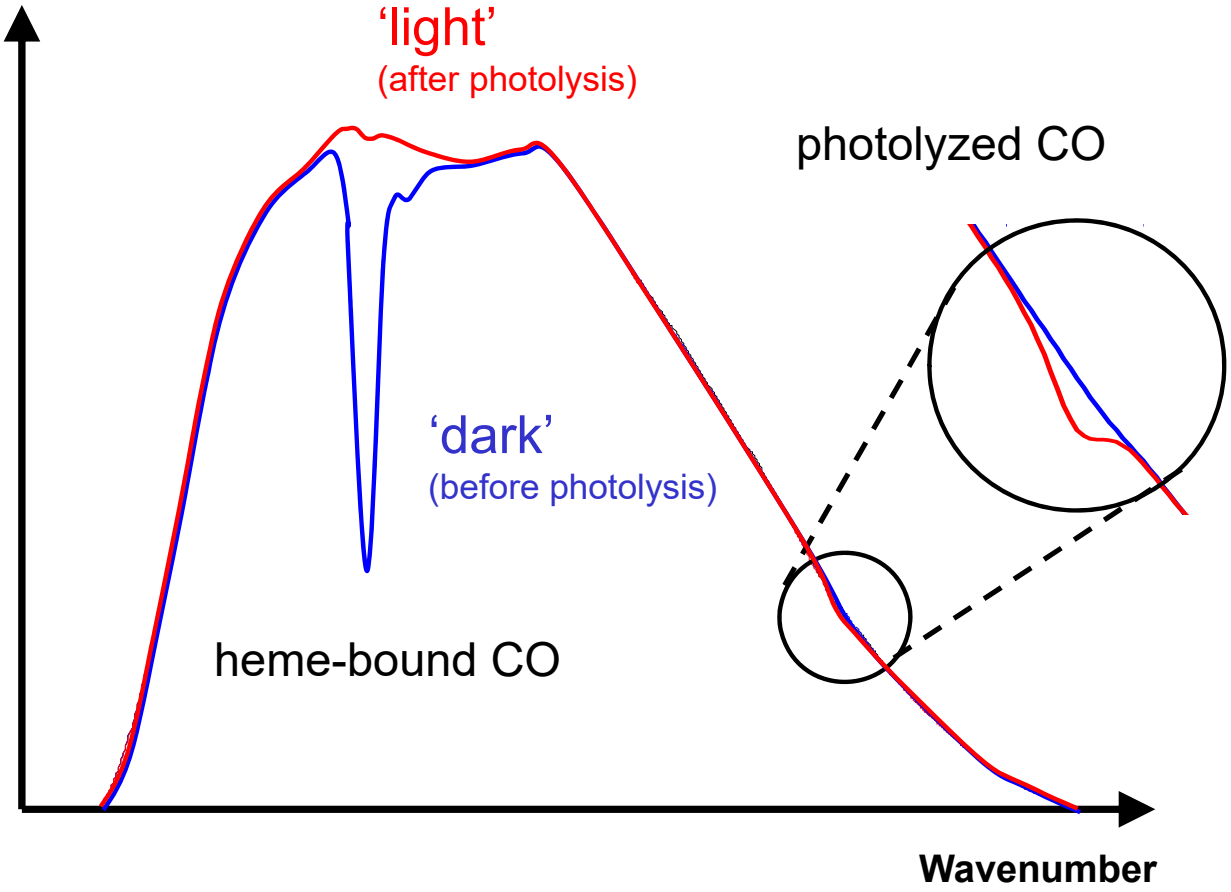

Carbonmonoxy myoglobin (MbCO):
Blue line: transmission of a MbCO sample with CO bound to the heme.
Red line: transmission of a MbCO sample after photolysis (at ~10 K), photodissociated ligands give rise to new bands.

Photolysis Difference Spectroscopy II

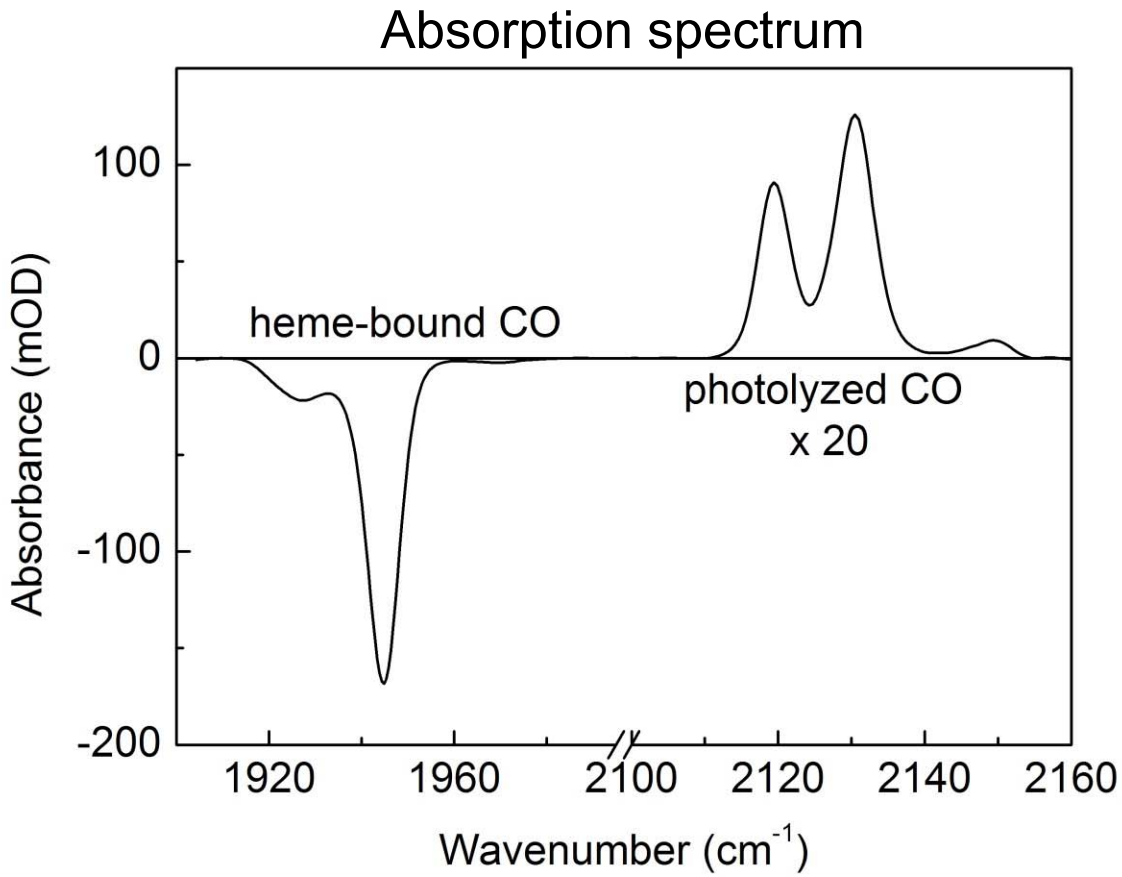

Photolysis Difference Spectroscopy III

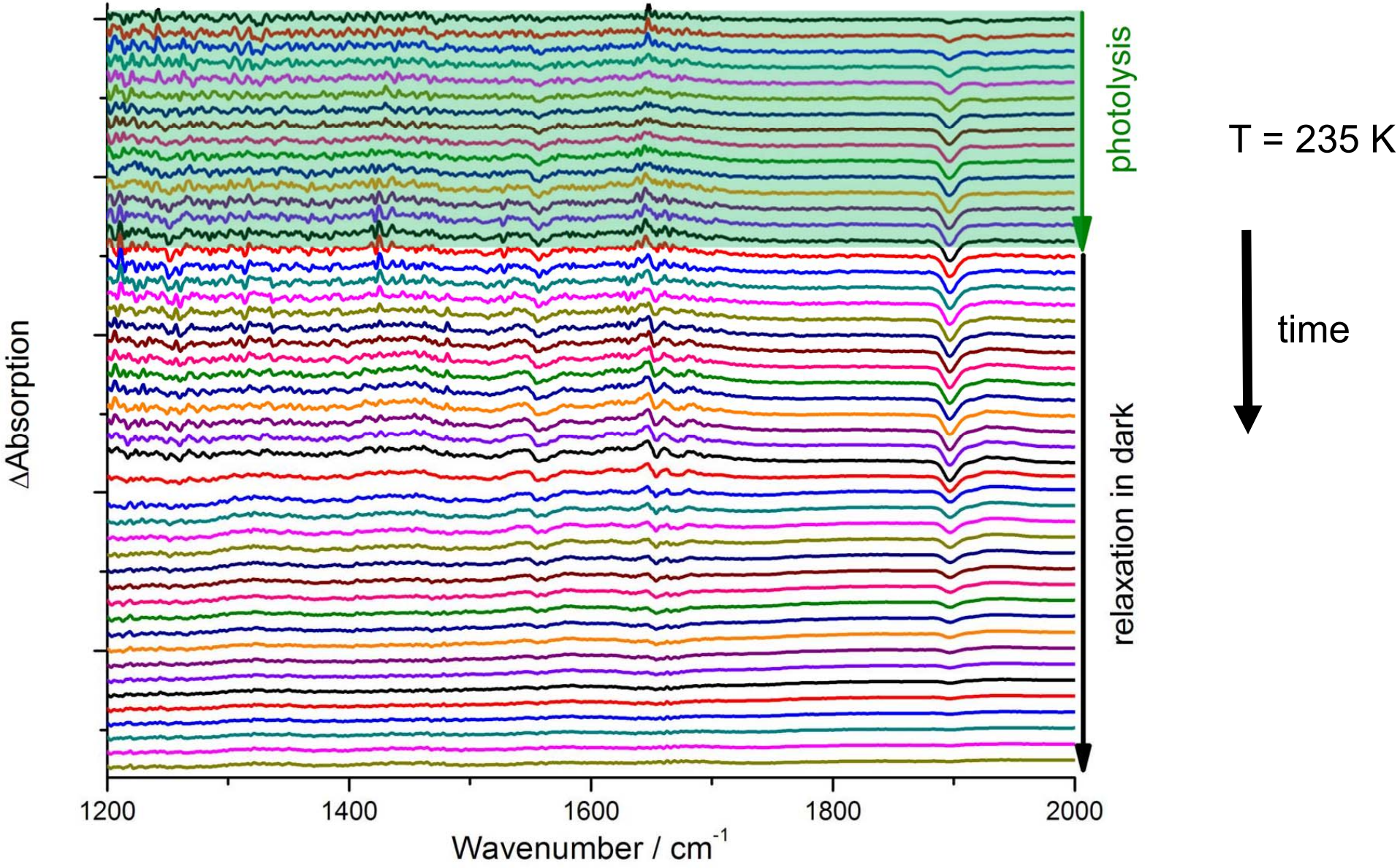

Photolysis of Indoleamine 2,3-dioxygenase (IDO)-CO

Isotope Effect in Cytochrome c Oxidase I

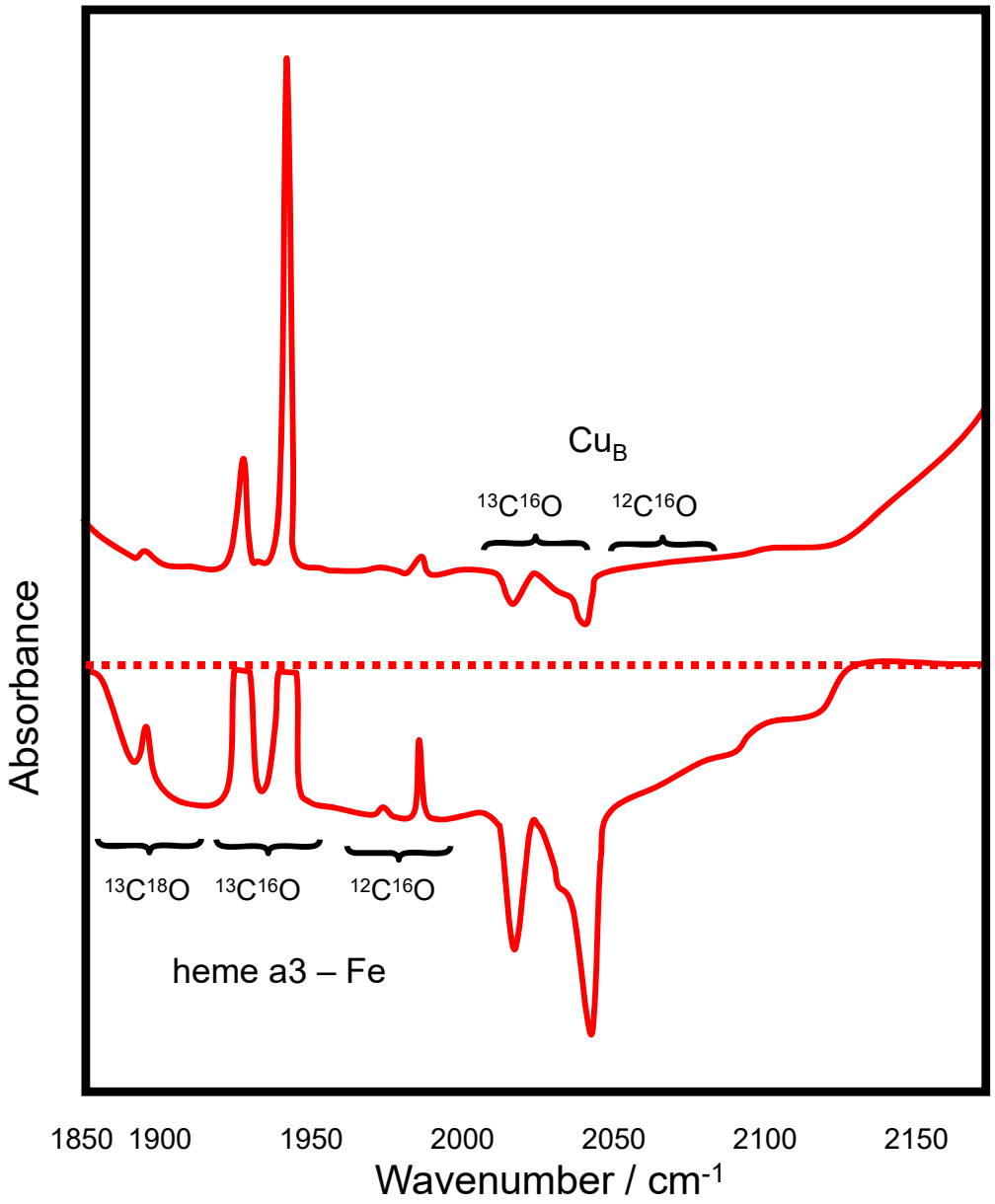

IR absorbance difference spectrum of isotope-enriched CO, coordinated to the central Fe of a heme a_3 group in the dark, minus photolyzed CO coordinated to Cu_B after illumination.

The sample is a mitochondrial preparation of CO-bound cytochrome c oxidase from beef heart, from which solvent water has been extracted with glycerol. The data were recorded at a temperature of **10 K**
(From Fiamingo et al., J. Biol. Chem. 257 (1982) 1639 – 1650).

Isotope Effect in Cytochrome c Oxidase II

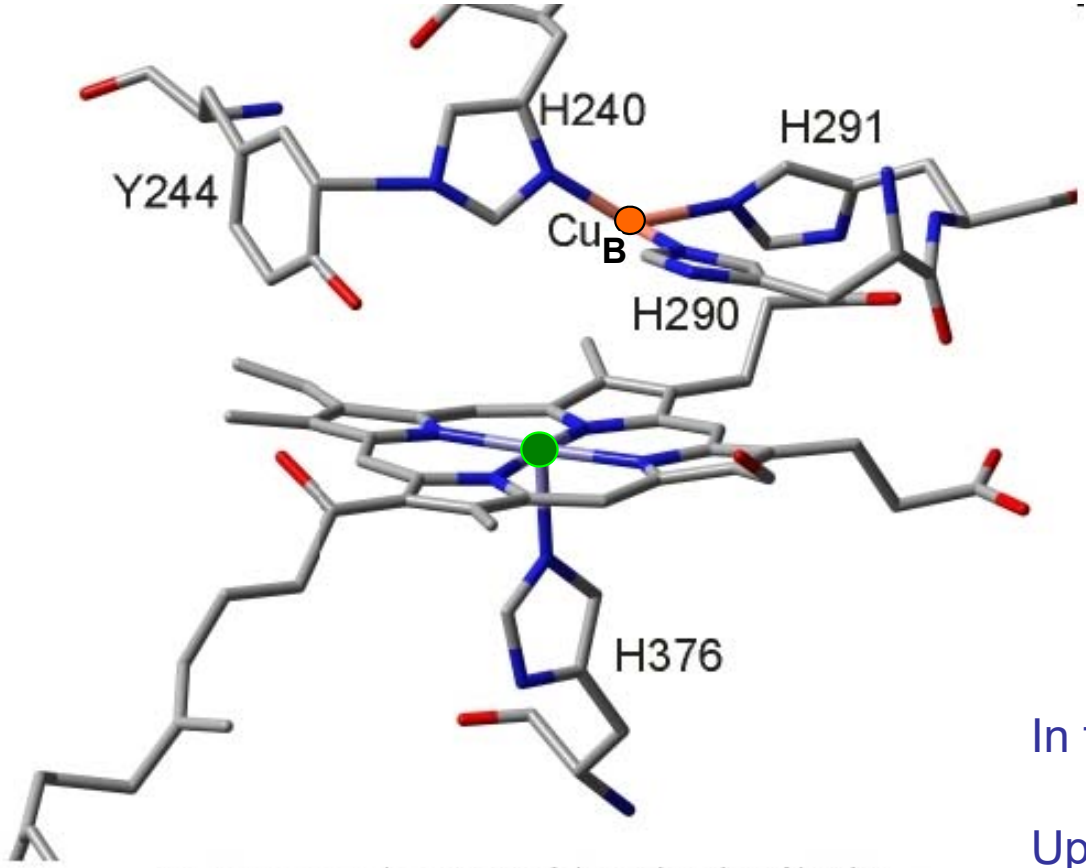

Figure 1: Crystal structure of the active site of bovine heart cytochrome c oxidase

CO is photolyzed from Fe ● and binds to Cu_B ●

In the dark, CO binds to the heme a_3 iron.

Upon photolysis, the CO coordinates with Cu_B before rebinding to Fe (T > ~140 K).

ATR: Avoiding the 'Water Problem'

Alternative to transmission technique:
ATR – Attenuated total reflection

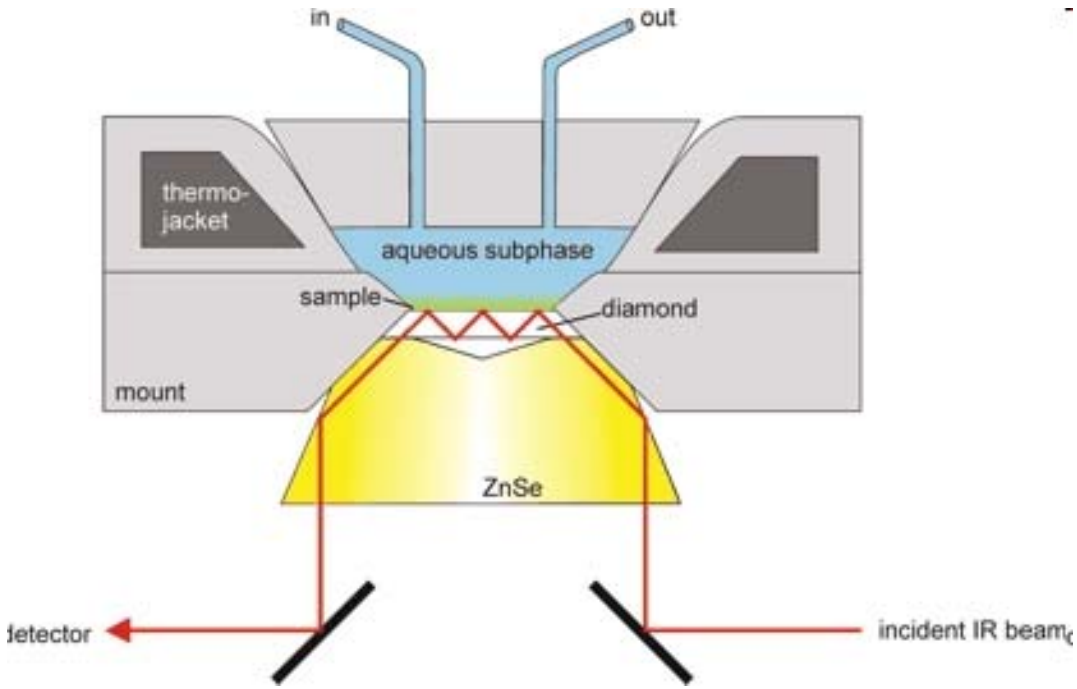

The IR beam is guided in an IR-transparent crystal by total reflection. The electromagnetic field may extend beyond the crystal surface for about one micron as a so-called ***evanescent field***. A protein sample prepared directly on the surface of the crystal is sensed by this evanescent wave and contributes to the absorption of the IR beam. The bulk water phase above is, due to the small penetration length (~1 µm) of the evanescent field, not sensed by the IR beam.

SEIRA: Surface-Enhanced IR Absorption

- Molecules adsorbed on ***metal island films*** or nanoscale particles exhibit 10 – 1000× more intense infrared absorption than without the metal.
- Electromagnetic (EM) interactions of the incident photon field with the ***metal*** and molecules are (mainly) responsible for the enhancement.

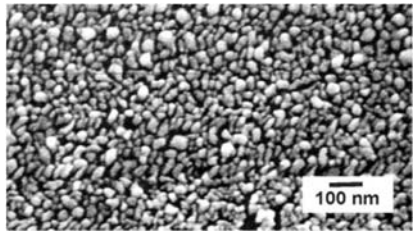

SEM image of a 10 nm thick Ag film vacuum-evaporated on Si

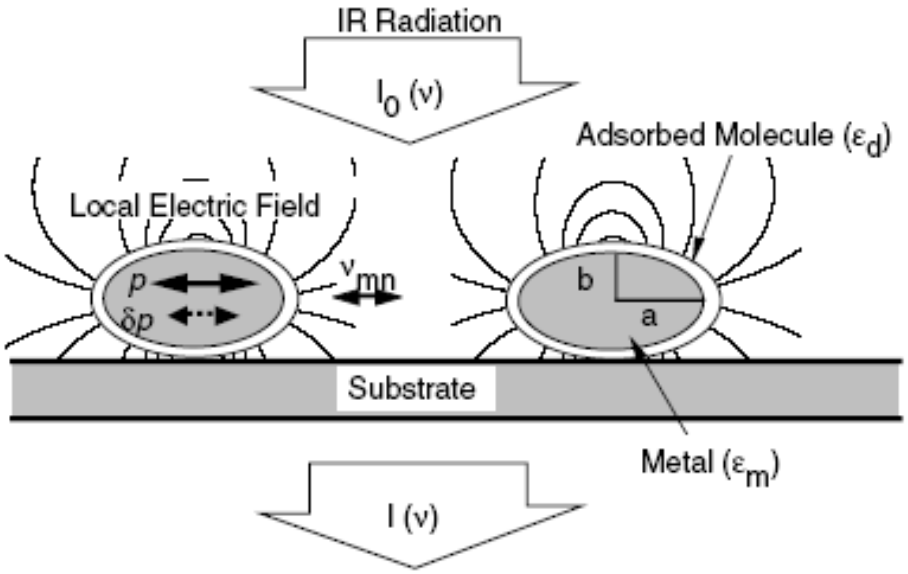

M. Osawa, Topics Appl. Phys. **2001**, 81, 163–187

The metal islands are polarized by the incident IR radiation through the excitation of a collective electron resonance, or localized plasmon modes, and the dipole *p* induced in an island generates a local EM field that is much stronger than the incident photon field around the island.

Combining ATR with SEIRA can give a signal enhancement of at least ~10^4.

SEIRA: Surface-Enhanced IR Absorption

Surface preparation

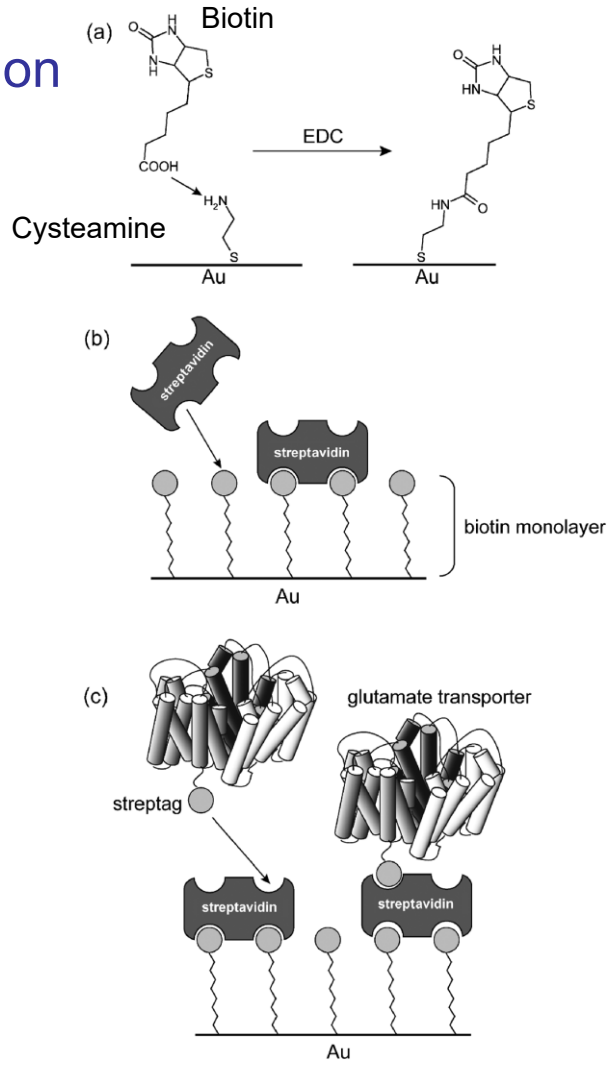

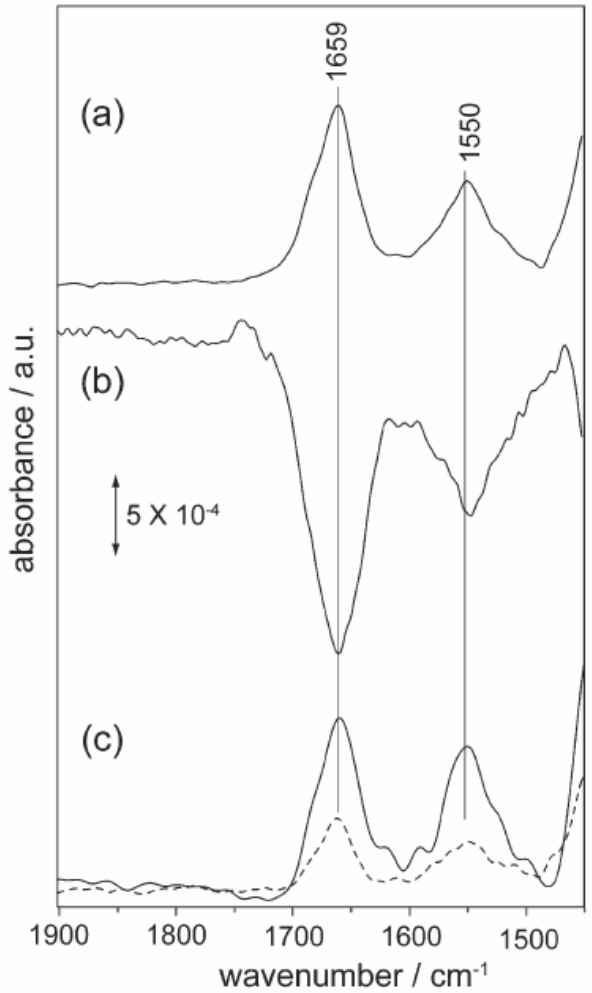

Fig. 6 SEIRA spectrum of (a) the bacterial glutamate transporter, *ecgltP*, specifically adsorbed *via* the N-terminal strep-tag to the streptavidin/biotin modified gold surface. (b) SEIRA spectrum of the same surface after removal of the *ecgltP*/streptavidin layer by the addition of 5 mM desthiobiotin. (c) Spectra of re-adsorbed *ecgltP* to the regenerated streptavidin/biotin modified gold surface (solid curve) and when the streptavidin/biotin layer is blocked by the addition of free biotin (dashed curve).

X. Jiang et al., Phys. Chem. Chem. Phys., 2008, 10, 6381–6387

Kinetic FTIR: Rapid-Scan / Step-Scan

- Techniques to observe fast dynamics (e.g., after photoexcitation)

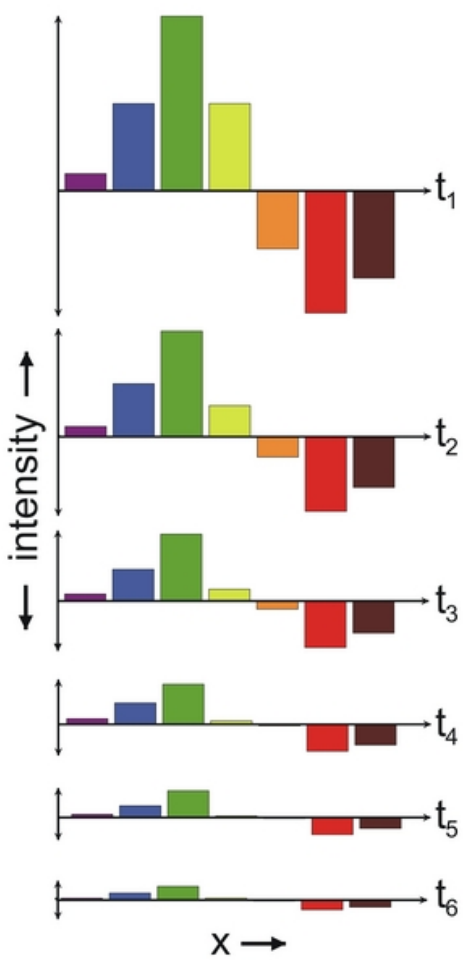

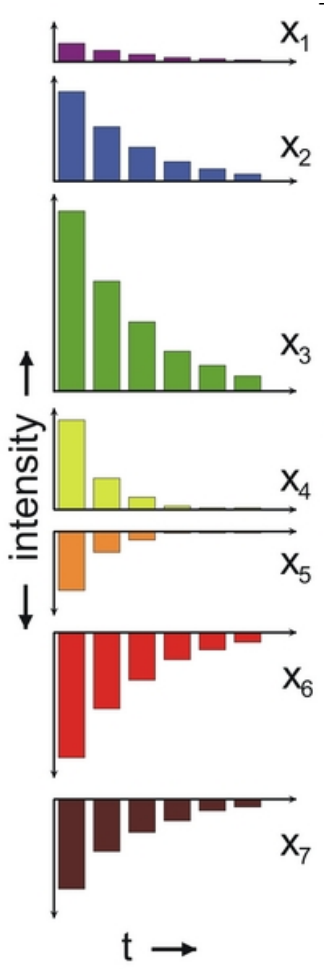

Rapid scan: Continuously perform fast scans (time resolution: ms), works for irreversible processes.

Step scan: stepwise movement of mirror (time resolution: ns - µs), needs repetitive process.

Step-Scan FTIR

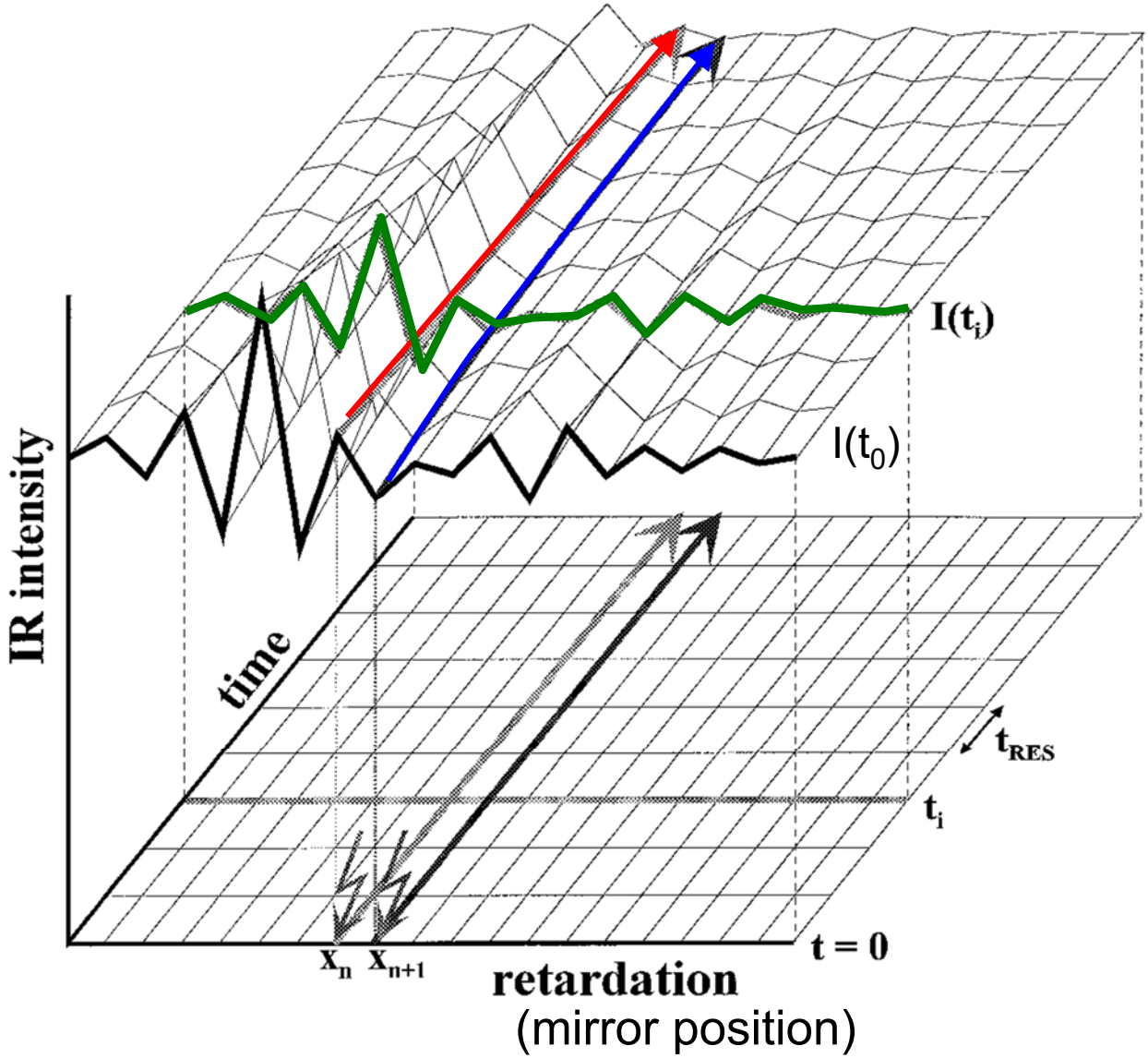

Step scanning requires samples that can be cycled through the same process many times.

Step-scan principle:

- Mirror is stopped at sampling positions x_n.
- Reaction is initiated (laser flash).
- Time dependence of the IR intensity is measured.
- After equilibration, scanner steps to the next position x_{n+1}, and the reaction is started again.
- After measuring at all sampling positions, the data are rearranged to time-dependent interferograms, $I(t_i)$.
- Fourier transformation yields the time-dependent spectra.

Rammelsberg et al., APPLIED SPECTROSCOPY, 51, 558 (1997)

Photocycle of Bacteriorhodopsin (bR)

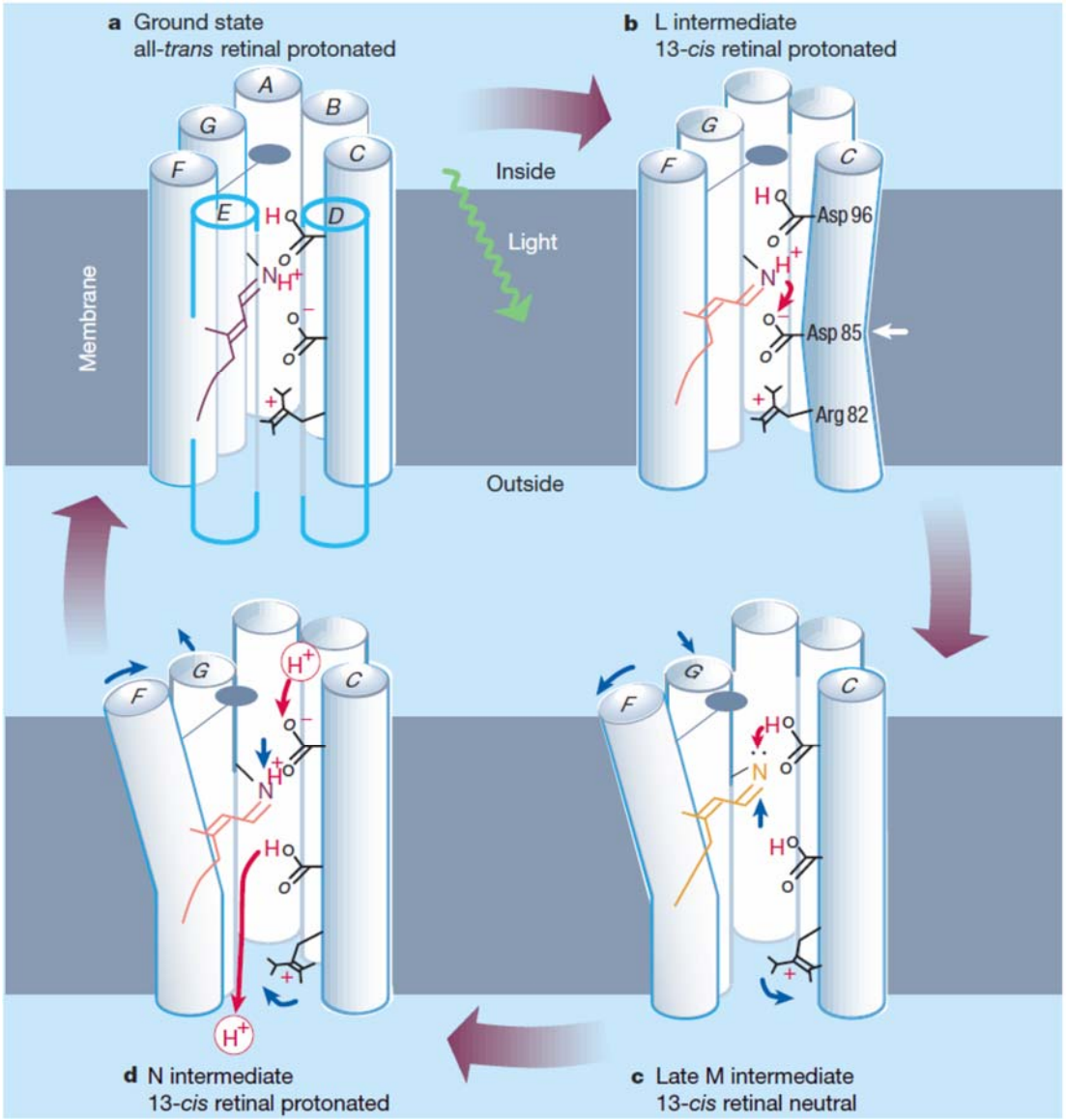

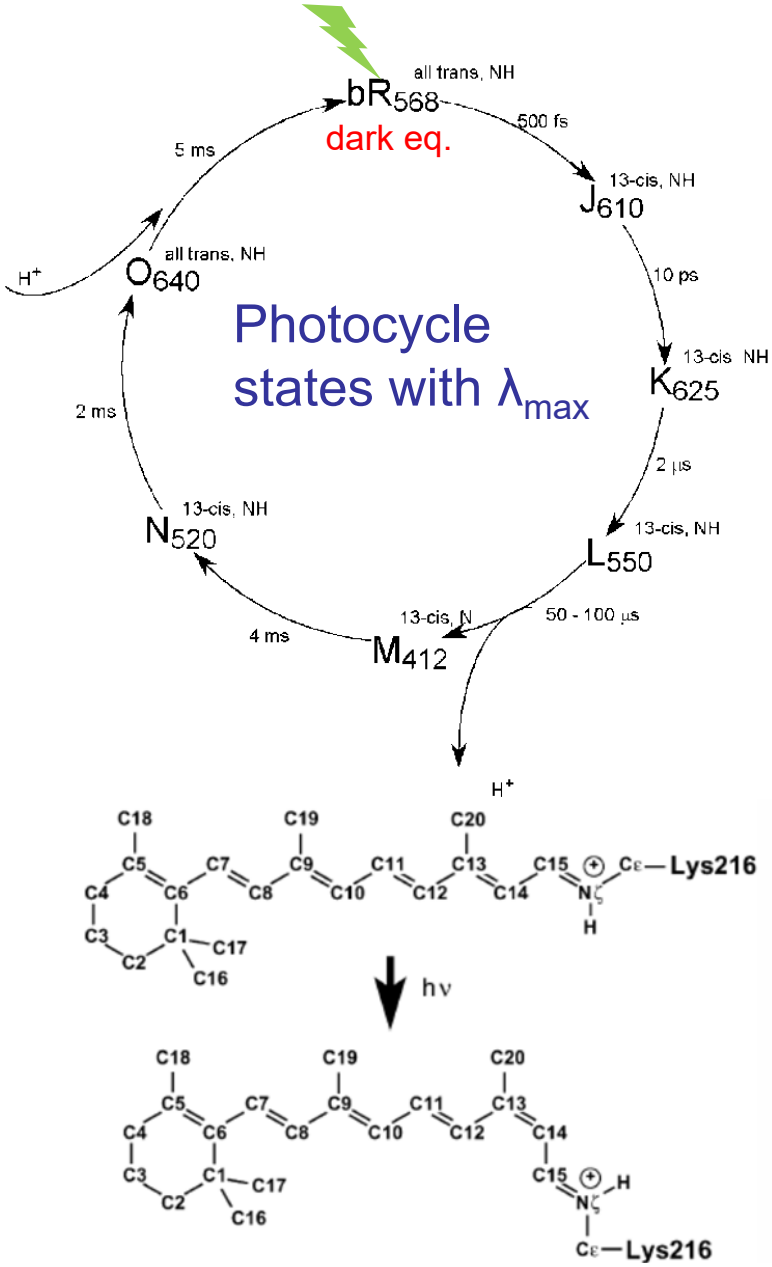

Step-Scan FTIR on Bacteriorhodopsin

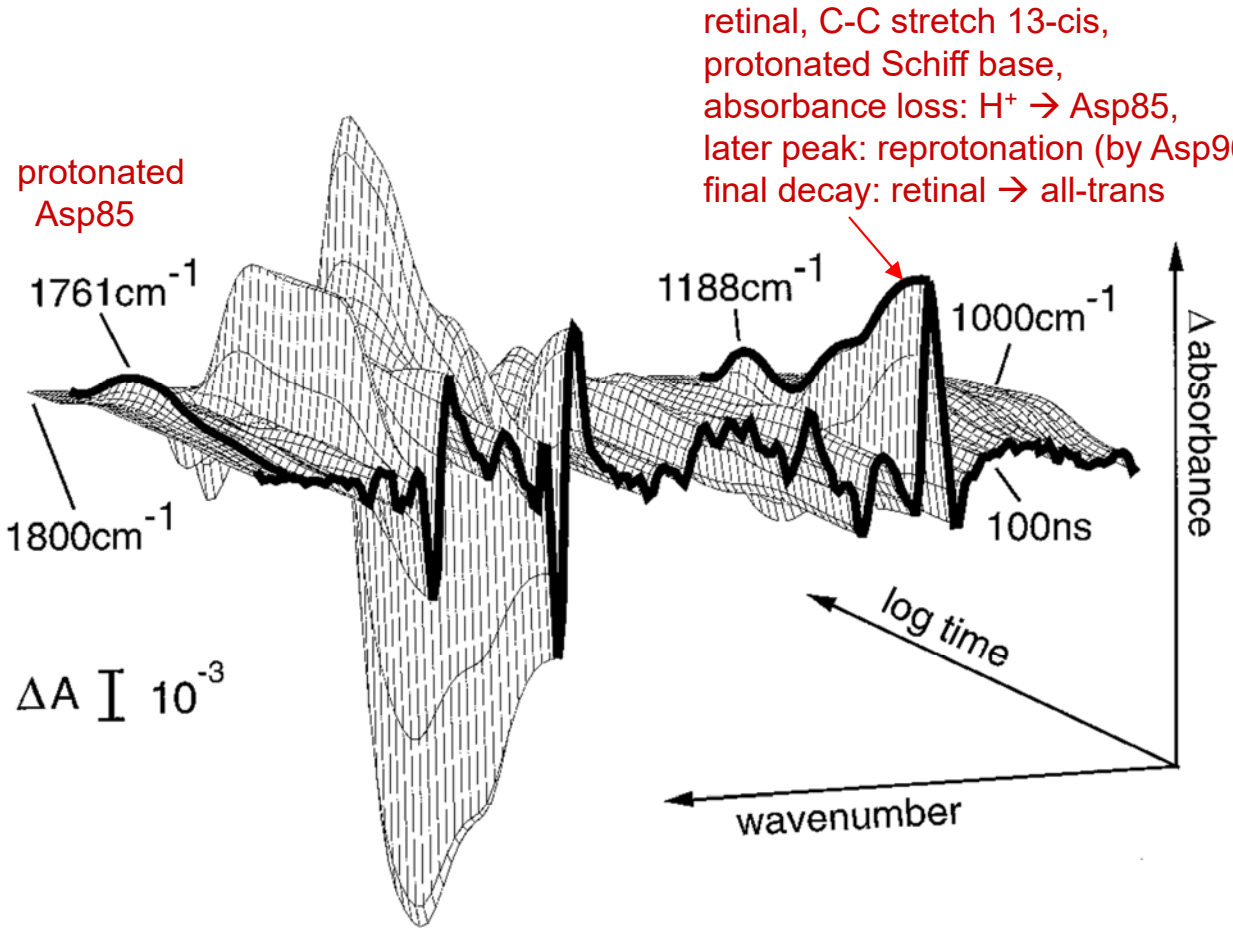

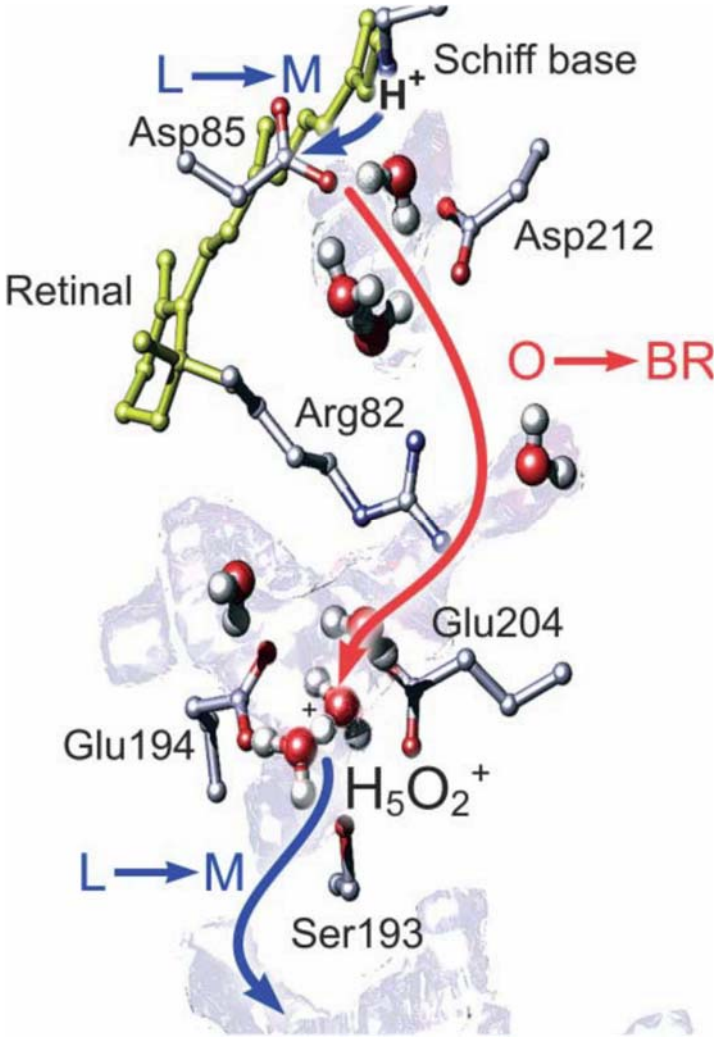

→ Schiff base proton is transferred to Asp85

Three-dimensional representation of the IR absorbance changes during the bacteriorhodopsin photocycle, measured between 1800 and 1000 cm^{-1} with 100-ns time resolution and 3-cm^{-1} spectral resolution.

Proton Movement

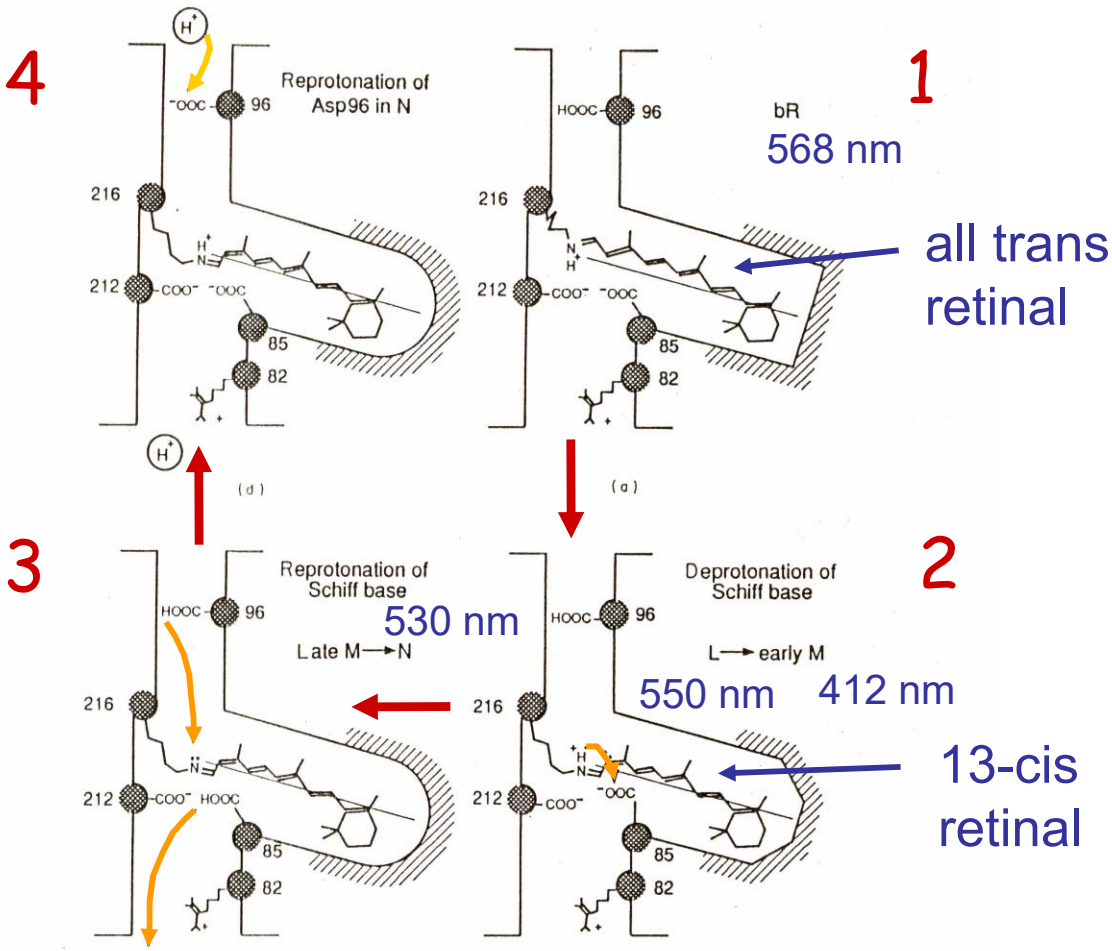

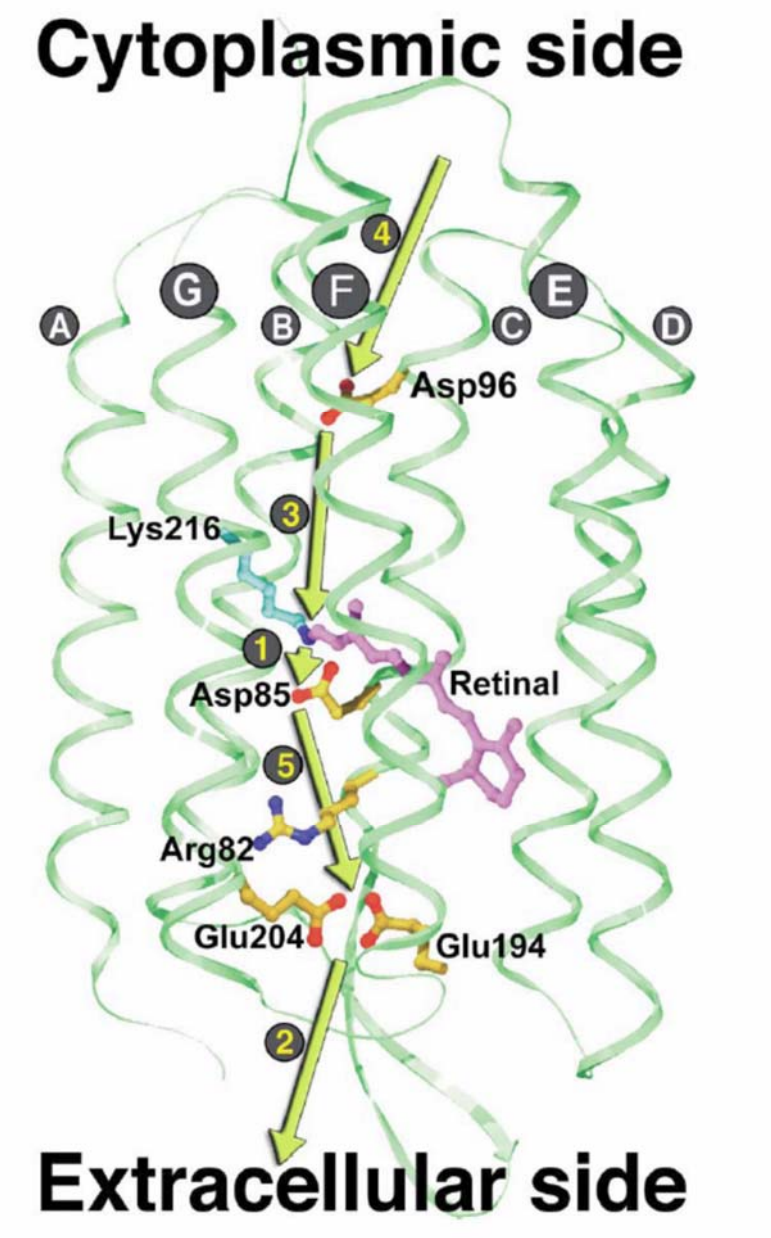

Biophysics II

Raman Scattering

Uli Nienhaus

Prof. G. U. Nienhaus, Vorlesungsunterlagen Biophysik II, SS 2023.
Nur zum KIT-internen, vorlesungsbegleitenden Gebrauch.
Weitergabe und anderweitige Nutzung verboten.

Raman Scattering I

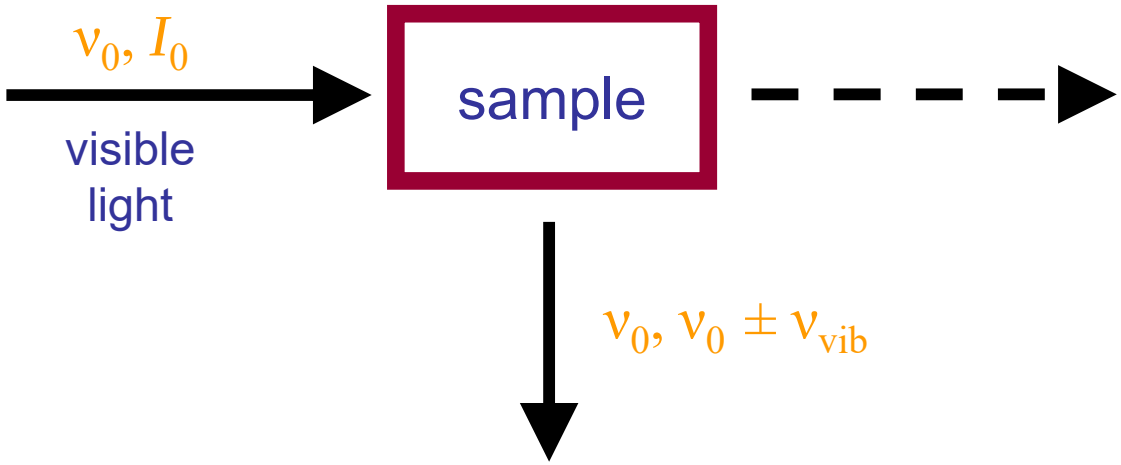

Rayleigh Scattering: ν_0, $10^{-3}\, I_0$

Raman Scattering: $\nu_0 \pm \nu_{vib}$, $10^{-6} \ldots 10^{-9}\, I_0$

Raman Scattering II

Physical explanation (classical): Energy $E = -\vec{\mu} \cdot \vec{E}$

incident EM-wave

$$\vec{\mu} = \alpha \vec{E} = \alpha \vec{E}_0 \cos(2\pi\nu_0 t)$$

induced dipole

polarizability

$$\alpha = \alpha_0 + \frac{\partial \alpha}{\partial Q} Q = \alpha_0 + \frac{\partial \alpha}{\partial Q} Q_0 \cos(2\pi\nu_{vib} t)$$

normal mode coordinate

$$\vec{\mu} = \left(\alpha_0 + \frac{\partial \alpha}{\partial Q} Q_0 \cos(2\pi\nu_{vib} t) \right) E_0 \cos(2\pi\nu_0 t)$$

$$= \alpha_0 E_0 \cos 2\pi\nu_0 t + \frac{\partial \alpha}{\partial Q} Q_0 E_0 \frac{1}{2} \left[\cos 2\pi(\nu_0 + \nu_{vib})t + \cos 2\pi(\nu_0 - \nu_{vib})t \right]$$

Rayleigh scattering

anti-Stokes

Stokes

Raman scattering

Raman Excitation Processes

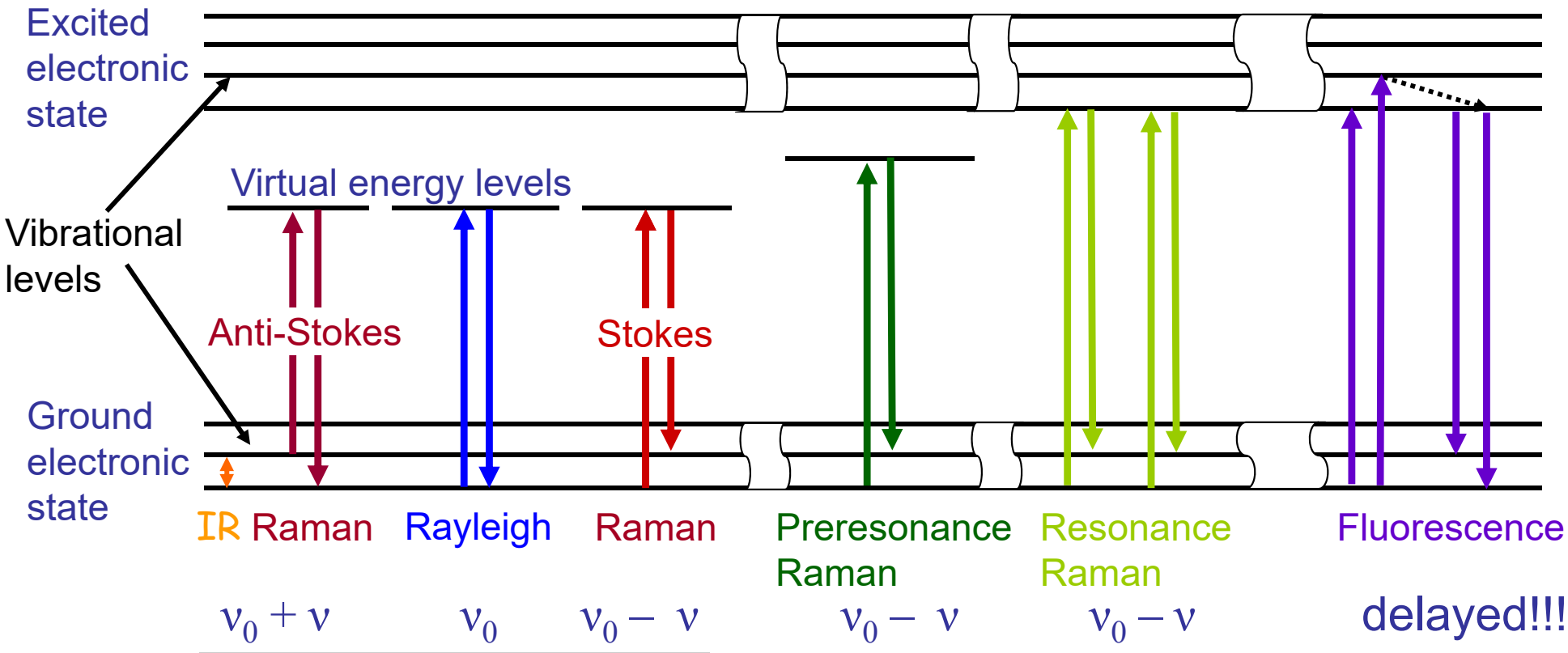

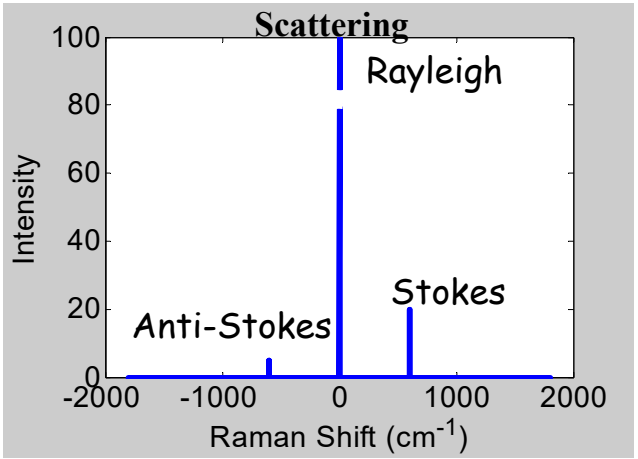

Raman Spectroscopy – Band Assignment

- Calculations: Quantum chemical, normal mode analysis
- Model systems (e.g., only cofactor instead of whole protein)
- Isotope effect
- Structure modification (e.g., mutation or chemical)
- Environmental changes: redox potential, pH, p, T, cosolvents

Raman Scattering Apparatus

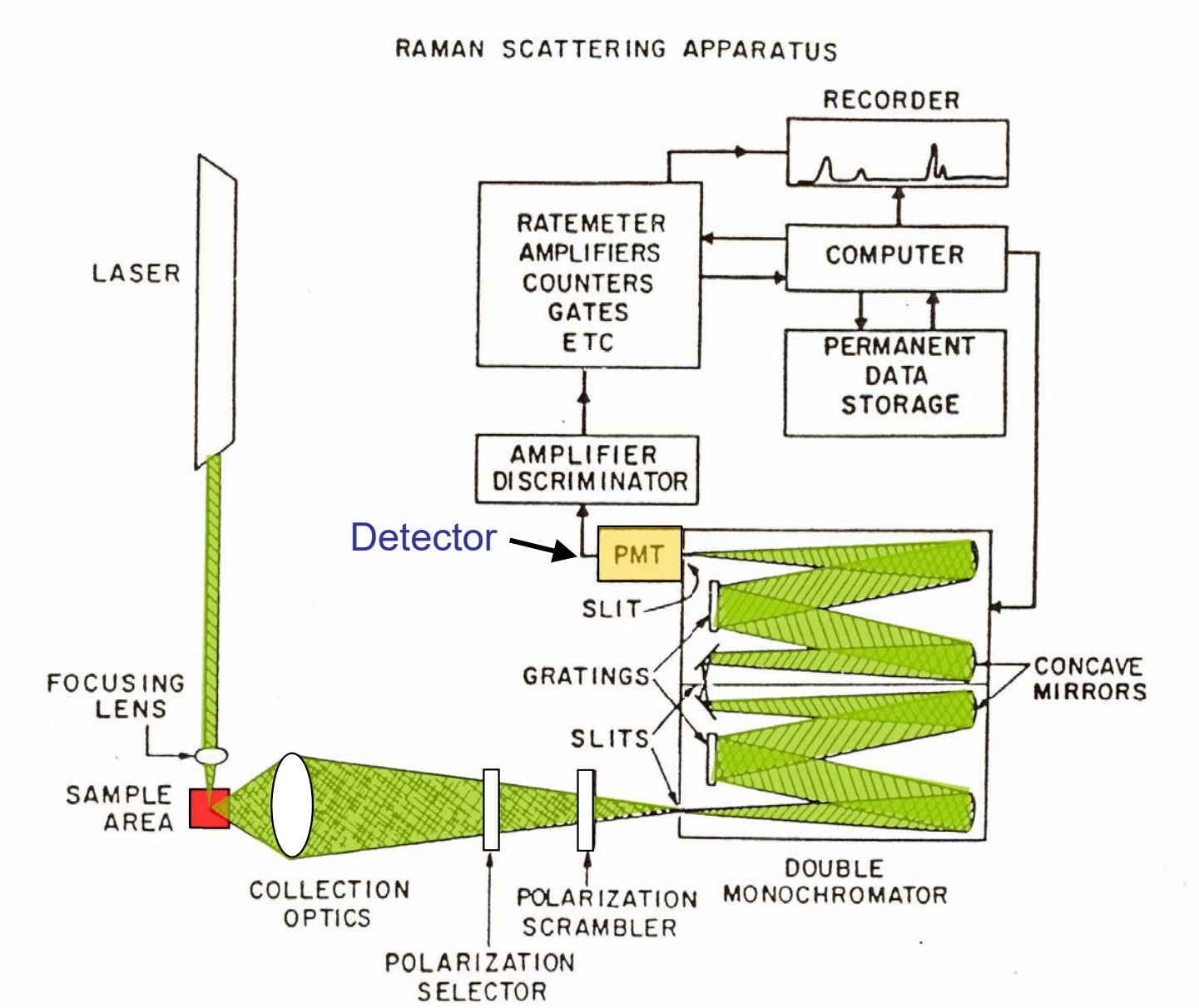

Proteins: T Dependence of RNase A

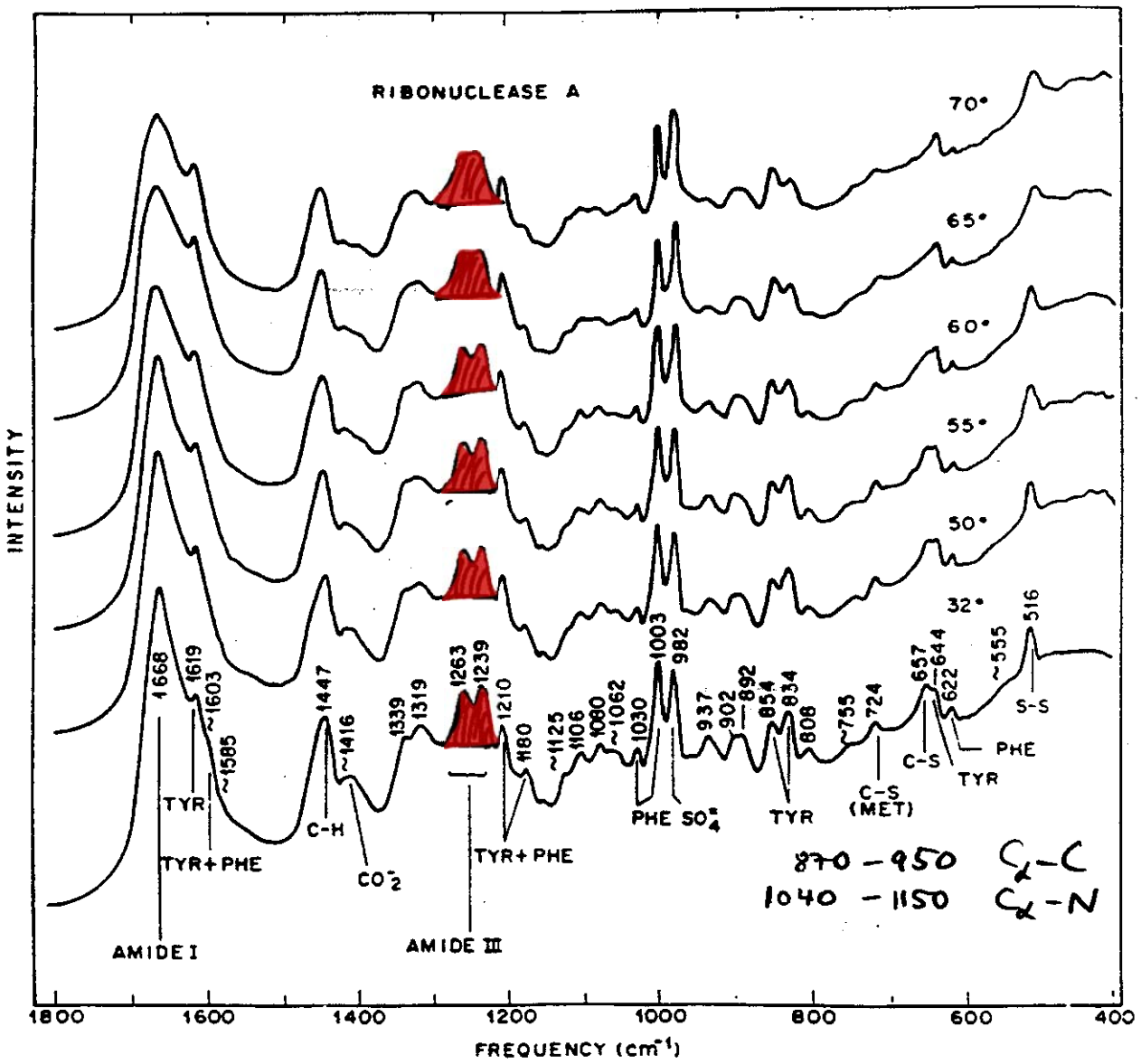

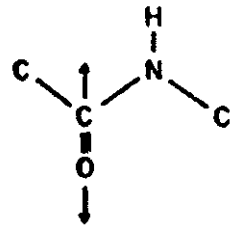

AMIDE I
1645 – 1680 cm⁻¹

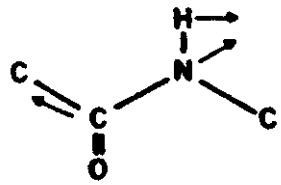

AMIDE III
1230 – 1300 cm⁻¹

32°C:
30 res. α-helix (1265)
40 res. β-sheet (1240)
54 res. intermediate (1250)

with increasing T:
→ 1250 cm^{-1} line increases
→ random coil

Nucleic Acids

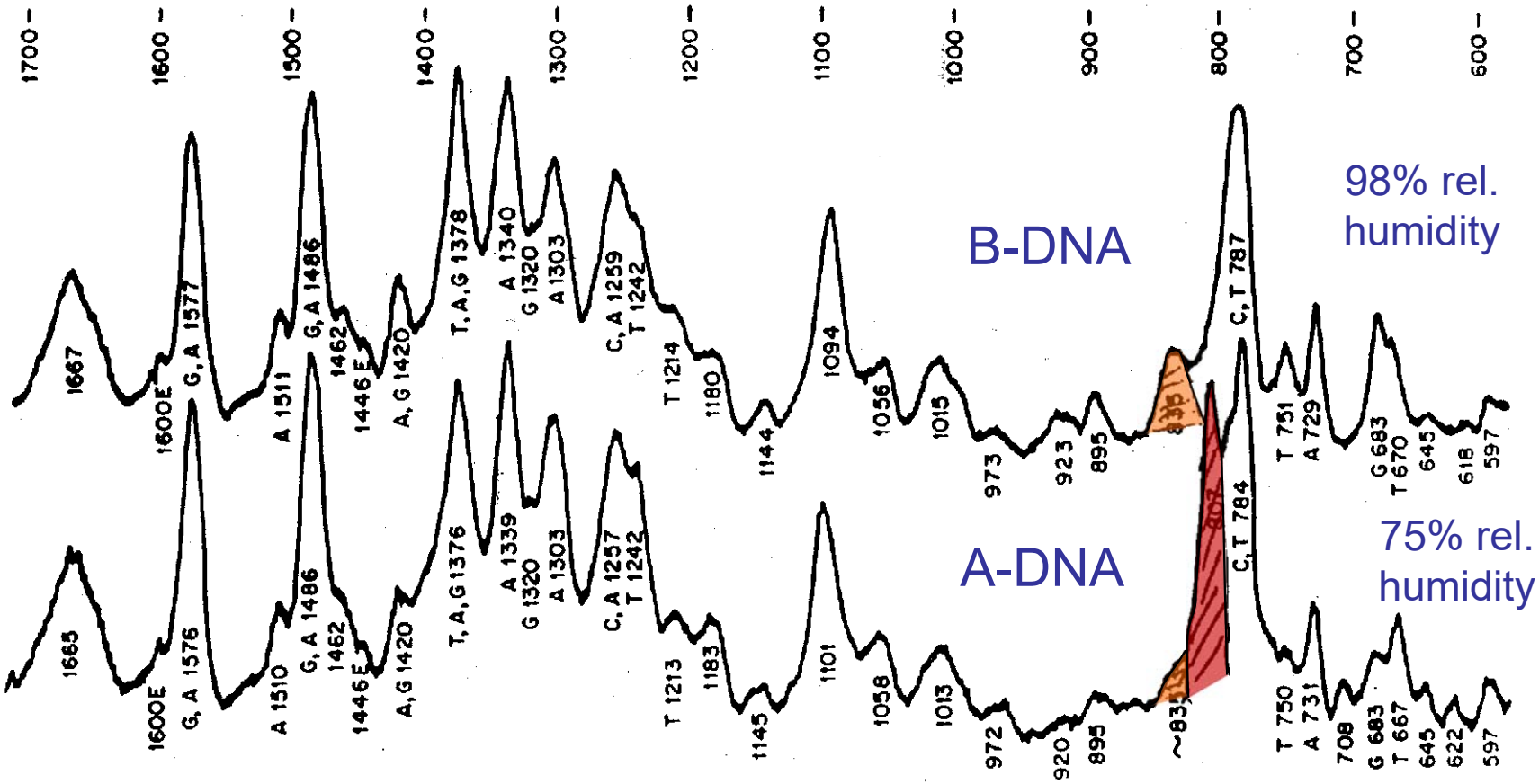

Raman spectra of calf thymus DNA at different relative humidities.

phosphodiester symmetric stretch

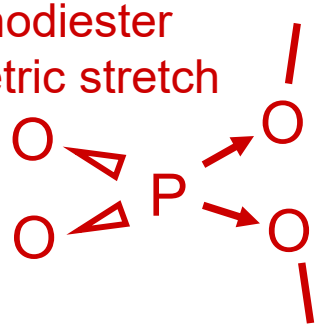

Phospholipids and Membranes

Raman modes of phospholipids and membranes:

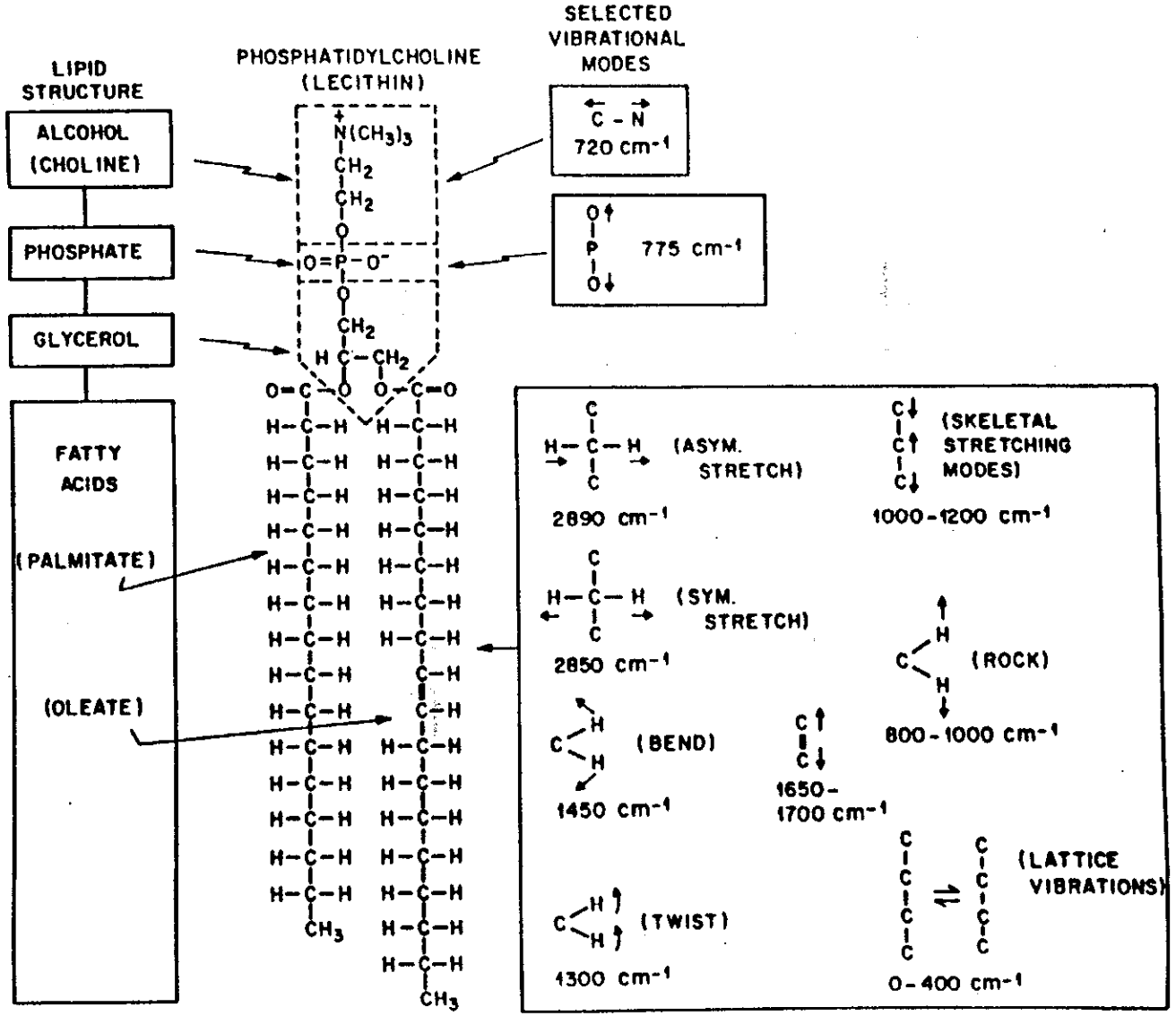

Resonance Raman Spectroscopy

- Energy of the exciting laser is tuned to an electronic transition of the molecule.
- Extremely useful for large biomolecules with (non-fluorescent!) chromophores (e. g., heme) embedded in their structures.
- Resonance enhancement occurs only for vibrational modes associated with the chromophore, thus reducing the complexity of the spectrum.
- Key advantage over traditional Raman spectroscopy: enormous increase in the intensity of Raman peaks (up to 10^6).
- Disadvantage of resonance Raman: peak heights depend on the amplitude of the vibration and on the unknown coupling strength between the vibration and the resonantly excited electronic state.

Dependence on Excitation Wavelength

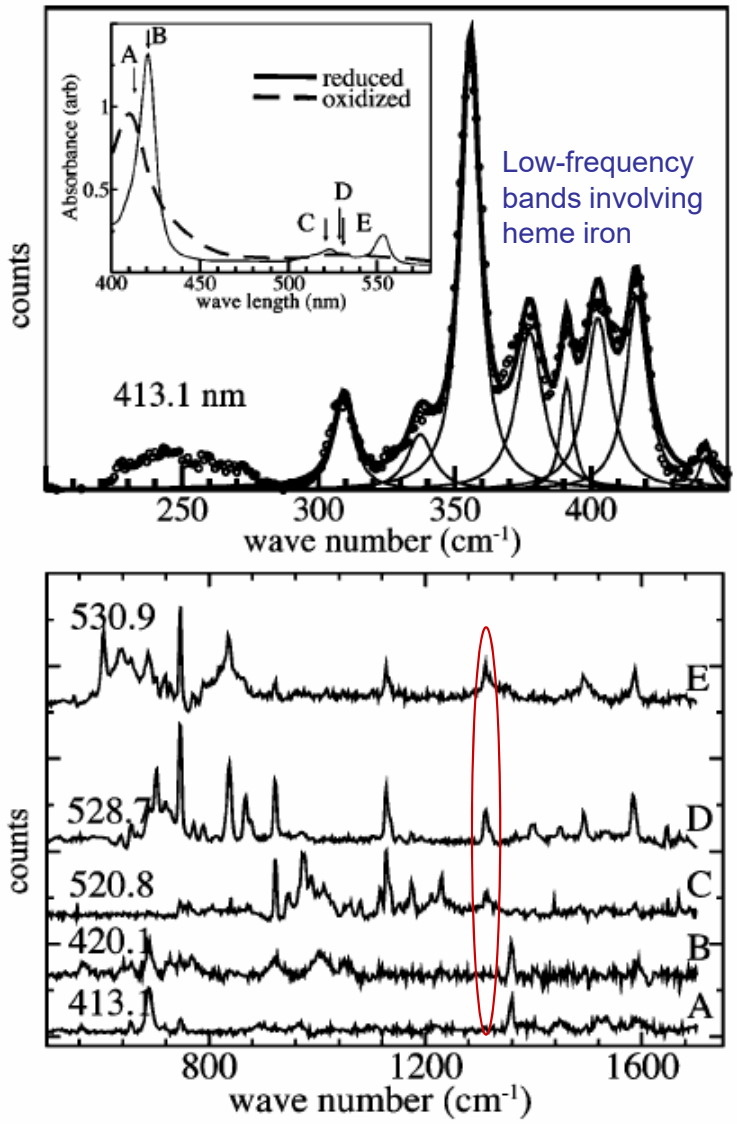

Low-frequency bands involving heme iron

Amplitudes of peaks change significantly and unpredictably from one wavelength to the next!

Cytochrome f: ~ 300 aa, 32 kDa, the largest of eight subunits of the membrane-bound b_6f complex in chloroplasts

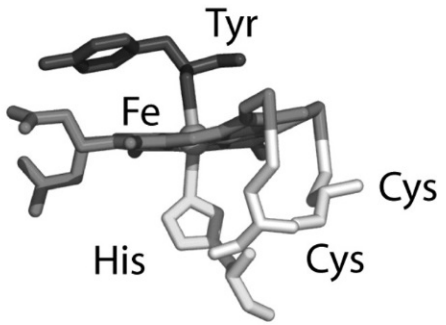

Figure 3. Raman spectroscopy on cytochrome *f* (reduced). Top, inset: Absorption spectra for cytochrome *f* (reduced and oxidized) showing the peaks relevant for resonance excitation. Labeled arrows denote wavelengths used for Raman measurements: A, 413.1 nm; B, 420.1 nm; C, 520.8 nm; D, 528.7 nm; and E, 530.9 nm. Top: Raman spectrum at 413.1 nm (circles), results of peak fitting from 280 to 450 cm^{-1}, using Voigt trial functions (thin lines), and the total best fit curve (thick line). Bottom: Raman spectra for all five wavelengths for 450–1700 cm^{-1}; the variability of peak heights with wavelength illustrates the difficulty of assessing amplitudes of vibrational modes from resonant Raman spectra.

Adams et al., J. Phys. Chem. B 110 (2006) 530.

Time-resolved Resonance Raman Scattering: Pump-probe Experiment on Hemoglobin

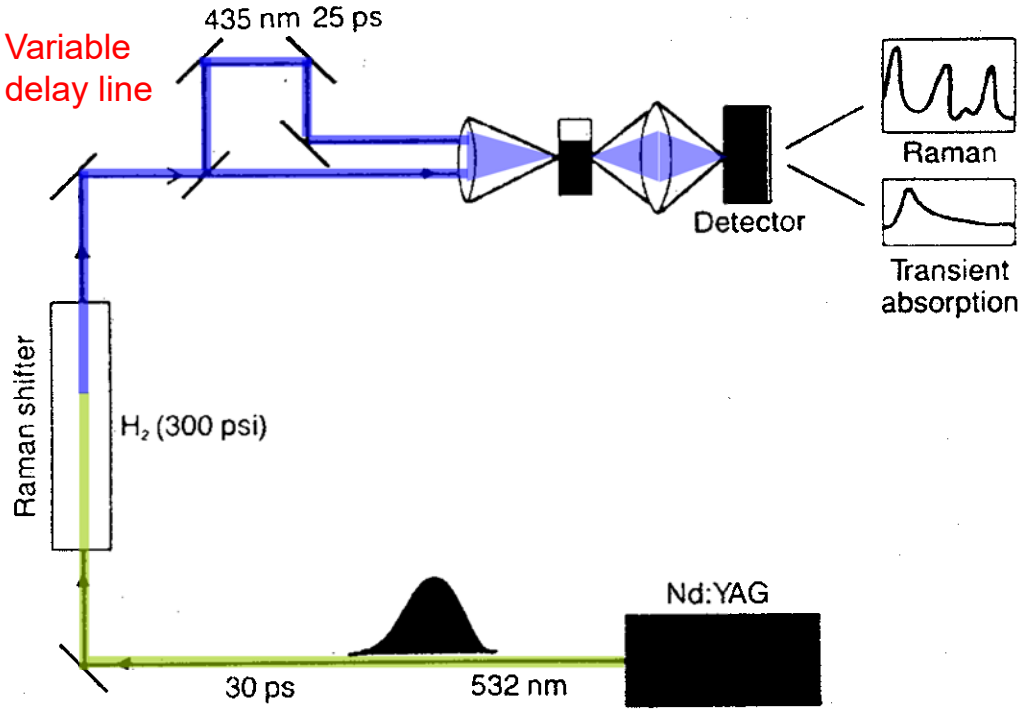

Hemoglobin active site

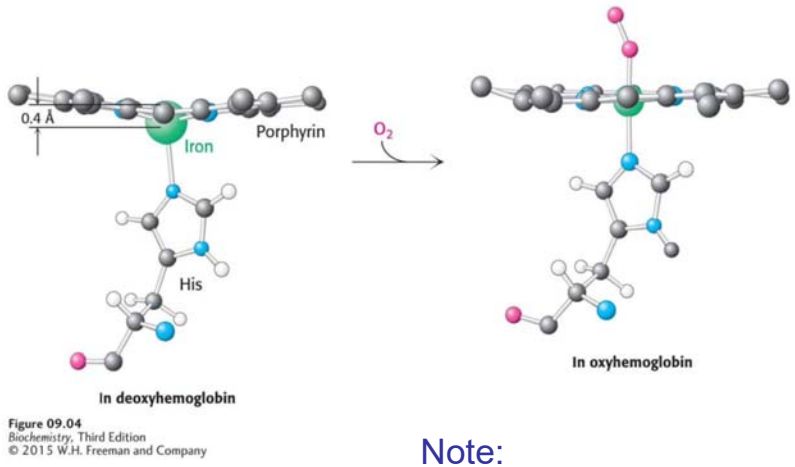

Figure 09.04
Biochemistry, Third Edition
© 2015 W.H. Freeman and Company

Note:
1. Fe displacement
2. Fe-His bond tilted

Experimental setup used to generate and monitor both picosecond time-resolved Raman spectra and transient absorption spectra.
1st (pump) pulse: photodissociates O_2 from hemoglobin
2nd (probe) pulse: excites Raman transition (also used for absorption measurement)

$$HbO_2 + h\nu\ (25\ ps) \rightarrow Hb^* + O_2 \rightarrow HbO_2$$

Hb*: Photoproduct, deligated Hb shortly after ligand photodissociation

Fe-His Stretching Bands of Deoxy Hb and Hb*

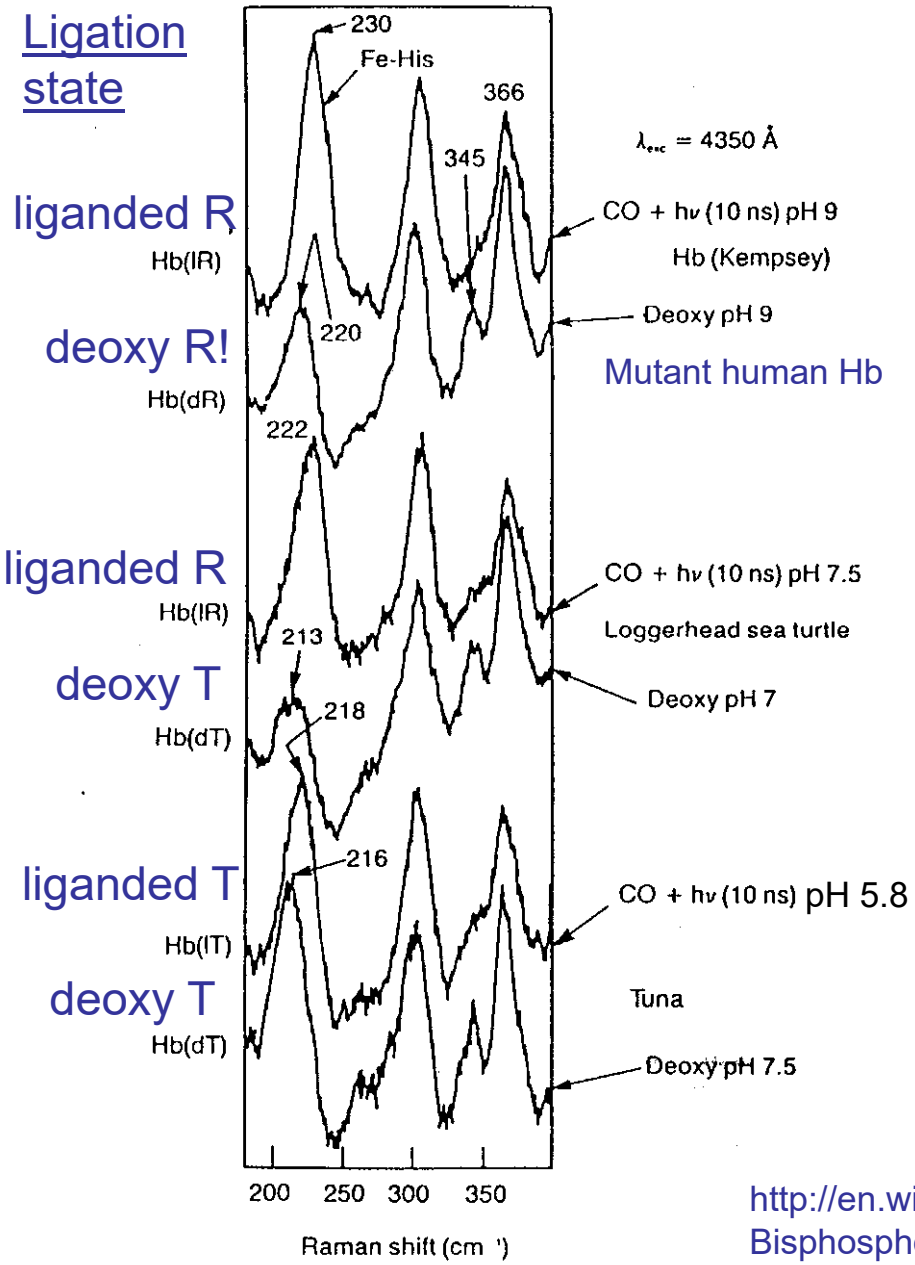

Low-frequency part of resonance Raman spectra of different equilibrium and non-equilibrium structures of deoxy hemoglobin generated with a 10-ns laser pulse.

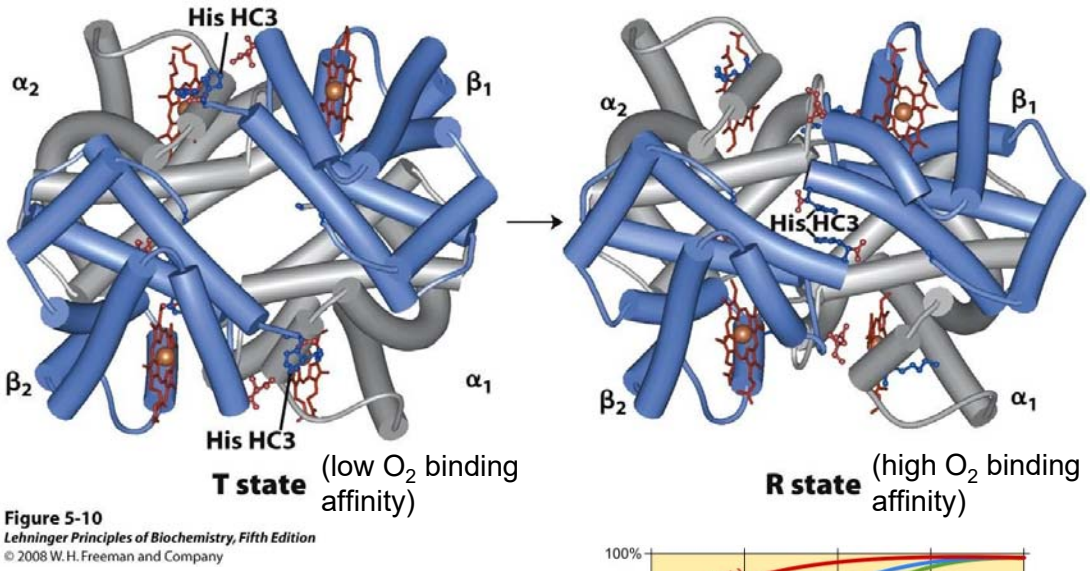

T state (low O_2 binding affinity)

R state (high O_2 binding affinity)

Figure 5-10
Lehninger Principles of Biochemistry, Fifth Edition
© 2008 W. H. Freeman and Company

R-T transition in hemoglobin (cooperativity).

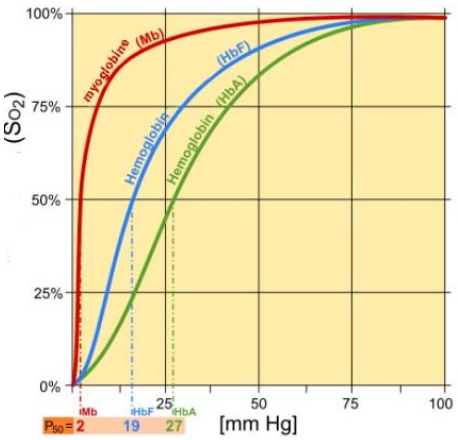

http://en.wikipedia.org/wiki/2,3-Bisphosphoglyceric_acid#mediaviewer/File:Hb.jpg

Deoxy Hemoglobin

Systematic variation of Fe-His stretching frequency (only active in 5-coord. heme):

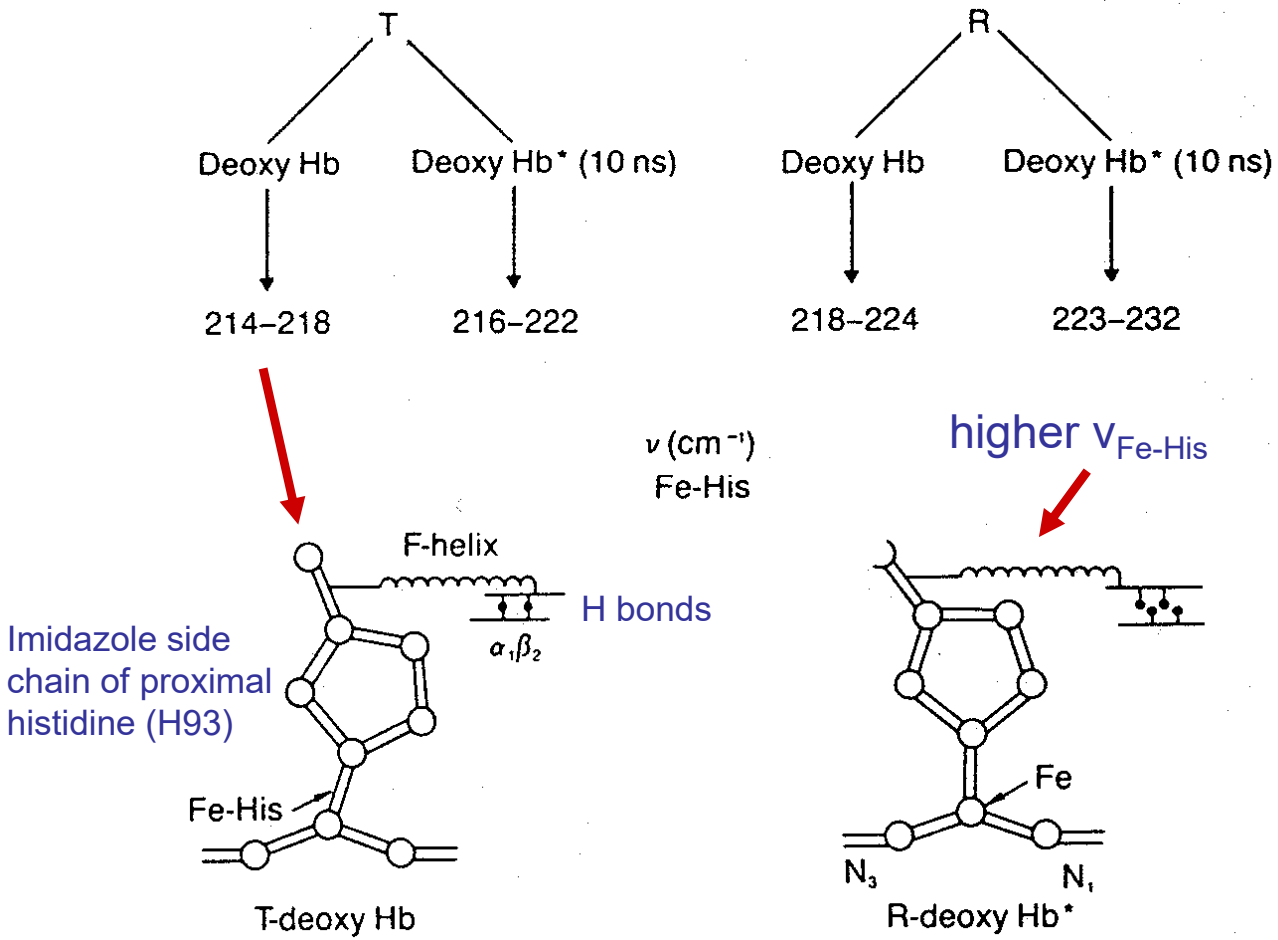

Conclusions:

Short-time (ps/ns) photoproducts (Hb*) are intermediates with fast ligand dissociation and heme displacement but no tilt of the Fe-His bond.

The F helix shift accompanying the histidine tilt happens much later in the RT transition (microseconds).

Surface-Enhanced Raman Scattering (SERS)

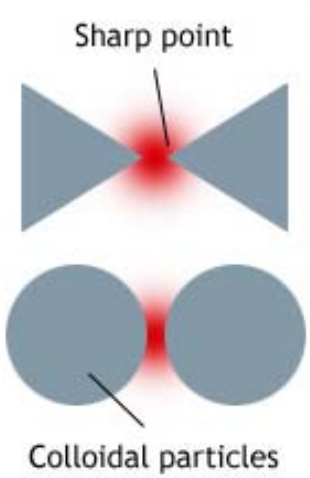

A molecule adsorbed on a rough metal surface can produce a Raman signal up to 12 orders of magnitude more intense than on a flat substrate → Single-molecule sensitivity!

Enhancement mechanisms:

- Strong enhancement of the local electro-magnetic field in the proximity of sharp points of textured metals [Au, Ag, Cu], or in the nano-scale gaps between colloidal particles featuring localized plasmon excitations.

- Charge-transfer reaction between surface and (adsorbed) molecule (enhancement 10^2 – 10^3).

But: enhancement effect only short ranged: 2 – 3 nm!

SERS: Principle

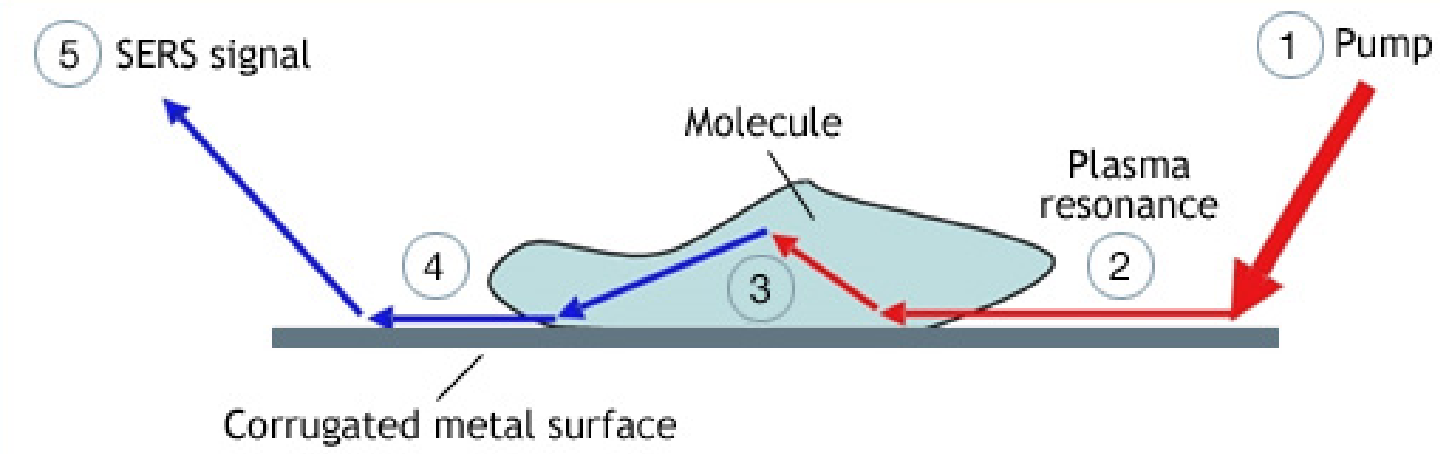

(1) laser light incident on the corrugated metal substrate (see SEIRA!)
(2) plasmon excitation
(3) light scattered by the molecule
(4) Raman scattered light transferred back to plasmons and scattered in air
(5) Plasmons in the metal act as antennas, which assist in coupling light into molecules close to the surface and couple out photons into specific directions. The enhanced coupling both into and out of the molecule amplifies the Raman signal. Plasmon properties – such as wavelength and width of its resonance – depend on the nature of the metal surface and on its geometry.

SERS Surface Preparation

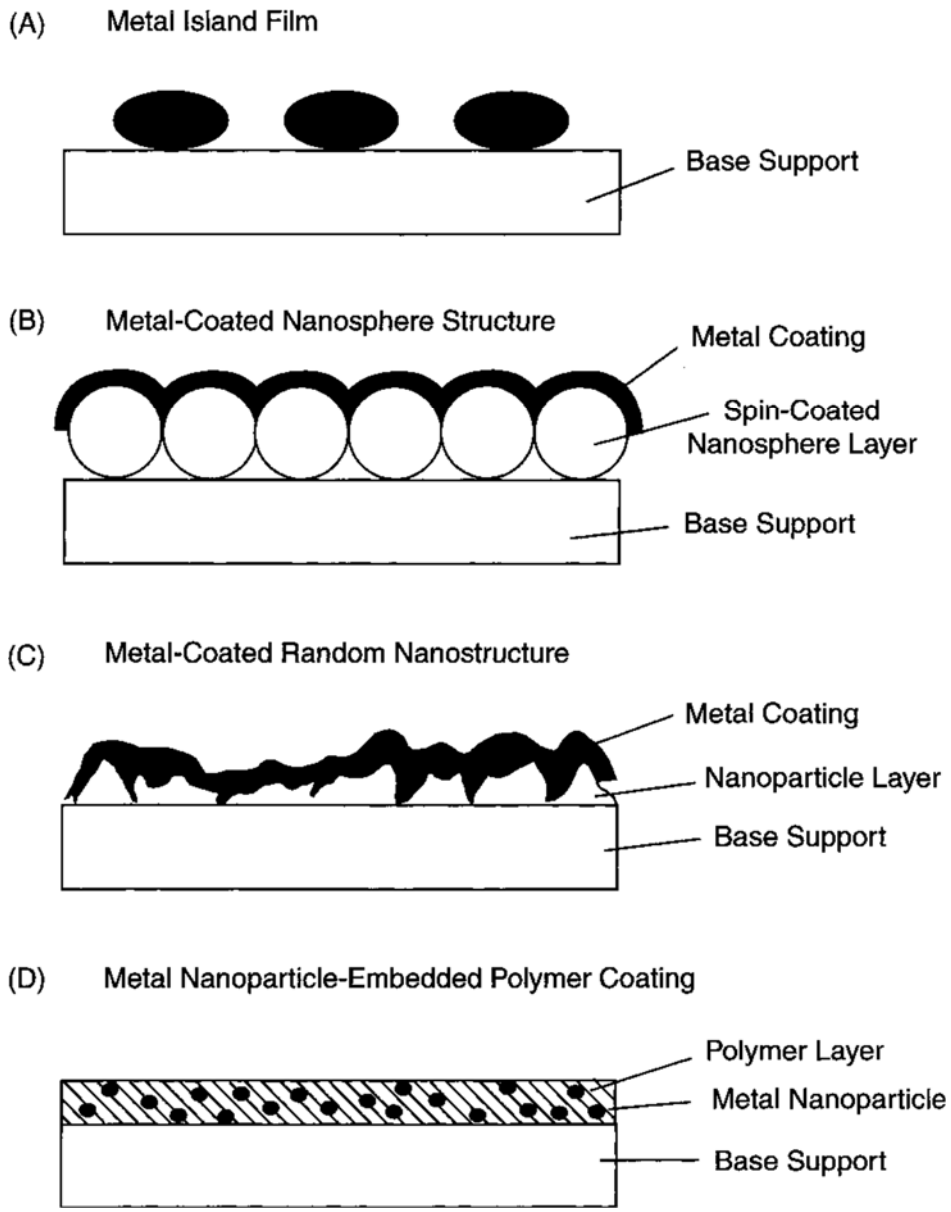

SERS Application: Detection of DNA

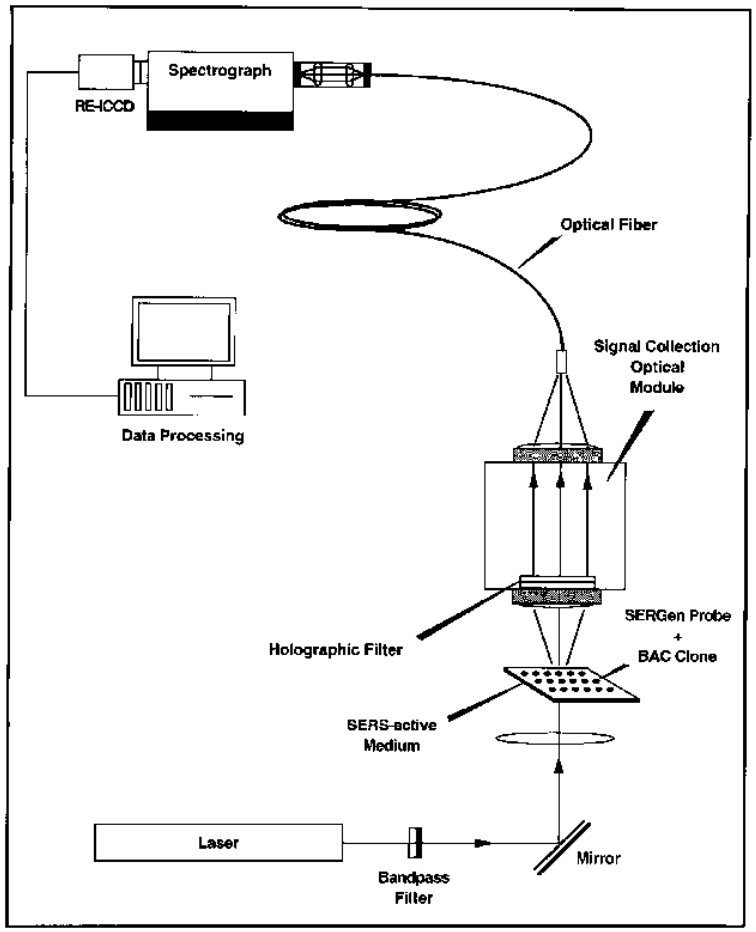

Instrumental set-up for spectral recording of individual spots of SERGen probes.

Vo-Dinh et al., *J. Raman Spectrosc.* **30**, 785–793 (1999)

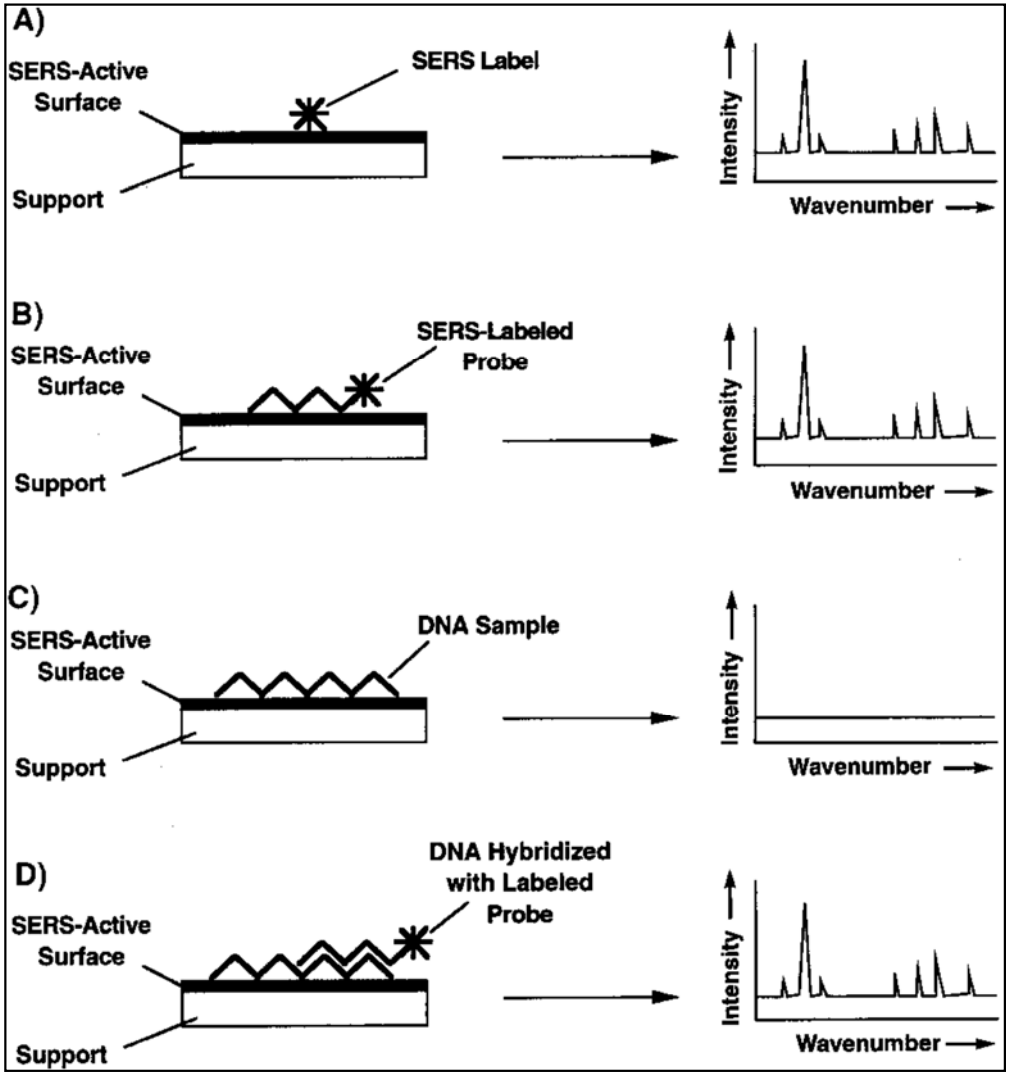

Schematic diagram of DNA hybridization and SERGen detection. (A) Selection of a SERS-active label; (B) detection of a SERS-labeled DNA probe; (C) no detection for an unlabeled DNA probe; (D) detection of DNA hybridized to a labeled probe.

Biophysics II

Exploring the Energy Landscape of Proteins

Uli Nienhaus

Prof. G. U. Nienhaus, Vorlesungsunterlagen Biophysik II, SS 2023.
Nur zum KIT-internen, vorlesungsbegleitenden Gebrauch.
Weitergabe und anderweitige Nutzung verboten.

Exploration of Protein Conformational Energy Surfaces

$$E = E_{el.} + E_{vib.} + E_{rot.} + E_{conf.}$$

- the term $E_{conf.}$ takes into account that proteins with identical sequences can have different internal energies due to variations in conformation.

Funnel-shaped conformational energy landscape

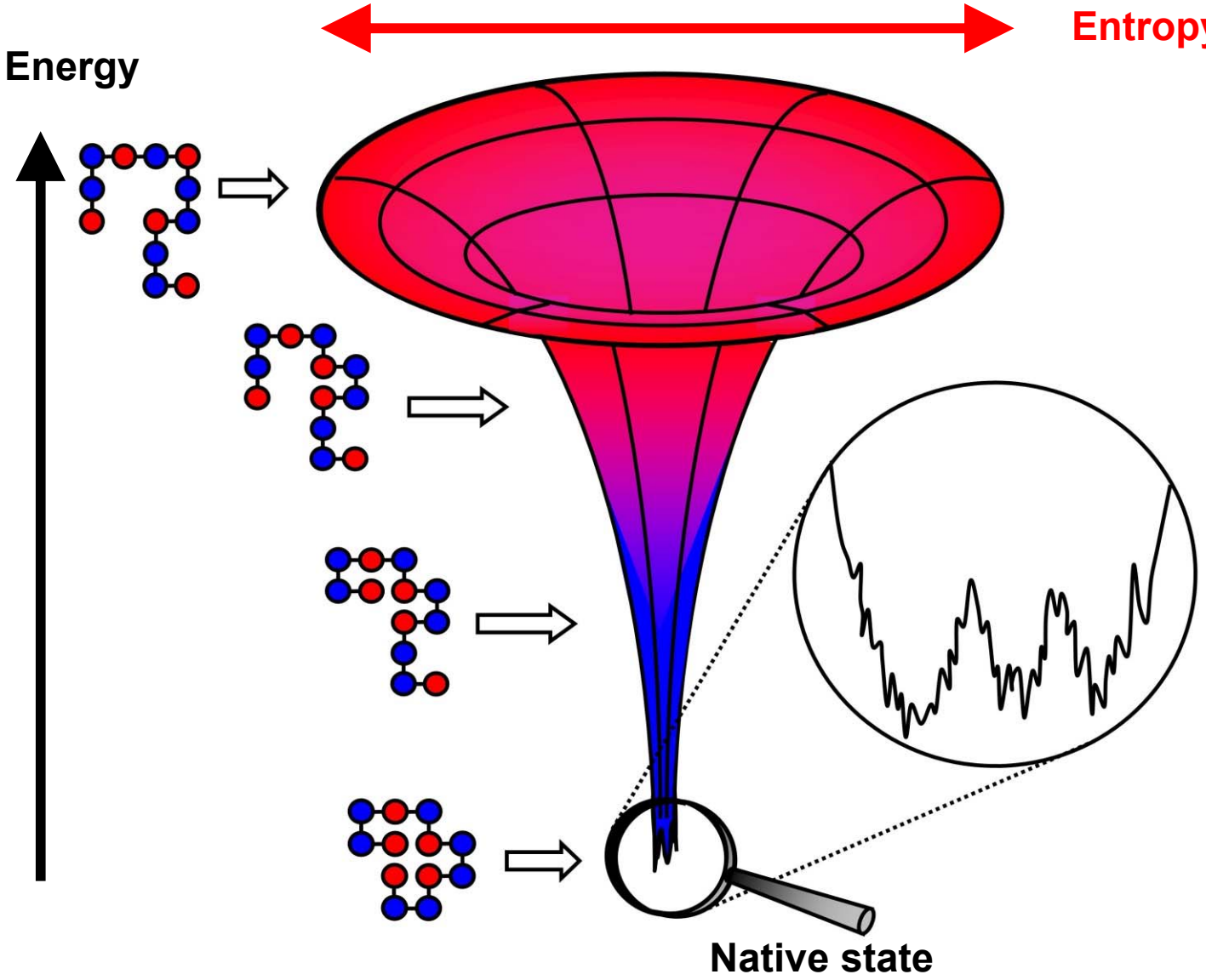

Energy landscape governs structure, dynamics, function

Nienhaus and Young, Encyc. Appl. Phys. 15 (1996) 163.

Onuchic
Wolynes
Bryngelson
Luthey-Schulten
Go
Dill
Thirumalai
Shakhnovich

Protein States and Conformational Substates

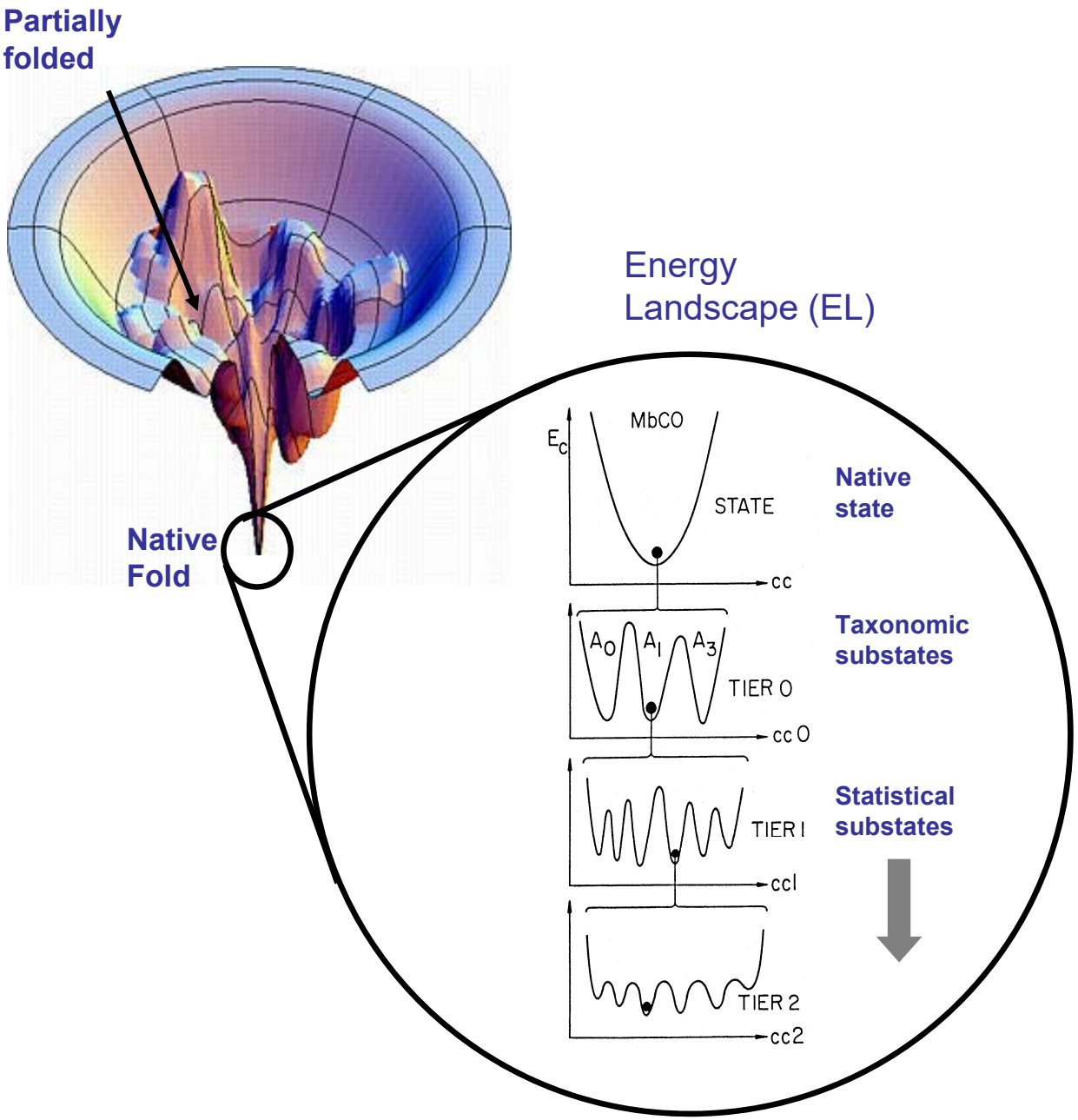

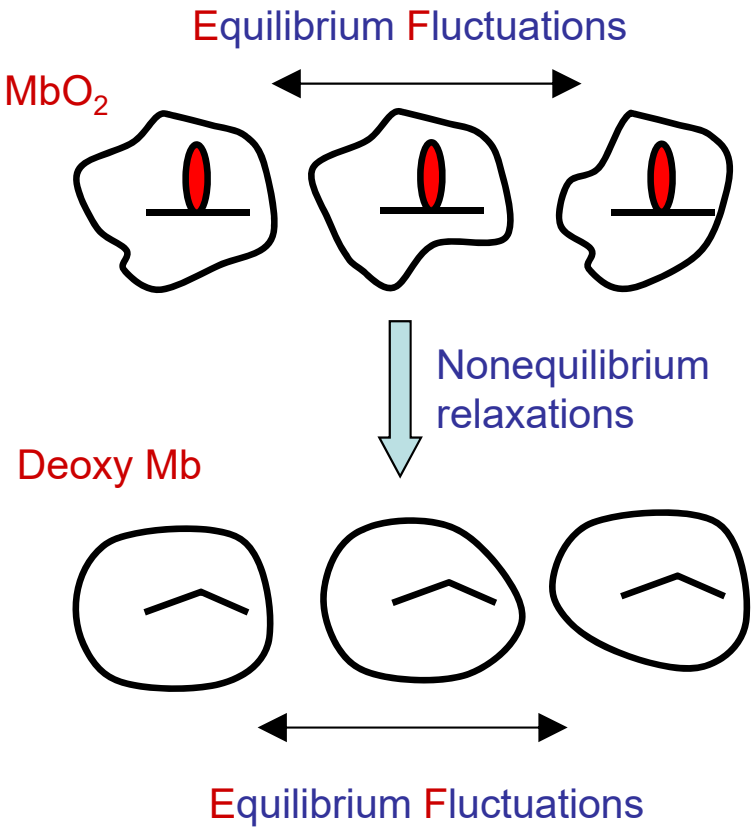

Aim: Explore properties of EL by measuring transitions between states and substates

Spectroscopy and Protein Dynamics I

Frequently, one focuses on dynamic processes (fluctuations and relaxations) that involve a few (often only two) states or substates only.

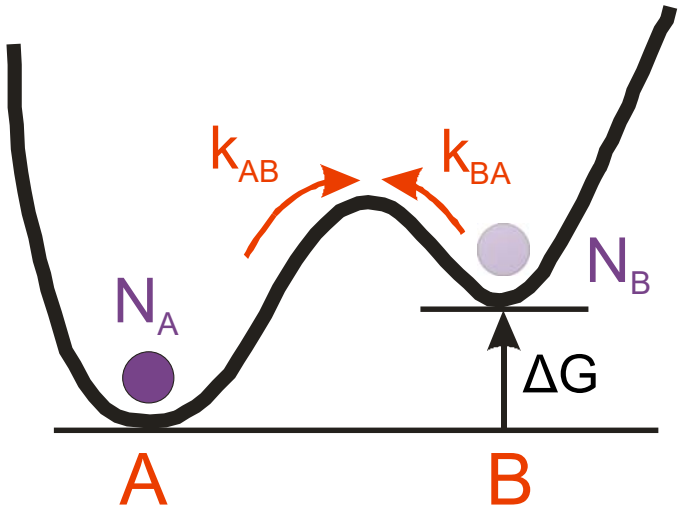

In equilibrium: $N_A \cdot k_{AB} = N_B \cdot k_{BA}$

$$\frac{N_B}{N_A} = \frac{k_{AB}}{k_{BA}} \equiv K$$

$$K = \exp(-\Delta G / RT)$$

$$= \exp(\Delta S / R)\exp(-\Delta H / RT)$$

To understand kinetic mechanisms, one aims to measure the associated rate coefficients over a wide range of temperatures (and other parameters such as pressure, viscosity etc.)

Spectroscopy and Protein Dynamics II

Quantitative determination of kinetic parameters

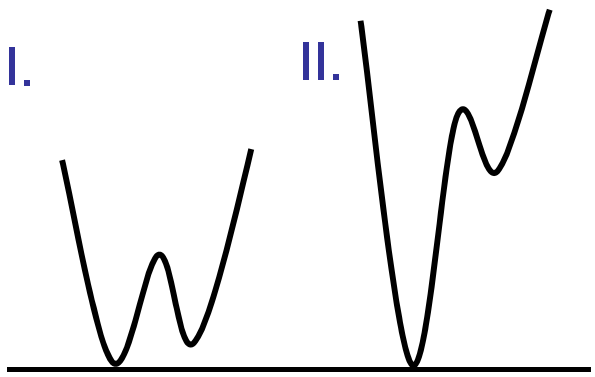

distinguish 2 cases:

I. ΔG small (~kT), $N_A \sim N_B$
II. ΔG large (>>kT), $N_B \sim 0$

Case I (ΔG small):

Relaxation methods

Apply a sudden, small perturbation to the system:

- T-jump
- p-jump
- E-field jump

Dispersion methods

Fluctuation methods

Case II (ΔG large):

Photoexcitation (flash photolysis, photo-isomerization, light-induced electron transfer)
pulse radiolysis, fast mixing…

Case I: Temperature Jump Relaxation

Temperature jump applied to a two-state system

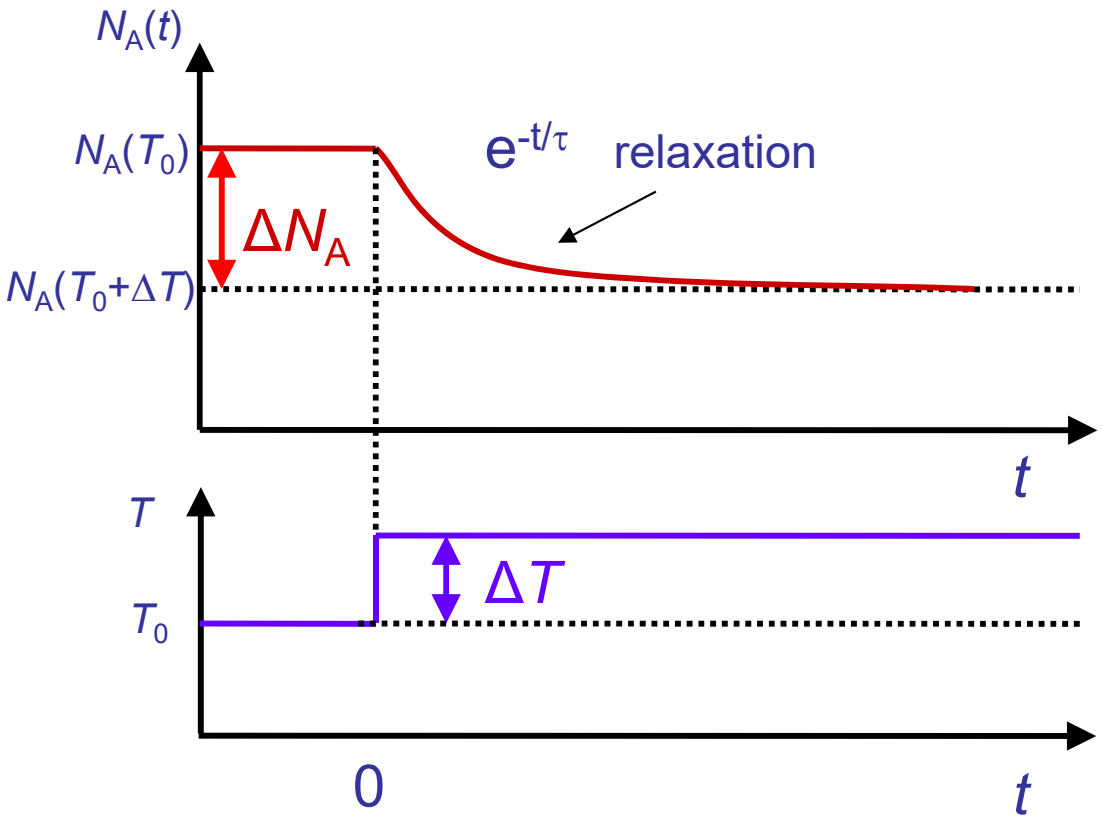

$$\frac{dN_A}{dt} = k_{BA}N_B - k_{AB}N_A$$

with $N_A + N_B = 1$ (normalization)

$$\frac{dN_A}{dt} = k_{BA}(1 - N_A) - k_{AB}N_A$$

$$N_A(t) = N_A(\infty) + \Delta N_A\, e^{-t/\tau}$$

$$\left.\begin{aligned} \frac{1}{\tau} &= k_{BA} + k_{AB} \\ K &= \frac{k_{AB}}{k_{BA}} \end{aligned}\right\}$$

2 equations for 2 rate coefficients

T-jump – Joule and Microwave Heating

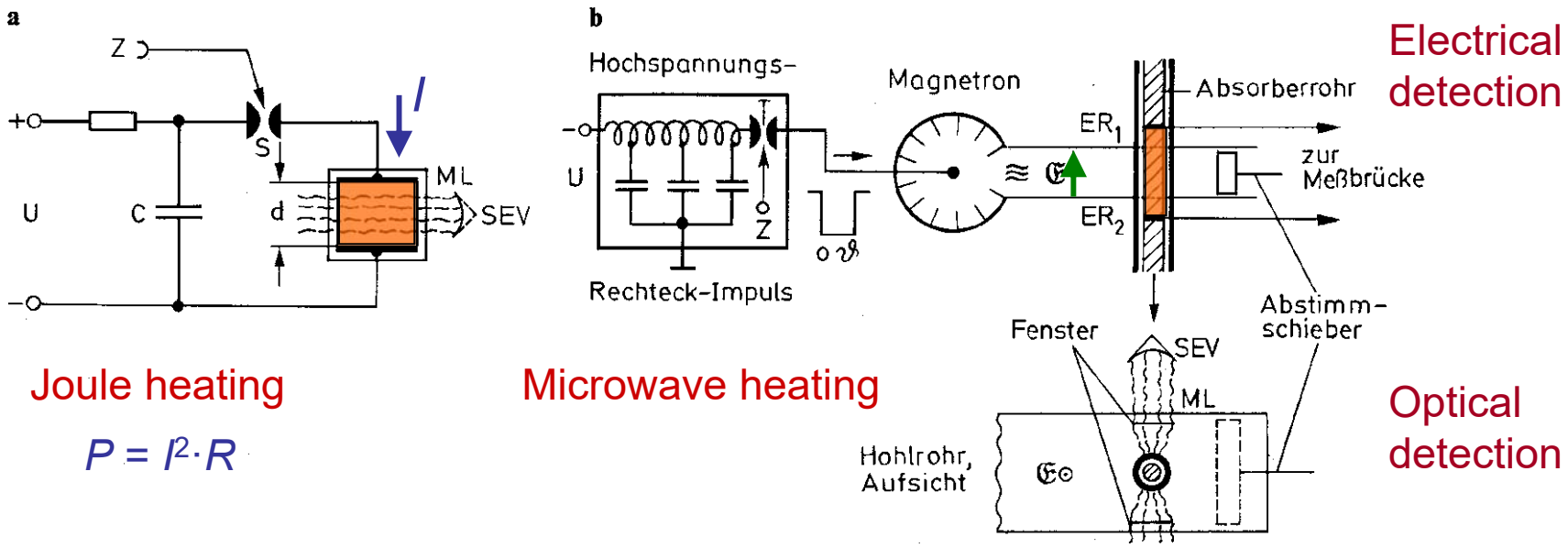

Joule heating

$P = I^2 \cdot R$

Microwave heating

Schematic drawings of devices for generating rapid temperature jumps: **a)** Heating by a current pulse, *U* high voltage, 10-50 kV; *C* pulse discharge capacitor; *Z* trigger pulse; *S* spark gap; *ML* monitoring light; *d* separation between electrode plates; SEV light detector (photomultiplier, photodiode). **b)** Heating by microwave pulse, *Z* Thyratron (controlled rectifier); ϑ pulse duration; E vector of microwave field. *In side view*: conductometric detection: ER_1, ER_2 electrode rings. *In top view*: photometric detection as in a).

Ultrafast T-jump Using Pulsed NIR Light

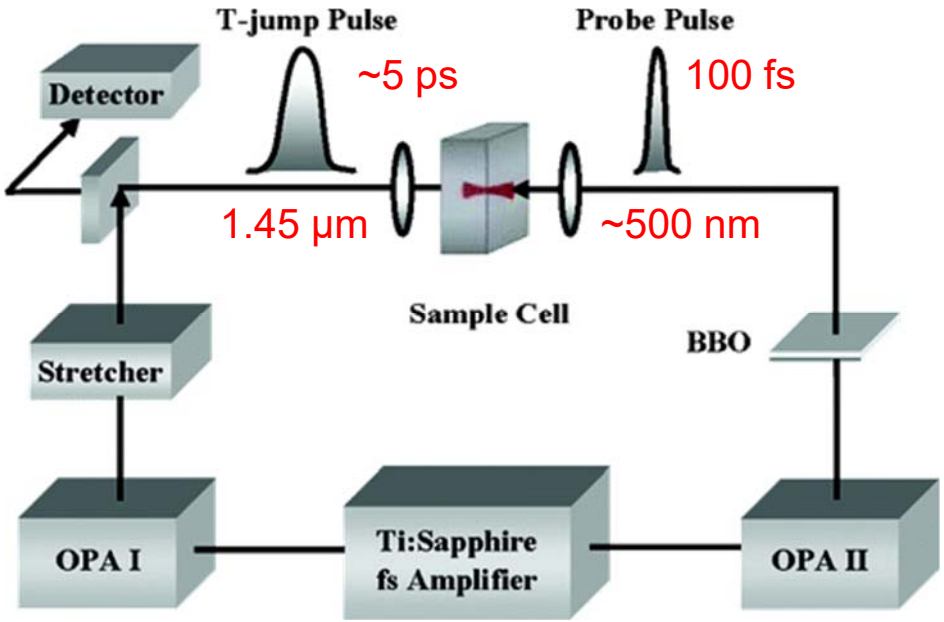

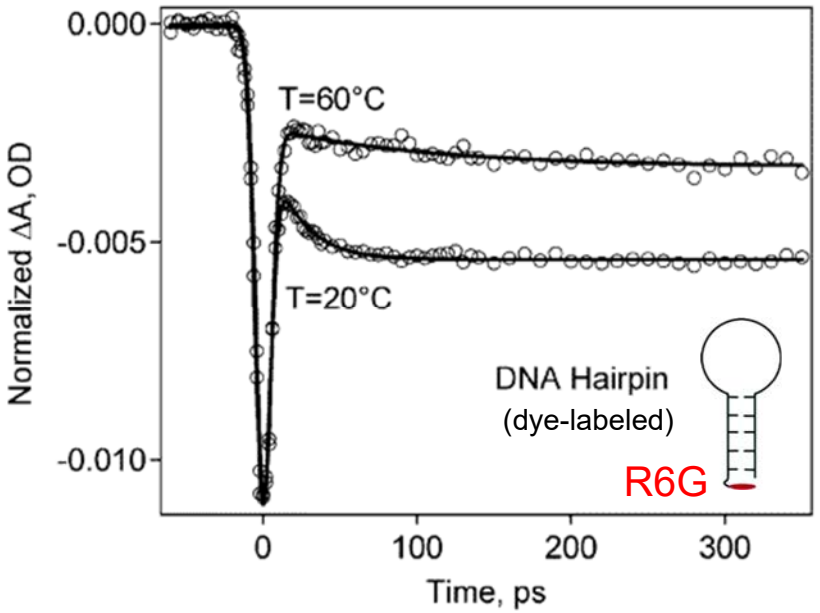

Pulses were generated by two OPA systems pumped by a Ti:sapphire amplifier with a repetition rate of 200 Hz. The T-jump pulse was set to 1.45 μm (OH stretch overtone band) with a typical energy of 15 μJ, stretched to 5−20 ps. The time-delayed probe pulse (100 fs) has much less energy (<1 nJ) and was tuned to different wavelengths to monitor absorption changes of interest. The sample was held in a 100 or 300 μm thick flat capillary cell and was placed in a temperature-controlled cell holder with minimal disturbance of alignment. Δ T < 20°C.

~20 ps dynamics at temperatures below the melting of DNA (60 °C in high [salt] solution) reflects water reorientation.

Single strand destacking: ~1 ns.

Hairpin destacking: microseconds.

Ultimate speed limit: water thermalization by hydrogen bonds, ~5 ps

Ma, Wan, Zewail, *J. Am. Chem. Soc.*, 2006, 128, 6338.
Ma, Wan, Wu, Zewail, *Proc. Natl. Acad. Sci. USA* 104, 712 (2007).

In-vivo T-jump Using Laser Heating

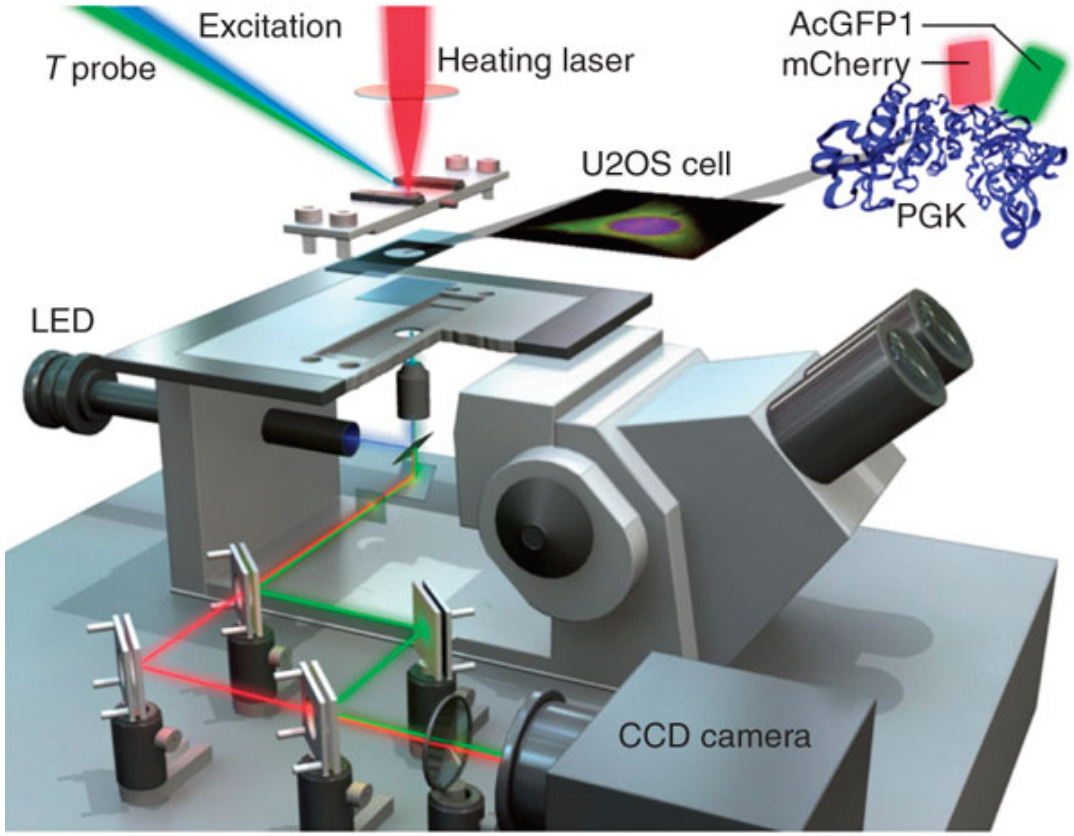

Phosphoglycerate kinase (PGK), labeled with a FRET pair of fluorescent proteins.

Cells in the imaging chamber are illuminated by the blue LED or the argon ion laser (458 nm) to excite the FRET donor. The green laser (532 nm) probes the temperature (T probe) inside the cell by exciting the acceptor directly. A heating (infrared) laser (2,200 nm) initiates the temperature jump. The two-color fluorescence images are projected onto a CCD camera capable of recording millisecond time resolution movies of PGK folding/unfolding kinetics in the cell.

Protein folding stability and dynamics imaged in a living cell
Ebbinghaus et al., Nature Methods 7, 319 - 323 (2010)

Laser Heating – Temperature Profiles

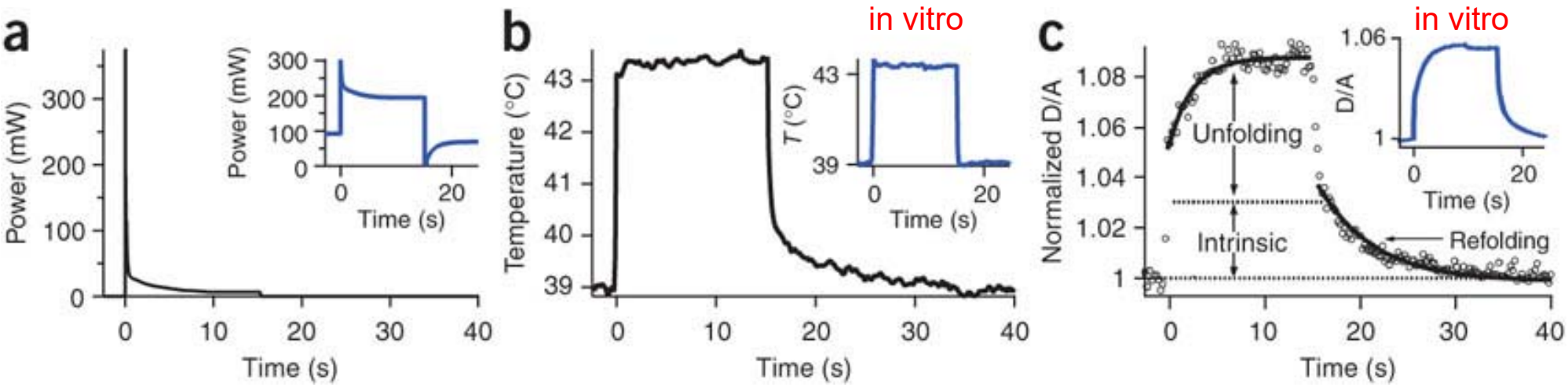

(a) Laser profiles for a **fast** upward temperature jump of 4 °C and for a <50 ms downward jump (inset).

(b) Corresponding temperature profiles measured directly in a U2OS cell and in vitro (inset) by mCherry fluorescence intensity (exc. 532 nm). The mCherry protein has a pronounced temperature dependence of its fluorescence quantum yield.

(c) Protein unfolding (t = 0 – 15 s) and refolding (t = 15 – 40 s) in a U2OS cell and in vitro (inset). The initial fast rise contains an unresolved burst phase and an intrinsic fluorescence baseline. The subsequent resolved phase monitors unfolding of the PGK fusion construct. After the temperature jump is switched off, the protein refolds to the original baseline, indicating complete reversibility both in the cell and in vitro.

Protein folding stability and dynamics imaged in a living cell
Ebbinghaus et al., Nature Methods 7, 319 - 323 (2010)

T-jump Experiments in vitro and in vivo

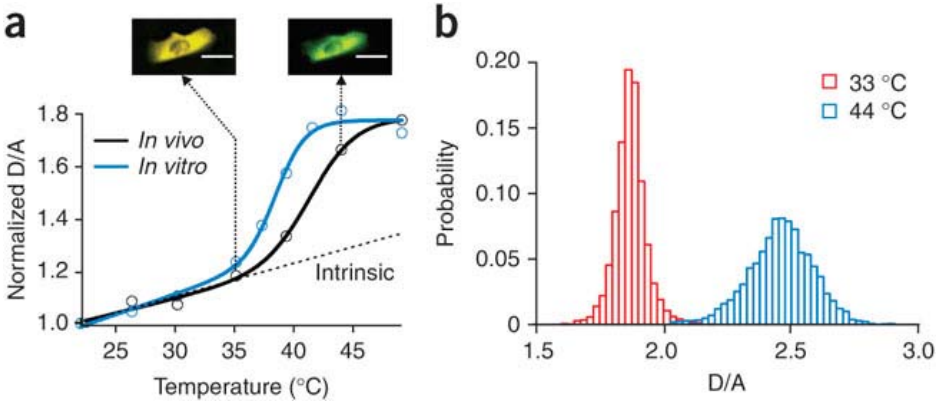

(a) Sigmoid fit to the *in vivo* D/A ratio upon thermal denaturation compared to *in vitro*. The dotted line shows the intrinsic native state fluorescence baseline. Scale bars, 20 μm.

(b) FRET D/A distributions at the indicated temperatures.

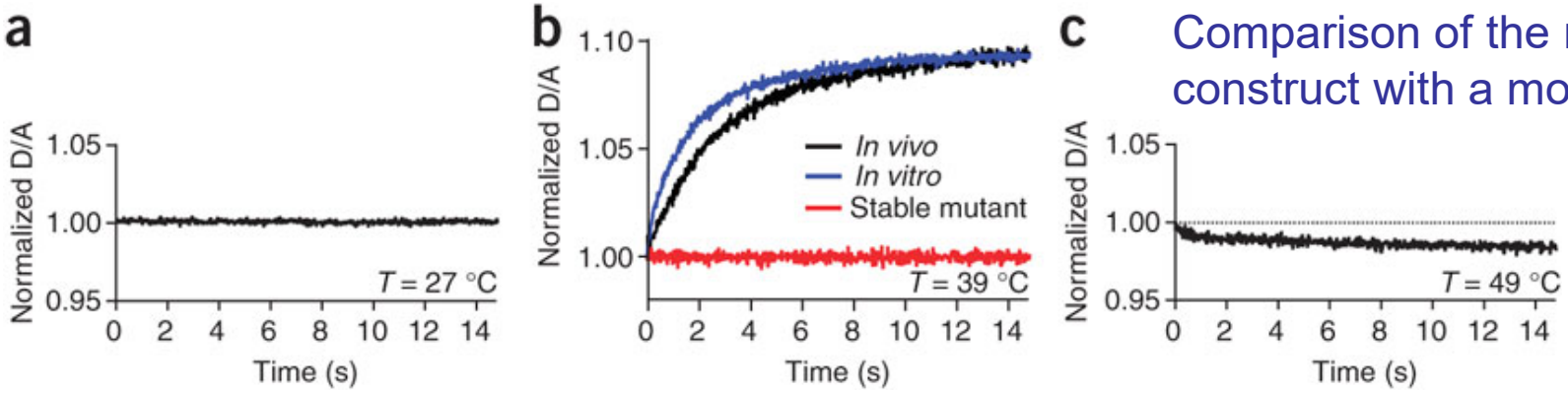

Comparison of the native PGK construct with a more stable mutant

(a) Normalized D/A after a temperature jump from **27 to 31 °C** on the folded state baseline showed **no unfolding** of the less stable PGK after the jump.

(b) Normalized D/A after a temperature jump from **39 to 43 °C**, near the melting temperature, resolves **unfolding** of the less stable construct in vitro and in vivo but not for the more thermally stable mutant.

(c) Normalized D/A after a temperature jump from **49 to 53 °C** on the unfolded baseline, showing **no additional unfolding** of the less stable protein. Instead a small decrease of the D/A was observed, presumably owing to aggregation and intermolecular FRET.

Protein folding stability and dynamics imaged in a living cell
Ebbinghaus et al., Nature Methods 7, 319 - 323 (2010)

Case I: Dispersion Methods

- Apply periodic (sinusoidal) perturbation:
  - E-field
  - sound
  - light

$\Rightarrow$ sinusoidally varying concentration of reactants/products:

$$\Delta C(t) = A(\omega)\sin(\omega t - \phi)$$

The relaxation time τ can be obtained from the ω-dependencies of the amplitude or phase:

$$A(\omega) = \Delta C^{\circ} / \sqrt{1+\omega^2 \tau^2}$$

$$\phi(\omega) = \arctan(\omega\tau)$$

The principle was already discussed for phase fluorometry!!!

Case I: Fluctuation Methods

Observe fluctuations of small ensembles or even single molecules

Number fluctuations in equilibrium

$$\left\langle \left(\frac{\delta N}{N} \right)^2 \right\rangle = \frac{1}{\langle N \rangle}$$

Monitor structural fluctuations in equilibrium

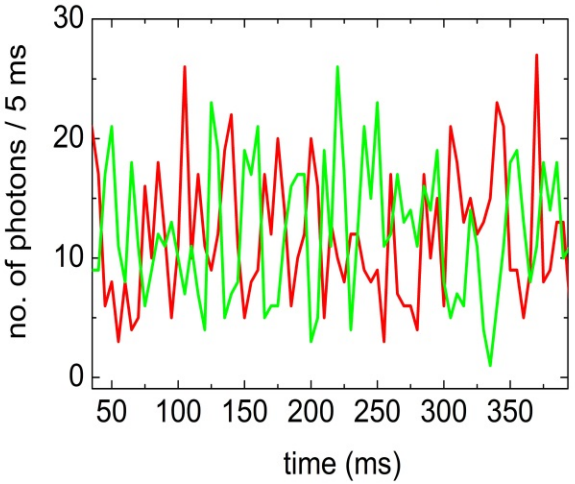

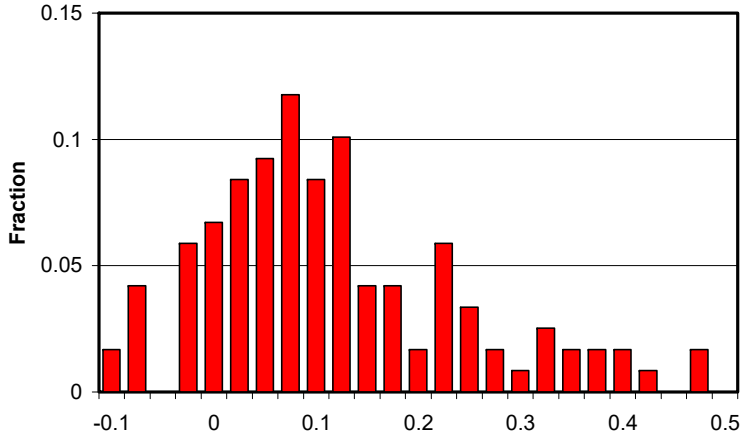

Determine distribution functions of relevant observables

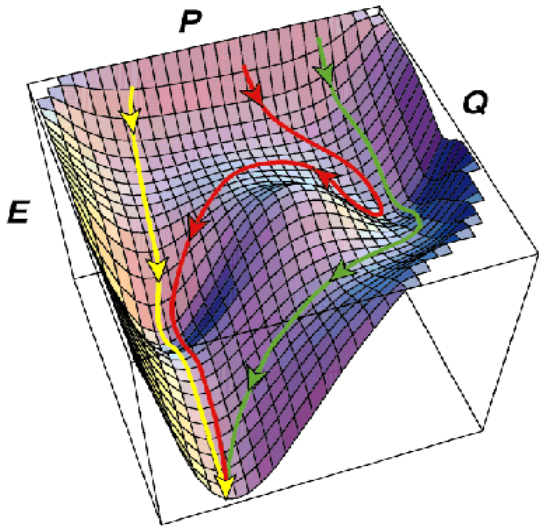

Measure time trajectories and reaction pathways under non-equilibrium conditions w/o need to synchronize a heterogeneous ensemble

Confocal Microscopy

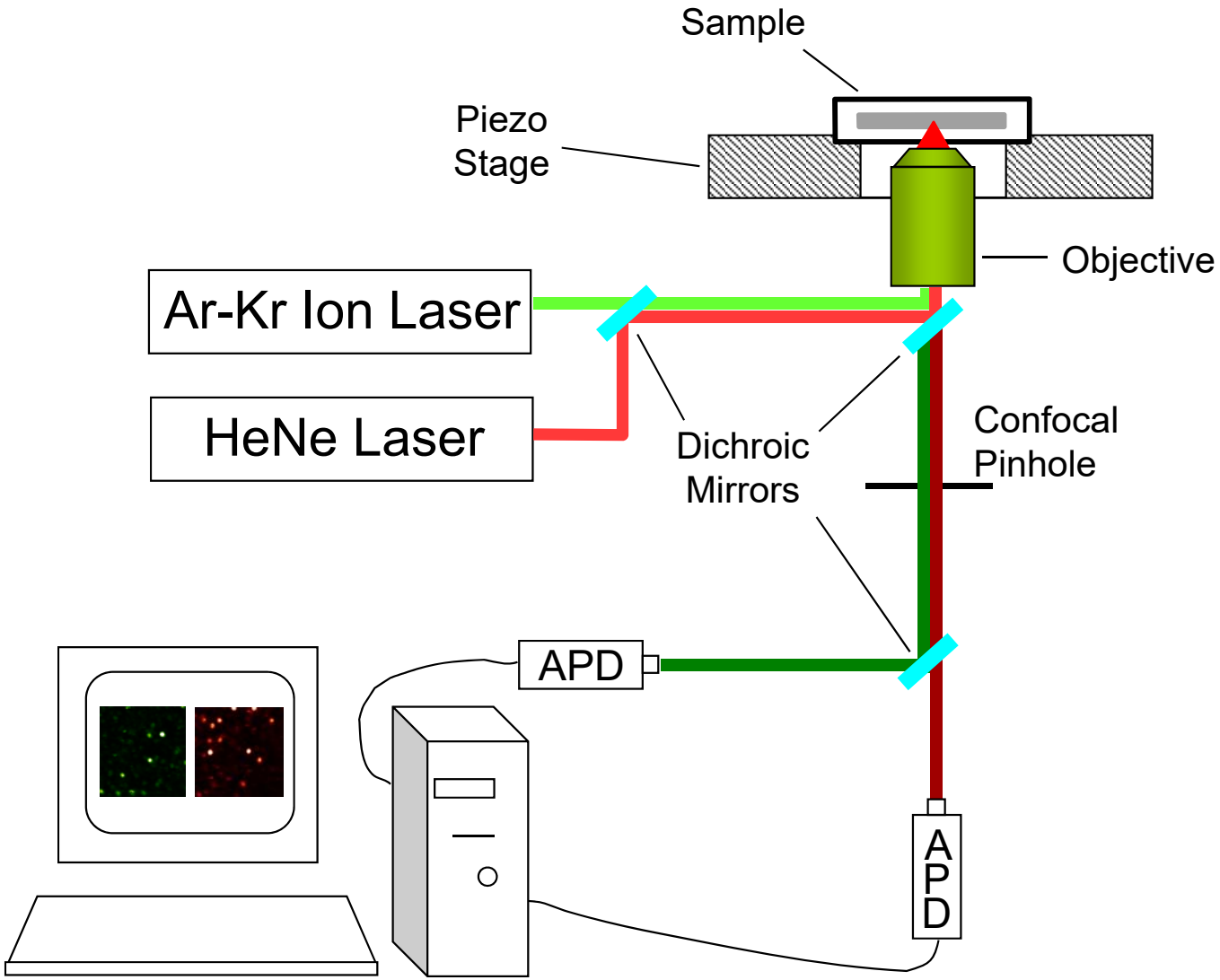

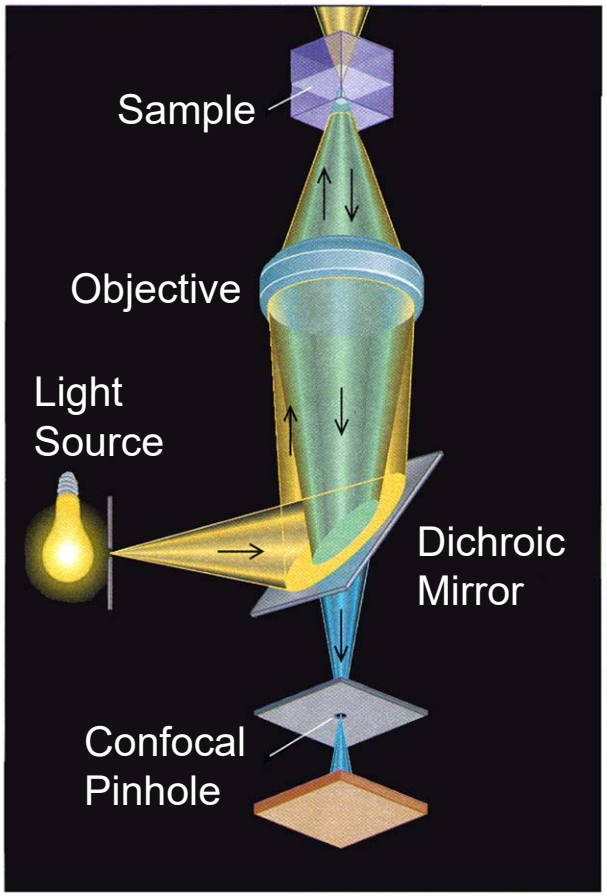

Axial sectioning, observation volume ca. 1 μm^3 = 1 fL

Conformational Changes in 3-Helix RNA Junctions Bound to Glass Surfaces

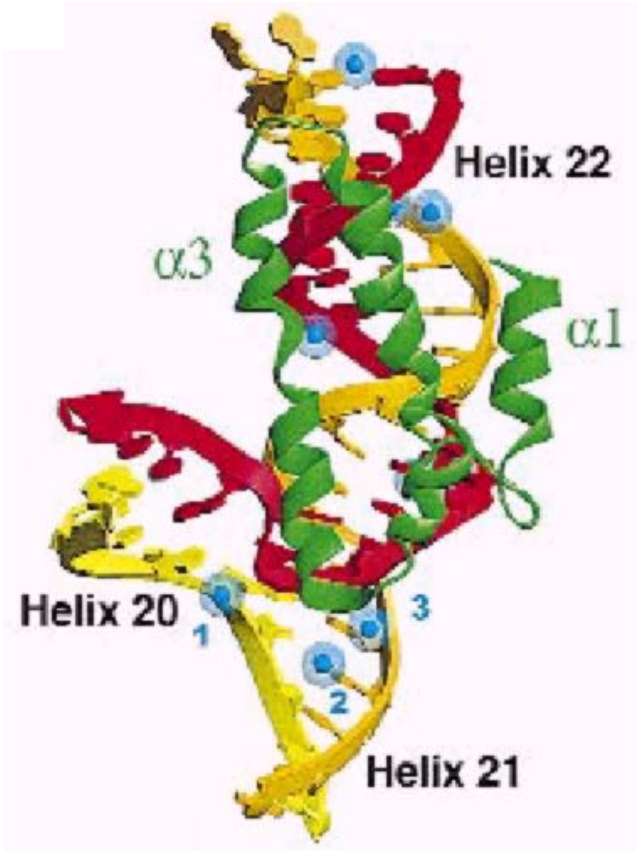

Fragment of 16S RNA of the prokaryotic 30S ribosomal subunit, which binds S15 protein upon assembly!

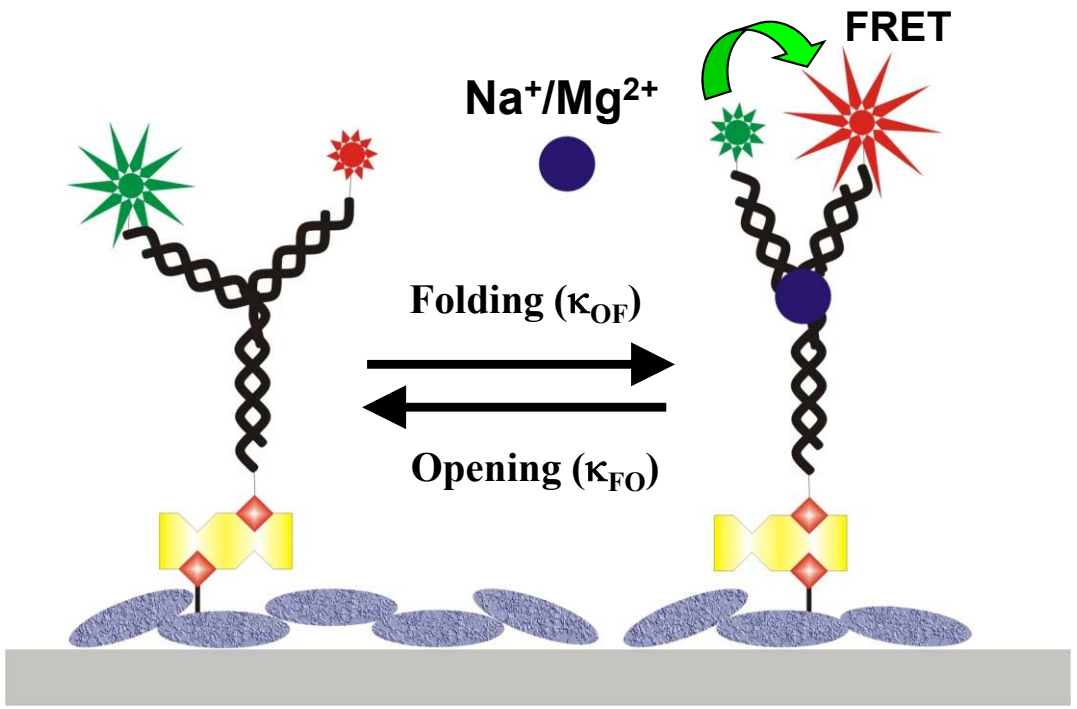

- **Biotinylated BSA adsorbed to glass**
- **Coupling via streptavidin/biotin**
  - **simple procedure**
  - **low background**
  - **weak unspecific binding**

Kim, Nienhaus, Ha, Orr, Williamson, Chu, *Proc. Natl. Acad. Sci. USA* 99 (2002) 4284.

Fluorescence Resonance Energy Transfer

FRET Efficiency:

$$E = 1 - \frac{I_{D(w/A)}}{I_{D(w/o\ A)}}$$

FRET depends on:

- **spectral properties of D and A**
- **relative orientation of D and A**
- **D-A separation**

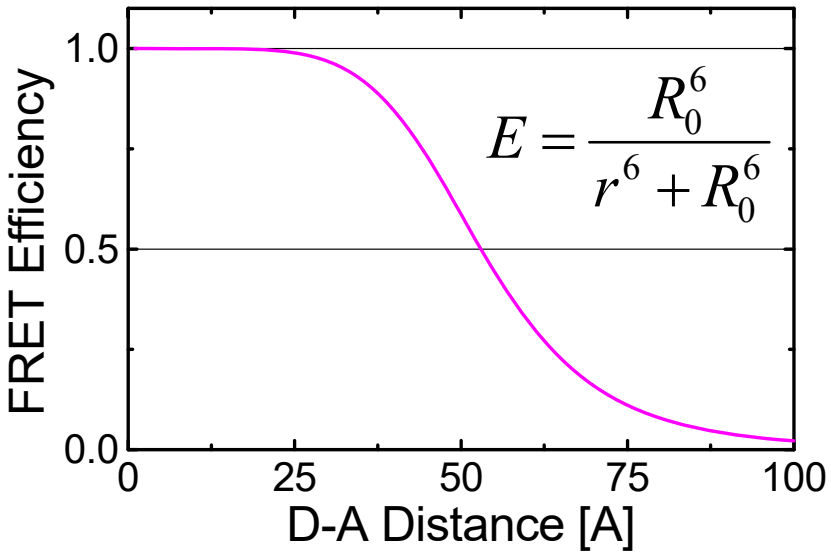

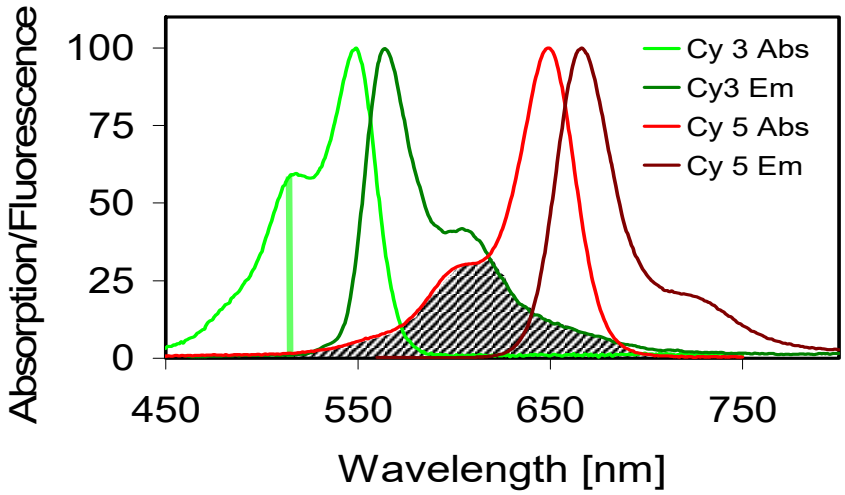

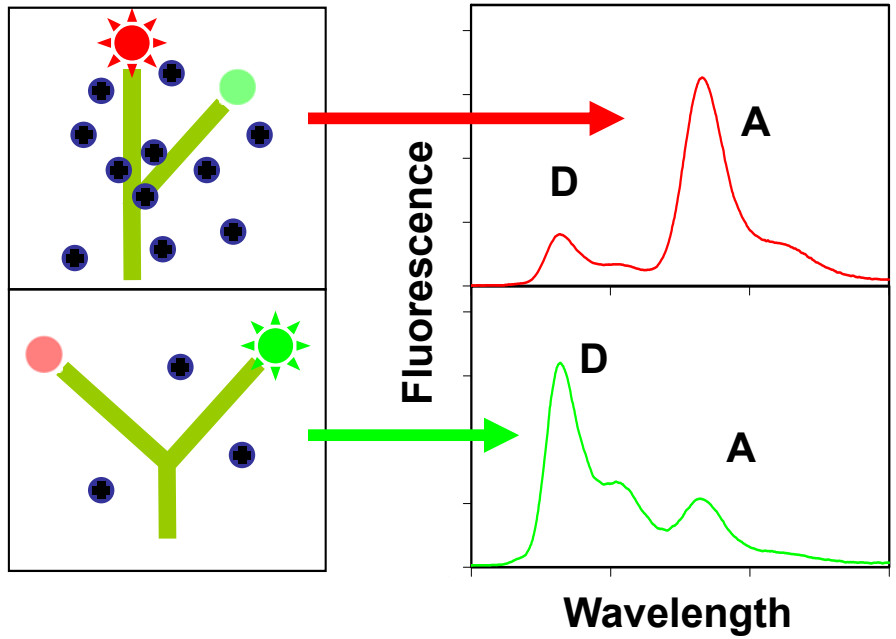

Metal Ion-induced Conformational Change of Single RNA Junctions

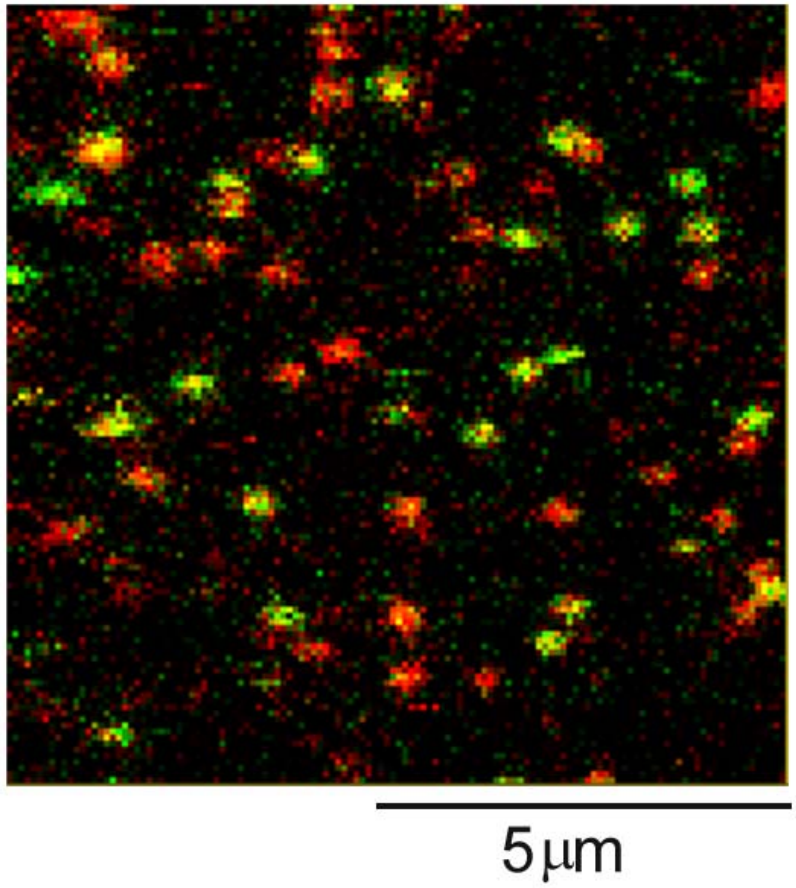

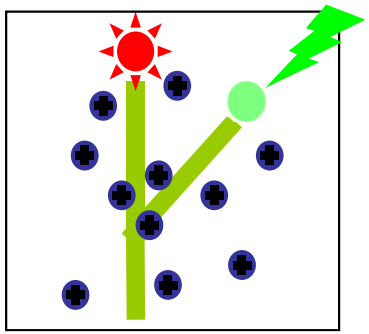

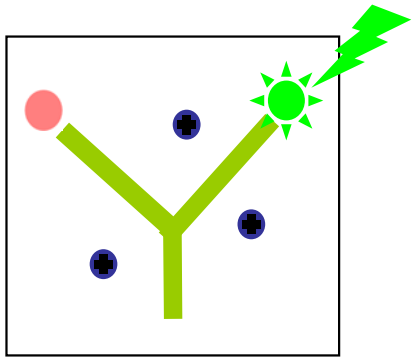

Images, ~128 x 128 px,
5 ms dwell time per pixel

Mg^{2+} Concentration Dependence

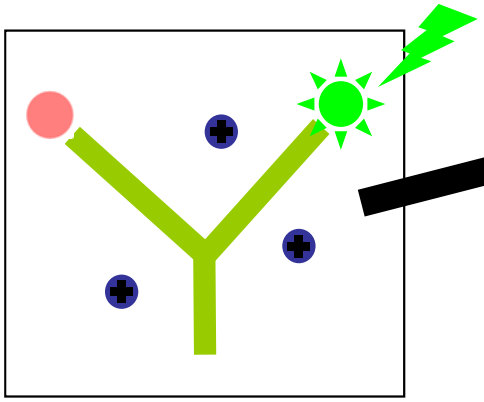

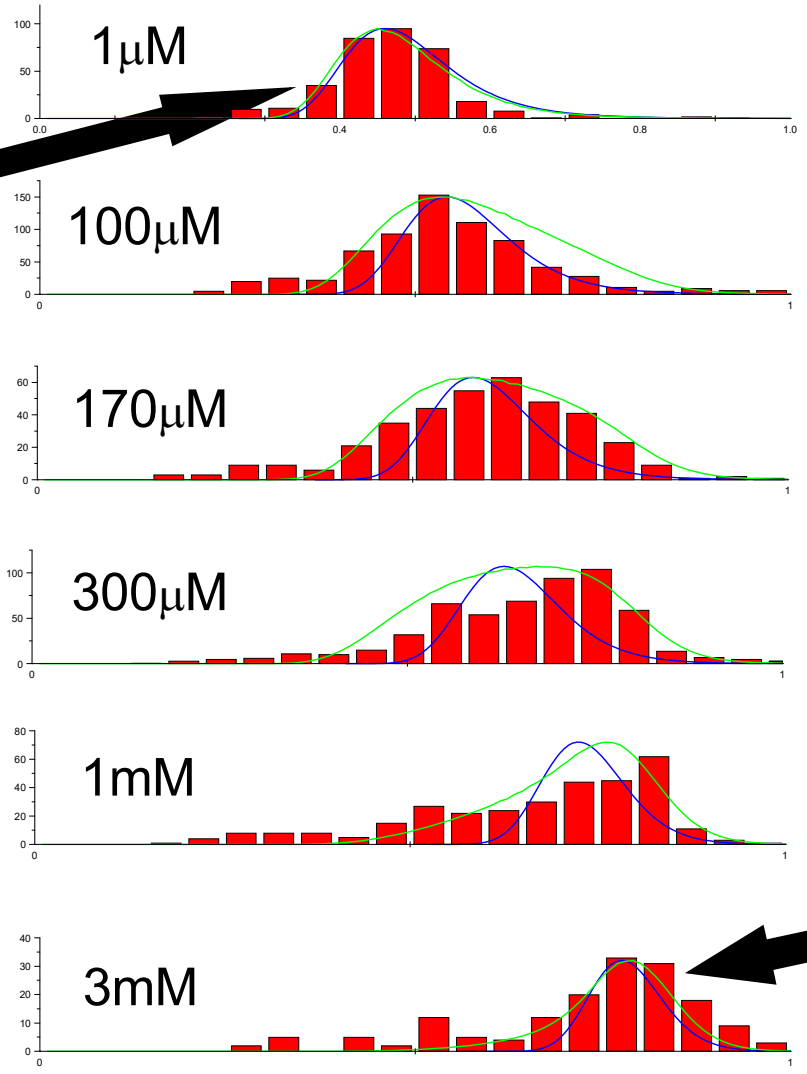

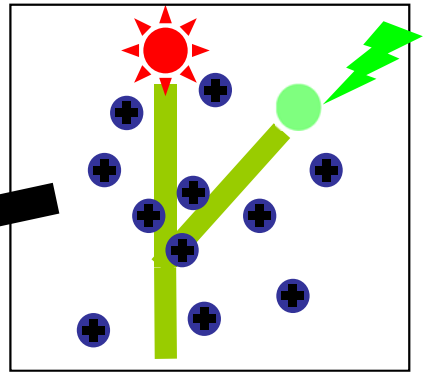

FRET histograms: # of molecules plotted as a function of proximity factor (”FRET efficiency“).

$I_A/(I_A+I_D)$ (FRET scale)

Real-time Single RNA Folding/Unfolding by Mg^{2+} Buffer Exchange

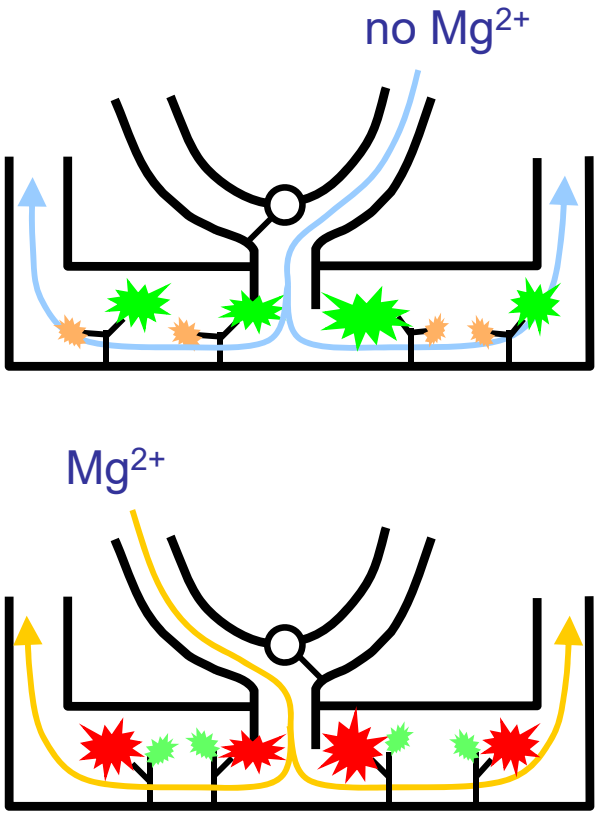

relaxation experiments with individual RNA molecules

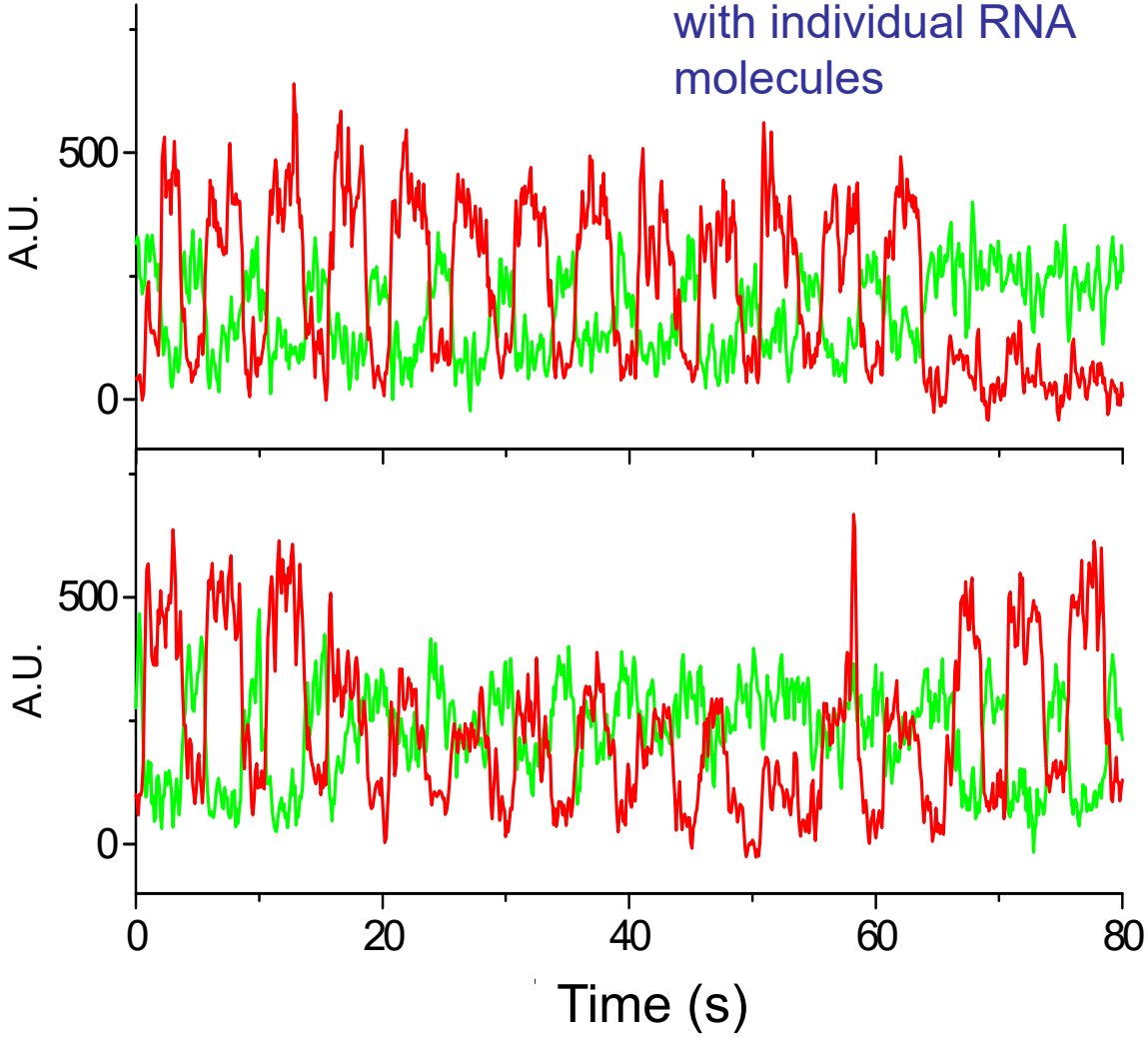

Donor / Acceptor Fluorescence Fluctuations

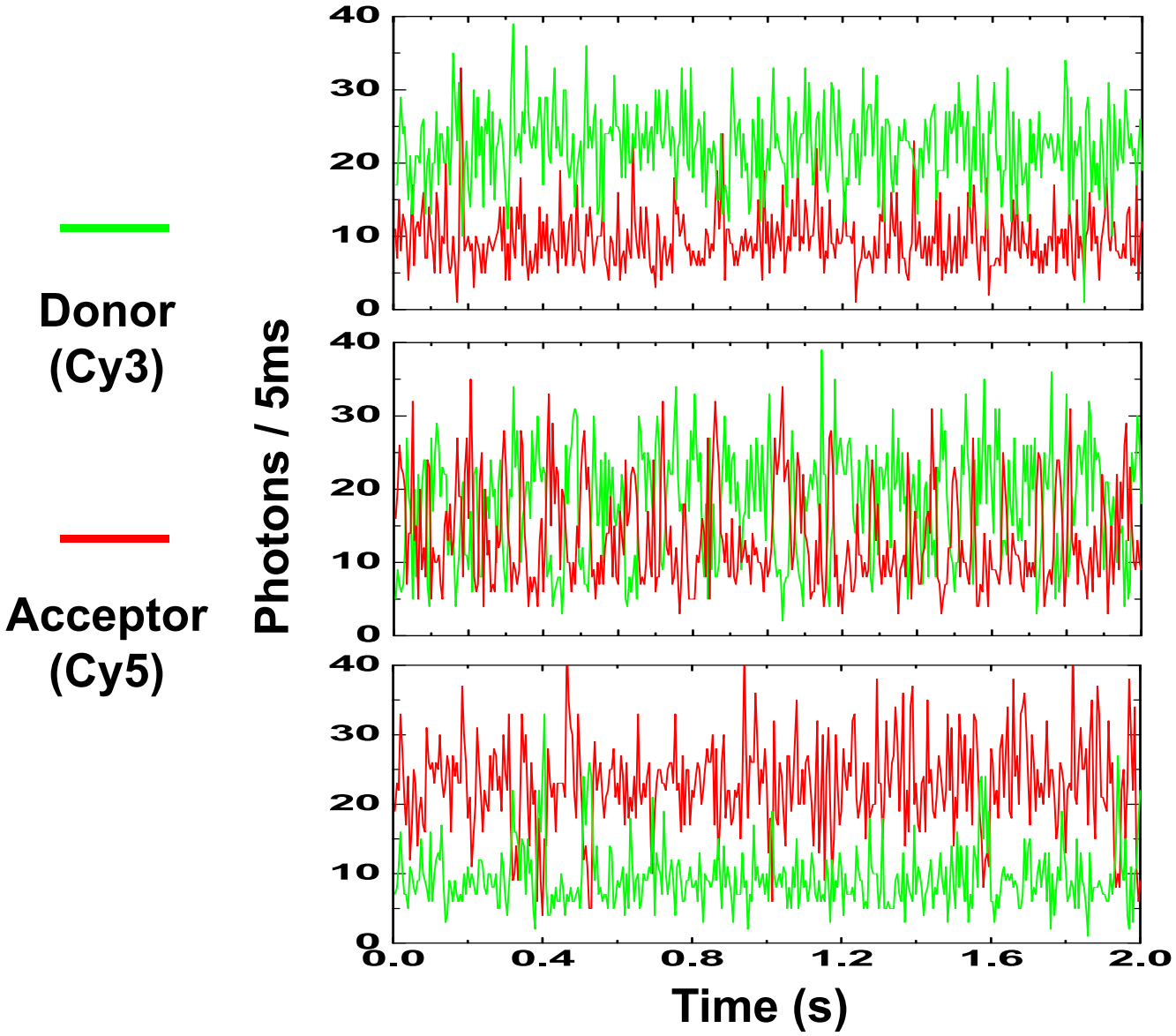

Time traces reveal equilibrium & dynamics

Single-Molecule Fluorescence Correlation Spectroscopy

Pair correlation function: $G_{XY}(\tau) = \dfrac{\langle \delta I_X(t)\ \delta I_Y(t+\tau)\rangle}{\langle I_X(t)\rangle\langle I_Y(t)\rangle}$

X = Y: autocorrelation
X ≠ Y: cross-correlation

$$I(t) = \langle I \rangle + \delta I(t)$$

Stochastic fluctuations between two states:

$$\mathrm{RNA(O)} \underset{\kappa_{OF}}{\overset{\kappa_{FO}}{\rightleftharpoons}} \mathrm{RNA(F)}$$

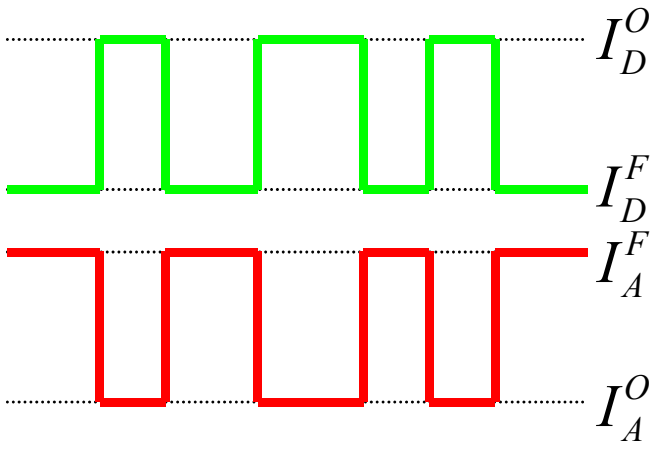

$$AC_{A(D)}(\tau) = \frac{\left(I^F_{A(D)} - I^O_{A(D)}\right)^2}{\left(\kappa_{OF} I^F_{A(D)} + \kappa_{FO} I^O_{A(D)}\right)^2} \kappa_{OF}\kappa_{FO} \exp\left[-\lambda_R \tau\right]$$

$$CC(\tau) = \frac{\left(I^F_D - I^O_D\right)\left(I^F_A - I^O_A\right)}{\left(\kappa_{OF} I^F_D + \kappa_{FO} I^O_D\right)\left(\kappa_{OF} I^F_A + \kappa_{FO} I^O_A\right)} \kappa_{OF}\kappa_{FO} \exp\left[-\lambda_R \tau\right]$$

with $\lambda_R = \tau_R^{-1} = \kappa_{FO} + \kappa_{OF}$

Random telegraph process (two-level continuous time-Markov process)

Kim et al., *Proc. Natl. Acad. Sci. USA* 99 (2002) 4284.

Correlation Functions from a Single RNA Junction

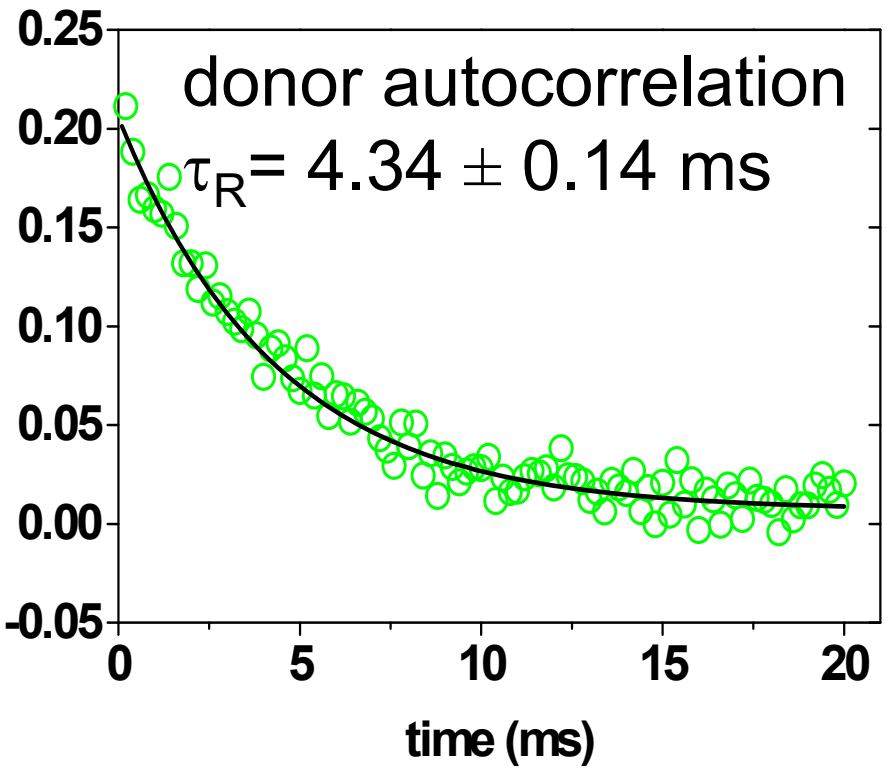

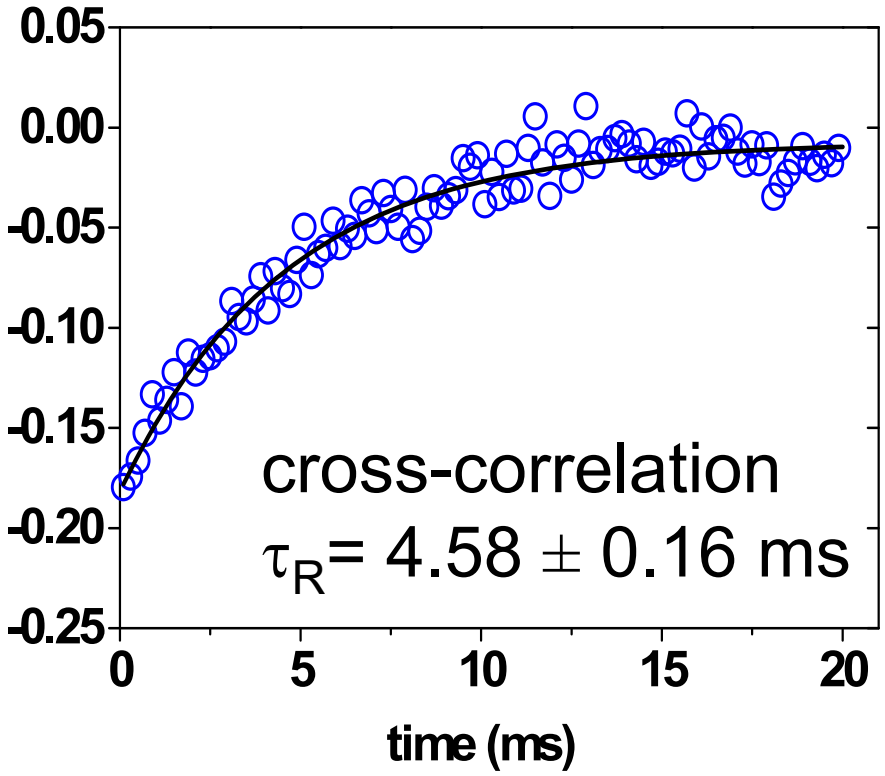

$$G_{XY}(\tau) = \frac{\langle \delta I_X(t)\ \delta I_Y(t+\tau) \rangle}{\langle I_X(t) \rangle \langle I_Y(t) \rangle}$$

$[Mg^{2+}]$ = 200 μM

Variation of $[Mg^{2+}]$ yields further insights.

Fluorescence Correlation Spectroscopy (FCS)

Experiments on freely diffusing molecules!

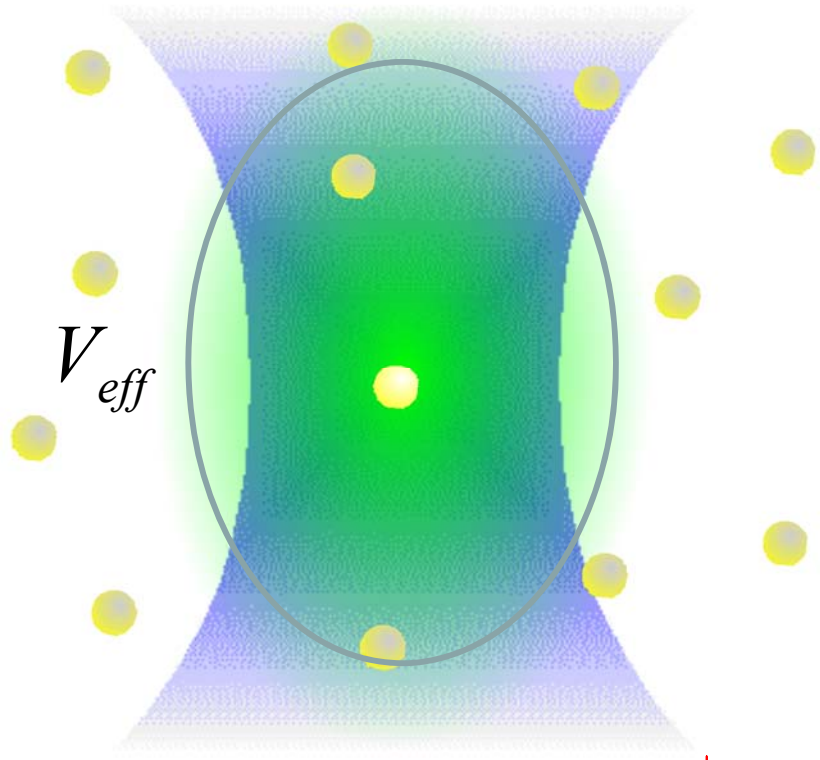

- **Translational Diffusion**
- **Rotational Diffusion**
- **Fluorescence Lifetimes**
- **Molecular Brightness**
- **Spectral Shifts**
- **FRET**
- **Multiplex Detection**
- **Coincidence Analysis**

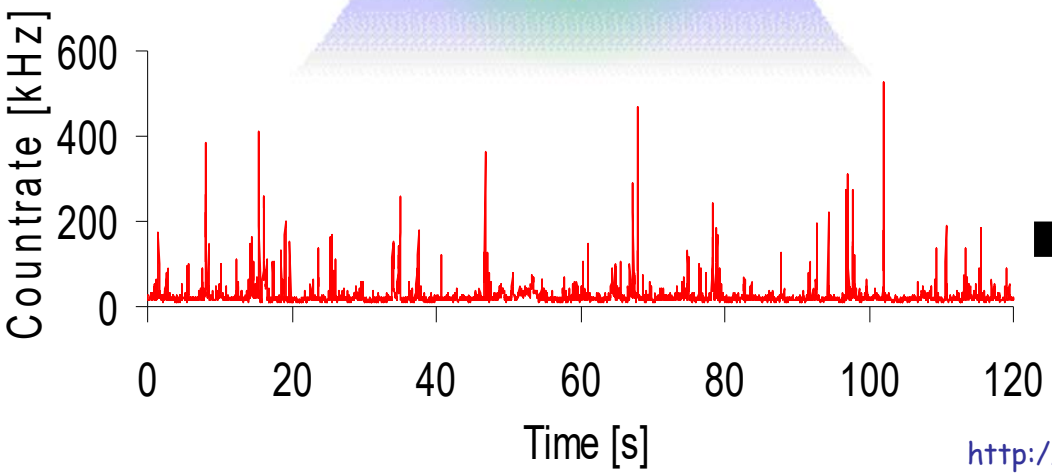

Amplitude statistics: PCH

Time correlations: FCS

http://research.stowers-institute.org/wiw/external/Technology/FCS/index.htm

FCS on Diffusing Molecules

Data collection

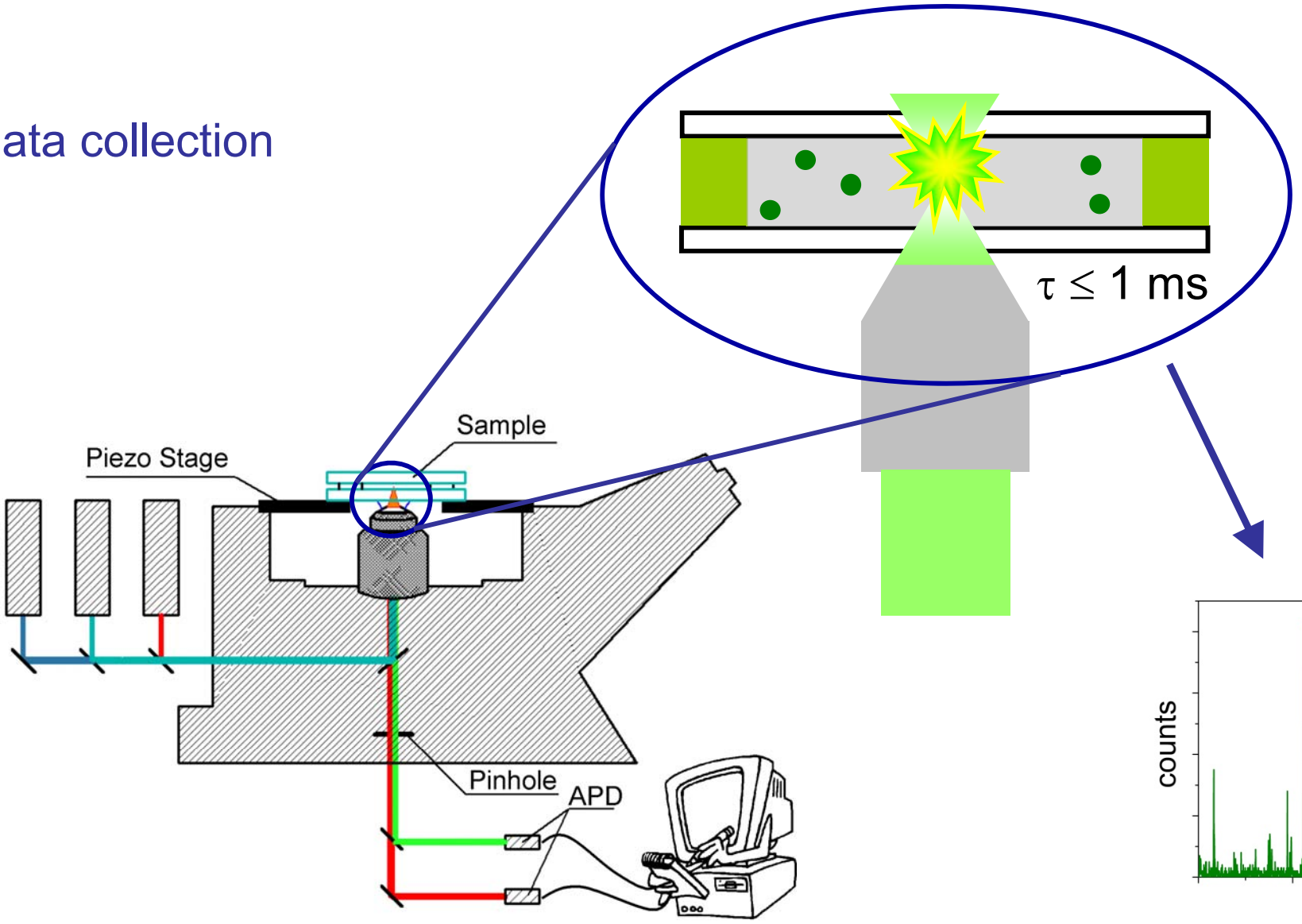

ACF of Freely Diffusing Molecules I

The fluorescence intensity is given by:

$$F(t) = \kappa Q \int d\mathbf{r}\, W(\mathbf{r}) C(\mathbf{r},t)$$

where κ is a scaling factor (dependence on laser power, detection efficiency)

Q = $\varepsilon\,\phi$; Brightness (absorption coeff. × QY)

$W(\mathbf{r}) = I(\mathbf{r})S(\mathbf{r})X(\mathbf{r})$; Probe Volume

$C(\mathbf{r},t)$ = Number Density

$I(\mathbf{r})$ = laser intensity profile
$S(\mathbf{r})$ = Sample extent
$X(\mathbf{r})$ = Detection volume

The autocorrelation function (ACF) is given by:

$$G(\tau) = \frac{\langle \delta F(0)\delta F(\tau)\rangle}{\langle F\rangle^2} = \frac{\iint d\mathbf{r}d\mathbf{r}'\, W(\mathbf{r})W(\mathbf{r}')\langle \delta C(\mathbf{r},\tau)\delta C(\mathbf{r}',0)\rangle}{\left[\langle C\rangle \int d\mathbf{r}\, W(\mathbf{r})\right]^2}$$

ACF of Freely Diffusing Molecules I

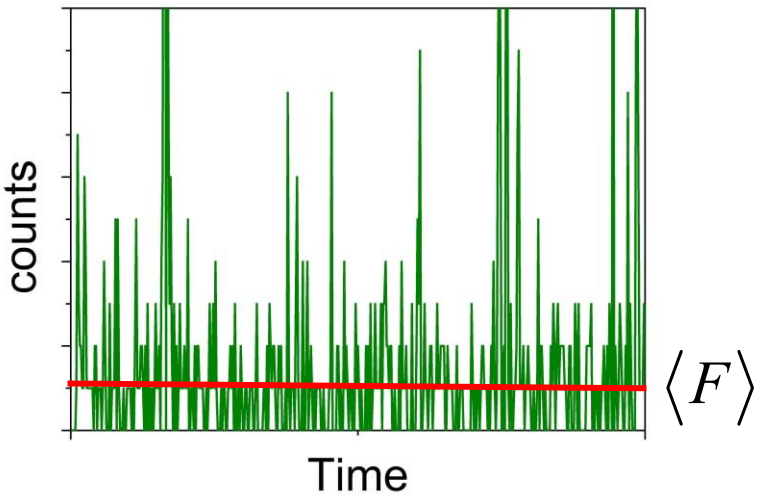

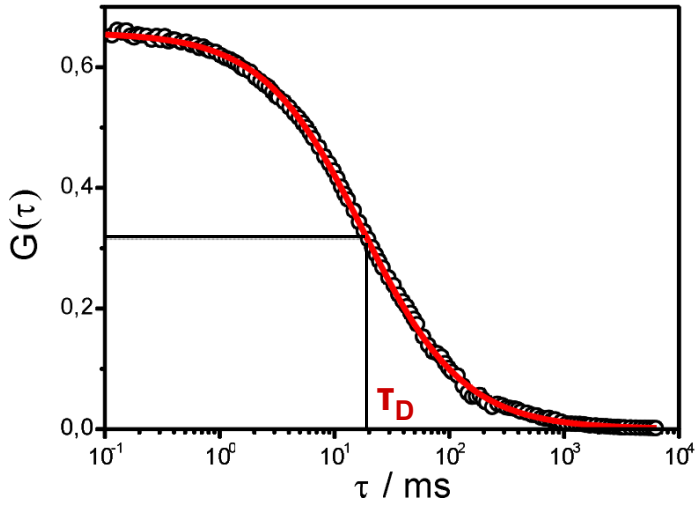

$$F(t) = \langle F \rangle + \delta F(t)$$

Fluorescence Signal

$$G(\tau) = \frac{\langle \delta F(t)\, \delta F(t+\tau) \rangle}{\langle F \rangle^2}$$

Autocorrelation function

$$G(\tau) = \frac{\gamma}{\langle N \rangle} \left(1 + \frac{\tau}{\tau_D}\right)^{-1} \left(1 + \left(\frac{r_0}{z_0}\right)^2 \frac{\tau}{\tau_D}\right)^{-\frac{1}{2}}$$

$$\langle N \rangle = \langle C \rangle V_{eff} = \langle C \rangle r_0^2 z_0 \left(\frac{\pi}{2}\right)^{3/2}$$

Diffusional autocorrelation function for 3D Gaussian volume: $\gamma = \frac{\int I^2 dV}{\int I dV} = \left(\frac{1}{2}\right)^{3/2}$

$$\tau_D = \frac{r_0^2}{4D}$$

← Diffusion coefficient

Diffusional correlation time

Application of FCS: Binding Studies

Nanoparticle-protein interaction

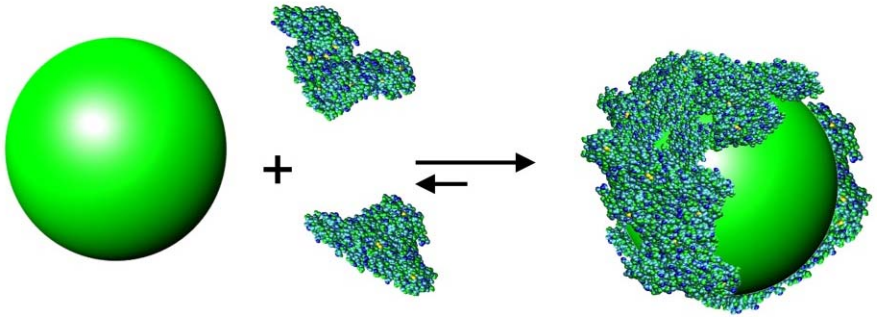

nanoparticle protein

$$D = \frac{k_B T}{6\pi\eta R_H}$$

Hydrodynamic radius of the molecule

Stokes-Einstein law (for translational diffusion)

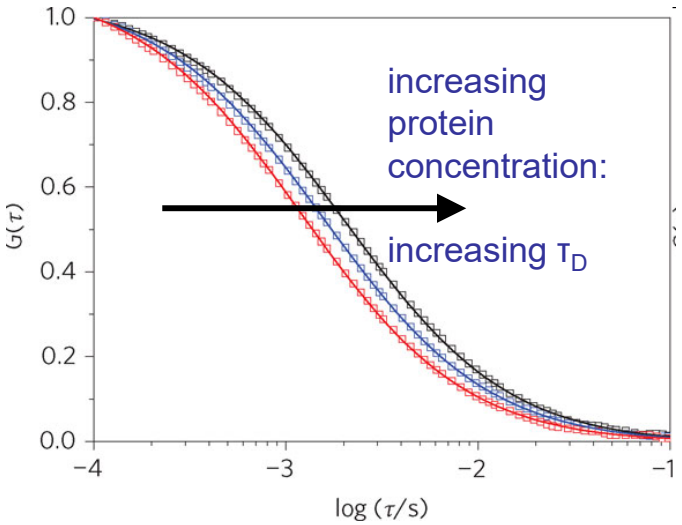

Autocorrelation curves

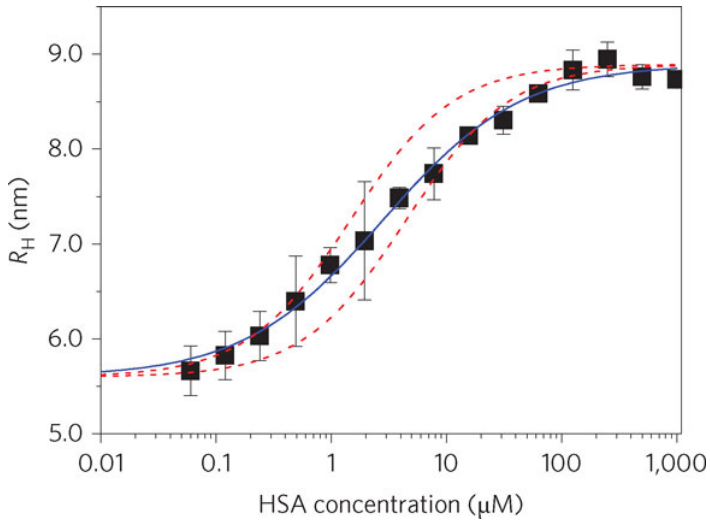

Binding curve

Röcker et al., Nature Nanotechnology 4 (2009) 577-580.

Case II: ΔG large, $N_B \sim 0$

- need to apply a major perturbation:

stopped flow or continuous flow:

rapid mixing of reactants using a fine nozzle. In stopped flow, a cuvette is filled once and the reaction is monitored transiently. In continuous flow, the reaction is monitored in steady state as a function of the distance behind the nozzle. Dead time: μs - ms.

pulse radiolysis:

Bombarding samples with microsecond pulses of high energy electrons (MeV) from a linear accelerator.

photoexcitation:

Short laser pulses (1 ps < τ < 1 μs) can be employed to initiate photon-induced electron transfer, chromophore isomerization, or photolysis of ligands from (heme) proteins.

Flash Photolysis

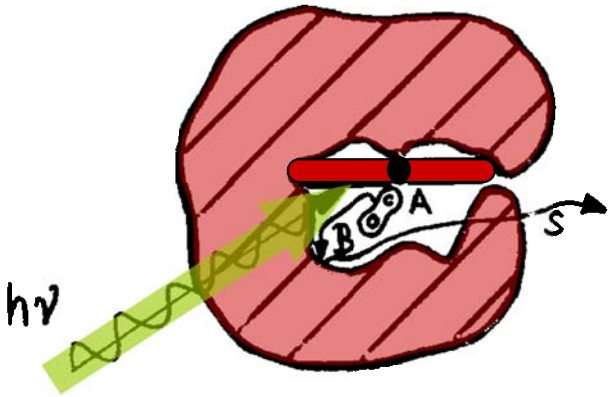

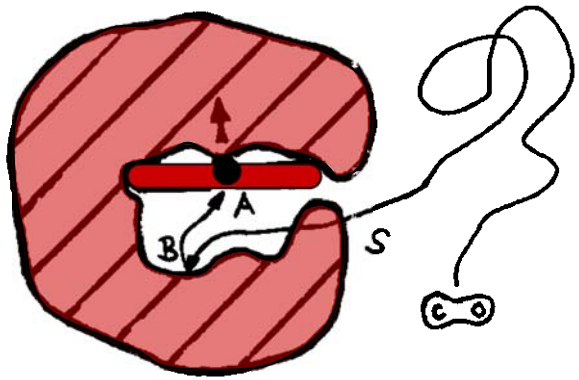

Rebinding

Photodissociation,
e.g., of heme proteins
such as MbCO

Protein motions:
r → t relaxation, fluctuations

Experimental realizations:

- pump / probe
- transient recording

Transient spectroscopy: Kinetic Spectrometer

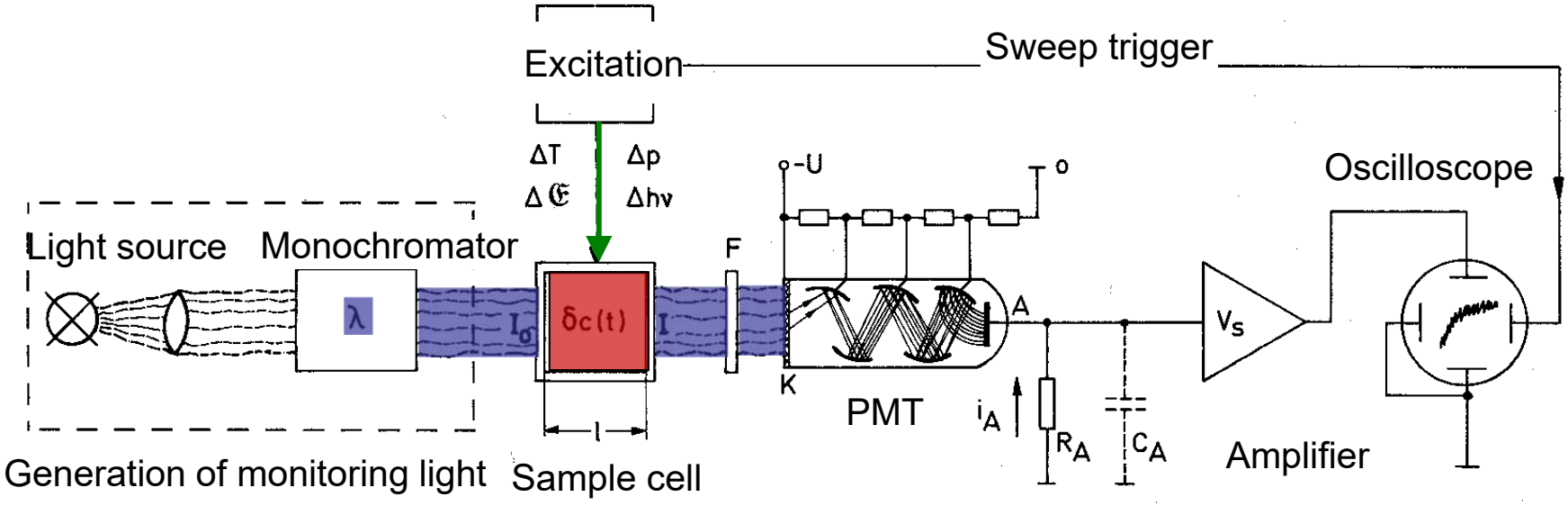

Schematic drawing of a kinetic pulse spectrophotometer. PMT photomultiplier tube, K photo cathode; A anode; U cathode voltage (ca. -500 V for absorption measurements); F interference filter used with light pulse excitation to block off scattered light of the flash; λ wavelength; R_a load resistor; C_a stray capacity at the anode.

Porter [Norrish et al., Nature 164 (1949) 658 (Spectrograph)], Witt [Witt et al., Z. physik. Chemie N.F. 20 (1953) 193 (flash-pulse-photometer)] and Rüppel [Rüppel et al., Ber. Bunsenges. 68 (1964) 340 (repetitive pulse-photometer)].

Flash Photolysis (VIS, NIR, IR)

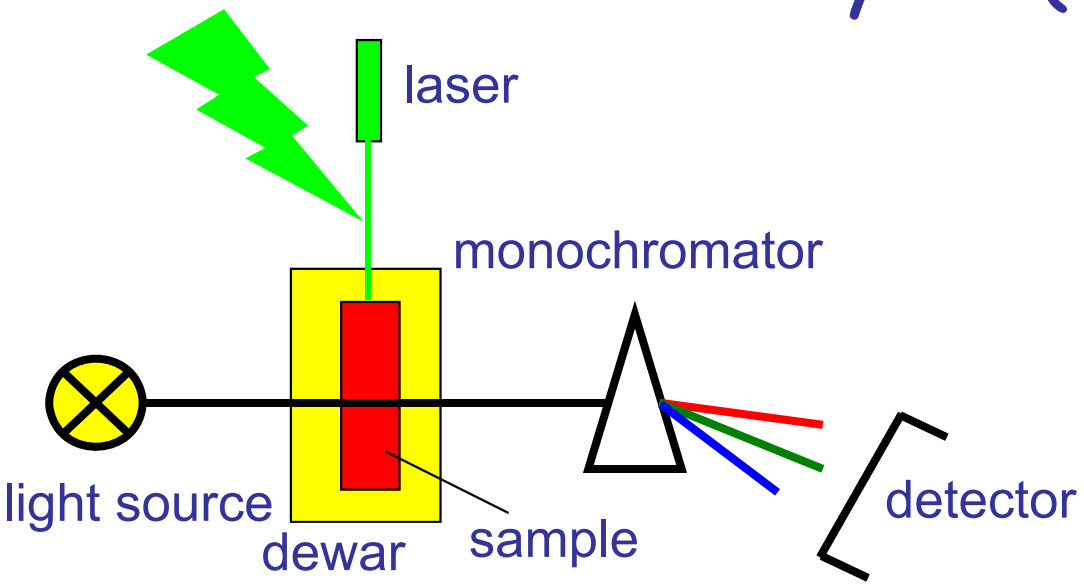

290 K

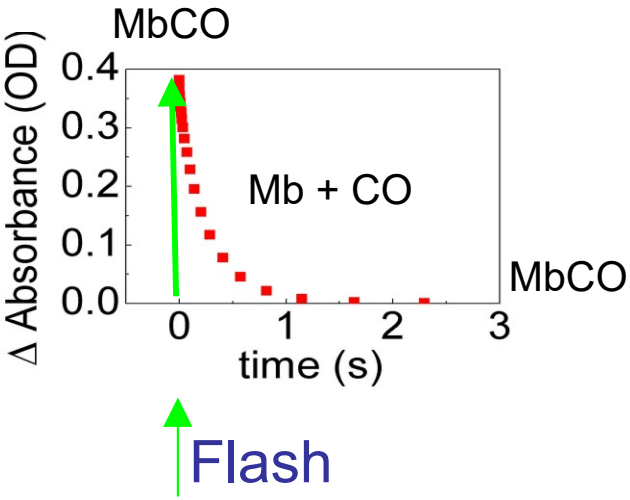

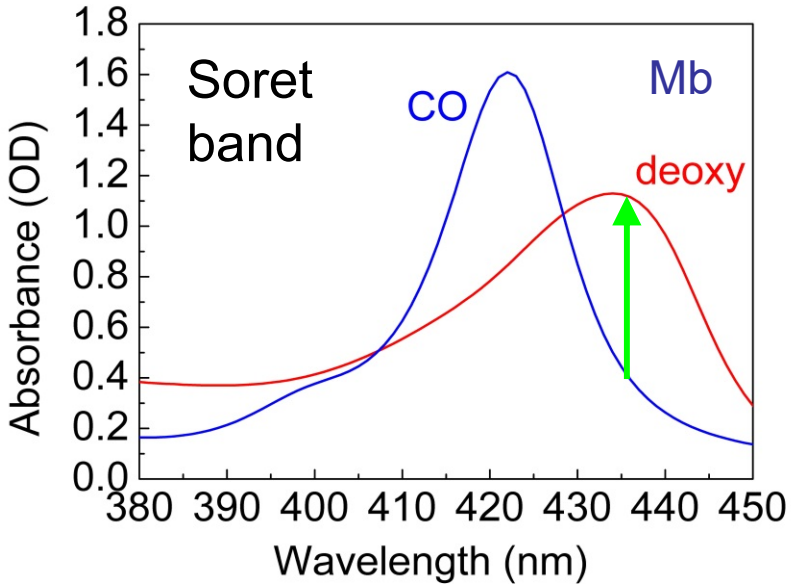

100 K

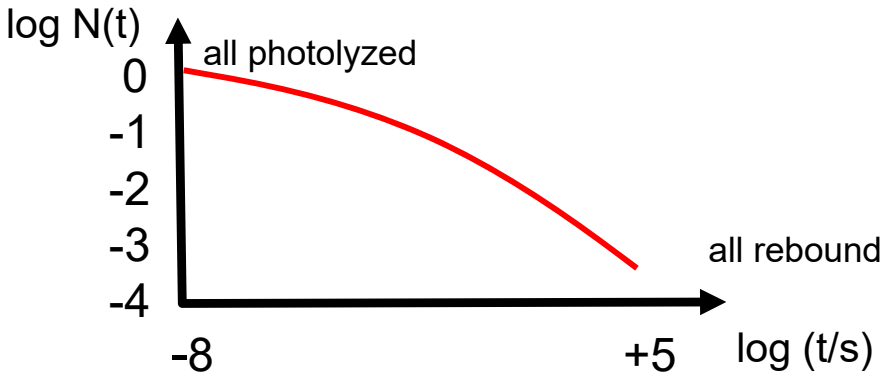

Biophysics II

Spectroscopic Evidence of Conformational Substates in Proteins

Uli Nienhaus

Prof. G. U. Nienhaus, Vorlesungsunterlagen Biophysik II, SS 2023.
Nur zum KIT-internen, vorlesungsbegleitenden Gebrauch.
Weitergabe und anderweitige Nutzung verboten.

Experimental Evidence of Protein Conformational Heterogeneity

Experimental parameters measured on protein ensembles are not sharp, but distributed.

- Debye-Waller and Lamb-Mössbauer factors in x-ray and γ-ray scattering/absorption experiments are indicative of structural heterogeneity.

- **Ligand binding reactions** (as well as conformational changes and electron transfer reactions) show non-exponential kinetics at cryogenic temperatures.

- Spectral lines (electronic and vibrational transitions) are inhomogeneously broadened.
  - **spectral hole burning**
  - **kinetic hole burning**

Conformational Substates

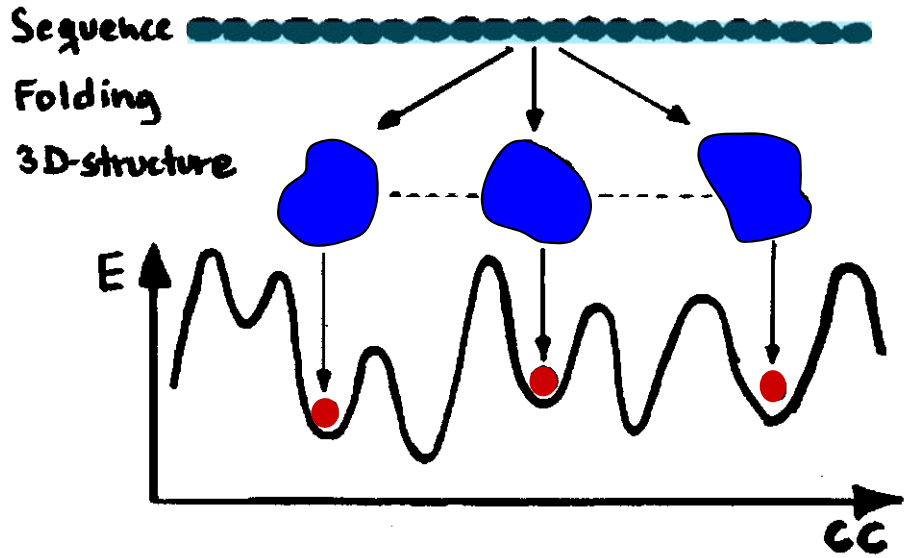

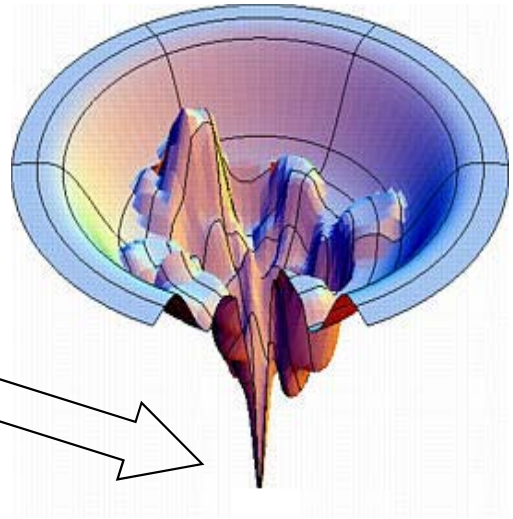

Conformational substates (CS):

- same overall structure, details differ
- same function, rates may differ

low temperature / short times: static distributions

high temperature / long times: fluctuations between CS

rugged conformational energy landscape → complex system

Complex Systems I

Glasses are liquids with arrested motions

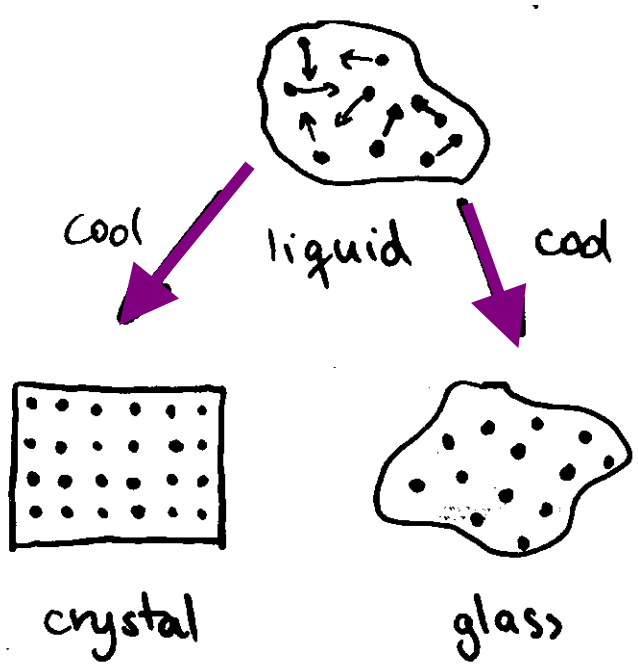

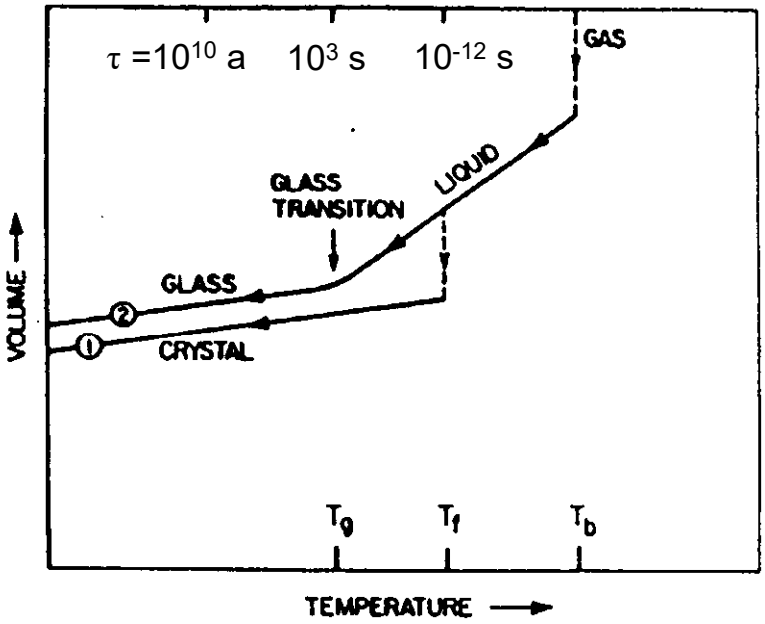

- Glasses, spin glasses, synthetic polymers and biomolecules share essential properties:
  - distributions of characteristic time scales of motion
  - non-Arrhenius temperature dependence of time scales
  - metastability
- They are all complex systems characterized by rugged energy landscapes.

Complex Systems II

Disorder

crystal

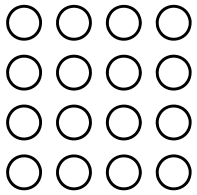

symmetry
periodicity

glass

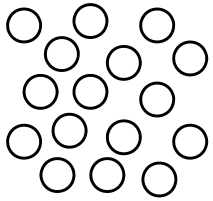

randomness
aperiodicity

Frustration

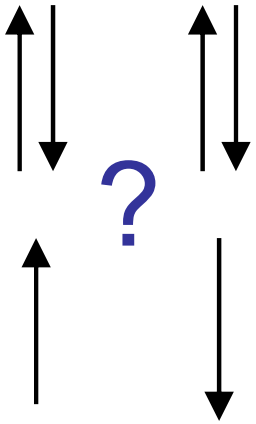

spin glass

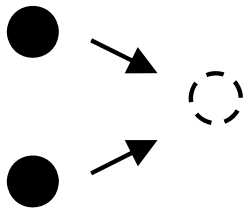

Biomolecules

Competition for vacant
sites (steric constraints)

Conformational Heterogeneity: Model System Myoglobin (Mb)

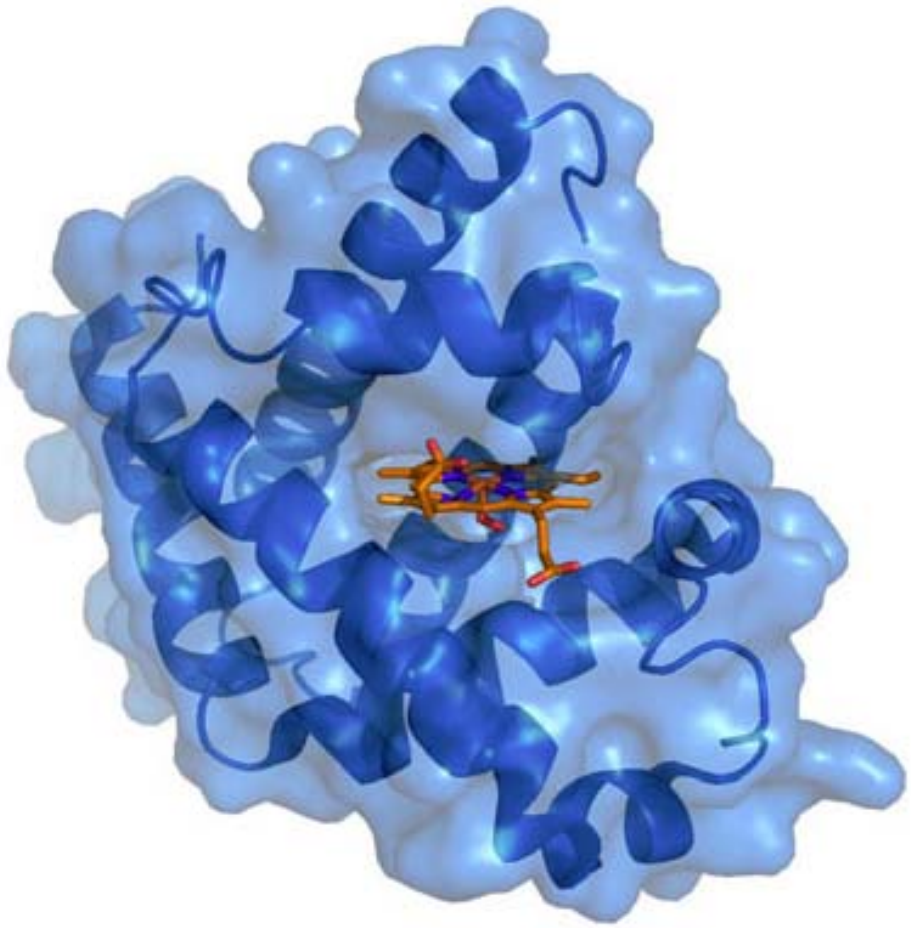

- Mb has a simple function: reversible ligand (O_2, CO, NO) binding at the heme iron.
- First x-ray structure solved at atomic resolution (1960):
  - 153 amino acids
  - 8 α-helices
  - 1 heme group
- In x-ray structures, the mean square displacements of the atoms are large. There are also multiple occupancies of side chains.

Ligand Binding at Low Temperature

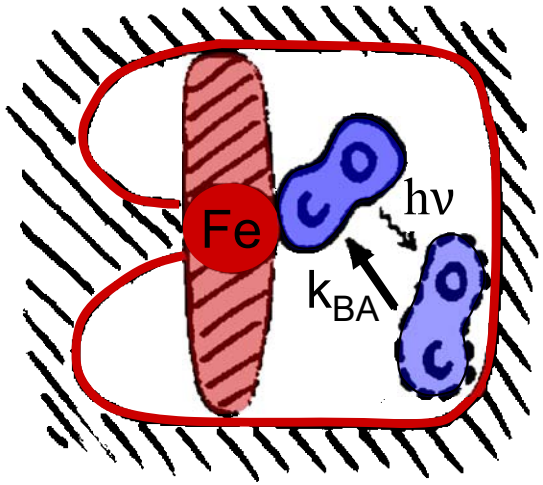

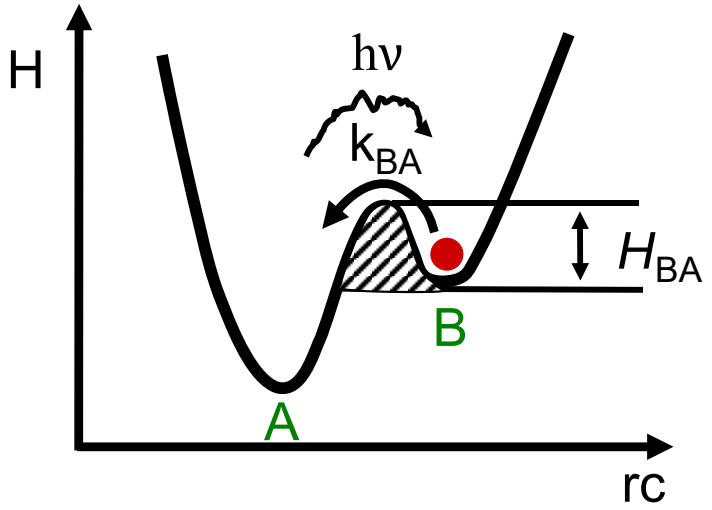

Below ~ 180 K:
CO remains in heme pocket after photolysis

$$N(t) = e^{-k_{BA}t}$$

$$k_{BA} = A_{BA} e^{-H_{BA}/RT}$$

Arrhenius law

A: CO bound
B: CO in heme pocket
H_{BA}: barrier associated with bond formation

Austin et al., Biochemistry 14 (1975) 5355.

Structural Changes at Low Temperature

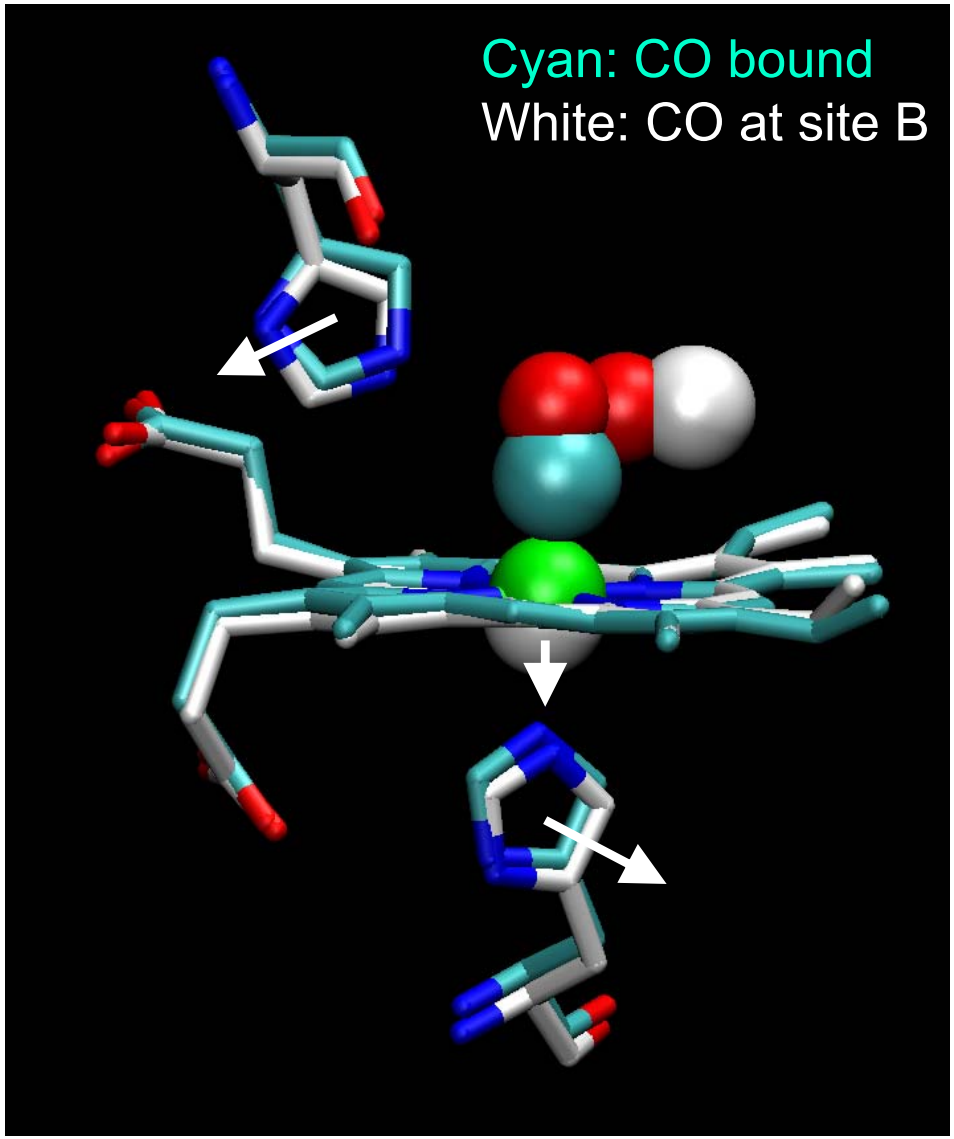

CO photolysis causes minor structural displacements (T<100 K), the CO ligand remains very close to the heme iron.

Photoproduct structures:

Schlichting et al., Nature 317 (1994) 808.
Teng et al., Nature Struct. Biol. 1 (1994) 701.
Hartmann et al., PNAS 93 (1996) 7013.

Flash Photolysis – Nonexponential Rebinding

Austin et al., Biochemistry 14 (1975) 5355.

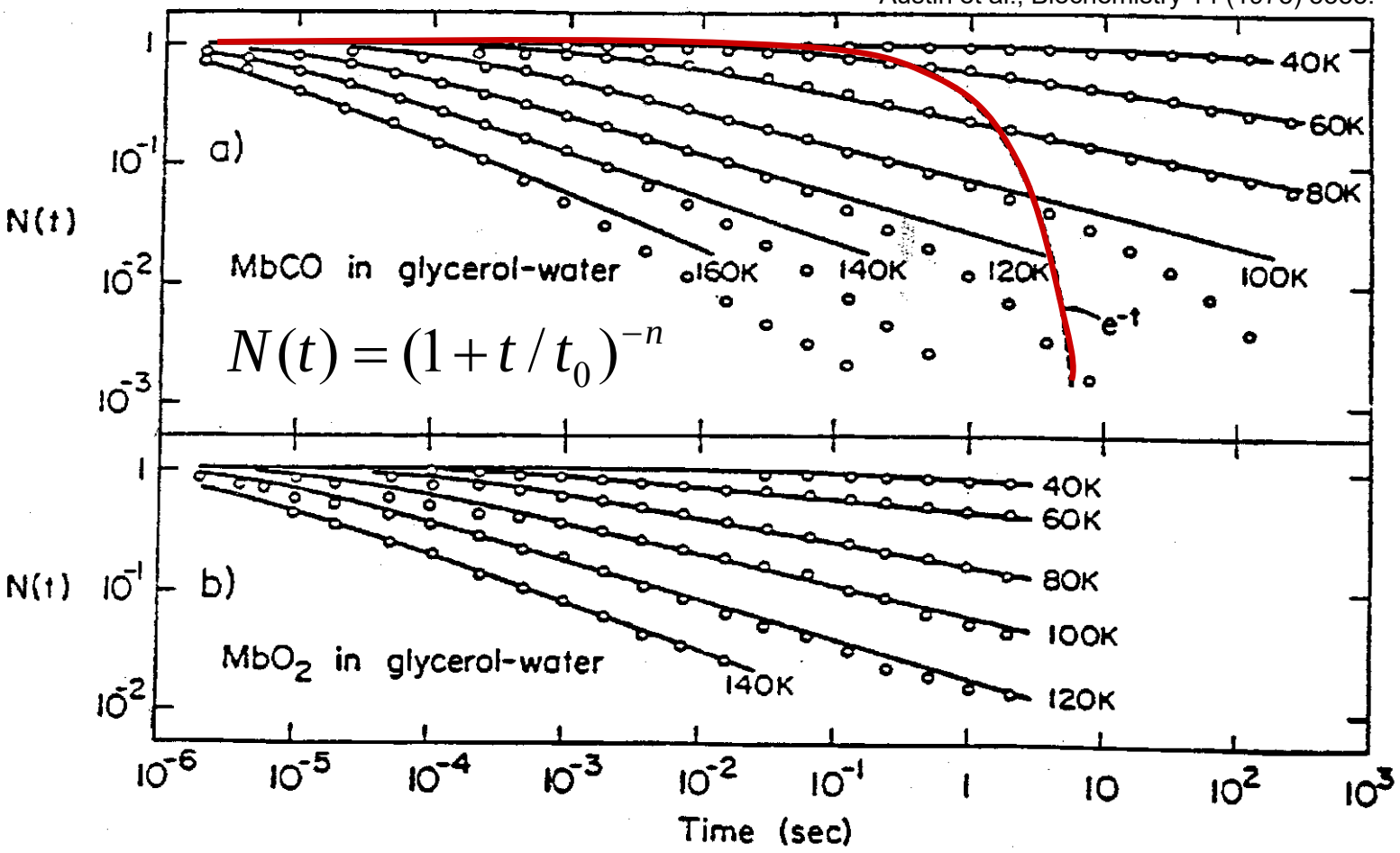

Kinetic trace measured with flash photolysis in the visible (436 nm) can be described at each temperature with a distribution of rate coefficients: $N(t;T) = \int f(k_{BA};T)\, e^{-k_{BA}t}\, \mathrm{d}\log k_{BA}$

Enthalpy Barrier Distributions

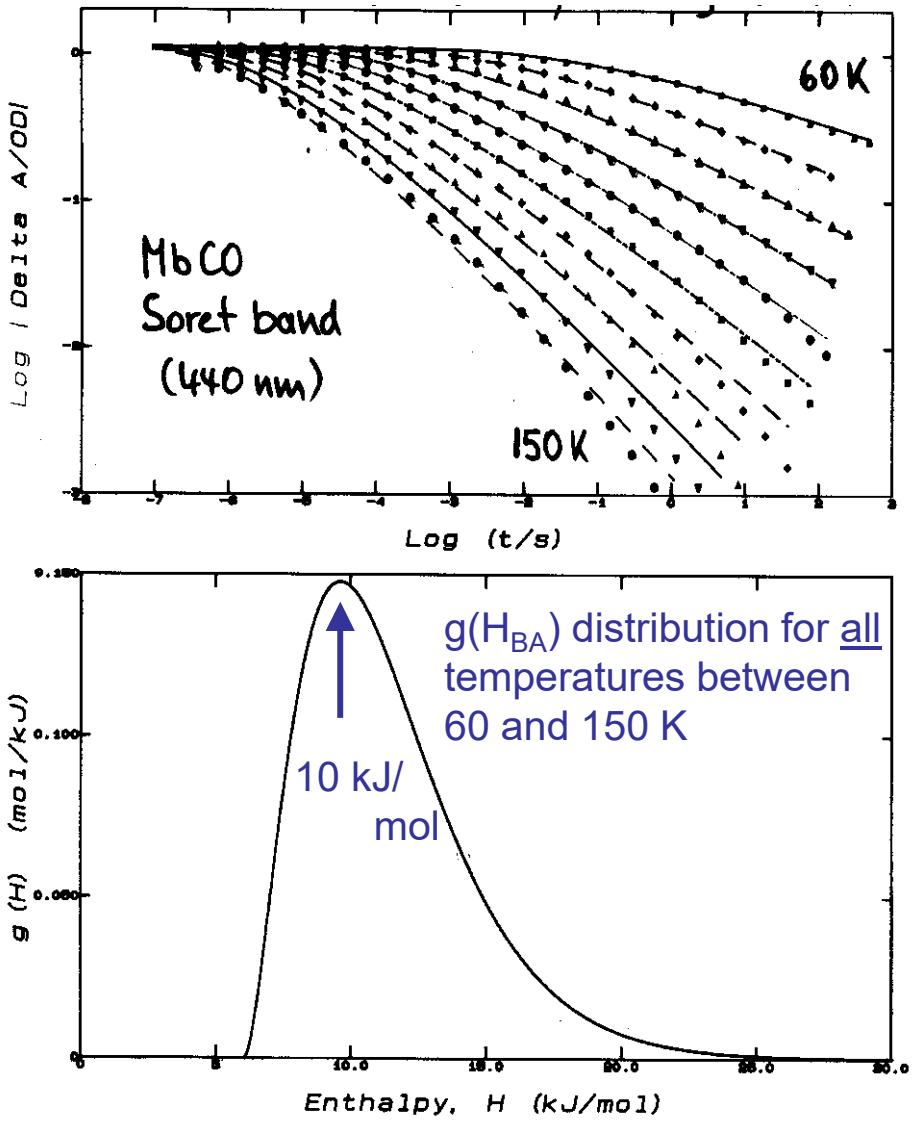

Steinbach et al., Biochemistry 30 (1991) 3988.

A single enthalpy barrier distribution, g(H), allows us to model all kinetic traces between ~50 and 150 K:

$$N(t) = \int g(H_{BA}) e^{-k_{BA} t} \, dH_{BA}$$

with $$k_{BA} = A_{BA} e^{-H_{BA}/RT}$$

functional heterogeneity → structural heterogeneity

Spectral Hole Burning: Principle

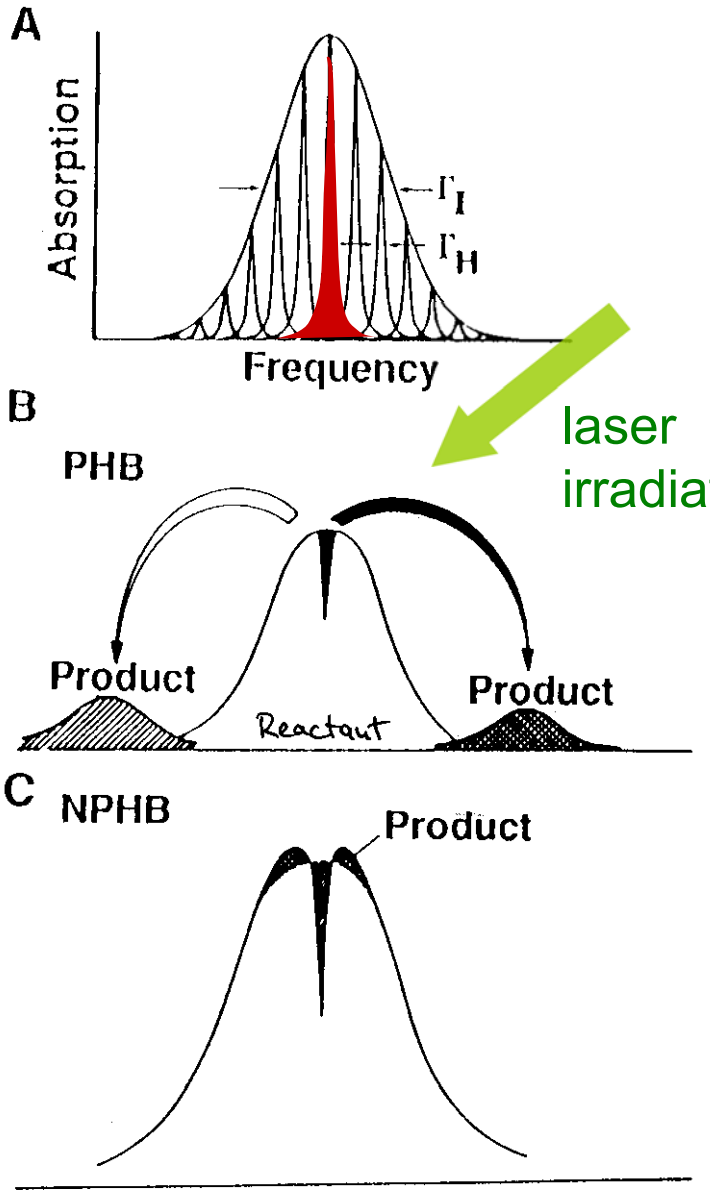

laser irradiation

Inhomogeneously broadened absorption band with a width Γ_I. The homogeneous bands of width Γ_H of the individual electronic transitions are hidden within the broad inhomogeneous absorption band.

photochemical hole burning

photophysical hole burning

Laser-induced spectral hole burned at frequency ν_1. The photoproduct absorbs at a different frequency.

Spectral Hole Burning in PP IX-Mb

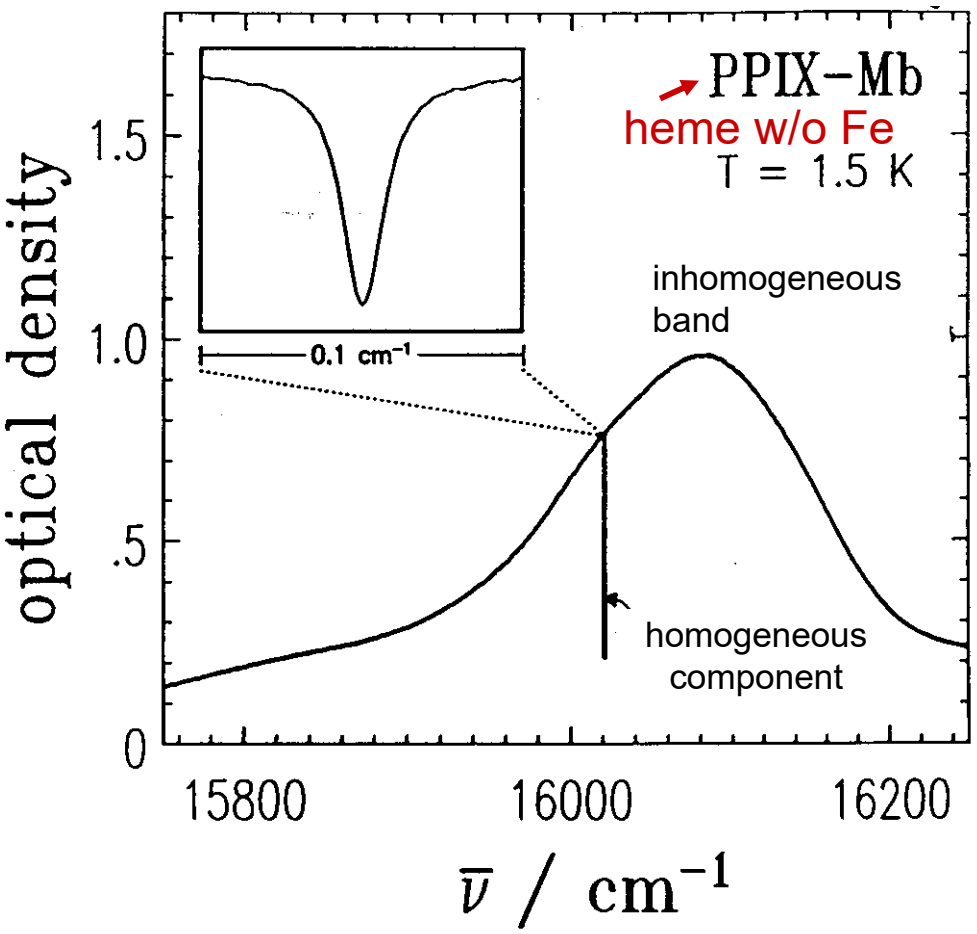

A narrow-band tunable laser is used to burn a hole (with high power). Subsequently, the laser is tuned across the absorption band to measure the absorbance.

1 GHz = 1 ns^{-1} ≅ 4.13 μeV ≅ 0.03 cm^{-1}

Hole Burning and Temperature Cycling

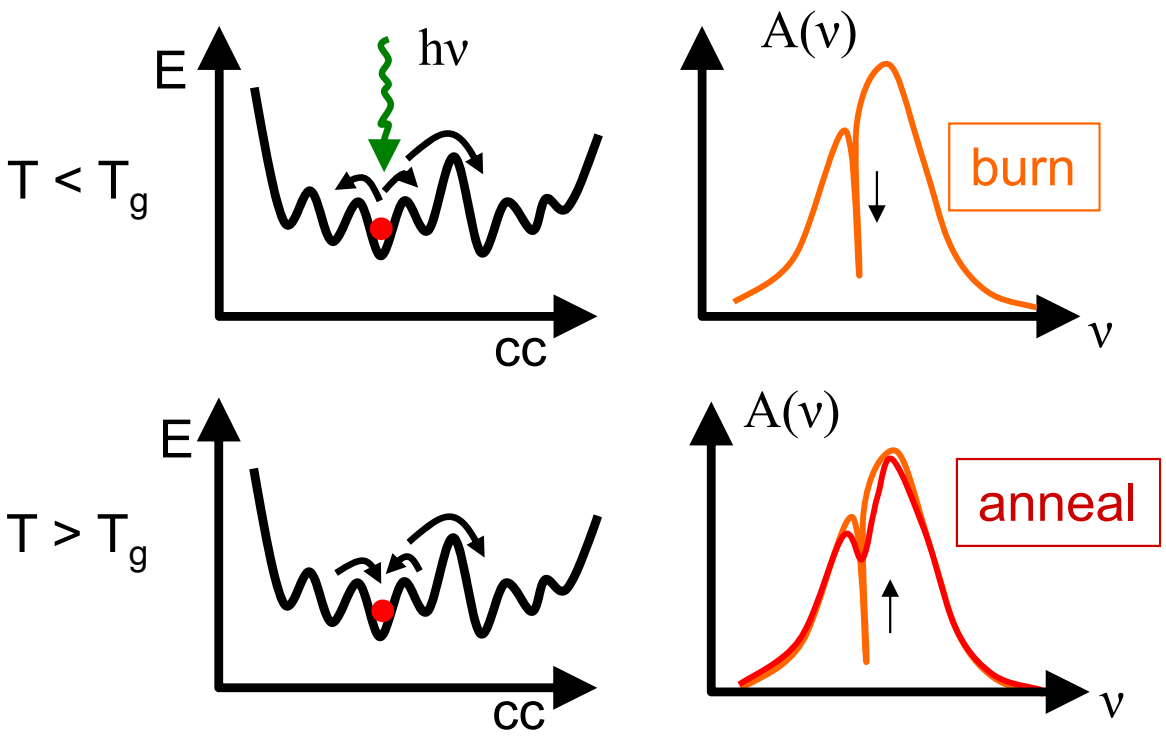

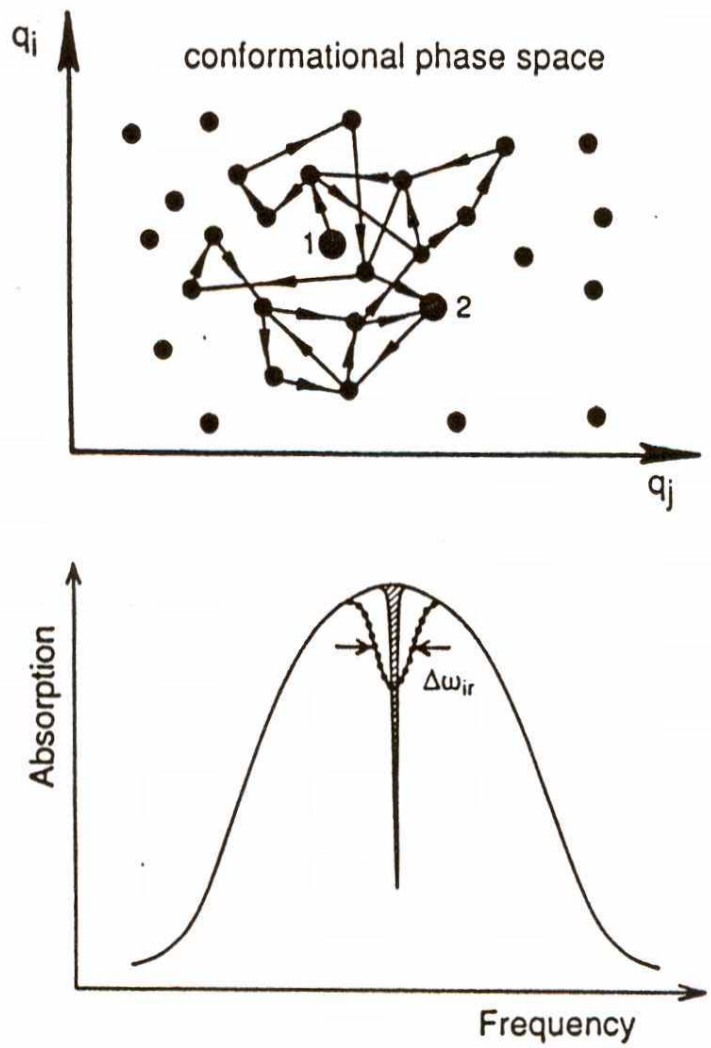

A spectral hole as a conformation space marker.
The sharp hole is burned at the lowest temperature, when the protein is in substate 1. As a consequence of cyclic temperature variation, the protein is trapped in substate 2. The process of structural detrapping and retrapping is reflected in a broadening of the hole ($\Delta\omega_{ir}$).

Hole Burning Spectroscopy: Energy Transport in Antenna Complexes

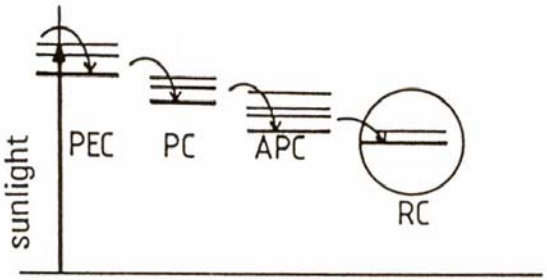

Energy level scheme of the antenna system of blue-green and red algae.

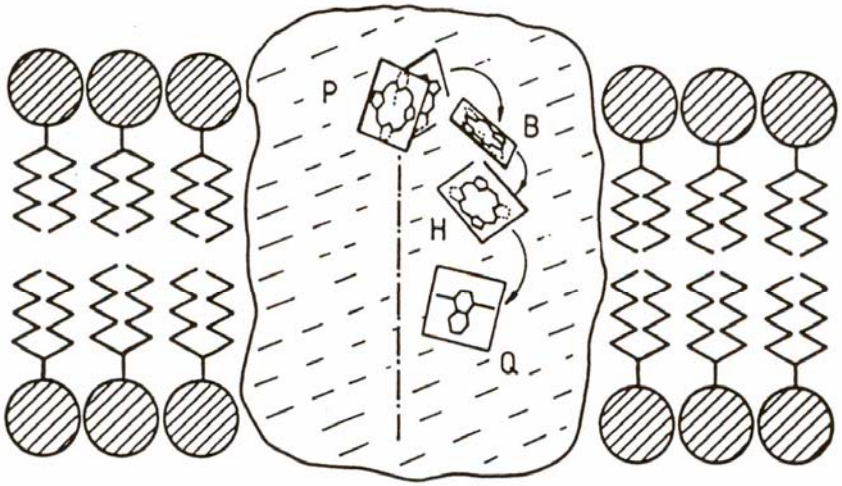

FIG. 7. Reaction center with the active branch. P, Special pair; B, bacteriochlorophyll; H, bacteriopheophytin; Q, quinone. The inactive branch is symmetrically arranged.

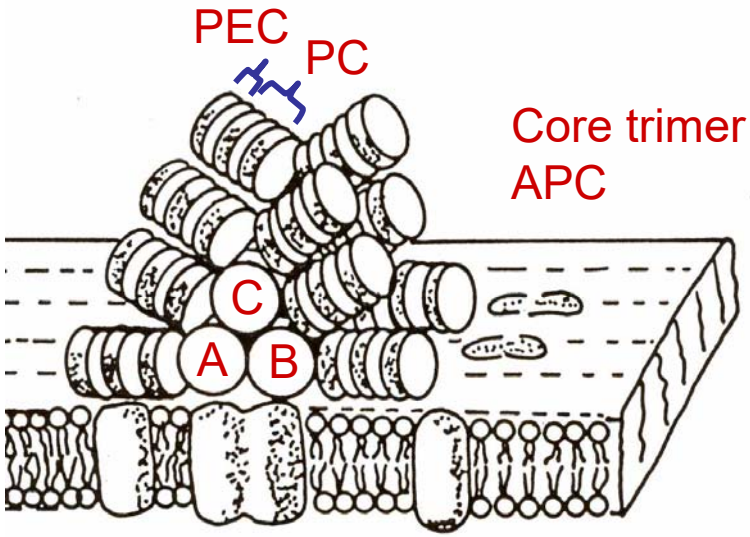

Antennas (phycobilisomes), membrane, and reaction center.

phycoerythrocyanin (PEC)
phycocyanin (PC)
allophycocyanin (APC)

Friedrich, Methods Enzymol., 246, 226 (1995)

Temperature Dependence of Hole Width

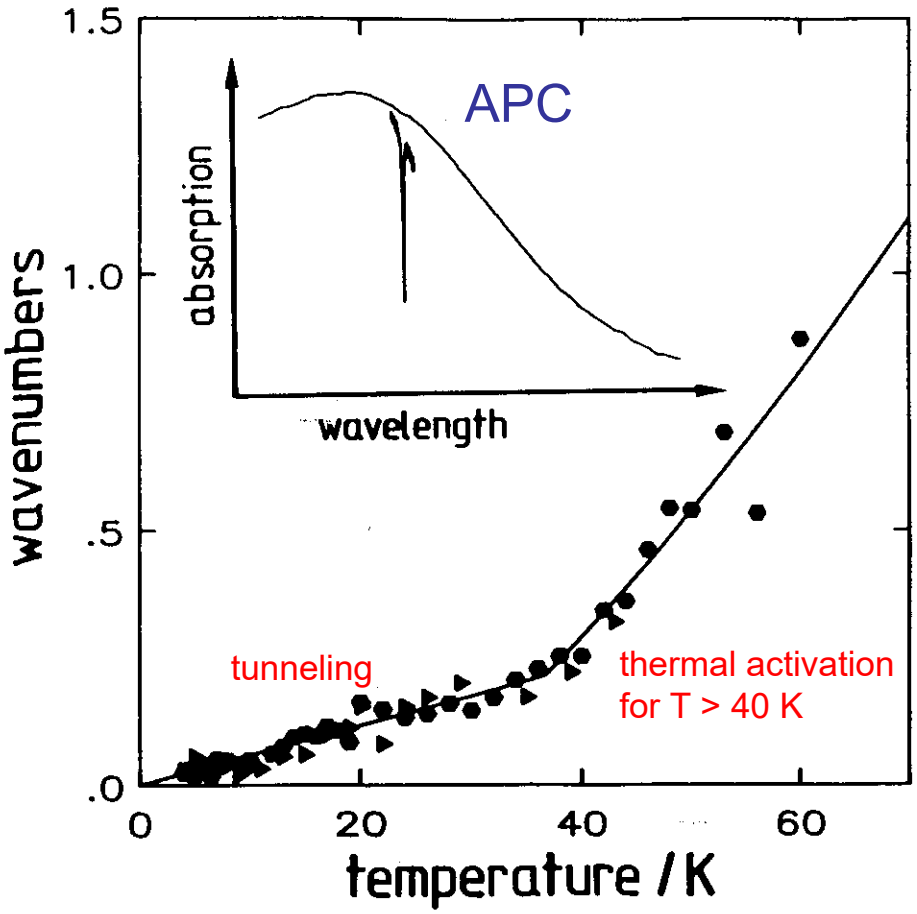

Thermally irreversible broadening $\Delta\omega_{ir}$ of an optical hole (inset) as measured by a temperature cycling experiment. Burning temperature: 4.2 K, laser frequency 6573 Å, sample: phycobilisomes of the alga *Mastigocladus laminosus* in sucrose/ phosphate buffer glass. Also shown is part of the inhomogeneously broadened absorption line between 6500 and 6650 Å.

Köhler & Friedrich, J. Chem. Phys. 90, 1270 (1989)

Two-Level Systems

- Activated barrier crossing
- Tunneling

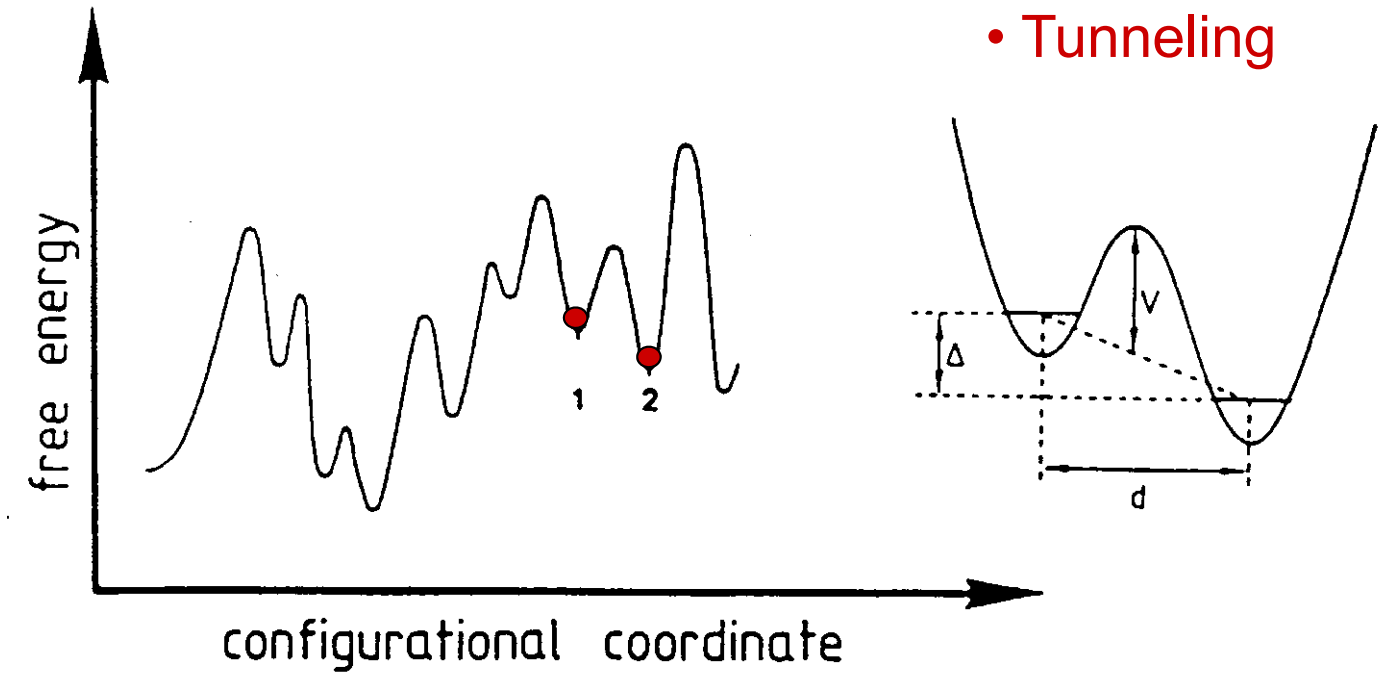

Cut through the configuration space of a large protein along a fictive coordinate. The simplest element which allows for conformational relaxation (e.g., from 1 to 2) is a double well potential.

Kinetic Hole Burning

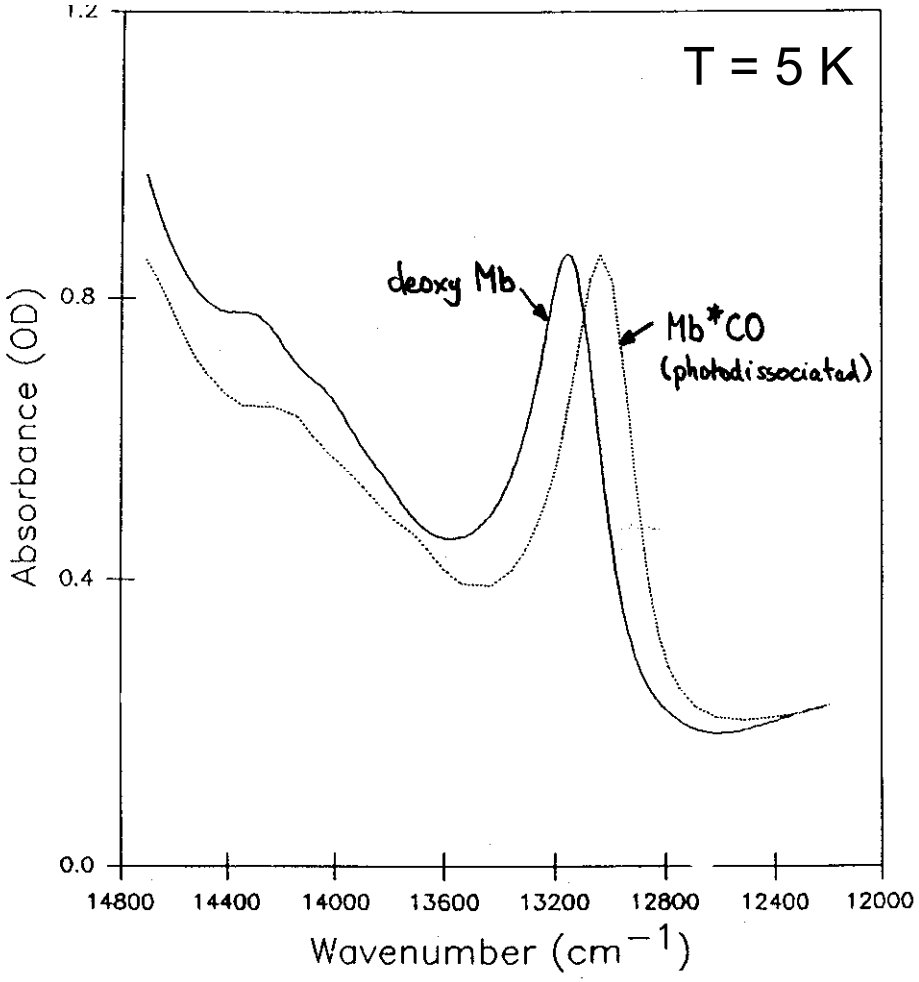

Band III

- Weak absorption band at ~760 nm in high-spin ferrous (Fe^{2+}) heme proteins (Mb, Mb*CO, Mb*O_2)
- charge-transfer transition

  porphyrin $\pi \rightarrow Fe^{2+}$ (d_{yz}).

Kinetic Hole Burning in Band III

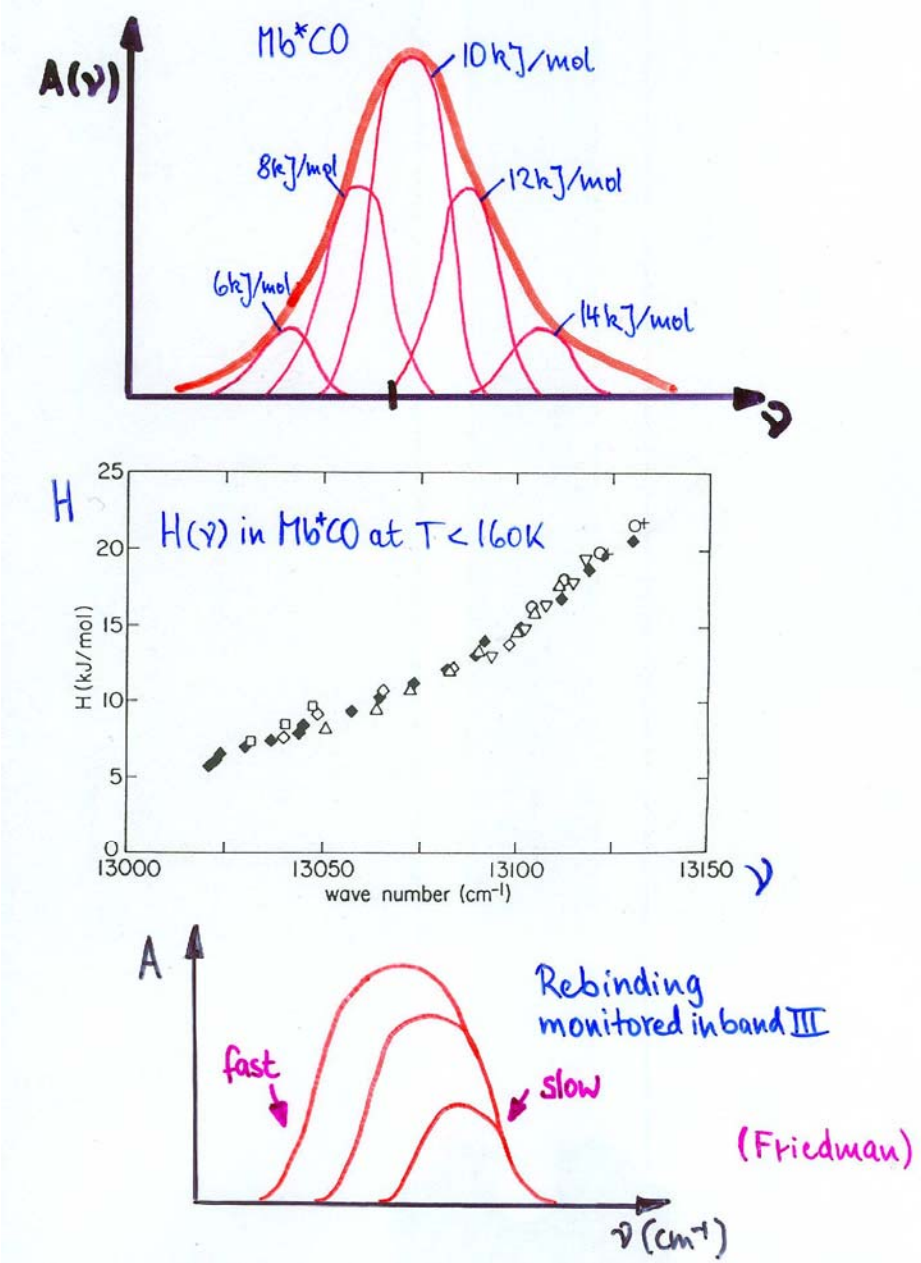

Spectra measured during a temperature ramp 4 – 140 K

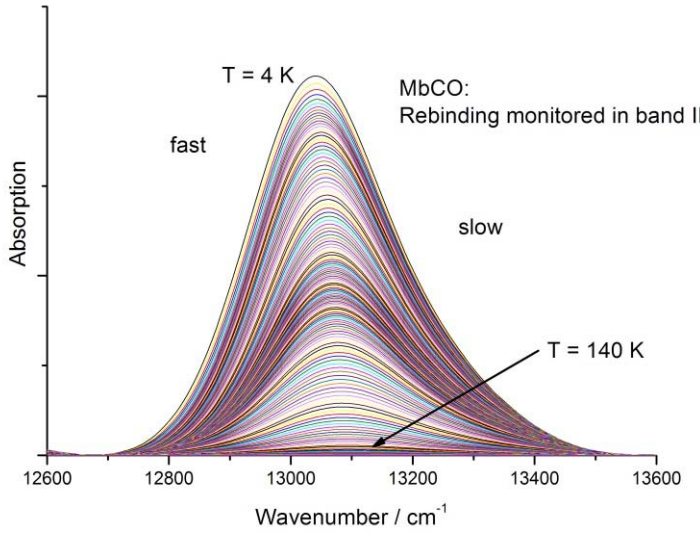

Kinetic Hole Burning in Band III

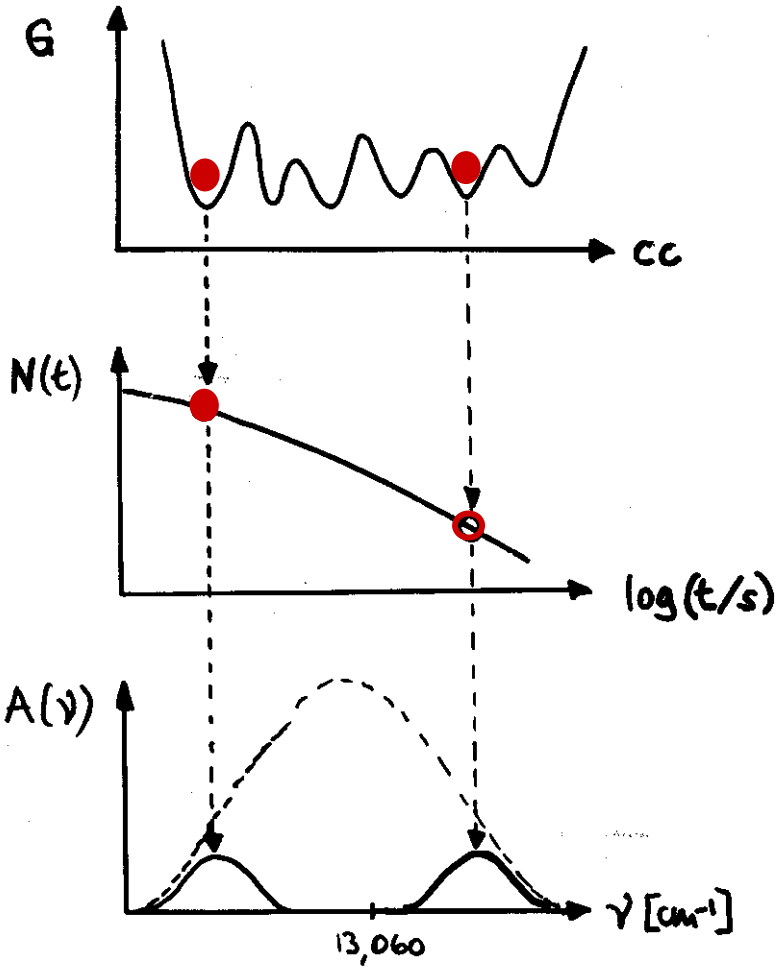

Substates CS

Rebinding $k \sim 1 / t$

Band III spectrum

Biophysics II

Energy Landscapes and Taxonomic Substates in MbCO

Uli Nienhaus

Prof. G. U. Nienhaus, Vorlesungsunterlagen Biophysik II, SS 2023.
Nur zum KIT-internen, vorlesungsbegleitenden Gebrauch.
Weitergabe und anderweitige Nutzung verboten.

Exploring the Energy Landscape of Proteins

- Investigate topography of EL
  - coarse structure, basic features
- Relation spatial structure $\leftrightarrow$ EL

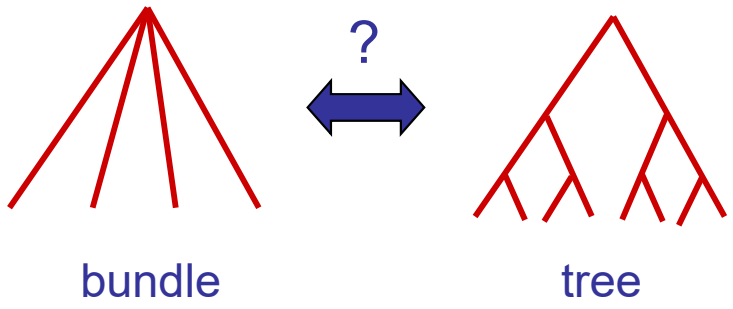

- Dynamics in the EL
  - nonexponential, non-Arrhenius relaxations
- Connection EL $\leftrightarrow$ function
  - characterize functionally relevant states

Computational Approaches I

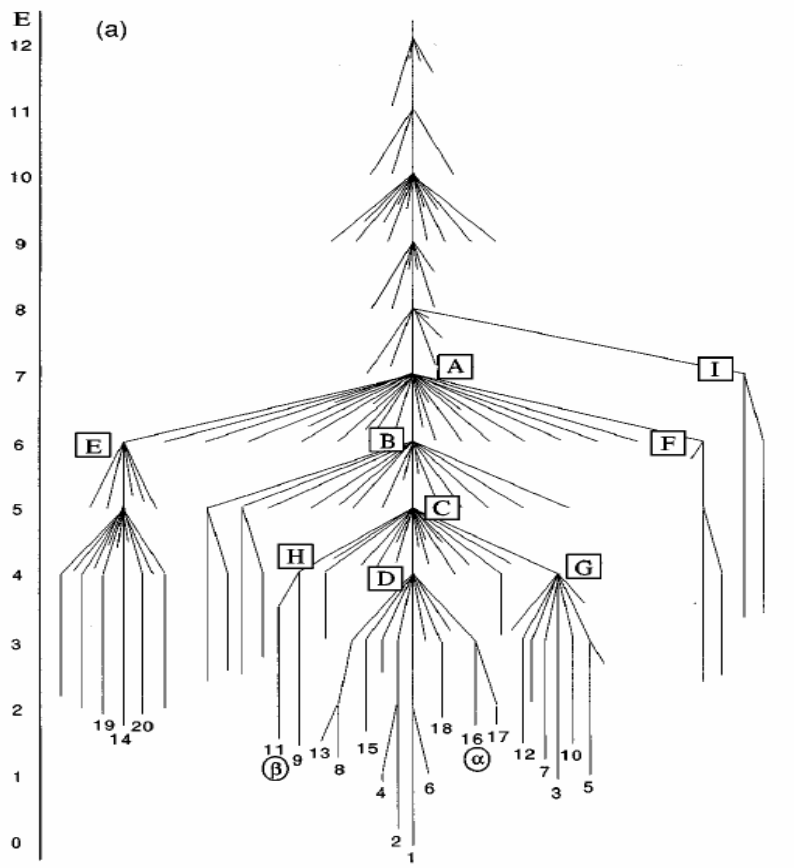

Conformational analysis of a tetrapeptide (isobuturyl-Ala_3-NH-CH_3)

Czerminski & Elber, PNAS 86 (1989) 6963.
Becker & Karplus, J. Chem. Phys. 106 (1997) 1495

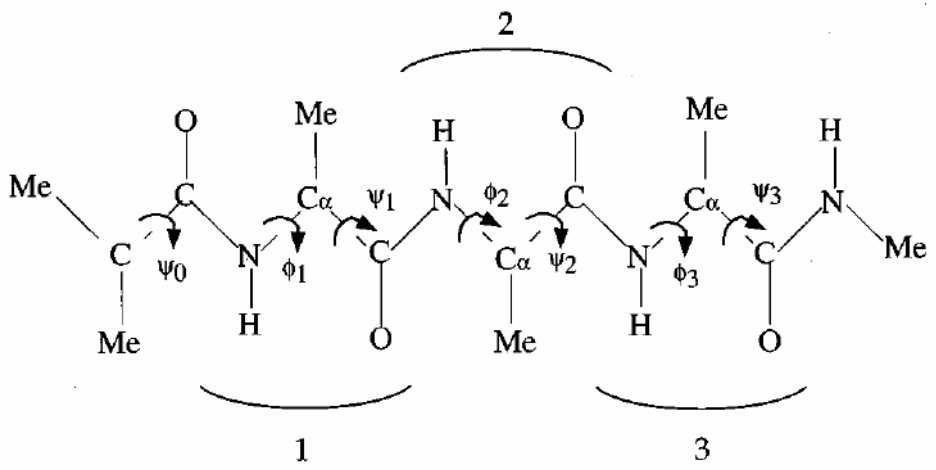

- 72-dimensional conformation space (CH_3 'extended atom')
- 139 PE minima
- 393 barriers separating minima

Computational Approaches II

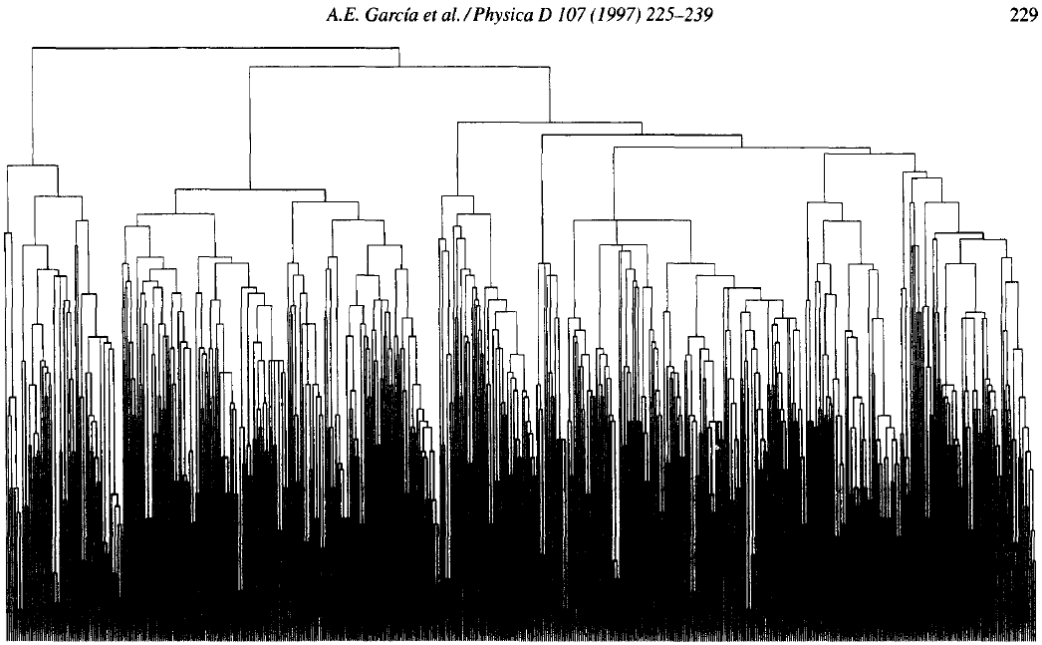

Hierarchical tree of conformations from a 5.1 ns simulation of the small protein crambin.

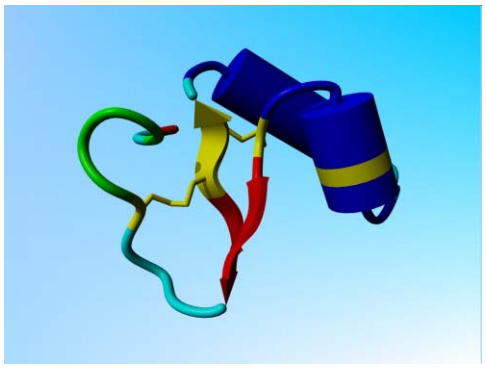

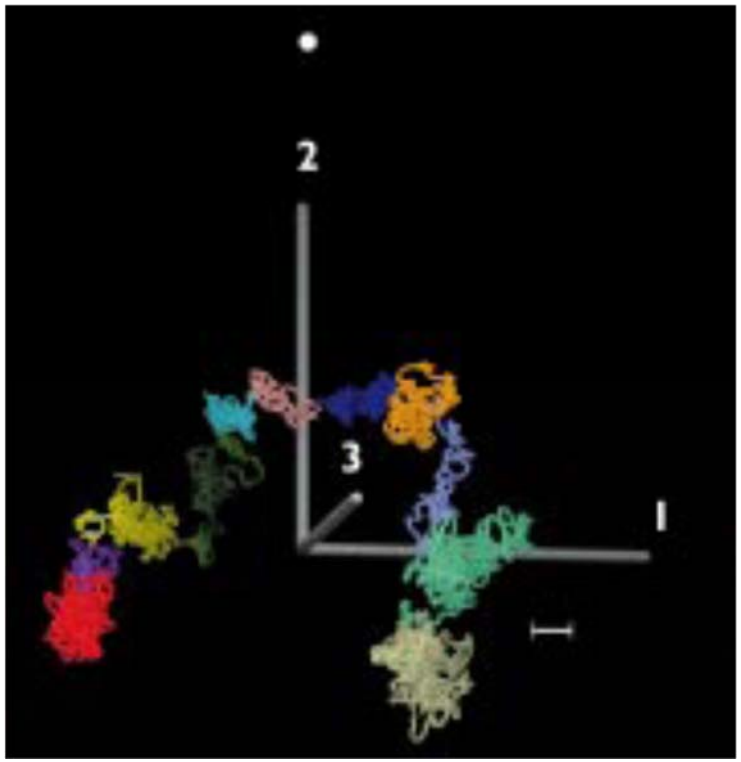

Configuration space projection for 1 ns of Mb dynamics. The readily apparent 'beads on a string' are each colored differently and correspond to global conformational substates of the protein.

Andrews et al., Structure 6 (1998) 587

Hierarchy of Substates in MbCO

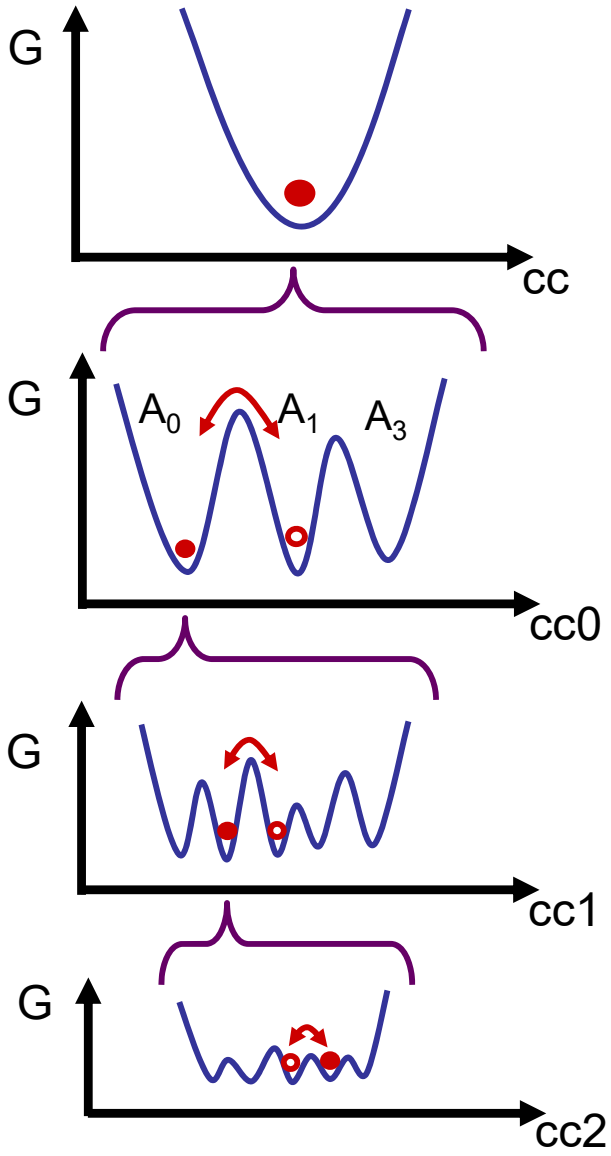

CS0

A substates/
Taxonomic substates
(show different IR, Raman signatures)

CS1

Statistical substates
(nonexponential rebinding)

CS2

(hole burning, calorimetry)

H. Frauenfelder (1922-2022)

Conformational Dynamics

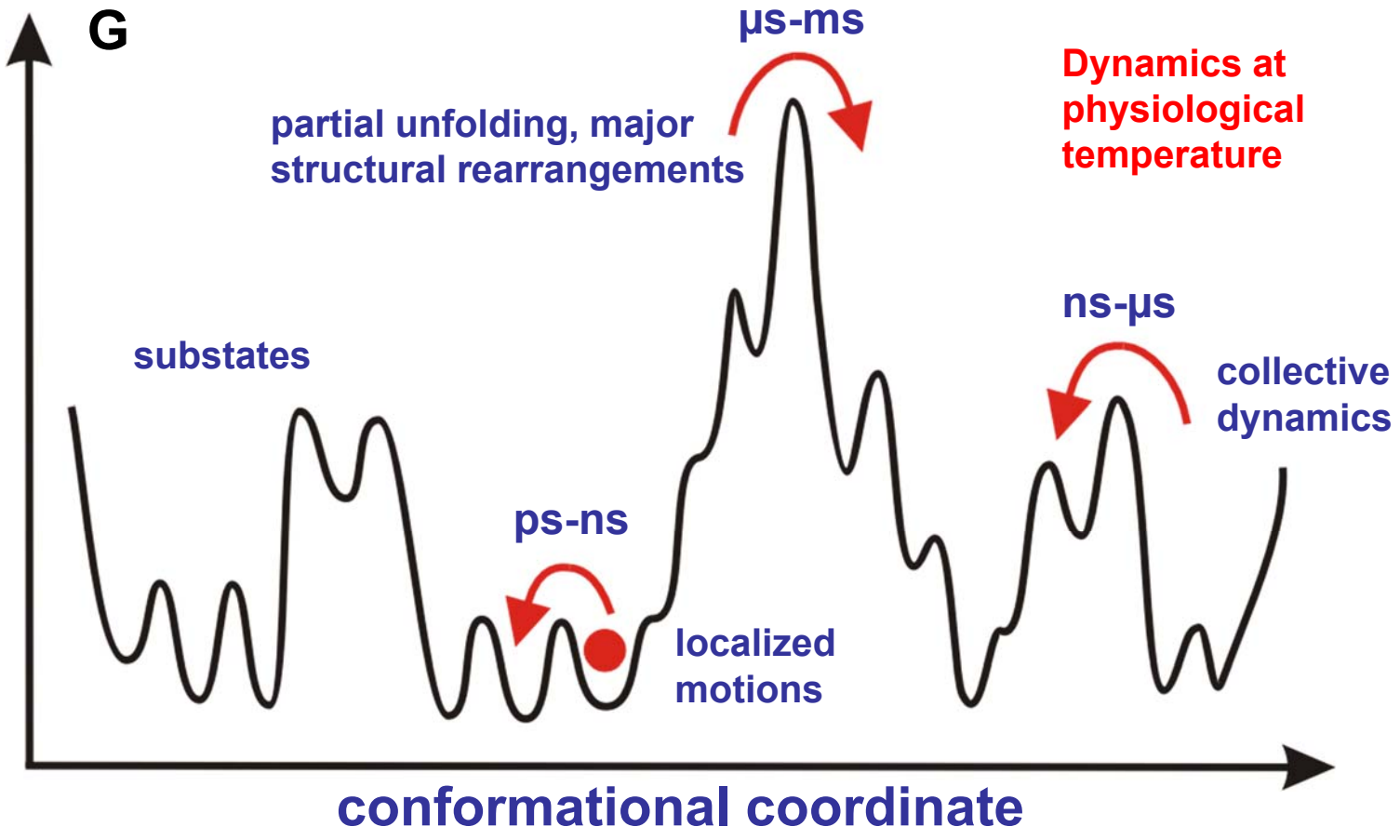

MbCO: Taxonomic Substates I

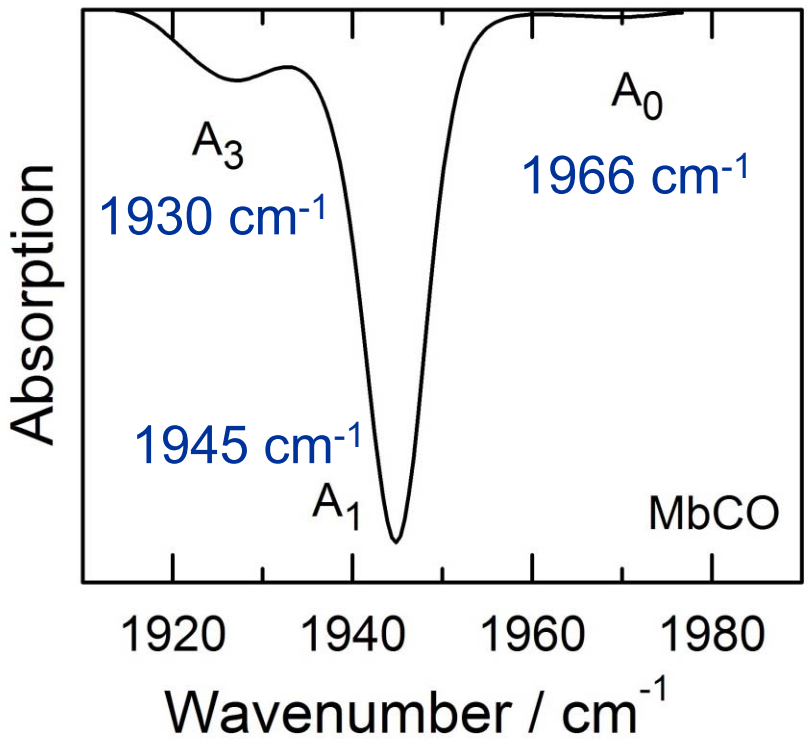

Photolysis difference FTIR spectra

A substates: CO bound to heme iron:

$1920\ cm^{-1} < \nu < 1980\ cm^{-1}$

compare to CO gas: $\nu = 2143\ cm^{-1}$

Line positions reflect protein-ligand interaction.

The relative populations of A substates depend on external parameters (*T*, *p*, pH, hydration).

MbCO: Taxonomic Substates II

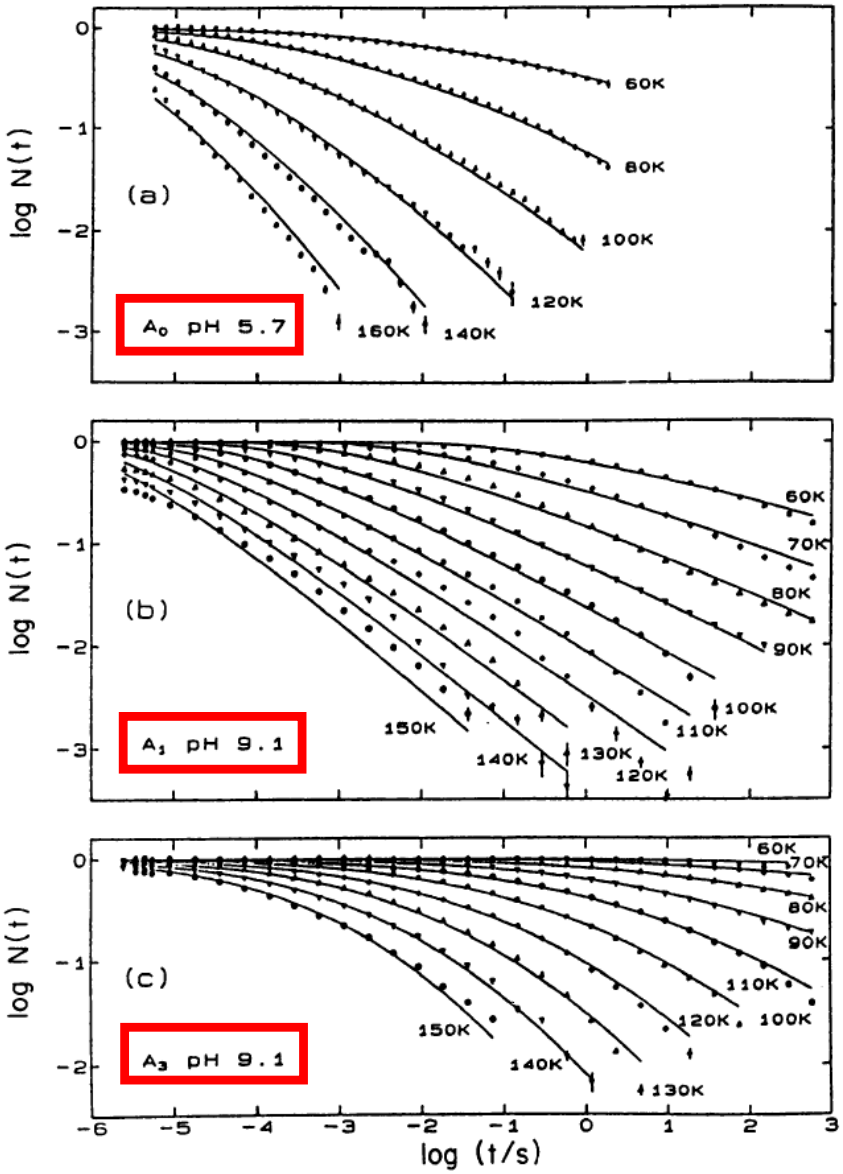

Low temperature kinetics of MbCO measured by flash photolysis with monitoring the absorption changes in the mid-infrared in the A substates (1930, 1945, 1966 cm^{-1}).

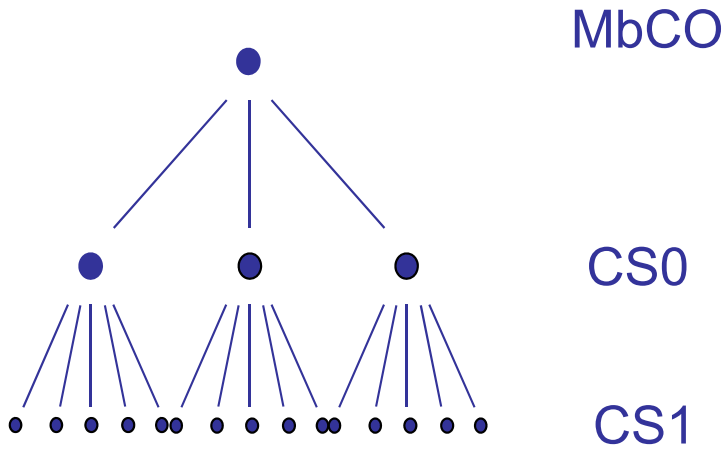

MbCO: Taxonomic Substates III

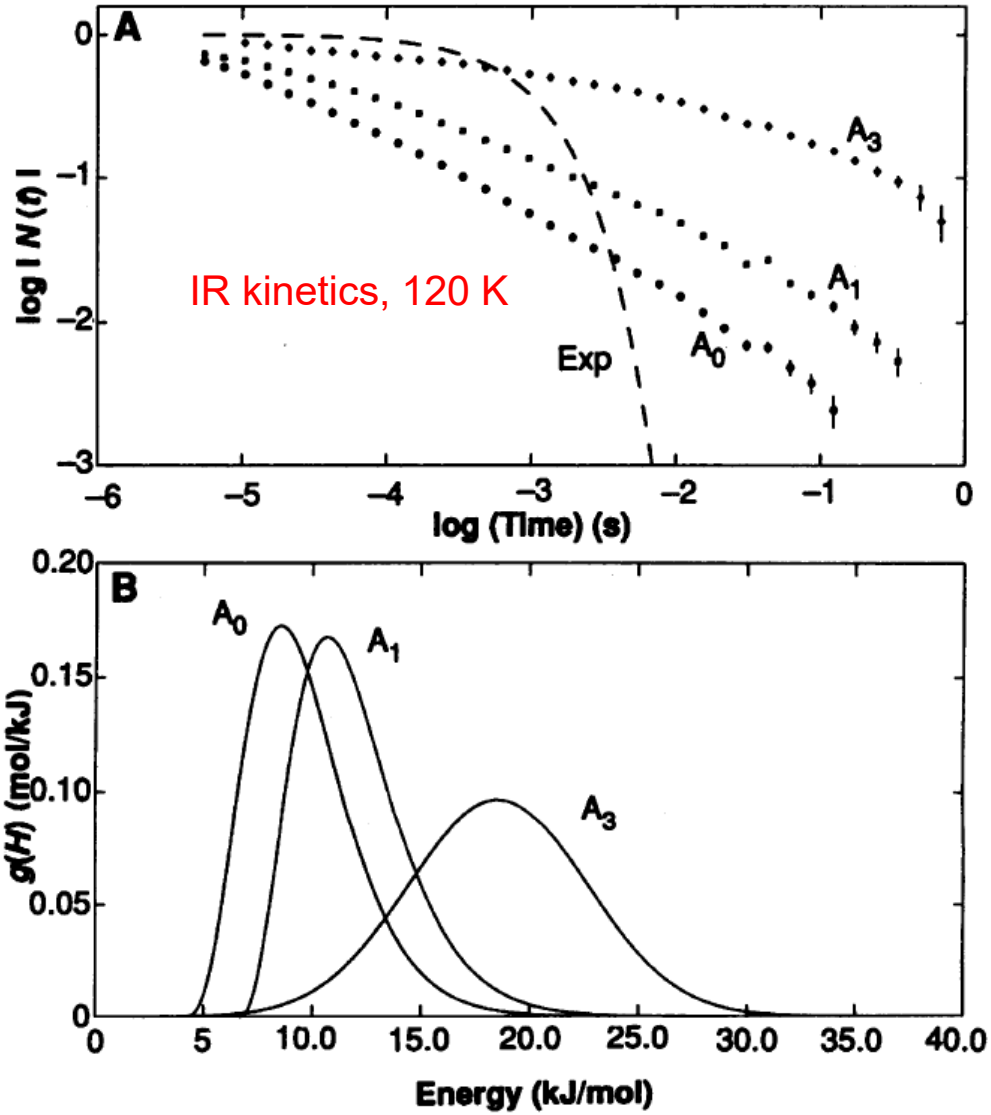

Low temperature barrier distributions

$$N_{A_i}(t) = \int dH\, g_{A_i}(H)\, e^{-k(H)t}$$

with

$$k(H) = A\frac{T}{T_0}\, e^{-H/RT}$$

Different g(*H*) for each A substate!
(also different pre-exponentials!)

Frauenfelder et al., Science 254 (1991) 1598

A States: pH Effect on Function at Room T

- CO association kinetics at room T: (p_{CO} = 1 atm)

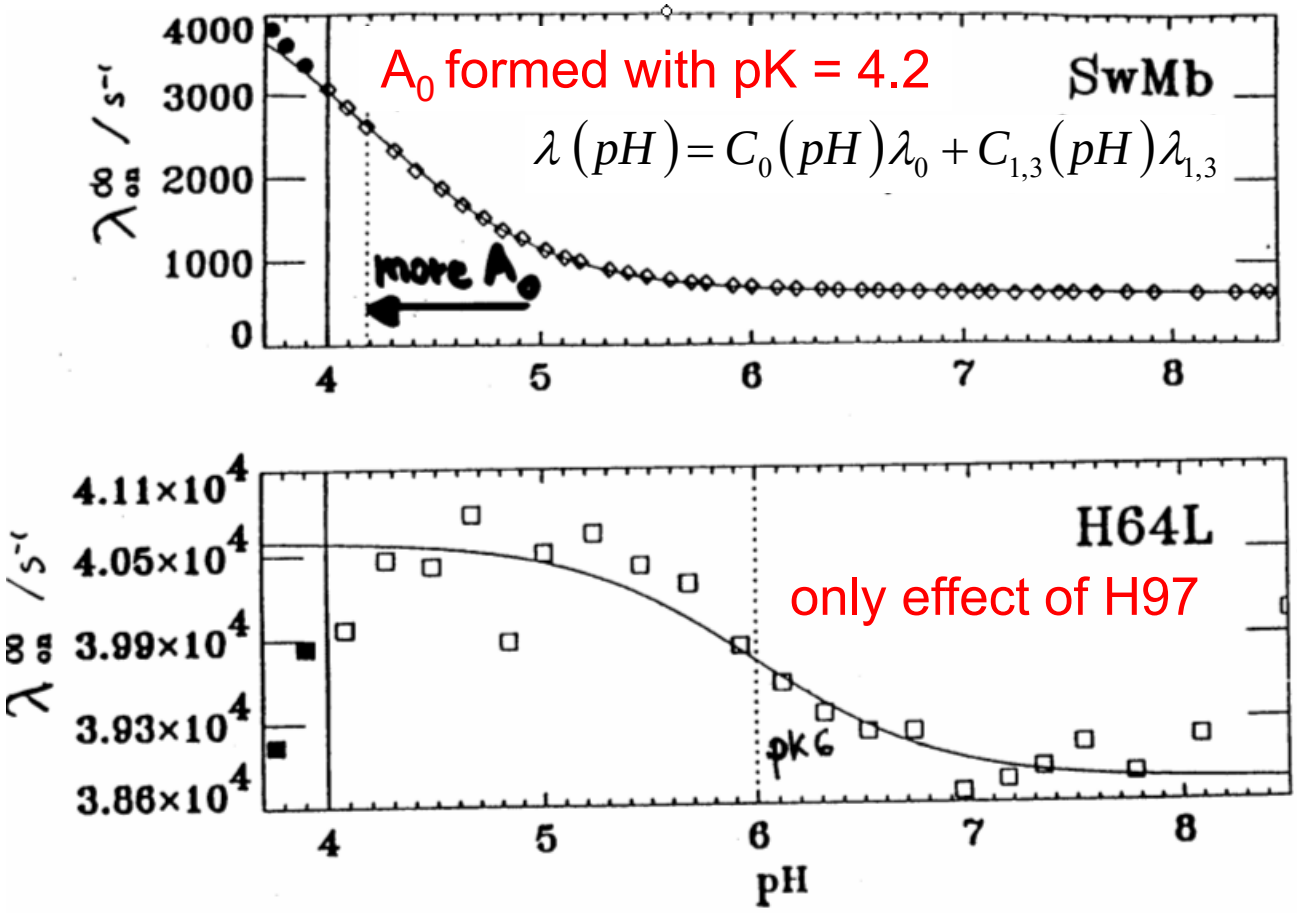

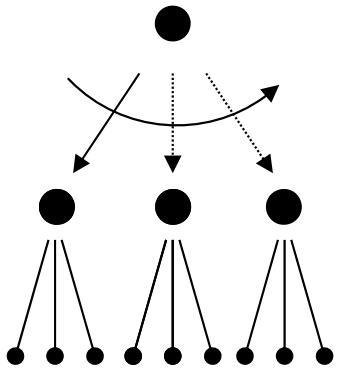

pH Dependence of A Substates II

Protonation: one possible mechanism to generate or influence taxonomic substates

Likely candidates:

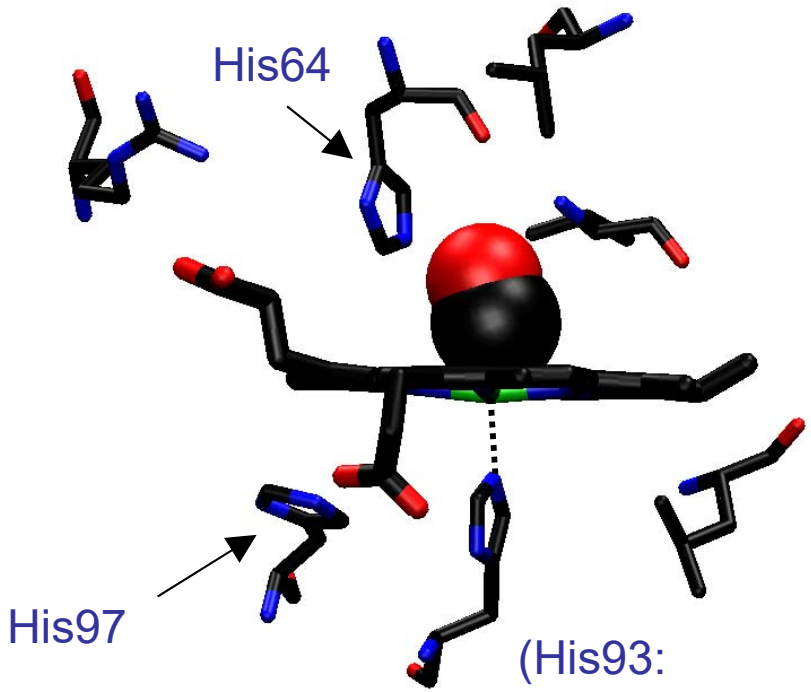

X-ray Structures of $A_{1,3}$ and A_0

MbCO

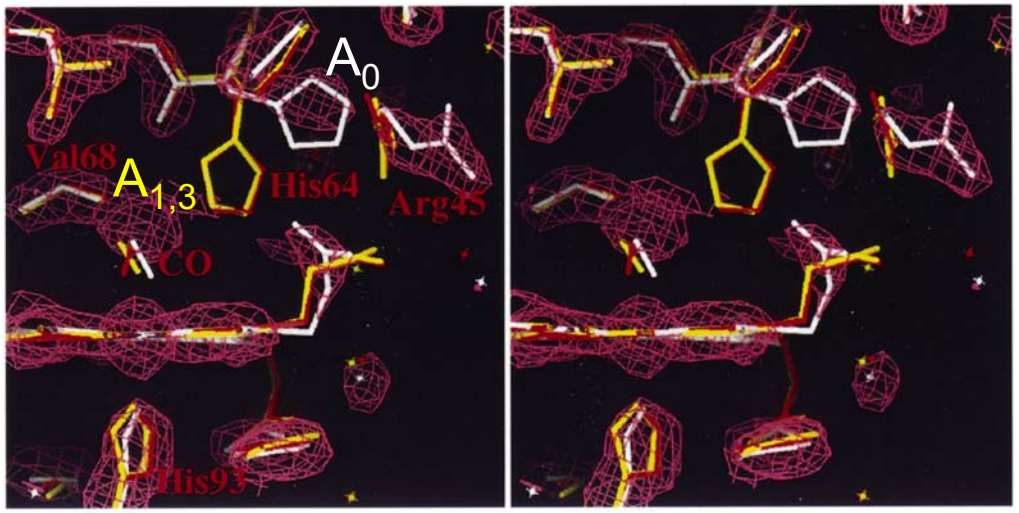

white : pH 4
yellow: pH 5
red : pH 6

deoxyMb

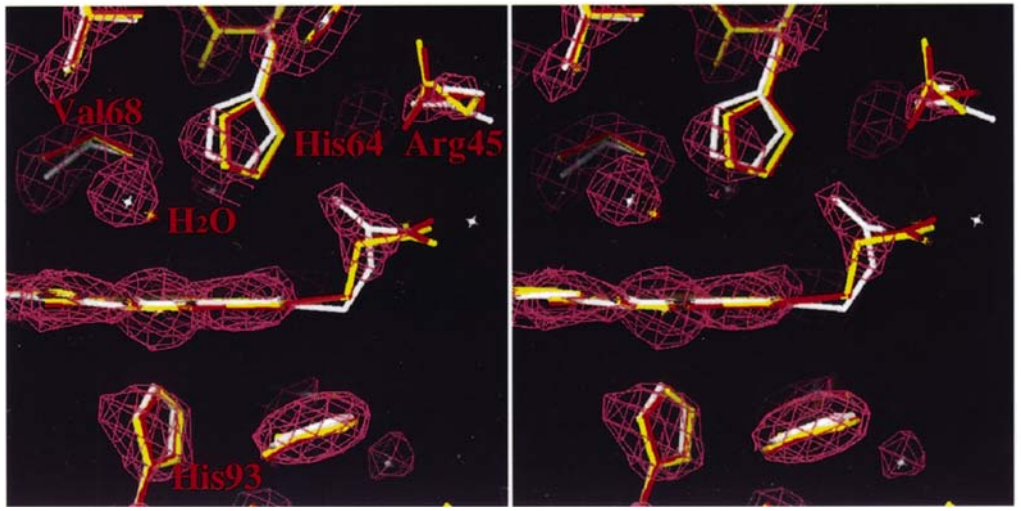

Yang & Phillips,
J. Mol. Biol. 256 (1996) 762

A_1 and A_3

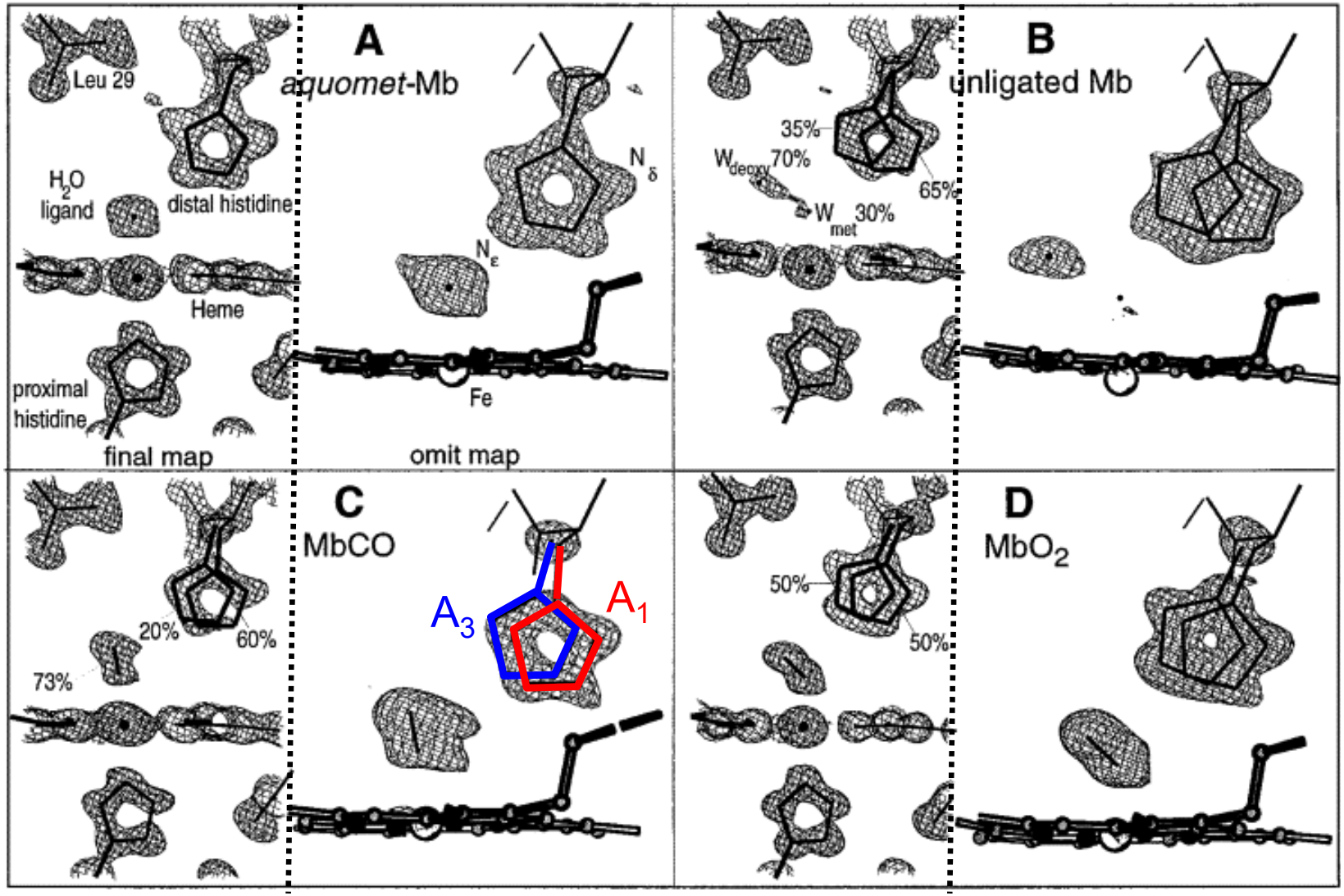

Vojtechovsky et al., Biophys. J. **77** (1999) 2153–2174

Charge Effects on ν_{CO}

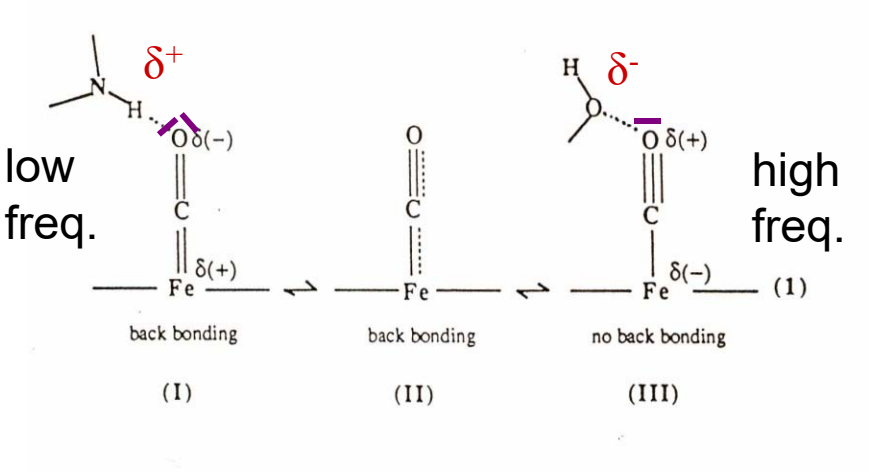

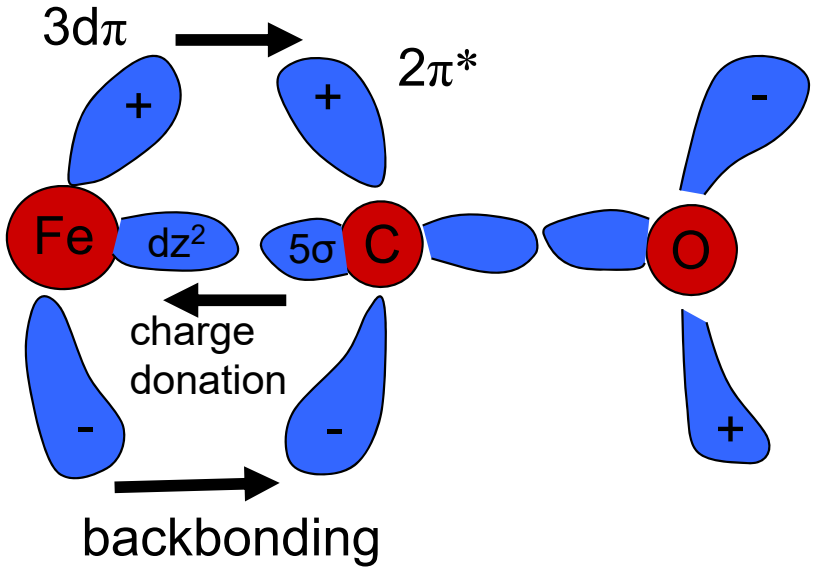

π - backbonding mechanism

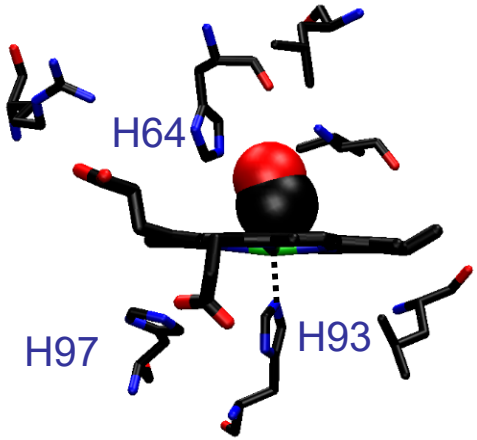

- apolar heme pocket (H64A/V/L/I mutants): ν_{CO} ~ 1970 cm^{-1}
- lower CO frequency: positive charge near ligand oxygen,
  → H64 side chain
- higher CO frequency with protonated H97:
  removal of charge density at Fe atom leads to less backbonding

Biophysics II

Ligand Binding to Heme Proteins under Physiological Conditions

Uli Nienhaus

Prof. G. U. Nienhaus, Vorlesungsunterlagen Biophysik II, SS 2023.
Nur zum KIT-internen, vorlesungsbegleitenden Gebrauch.
Weitergabe und anderweitige Nutzung verboten.

1972: CO Binding at Ambient Temperature

'The results on myoglobin (Mb) present no problem; indeed, they are just what would be expected for a simple one-site molecule that undergoes no conformational change on ligand binding, has no Bohr effect, and, of course, no cooperativity, and whose reaction with CO under all conditions can be described as a simple one-step process:'

$$Mb + CO \underset{\lambda_{off}}{\overset{\lambda'_{on}}{\rightleftharpoons}} MbCO; \quad K = \frac{\lambda'_{on}}{\lambda_{off}} = \frac{1}{[\mathrm{CO}]_{1/2}} = \Lambda_a$$

M. Brunori et. al., Proc.Nat.Acad.Sci. USA 69, 868-871 (1972).

1972: CO Binding at Ambient Temperature

Flash photolysis

$$Mb + CO \underset{\lambda_{off}}{\overset{\lambda'_{on}}{\rightleftharpoons}} MbCO; \quad K = \frac{\lambda'_{on}}{\lambda_{off}} = \frac{1}{[CO]_{1/2}} = \Lambda_a$$

Take [MbCO(t = 0)] = 0; [CO] >> [Mb]

[Mb(t)] = $A \cdot \exp[-\lambda t] + B$

[MbCO(t)] = $A \cdot (1 - \exp[-\lambda t])$

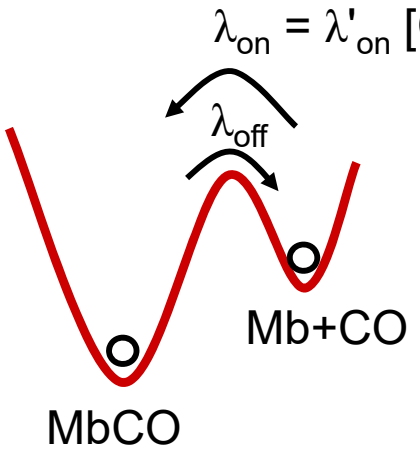

$$\lambda = \lambda'_{on}[CO] + \lambda_{off}$$

$$A = N\frac{\Lambda_a[CO]}{1+\Lambda_a[CO]}$$

$N = A + B$ const.

	λ'_{on} (s^{-1} M^{-1})	λ_{off} (s^{-1})	Λ_a (M^{-1})
CO	5 x 10^5	1.9 x 10^{-2}	2.7 x 10^7
O_2	1.7 x 10^7	15	1.1 x 10^6

ratio 1:25

Temperature-dependent CO Binding

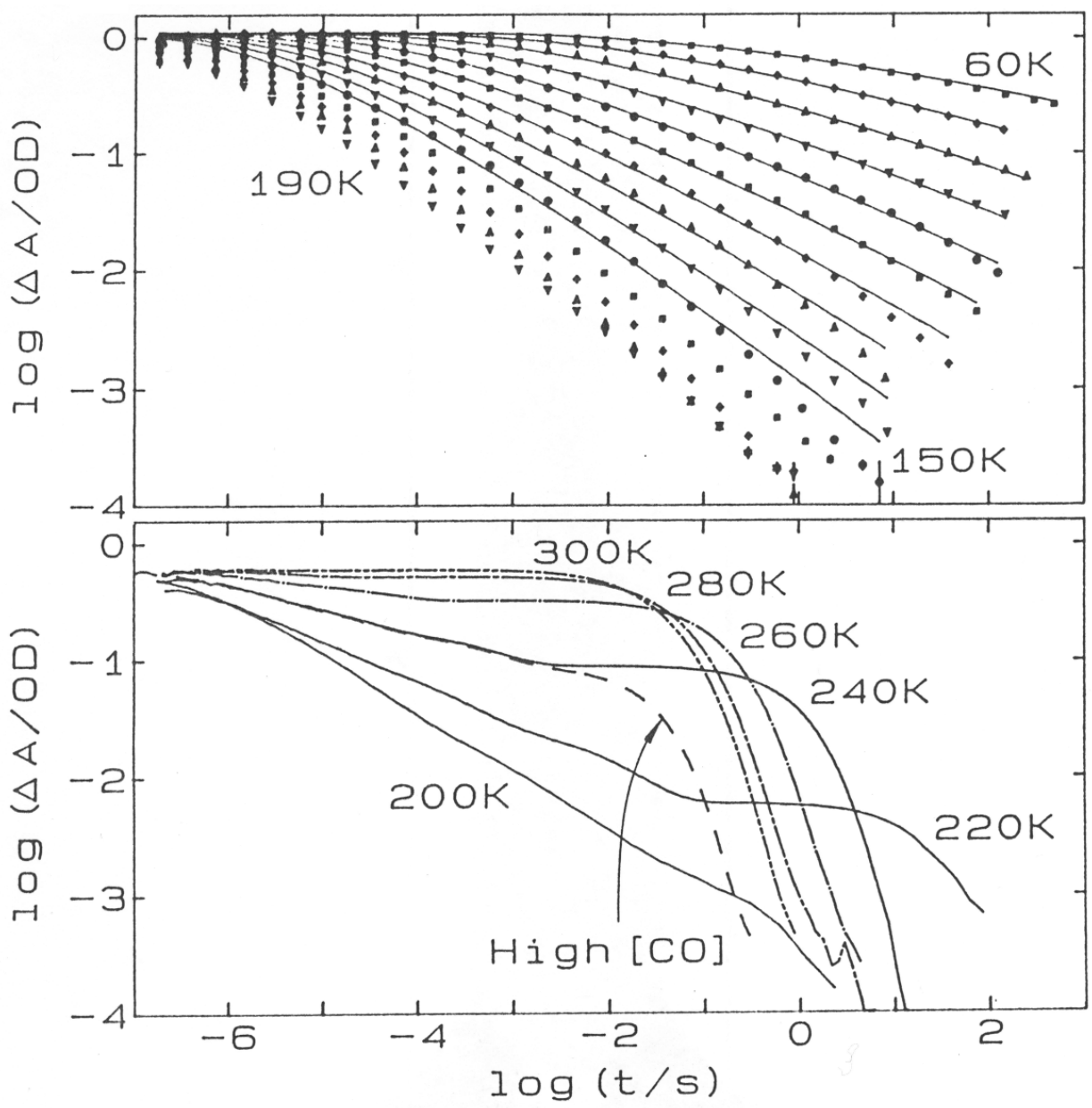

nonexponential rebinding

multiple rebinding steps

T > 210 K:
Protein Fluctuations and Ligand Escape

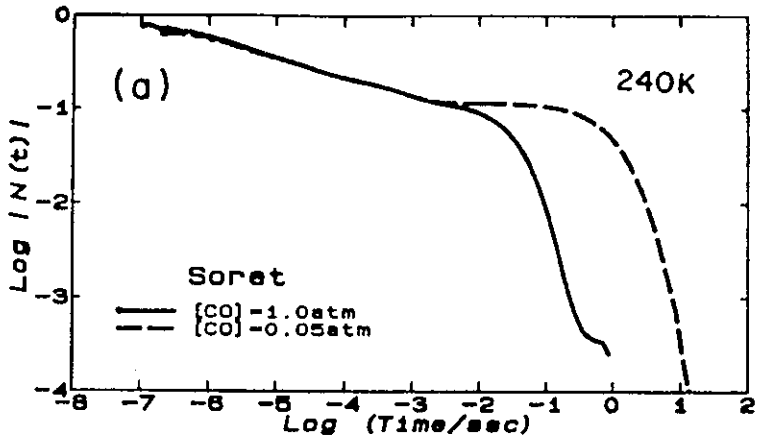

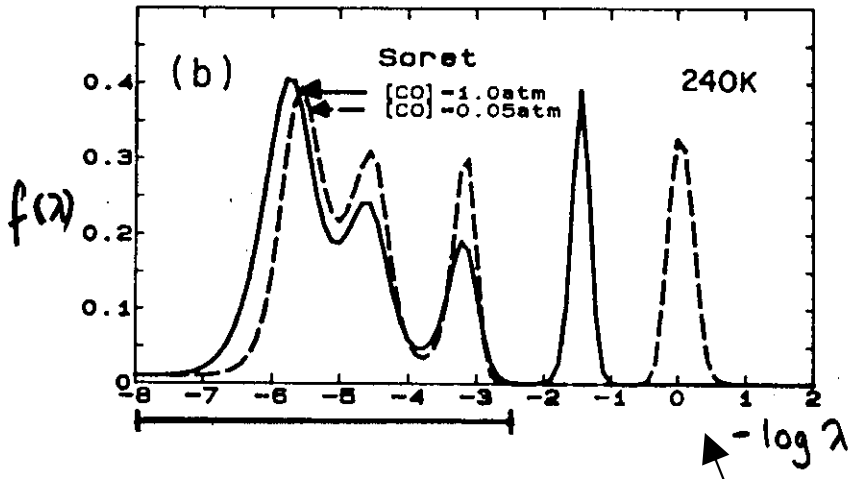

$$N(t) = \int f(\lambda)\, e^{-\lambda t}\, d\left(\log \lambda\right)$$

normalized to N(0) = 1!

internal rebinding

CO binding from solvent (because it changes with [CO])

Reaction Energy Landscape

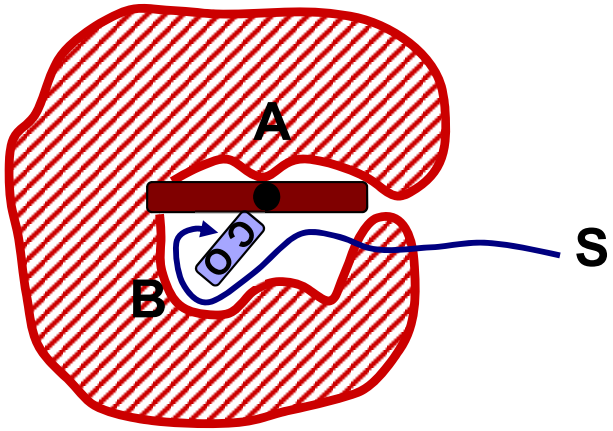

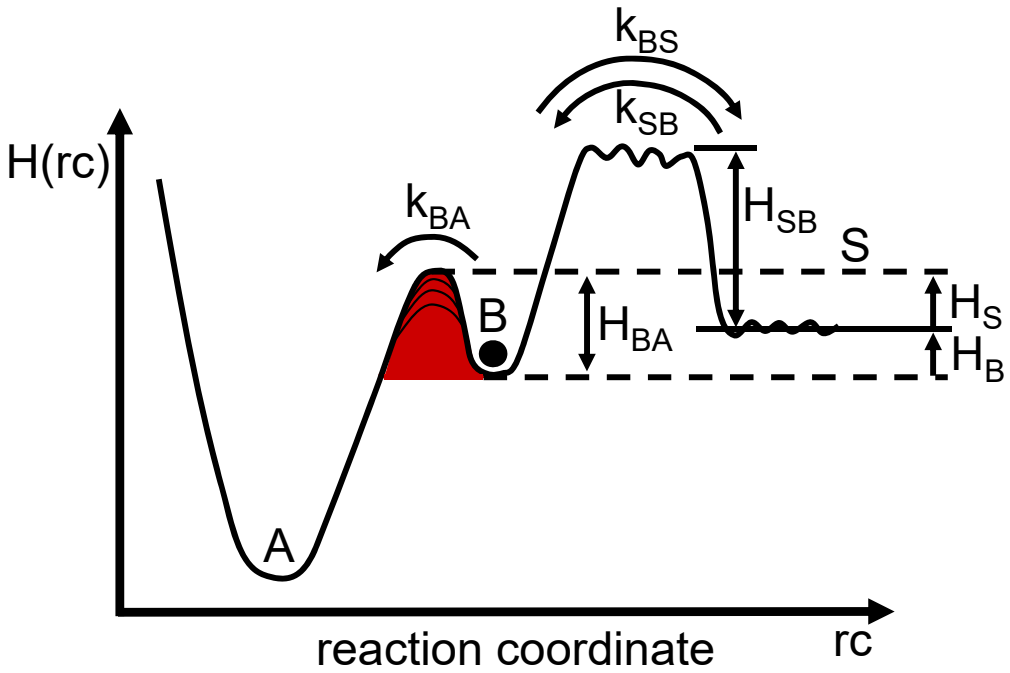

Three-Well Model I

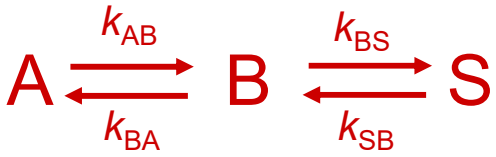

$$\frac{dN_A}{dt} = -k_{AB}N_A + k_{BA}N_B$$

$$\frac{dN_B}{dt} = k_{AB}N_A - (k_{BA} + k_{BS})N_B + k_{SB}N_S$$

$$\frac{dN_S}{dt} = k_{BS}N_B - k_{SB}N_S$$

Normalization: $N_A + N_B + N_S = 1$

Initial condition: $N_B = 1$; $N_A = N_S = 0$ (t = 0, after flash)

Solution straightforward, but clumsy and non-intuitive.

Three-Well Model II

Simplification: $k_{AB} = 0$; $k_{SB} << k_{BA}, k_{BS}$

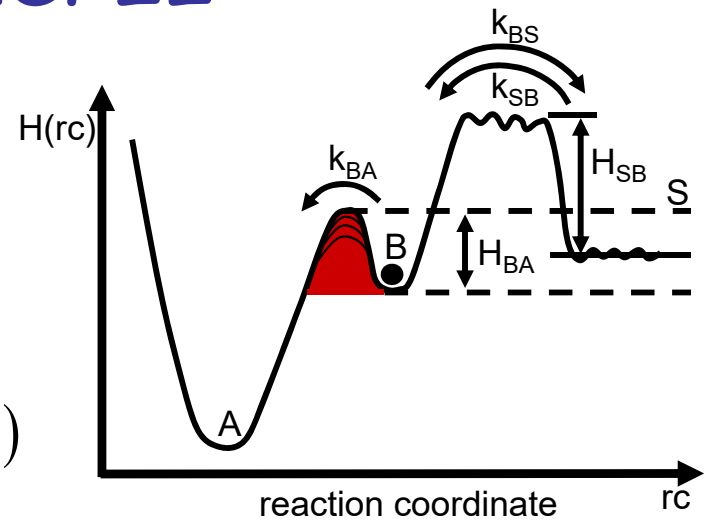

$$\Longrightarrow \quad N(t) = 1 - N_A(t) = N_B(t) + N_S(t)$$
$$= N_I \exp(-\lambda_I t) + N_S \exp(-\lambda_S t)$$

Separation into two distinct processes!

$$N_I = \frac{k_{BA}}{k_{BA} + k_{BS}} \quad ; \quad N_S = \frac{k_{BS}}{k_{BA} + k_{BS}}$$

$$\lambda_I = k_{BA} + k_{BS}$$

$$\lambda_S = k_{BA} \cdot P_B \cdot N_S = k_{BA} \cdot \frac{k_{SB}}{k_{BS}} \cdot \frac{k_{BS}}{k_{BA} + k_{BS}} = k_{SB} \cdot N_I$$

pocket occupation factor

A 'Model' for the 3-Well Model I

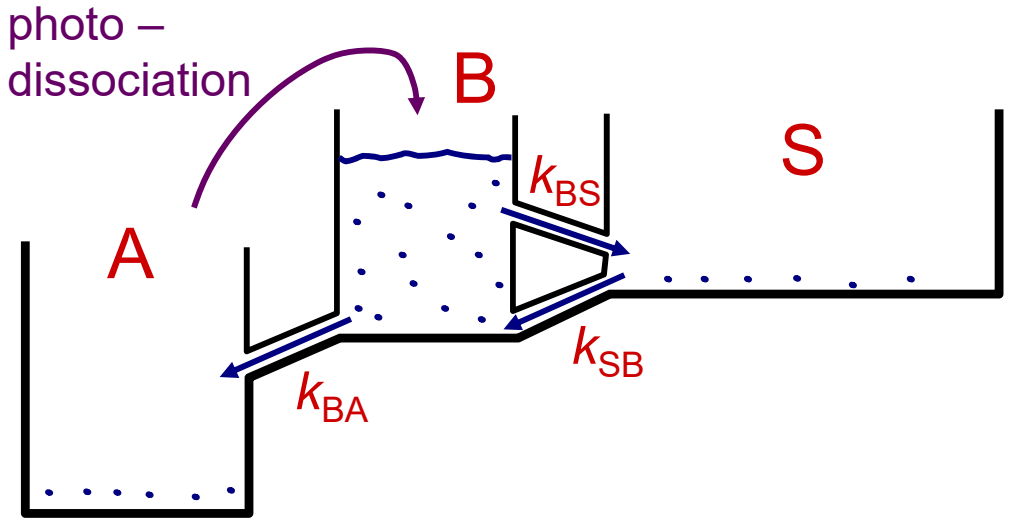

- The fraction that returns from B directly is given by $k_{BA} / (k_{BA} + k_{BS}) = N_I$.
- Depletion of B occurs with $k_{BA} + k_{BS} = \lambda_I$.
- The fraction that returns from S is given by $k_{BS} / (k_{BA} + k_{BS}) = N_S$.
- Depletion of S is given by $k_{SB} \cdot N_I = \lambda_S$:

  = Probability of returning to B (= k_{SB}) times probability to go to A.

A Model for the 3-Well Model II

Which step governs ligand association?

- Two limiting cases:

$$(i) \quad N_S \approx 1 \quad \rightarrow \quad k_{BA} << k_{BS} \quad \rightarrow \quad \lambda_S = k_{SB} \cdot \frac{k_{BA}}{k_{BA} + k_{BS}} \approx k_{BA} \frac{k_{SB}}{k_{BS}}$$

$$(ii) \quad N_S << 1 \quad \rightarrow \quad k_{BA} >> k_{BS} \qquad \lambda_S = k_{SB} \cdot \frac{k_{BA}}{k_{BA} + k_{BS}} \approx k_{SB}$$

MbCO at 300 K: case (i)
MbO_2 at 300 K: $N_S \approx 75\%$ → toward case (ii)

Low T (<240 K): $N_S << 1$ → case (ii)

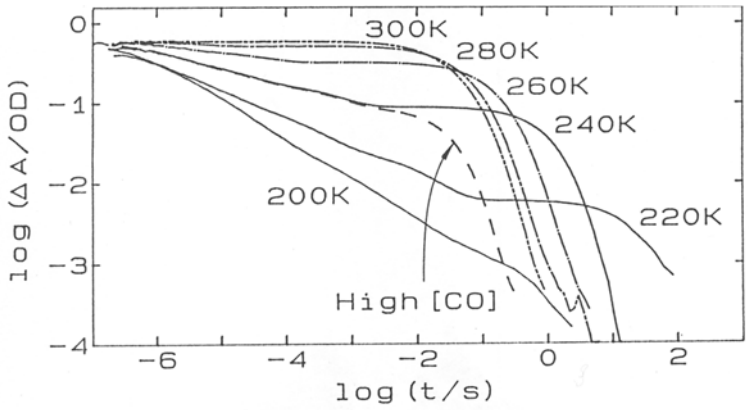

3-Well Model: Further Complications

- inner barrier distributed
- multiple interior CO binding sites
- entry/exit: fluctuating gate,
  not static barrier!
- A substates, pH
- dependence on ligand type (O_2, CO, NO, …)

Occupancy of Interior Binding Sites

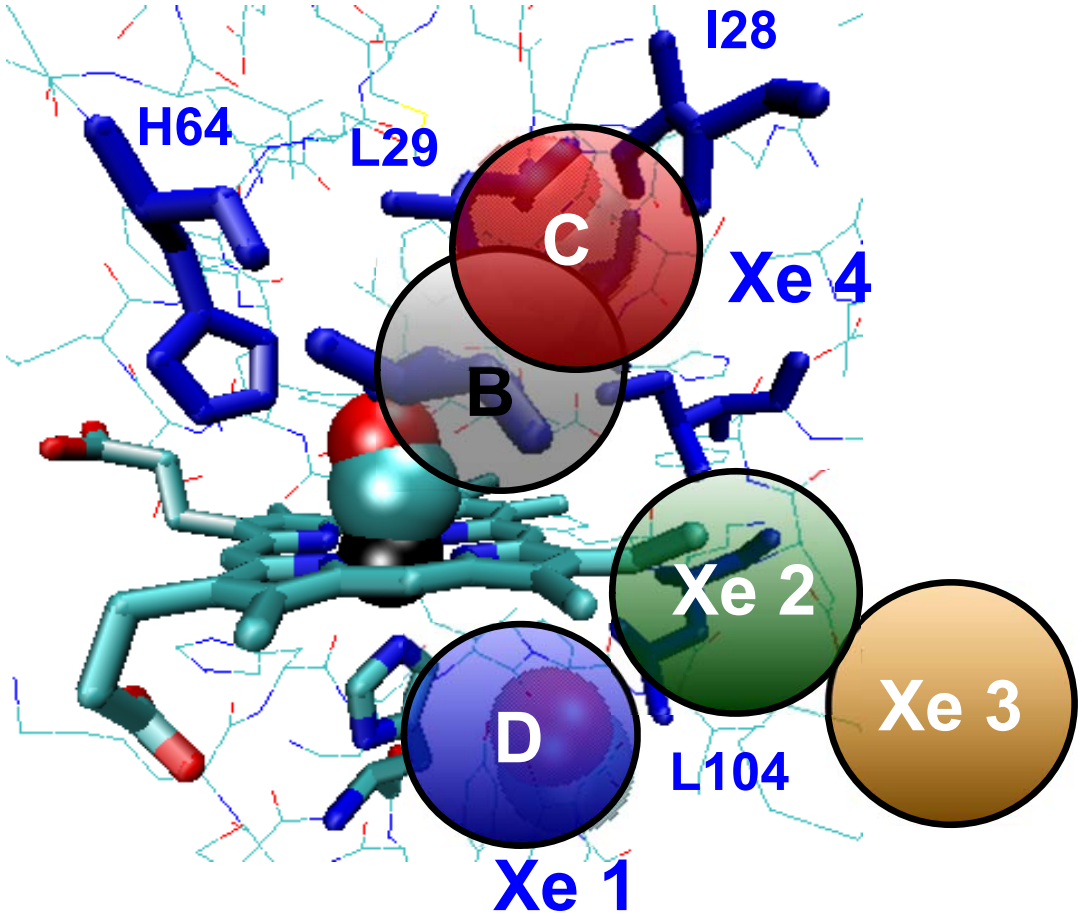

Internal cavities give rise to:

- more efficient ligand escape from Mb
- less efficient ligand rebinding from site B

Experimental Approach:

Physical Method:

Addition of xenon gas

Xenon and photolyzed ligand will compete for free volumes.

Chemical Method:

Protein engineering

Point mutations are introduced to specifically block cavities and / or migration pathways.

Entry and Exit of Ligands I

- MD calculations using x-ray structure
- Entry/exit are concerted motions of protein-ligand system, extreme cases: diabatic / adiabatic.

Diabatic calculation (Case & Karplus, 1979)

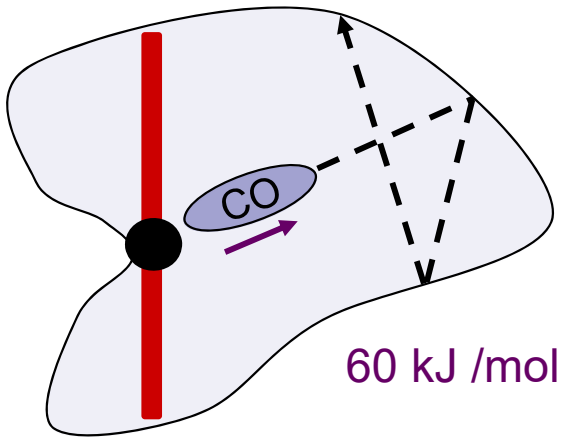

- CO bounces around elastically and explores potential
- Test particle taken smaller than CO molecule
- Exit barrier:

Calculation	400 kJ/mol (~2 pathways)
Experiment	~ 12 kJ/mol

Entry and Exit of Ligands II

Side chain rotation in the model

- take most probable pathway
- side chain rotations of HisE7 / Thr E10 / Val E11

  increase protein energy by 30 kJ/mol, but produce exit barrier of 20 kJ/mol

Adiabatic calculation

- minimize energy of molecule with given CO position. Move CO, minimize energy, repeat steps ……

  → multiple exit pathways??? --- NO!!!

Computational Analysis of Exit Channel

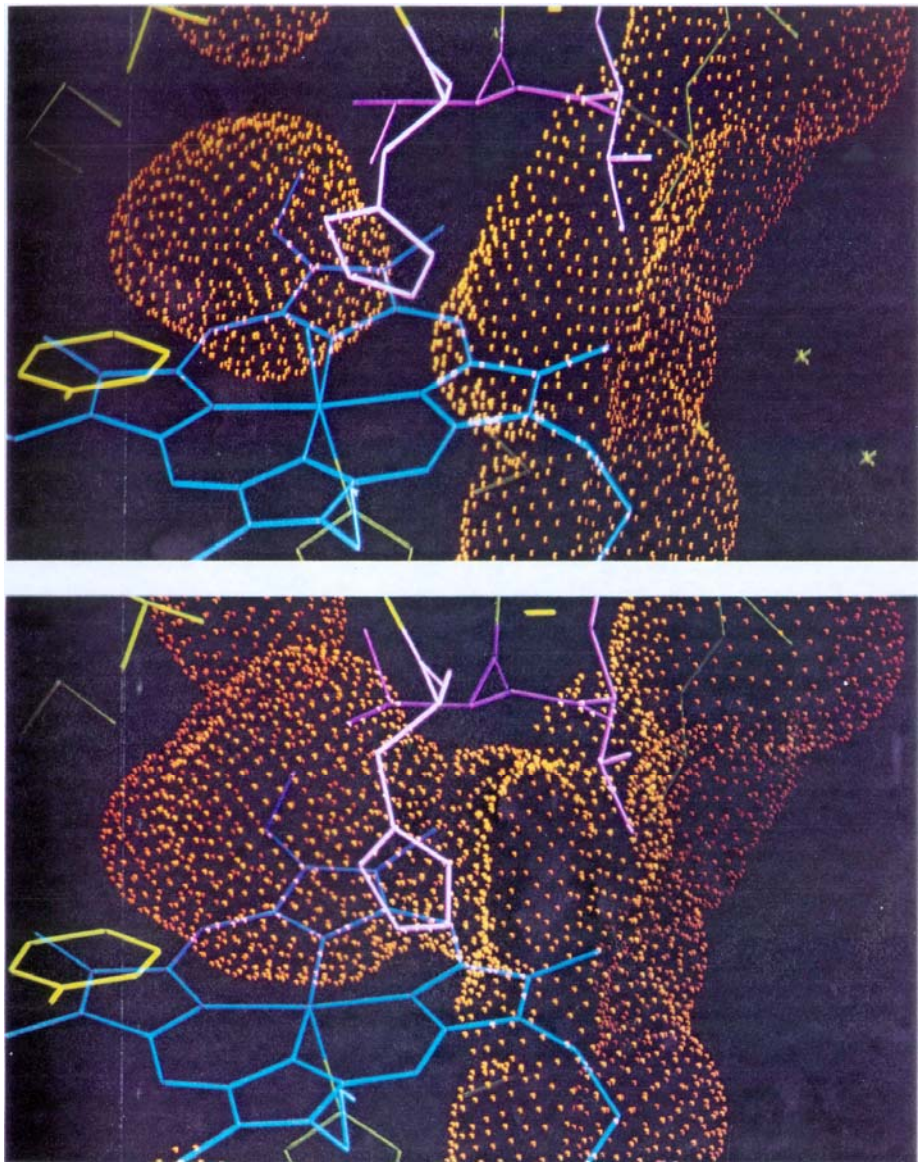

CHANNEL OF ESCAPE for an oxygen molecule bound to the heme group of a myoglobin molecule is opened by the rotations of three amino acid side chains.

The top image shows the static structure of myoglobin determined by X-ray crystallography. There is no path from the surface of the molecule (orange dots) to a pocket inside the molecule just above the heme group (blue). The pocket is near the site where the heme group's iron atom binds an oxygen molecule.

In the bottom image the side chains of three amino acids (purple) have been rotated. As a result an escape channel opens. The positions of the other backbone and side-chain atoms (green) are unchanged in this simulation. If the structure of the myoglobin molecule were rigid, so that the rotations of side chains were impossible, an oxygen molecule might take billions of years to enter or leave the binding site. Detailed simulations suggest that an oxygen molecule encounters a succession of barriers, so that it moves in a "random walk" much like that of a small molecule in a liquid.

'Molecular Doorstops' - Experimental Approaches I

- Phenyl hydrazine ( - NH – NH_2) reacts with myoglobin and leaves the bulky phenyl group as ligand (Ringe et al., Biochem. 23 (1984) 2)
- similar approach: use of isocyanide ligands: C = N – R (Johnson et al., JMB 207 (1989) 459)

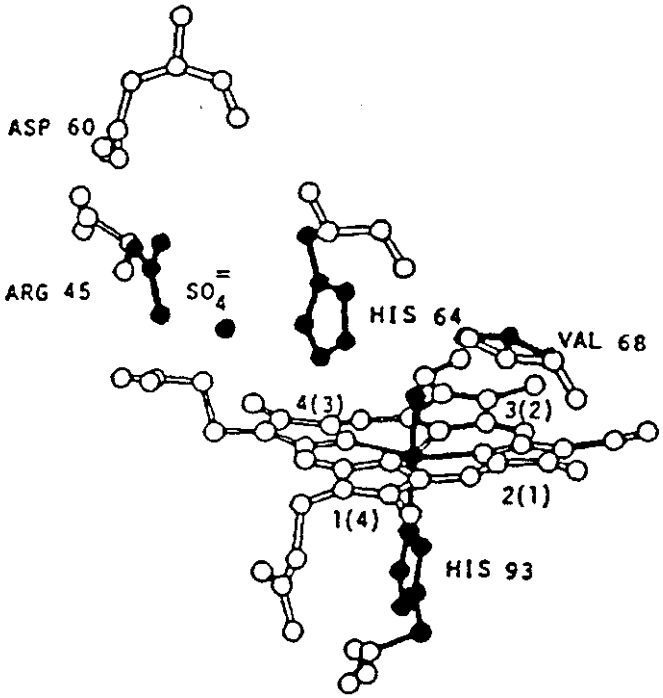

Drawing of the residues around the heme in metmyoglobin that are involved in the formation of a channel when phenylhydrazine is added. The iron atom, bound water molecule, sulfate ion and amino acid side chains undergoing changes are indicated in black.

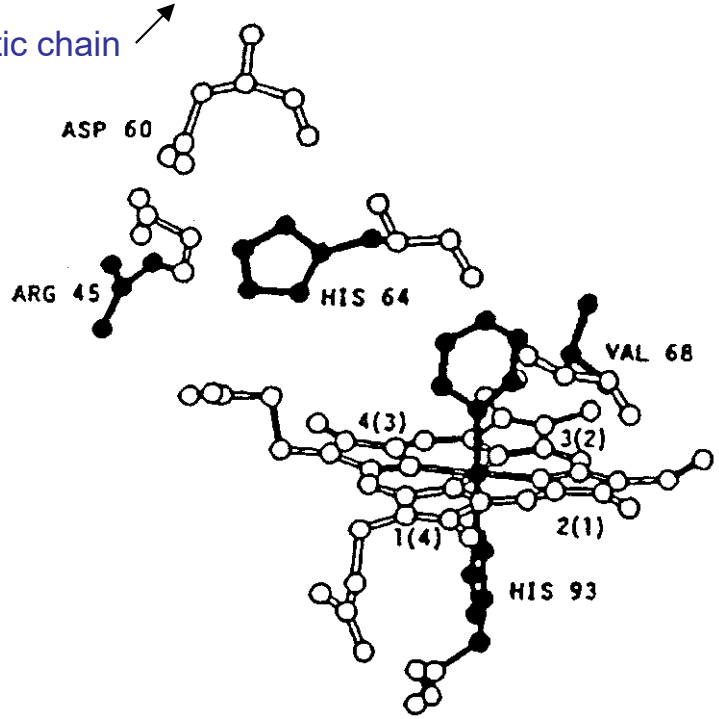

Drawing of the residues around the heme in myoglobin with phenyl bound to the iron atom. Asp-60(E3) and Arg-45(CD3) are close enough to catch one other to form an ion pair. The iron atom, phenyl group and amino acid side chains, which have moved as a consequence of the phenyl group, are indicated black.

'Molecular Doorstops' - Experimental Approaches II

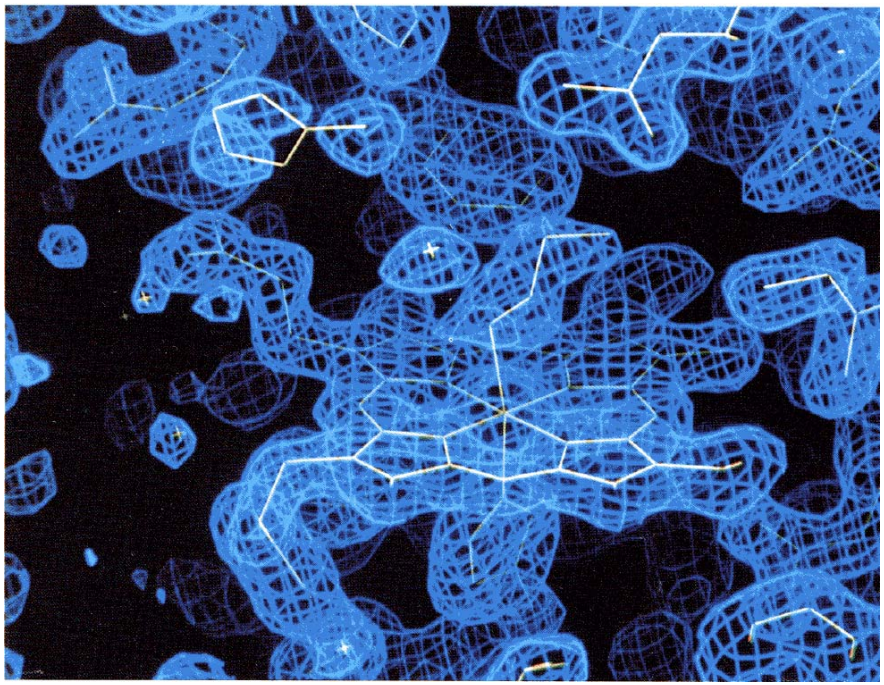

Ethyl-isocyanide
CO
O_2

Opening of the histidine gate

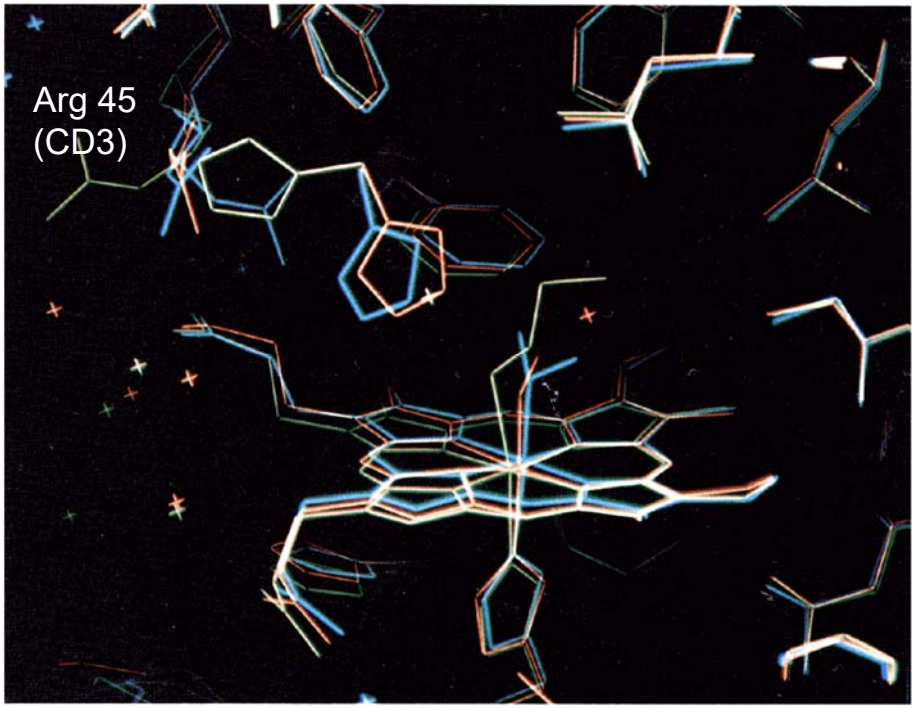

Johnson et al., JMB 207 (1989) 459

Biophysics II

Brief Sketch of Reaction Theory

Uli Nienhaus

Prof. G. U. Nienhaus, Vorlesungsunterlagen Biophysik II, SS 2023.
Nur zum KIT-internen, vorlesungsbegleitenden Gebrauch.
Weitergabe und anderweitige Nutzung verboten.

Reaction Theory

- example: geminate (!) rebinding after photodissociation

$$Mb^*O_2 \xrightarrow{k_{BA}} MbO_2$$

- reaction velocity:

$$\upsilon_r = \frac{-d[Mb^*]}{dt} = k_{BA}[Mb^*]$$

- question: which physical parameters govern the rate coefficient k_{BA} ?

Collision Theory

Assumptions:

- reaction takes place through collisions of molecules in the gas phase
- only collisions with sufficient energy will lead to reactive events

$$k = A\, e^{-E_a / kT}$$

Arrhenius law

frequency of collisions, $\propto T^{1/2}$

fraction with sufficient kinetic energy

- Arrhenius law frequently observed empirically.
- Arrhenius plot

$$\ln k = \ln A - \frac{E_a}{k}\left(\frac{1}{T}\right)$$

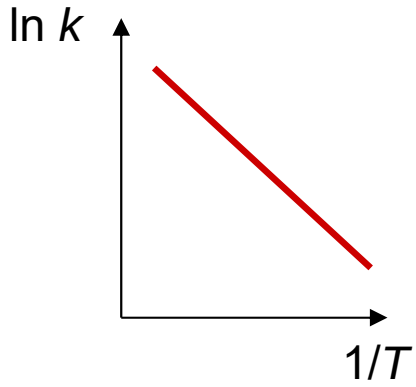

Arrhenius Transitions and Tunneling I

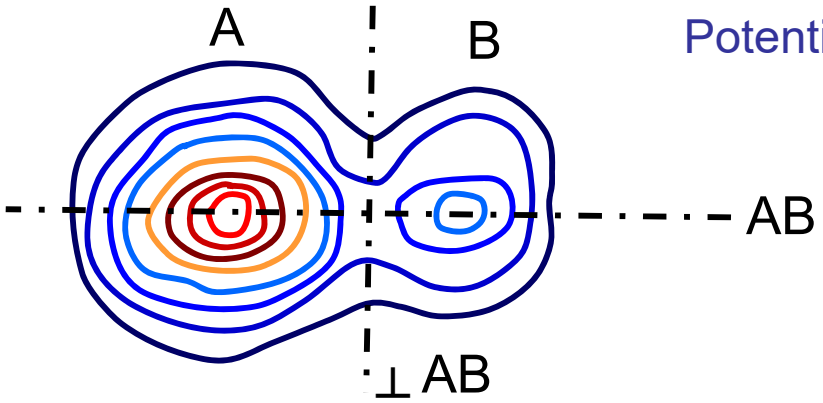

Potential energy map

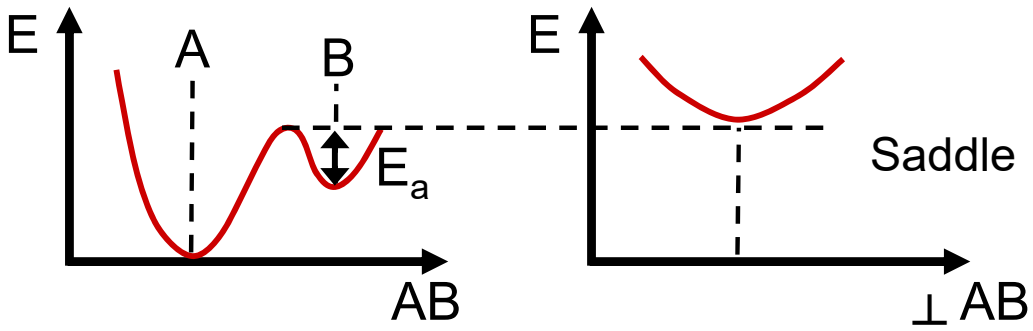

- transitions from one well to the other (reactant → product) correspond to chemical reaction.

modeled as single particle motion!

Arrhenius Transitions and Tunneling II

- quantized energy levels:

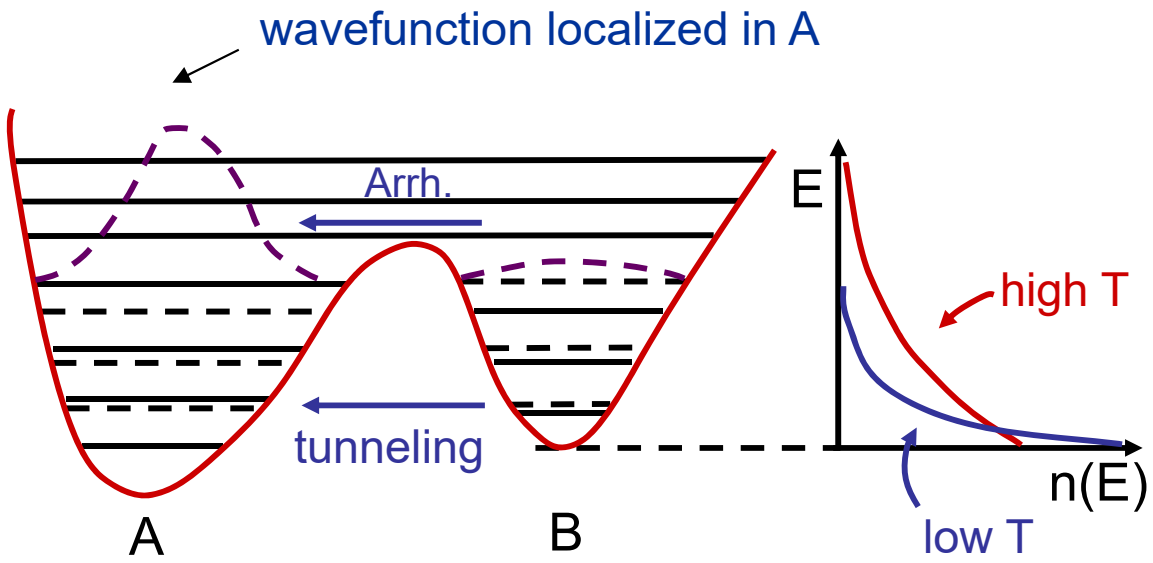

- low T: tunneling dominates
  Note: deexcitation in well A necessary !
- high T: thermal activation dominates

Transition State Theory (TST) I

- activated complex theory, ‘absolute‘ rate theory
- widely accepted in chemistry, although theory has problems with reactions in the condensed phase. Nevertheless, useful starting point.
- two-well model:

$$\frac{\int_{\Delta G_{BA}^{\neq}}^{\infty} e^{-\Delta G/RT}\, d\,\Delta G}{\int_{0}^{\infty} e^{-\Delta G/RT}\, d\,\Delta G} = e^{\frac{-\Delta G_{BA}^{\neq}}{RT}}$$

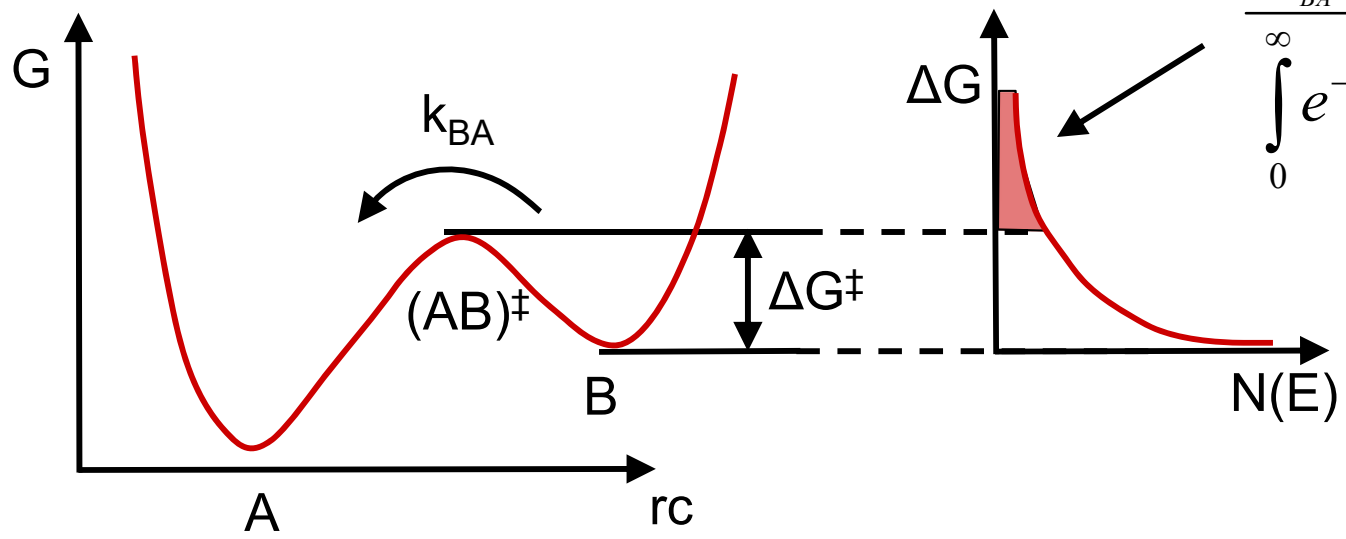

Transition State Theory (TST) II

- theory introduces an activated complex $(AB)^{\ddagger}$ → in equilibrium with B
- activated complex decays with frequency ν of a 'critical vibration'
- rate coefficient k_{BA} is then given by

Partition function of vibration

$$k_{BA} = \nu \cdot Z_{\nu} \exp[-\Delta G^{\neq} / RT]$$

frequency of vibration — equilibrium population of transition state

- critical vibration has a low frequency ⇒ highly excited

$$Z_{\nu} = \sum_{n} e^{-\frac{(n+1/2)h\nu}{kT}} = \frac{e^{-h\nu/2kT}}{1-e^{-h\nu/kT}} = \frac{1}{2\sinh(h\nu/2kT)} \approx \frac{kT}{h\nu}$$

$$\Rightarrow \quad \underline{\underline{k_{BA} = \frac{kT}{h} e^{-\Delta G^{\neq}/RT}}} = \underbrace{\frac{kT}{h} e^{\Delta S^{\neq}/R}}_{\text{preexponential}} \underbrace{e^{-\Delta H^{\neq}/RT}}_{\text{Arrhenius exponential}}$$

Problems with TST Ansatz

Assumptions:

- Thermal equilibrium between reactants and activated complex is maintained.
- Reactive trajectory crosses the barrier only once.
- Classical treatment.
- Well-defined energy surface exists (adiabatic reaction).
- Friction is not properly accounted for.

Kramers Theory

- Proteins are complex dynamic systems, and motions of the protein itself and the solvent shell around it will affect the rate of protein reactions.

- The reaction surface of proteins is multidimensional, and the treatment is such that one (or a few) coordinate(s) is (are) singled out as reaction coordinate(s), which exchange(s) energy and momentum with all the other coordinates. $\Rightarrow$ friction

  Friction $\leftrightarrow$ fluctuating forces

  Dissipation - Energy - Fluctuations

H. Kramers, Brownian motion in a field of force and the diffusion model of chemical reactions, Physica 7 (1940) 284.

Qualitative Picture I

Friction is quantified by velocity autocorrelation time – 'average time of motion with constant velocity':

$$\tau_v = m / \zeta$$

m: effective mass

ζ: friction coefficient

Low friction:
~ballistic motion

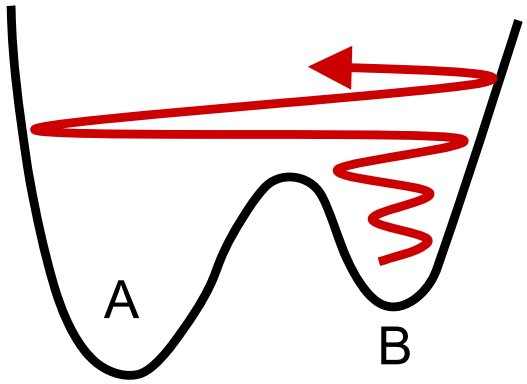

difficulty of deexcitation in well A and excitation in well B

High friction:
Brownian motion, random walk

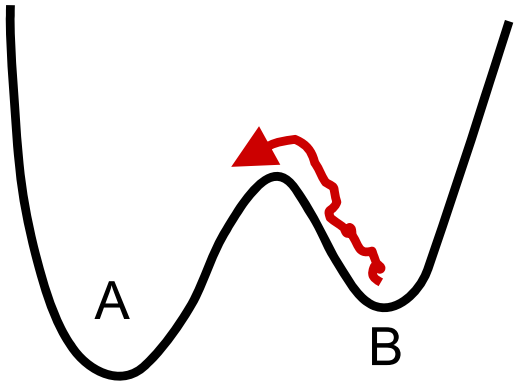

crossing of the barrier many times

Qualitative Picture II

Stokes's law:

$\zeta = 6 \pi \eta a$

η: viscosity

a: characteristic linear distance

Kramers's result:

$k = \kappa k_{TST}$

κ: transmission coefficient

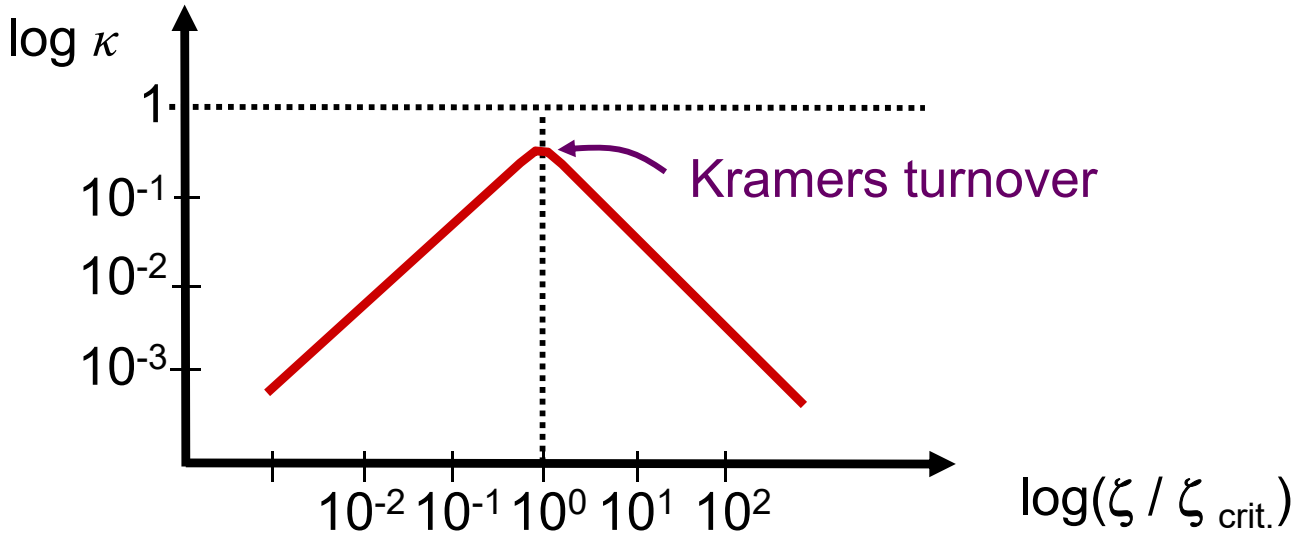

Kramers Equation – Experimental Evidence I

Isomerization energy barriers for ground-state stilbene (lower curve) and excited-state stilbene (upper curve).

One-dimensional potential energy surfaces are schematic. A large barrier separates the *cis* and *trans* isomers only on the ground-state surface.

In this one-dimensional model the reaction coordinate involves twisting about the carbon-carbon double bond. The isomerization of either isomer in the excited state to the other isomer is postulated to occur via the same intermediate, for which the twisting angle Θ is 90°.

Arrows through the structure diagram of each isomer: direction of the dipole moment associated with the transition from the ground state to the first excited state.

The time constants indicated refer to measurements in hexane solution.

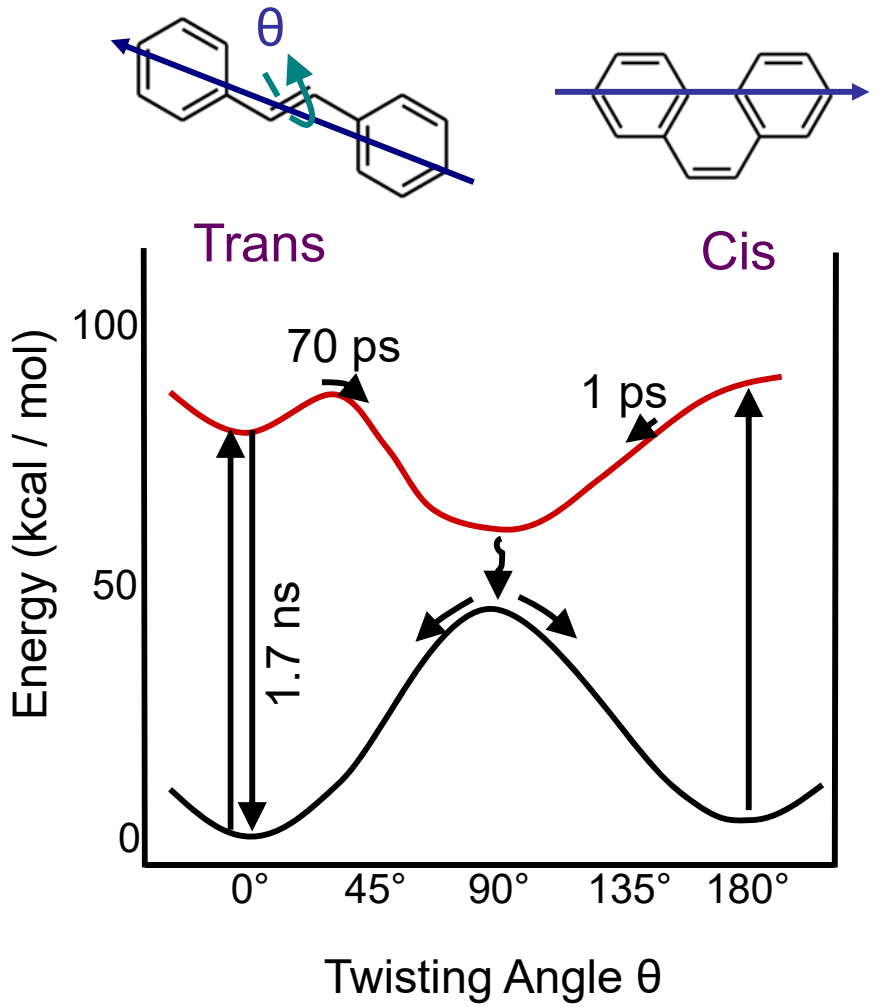

Fleming & Wolynes
Physics Today
(1990) 43: 36-43

Kramers Equation – Experimental Evidence II

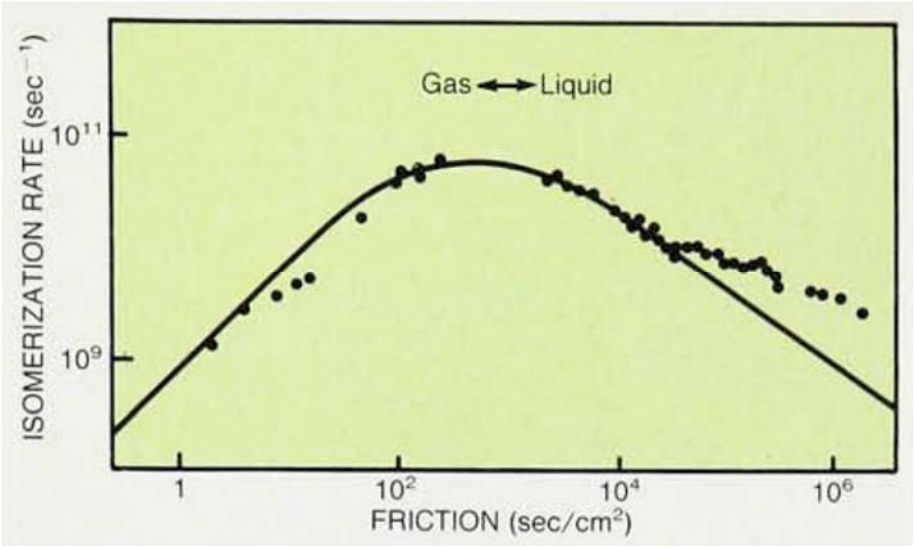

Fleming & Wolynes
Physics Today
(1990) 43: 36-43

Isomerization rate of *trans-stilbene* as a function of friction, showing the Kramers turnover.

Solid line: calculation by Jürgen Troe and coworkers (University of Göttingen).

Deviation at high friction may be due to frequency-dependent friction. At high friction it is also likely that the proportionality between the inverse diffusion coefficient and friction breaks down, even for low-frequency motions.

Collective Rate Processes I

- So far, we have only considered simple barrier crossing events. Proteins, however, are densely packed, and a conformational change may involve multiple, distributed barriers.

  Example:

  rotation of an internal sidechain in a protein:

  - low T: strong hindrance, multiple barriers,
    collective motion, *E*-surface temp. dependent
  - high T: thermal fluctuations of surrounding residues
    allow almost free motion

- Nonexponential dynamics
- Arrhenius relation not applicable

Collective Rate Processes II

- Structural dynamics in glass-forming liquids and (bio)polymers shows properties of collective transitions:

nonexponential dynamics

$$\Phi(t,T) = e^{-(k(T)t)^{\beta}}$$

Rudolf Kohlrausch
Friedrich Kohlrausch

usually, 0.2 << β << 1

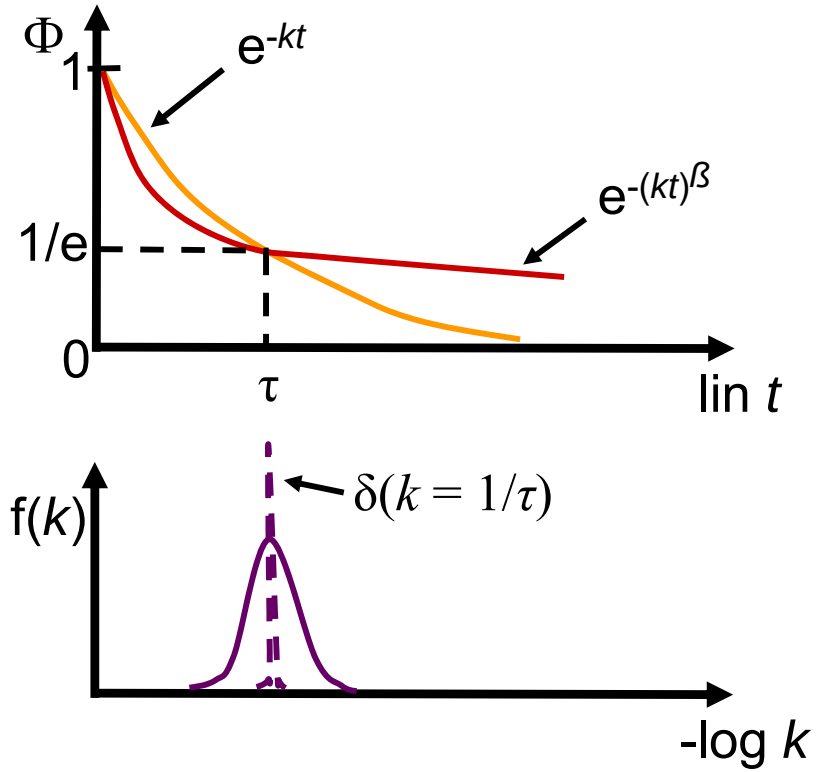

Collective Rate Processes III

Non-Arrhenius Temperature Dependence

$$k = A_A\, e^{-E_A/RT}$$

"α - relaxation"

E_A = 50 kJ/mol; A_A = 10^{18} s^{-1}

curved Arrhenius plot

barriers effectively temp. dependent !

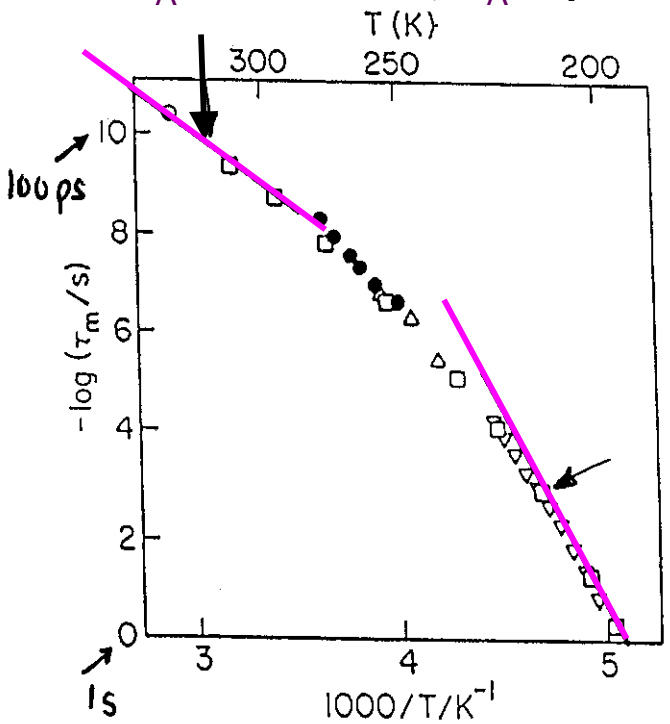

E_A = 140 kJ/mol
A_A = 10^{36} s^{-1}

prefactors unreasonably large

Relaxation/fluctuation times in glycerol obtained with different techniques. Mössbauer effect (●), dielectric susceptibility (□), ultrasonic relaxation (△), specific heat spectroscopy (▽), and Brillouin scattering (○).

Collective Rate Processes IV

Alternative Parameterization

Vogel-Fulcher law

$$k = A_{VF}\, e^{-E_{VF}/R(T-T_0)}$$

$$k = A_F\, e^{-\left(\frac{E_F}{RT}\right)^2}$$

Ferry's law

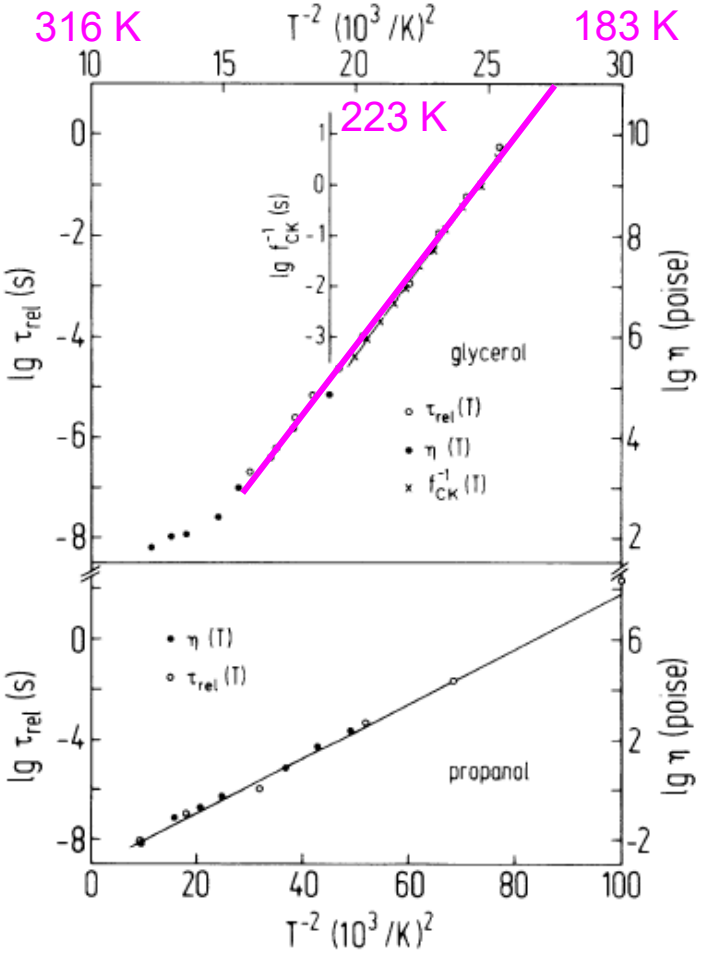

Comparison of the T dependences of η and dielectric relaxation time for propanol and glycerol. f_{ck} is the peak frequency of the imaginary part of the product of specific heat and thermal conductivity.

H. Bässler, PRL 58 (1987) 767

Biophysics II

Quantum Tunneling in Ligand Binding to Heme Proteins

Uli Nienhaus

Prof. G. U. Nienhaus, Vorlesungsunterlagen Biophysik II, SS 2023.
Nur zum KIT-internen, vorlesungsbegleitenden Gebrauch.
Weitergabe und anderweitige Nutzung verboten.

Tunneling in Ligand Binding to Heme Proteins

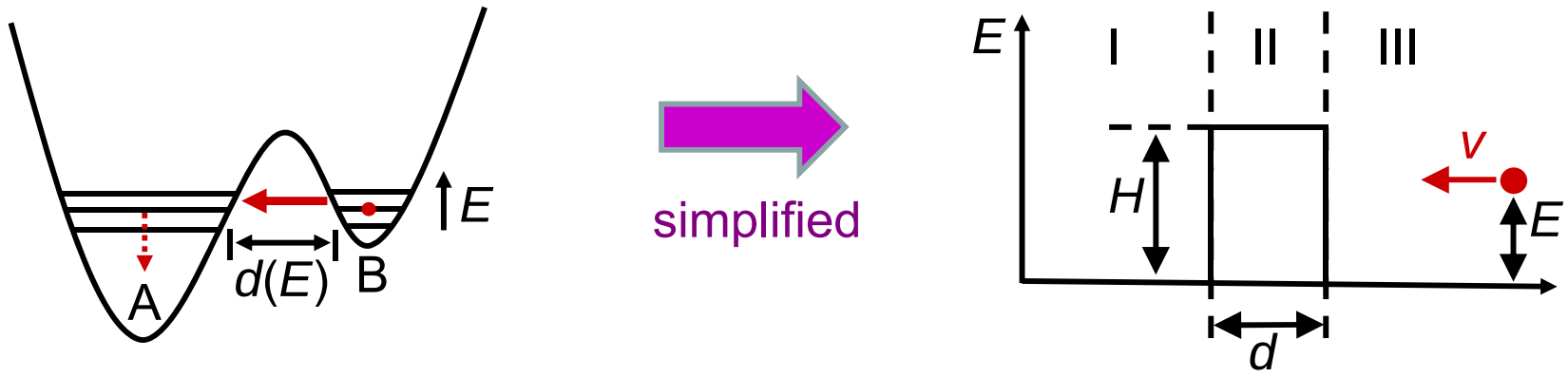

- square well simplest model for tunneling
- wave functions are simple plane waves in regions I, III, and a decaying exponential in region II
- transmission coefficient *TC* (ratio of incident/transmitted probability currents) is given by

$$TC = e^{-2\kappa d/\hbar} \quad , \quad \kappa = \sqrt{2M(H-E)}$$

$$k_t = A_t(T)\, e^{-\gamma \underbrace{\sqrt{2M(H-E)}\, d/\hbar}_{\text{Gamow factor}}}$$

γ = 2 for rectangular barrier
4/3 for triangular barrier
$\pi/2$ for parabolic barrier

- for $T = 0$, only tunneling is possible. With increasing T, change to Arrhenius behavior.

How to Recognize Tunneling I

- 2 characteristic features:
    1. weak T dependence for $T \rightarrow 0$.
    2. pronounced mass dependence

Temperature dependence

- low T kinetics much faster than predicted by Arrhenius law using parameterization at higher T (> 30 – 50 K):

$$N(t) = \int g(H) e^{-\left[A\frac{T}{T_0} e^{-H/RT} \right] t} \, dH$$

How to Recognize Tunneling II

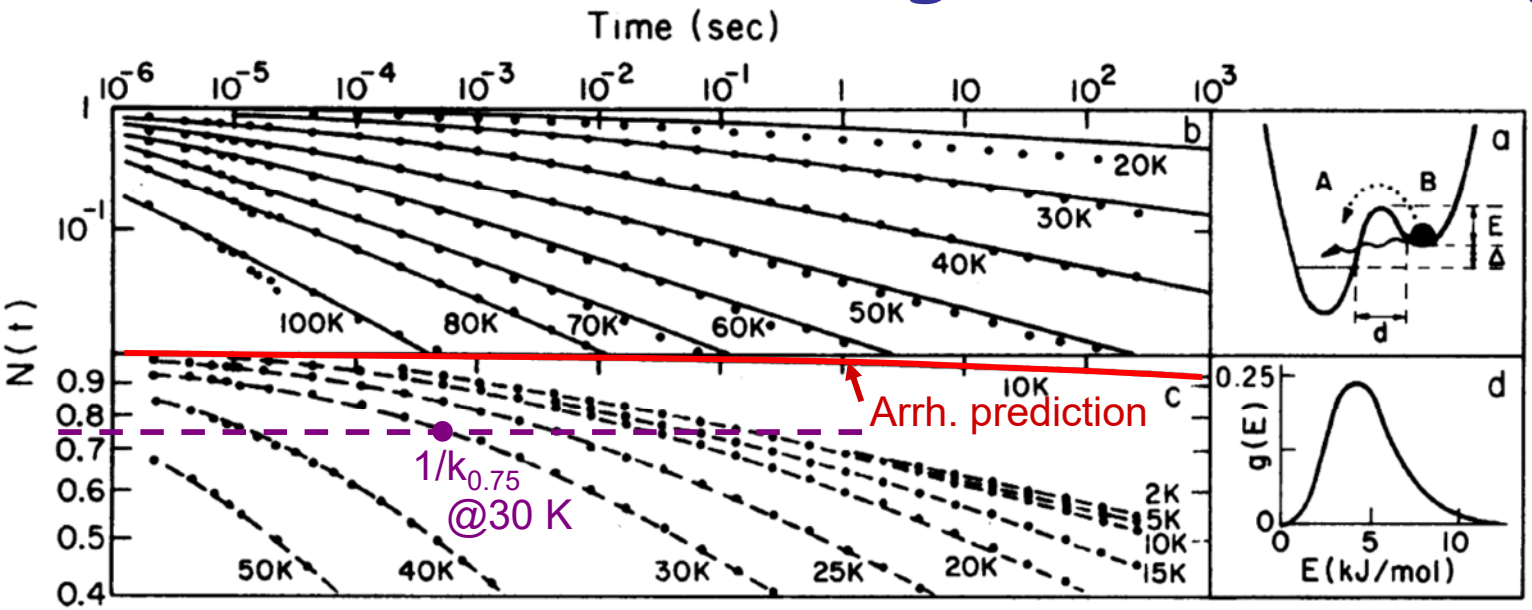

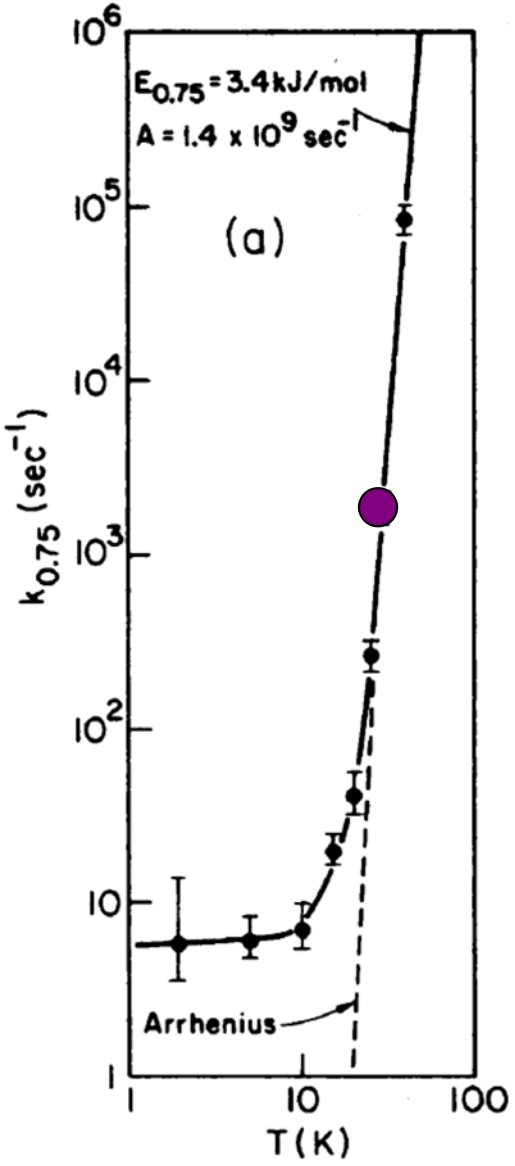

(a) System in well B can move to A by hopping over the barrier or by tunneling through it.

(b) Rebinding of CO to hemoglobin β-chains (βHb) after photodissociation. $N(t)$: fraction of βHb molecules that have not rebound CO at time t after the laser flash.

(c) Same data as (b), but plotted with expanded $N(t)$ scale. The solid line labeled 10 K indicates $N(t)$ as expected without tunneling.

d) Activation energy spectrum for βHb CO. The solid lines in (b) are calculated with $g(E)$ shown here.

Right: The rate coefficient $k_{0.75} = 1/t_{0.75}$ (from c) plotted as a function of log T. The steeply dropping part corresponds to the classical Arrhenius hopping over the barrier. The observed rate is much faster than the classical one for $T < 20$ K and provides evidence of quantum-mechanical tunneling.

Alberding et al., Science 192 (1976) 1002

How to Recognize Tunneling III

Mass dependence (isotope effect)

- even thermally activated rate processes are mass dependent, weakly though! ($\omega_B = \sqrt{D/m}$) .

- tunneling, by contrast, exhibits exponential **mass** dependence.

  → study rebinding as a function of ligand mass (use isotopes!)

- rate coefficients for light (*l*) and heavy (*h*) isotopes:

$$\left.\begin{aligned} k_l &= A\exp[-C\sqrt{M_l}] \\ k_h &= A\exp[-C\sqrt{M_h}] \end{aligned}\right\} \quad \ln\frac{k_l}{k_h} = C\left(\sqrt{M_h} - \sqrt{M_l}\right) \quad ①$$

- coefficient C given by:

$$C = \ln\left(\frac{A}{k_l}\right)\cdot\frac{1}{\sqrt{M_l}} \quad ②$$

How to Recognize Tunneling IV

Mass dependence (isotope effect)

- plug ② into ①:

Multiply by one!

$$\ln\frac{k_l}{k_h} = \ln\left(\frac{A}{k_l}\right)\cdot\frac{\sqrt{M_h}-\sqrt{M_l}}{\sqrt{M_l}} \qquad \left(\times\frac{\sqrt{M_h}+\sqrt{M_l}}{\sqrt{M_h}+\sqrt{M_l}}\right)$$

$$\Longrightarrow \quad \ln\frac{k_l}{k_h} \approx \ln\left(\frac{A}{k_l}\right)\cdot\frac{\Delta M}{2M}$$

$\Delta M = M_h - M_l$

$M \approx (M_h + M_l) / 2$

$\Delta M << M$

Ratio k_l/k_h gets large for long times (k_l small)

- for single-valued k: no choice
- for distributions: pick small k-values (long times)!

Experimental Determination I

- problem: rebinding curves flat at low T, isotope effect small.
  → high precision needed !
- cannot use two samples prepared separately using different ligand isotopes.
- solution: measure CO kinetics by FTIR in the infrared, where CO with different isotope composition can be easily distinguished.

MbCO substate A_1:

$^{12}C^{16}O$	1945 cm^{-1}
$^{13}C^{16}O$	1901 cm^{-1}
$^{12}C^{18}O$	1902 cm^{-1}

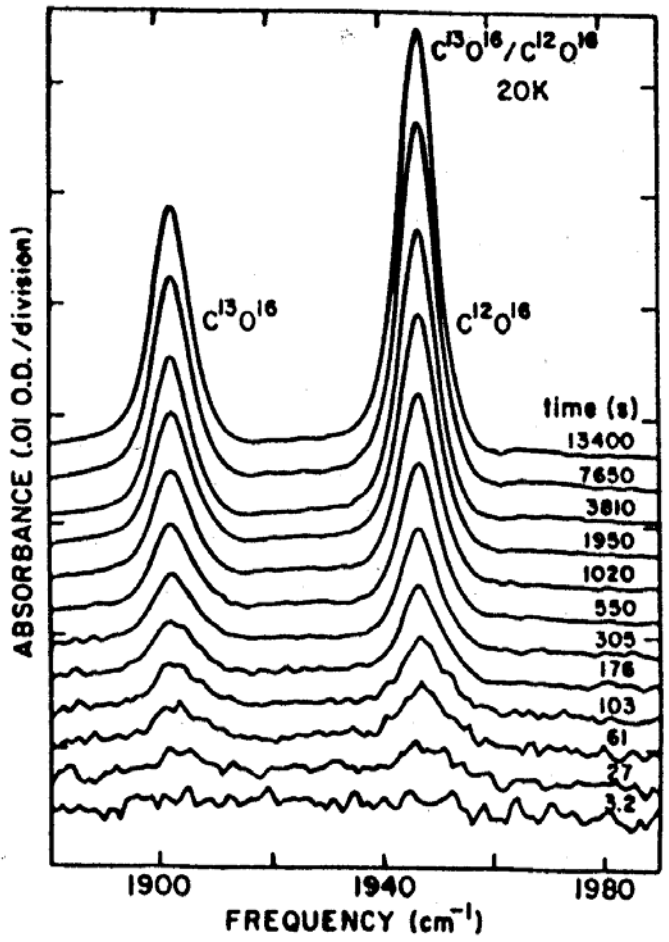

Experimental Determination II

kinetics
calculated from
areas of IR bands

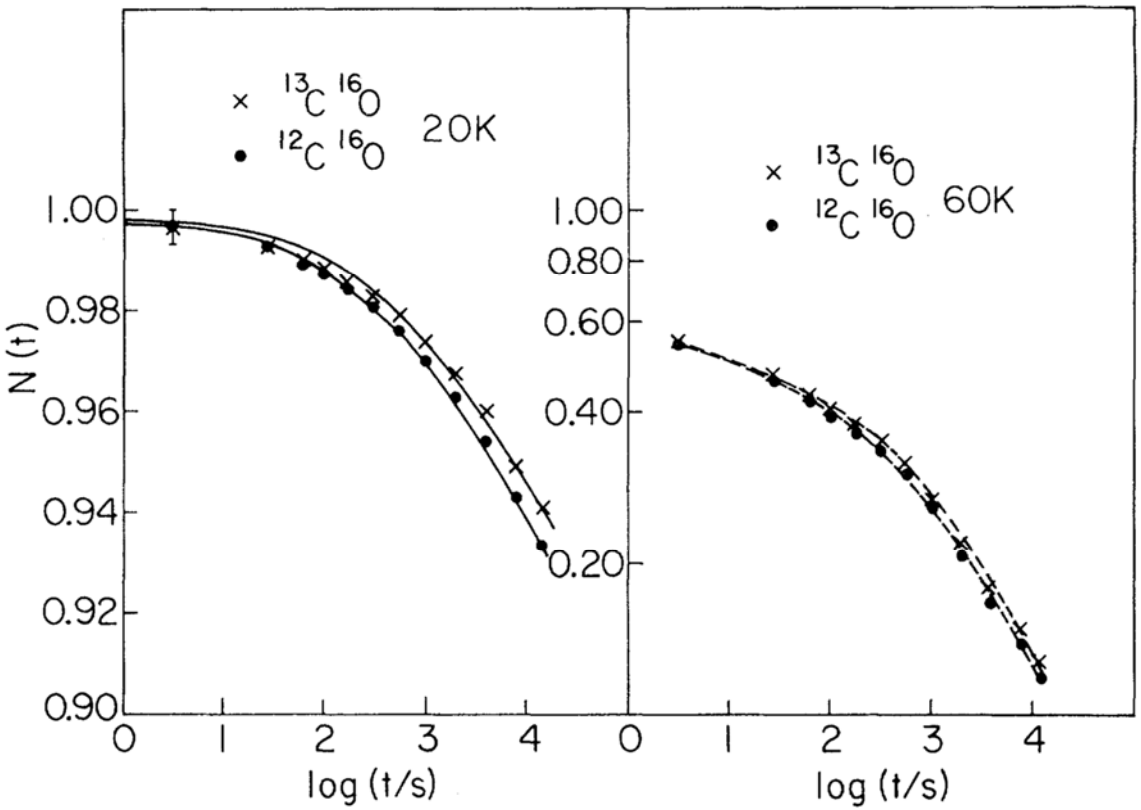

Alben et al., Phys. Rev. Lett. 44 (1980) 1157.

Experimental Results I

Values of k_l/k_h ($\approx t_h/t_l$ for the same rebinding fraction) at $\approx 10^3$ s and values of $\Delta M/M$, the relative mass change, in the binding of carbon monoxide to myoglobin. The model calculations refer to point particles moving in fixed potentials.

Quantity		$^{12}C^{16}O$ vs $^{13}C^{16}O$	$^{12}C^{16}O$ vs $^{12}C^{18}O$
Experimental: k_l/k_h	60 K	1.20 ± 0.05	1.15 ± 0.05
	20 K	1.53 ± 0.05	1.20 ± 0.05
→ $\Delta M/M$	(20 K)	0.040 ± 0.015	0.019 ± 0.007
Model: $\Delta M/M$			
M is the mass of	CO	0.035	0.069
	C	0.080	0
	O	0	0.118
M is the reduced mass of	CO-Fe	0.023	0.045
	C-Fe	0.066	0
	O-Fe	0	0.090

Small!!!
→ Oxygen does not move much

Alben et al., Phys. Rev. Lett. 44 (1980) 1157

Experimental Results II

- rate coefficients are mass dependent, indicative of tunneling.
- from rebinding data, $\Delta M/M$ can be calculated.
- experimental $\Delta M/M$ can be compared with theoretical expression, using different assumptions about the mass that actually tunnels.
- comparison for ^{12}C / ^{13}C yields $\Delta M/M$ as expected for tunneling of CO.
- comparison for ^{16}O / ^{18}O yields much smaller mass dependence than expected for tunneling of CO.
- structural details important !

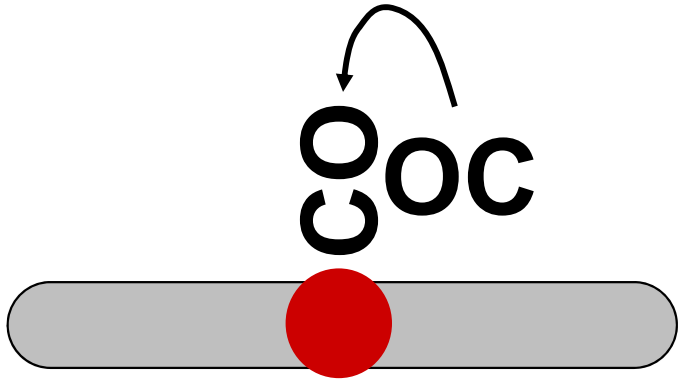

Biophysics II

Biological Energy Conversion

Uli Nienhaus

Prof. G. U. Nienhaus, Vorlesungsunterlagen Biophysik II, SS 2023.
Nur zum KIT-internen, vorlesungsbegleitenden Gebrauch.
Weitergabe und anderweitige Nutzung verboten.

Evolution of Bioenergetic Systems

- The first living cells appeared ~3.5 billion years ago, when the earth was a mere 1 billion years old.
- Early metabolic pathways presumably involved fermentation of geochemically produced organic molecules (sugars → acids) to produce ATP and reducing power (NADH/NADPH).
- Acidification led to the evolution of proton pumps that removed protons from the cells.
- Eventually, proton pumps were integrated into electron transport chains.
- As the supply of geochemically produced foodstuffs dwindled, photosynthesis was invented by sulfur bacteria, which used it for extracting high-energy electrons from H_2S.
- About 2 billion years ago, cyanobacteria finally managed to use the abundant source H_2O as an electron donor.
- This process led to a major ecological catastrophe because the production of O_2 from water splitting produced an oxidative environment that was highly poisonous for many organisms at that time.
- Further evolution led to the development of aerobic respiration, by which sugar, in the presence of oxygen, can be metabolized much more efficiently (2 ATP / molecule glucose without O_2 vs. 30 with O_2).

Bioenergetics

Energy conversion takes place in bacteria and cell organelles (mitochondria and chloroplasts) of plants and animals. They contain their own DNA and are believed to have evolved from prokaryotes that were engulfed by primitive eukaryotes.

Mitochondria: convert energy derived from chemical fuels – respiration

$[CH_2O] + O_2 \rightarrow CO_2 + H_2O$

ΔG

actually:

$CH_2O + O_2 + H_2O^* \rightarrow CO_2^* + 2\ H_2O$

*denotes a particular O

Chloroplasts: convert energy derived form sunlight – photosynthesis

$CO_2 + H_2O \rightarrow [CH_2O] + O_2$

$h\nu$

actually:

$CO_2 + 2\ H_2O^* \rightarrow CH_2O + H_2O + O_2^*$

Although respiration and photosynthesis are often presented as the reverse of each other, the underlying fundamental processes are rather similar.

Chemiosmosis

Universal energy conversion mechanism that connects electron flow, proton gradient, and ATP synthesis (Mitchell 1961). Energy is stored in a pH gradient or electrostatic potential of a membrane on which the energy-converting proteins are arranged.

$$\Delta \tilde{\mu}_{H^+} = F \cdot \Delta\Psi - 2.3\, RT\ \Delta pH$$

Faraday constant = e · N_A

ln 10

Chemiosmotic Coupling I

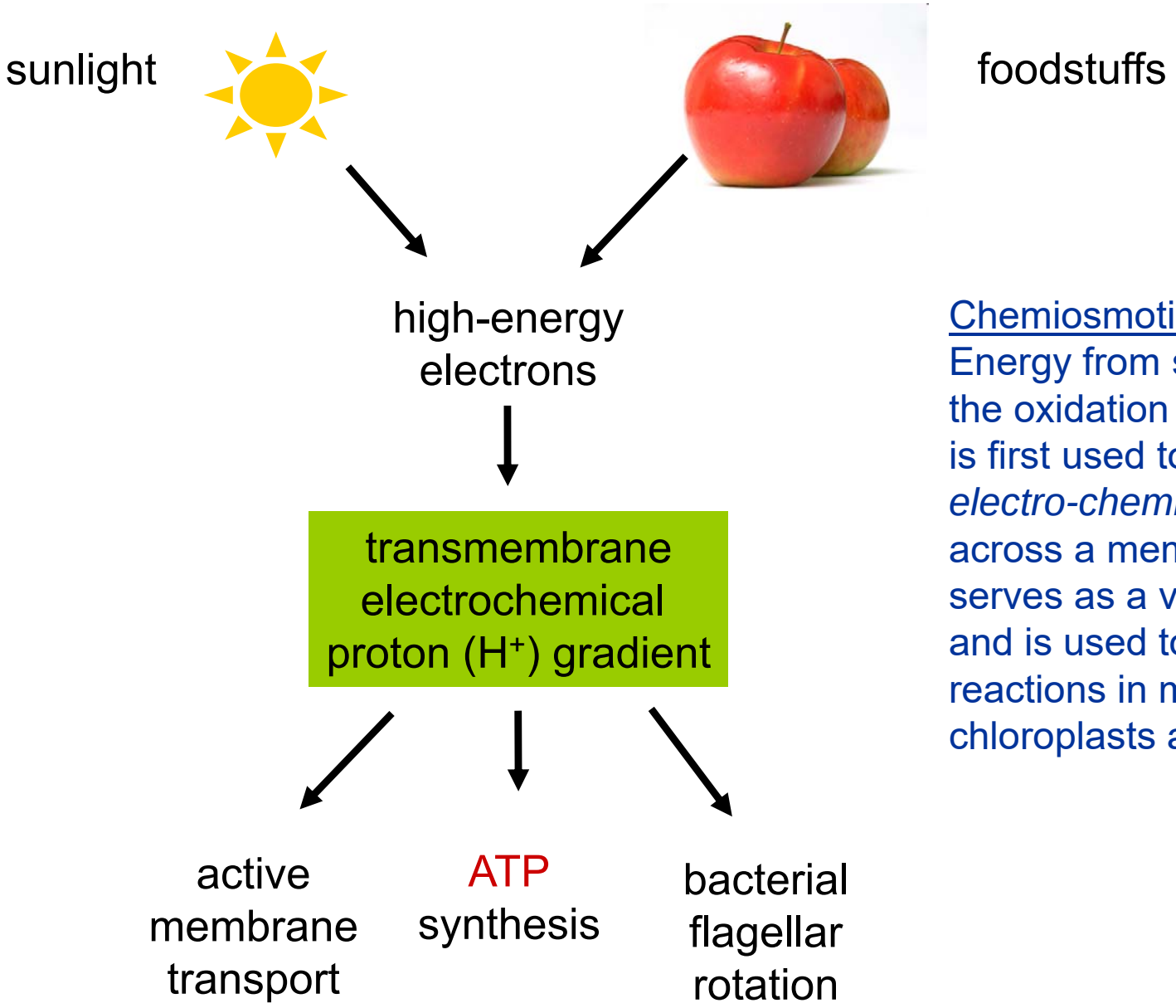

Chemiosmotic coupling:
Energy from sunlight or the oxidation of foodstuffs is first used to create an *electro-chemical proton gradient* across a membrane. This gradient serves as a versatile energy store and is used to drive a variety of reactions in mitochondria, chloroplasts and bacteria.

Chemiosmotic Coupling II

Chloroplast

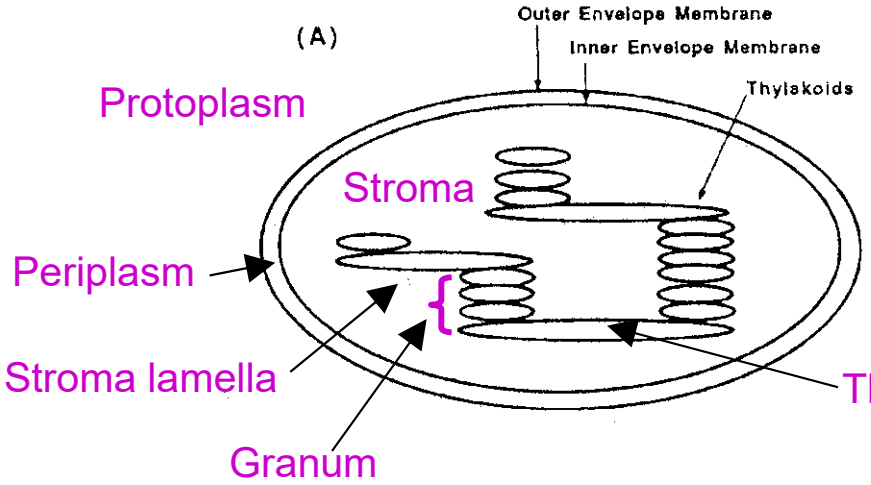

Diameter ~ 5 μm

Gram-negative bacterium (e. g., *E. coli*)

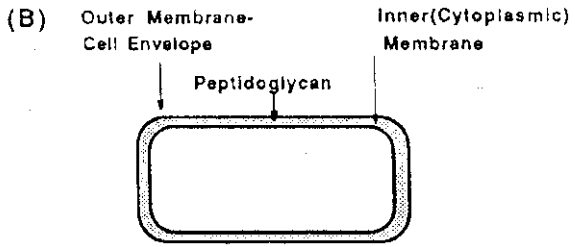

Mitochondrion

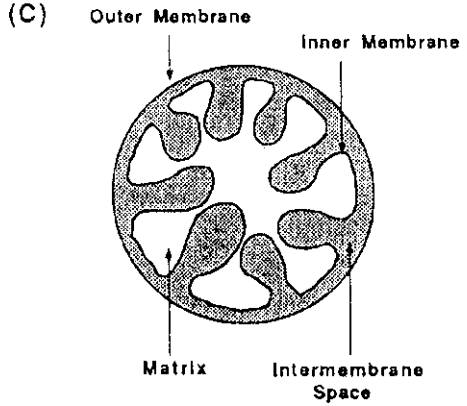

Chemiosmotic Coupling III

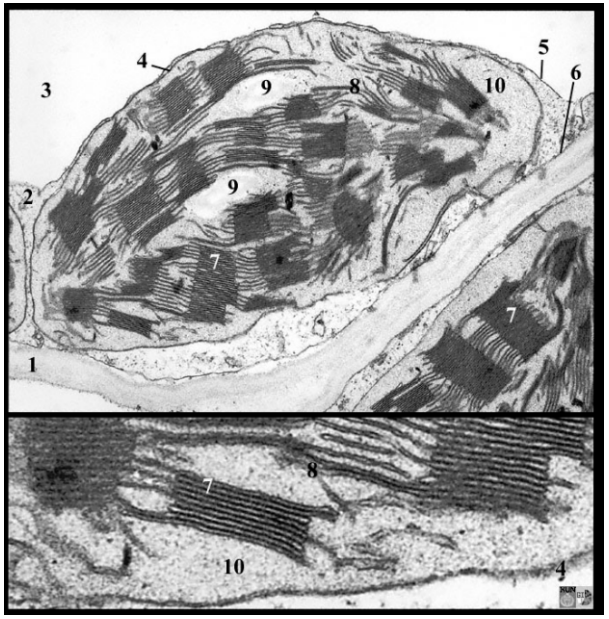

Chloroplast in a tobacco leaf
(transmission electron microscopy):
1 cell wall, 2 cytoplasm, 3 vacuole,
4 chloroplast envelope (2 membranes),
5 tonoplast, 6 plasma membrane, 7 grana,
8 stroma thylakoids, 9 starch grains, 10 stroma

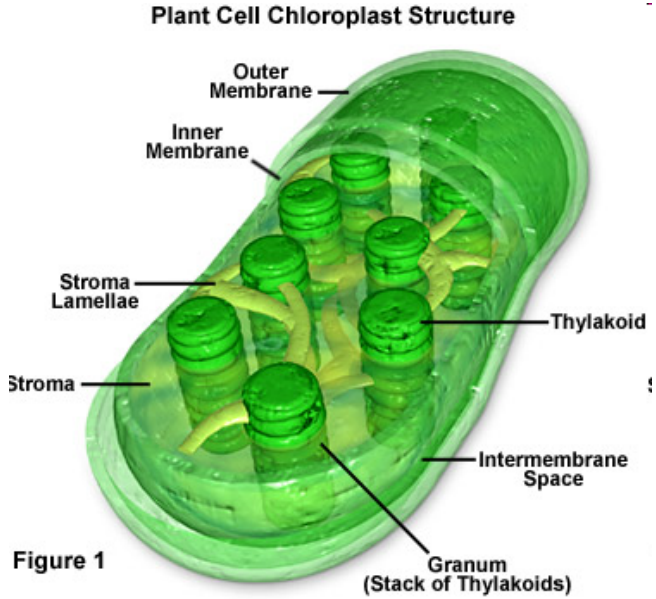

mitochondrion 1 - 2 µm x 0.5 - 1.0 µm.
chloroplast is approximately 5 µm across
(based on Keegstra et al., 1984)

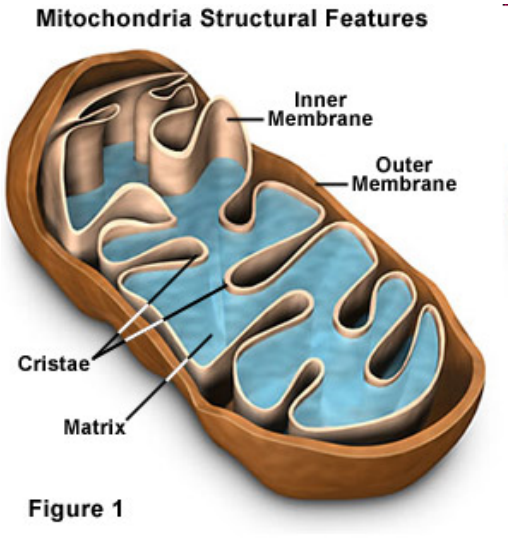

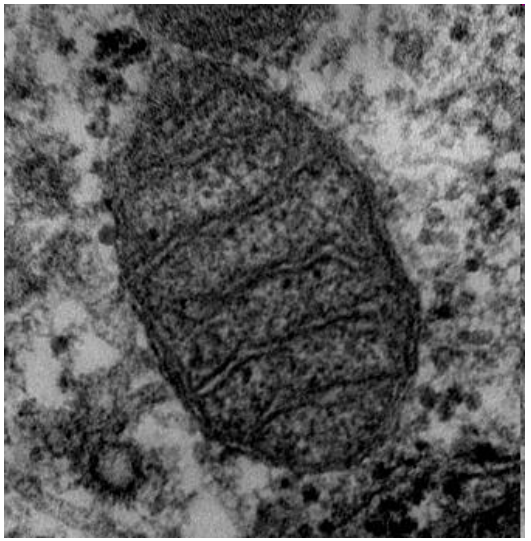

Chemiosmotic Coupling IV

across inner membrane

across thylakoid membrane

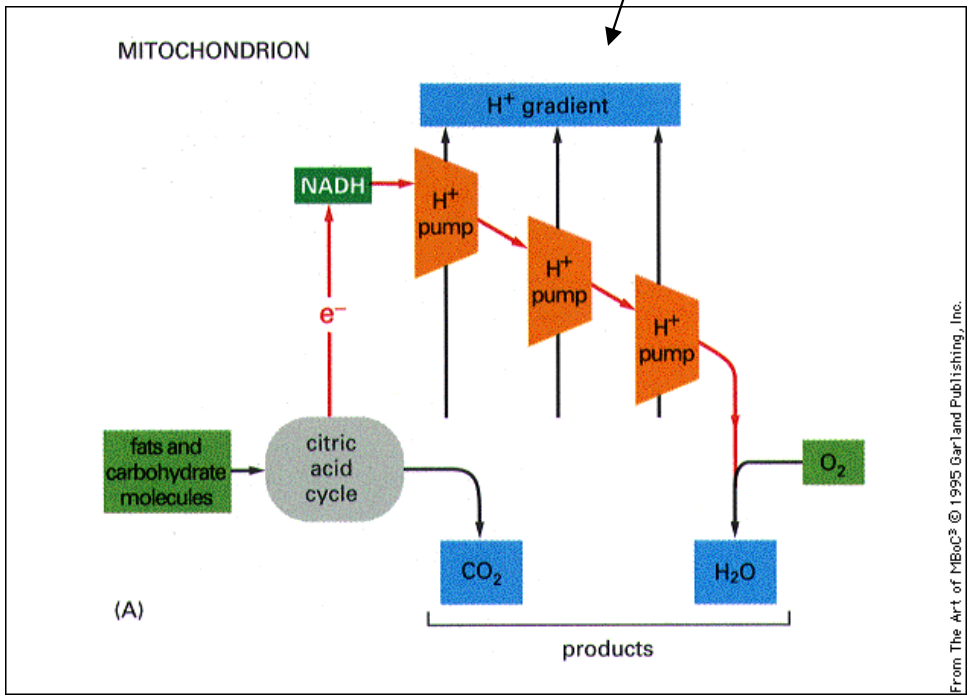

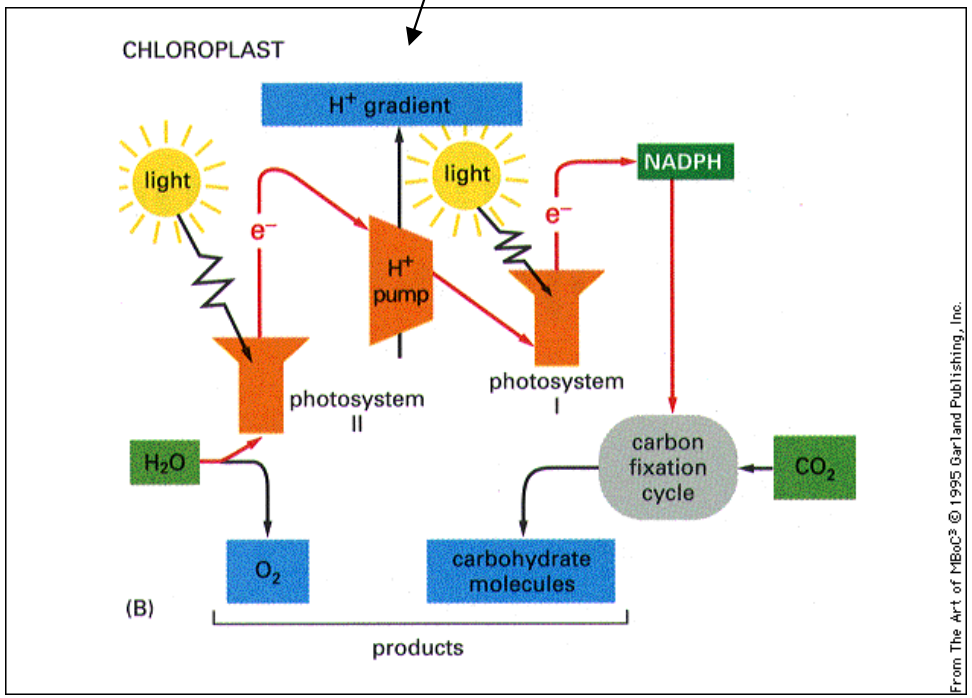

Plant Photosynthesis I

Photosynthesis in plants can be subdivided into a photophysical primary process, light-induced charge separation, and two subsequent (dark) biochemical processes, CO_2 fixation, and ATP synthesis.

Light-induced charge separation

- two steps: $h\nu_{680\ nm} \approx 1.8$ eV

1. Photosynthetic water splitting:

   $H_2O \rightarrow \frac{1}{2} O_2 + 2 H^+ + 2 e^- + \Delta G_1$ (0.816 eV)

2. Transfer of electrons to $NADP^+$

   $NADP^+ + 2 e^- + H^+ \rightarrow NADPH + \Delta G_2$ (0.342 eV)

Plant Photosynthesis II

- charge separation occurs in large, membrane-spanning protein complexes, called reaction centers (RC), which are oriented parallel in the thylakoid membrane. The result of the primary process is light-induced transfer of electrons from the lumen to the stroma and protons in the opposite direction. The energy is stored in NADPH and $\Delta pH \approx 3 - 3.5$.

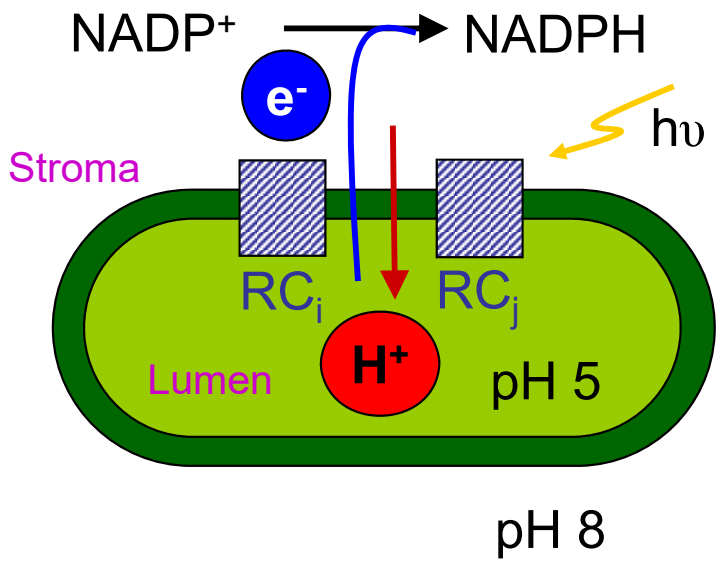

$\Delta\Psi \approx 0$ because thylakoid membrane is permeable for Mg^{2+} and Cl^{-}.

(Mitochondria: $\Delta pH \approx 1$, and $\Delta\Psi$ is significant)

Plant Photosynthesis III

Dark reactions:

1. Proton gradient is used by ATP synthase to catalyze the reaction

$ADP^{3-} + PO_4^{3-} + 2\ H^+ \rightarrow\ ATP^{4-} + H_2O$ (often written as ADP + $P_i \rightarrow$ ATP +H_2O)

2. NADPH is a strong reductant (electron donor).
   Together with ATP, it can convert CO_2 to CH_2O

$$CO_2 + 2\ NADPH + 3\ ATP^{4-} + 2\ H_2O \rightarrow$$
$$[CH_2O] + 2\ NADP^+ + 3\ ADP^{3-} + 3\ HPO_4^{2-} + H^+$$

Plant Photosynthesis IV

Scheme (a) below shows the net transfer of atoms and charges. The first step in plants, however, is the one depicted in (b), where CO_2 is coupled to ribulose-1.5-bisphosphate by the enzyme ribulose bisphosphate carboxylase (RuBisCo) in the stroma. This enzyme is very inefficient (3 – 10 s^{-1}), thus many copies are needed; it can be up to 50% of the total amount of chloroplast protein mass.

In the Calvin-Benson (CO_2-fixation) cycle, the intermediate is split into two molecules of 3-phosphoglycerate.

→ further biosynthesis of sugars, amino acids, fatty acids.

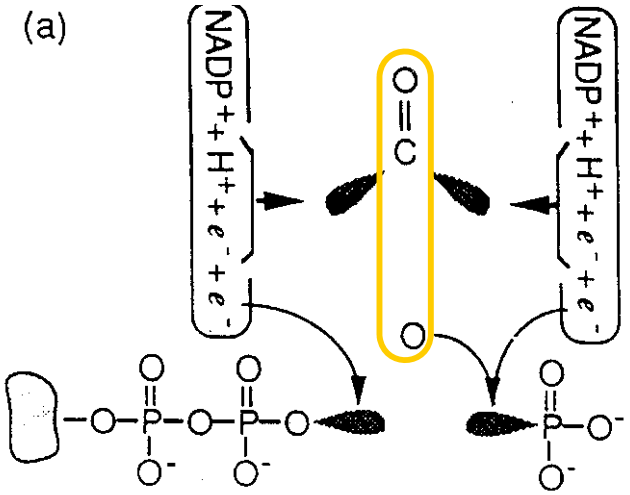

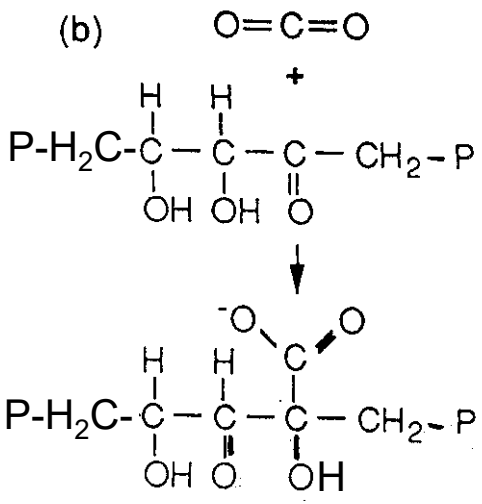

← 5 carbons

← 6 carbon intermediate

Photosynthetic Apparatus I

- chloroplasts have the ability to use water as an electron donor. To generate NADPH (redox potential ~ −320 mV) from water (redox potential ~ +830 mV), two photosystems are employed:

  PS I (P700)

  PS II (P680) - water splitting enzyme

- clear evidence of two reaction centers was obtained by measuring the photosynthesis yield (O_2 production) as a function of wavelength.

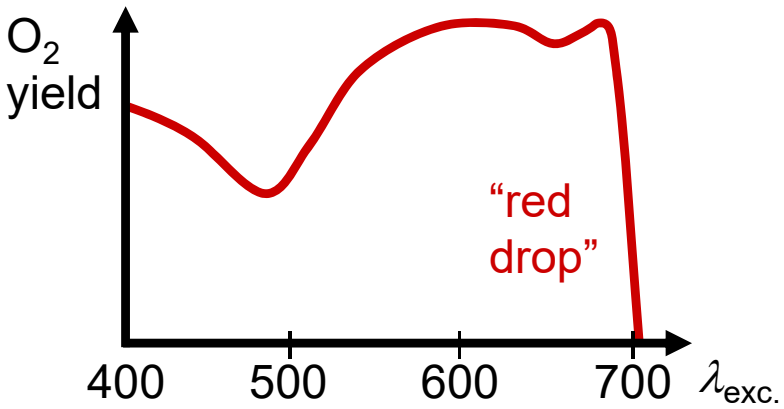

Excitation can only happen for $\lambda < \lambda_{crit.}$.
For 690 nm < λ < 705 nm, only PSI can be excited → no photosynthesis possible.

Photosynthetic Apparatus II

- Photosystem II contains a Mn_4CaO_5 cluster that extracts electrons from water:

$$2\ H_2O \xrightarrow{4\ h\nu} O_2 + 4\ H^+ + 4\ e^-$$

loss of synchronization
(misses, double hits)

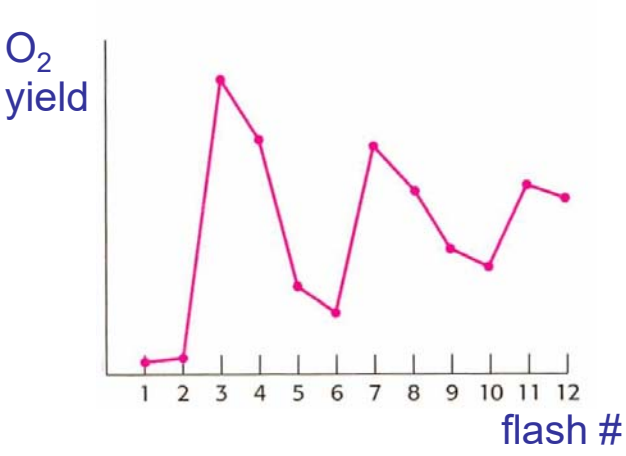

dark: ~ 75% S_1, 25% S_0

(L. Stryer)

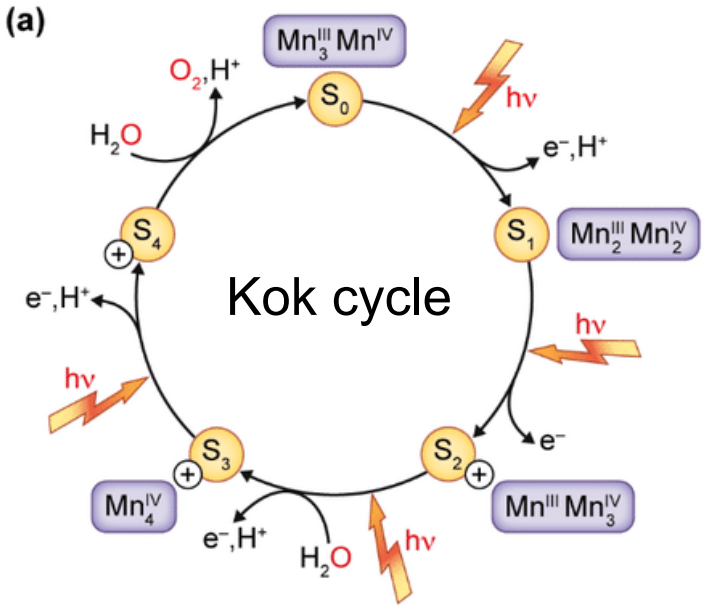

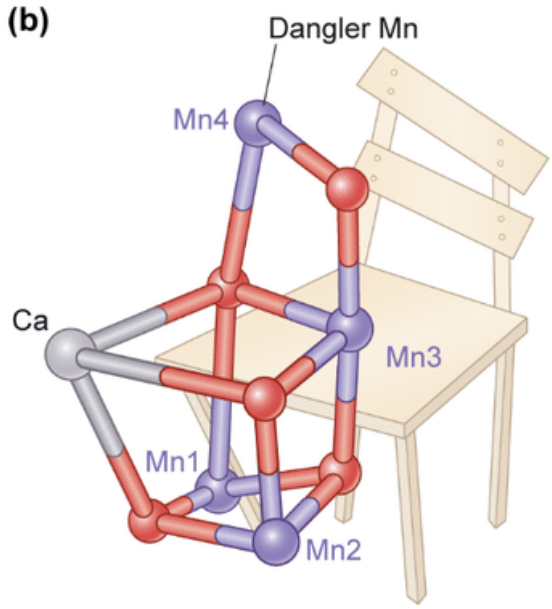

Mn_4CaO_5

'Z - Scheme' I

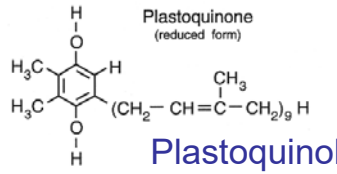

Plastoquinol

Plastocyanin
(small blue copper protein)

Water splitting

Energy of electrons

Primary acceptor

H_2O

$2\ H^+ + \frac{1}{2}\ O_2$

Light

P680

Photosystem II
(PS II)

Electron transport chain

Pq

Cytochrome complex

Cyt b_6-f complex

Pc

ATP

Primary acceptor

P700

Photosystem I
(PS I)

Electron transport chain

Fd

$NADP^+$ reductase

$NADP^+ + 2\ H^+$

$NADPH + H^+$

Light

Direction of electron flow

Net reaction:

$2\ H_2O + 2\ NADP^+ \xrightarrow{h\nu} O_2 + 2\ NADPH + 2\ H^+$

Ferredoxin:

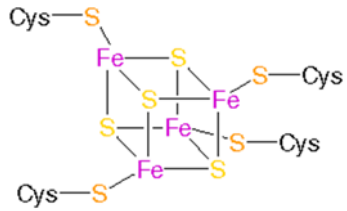

$Fe^{3+} \rightarrow Fe^{2+}$

e^-

(2 S – 2 Fe)
(3 S – 3 Fe)
(4 S – 4 Fe)

'Z - Scheme' II

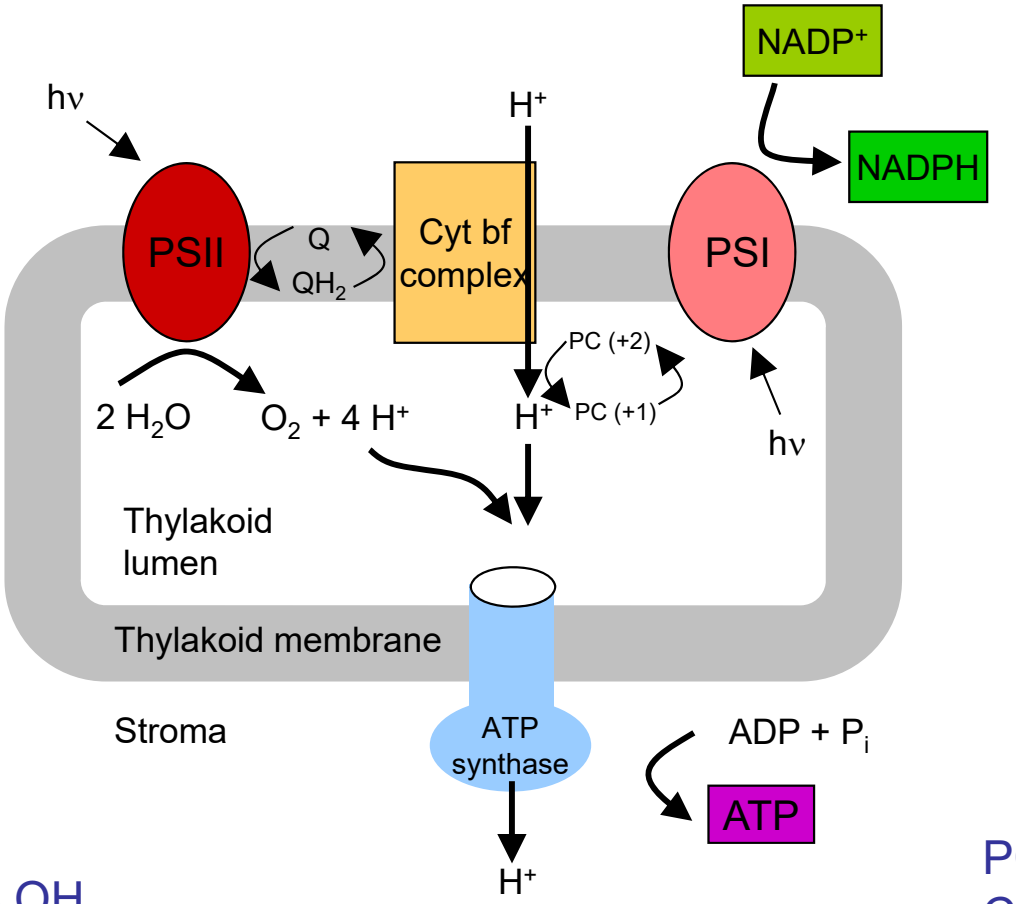

Q: Plastoquinone

$Q + 2\ H^+ + 2\ e^- \rightarrow QH_2$

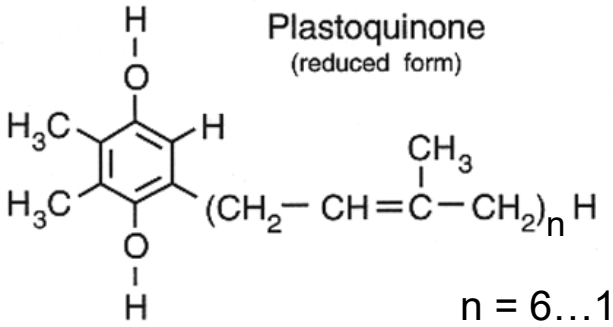

n = 6…10

PC: Plastocyanin

$Cu^{2+} + e^- \rightarrow Cu^+$

PSI and ATP Synthase are located in unstacked parts of thylakoid membrane.

Experimental Tests of the Chemiosmotic Hypothesis I

- According to Mitchell, ATP production is coupled to an electrochemical proton gradient.

$$ADP + P_i + n\ H^+_{in} \rightleftharpoons ATP + H_2O + n\ H^+_{out}$$

reversible !

- The total electrochemical potential of the proton is

$$\Delta\mu_{H+} = RT\ \ln\left([H^+_{out}] / [H^+_{in}]\right) + F\ \Delta\Psi$$

- Evidence:
  1. ATP production increases strongly with ΔpH.
  2. ΔpH gradients induced by light are relaxed faster if [ADP] is increased.

Experimental Tests of the Chemiosmotic Hypothesis II

- ATP production needs a free energy of 0.35 eV.
  → H^+ chemical potential should have a threshold.
  ~ 140 meV ⇒ 3 H^+ needed.

ATP synthesis

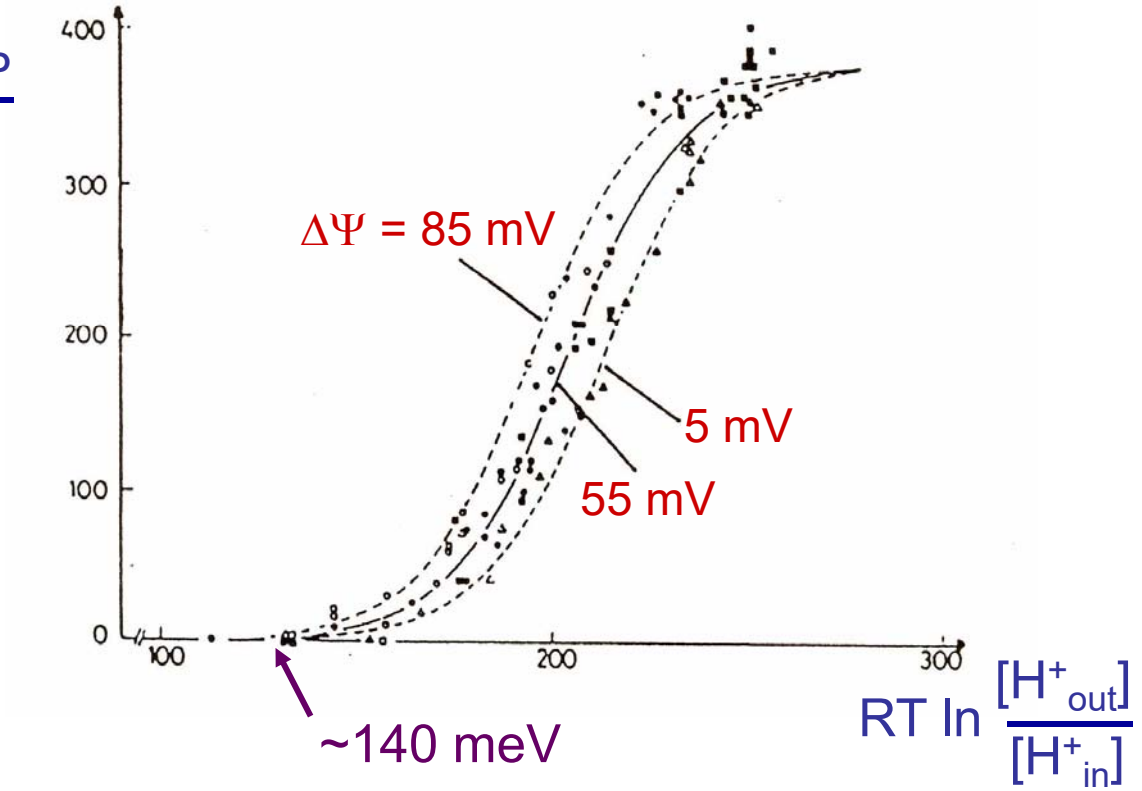

ΔΨ shifts curves
⇒ equivalence of concentration gradient and potential gradient

Equivalence of Light-driven and E-field-driven ATP Synthesis I

- Application of an electric field allows one to generate voltages of the order of ~ 100 mV across the membranes.
- Only on one side of the 1-μm vesicle does the voltage have the proper orientation to drive ATP synthesis.

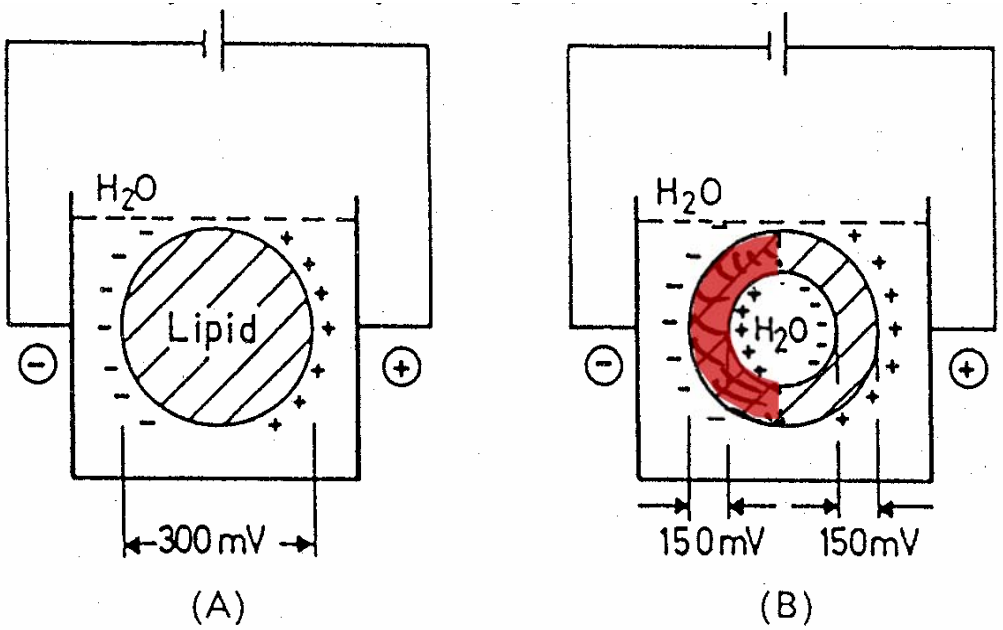

Principle of the external electric field method: Two electrodes in aqueous solution are separated by 1 mm and 300 V are applied, so that the field strength is 3,000 V/cm. The voltage across 1 μm (10^{-4} cm) distance is then 300 mV (A), distributed as 150 mV across the two high resistance sides (B). The opposite polarity across the lipid annulus induced by the electrode plates on the two sides of the vesicle is shown.

(Witt, 1979)

Equivalence of Light-driven and E-field-driven ATP Synthesis II

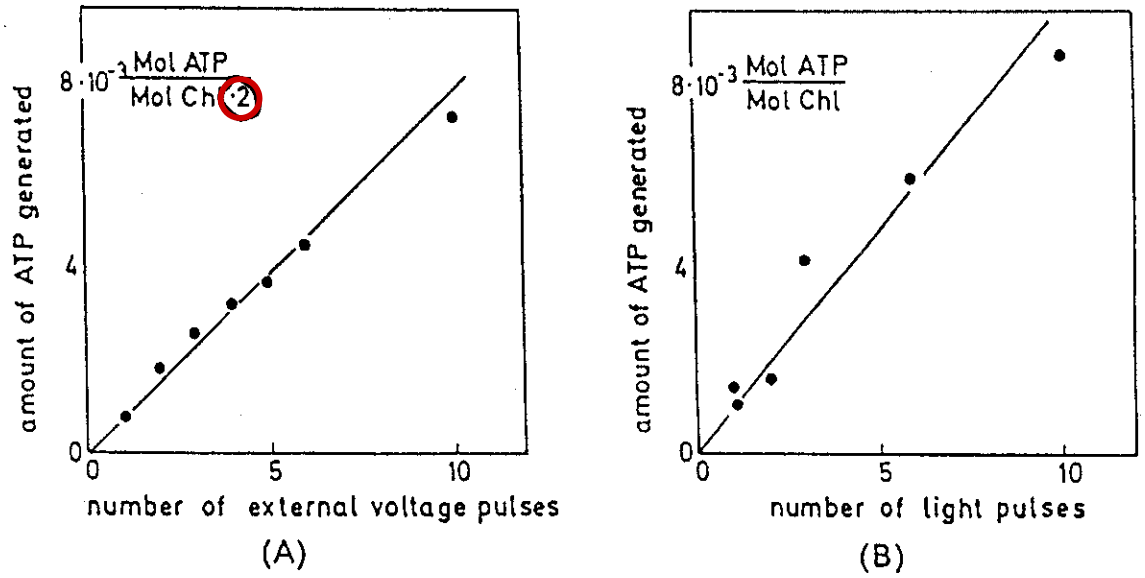

Yield of ATP formation driven by external voltage pulses in the dark (A) and by light pulses (B). Duration of both pulses = 30 ms (Witt, 1979).

Biophysics II

Photosynthesis Apparatus of Purple Bacteria

Uli Nienhaus

Prof. G. U. Nienhaus, Vorlesungsunterlagen Biophysik II, SS 2023.
Nur zum KIT-internen, vorlesungsbegleitenden Gebrauch.
Weitergabe und anderweitige Nutzung verboten.

Photosynthetic Apparatus of Purple Bacteria

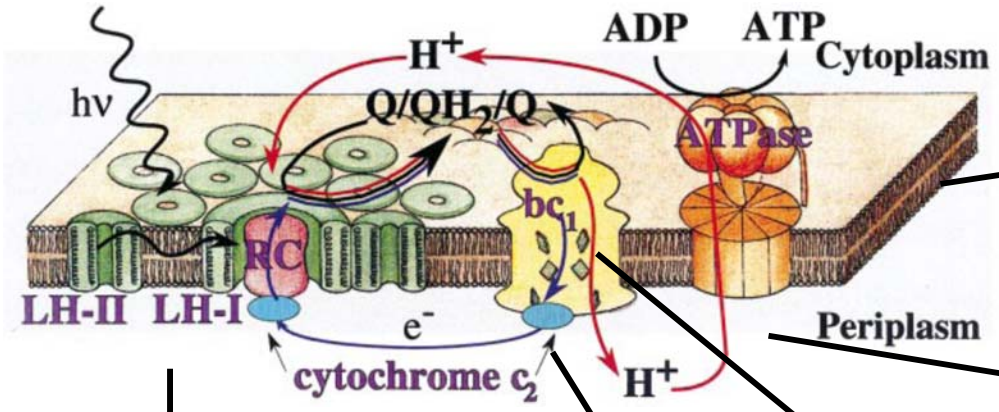

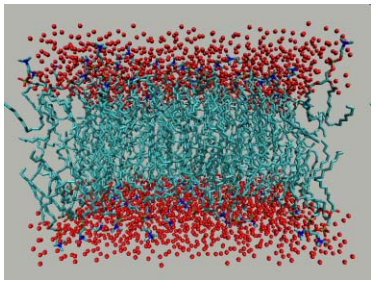

POPC membrane

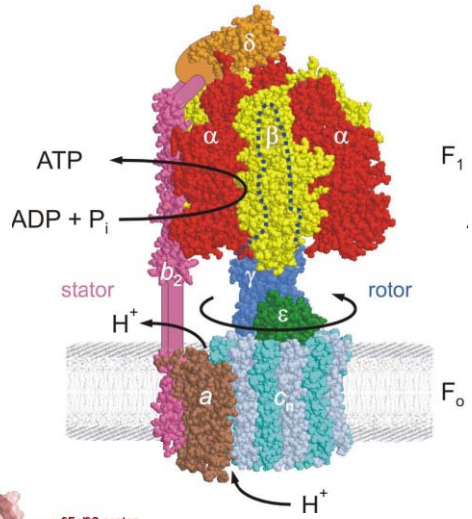

F_1-ATPase

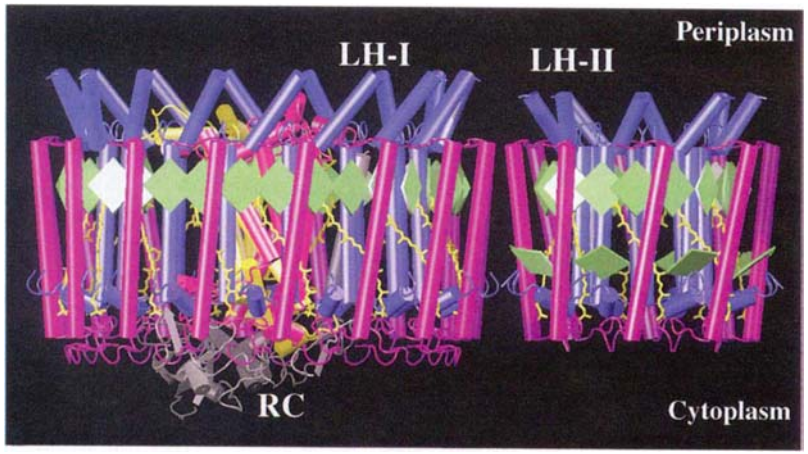

Light harvesting complex
and photosynthetic reaction center

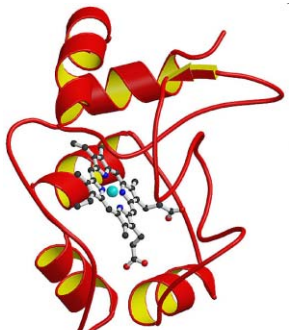

Cytochrome c2
(Rhodobacter capsulatus)

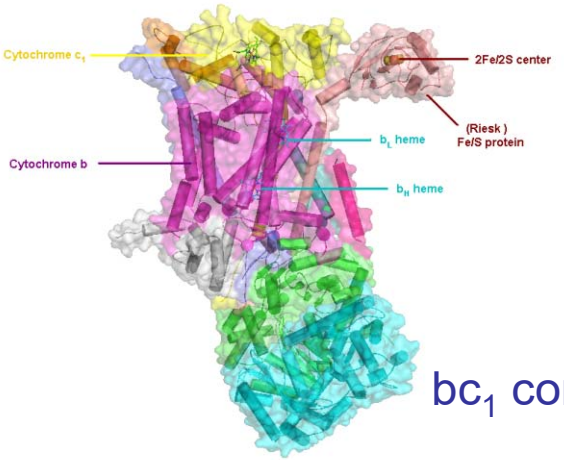

bc_1 complex

Electron Transport Chains

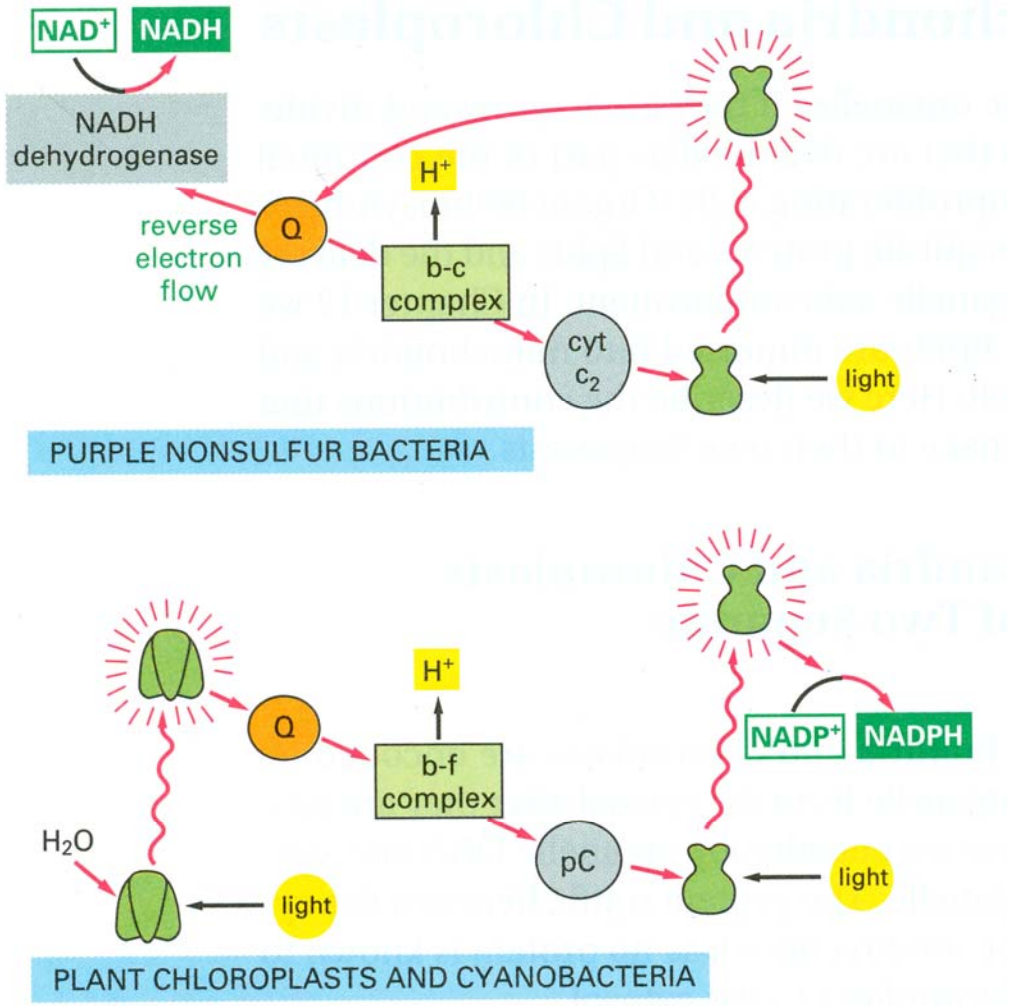

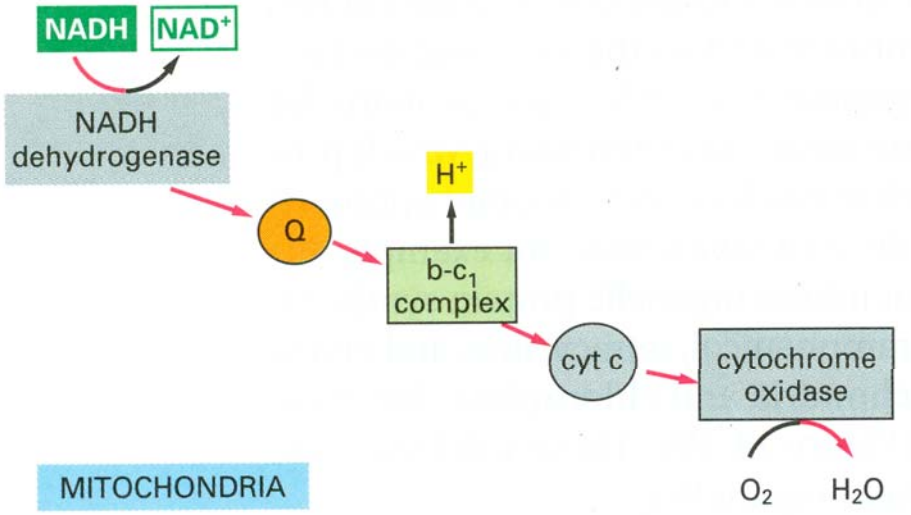

Structure of Light Harvesting System

RC turnover : ~ 1000 s^{-1}

Sunlight : 0.1 – 10 s^{-1}

⇒ need for light-harvesting complexes

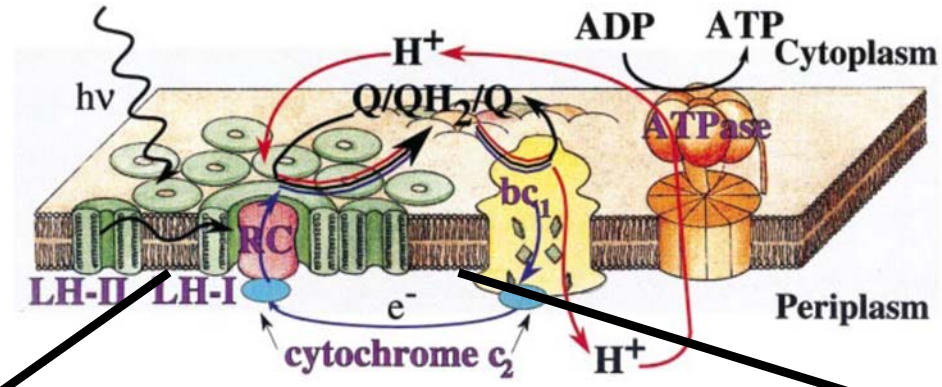

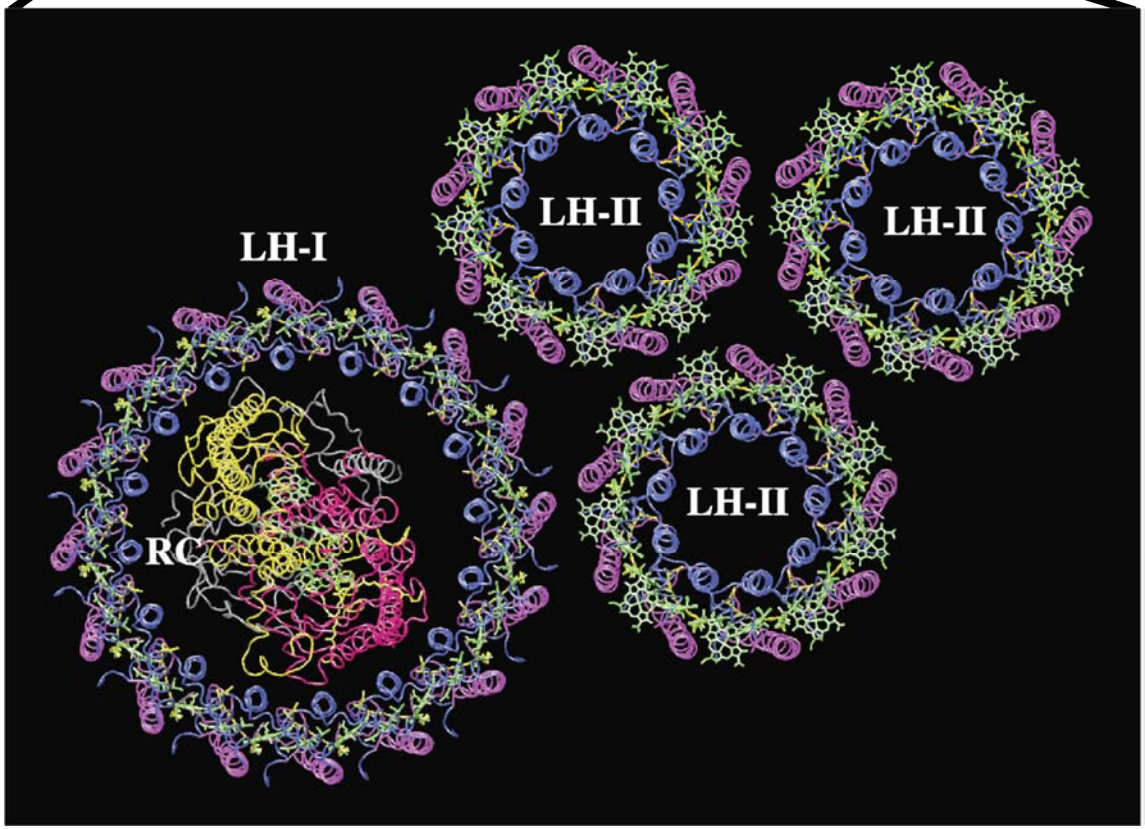

Photosynthetic Unit
PSU

Photosynthesis Pigments I

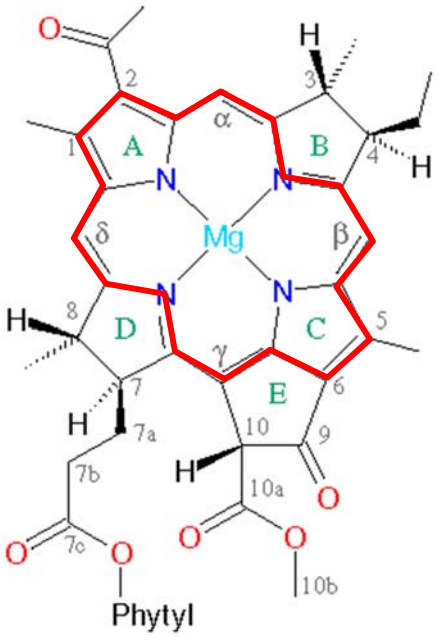

Bacteriochlorophyll a

In Chl b /BChl b:
$CH_3 \rightarrow C{=}O$
H

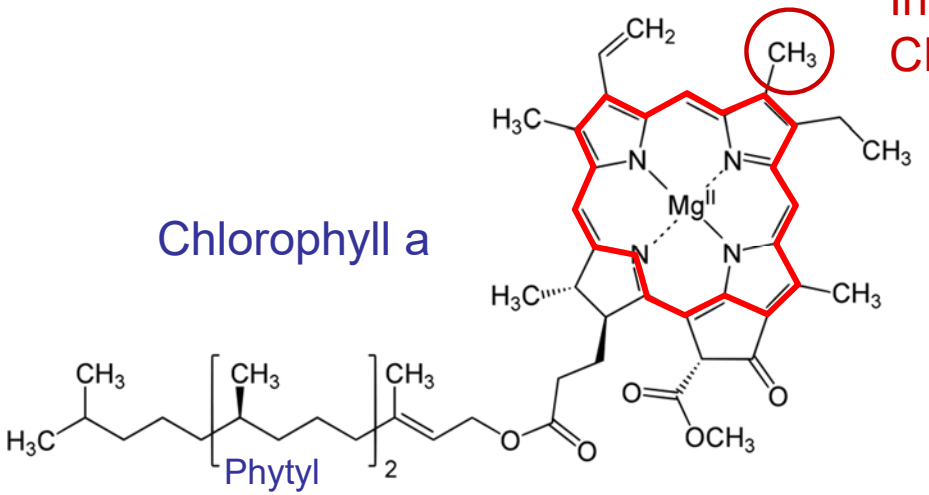

Chlorophyll a

Carotenoids:

2 functions:

- quench Chl triplet state (avoid singlet O_2)
- absorb sunlight in a different spectral region

β-Carotene

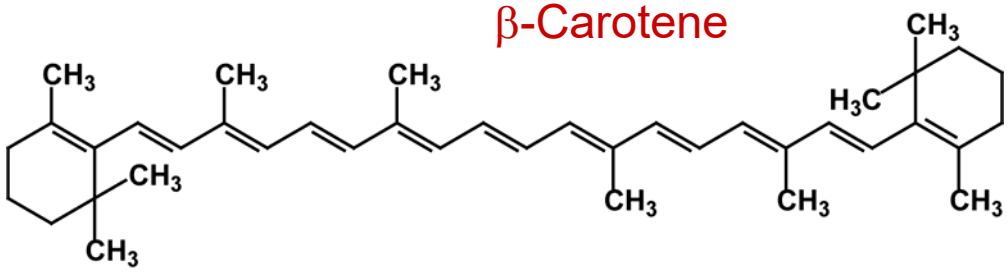

Photosynthesis Pigments II

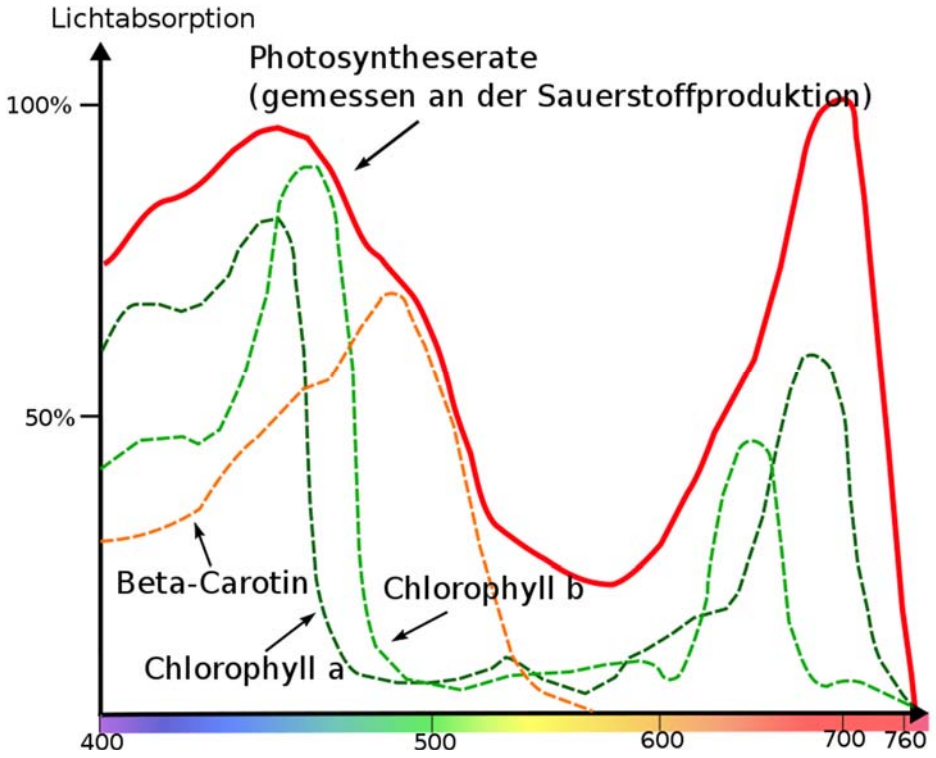

wavelength / nm

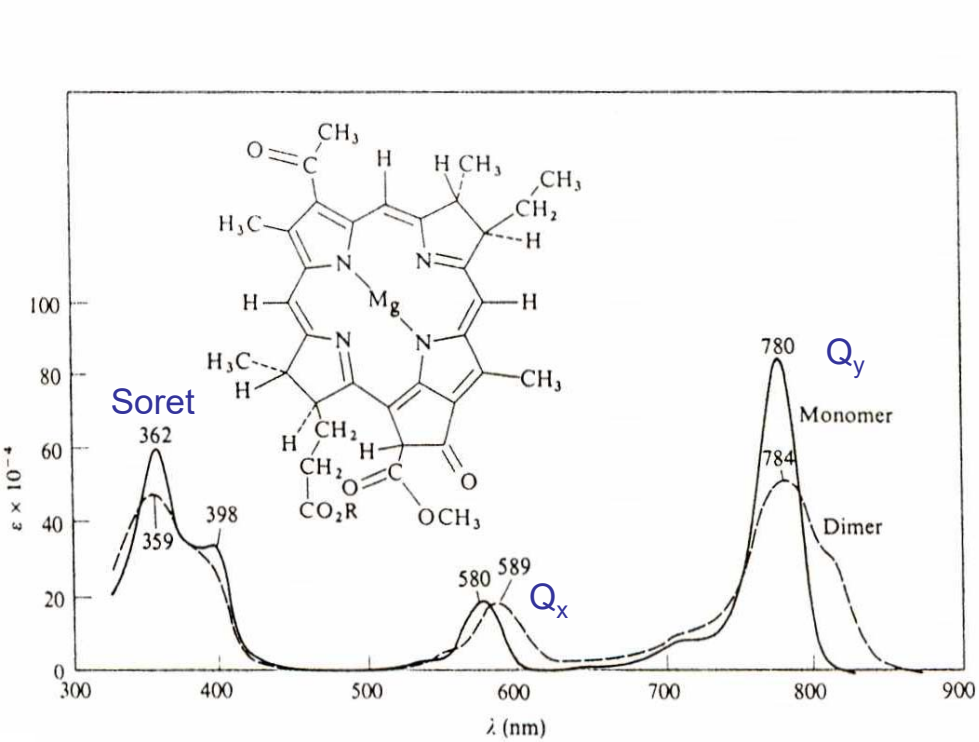

Monomer and dimer spectra of bacteriochlorophyll: splitting of the longest-wavelength Q_y band

(Sauer et al. JACS 88, 2681 (1966))

Electronic Excitation and Deexcitation

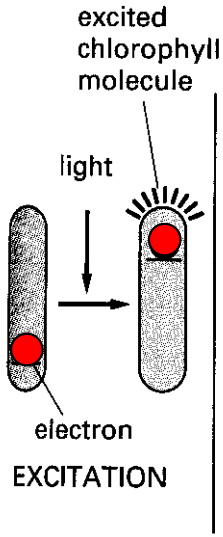

POSSIBLE DECAY PATHWAYS

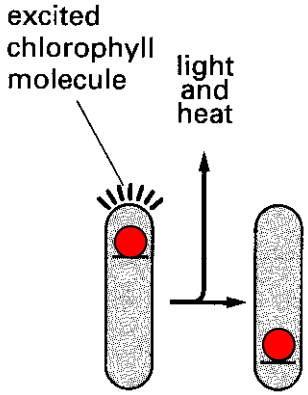

1 decay by giving off light and heat

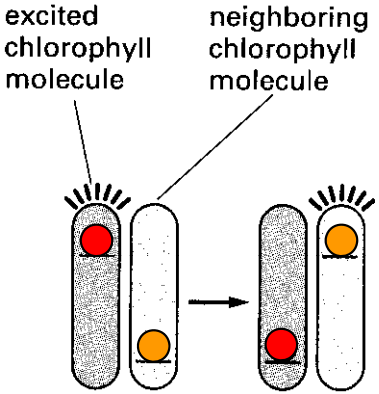

2a decay by resonance energy transfer
- only possible if transitions optically allowed! (Förster)

2b decay by electron exchange (Dexter)

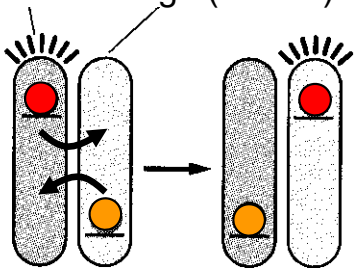

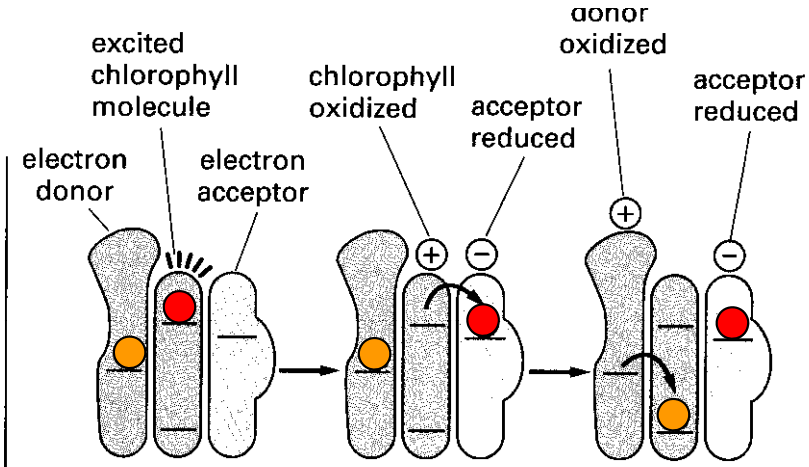

3 decay by successive electron transfers

Strong coupling of chlorophylls in LH leads to delocalized excitations (excitons).

Exciton Migration from Antenna Complexes to Reaction Center

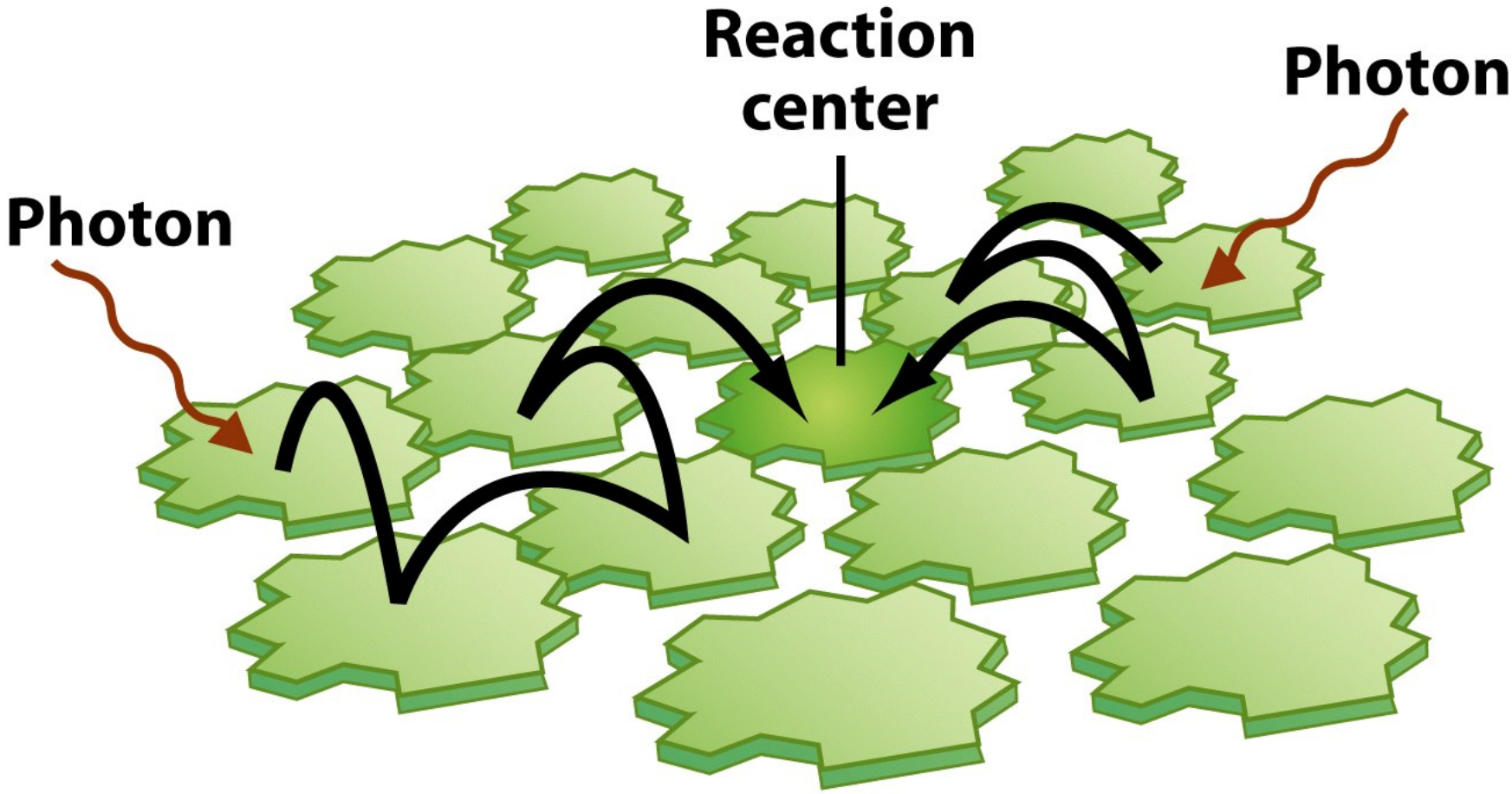

Cascade of Electronic Excitation Transfer in the Bacterial PSU

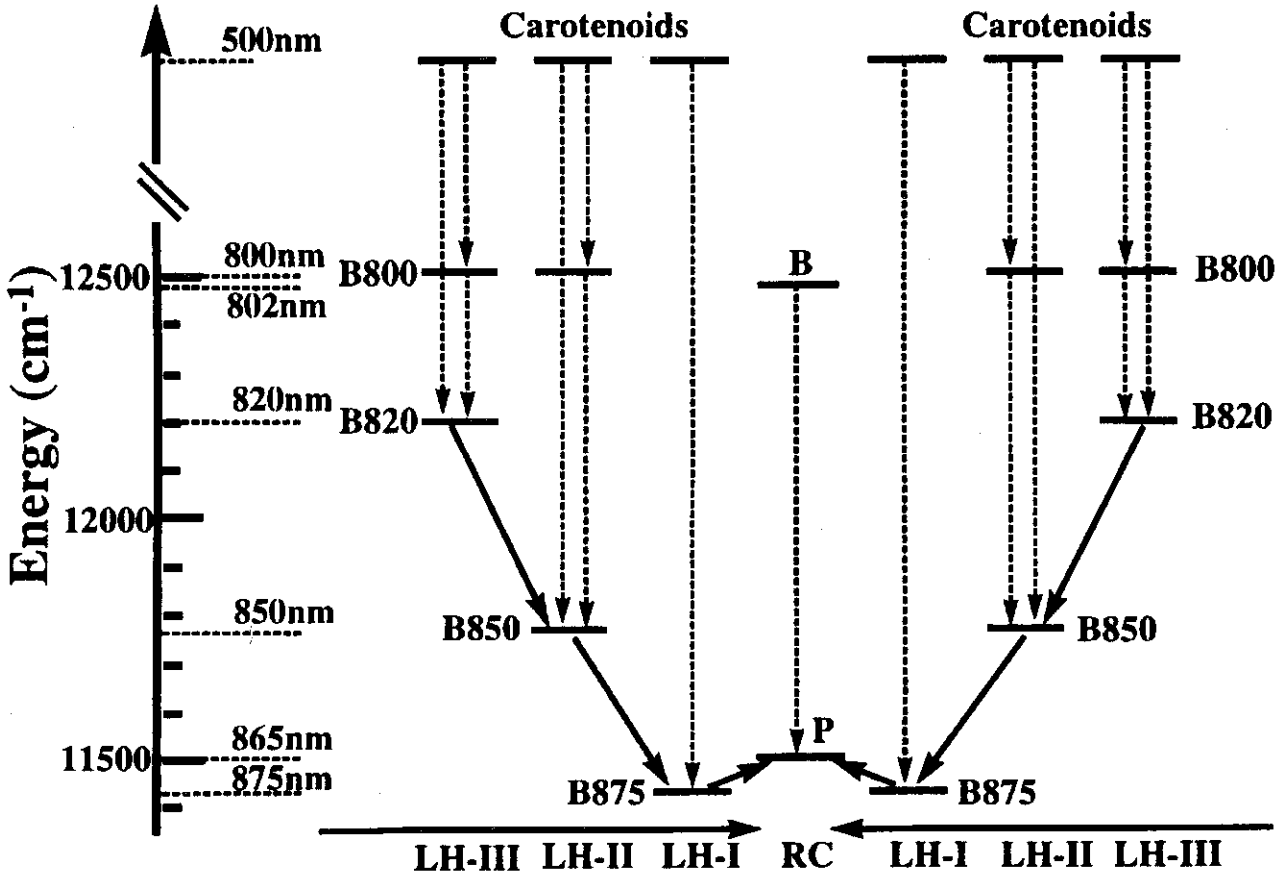

Light Harvesting Complex II of Rhodospirillum (Rs.) molischianum I

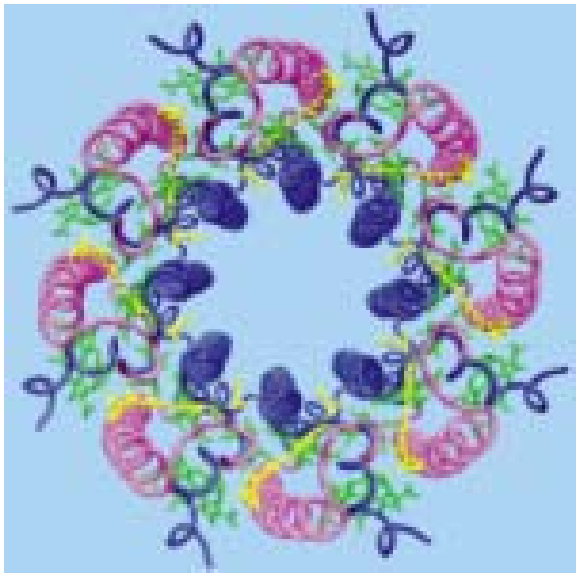

top view

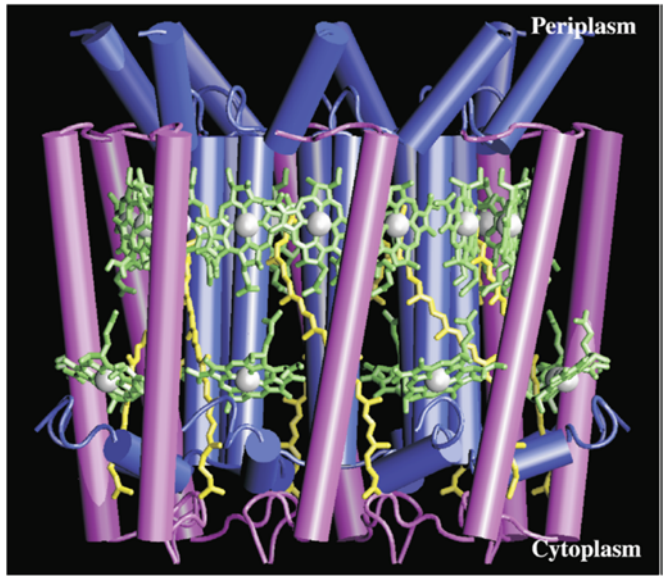

side view

Light Harvesting Complex II of Rs. molischianum II

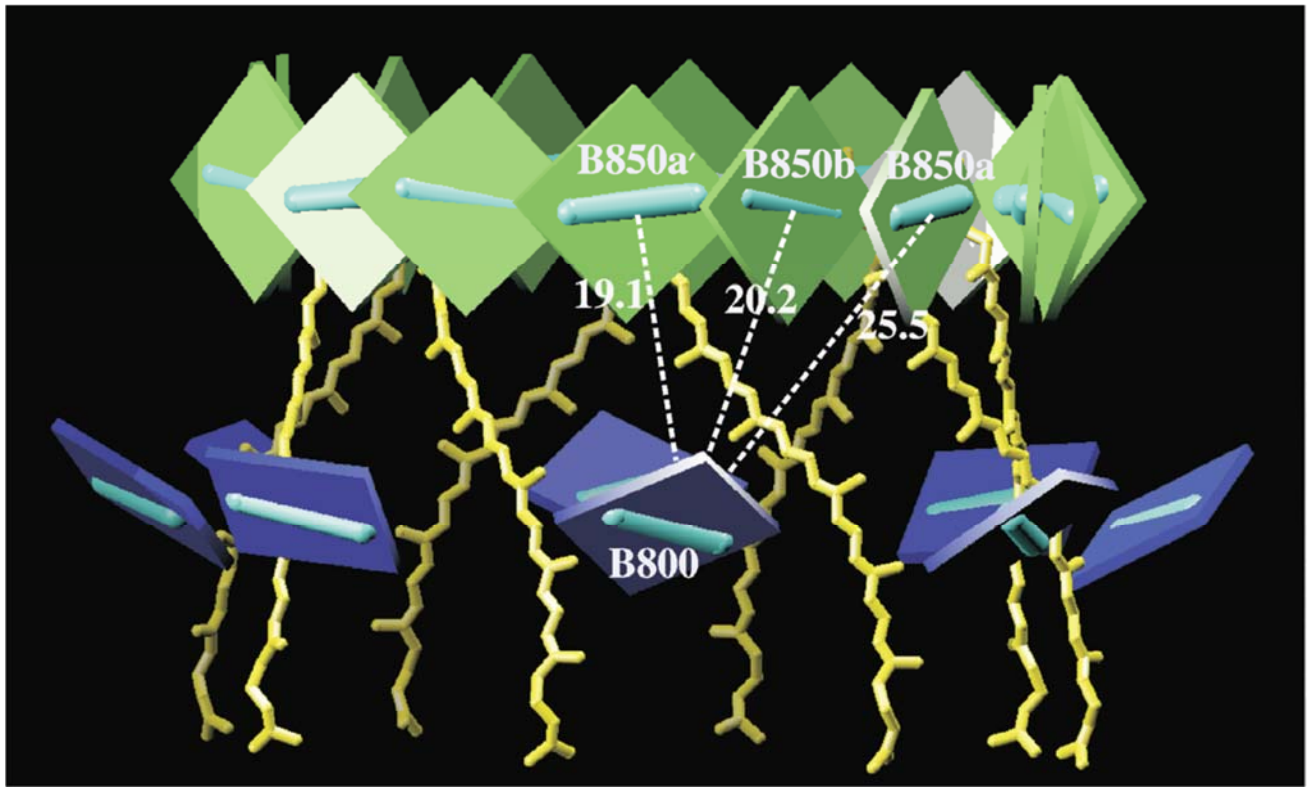

Förster:
Qy (B800)
→
Qy (B850)

Arrangement of chromophores in LH-II of *Rs. molischianum.* Bacteriochlorophylls (BChls) are represented as squares; 16 B850 BChls are arranged in the top ring and 8 B800 BChls in the bottom ring. Carotenoids (lycopenes) are shown in a licorice representation. Bars connected with the BChls represent the Q_y transition dipole moments. Representative distances between central M_g atoms of B800 BChl and B850 BChl are indicated (in Å). The B850 BChls bound to the α-apoprotein and the β-apoprotein are denoted as B850a and B850b, respectively; bacteriochlorophyll B850a' is bound to the (left) neighboring heterodimer.

Hu et al., J. Phys. Chem. B 101 (1997) 3860

Light Harvesting Complex II of Rs. molischianum III

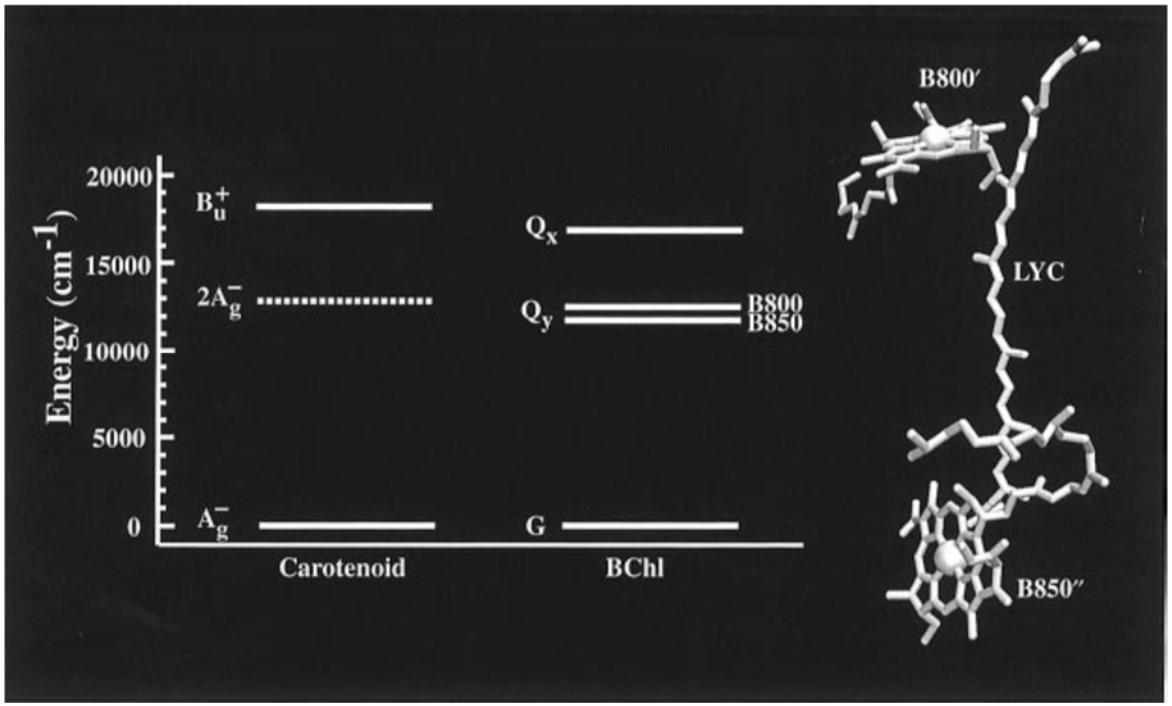

Contacts between B800, B850 BChls and lycopene (LYC) in LH-II as well as the energies of the electronic ground and excited states of the chromophores. Solid lines represent spectroscopically measured energy levels. The dashed line indicates the estimated energy of the $2A_g$ state of lycopene (carotenoid). B850a'' stands for the B850 BChl-a bound to the α-apoprotein of the right-hand side neighboring $\alpha\beta$-heterodimer, and the B800' for the B800 BChl-a bound to the left-hand side neighboring $\alpha\beta$-heterodimer.

Hu et al., J. Phys. Chem. B 101 (1997) 3860

Photosynthetic Reaction Center

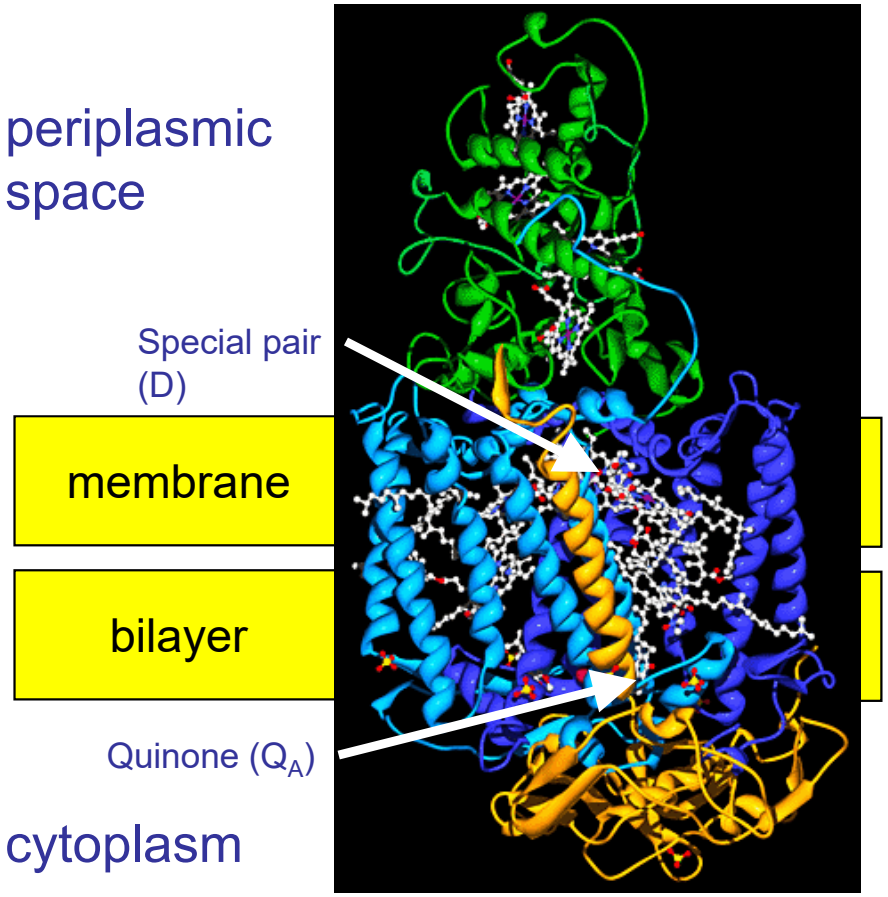

3-D structure of the photosynthetic reaction center from the purple bacterium *Blastochloris viridis*.

The structure consists of four protein subunits, which are represented as ribbons and colored light blue (subunit L), blue (subunit M), brown (subunit H), and green (cytochrome).

Bound within the proteins are molecules that carry out the function of the reaction center; these are represented as ball-and-stick models, with colors white (carbon atoms), blue (nitrogens), red (oxygens), and yellow (sulfurs).

In vivo, the reaction center is located in the cell membrane of the bacterium, with the cytochrome protruding on the outside and the bottom part of the subunit H protruding on the inside.

Arrangement of the RC Cofactors

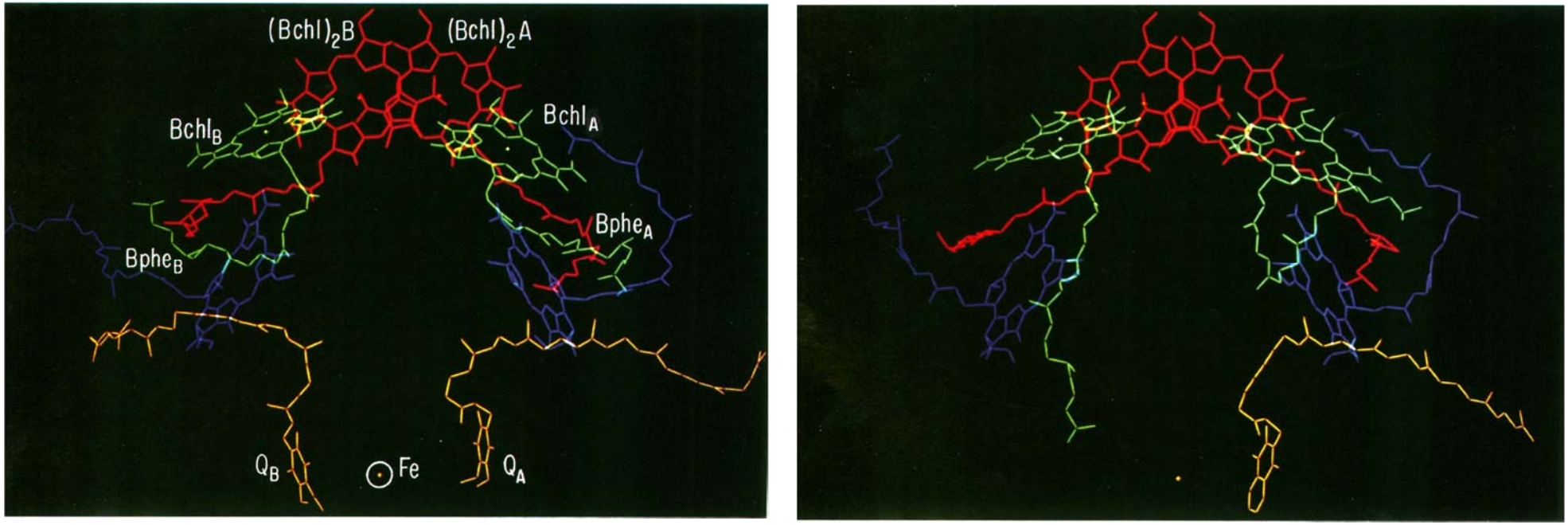

Cofactor structures of the RC from *Rb. sphaeroides* (left) and from *Bl. viridis* (right). The 2-fold symmetry axis is aligned vertically in the plane of the paper. Electron transfer proceeds preferentially along the A branch. The periplasmic side of the membrane is near the top and the cytoplasmic side is near the bottom of the structure.

Allen et al., Proc. Natl. Acad. Sci. USA 84 (1987) 5732

Electron Transfer Pathway I

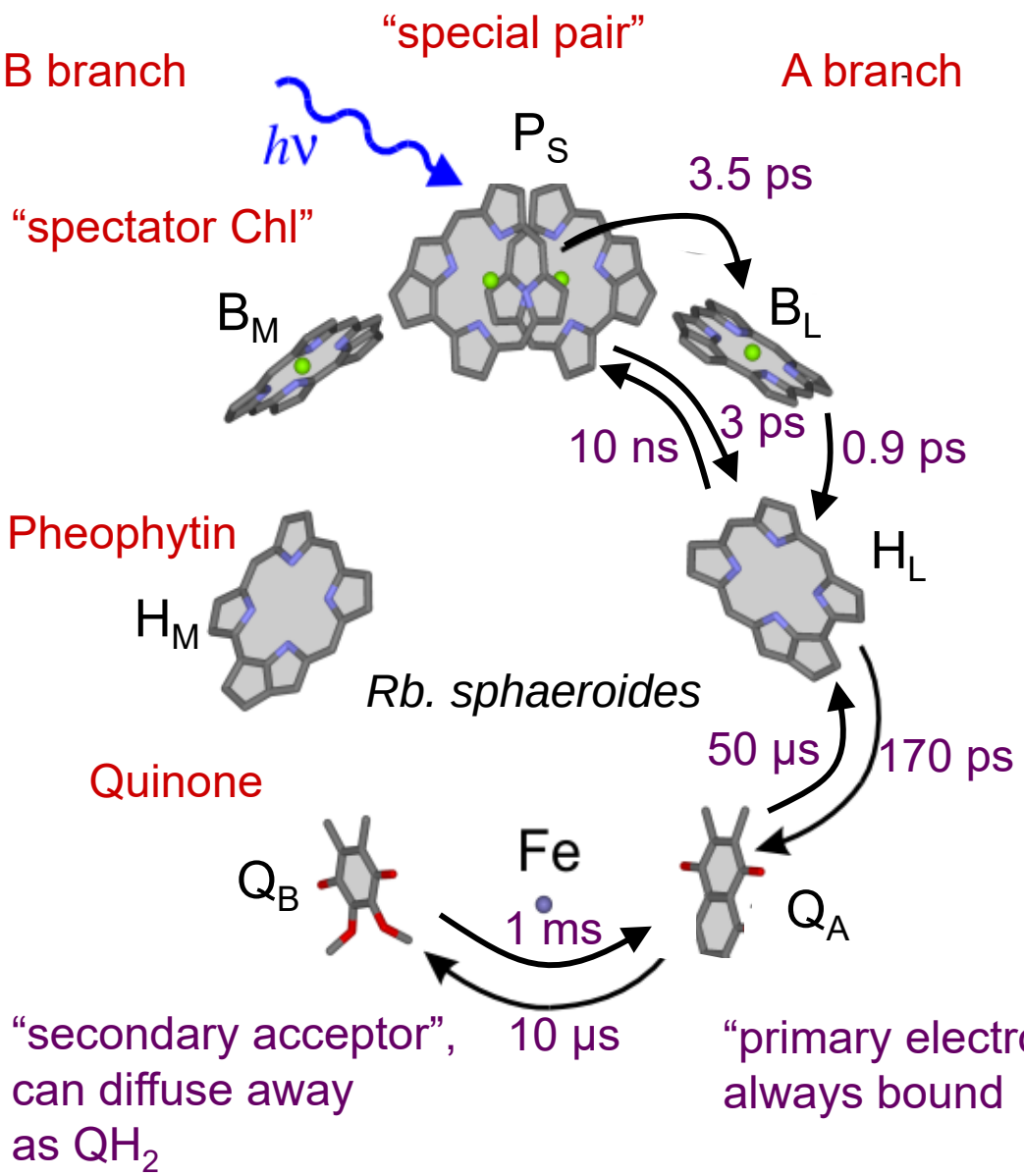

① Photoexcitation leads to electron transfer to Q_B.

② The cycle repeats a second time, and Q_B binds two protons (QH_2) and diffuses into the membrane.

③ A new Q_B binds and the process repeats itself.

Electron Transfer Pathway II

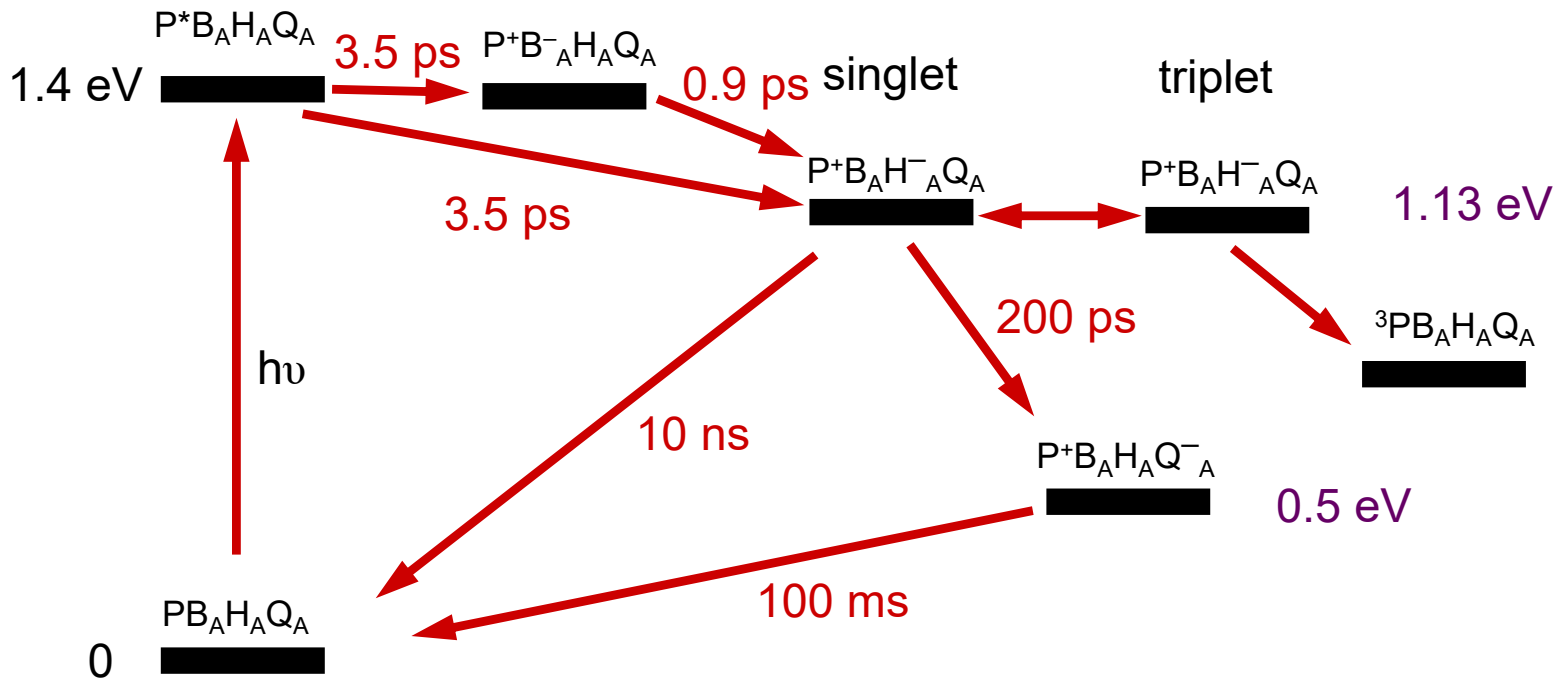

- Back-reactions are 100- to 1000-fold slower than the forward reactions. Therefore, the quantum yield is close to 1.
- The price paid for the high yield is the loss of ~ 2/3 of the free energy.

Energy Conversion in *Blastochloris viridis*

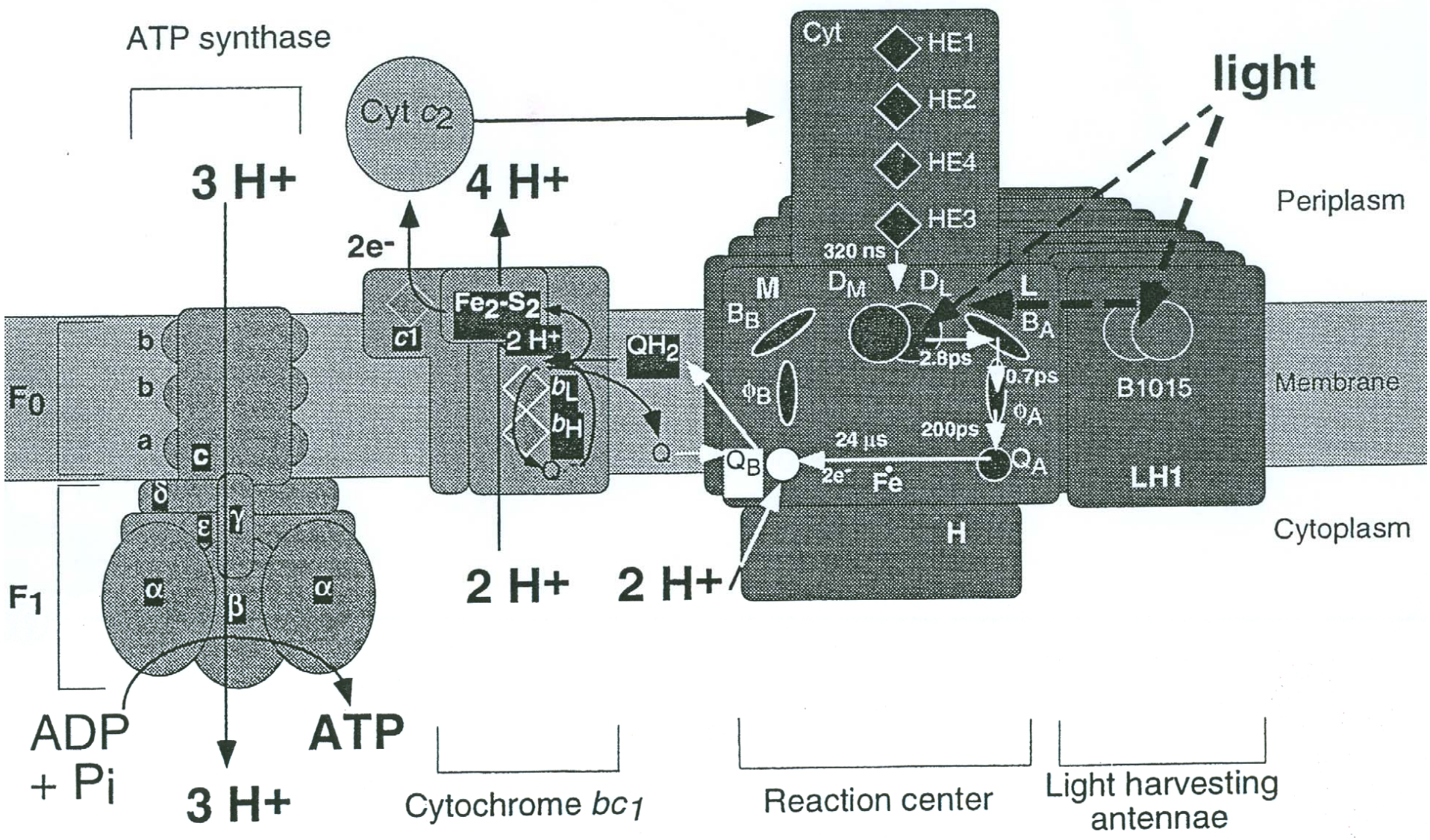

Biophysics II

Energy Storage and Transfer in Photosynthetic Antenna Complexes of Purple Bacteria

Uli Nienhaus

Prof. G. U. Nienhaus, Vorlesungsunterlagen Biophysik II, SS 2023.
Nur zum KIT-internen, vorlesungsbegleitenden Gebrauch.
Weitergabe und anderweitige Nutzung verboten.

Arrangement of Chlorophylls and their Q_y Transition Dipole Moments

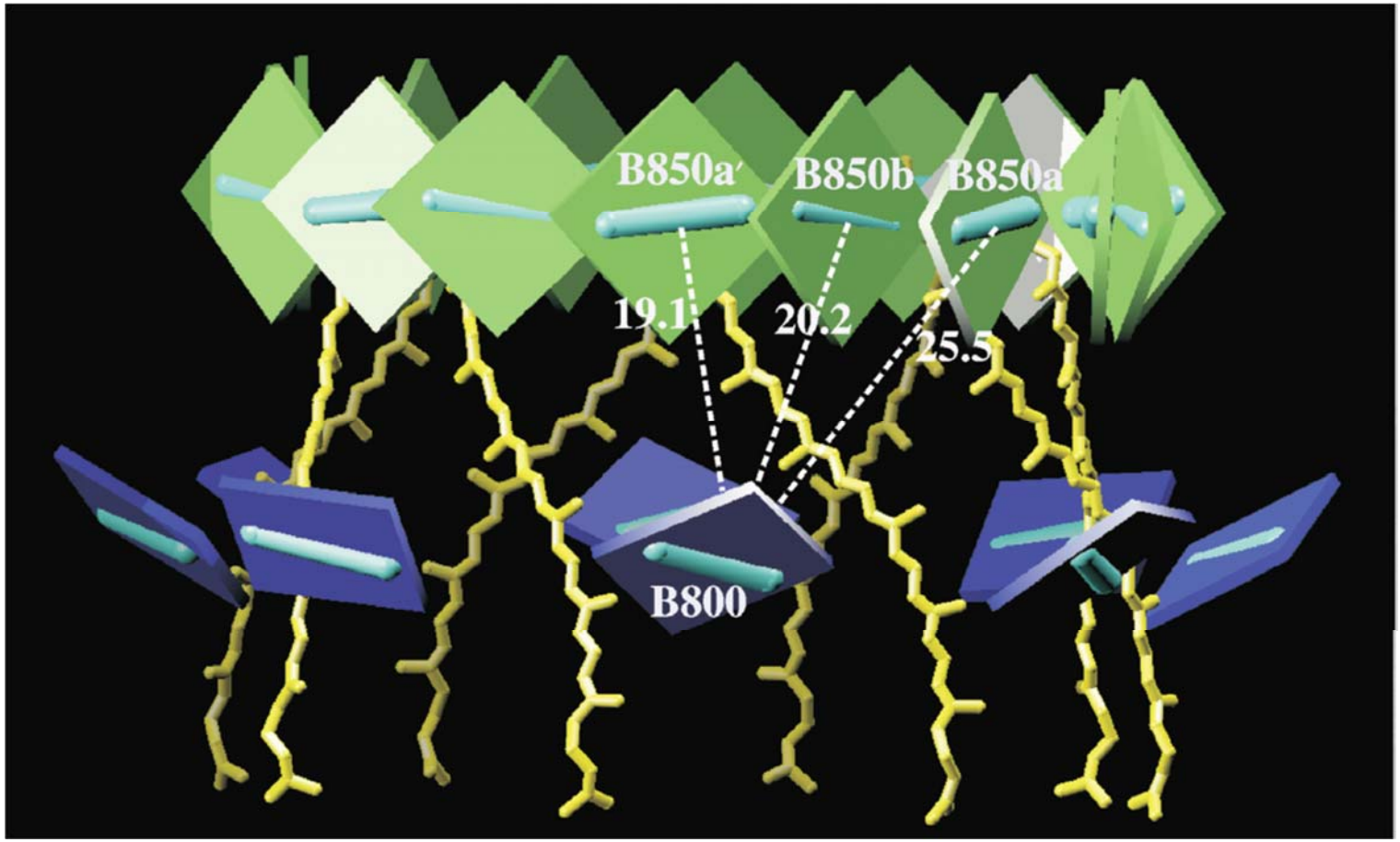

Hu et al., J. Phys. Chem. B 101 (1997) 3854

Energy Spectrum of Antenna Complexes

- In *Rs.* m*olischianum*, the structure of LH-II (LH-I) contains a 16 (32) – membered ring of B850 chlorophylls.

- The closeness of the chromophores suggests that excitations are not localized on individual chromophores, but rather delocalized over multiple chromophores and possibly the entire ring.

- The structure of LH-II (*Rs. molischianum*) is an octamer of dimers. For general reasons, the exciton energy spectrum is expected to show a doublet of octets:

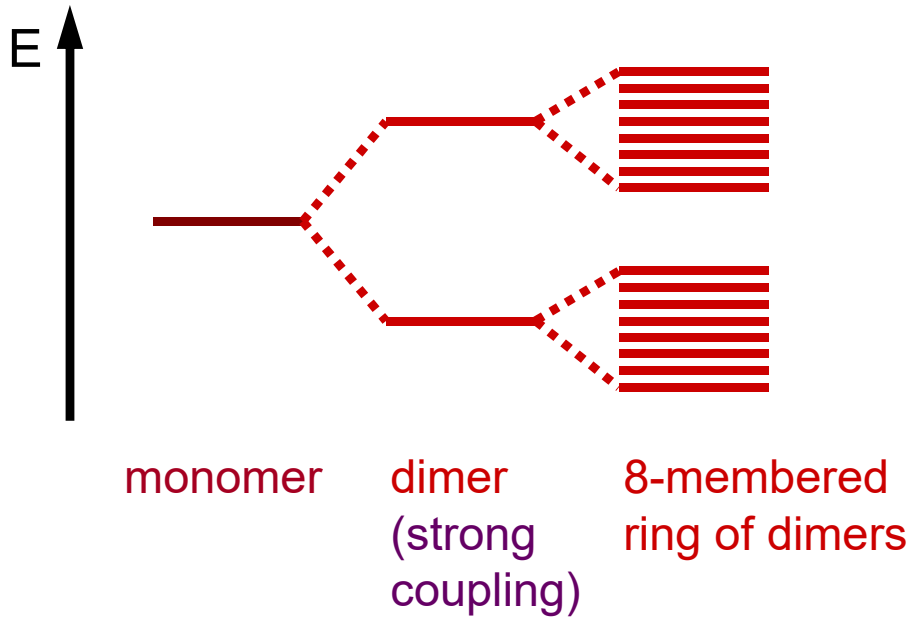

Dimer of Interacting Monomers

- Two energy eigenfunctions:

$$\psi_+ = \frac{1}{\sqrt{2}}(\psi_1 + \psi_2)$$

$$\psi_- = \frac{1}{\sqrt{2}}(\psi_1 - \psi_2)$$

- Positive interaction energies between next neighbors in LH.

- Antiparallel orientation in LH

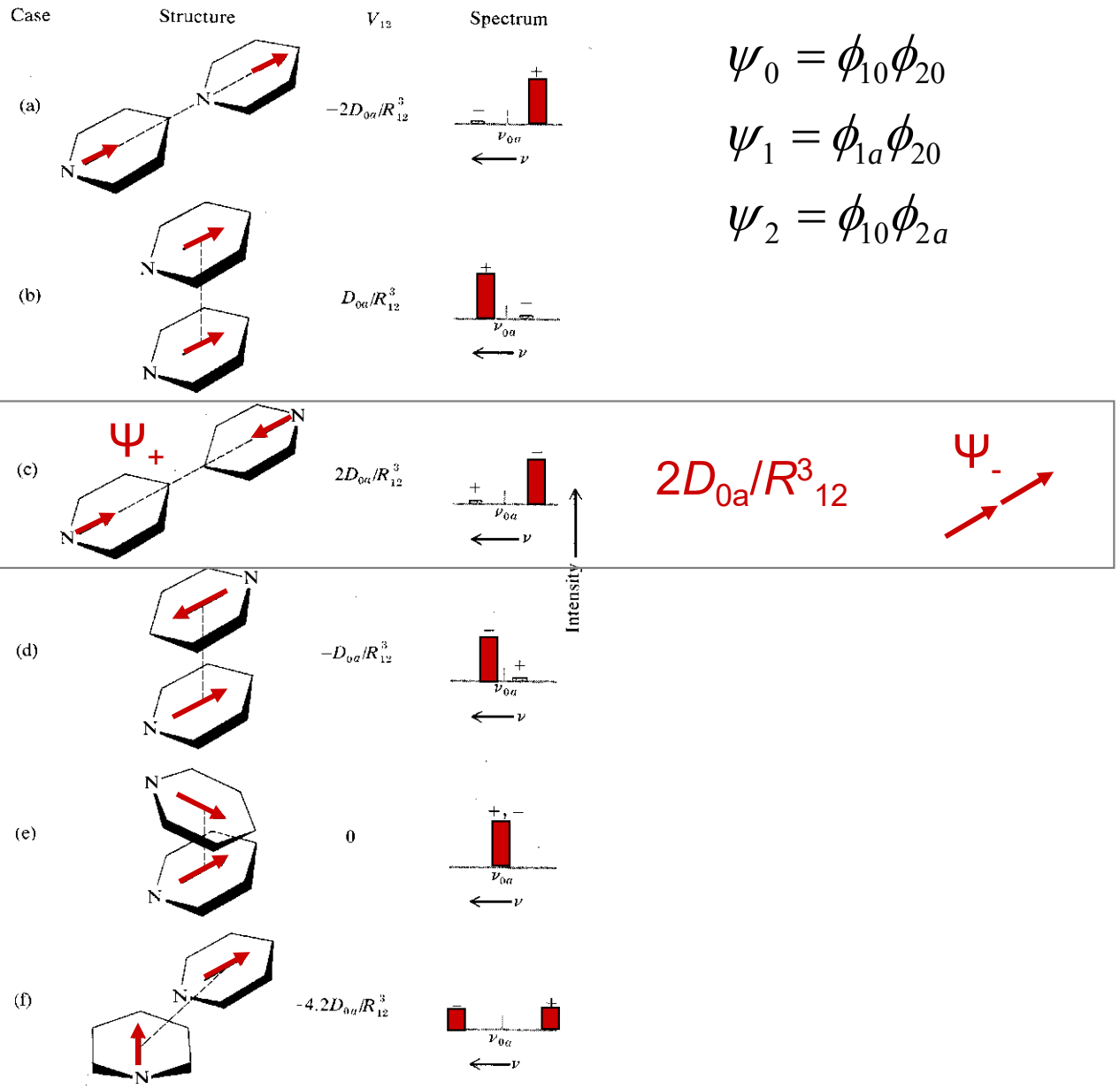

$$\psi_0 = \phi_{10}\phi_{20}$$

$$\psi_1 = \phi_{1a}\phi_{20}$$

$$\psi_2 = \phi_{10}\phi_{2a}$$

Cantor & Schimmel, Vol. II
Page 396

Quantum Mechanical Description I

- The relevant electronic excitations will be described in terms of single BChl Q_y excitations:

$$|\alpha\rangle = \Psi_1(g)\Psi_2(g) \cdots \Psi_{\alpha-1}(g)\Psi_\alpha(\mathbf{Q_y})\Psi_{\alpha+1}(g) \cdots \Psi_{2N}(g) \qquad (1)$$

orthonormal: $\langle\alpha|\alpha'\rangle = \delta_{\alpha,\alpha'}$

- Interactions between chromophores:

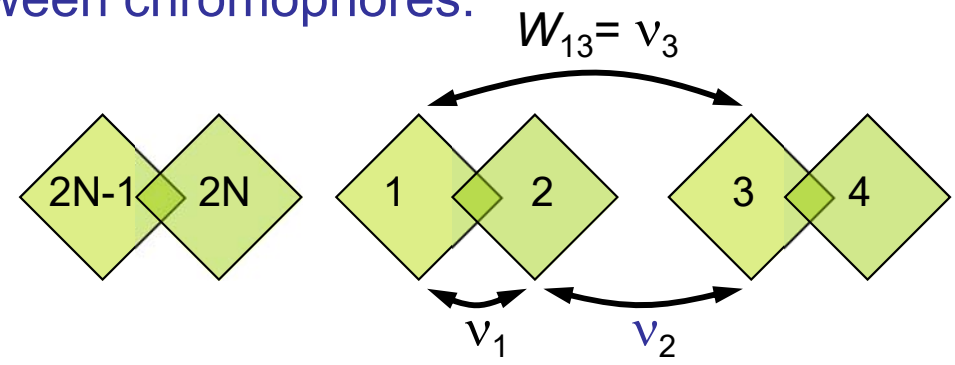

$$W_{12} = W_{21} = W_{j,\,j+1} = W_{j+1,\,j} = \nu_1 \qquad j = 1, 3, 5, 7 \cdots$$

$$W_{23} = W_{32} = W_{j,\,j+1} = W_{j+1,\,j} = \nu_2 \qquad j = 2, 4, 6, 8 \cdots$$

$$W_{13} = W_{31} = W_{j,\,j+2} = W_{j+2,\,j} = \nu_3 \qquad j = 1, 3, 5, 7 \cdots$$

Quantum Mechanical Description II

- all other couplings:

unit vectors!
Magnitude of dipolar strength |D| and dielectric coefficient ε are absorbed in C.

$$W_{jk} = C\left(\frac{\vec{d}_j \vec{d}_k}{r_{jk}^3} - \frac{3\left(\vec{r}_{jk}\cdot\vec{d}_j\right)\left(\vec{r}_{jk}\cdot\vec{d}_k\right)}{r_{jk}^5}\right)$$

$$C = \nu_3\left(\frac{\vec{d}_1\cdot\vec{d}_3}{r_{13}^3} - \frac{3\left(\vec{r}_{13}\cdot\vec{d}_1\right)\left(\vec{r}_{13}\cdot\vec{d}_3\right)}{r_{13}^5}\right)^{-1}$$

- ν_1 = 806 cm^{-1}, ν_2 = 377 cm^{-1}, ν_3 = –152 cm^{-1} are determined from quantum mechanical calculations; the $\vec{r}_{jk}$ are taken from the structure, and ν_3 is used to determine the constant *C*, which is affected by the dipolar strength of Chl and the dielectric coefficient of the protein.

Eigenvalue Problem for LH-II Hamiltonian I

The effective Hamiltonian in the basis (1) (on slide 5) for k = 1, 2,...16 can be written

$$\hat{H} = \begin{pmatrix} \varepsilon & \nu_1 & W_{1,3} & W_{1,4} & \cdots & \cdot & W_{1,2N-1} & \nu_2 \\ \nu_1 & \varepsilon & \nu_2 & W_{2,4} & \cdots & \cdot & W_{2,2N-1} & W_{2,2N} \\ W_{3,1} & \nu_2 & \varepsilon & \nu_1 & \cdots & \cdot & W_{3,2N-1} & W_{3,2N} \\ W_{4,1} & W_{4,2} & \nu_1 & \varepsilon & \cdots & \cdot & \cdot & \cdot \\ \cdot & \cdot & \cdot & \cdot & \cdots & \cdot & \cdot & \cdot \\ \cdot & \cdot & \cdot & \cdot & \cdots & \cdot & \cdot & \cdot \\ \cdot & \cdot & \cdot & \cdot & \cdots & \cdot & \cdot & \cdot \\ \cdot & \cdot & \cdot & \cdot & \cdots & \varepsilon & \nu_2 & W_{2N-2,2N} \\ \cdot & \cdot & \cdot & \cdot & \cdots & \nu_2 & \varepsilon & \nu_1 \\ \nu_2 & \cdot & \cdot & \cdot & \cdots & W_{2N,2N-2} & \nu_1 & \varepsilon \end{pmatrix} . \quad (2)$$

For the B850 system of LH-II, the 16-dimensional Hamiltonian (2) can be written in a form that reflects the dimeric structure of the chlorophyll aggregate with C_8 symmetry

$$\hat{H} = \begin{pmatrix} \hat{H}_{11} & \hat{H}_{12} & \cdots & \hat{H}_{18} \\ \hat{H}_{21} & \hat{H}_{22} & \cdots & \hat{H}_{28} \\ \cdot & \cdot & \cdots & \cdot \\ \cdot & \cdot & \cdots & \cdot \\ \cdot & \cdot & \cdots & \cdot \\ \cdot & \cdot & \cdots & \cdot \\ \cdot & \cdot & \cdots & \cdot \\ \hat{H}_{81} & \hat{H}_{82} & \cdots & \hat{H}_{88} \end{pmatrix} . \quad (3)$$

Eigenvalue Problem for LH-II Hamiltonian II

In (3), the $\hat{H}_{jk}$ are actually 2 × 2 matrices which can be identified through comparison with (2). One can readily verify, for example,

$$\hat{H}_{11} = \begin{pmatrix} \varepsilon & \nu_1 \\ \nu_1 & \varepsilon \end{pmatrix}, \quad \hat{H}_{12} = \begin{pmatrix} W_{13} & W_{14} \\ \nu_2 & W_{24} \end{pmatrix} \quad .$$

The C_8 symmetry of the chlorophyll aggregate implies the symmetry property

$$\hat{H}_{jk} = \hat{H}_{j+m,k+m}\,, \quad m = 1, 2, \ldots 8\,. \qquad (4)$$

Note: $W_{ij} = W_{ji}$ (symmetric coupling)
$\Rightarrow$ $\hat{H}_{ij} = \hat{H}_{ji}^{+}$ (transpose)

Eigenvalue Problem for LH-II Hamiltonian III

- Because of cyclic boundary conditions ($\Psi(s) = \Psi(s + M \cdot L)$, s = coordinate on the circle, L circumference, M integer), the eigenvectors of Hamiltonian (3) can be written:

$$|n,\beta\rangle = \frac{1}{\sqrt{N}} \sum_{k=1}^{N} \exp\left(2\pi i n \frac{k}{N}\right) |k,\beta\rangle$$

- k: cyclic label (1, 2….N, 1, 2….N, 1, 2..)
- N = 8 for LH-II
- 2D vector representing state of dimer, (ψ_-:β = 1; ψ_+: β = 2).

with $|k,\beta\rangle^+ = (0 \cdots 1 \cdots 0) v^+_{k\beta}$

orthonormal — k^{th} dimer position

$$|n,\beta\rangle = \frac{1}{\sqrt{8}} e^{2\pi i n \frac{1}{8}} \begin{pmatrix} 1 \\ 0 \\ 0 \\ \vdots \\ 0 \end{pmatrix} v_{1\beta} + \frac{1}{\sqrt{8}} e^{2\pi i n \frac{2}{8}} \begin{pmatrix} 0 \\ 1 \\ 0 \\ \vdots \\ 0 \end{pmatrix} v_{2\beta} + \frac{1}{\sqrt{8}} e^{2\pi i n \frac{3}{8}} \begin{pmatrix} 0 \\ 0 \\ 1 \\ \vdots \\ 0 \end{pmatrix} v_{3\beta} \quad \ldots \quad = \frac{1}{\sqrt{8}} \begin{pmatrix} e^{2\pi i n \frac{1}{8}} v_{1\beta} \\ e^{2\pi i n \frac{2}{8}} v_{2\beta} \\ e^{2\pi i n \frac{3}{8}} v_{3\beta} \\ \vdots \\ e^{2\pi i n \frac{8}{8}} v_{8\beta} \end{pmatrix}$$

(N = 8)

- Eigenvalue problem

$$\hat{H} |n,\beta\rangle = E_{n,\beta} |n,\beta\rangle$$

Eigenvalue Problem for LH-II Hamiltonian IV

- Eigenvalue problem (N = 8)

$$\begin{pmatrix} \hat{H}_{11} & \hat{H}_{12} & \hat{H}_{13} & \cdots & \hat{H}_{18} \\ \hat{H}_{21} & \hat{H}_{22} & & & \\ \hat{H}_{31} & & \ddots & & \vdots \\ \vdots & & & \ddots & \\ \hat{H}_{81} & & \cdots & & \hat{H}_{11} \end{pmatrix} \begin{pmatrix} e^{2\pi i n\frac{1}{8}} v_{1\beta} \\ e^{2\pi i n\frac{2}{8}} v_{2\beta} \\ e^{2\pi i n\frac{3}{8}} v_{3\beta} \\ \vdots \\ e^{2\pi i n\frac{8}{8}} v_{8\beta} \end{pmatrix} = E_{n,\beta} \begin{pmatrix} e^{2\pi i n\frac{1}{8}} v_{1\beta} \\ e^{2\pi i n\frac{2}{8}} v_{2\beta} \\ e^{2\pi i n\frac{3}{8}} v_{3\beta} \\ \vdots \\ e^{2\pi i n\frac{8}{8}} v_{8\beta} \end{pmatrix}$$

$$\hat{H}_{j1}\left(e^{2\pi i n\frac{1}{N}} v_{1\beta}\right) + \hat{H}_{j2}\left(e^{2\pi i n\frac{2}{N}} v_{2\beta}\right) + \cdots = E_{n,\beta}\left(e^{2\pi i n\frac{j}{N}} v_{1\beta}\right) \qquad \text{all } v_{k\beta} \text{ equal: } \quad v_{k\beta} = v_{n\beta}$$

$$\sum_{k=1}^{N} \hat{H}_{jk}\left(e^{2\pi i n\frac{(k-j)}{N}}\right) \cancel{e^{2\pi i n\frac{j}{N}}} v_{n\beta} = E_{n\beta} \cancel{e^{2\pi i n\frac{j}{N}}} v_{n\beta}$$

- From the symmetry property (4) (on slide 8) one can see that

$$\hat{h}_n = \sum_{k=1}^{N} \hat{H}_{jk}\left(e^{2\pi i n\frac{(k-j)}{N}}\right)$$

does not depend on *j*, so that

$$\hat{h}_n v_{n\beta} = E_{n\beta}\, v_{n\beta}.$$

- From this equation, the spectrum can be calculated.

Exciton Energy Spectrum

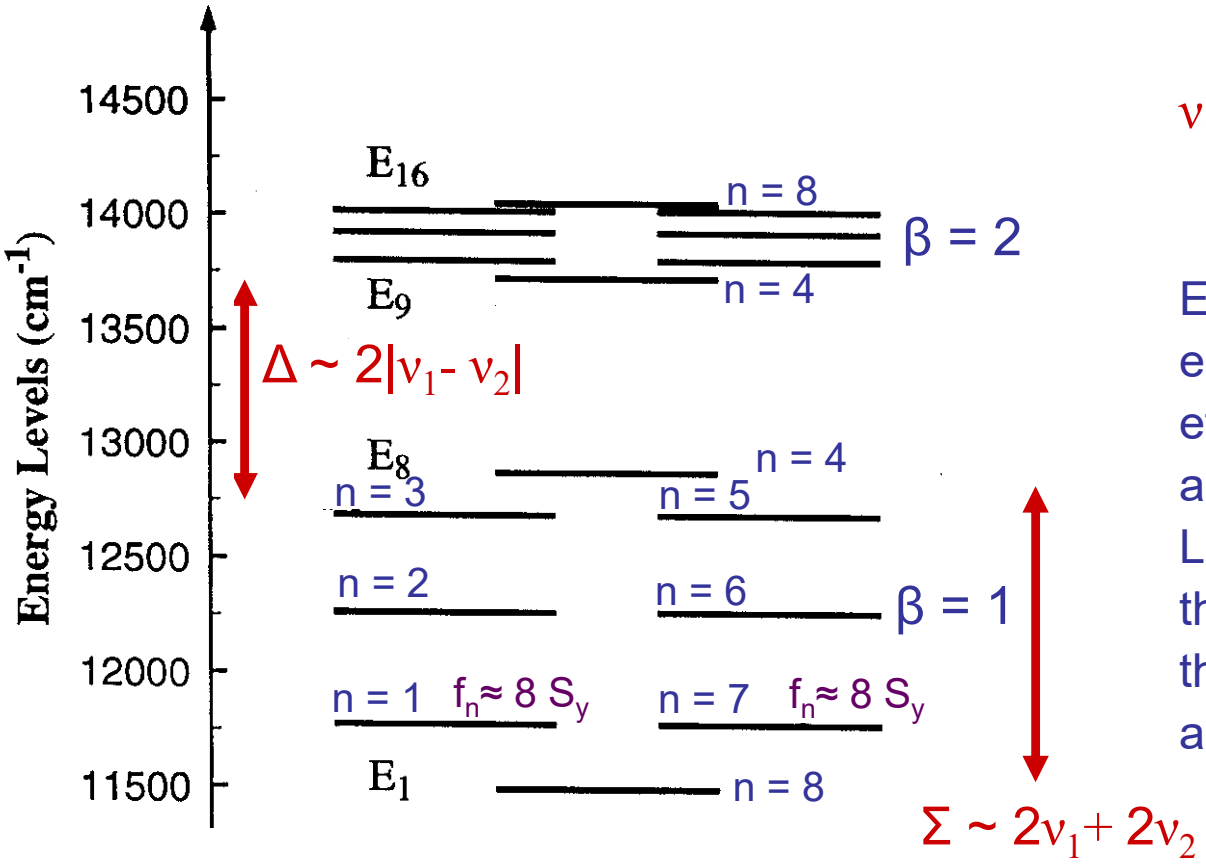

$\nu_1 > 0, \quad \nu_2 > 0, \quad \nu_1 > \nu_2$

Energies associated with the eigenstates (exciton states) of the effective Hamiltonian describing the aggregate of B850 chlorophylls in LH-II. The ε value was chosen such that the energies E_2, E_3 coincide with the spectral maximum of the circular aggregate at 850 nm (11765 cm^{-1}).

Oscillator strength f_n is close to zero everywhere except for the degenerate pair E_2/E_3 .

Properties of Exciton States

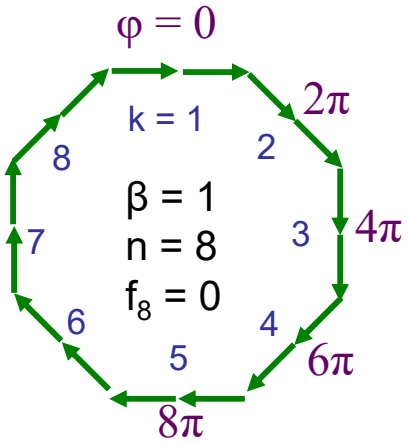

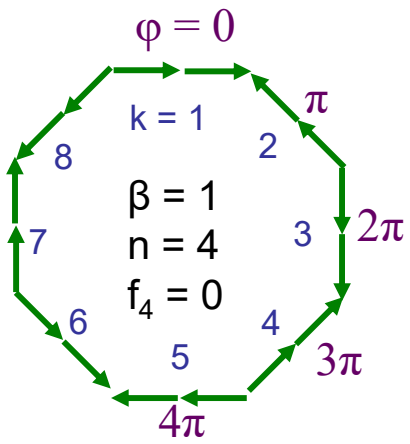

n = 8, lowest excited state, carries no oscillator strength;
n = 4, highest exciton state for for β = 1 ($\rightarrow\rightarrow$ in dimer).

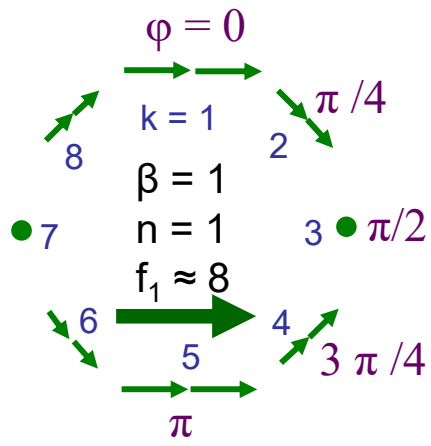

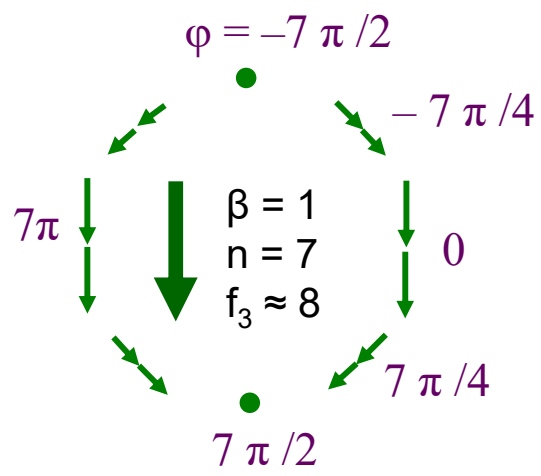

n = 1 and n = 7 carry all the oscillator strength!

The upper octet has β = 2 ($\leftarrow\rightarrow$ in dimer), and all states have vanishing oscillator strengths (β = 2, n = 8 has f ~ 0.25, all others much less)!

The lowest exciton state cannot radiate and thus is an efficient energy storage device!

Pigment Organization in the Bacterial Photosynthetic Membrane

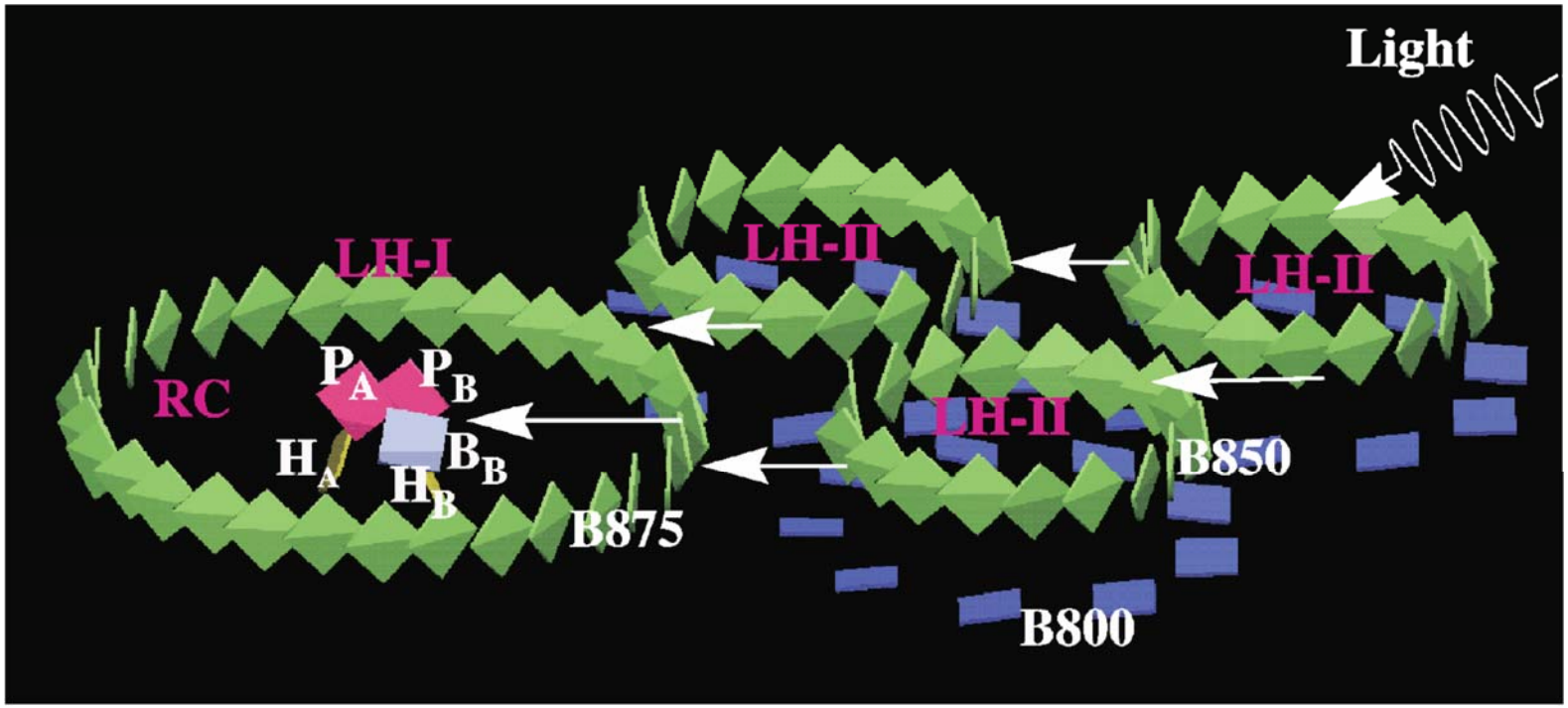

Excitation Transfer LH-II → LH-II I

- A two-ring LH-II system can be described by a Hamiltonian matrix of dimension 32:

$$\hat{H} = \begin{pmatrix} \hat{R}_{11} & \hat{R}_{12} \\ \hat{R}_{21} & \hat{R}_{22} \end{pmatrix}$$

$\hat{R}_{11}$ and $\hat{R}_{22}$ represent couplings within rings 1 and 2, and $\hat{R}_{12}(i,j) = W_{ij}$, where *i* = 1...16 is the index on ring 1, and *j* on ring 2, describes the coupling between rings 1 and 2; $\hat{R}_{12} = \hat{R}_{21}{}^{+}$.

- The problem becomes much simpler if we only consider the lowest exciton state of ring 1, $|w^1{}_1\rangle$, and ring 2, $|w^2{}_1\rangle$. The dynamics of the two-state system is then governed by the Hamiltonian

$$H^{1} = \begin{pmatrix} < w_1^1 \mid \hat{H} \mid w_1^1 > & < w_1^2 \mid \hat{H} \mid w_1^1 > \\ < w_1^1 \mid \hat{H} \mid w_1^2 > & < w_1^2 \mid \hat{H} \mid w_1^2 > \end{pmatrix} = \begin{pmatrix} E_0 & A \\ A & E_0 \end{pmatrix}$$

symmetry !

Excitation Transfer LH-II → LH-II II

The wave function is given by $\psi = c_1(t)\,|\,w_1^1\rangle + c_2(t)\,|\,w_1^2\rangle,$

and the time evolution is given by

$$i\hbar\frac{\partial c_1}{\partial t} = E_0\,c_1 + A\,c_2$$

$$i\hbar\frac{\partial c_2}{\partial t} = A\,c_1 + E_0 c_2$$

with initial conditions: $c_1\,(0) = 1,\ c_2\,(0) = 0.$

Solution (Feynman III – Ch. 8):

F. Hund, Z. Phys. 43 (1927) 805

$$c_1(t) = \exp\left[-\frac{i}{\hbar}E_o\,t\right]\cos\frac{At}{\hbar}$$

$$c_2(t) = -i\exp\left[-\frac{i}{\hbar}E_o\,t\right]\sin\frac{At}{\hbar}$$

Excitation Transfer LH-II → LH-II III

- probability to find excitation on ring 2 if it is on ring 1 at $t = 0$:

$$|c_2|^2 = \sin^2 \frac{\langle w_1^2 \mid \hat{H} \mid w_1^1 \rangle}{\hbar} t$$

- calculation yields $\langle w_1^2 \mid \hat{H} \mid w_1^1 \rangle = 2.33\ \mathrm{cm}^{-1} \quad \Rightarrow \quad \tau = 7\ \mathrm{ps}$

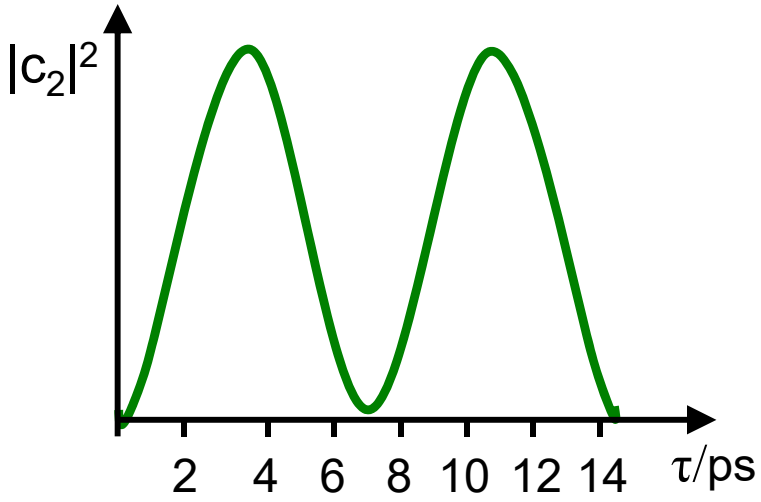

Energy Transfer LH-II → LH-I

- Calculation similar to the one sketched before, just that the Hamiltonian matrix now has a dimension 16 + 32 = 48.

- A simplified treatment is again possible. The lowest exciton level of LH-II is close to E_2/E_3 of LH-I, which are thus expected to be the energy-accepting states.

  Matrix element $\langle w_1^1 | \hat{H} | w_2^2 \rangle \approx 5 \text{ cm}^{-1}$

  $\Rightarrow$ τ = 3.3 ps , in agreement with experimental observations.

Energy Transfer LH-I → RC I

The simplest model takes into account the lowest energy exciton state $|1\rangle$ of LH-I and the dimer states Q_y of the special pair, $|2\rangle$ and $|3\rangle$:

$$\hat{H}_1 = \begin{pmatrix} \varepsilon_1 & \nu_{12} & \nu_{13} \\ \nu_{12} & \varepsilon_2 & \nu_{sp} \\ \nu_{13} & \nu_{sp} & \varepsilon_2 \end{pmatrix}$$

ε_1 = 11,335 cm^{-1}
ε_2 = 12,560 cm^{-1}
ν_{sp} = 1,000 cm^{-1} ?!
ν_{12} = 0.46 cm^{-1}
ν_{13} = 0.50 cm^{-1}

$\varepsilon_2 - \nu_{sp}$ = 11,560 cm^{-1} (865 nm)

} ~symmetric LH-I RC complex

With this Hamiltonian, the coupling of $|1\rangle$ to the lower energy dimer state is 0.028 cm^{-1} ⇒
τ = 595 ps in the case of perfect resonance.
However, the observed transfer time is $\tau \approx 35$ ps.

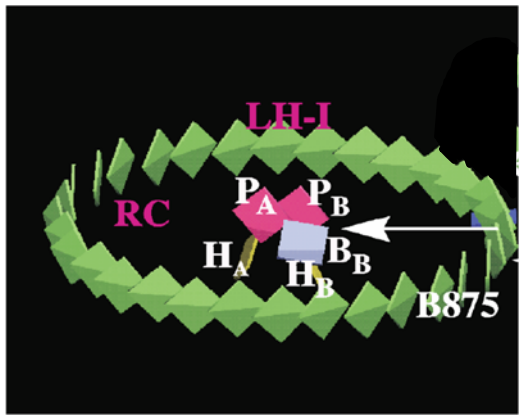

Energy Transfer LH-I → RC II

- Conclusion: simple model is insufficient. Taking the accessory chlorophylls also into the model,

Q_y states |4> and |5>

$$\hat{H}_2 = \left(\begin{array}{ccc:cc} \varepsilon_1 & \nu_{12} & \nu_{13} & \nu_{14} & \nu_{15} \\ \nu_{12} & \varepsilon_2 & \nu_{sp} & W_{24} & W_{25} \\ \nu_{13} & \nu_{sp} & \varepsilon_2 & W_{34} & W_{35} \\ \hdashline \nu_{14} & W_{24} & W_{34} & \varepsilon_3 & W_{45} \\ \nu_{15} & W_{25} & W_{35} & W_{45} & \varepsilon_3 \end{array}\right)$$

which yields a transfer time $\tau \approx 65$ ps. Consequently, the accessory chlorophylls are important for the energy transfer LH-I → RC .

Energy Transfer Processes

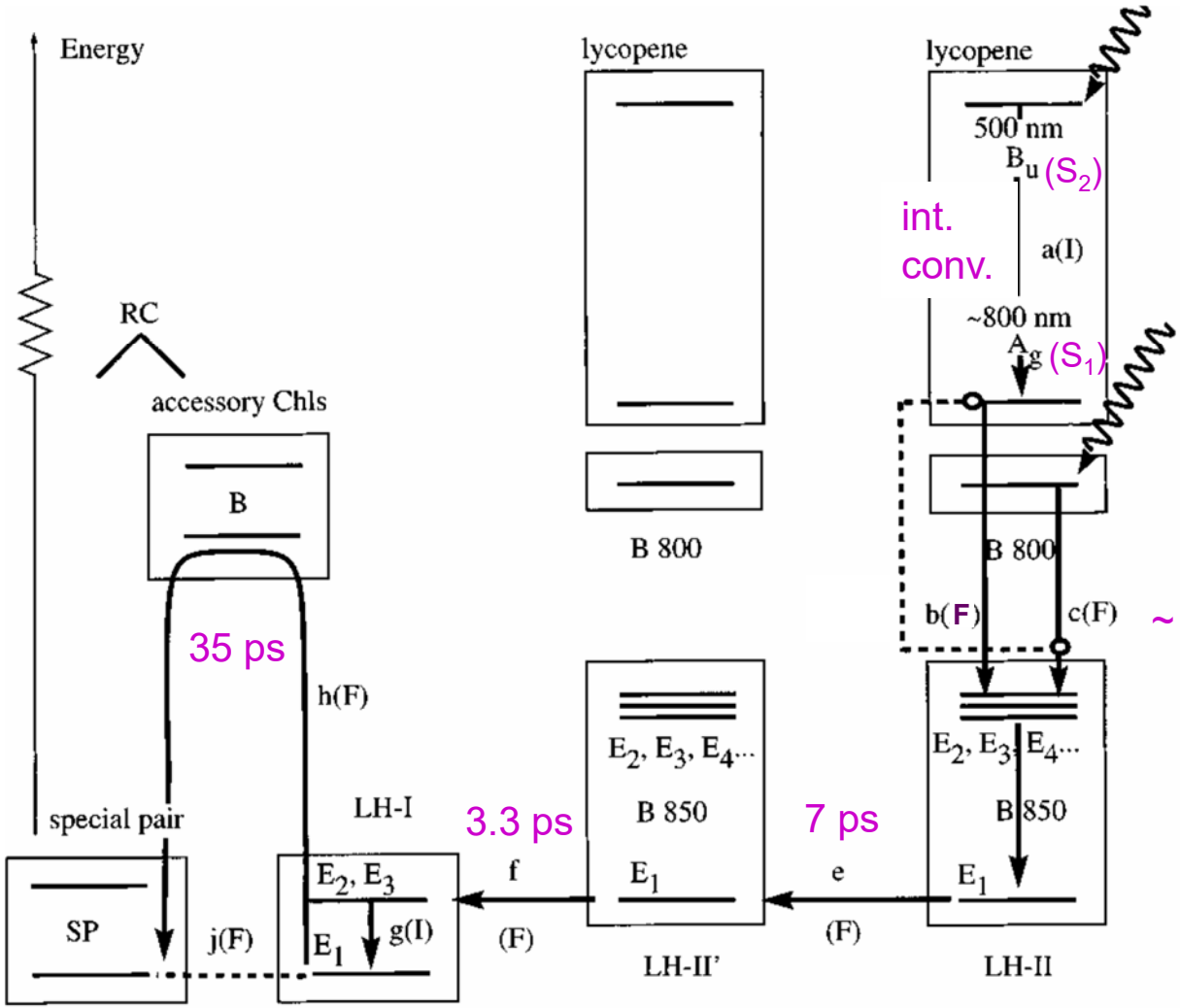

Hu et al., J. Phys. Chem. B 101 (1997) 3854-3871

Biophysics II

Electron Transfer in Biology

Uli Nienhaus

Prof. G. U. Nienhaus, Vorlesungsunterlagen Biophysik II, SS 2023.
Nur zum KIT-internen, vorlesungsbegleitenden Gebrauch.
Weitergabe und anderweitige Nutzung verboten.

Electron Transfer in Biology – Theory and Experiment

- Electron transfer plays a crucial role in energy transduction in biological systems. Both photosynthesis and respiration are based on the principle of vectorial transport of electrons and protons across a membrane.

- Here, our goal is to understand which physical parameters govern the electron transfer process.

- With this knowledge, can we design better biological devices, or is, for example, the photosynthetic reaction center the “ultimate exciton-separating machine” ?

- More specifically, can we understand
  - why the ‘B’ branch in RCs is not used?
  - why does Mother Nature take more than one redox pair to span the membrane?
  - what makes the forward rates in RCs so much faster than the backward rates, leading to QY ≈ 1?

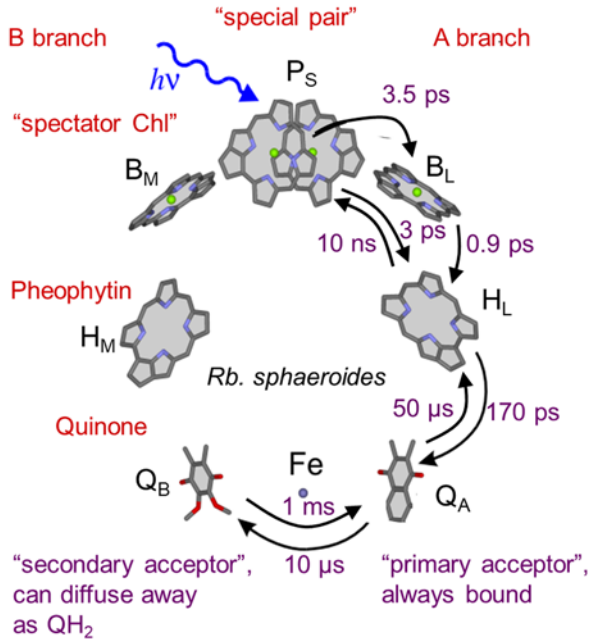

Classical (Marcus) ET Theory I

- The classical version of electron transfer theory was developed by Rudy Marcus (Nobel Prize 1992) in the 1950s/1960s. It deals primarily with ET between ion-ion pairs in solution and ion-electrode interactions, but is readily adapted to intramolecular ET in biological complexes with fixed donor-acceptor displacements.

- Marcus started with the concept of an encounter complex D··A with weak donor-acceptor interactions (otherwise the observed reaction rates should have been much faster). Marcus developed a theory that incorporates the ideas of energy conservation and the Franck-Condon principle (introduced to this problem earlier by Libby). FC principle: “sudden” change of electronic configuration without change of nuclear coordinates.

Classical (Marcus) ET Theory II

Electron Transfer in Solution

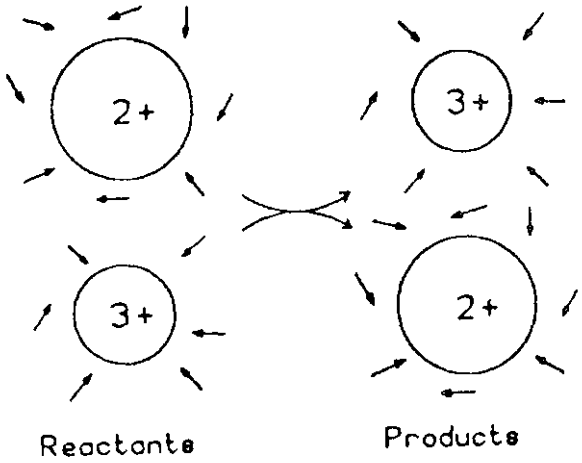

$$Fe^{2+} + Fe^{*3+} \rightarrow Fe^{3+} + Fe^{*2+} \quad (1)$$

Typical nuclear configurations of the reactants, products, and surrounding solvent molecules in Reaction 1. The longer M-OH_2 bond length in the 2+ state is indicated schematically by the larger ionic radius.

Potential Energy Surfaces, Profile

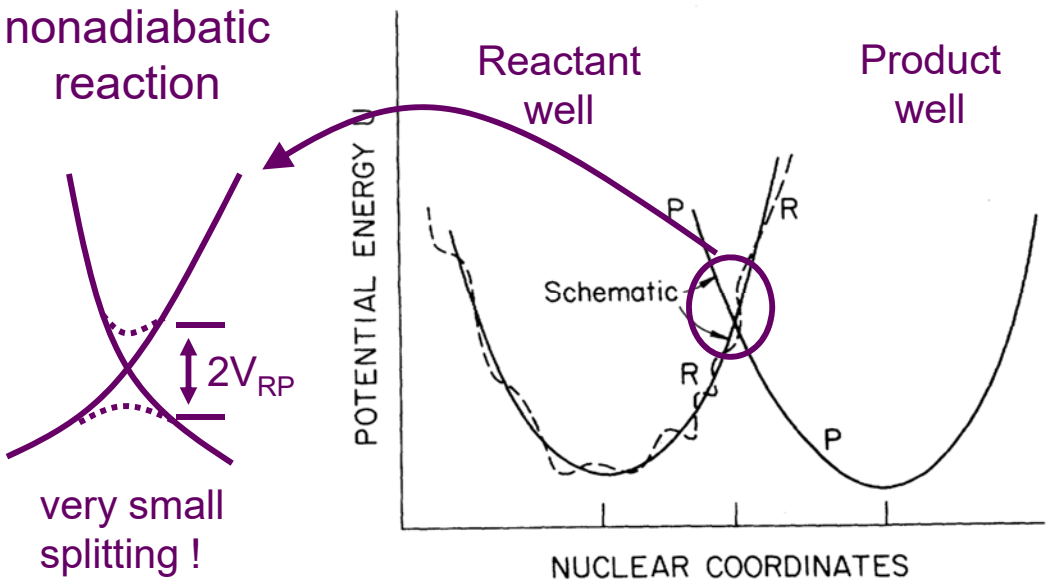

Profile of potential energy surfaces for reactants plus environment, R, and for products plus environment, P. Solid curves: schematic. Dashed curve: schematic but somewhat more realistic.

R. A. Marcus, Rev. Mod. Phys., 65 (1993) 599.

Classical (Marcus) ET Theory III

- the electronic system is represented by two wells (1) and (2). The finite size of the barrier gives rise to a coupling that enables the transition to occur.

- the system fluctuates into the region where the levels cross. There, it can switch to the product curve (energy conservation!) and relax to the bottom of the product well.

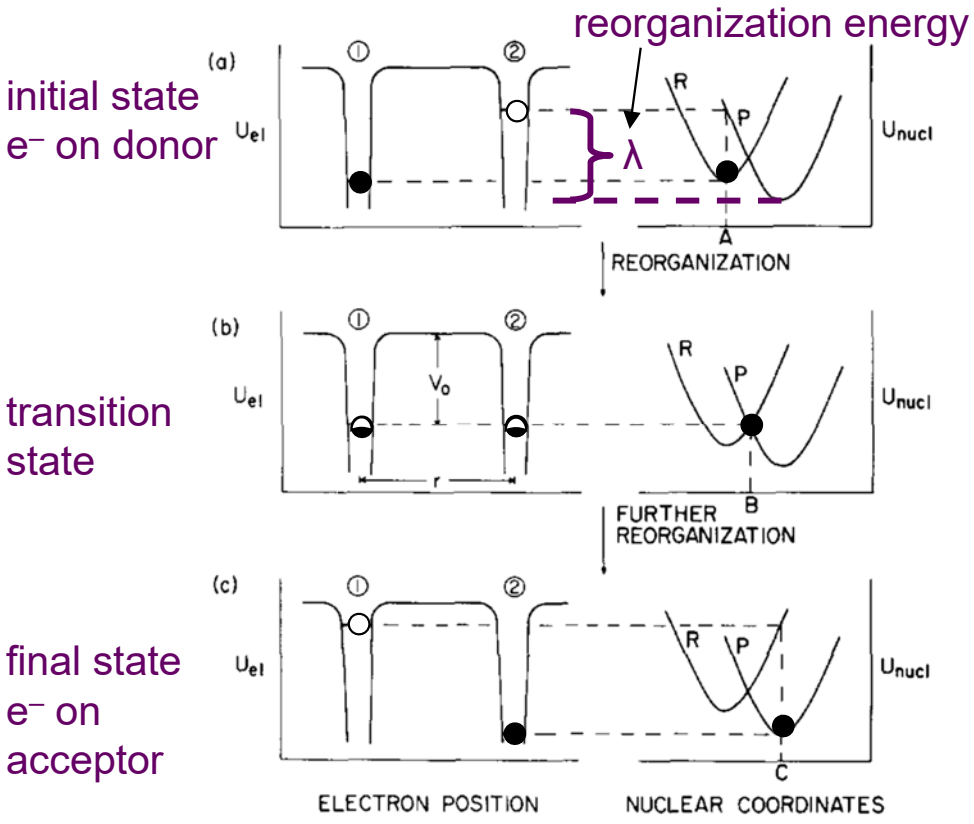

Electronic potential-energy curves (left) and corresponding (nuclear) potential-energy curves (right). Electronic energies in the two wells are indicated on the left for three nuclear configurations A, B, and C for the reaction $red_1 + ox_2 \rightarrow ox_1 + red_2$. The levels in the well are vertical ionization energies: the filled and open circles denote, respectively, ionization of the reduced state at its equilibrium nuclear configuration and at the equilibrium configuration appropriate to its oxidized state; the half-filled circles refer to ionization of the reduced state at the nuclear configuration appropriate to the intersection region. The level in well 1 is initially occupied in (a) and the level in well 2 in (c) .

Marcus Equation I

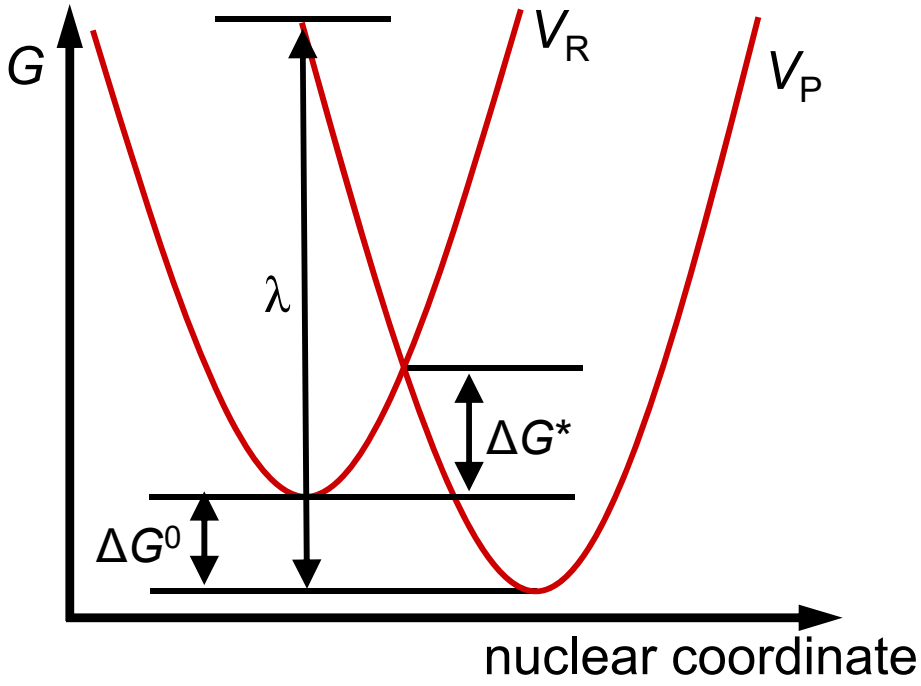

Arrhenius expression

$$k = A\, e^{-\Delta G^*/k_B T}$$

$$\Delta G^* = \frac{\left(\lambda + \Delta G^0\right)^2}{4\lambda}$$

reorganisation energy

'*A*' contains attempt frequency and electronic coupling (tunneling probability ~ $e^{-\beta r}$).

$$k = \frac{2\pi}{\hbar} V_0^2\, e^{-\beta R}\, \frac{1}{\sqrt{4\pi\lambda k_B T}}\, e^{-\frac{\left(\lambda+\Delta G^0\right)^2}{4\lambda k_B T}}$$

(general expression)

Marcus Equation II

The Inverted-Region Effect

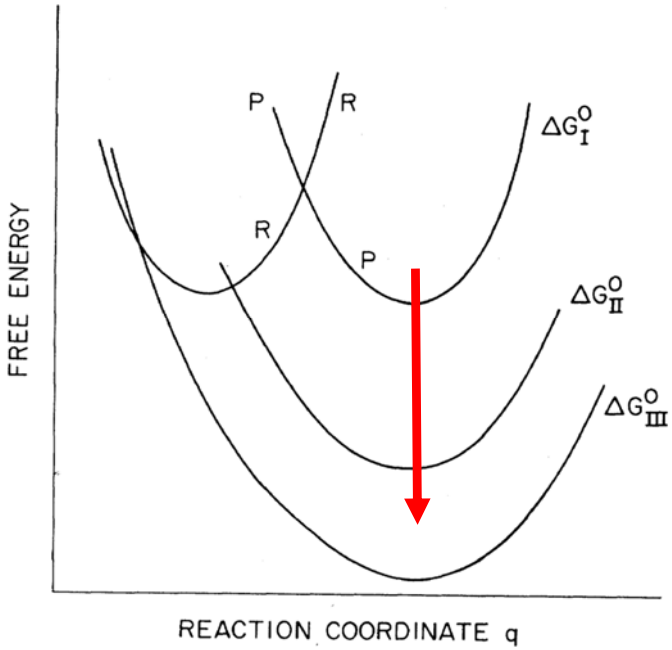

Plot of the free energy *G* vs. the reactants (R) and products (P) for three different values of ΔG^0, in the cases I to III indicated below.

Experimental Confirmation of Inverted Region

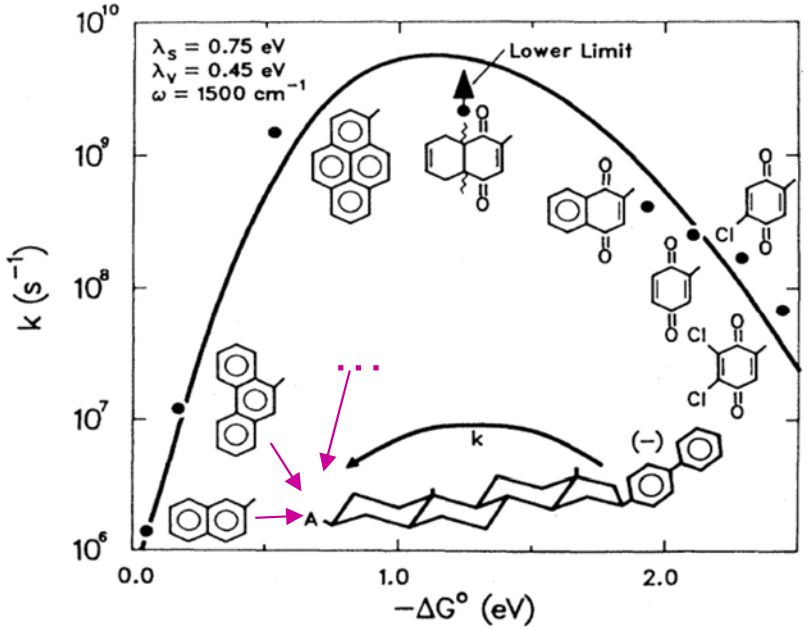

Inverted region effect in chemical electron transfer reactions (Miller et al., JACS 106 (1984) 3047).

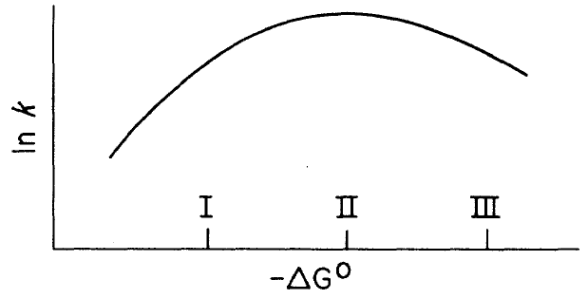

Plot of ln *k* vs $-\Delta G^0$. Points I and III are in the normal and inverted regions, respectively, while point II, where ln *k* is at its maximum, occurs at $-\Delta G^0 = \lambda$.

Quantum-Mechanical Theory I

We consider two states, a ≡ DA, and b ≡ D^+A^-. A weak coupling exists so that the (metastable) state a transforms into b in a nonadiabatic transition, which is irreversible because of

- a dense set of states in b
- vibrational relaxation.

Using the Born-Oppenheimer approximation, the wave functions of states a and b are given by

$$\psi_{a,v} = \phi_a(\vec{r};\vec{q})\,\chi_{av}(\vec{q}) \qquad H = H_0 + V,$$

$$\psi_{b,w} = \phi_b(\vec{r};\vec{q})\,\chi_{bw}(\vec{q}) \quad \leftarrow \text{ these are eigenstates of } H_0$$

electronic / nuclear parts of wave function

The nuclear motions are governed by the multidimensional energy surfaces $U_a(\vec{q})$ and $U_b(\vec{q})$, $\vec{q}$ are the normal modes.

v, *w* represent two sets of vibrational quantum numbers.

Jortner, BBA 594 (1980) 193-230

Quantum-Mechanical Theory II

A weak coupling (one-electron two-center exchange interaction) exists between a and b,

$$V_{av,bw} = \int d\vec{r} \int d\vec{q}\, \phi_a(\vec{r},\vec{q})\chi_{av}(\vec{q})\hat{V}(\vec{r})\phi_b(\vec{r},\vec{q})\chi_{bw}(\vec{q})$$

which affects the electronic part of the wave function only (Condon approximation)

$$V_{av,bw} = \langle \phi_a \mid \hat{V} \mid \phi_b \rangle \langle \chi_{av} \mid \chi_{bw} \rangle$$

The microscopic rate coefficient *k* for the nonadiabatic transition a $\rightarrow$ b is given by Fermi's Golden Rule:

$$k_{ab}^{v} = \frac{2\pi}{\hbar} \sum_{w} |V_{av,bw}|^2 \, \delta(E_{bw} - E_{av})$$

av $\rightarrow$ any bw

$$= \frac{2\pi}{\hbar} |V|^2 \cdot \sum_{w} |\langle \chi_{av} \mid \chi_{bw} \rangle|^2 \, \delta(E_{bw} - E_{av})$$

$$V = \langle \phi_a \mid \hat{V} \mid \phi_b \rangle$$

Quantum-Mechanical Theory III

Usually, it is assumed that the electron transfer process occurs from an initial vibrational manifold in thermal equilibrium:

$$k_{ab} = \frac{2\pi}{\hbar} |V|^2 \, FC$$

thermally averaged Franck-Condon factor

electronic coupling matrix element

$$FC = \sum_v \sum_w \rho_v \, |\langle \chi_{av} | \chi_{bw} \rangle|^2 \, \delta(E_{bw} - E_{av})$$

$$\rho_v = \frac{\exp(-E_{av} / k_B T)}{\sum_v \exp(-E_{av} / k_B T)}$$

$$|V|^2 \approx |V_0|^2 \, e^{-\beta R} \quad \rightarrow \quad \text{Gamow}$$

β = 0.7 Å^{-1} : covalent bonds
β = 2.8 Å^{-1} : vacuum
β = 1.4 Å^{-1} : proteins

factor 10 every 1.7 Å!

Quantum-Mechanical Theory IV

BOX 1 Equations and parameters of electron transfer

Equation/symbol		Definition

$$k_{et} = \frac{2\pi}{\hbar} V_R^2 FC \qquad (1)$$

Electron-transfer rate: Fermi's golden rule derived from quantum mechanical perturbation theory applied to non-adiabatic reactions

V_R^2	Electronic coupling	Quantum mechanical matrix element coupling reactant and product electronic wavefunctions.
FC	Franck–Condon-weighted density of states	Integrated overlap of reactant and product nuclear wavefunctions of equal energy.
$\hbar$	Planck's Constant	

$$V_R^2 = V_0^2 \exp(-\beta R) \qquad (2)$$

Electronic coupling reflecting simple exponential decay of electronic wavefunctions with distance

V_0^2	Maximum electronic coupling	
R	Distance	Centre of edge atom of donor to centre of edge atom of acceptor.
β	Beta	Exponential coefficient of decay of electronic coupling with R.

Moser et al., Nature 355 (1992) 796.

Quantum-Mechanical Theory V

$$FC = (4\pi\lambda kT)^{-1/2} \exp -[(-\Delta G^\circ - \lambda)^2/4\lambda kT] \qquad (3a)$$

Marcus classical form of overlap of harmonic oscillator wavefunctions with identical frequencies[3]

λ	Reorganization energy	Energy required to distort nuclear configuration of product state into the geometry of the reactant state without electron transfer. Generally rises with the increased polarity of the redox centre environment.
$-\Delta G^\circ$	Free energy	Difference between reactant and product state
k	Boltzman constant	

$$FC = (\hbar\omega)^{-1} \exp[-S(2n+1)] \left(\frac{n+1}{n}\right)^{P/2} I_p[2S\sqrt{n(n+1)}] \qquad (3b)$$

Quantum-corrected Marcus-type expression of Levich and Dogonadze[7] and of Jortner[8]. Other expressions explicitly combine quantum high-frequency and classical low-frequency motion[8].

$\hbar\omega$	Characteristic frequency	Reorganization energy-weighted average of frequencies of harmonic oscillators coupled to electron transfer, in energy units. Vibrations involving solvent, protein medium and redox cofactors range from <10 meV to >200 meV.
$S = \lambda/\hbar\omega$		Characteristic frequency normalized λ.
$P = -\Delta G^\circ/\hbar\omega$		Characteristic frequency normalized free energy.
$n = [\exp(\hbar\omega/kT) - 1]^{-1}$		Average harmonic oscillator vibrations level populated at temperature T.
$I_p()$	Modified Bessel function of order P	

$$FC = (2\pi\sigma^2)^{-1/2} \exp[-(\Delta G - \lambda)^2/2\sigma^2] \qquad (3c)$$

Semiclassical Hopfield expression[9]. This simple gaussian form is usually quite similar to equation (3b)

$\sigma^2 = \lambda\hbar\omega \coth(\hbar\omega/2kT)$	Variance of distribution with quantum correction for low temperatures.

Franck-Condon factor:

3a) Classical expression,
valid if $\hbar\omega_i \ll kT$
for all vibrations coupled to ET

3b) Coupling to a single, "effective" mode.

3c) High T limit: coth → 1/x ➔ $\sigma^2 = 2\lambda kT$ (Marcus)
Low T limit: coth → 1 ➔ $\sigma^2 = \lambda\hbar\omega$
($\hbar\omega/2$ instead of kT)

Moser et al., Nature 355 (1992) 796.

Franck-Condon Factors

$\hbar\omega > kT$:
only vibrational ground state of donor potential occupied

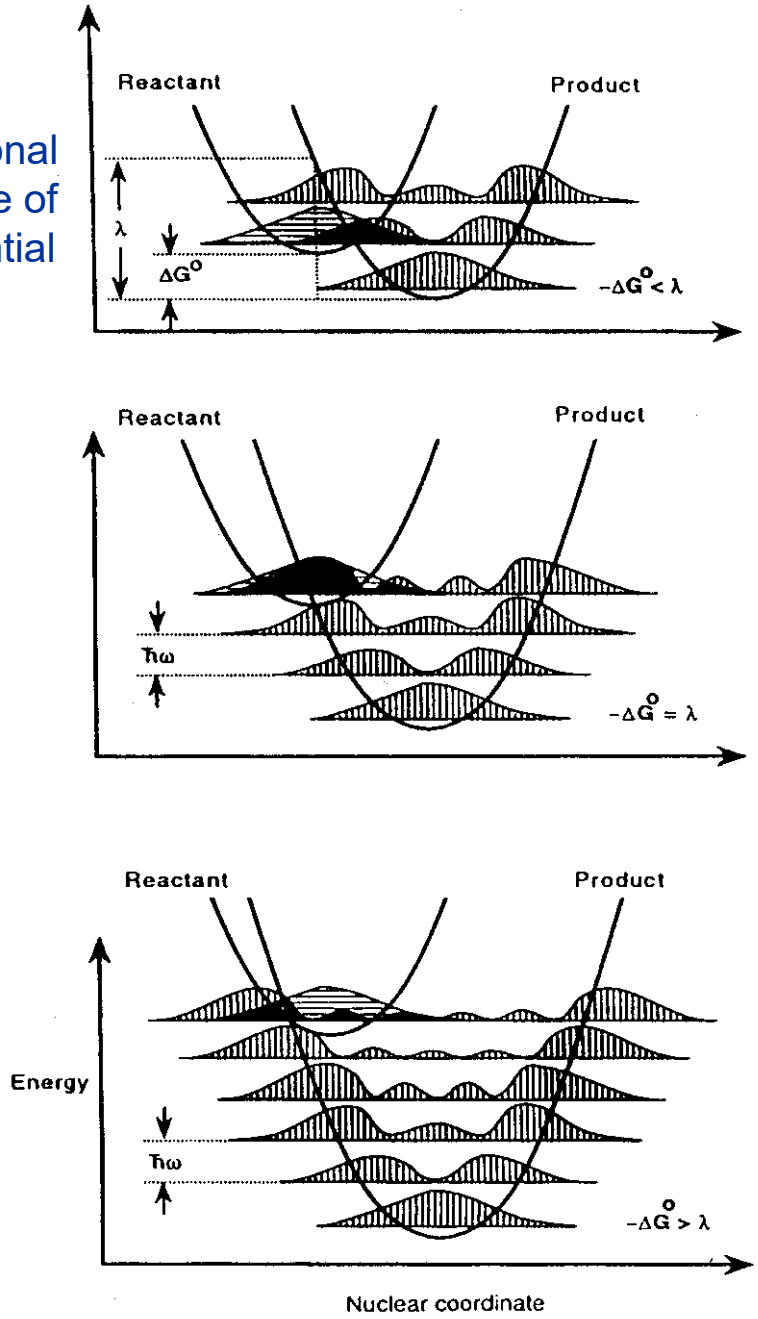

Intersecting parabolic potential energy surfaces represent classical reactant and product harmonic oscillators for three electron-transfer reactions with different free energies.

Quantum mechanical harmonic oscillator wavefunctions $|\Psi|^2$ are superimposed on these parabolas.

Franck-Condon factors are proportional to the overlap of reactant nuclear wavefunctions (horizontal shading) and product wavefunctions (vertical shading).

Overlap will be maximal when the free energy of the reaction ($-\Delta G^0$) matches the reorganization energy (λ). λ, held constant in this figure, represents the energy required to move along the product potential surface as the nuclear geometry is distorted from the average product configuration to the average reactant configuration.

Harmonic oscillator energy levels are separated by quantum energy $\hbar\omega$. For clarity, only the lowest energy-reactant vibrational state is shown, corresponding to a Boltzmann thermal energy $kT << \hbar\omega$.

Redox Cofactor Arrangements

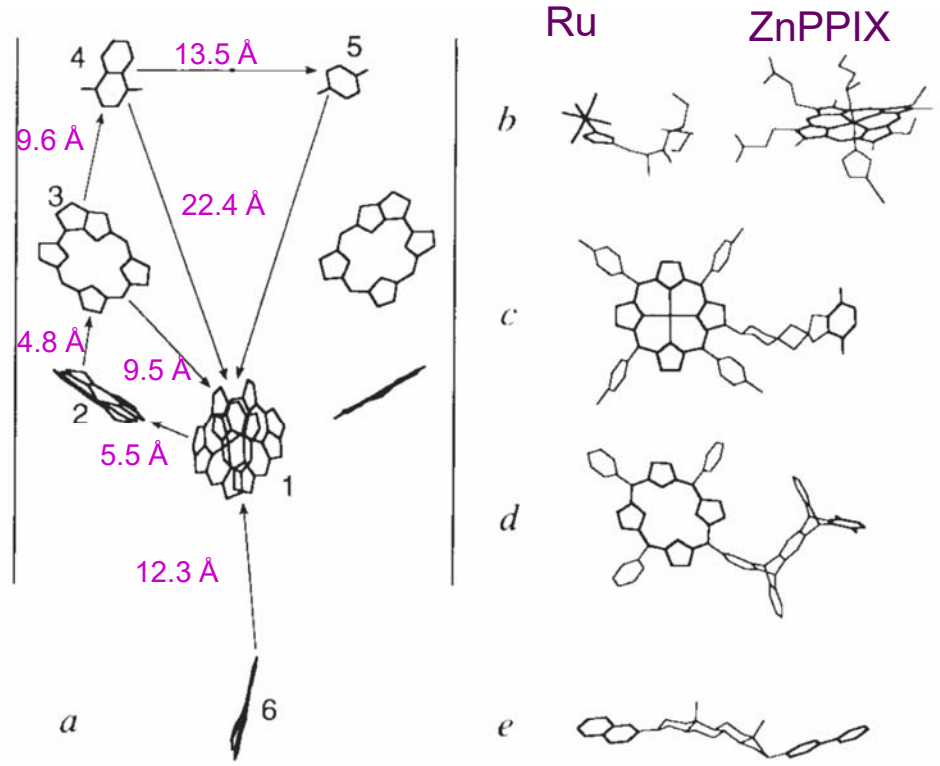

Representative structures of electron-transfer systems with well defined donor-acceptor distances. **(a)** Geometry of the cofactors of the photosynthetic RC of *Bl. viridis*. After light excitation of the bacteriochlorophyll dimer (1) electron transfer progresses sequentially through bacteriochlorophyll monomer (2), bacteriopheophytin (3), primary quinone (4), and secondary quinone (5). The resultant positively charged oxidized dimer ($BChl_2^+$) can be rereduced by the nearest of four bound haem cytochrome c (6). Arrows: physiologically productive charge separations and non-productive charge recombinations. Vertical lines: rough dimension of the membrane profile across which the light-driven electron transfer generates transmembrane potential. The two cofactors symmetric to 2 and 3 do not seem to be involved as redox intermediates and their function is uncertain.

(b) Semisynthetic system of ruthenated histidine 39 (left) and zinc-substituted haem (right) of a cytochrome c from *Candida krusei*. **(c)** Porphyrin-quinone pair linked covalently by a saturated spirocyclobutane bridge containing one cyclobutane unit. **(d)** Porphyrin-quinone pair linked covalently by the pentiptycene bridge containing four aromatic rings. **(e)** Naphthalene-biphenyl pair linked covalently by steroid bridge and activated by pulse radiolysis. Donor and acceptor redox centers are illustrated with thicker lines than the amino acids and bridging groups.

Free Energy Dependence of ET Rates

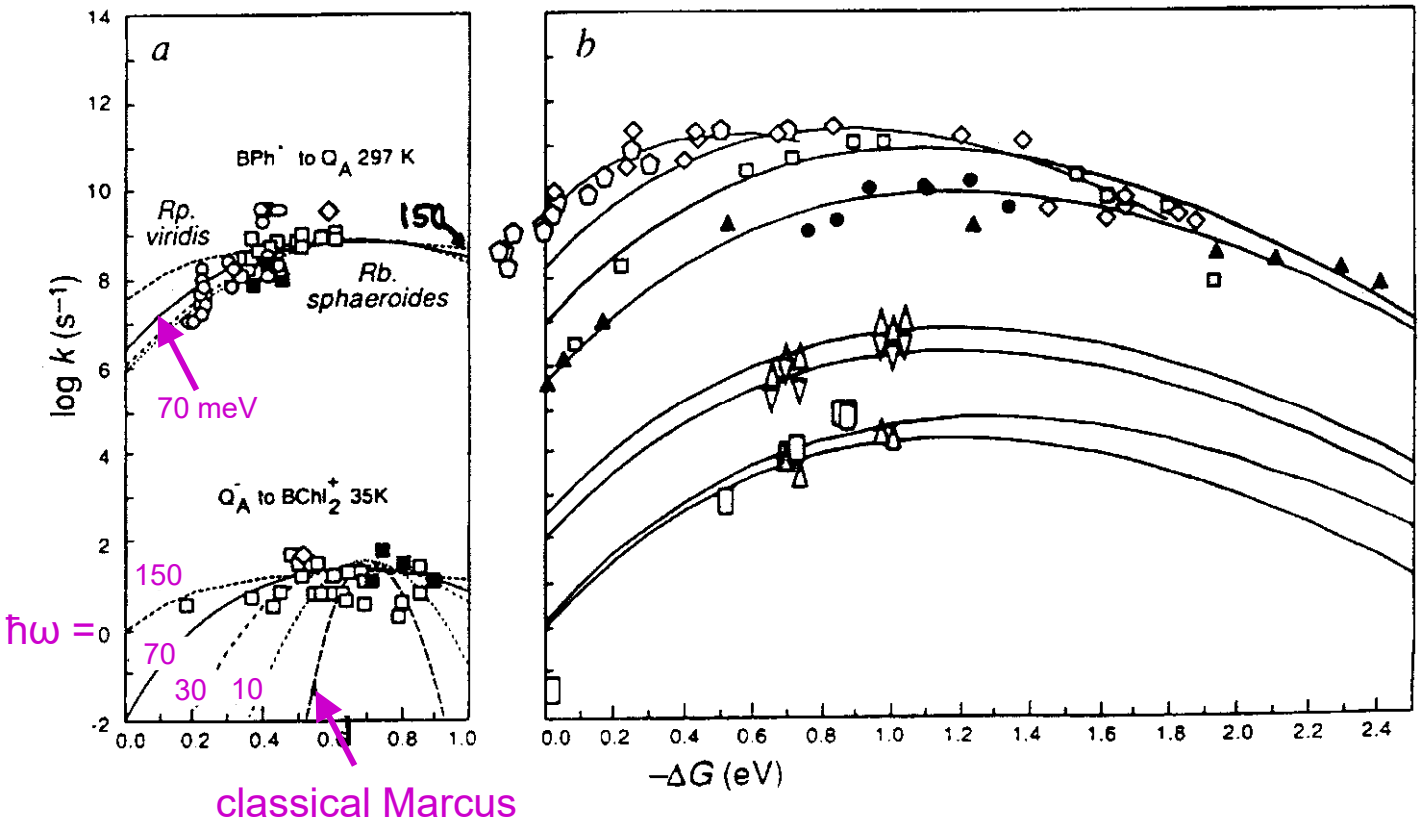

Free energy dependence of electron transfer rates in various systems.

(a) BPh^- to Q_A and Q_A^- to $BChl_2^+$ in photosynthetic RCs. The free energy was changed by replacing the native Q_A with other compounds with different electrochemistry. *Rb. sphaeroides*: native quinone (◇), non-native quinones (□), non-quinonoids (■); *Rp. viridis*: native quinone: (⬭), non-native quinones (○). The data are fits with the quantized Marcus expression (Eq. 3b, Slide 12) with λ = 0.7 eV for both reactions, $\hbar\omega$ is varied as shown in the figure.

(b) Semisynthetic ruthenium-cytochrome c (▽, △) and ruthenium-myoglobin systems (□); bridged porphyrin-quinone (◇), (▯), (●); biphenyl-acceptor (▲) and diiridium-pyridinium (▣) molecules. A common value of $\hbar\omega$ of 70 meV with the published values of λ were used to fit all the data (T ~ 290 K).

Rate versus Distance Relation

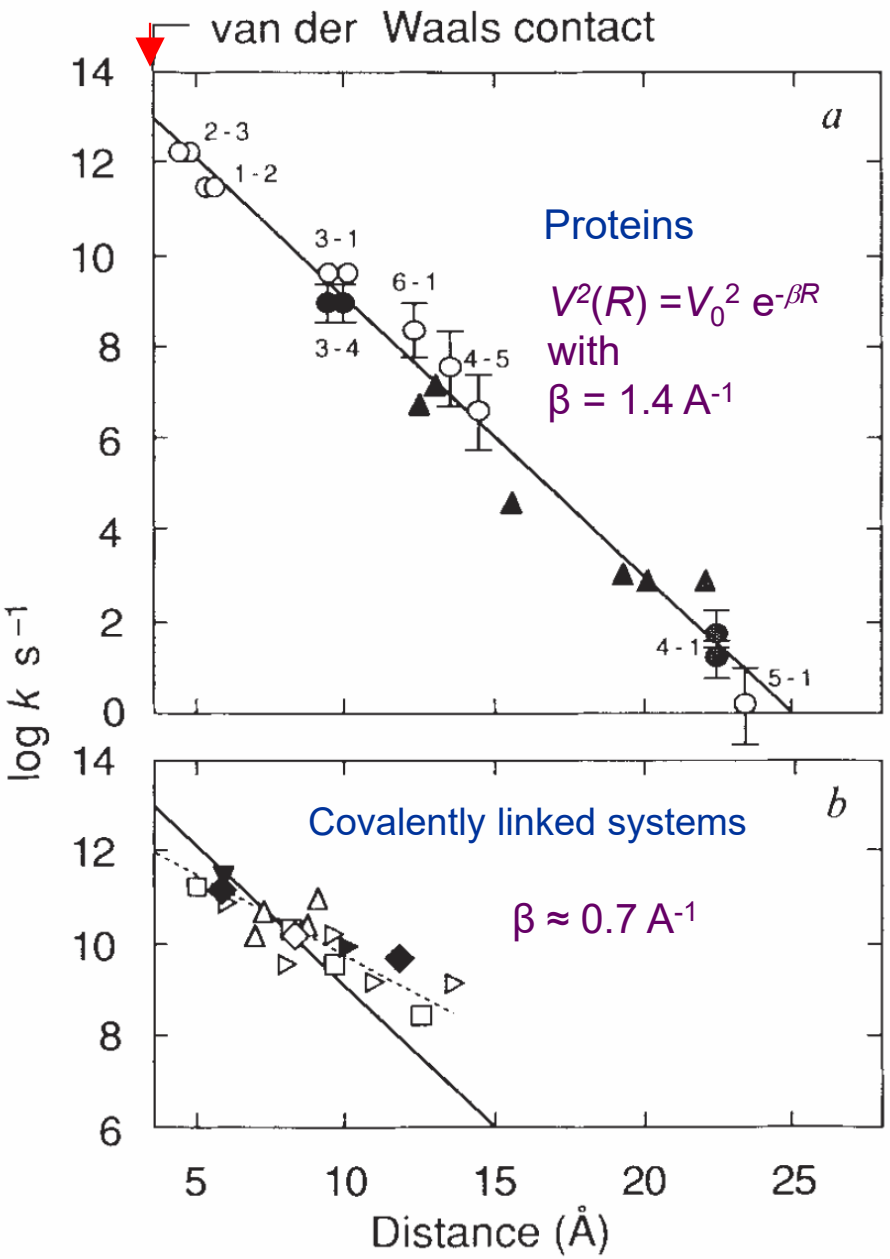

Free-energy optimized rate versus edge-to-edge distance relationship for electron transfer.

(a) Proteins, including the photosynthetic RC (○) and semi-synthetic Ru-cyt c and Ru-Mb (△); filled symbols refer to previous figure. Numbers refer to cofactors involved in photosynthetic charge separation in the reaction centre: $BChl_2$ (1), BChl (2), BPh (3), Q_A (4), Q_B (5) and cyt c (6). Error bars are associated with uncertainties in rate optima: for cyt c to $BChl_2^+$ the error bars span a λ range of 0.7 to 1.0 eV; for Q_A^- to Q_B and Q_B^- to $BChl_2^+$ which may have quite polar environments, the error bars span a λ range of 0.7 to 1.3 eV.

(b) Covalently linked systems. Triangles represent bridges incorporating aromatic groups: triptycene (▽), pentiptycene (△), others (▷). Quadrilaterals represent bridges without aromatic groups: spirocyclobutanes (0-3 units; □), others (◇). Filled symbols refer to previous figure.

The fitted line of (a) represents a simple exponential decay with β of 1.4 Å^{-1}. Distance is defined as center of edge atom of donor to centre of edge atom of acceptor; thus the vertical line at 3.6 Å represents van der Waals contact.

Engineering ET Proteins I

- At room temperature, an empirical Marcus-type relationship can be used to calculate the rate coefficient as a function of the (edge-to-edge) distance and the two parameters λ, ΔG:

"Dutton's ruler"

in [s^{-1}] ↙ R in [Å] ↙

$$\log k_{ET} = 15 - 0.6\,R - 3.1\,\frac{(\Delta G + \lambda)^2}{\lambda}$$

↖ energies in [eV]

Here, the factor 0.6 = β/ln 10, with β = 1.4 $Å^{-1}$, and the factor 3.1 = (ln 10 · 2 $\hbar\omega$)$^{-1}$, where $\hbar\omega \approx 70$ meV ("effective" mode) is assumed (Eq. 3b, Slide 12, low T limit).

- With this relation, we can investigate the design principles of ET proteins.

Engineering ET Proteins II

Distances

- The chemi-osmotic membrane system demands ET over at least 35 Å in the low-dielectric profile of the membrane.

- It is impossible to have ET between two redox centers separated by 35 Å at a rate comparable with the submillisecond lifetime of encounter complexes with, e.g., cyt c or quinones.

  $\Rightarrow$ at least two sequential ET processes are necessary.

- RCs have an even more severe time constraint: since the lifetime of the electron donor in the excited state is only on the order of nanoseconds, the initial transfer must happen on a subnanosecond scale.

  $\Rightarrow$ Photosynthetic RCs need at least three steps:
  (e.g., $P^* \rightarrow H_A \rightarrow Q_A \rightarrow Q_B$).

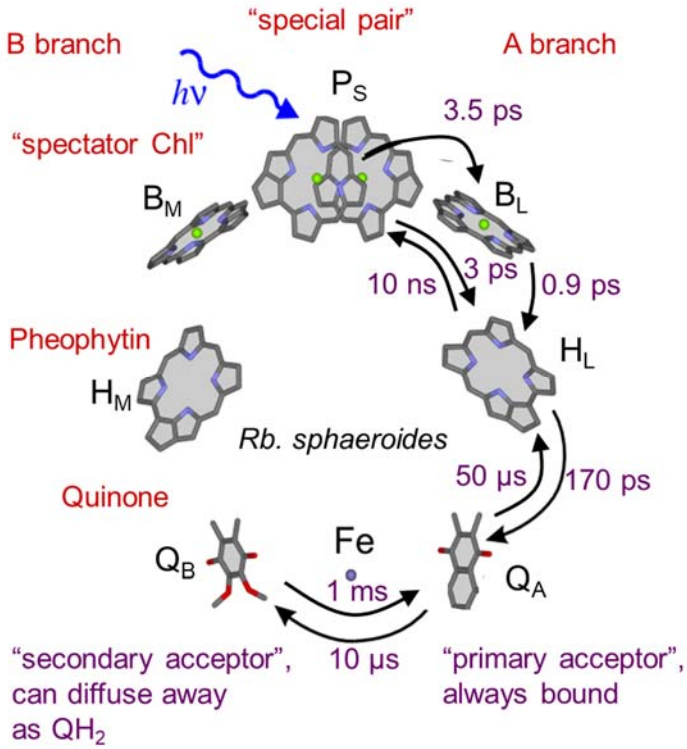

Franck-Condon Factors I

- Natural systems want to minimize free energy expenditure in forward direction (ΔG). However, a decrease is necessary to avoid thermal repopulation of the donor state.

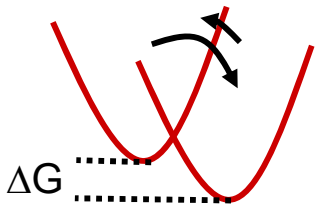

- Delocalized systems (Chl, Phe, Q) in a low-dielectric environment are employed because they have small λ values (typically ~600 − 800 meV).

- Initial charge separation competes with large ΔG back reaction over the same distance. A small $\lambda \approx 300$ meV in this step may reflect selection pressure to push the back reaction into the inverted region, thereby creating a large barrier.

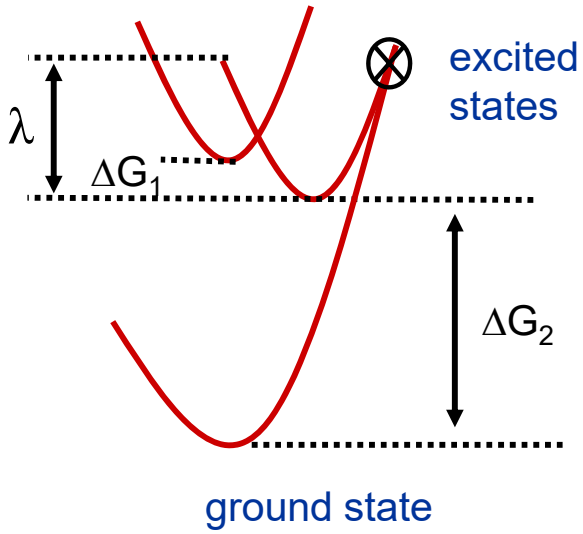

Franck-Condon Factors II

- The B branch of RC is inactive in spite of the same ET distances ($k_M < 0.01\ k_L$) because of the FC factor. Presumably, $\lambda \approx 600$ meV (?) and $\Delta G \approx +200$ meV (?) for the primary step.

- ΔG values for return of electron from Q_A^- and Q_B^- are similar, yet it is more stable on Q_B^- (seconds instead of ~ 100 ms). Fairly polar Q_B site provides large λ .

- Two-step initial charge separation can be rapid, and recombination over longer distance is slower ($e^{-\beta R}$!).

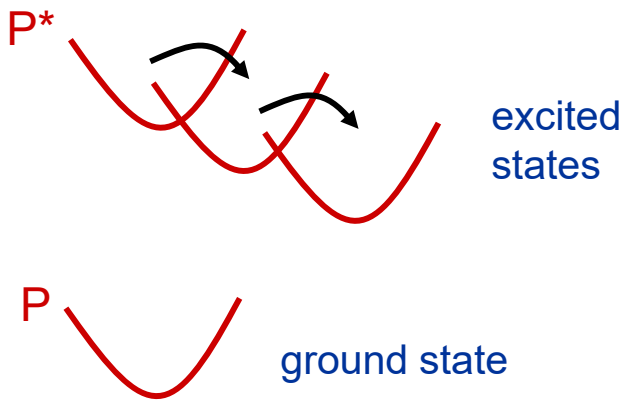

De novo RC Design I

- Assume edge-to-edge distance of primary donor and terminal acceptor 41 Å .
- Assume photon energy ~ 1.4 eV. ← 870 nm (peak absorption of special pair in *Rh. sphaeroides*)
- A three-step design leads to 20 ns charge separation at 99% efficiency.
- From 1.4 eV input, ~ 0.8 eV can be achieved (theoretically!) as chemical potential, compared with 0.4 eV for native RCs !

De novo RC Design II

Possible arrangements of redox centers for efficient charge separation in a hypothetical photosynthetic protein. The overall distance of charge separation between C and Q is represented as the same distance as cytochrome c to Q_A electron transfer of the photosynthetic reaction center.

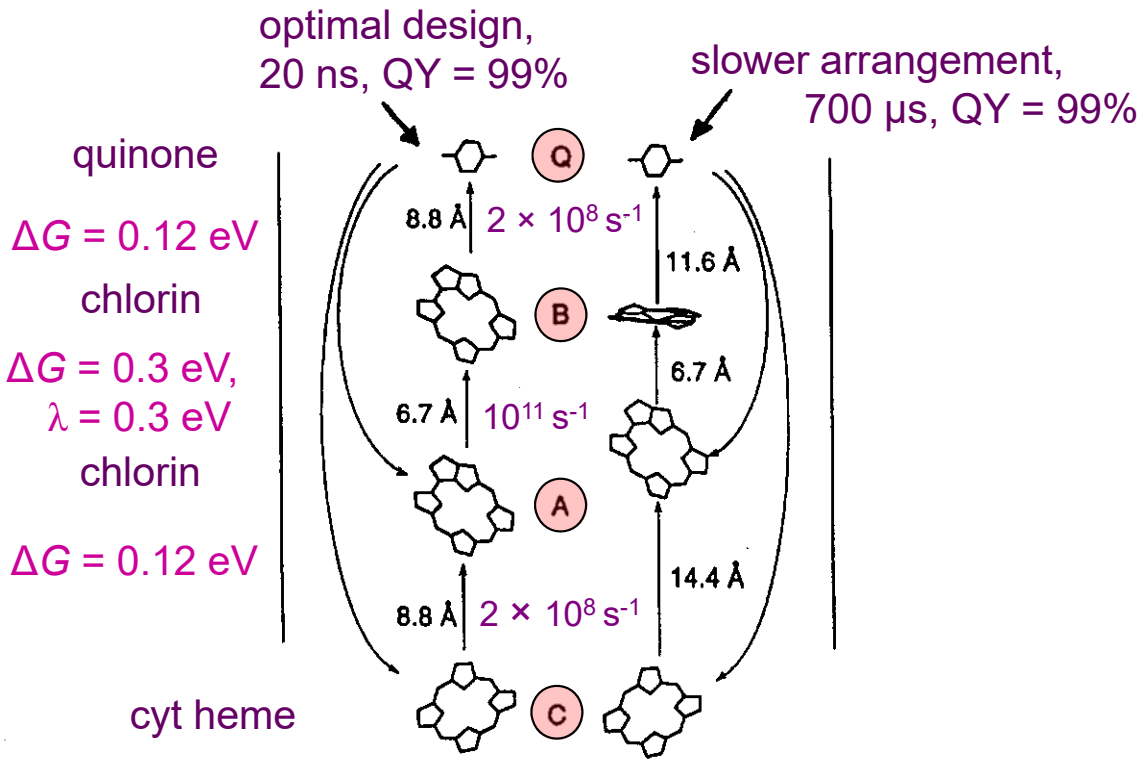

A and B: chlorin-type redox centers that function as absorber of light energy and electron-transfer intermediate, respectively.

Distances and free energies of reactions are chosen according to the first order description of intraprotein electron transfer, to achieve 99% quantum efficiency in charge separation across a low dielectric membrane with millisecond or better stability and minimum consumption of free energy. The optimum geometry of redox centers is presented in the left half of the figure (with ET rates), poor orientation of redox center B is shown on the right.